

FUNDAMENTAL STRATIGRAPHIC, SEDIMENTOLOGIC, AND PETROPHYSICAL
ELEMENTS OF HETEROZOAN CARBONATES: GRAIN-RICH FINING- AND
SHOALING-UPWARD CYCLOTHEMS AND CLINOTHEMS

BY

Tony Michael Pugliano

Submitted to the graduate degree program in Geology
and the Graduate Faculty of the University of Kansas
in partial fulfillment of the requirements for the degree of
Master of Science.

Robert H. Goldstein, Co-chairperson

Evan K. Franseen, Co-chairperson

Committee members*

*
John Doveton

Date defended: 12/31/2015

The Thesis Committee for Tony Michael Pugliano certifies
that this is the approved Version of the following thesis:

FUNDAMENTAL STRATIGRAPHIC, SEDIMENTOLOGIC, AND PETROPHYSICAL
ELEMENTS OF HETEROZOAN CARBONATES: GRAIN-RICH FINING- AND
SHOALING-UPWARD CYCLOTHEMS AND CLINOTHEMS

Committee:

Robert H. Goldstein, Co-chairperson

Evan K. Franseen, Co-chairperson

John Doveton

Date approved: 12/31/2015

Abstract

Tony Michael Pugliano, M.S.
Department of Geology, December 2015
The University of Kansas

This research documents Pliocene and Miocene outcrops from SE Spain to evaluate controls on stratigraphic architecture and petrophysical properties of carbonate rocks of the heterozoan association. It shows that grain-rich, fining updip clinothems and fining-upward cyclothem are expected to form in heterozoan carbonate systems, and depending on degree of diagenetic alteration, some of these fundamental units of stratigraphic architecture have predictable petrophysical properties.

The Pliocene outcrop is a lowstand shaved-shelf system, forming a single prograding clinothem. Ten lithofacies are distributed along six depositional profiles that reflect four different environmental settings. Hypothetical progradation of each of these depositional profiles would form six end-member fining-updip and fining-upward, grain-rich clinothems. Proximal facies are the finest, and are composed of sorted bryozoan-coralline algae packstones. More distal facies are poorly sorted, rhodolith and bivalve rudstones.

Miocene deposits are composed of seven cyclothem, which drape and onlap a gently sloping surface. In proximal settings, cyclothem consist of poorly sorted rudstone facies that coarsen upward and then fine upward to a cross-bedded, well-sorted packstone. In medial to distal settings, cyclothem are coarse rudstone at the base, which fines upward to packstone. The most distal cycles consist of basal hemipelagic wackestones that are overlain by rudstone and packstone facies. Most typically, the cyclothem are coarse-grained facies at the base, interpreted to form during transgression, and overlain by a finer packstone, interpreted to form during a relative fall in sea level. The fine grain size is interpreted to form as waves rework coarse sediments into sorted,

abraded sands, creating a fining-upward trend. Bryozoans are most abundant in proximal areas and average 54% of the total sediment, bivalves dominate medial regions with 40%, and coralline algae in distal regions with averages of 33%.

The shoaling- and fining-upward, grain-rich cycles from the Miocene develop primarily from relative sea level and paleotopographic position. Using tilt-corrected paleotopography and interpretations of depositional environment from lithofacies, a quantitative sea-level curve has been developed and indicates typical sea-level amplitudes of 24-67m, with two outlier amplitudes that reach up to 116m.

In the Pliocene clinotherm, sorted packstones have 51% average porosity and 6,230md median permeability, whereas rudstone facies have 42% and 2,538md. Dolomitized Miocene packstones have 32% average porosity and 313md median permeability, and dolomitized rudstones have 36% average porosity and 115md median permeability, whereas least-altered Miocene packstones have 43% average porosity and 5,279md median permeability, and rudstones have 40% average porosity and 1,800md median permeability. These data indicate that sorted packstones have the highest original petrophysical values. Where diagenetically altered, packstones are more altered than genetic rudstones and therefore have higher variability. Originally high permeability of packstones appears to allow for enhanced diagenetic fluid flow, leading to increased alteration. In Pliocene and Miocene deposits that have not been extensively altered, and that lack calcisilt-rich caps, vertical depositional profiles show an upward increase in petrophysical values associated with upward shoaling. In diagenetically altered deposits, this predictable trend becomes more variable, and is commonly reversed.

These data indicate that heterozoan systems that have not been extensively diagenetically altered form petrophysical trends that are predictable based on the stratigraphic architecture and facies distribution of grain-rich shoaling- and fining-upward cycles. These outcrop analogs have

been developed into eight 3D Petrel™ reservoir-analog models and facies models to aid in predicting the distribution of reservoir character in similar deposits in the subsurface. The results establish controls that predict facies distribution and depositional trends to enable the modeling of petrophysical properties of heterozoan reservoirs in the subsurface of SE Asia, offshore Venezuela, and elsewhere.

Table of Contents

ABSTRACT.....	III
LIST OF FIGURES AND TABLES.....	IX
ACKNOWLEDGEMENTS	X
CHAPTER 1: Introduction.....	1
CHAPTER 2: Fundamental Elements of Stratigraphic Architecture in Heterozoan Carbonates: Grain-Rich Fining-and-Shoaling-Upward Cyclothems and Clinothems	4
Abstract.....	4
Introduction.....	5
Geologic Setting.....	8
Methodology	13
Pliocene stratigraphic architecture	15
Clinothem Geometry.....	15
Depositional Profiles (DP) of Facies on Clinothem Slopes.....	19
Pliocene Lithofacies and Interpretations	20
Silty Packstone.....	24
Sand-Gravel Packstone Association	26
Bioclastic Rudstone Association.....	30
Rhodolith-Bivalve Rudstone Association.....	32
Miocene Stratigraphic Architecture.....	36
Draping and Onlapping Cyclothems.....	36
Miocene Lithofacies and Interpretations... ..	37
Cross-Bedded Packstone Association.....	41
Bryozoan-Bivalve Rudstone Association	46
Bivalve Rudstone Association	48
Coralline Algae Rudstone Association	51
Planktonic Foraminifera Wackestone and Packstone Association	53
Miocene Cyclothems	56
Proximal Cyclothems.....	57
Medial Cyclothems	57

Distal Cyclothems	58
Discussion and Controls	58
Paleotopography and Substrate	58
Energy regime	61
Relative Sea Level	63
Sequence Architecture: Grainy fining- and shoaling-upward cyclothems	73
Application to the Subsurface	74
Conclusions	76
References Cited.....	79
CHAPTER 3: Controls on the Petrophysical Character of Grain-Rich Fining-Upward Cyclothems and Clinothems in Heterozoan Carbonates.....	87
Abstract.....	87
Introduction.....	88
Geologic Setting.....	89
Methodology	93
Lithofacies and Stratigraphy	94
Diagenesis.....	97
Pliocene diagenesis	97
Miocene diagenesis	98
Pore type Distribution and Classification.....	102
Petrophysical dataset	105
Descriptive Statistics.....	105
Petrophysical Correlations... ..	114
Petrophysical Distribution in Fining-Upward Trends... ..	122
Pliocene.....	122
Miocene.....	124
Discussion- Controls on Petrophysical Heterogeneity... ..	125
Grain Constituents... ..	127
Rock Texture and Grain Sorting	128
Sedimentary Structures	129
Diagenesis	130

Grain-Rich Shoaling- and Fining-Upward Cycles.....	134
Subsurface Implications	135
Reservoir Modeling	136
Reservoir analogs	144
Conclusions.....	145
References Cited.....	149
APPENDICES	154
Appendix I Measured Stratigraphic Sections	154
Appendix II Lithofacies.....	174
Appendix III Petrography.....	184
Appendix IV Grain Size Measurements and Sorting.....	251
Appendix V Diagenesis and Mineralogy	284
Appendix VI Miocene Paleobathymetric Quantification Data.....	291
Appendix VII Petrophysical Dataset and Correlations.....	292
Appendix VIII T & F Test Results.....	324
Appendix IX Petrel Input Data	326
Appendix X Reservoir Analog Workflow	333
Appendix XI Petrel Facies Models.....	336
Appendix XII Petrel Petrophysical Models.....	338
Appendix XIII Petrel Volumetric Calculations.....	340
Appendix XIV Compaction Algorithms.....	343

List of Figures & Tables

Chapter 2:

Figure 1 Location Map	9
Figure 2 Paleotopographic Maps	11
Figure 3 Miocene Stratigraphic Section	12
Figure 4 Key	16
Figure 5 Pliocene Photomosaic and Interpretations	17
Figure 6 Pliocene Organism Distribution	18
Figure 7 Pliocene Cross Section	18
Figure 8 Pliocene Depositional Profiles	22
Figure 9 Pliocene Grain Sorting Analysis	25
Figure 10 Packstone Facies and Photomicrographs	28
Figure 11 Rudstone Facies and Photomicrographs	34
Figure 12 Rhodolith Facies and Photomicrographs	35
Figure 13 Miocene Photomosaic	37
Figure 14 Miocene Cross Section	38
Figure 15 Miocene Organism Distribution	39
Figure 16 Miocene Grain Sorting Analysis	44
Figure 17 Wackestone Facies and Photomicrographs	55
Figure 18 Miocene Cycle Patterns	56
Figure 19 Miocene Cyclothem Development Model	66
Figure 20 Miocene Quantitative Relative Sea-Level Curve	68
Table 1 Pliocene Lithofacies Description	23
Table 2 Miocene Lithofacies Description	41

Chapter 3:

Figure 1 Location Map	90
Figure 2 Miocene Stratigraphic Section	92
Figure 3 Paleotopographic Maps	93
Figure 4 Pliocene and Miocene Cross Sections	96
Figure 5 Diagenetic Facies Photomicrographs	101
Figure 6 Dolomite Distribution along Ricardillo	102
Figure 7 Pores Type Distribution Photomicrographs	103
Figure 8 Sorted and Silty Packstone Pore Space Photomicrograph	104
Figure 9 Porosity Box and Whisker Plots	106
Figure 10 Diagenetic Porosity Box and Whisker Plots	106
Figure 11 Permeability Box and Whisker Plots	108
Figure 12 Diagenetic Permeability Box and Whisker Plots	109
Figure 13 Full Petrophysical Dataset Compared by Diagenetic facies	115

Figure 14 Dolomite and Moldic Porosity Correlation	116
Figure 15 Lithofacies Petrophysical Distribution	119
Figure 16 Grain Size and Petrophysical Distribution (Pliocene)	120
Figure 17 Rock Texture and Petrophysical Distribution	121
Figure 18 Sorting and Petrophysical Distribution (Pliocene)	122
Figure 19 Pliocene Petrophysical Vertical Distribution in Cycles	123
Figure 20 Miocene Petrophysical Vertical Distribution in Cycles	126
Figure 21 Compaction Algorithms	136
Figure 22 Pliocene Facies and Permeability Petrel Models	141
Figure 23 Miocene Facies, Porosity, and Permeability Petrel Models	143
Table 1 Diagenetic Facies Description	98
Table 2 Sedimentary Structures T Test Results	108
Table 3 Pliocene Lithofacies Petrophysical Dataset Summary	110
Table 4 Miocene Lithofacies Petrophysical Dataset Summary	111
Table 5 Miocene Diagenesis Petrophysical Dataset Summary	112
Table 6 Petrophysical Comparison between Lithofacies and Diagenesis	112
Table 7 Summary Table of Petrophysical Values by Textures and t- and F-test Results	114

ACKNOWLEDGMENTS

I would like to thank my advisors, Dr. Robert Goldstein and Dr. Evan Franseen for their support and assistance during my graduate work. I am grateful for the knowledge that they imparted to help me develop skills in scientific thinking, researching, and writing. Their insight and one-on-one teaching is one of the most beneficial things I received throughout my graduate studies. In addition, I am grateful for the funding they helped provide for this research, and for their devoted efforts towards the development and advancement of the KICC. The opportunity to add to their ongoing research in the Cabo de Gata of Spain, and the chance to do research in such amazing outcrops has been tremendously beneficial. I appreciate that they challenged me to develop new skills by providing me with the opportunity to have such an interdisciplinary thesis. I would also like to thank my undergraduate advisor Dr. Forest Gahn for opening up the world of carbonates to me and allowing me to have research opportunities in both ancient and modern carbonates as an undergraduate.

I thank the KU Department of Geology for providing coursework that allowed for studying the geosciences in the classroom, lab, and in the field. Dr. Hassan Eltom was generous of his time and willing to answer questions and assist me in my usage of PetrelTM. I gratefully acknowledge the Kansas Geologic Survey for the use of their facilities and specifically to Dr. John Doveton for his willingness to serve on my committee, and for his help in teaching me the skills in statistics and petrophysics that were necessary for this research. In addition, I would like to thank Dr. Jon Smith and Dr. Greg Ludvigson for allowing me to use their stepping stage and point counting software. Lastly from the KGS, I would like to thank Dave Laflen for letting me use the drill press to core my samples.

Wayne Dickerson and Mark Mercer are acknowledged for making hundreds of high quality thin sections for me, and Weatherford Labs for their affordable core plug measurements. KICC, AAPG, and SEPM provided grants to aid in this research, and hosted conferences that allowed me to display and promote my work.

I would like to thank my family for providing me the opportunity to grow up in an environment where I could learn and have many opportunities to determine what I enjoy doing. All of the love and guidance I received helped me to develop the skills that I have today and have gotten me to where I am. Lastly, I would like to thank my wife Sarah, not only for being my lovely field assistant, but for supporting me throughout graduate school and pleasantly dealing with my absence from home during all of the late nights and long days of coursework, research, and travel.

Chapter 1: Introduction

Heterozoan carbonates (e.g. James 1997) are common in the modern and in the stratigraphic record, yet there remains a dearth of broadly applicable stratigraphic, sedimentologic, and reservoir models to help in understanding them. If there are attributes that appear repeatedly in heterozoans, then those attributes could lead to useful models for understanding, and for prediction in the subsurface. This research is focused on a study of two exceptional exposures of heterozoan carbonates in the Cabo de Gata region of southeastern Spain, which allow for testing of hypotheses related to updip-downdip depositional trends, stratigraphic architecture, and reservoir character.

Previous work by Dillelt et al. (2004) has demonstrated that in one of these exposures, the Pliocene of the Carboneras basin, there is a lowstand clinothem that preserves paleotopography. The study showed that facies tended to fine up the depositional-dip, due to increases in abrasion and fragmentation from wave base on the top of the clinothem. Previous work by Toomey et al. (2003) on the Miocene deposits of the Ricardillo exposure noted multiple fining-upward cycles that draped and onlapped a gently sloping surface. The fining-upward trend was interpreted to result from relative falls in sea level and increased abrasion associated with wave base effects. These two areas, both of which show evidence for coarsening in deeper waters and fining in shallower waters, provide the record to evaluate if there are predictable updip-downdip trends that could lead to a fundamental model of stratigraphic architecture that could be broadly applicable to many heterozoan systems. Moreover, the outcrops allow for a comparison between those depositional trends and petrophysical properties, to determine if there is a predictable reservoir unit that can be helpful in modeling heterozoan reservoir performance. The effect of diagenesis on petrophysical properties can be evaluated as well, as the Pliocene outcrops have experienced

little diagenetic alteration and the Miocene outcrops have received significant calcite cement, and have been extensively dolomitized (Li et al. 2013; 2014).

The data, results, and interpretations of this thesis are presented as two papers and comprise Chapters 2 and 3. Chapter 2 describes, classifies, and quantifies properties from a total of 23 heterozoan carbonate lithofacies from both field areas and explains the stratigraphic architecture and cycle patterns that these lithofacies construct. The mechanisms behind the development of these trends include: paleotopography, climate, nutrients, energy regime, and relative sea level, and are also discussed in this chapter. Although the Pliocene and Miocene deposits form under different depositional settings, at different scales, and with a different sea-level history, fining- and shoaling-upward depositional trends are developed in both systems. Therefore, this research proposes that this depositional pattern should lead to fundamental building blocks for heterozoan carbonates that can be used to better understand stratigraphic architecture and facies distribution. The result is that grain-rich fining-upward cyclothem and fining-updip clinothem emerge as fundamental stratigraphic units in heterozoan systems. This chapter is formatted according to the Journal of Sedimentary Research publication style.

Chapter 3 details petrophysical properties for heterozoans within the context of grain-rich fining-upward cyclothem and fining-updip clinothem, and the amount and type of diagenetic alteration. In the relatively unaltered deposits, the stratigraphic architecture leads to predictable petrophysical properties. In units in which a capping calcisilt-rich facies (interpreted as shallow sea grass environments) was absent, fining-upward and fining-updip is associated with increased porosity and permeability, associated with fining. Where the calcisilt-rich facies is present, there is a capping facies of lower porosity and permeability. The data on the least diagenetically altered

deposits show that these trends may be preservable in the subsurface, but where diagenetic alteration has been significant, they are totally obscured, and in some cases, inversed. This chapter is formatted according to the American Association of Petroleum Geologist Bulletin publication style.

REFERENCES CITED

- Dillett, P.M., Goldstein, R.H., Franseen, E.K., 2004, Paleotopographic and sea-level controls on the sequence stratigraphic character of a heterozoan carbonate succession: Pliocene, Carboneras Basin, southeast Spain: Master's Thesis, University of Kansas, Lawrence, 119 pp.
- James, N. P., 1997, The cool-water carbonate depositional realm, in James, N.P. and Clarke, J.A.D., eds., Cool-water Carbonates: SEPM, Special Publication 56, p. 1-20.
- Li, Z., Goldstein, R.H., and Franseen, E.K., 2013, Ascending Freshwater Mesohaline Mixing: A New Scenario for Dolomitization: *Journal of Sedimentary Research*, v. 83, p. 277-283.
- Li, Z., Goldstein, R.H., and Franseen, E.K., 2014, Climate, duration, and mineralogy controls on meteoric diagenesis, La Molata, southeast Spain: Interpretation, *Journal of SEG/AAPG*, v. 2, p. 111-123.
- Toomey, N., Goldstein, R.H., Franseen, E.K., 2003, Controls on Sequence Stratigraphy in Upper Miocene Carbonates of Cerro De Ricardillo, Southeastern Spain: Master's Thesis, University of Kansas, 146 pp.

Chapter 2:

Fundamental Elements of Stratigraphic Architecture in Heterozoan Carbonates:

Grain- Rich Fining-and-Shoaling-Upward Cyclothem and Clinothem

Tony M. Pugliano, Robert H. Goldstein, and Evan K. Franseen

*Department of Geology, the University of Kansas, 1475 Jayhawk Boulevard, 120 Lindley Hall,
Lawrence, KS, 66045, USA*

ABSTRACT

Heterozoan carbonates form broad extensive ramps and are common in ancient and modern systems with meso-eutrophic conditions and cooler waters (<20°C). Although heterozoan carbonates are widespread throughout the geologic record, there are many unknown characteristics regarding stratigraphic architecture, sedimentology, facies distribution, diagenesis, and reservoir character. Late Miocene and early Pliocene intervals of temperate climate allowed for the deposition of heterozoan carbonates on the flanks of underlying volcanic basement and older carbonate strata in SE Spain. The heterozoan carbonate complexes of the Cabo de Gata region provide ideal outcrop analogs for evaluating characteristics and controls on properties of such deposits. Pliocene deposits are composed of a prograding clinothem with six depositional profiles, reflecting four depositional environments in the basin. The clinothem shows trends that fine updip, from rudstones in distal regions to packstones in proximal regions. Proximal facies contain sorted and unsorted bryozoan-coralline algae packstones; time equivalent strata immediately downdip, are poorly sorted, rhodolith and bivalve-rich rudstones. In contrast, Miocene strata are composed of stacked cyclothem; each cyclothem consists of basal transgressive, coarse-gravel rudstones and an upper regressive, cross-bedded mud-poor packstone. During shoaling, waves reworked coarse sediments into sorted, abraded sands,

creating a fining-upward trend. Miocene cyclothems form predictable patterns that are dependent on paleotopographic position. Cyclothems are composed of three facies deposited on the proximal ramp: two poorly sorted rudstone facies that coarsen upward and are sharply overlain by a cross-bedded, moderate to well-sorted packstone. Medial and distal cyclothems are composed of two facies: a coarse rudstone overlain by a cross-bedded, moderate to well-sorted packstone. The most distal cyclothems consist of basal hemipelagic wackestones overlain by rudstone and packstone facies. The Miocene strata are similar to the Pliocene clinothem in that fossil constituents show peak amounts of bryozoans in the proximal ramp, bivalves in the middle ramp, and coralline algae and rhodoliths in distal regions of the ramp. In the Miocene outcrops, hemipelagic/turbidites and grain-rich debrites are deposited in the deepest water environments. Paleotopography and facies distribution allows for the quantification of relative sea-level changes. Typical amplitudes range from 24 to 67m and reflect glacioeustatic fluctuations in sea level common during the Miocene. Fining-updip depositional trends and fining-upward shoaling cycles are proposed as a fundamental depositional motif in shallow, grain-dominated heterozoan carbonate deposits. This model can be applied to other ancient and modern systems, especially to Miocene deposits throughout the Mediterranean and South China Sea.

INTRODUCTION

The stratigraphic record and modern depositional settings show that heterozoan carbonates are abundant worldwide. The term *heterozoan carbonates* describes carbonate complexes and ecosystems composed of heterotrophic filter feeders and coralline algae that lack abiotic grains, are predominately calcite, precipitate minor abiotic cement, produce little mud, are light independent (with the exception of coralline algae), thrive in mesotrophic-eutrophic

conditions, and are temperature independent (James 1997). Heterozoans do not form shallow-water mounds, reefs, bioherms, large shoals, or barriers and therefore are exposed to the effects of high physical energy, causing abrasion, erosion, winnowing, and the development of hardgrounds and surfaces of non-deposition above fairweather wave-base (James 1997; Bassi 2006).

Although these systems dominate temperate, polar, oligophotic, and eutrophic systems, the majority of research in carbonate sedimentology, stratigraphy, and reservoir character has focused on photozoan systems. Previous work on heterozoan carbonates, both ancient (Lees and Buller 1972; Lees 1975; Carannante et al. 1981, 1988; Simone and Carannante 1988; Nelson et al. 1988; Scoffin 1988; Scoffin and Bowes 1988; Boreen and James 1993; Martin and Braga 1994; Martin et al. 1996; Franseen et al. 1997; James 1997; James and Clarke 1997; Betzler et al. 2000, Schlager 2000, 2003, 2005) and modern (James 1997; James et al. 1992, 1994, 1999, 2000, 2001; Freiwald 1998; Michel et al. 2011), has furthered the understanding of lithofacies characterization and depositional controls. Despite this body of research, there are still many unknowns regarding microfacies analyses, facies distribution, depositional trends, stratigraphic packaging, and reservoir character.

Miocene and Pliocene heterozoan carbonate complexes of the Cabo de Gata region of SE Spain (Fig. 1) provide ideal outcrops for measuring, describing, and modeling sedimentologic and reservoir properties of such deposits. In particular, Pliocene heterozoans of the Carboneras Basin were deposited in association with a shaved-shelf system (e.g. James 1994) and include a grain-rich prograding clinothem with fining-updip depositional profiles (Dillett et al. 2004). Miocene heterozoan carbonates of the Ricardillo area contain stacked, laterally extensive packages of partially dolomitized cyclothem. There are two types: one that shoals

and fines upward (Toomey et al. 2003); and another that deepens and coarsens upward at its base, and shoals and fines upward at its top.

These grainy, fining-updip, and fining-and-shoaling-upward trends are distinctly different depositional patterns compared to what has been modeled for photozoan carbonate systems and are in stark contrast to the more common coarsening-upward or coarsening-updip motifs found in photozoan systems. We propose that these depositional patterns should be considered as fundamental building blocks that can be used to better understand the stratigraphic architecture of heterozoan carbonates.

The two southeastern Spain localities are ideal for calibrating the origin of fundamental elements of stratigraphic architecture. The Pliocene deposits of the Carboneras basin (Fig. 1, 2) preserve clinoform morphologies, which allow for calibration of depth differences of various facies, as well as variants that may represent temporal changes in updip-downdip facies pattern. Miocene deposits of the Ricardillo area (Fig. 1, 2) preserve similar facies to those in the Pliocene, but their architecture is preserved as cyclothems. The Pliocene clinothem is the key calibration for quantifying the processes of sea-level variation that give rise to the Miocene cyclothems. In so doing, this research quantitatively documents fundamental aspects of facies variation in heterozoan carbonates and tests hypotheses of what controls lead to the construction of fundamental depositional units. It considers relative fluctuations in sea level, paleotopography of substrate, nutrients, physical energy effects, sediment transport mechanism, and organismal response to depositional setting. Data include stratigraphy, lithologic texture, sedimentary structure, and paleotopography from field studies; and fossil content and distribution, relative grain size, and sorting from thin sections.

GEOLOGIC SETTING

The Carboneras Basin and Cerro de Ricardillo areas (Fig. 1, 2) contain heterozoan carbonate complexes deposited in the Cabo de Gata volcanic province of southeastern Spain. During the Alpine orogeny (Cretaceous-Seravallian), this region was affected by north-south compressional stress due to the collision of the African tectonic plate with the Iberian and European plates. During the mid-late Miocene, compressional stress shifted to the northwest, creating a shear zone with strike-slip faults and pull apart basins, causing extension and the eruption of calc-alkaline dacite and rhyolite (Lopez- Ruiz et al. 1980; Rehault et al. 1985; Montenat et al. 1987; Platt and Vissers 1989; Montenant et al. 1990; Sanz de Galdeano and Vera 1992; Serrano 1992; Martin et al. 2003). These volcanics, and preexisting metamorphic basement, were subsequently eroded, faulted, and highly fractured (Franseen 1989) forming an archipelago with interconnected basins and straits (Esteban 1979; Esteban and Giner 1980; Sanz de Galdeano and Vera 1992; Esteban 1996; Franseen and Goldstein 1996; Franseen et al. 1998).

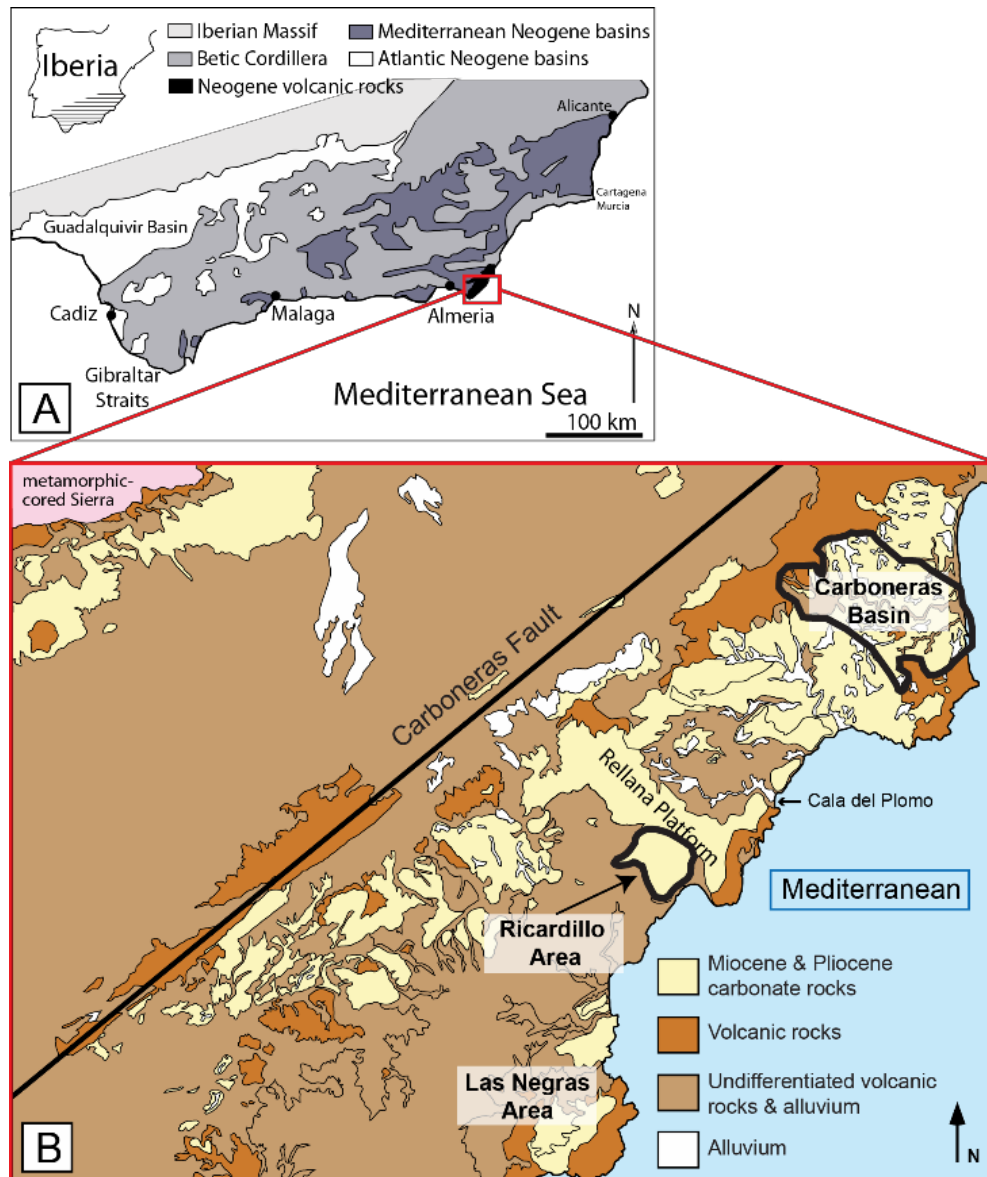


Figure 1: A) Location map of Neogene basins in the Betic Cordillera of southern Spain. The red box outlines the Cabo de Gata volcanic province. Modified from Gibbons and Moreno (2003). B) Generalized geologic map of the Cabo de Gata region and location of the Ricardillo area and the Carboneras Basin. Modified from Instituto Geologico y Minero de Espana (1981).

After volcanism had primarily ceased, temperate climate (Franseen et al. 1998) allowed for the deposition of heterozoan carbonates on the flanks of the volcanic highs throughout the Betic basins (Franseen et al. 1998). One of these volcanic highs was Cerro de Ricardillo, a homoclinal surface with a ~6 degree gradient overlain by ramp-like Miocene carbonates.

Ricardillo is currently at 309 meters elevation (Fernandez-Soler 1996). This peak is the highest in the area that is flanked by upper Miocene carbonates (Fig. 3), the oldest of which

correlate to strata with ages of 8.5 ± 0.1 Ma (Argon/Argon dating; Franseen et al. 1997; Franseen et al. 1998; Hess et al. 2011).

Further northeast, the Carboneras Basin experienced minor carbonate deposition during the Messinian (Fig. 1). Some propose it experienced a partial closing of the basin in the early Pliocene (Zanclean), creating an isolated embayment (Braga et al. 2003; Martin et al. 2003). Sea-level rise during the Zanclean (5.2-3.5 Ma) stage, created accommodation in this low-lying basin allowing for deposition of open-marine Pliocene heterozoan carbonates, comparable to those in the Miocene (Montenat et al. 1990; Franseen et al. 1993; Aquirre 1998; Goldstein and Franseen 2000). The southern part of the basin consists of a downlapping, prograding clinothem that formed in a shaved shelf system, and deposited during a lowstand (Dillett et al. 2004).

Post-depositional tectonic deformation is minor in the Cabo de Gata area, and is characterized by broad regional uplift and only minor tilting and faulting. For the most part, paleotopography is preserved (Esteban and Giner 1980; Franseen and Mankiewicz 1991; Franseen et al. 1993, 1997, 1998; Franseen and Goldstein 1996, Toomey et al. 2003; Dillett et al. 2004; Johnson et al. 2005; Hess et al. 2011; Sweeney et al. 2015), which allows facies paleobathymetry to be quantified. Minor tilting has been recognized to the northeast of Ricardillo (Hess 2011; Sweeney et al. 2015), therefore a -7m correction in elevation is applied to the proximal and medial regions of the Ricardillo area for this study.

Previous work has identified five depositional sequences in Miocene carbonate strata of the Las Negras area (DS1A, DS1B, DS2, DS3, TCC) (Franseen 1989; Franseen and Mankiewicz 1991; Franseen and Goldstein 1992, 1995, 1996; Franseen et al. 1993, 1997, 1998) and genetic units have been described and mapped in the Pliocene strata of the Carboneras Basin (Braga et al. 2003; Martin et al. 2004; Dillett et al. 2004). This research focuses on the Tortonian aged

DS2 sequences (Fig. 3) of cyclical heterozoan carbonates on Cerro de Ricardillo and the Zanclean aged prograding clinothem of the southern portion of the Carboneras Basin (Figs. 1, 2).

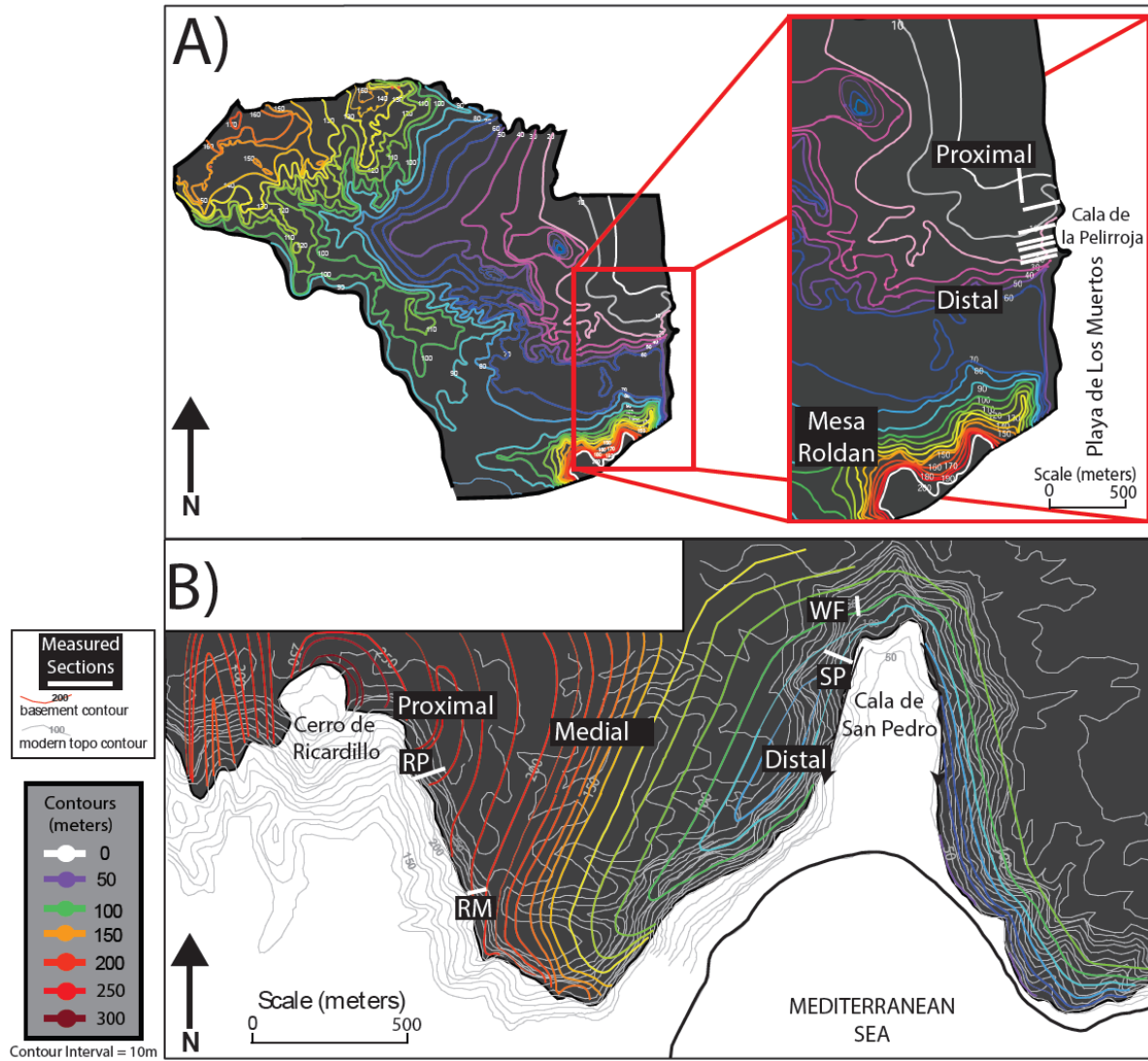


Figure 2: A) Map for the Carboneras Basin showing contours of modern-day elevation at the top of the Miocene strata, the surface onto which the Pliocene carbonates were deposited. This basin is 5.5 x 4.75 km across, however, this research only focused on the clinothem in the southeastern part of the basin just northeast of Mesa Roldan, in the Cala de la Pelirroja where the 7 measured sections are shown. Modified from Dillett et al. (2004). B) Map of the Ricardillo area showing contours of modern-day elevation at the contact between Miocene carbonate strata and underlying volcanics. The area is 1.5 x .93km across. The four measured sections from this study are labeled on the map. Modified from Toomey et al. (2003). These two areas are separated by the Rellana Platform and the Agua Amarga Basin.

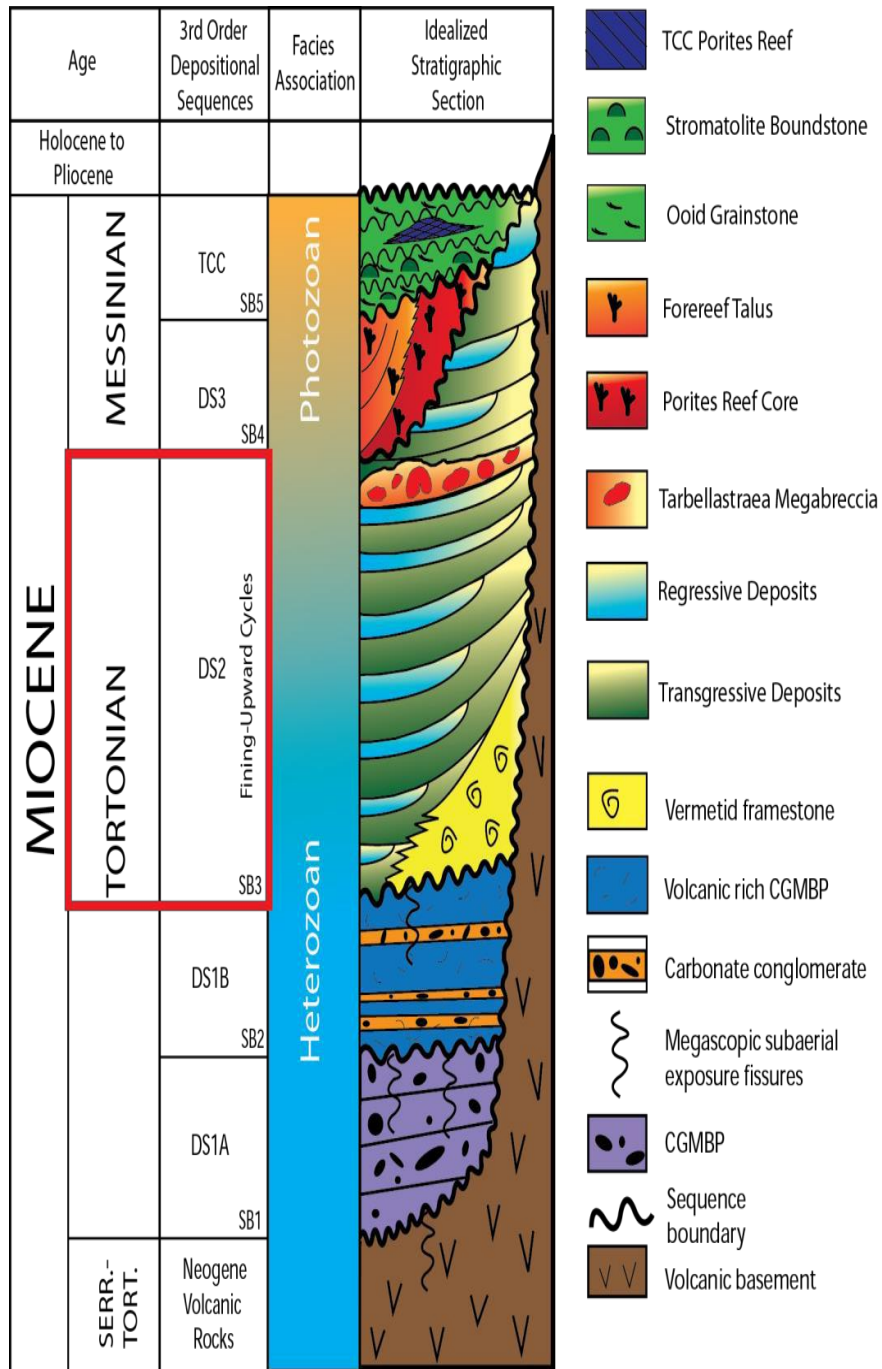


Figure 2: Generalized stratigraphic section for the Miocene-aged Cerro de Ricardillo area. The 3rd order sequence (DS2) containing the cyclic heterozoan deposits for this study is boxed in red. Five third-order depositional sequences are recognized throughout the region with multiple 5th order sequences in DS2 and the TCC. Modified from Toomey et al. (2003) and Franseen et al. (1998).

METHODOLOGY

Fieldwork was conducted on Cerro de Ricarillo, Cala de San Pedro, and the northern end of Playa de Los Muertos, in the Carboneras Basin of the Cabo de Gata region (Figs. 1 and 3). Locations of stratigraphic sections were determined based on exposure, accessibility, and paleotopographic location of the outcrop. Each section was measured and described at the centimeter scale. Lithofacies were classified by texture from Dunham (1962) and Embry and Klovan (1971). Hand samples were collected systematically from each lithofacies for petrographic and petrophysical analysis.

A total of 11 stratigraphic sections were measured, four from the Miocene of the Ricardillo area, and seven from the Pliocene of the Carboneras Basin. Of the Miocene sections, two were from Cerro de Ricardillo (36.4m and 25m in thickness), and two from Cala de San Pedro (75.7m and 21.4m in thickness). The Miocene sections were measured to document properties that change from proximal (230-309m elevation), medial (150-230m elevation), and distal portions of the ramp (90-150m elevation), while also capturing the 3D architecture of the exposure.

Five of the Pliocene sections were measured at Cala de la Pelirroja (6m, 27.3m, 6.4m, 16m, and 20.5m in thickness), and two were measured just to the north (22.8m, 14.6m in thickness; Appendix I). The seven sections cover the proximal to distal depositional profile of the clinothem. Sections ranging from the Miocene contact to the truncated surface of the clinothem (or close to) were measured at proximal (0-10m below truncated clinothem surface), medial (5-20m below truncated clinothem surface), and distal (20-45m below truncated clinothem surface) locations. Four supplementary sections were measured to document detailed

lateral facies changes along time-equivalent strata. These field measurements from both study areas, along with modern day elevations corrected for deformation (paleotopography), were used for stratigraphic correlations and to quantify lithofacies paleobathymetry.

A total of 333 thin sections were made at the University of Kansas and Petrographic Services and were used for petrographic analyses. Standard transmitted light and UV petrography was conducted on each sample. In some cases, where depositional fabrics were difficult to discern, paper filters were utilized to adjust lighting (e.g. Folk 1965). Approximately 250-300 point count measurements were collected at the Kansas Geological Survey using an electric stepping stage programmed for a regular grid for each sample to quantify the composition of lithofacies (e.g. Middleton et al. 1985; Flügel 2010). The number of point counts represents a statistically significant range specific to each lithofacies determined through JMicroVisionTM (Appendix III). One hundred grain size measurements were collected per sample on random points that intersected grains. The longest axis view of the grains in the 2D cut of the thin sections were used as representative of differences from sample to sample. Grain size measurements were converted into Φ values for sorting quantification and classification (e.g. Friedman 1962; Folk and Robles 1964; Flügel 2010). Miocene samples were stained using Alizarin Red-s Potassium Ferricyanide and dilute Hydrochloric acid (e.g. Lindholm and Finkelman 1972) to distinguish calcite from dolomite. Although not reported here (Chapter 3; Pugliano et al., 2015), background extraction micro-imaging analyses were then conducted to quantify dolomite content for Miocene samples. Petrographic analyses also included classifying pore types and their distribution, paragenesis of cements, and cement identification and classification (Chapter 3; Pugliano et al., 2015).

Lastly, 361 core plugs were taken for petrophysical analyses. Helium porosity, air

permeability, and grain density measurements were conducted through Weatherford Labs. Core plugs measured 2.54cm in diameter and 1.27-5cm in length. Plugs were cut and calibrated from hand samples at the Kansas Geological Survey.

PLIOCENE STRATIGRAPHIC ARCHITECTURE

Clinothem Geometry

The Pliocene clinothem is capped by a planar surface interpreted as representing erosion from the effects of wave base. Previous work conducted here includes interpretation of sea level, mapped genetic units and geometries, and general facies description (Dillett et al. 2004). Dillett et al. (2004) created a model showing that sand to gravel sized sediments are produced and abraded in updip environments above fairweather wave-base. These grains are then subsequently transported downdip and intermixed with coarser gravel and cobble sized grains that are forming from *in situ* growth of organisms. For this study, this relationship between grain size and depth relative to wave base has also been applied to the Miocene heterozoan carbonate complexes deposited in the Ricardillo area to calibrate the relationship between rudstone and packstone lithofacies.

In the southern part of the Carboneras Basin, where the clinoform geometry is well preserved (Fig. 5), bryozoans reach their peak grain abundance in proximal regions and decrease distally; bivalves peak in medial regions; and coralline algae content peaks in distal regions (Fig. 6). However, coralline algae is the dominant grain constituent throughout the clinothem. Benthic foraminifera (7%) and echinoids (8-10%) peak in proximal-medial regions. Planktonic foraminifera are rarely present in these outcrops, making up to 3% of total rock volume in only three samples.

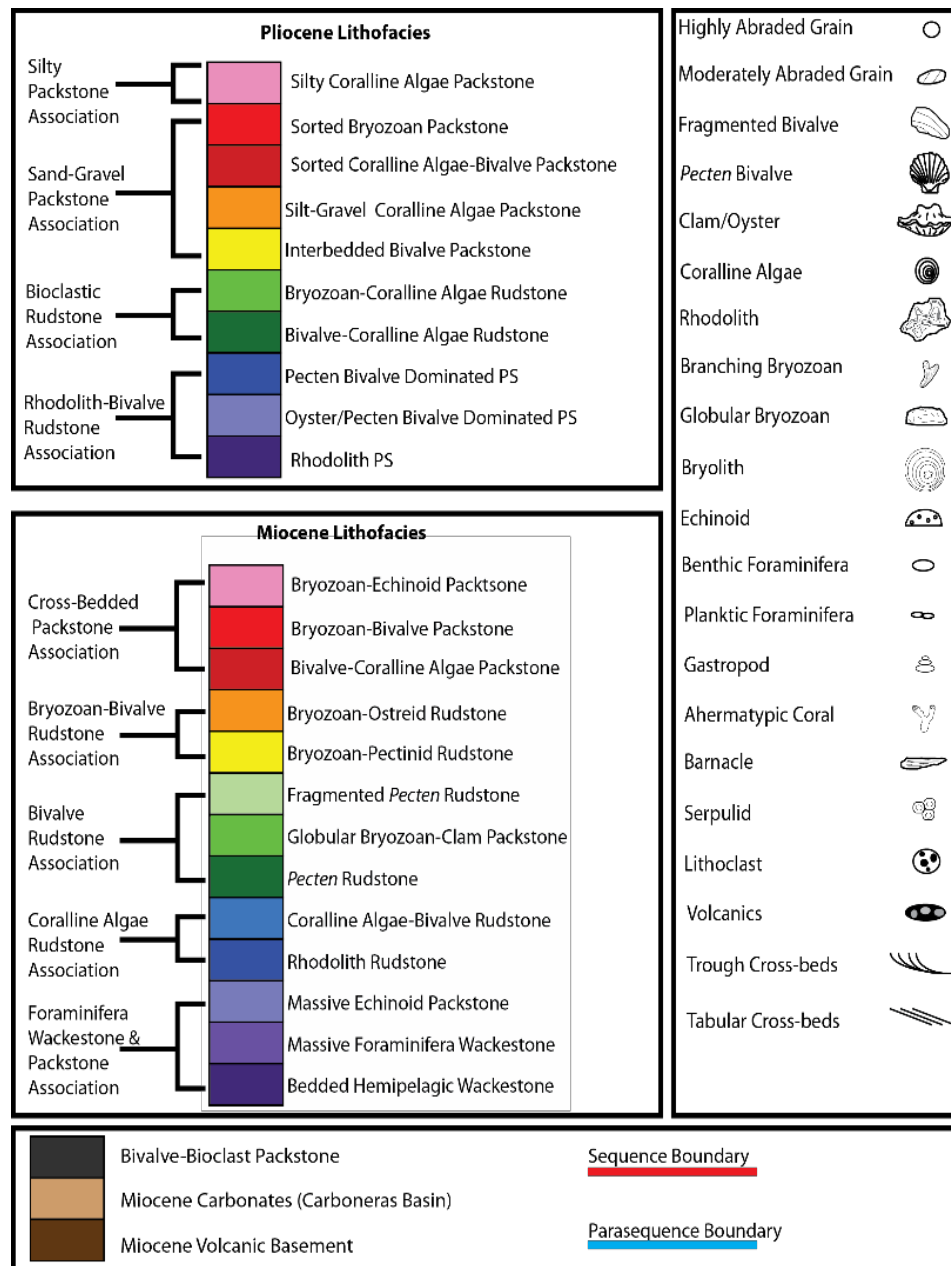


Figure 4: Key of symbols used in Figures 5, 7, 8, 14, 17, 21, and appendices.

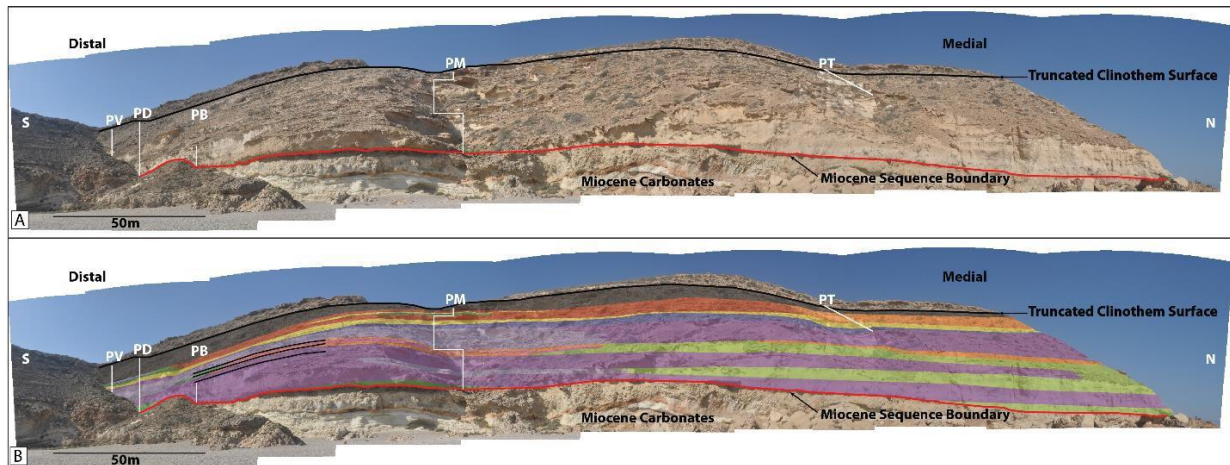


Figure 5: Photomosaic of the medial-distal region of the Pliocene clinothem along the beach cliffs of the Cala de la Pelirroja area. A) Uninterrupted clinothem marked with measured sections and basic labels. B) Clinothem with lithofacies distribution. Rhodolith Rudstone and Ostreid-Pectinid Rudstone facies dominate this part of the clinothem. The stratigraphic top of the clinothem remains dominated by packstone facies, even in this distal region. The far south (left) side of the clinothem carbonates downlap onto the unconformity on the top of the Miocene deposits and enter into the subsurface. Black lines highlight clinothem geometries.

The preserved geometries allow for the analysis of proximal to distal lateral facies variations along time-equivalent strata, and changes that occur as facies prograde and accommodation is reduced (Fig. 7). On the slopes of the clinothem, six time-equivalent depositional profiles (DP) have been identified, each profile consisting of two-to-seven facies. Four of these profiles are common depositional profiles and two are more minor in abundance (Fig. 8). The lateral distances of each of the facies on the profile is taken directly from field measurements. Depositional profiles transition along time-equivalent strata from the proximal regions of the clinothem at Dillet et al.'s (2004) interpreted wave-planation surface, down to the most distal parts of the clinothem where it downlaps onto the top of the Miocene.

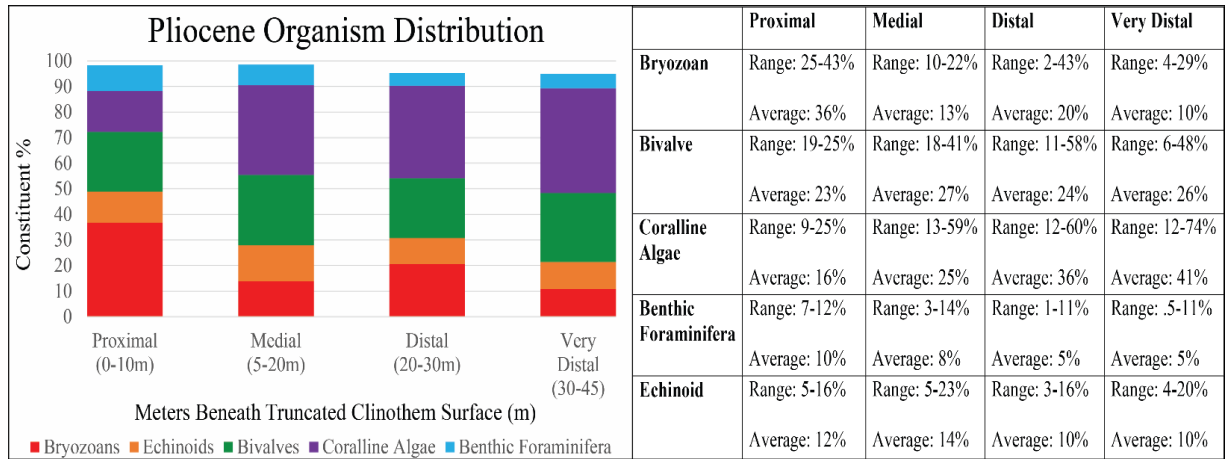


Figure 6: Paleotopographic distribution of organisms. Bryozoan content peaks in proximal regions, bivalves in medial regions, and coralline algae in distal regions. These trends are similar between the two study areas. However, coralline algae content in the Pliocene is much greater throughout the proximal and medial regions than found in the Miocene. The table shows ranges and averages of organism distribution. These values were measured through point counting of thin sections. Depths labeled beneath paleotopographic positions represent thicknesses beneath the truncated clinothem surface. Grain constituent percentages came from lithofacies within the stated ranges (Appendix III). This data has been normalized for grain constituents only, pore space, cement, and matrix were removed. Columns do not reach 100% as there are other minor grains present in each sample.

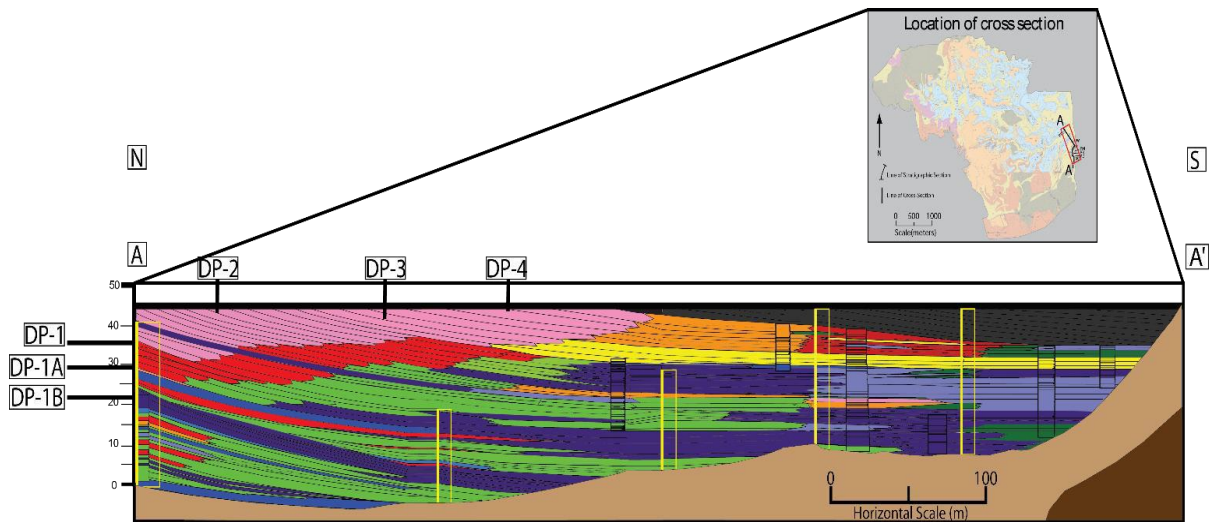


Figure 7: Cross section of the Pliocene clinothem at the southern end of the Carboneras basin. The cross section shows geometries mapped by Dillett et al. (2004). Ten lithofacies have been identified and described from proximal to distal along the clinothem slopes. Packstone facies are concentrated along proximal (northern) regions of the clinothem and prograde across the top. Rudstones with 12-15mm grain sizes span parts of the proximal and medial clinothem, but are absent in most of the distal areas, as these facies change laterally into the Rhodolith-Bivalve Rudstone Association that are composed of grains from 20-40+mm. Measured sections from this research are labeled on the clinothem, and are placed directly onto the clinothem, the locations of measured sections from Dillett et al. (2004) are marked in yellow boxes. Depositional profiles (DP) point to the particular strata that they represent. Modified from Dillett et al. (2004). Vertical scale is 2x exaggerated.

Depositional Profiles (DP) of Facies on Clinothem Slopes

DP-1 forms along the lower half of the clinothem as seen in Figure 7. This profile consists of the following proximal-distal lateral facies trend: Silty Coralline Algae Packstone - Sorted Bryozoan Packstone - Bryozoan-Coralline Algae Rudstone - Rhodolith Rudstone (Fig. 8). Rudstones make up the majority of the profile whereas the packstone facies has only a limited distribution, confined to the top of the clinothem. This profile is the most abundant of the depositional profiles and makes up ~44% of the total clinothem. Depositional profile abundance was calculated by comparing thickness of a particular depositional trend divided by the total thickness of the clinothem. Within DP-1 there are fluctuations in lateral facies trends and therefore two minor sub-profiles (variants on DP-1) have been described. These sub-profiles are not abundant and are interbedded with the DP-1 profile.

DP-1A (Fig. 8) consists of the following proximal-distal trend: Sorted Bryozoan Packstone - Bryozoan-Coralline Algae Rudstone - Rhodolith Rudstone - Bryozoan-Coralline algae Rudstone - Ostreid-Pectinid Rudstone - Rhodolith Rudstone - Bivalve-Coralline Algae Rudstone. Although this profile contains an abundance of lithofacies, each lithofacies has a minor lateral distribution along the clinothem slope, except for the Bryozoan-Coralline Algae Rudstone, which is the only dominant lithofacies along this profile.

DP-1B (Fig. 8) consists of the following proximal-distal trend: Sorted Bryozoan Packstone - Bryozoan-Coralline Algae Rudstone - *Pecten* Bivalve Rudstone - Rhodolith Rudstone - Bryozoan-Coralline Algae Rudstone - Rhodolith Rudstone. This profile is partially a synthetic profile in order to include the *Pecten* Packstone. The *Pecten* Packstone has a minor

and scattered distribution throughout the clinothem and therefore is included in this profile in its correct lateral position and with lithofacies that are typically found adjacent to it. The Rhodolith Rudstone is the only widely distributed lithofacies in this profile.

DP-2 stratigraphically overlies DP-1 and composes 22% of the overall clinothem. DP-2 (Fig. 8) consists of the following proximal-distal trend: Silty Coralline Algae Packstone - Sorted Bryozoan Packstone - Bryozoan-Coralline Algae Rudstone - Rhodolith Rudstone - Ostreid-Pectinid Rudstone. Whereas the Rhodolith Rudstone and Ostreid-Pectinid Rudstone are the dominant lithofacies along this profile, the packstone lithofacies have a wider lateral distribution compared to the DP-1 profiles.

DP-3 (Fig. 8) stratigraphically overlies DP-2 and is composed of two lithofacies: the Silty Coralline Algae Packstone and the Interbedded Bivalve Packstone. DP-3 composes 16% of the clinothem and has the most abundant packstone lithofacies distribution of any of the profiles.

DP-4 stratigraphically overlies DP-3 and is the capping profile of the clinothem. DP-4 (Fig. 8) composes 18% of the clinothem and consists of the following proximal-distal trend: Silty-Coralline Algae Packstone - Silt-Gravel Coralline Algae Packstone - Sorted Coralline Algae-Bivalve Packstone - Bivalve-Coralline Algae Rudstone - Ostreid-Pectinid Rudstone. The packstone lithofacies dominate this profile covering all proximal and medial parts of the clinothem, with rudstones only occurring distally.

PLIOCENE LITHOFACIES AND INTERPRETATIONS

The Pliocene clinothem contains 10 lithofacies, composing four lithofacies associations. These associations are subdivided based on grain size and grain constituents. Grain constituents for these deposits are diverse and are composed of: cheilostome, cyclostome, and fenestrina

bryozoans with globular, branching, and encrusting morphologies, including bryoliths (*Calpensia nobilis*) (e.g. Moissette et al. 2010). Geniculate and non-geniculate coralline algae and rhodoliths (*Mesolobus*, *Lithothamnion*), ostreids (*Crassostrea* and *Neopycnodonte*) (Martin et al. 2003) and pectinid (*Pecten*) bivalves. Less abundant organisms include echinoids (*Clypeaster*), benthic (Rotaliacea, Milionacea, and Textularia) and planktonic (*Globigerina*) foraminifera (rare), gastropods, serpulids, barnacles, ahermatypic corals, minor lithoclasts, volcanics (<1%), and calcisilt matrix. All facies are grain-rich, matrix-poor packstones and rudstones.

Table 1 contains detailed measurements and results from microfacies analyses. Texturally, facies show an excellent correlation between sorting and grain size (Fig. 9). The most fine-grained facies (coarse sand) have the best sorting. These finer-grained and well sorted facies are found updip on proximal clinothem slopes and tops, whereas the coarser-grained and poorly sorted facies are found downdip on the clinothem slopes (Fig. 9).

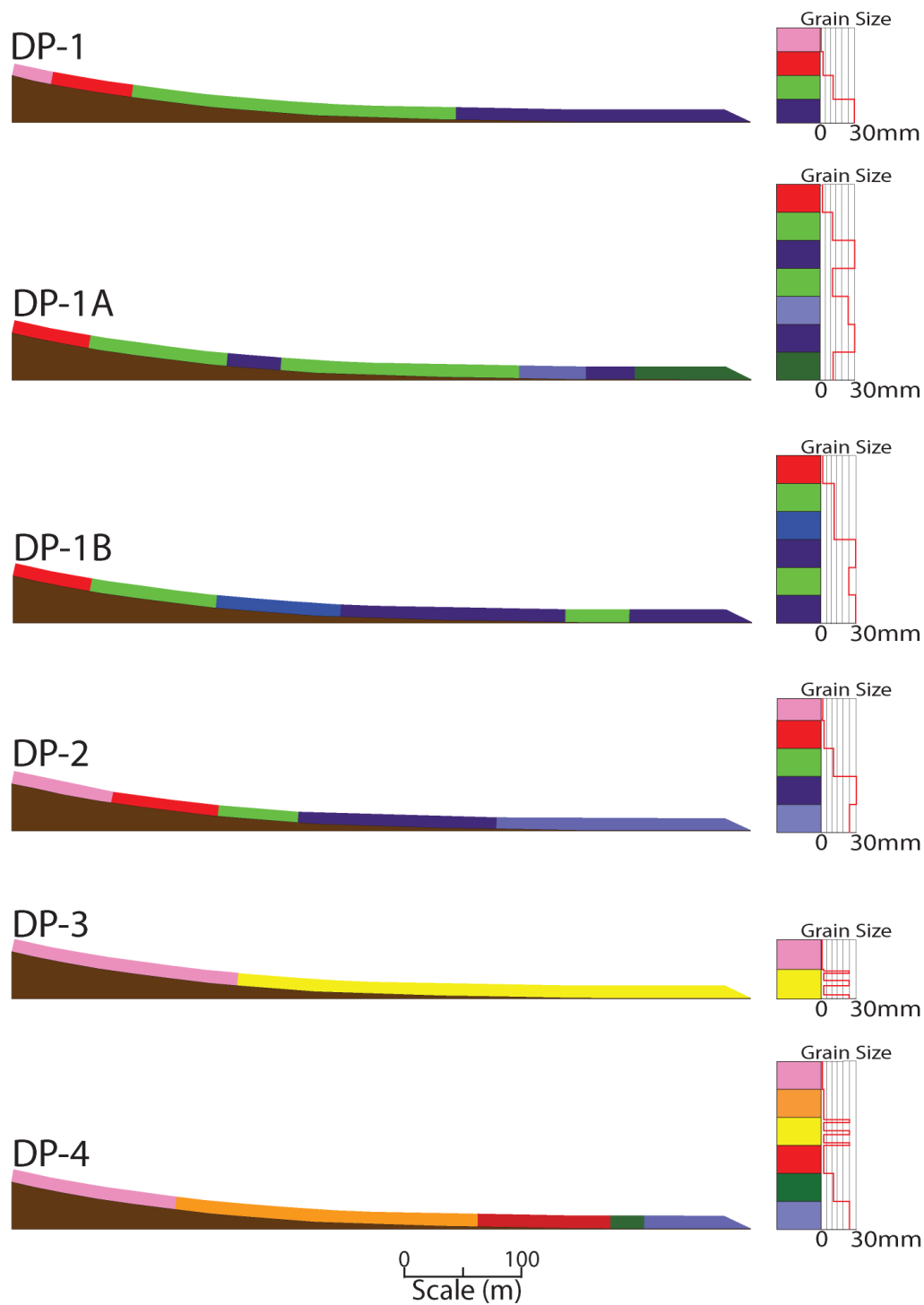


Figure 8: Pliocene depositional profiles. Six depositional profiles are found in the clinothem. DP-1 sub profiles are profiles that are similar to DP-1 but are not as volumetrically abundant. Figure 7 shows the lateral time-equivalent beds labeled along the clinothem. Each one of these profiles represents lateral facies changes measured and documented from fieldwork. Hypothetically, as each of these profiles would prograde they would form a vertical stratigraphic column that is represented adjacent to the lateral profiles. The adjacent grain size charts show that each of these profiles would form fining-upward cycles during shoaling. Rhodolith beds are the most abundant lithofacies, followed by Coralline Algae- Bivalve Rudstones. Overall rudstone facies are more abundant than packstone facies, similar to the Miocene.

Pliocene Lithofacies Description						
Facies Association	Lithofacies	Grain Constituents	Sorting vs. Grain Size	Grain Size	Sedimentary Structures	Depositional Mechanism
Silty Packstone	Silty Coralline Algae Packstone	Bryozoan: 16% Bivalve: 20% Coralline Algae: 25% Echinoid: 14% Benthic Foram: 8% Matrix: 10% Cement: 6% Other: 1%	σ_i : .9-1.1 Moderate $y = 16.949x^3 - 55.708x^2 + 60.194x - 20.36$ R = 1	Thin Section: .5-.67mm Outcrop: 1-2mm	-Massive -Horizontal Beds	-Moderate abrasion -Sediment transport: low-density flows -Baffling by grass beds
	Sorted Bryozoan Packstone	Bryozoan: 45% Bivalve: 18% Coralline Algae: 12% Echinoid: 9% Benthic Foram: 7% Matrix: 3% Cement: 5% Other: 1%	σ_i : .8-1.2 Well-Moderate $y = -0.4323x + 1.0835$ R = 0.39	Thin Section: .95-1.5mm Outcrop: 1-5mm	-Massive -Horizontal Beds -Sparse Graded Beds	- Moderate abrasion -Sediment transport: low-density flows
	Silt-Gravel Coralline Algae Packstone	Bryozoan: 21% Bivalve: 23% Coralline Algae: 29% Echinoid: 11% Benthic Foram: 7% Matrix: 5% Cement: 2% Other: 2%	σ_i : .8-1.7 Moderate-Poor $y = -0.2312x + 1.2558$ R = 0.12	Thin Section: .6-2.1mm Outcrop: 1-5mm	-Massive -Horizontal Beds -Sparse Graded Beds	-Moderate abrasion -Sediment transport: low-density flows -Baffling by grass beds
	Sorted Coralline Algae-Bivalve Packstone	Bryozoan: 12% Bivalve: 25% Coralline Algae: 28% Echinoid: 16% Benthic Foram: 10% Matrix: 2% Cement: 6% Other: 1%	σ_i : .7-1 Well-Moderate $y = -0.2191x + 0.8762$ R = 0.58	Thin Section: .75-1mm Outcrop: 1-5mm	-Massive	-Moderate abrasion -Sediment transport: low-density flows
Sand-Gravel Packstone Association	Interbedded Bivalve Packstone	Bryozoan: 13% Bivalve: 39% Coralline Algae: 18% Echinoid: 13% Benthic Foram: 7% Matrix: 3% Cement: 4% Other: 3%	Sand σ_i : .9-1.2 Moderate $y = 220.85x^4 - 232.83x^3 + 76.875x^2 - 8.4437x + 1.2688$ R = 0.69 Gravel σ_i : 1.1-1.7 Moderate-Poor $y = 0.2578x + 2.0531$ R = 0.99	Thin Section: .8-1.2mm Outcrop: 1-5mm	-Trough Cross-Beds -Interbedded Gravel-Sand Beds - Massive -Convex up shell orientation	- Moderate abrasion -Storm surge and return flow - Suspension - High energy
	Bryozoan-Coralline Algae Rudstone	Bryozoan: 33% Bivalve: 17% Coralline Algae: 21% Echinoid: 12%	σ_i : 1-1.7 Moderate-Poor	Thin Section: 1.7-3.9mm	-Massive -Sparse Graded Beds	-Minor abrasion -Sediment transport: low-density flows -In situ deposition

Rhodolith-Bivalve Rudstone Association		Benthic Foram: 4% Matrix: 6% Cement: 5% Other: 2%	$y = 1.0942e-0.239x$ R = 0.27	Outcrop: 12-15mm	- Concave up shell orientation	
	Bivalve- Coralline Algae Rudstone	Bryozoan: 9% Bivalve: 30% Coralline Algae: 27% Echinoid: 11% Benthic Foram: 5% Matrix: 2% Cement: 13% Other: 3%	$\sigma_i: 1-1.5$ Moderate-Poor $y = -1.9355x^2 - 2.1315x + 0.7818$ R = 0.78	Thin Section: 1.4- 2.4mm Outcrop: 12-15mm	-Massive - Concave up shell orientation	-Minor abrasion -Sediment transport: low-density flows - <i>In situ</i> deposition
	<i>Pecten</i> Rudstone	Bryozoan: 12% Bivalve: 30% Coralline Algae: 37% Echinoid: 8% Benthic Foram: 6% Matrix: 2% Cement: 4% Other: 1%	$\sigma_i: .9-1.9$ Moderate-Poor $y = 1.0444e-0.389x$ R = 0.7226	Thin Section: 2-8mm Outcrop: 25+mm	-Massive - Concave up shell orientation	- <i>In situ</i> deposition -Low energy
	Ostreid- Pectinid Rudstone	Bryozoan: 9% Bivalve: 34% Coralline Algae: 32% Echinoid: 9% Benthic Foram: 6% Matrix: 5% Cement: 2% Other: 3%	$\sigma_i: 1.1-2.3$ Moderate-Very Poor $y = -0.3399x^2 - 1.3316x + 0.764$ R = 0.579	Thin Section: 2-10mm Outcrop: 25+mm	-Massive - Concave up shell orientation	- <i>In situ</i> deposition -Low energy
	Rhodolith Rudstone	Bryozoan: 11% Bivalve: 17% Coralline Algae: 52% Echinoid: 7% Benthic Foram: 3% Matrix: 3% Cement: 5% Other: 2%	$\sigma_i: 1-2.3$ Moderate-Very Poor No correlation	Thin Section: 2-13mm Outcrop: 30+mm	- Massive	- <i>In situ</i> deposition -Moderate energy

Table 1: Pliocene lithofacies description. Summary table of diagnostic features for 10 lithofacies in the clinotherm in the southern end of the Carboneras Basin. The equations of lines and R² values for sorting values are based off of regression analyses from Figure 9.

Silty Packstone

Description.---Silty Coralline Algae Packstone (Table 1) is abundant in proximal regions and is only found in medial regions rarely (Fig. 7). Thicknesses of this lithofacies ranges from 1-3m. Dominant grains are coralline algae (24%) and bivalve fragments (20%). This lithofacies primarily occurs in massive beds. It is locally found in 20 cm-thick horizontal beds, and thin cm-thick graded beds. Silt-sized matrix in this facies is abundant in relation to the other grainy facies and calcisilt makes up ~10% of rock volume. Grains are moderately sorted, however, a portion of the sand grains are <125µm and, along with the calcisilt, fill intergranular pore space.

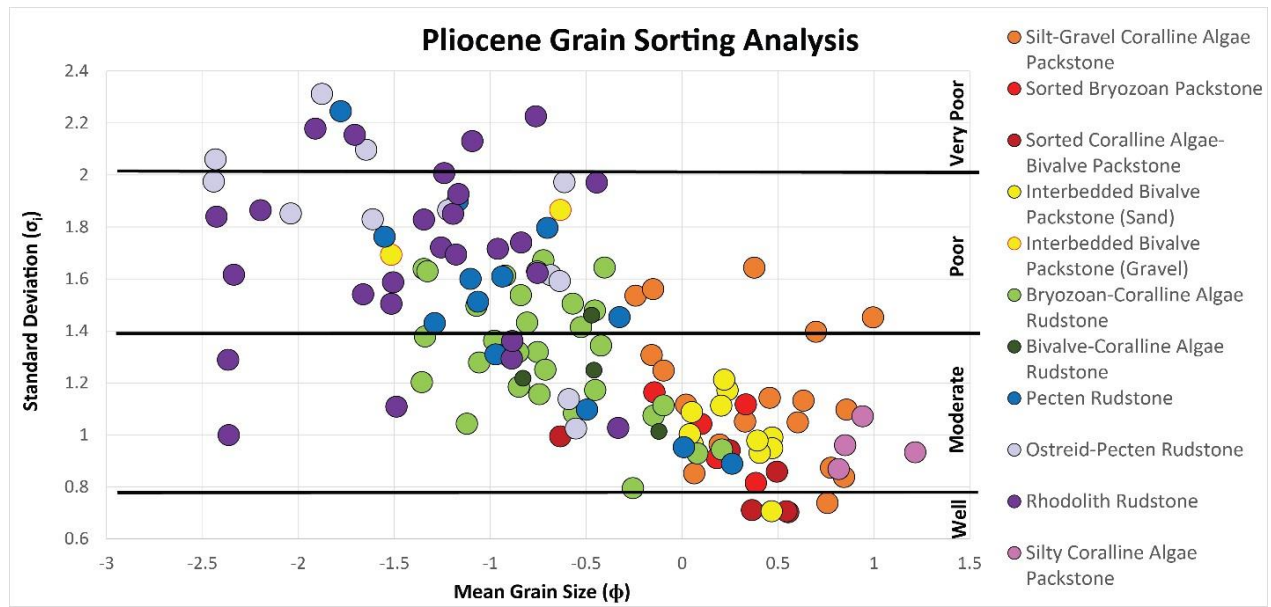


Figure 9: Quantitative sorting analysis of Pliocene lithofacies. This is based on measurements of grain size from petrographic analyses. The x-axis shows the mean grain size in ϕ values (grain size increases towards more negative values). The y-axis shows the standard deviation and allows for the quantification of grain sorting. Higher values indicate poorer sorting and are classified on the right of the graph. Lithofacies generally plot closely together. Equations of lines and R^2 values are located in Table 1. The equation for this entire dataset and the R^2 value is as follows: $y = 0.0547x^2 + 0.1515x - 0.3335x + 1.1132$, $R = 0.6524$

Interpretation.---This facies is the updip equivalent to the Sand-Gravel Packstone Association. Dilleet et al. (2004) interpreted the Silty Coralline Algae Packstone facies to form at depths of 8-18m and directly beneath wave base as evidenced by the wave planation surface truncating this lithofacies. The lack of cross-bedding and the abundance of silty matrix, suggest an environment below effective wave-base, where sediment accumulated from transport and suspension fall out.

The source of silt is interpreted to originate from the physical abrasion of grains above fairweather wave-base, which are transported and baffled by grasses on a broad flat surface on the top of the clinothem. This interpretation is consistent with the origin of silts that develop in modern heterozoans along the southern coast of Australia (O'Connell and James 2015). This most proximal region of the clinothem would have been shallow enough to support *Poseidonia oceanica* grass bed life (e.g. Moissette et al. 2007). Therefore a combination of this shallow shelf providing sufficient substrate for fine sediment accumulation, the baffling mechanism of *Poseidonia*

oceanica beds, and the proximity to the source of grain abrasion are a likely cause for the silt and fine sand content in this lithofacies.

Sand-Gravel Packstone Association

Description.---This lithofacies association consists of Sorted Bryozoan Packstone, Silty Coralline Algae Packstone, Sorted Coralline Algae-Bivalve Packstone, and Interbedded Bivalve Packstone. This association is primarily composed of sand-sized grains, however gravels are intermixed consistently in each of these lithofacies within the sands, making it a coarser association than the Silty Packstone.

The Sorted Bryozoan Packstone (Table 1) is distributed throughout the proximal part of the clinothem and has thicknesses of 1-3m. Bryozoan fragments compose 45% of this lithofacies and are disarticulated and fragmented with only robust branching bryozoan grains having any articulation preserved. These deposits are mostly massive and burrowed, with uncommon graded beds. Vertical burrows are abundant throughout this facies and are infilled with fine sands.

The Silt-Gravel Coralline Algae-Bivalve Packstone (Table 1) is deposited in a few thin beds in the most proximal parts of the clinothem and towards the top 1/3 of the clinothem in medial regions. Thicknesses range from 1.5-2.5m and beds are composed of 28% coralline algae and 23% bivalves as the main contributors. This lithofacies is more poorly sorted than others in this association and has a silty matrix content averaging 5%. This lithofacies is composed of centimeter scale horizontal beds (Fig. 10A) as well as massive beds, each with internal vertical burrows.

The Sorted Coralline Algae-Bivalve Packstone (Table 1D) has a limited distribution to only the top 1/3 of the clinothem in distal regions. Thicknesses range from 1-2.5m and beds are composed of 28% coralline algae and 25% bivalve. Mud content only reaches 1% in this facies.

Beds are massive; normally graded beds occur rarely. Meter scale vertical and horizontal infilled burrow networks are widespread, more so than any other lithofacies in this study.

The Interbedded Bivalve Packstone (Table 1) is found in the top 1/3 of the clinothem and ranges from medial to distal regions. Thicknesses range from 1.5-2.5m and beds are composed of 39% bivalves and 18% coralline algae. In medial regions, the basal 1m contains trough cross-bedding and sorted sands with scattered gravel. Above this basal level, and in the rest of the medial and distal parts of the clinothem, the cross-bedded strata pinch out and the rest of the lithofacies is composed of thin, alternating rudstone to packstone deposits. Ratios of the gravel to sand fraction of the alternating beds vary laterally. In medial areas the sorted sand-sized beds range from 40-60cm in thickness, however, further downdip this fraction becomes 10cm thick. The coarser fraction (20+mm) has the reverse distribution. In the coarser fraction, 70% of bivalve shells are oriented convex up, however further downdip in distal regions, this value decreases to 27%. Ten-to-fifteen centimeter long vertical infilled burrows are scattered throughout the medial regions of these deposits.

Grains in this association are all fragmented, fractured, slightly rounded and partially smoothed. Original textures are apparent, but are slightly altered by abrasion. The majority of grains are sand-sized (63 μ m-2mm), however, a portion of the grains are well above 2mm, and in some cases, whole rhodoliths are found throughout. This association contains a lesser amount of the sand-sized fraction than the one lithofacies that is further updip. With the exception of the Silt-Gravel Coralline Algae Packstone, all of the facies have well-moderate sorting and contain low calcisilt content (1%). Together with the Silty Packstone, they make up ~1/3 of the total clinothem volume.

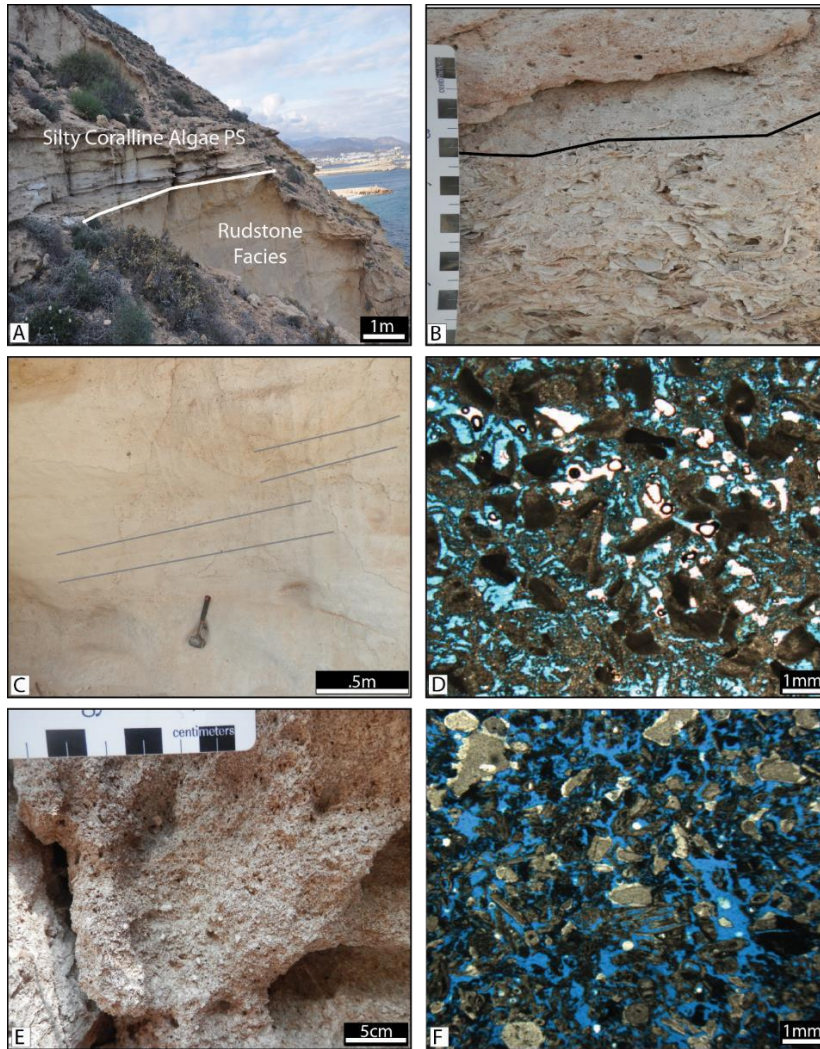


Figure 10: Photographs and photomicrographs of three packstone facies from the Miocene and Pliocene, and one transitional facies from the Miocene. This figure shows field and microscopic scale features of the Packstone Associations from both field areas. A) Silty Coralline Algae Packstone from a proximal section of the Pliocene clinothem overlying coarse rudstone facies. The thin horizontal beds displayed are characteristic of this facies. B) The sharp contact that is common between the rudstone and packstone lithofacies of the Miocene cyclothem. The black line shows the sharp contact. C) Outcrop photo of Coralline Algae-Bivalve Packstone. The tabular cross-beds are characteristic of the packstone facies from the Miocene, however, they are difficult to observe due to the nature of the outcrops. Illustrated lines show the orientation of the cross-beds. D) Photomicrograph of the same lithofacies as image C (Miocene). This facies has been extensively dolomitized, and has undergone dissolution. The majority of grains in this facies are abraded coralline algae. E) Close up field image of the Bryozoan-Echinoid Packstone (Miocene). Note the finer nature and loss of original texture on grains compared to the transitional bed shown in figure B. F) Photomicrograph of the facies from image E. This is an example of a calcitic (not dolomitized) facies from the Miocene. Note the abundant fragmented bryozoan and echinoid grains.

Interpretation.---This lithofacies association is the down-dip equivalent to the Silty Packstone. Dilleet et al. (2004) interpreted similar facies to accumulate at depths of 8-30m. The massive beds, thin horizontal beds, and scattered graded beds are interpreted to form from sediment transport of abraded grains that were produced and abraded above wave base and transported down dip through sediment gravity flows. As the abraded grains were moved further

downdip they were mixed with coarser *in situ* grains and became a less dominant feature (Dillet et al., 2004). The Silt-Gravel Coralline Algae Packstone has a higher (>5%) calcisilt fraction than others in the association and is interpreted to form from amounts of *Poseidonia oceanica* grass beds baffling sediment; possibly creating burrows and stabilizing sediment long enough to allow burrowing. The parts of this lithofacies that lack horizontal bedding are interpreted to have been abundant *Poseidonia oceanica* grass beds that baffled fine sediments.

The Interbedded Bivalve Packstone falls within the same depth range as the above lithofacies, however, it has a significantly different depositional mechanism. The trough cross-beds at the base of this lithofacies in proximal areas indicate reworking by high-energy tractive currents near or above fairweather wave-base. In addition to this, the decrease of the sand-sized fraction within this lithofacies downdip on the clinothem indicates a change in environmental condition, likely energy regime. Further evidence that these beds were deposited under a high-energy regime is the orientation of bivalve shells in the gravel beds. The transition from convex up bivalve shells in proximal areas to concave up and mixed orientation downdip indicates that the depositional setting lost energy as sediment was transported further downdip, away from the energy source, allowing suspension settling of shells (e.g. Bouma 1962). The convex up shell orientation in proximal regions makes sediment gravity flows an unlikely mechanism. The preserved horizontal beds and scattered vertical burrows indicate that bioturbation did not have a significant effect on shell orientation (e.g. Salazar et al. 1982), disproving the hypothesis that the specific shell orientation is caused by extensive bioturbation. In addition, the lack of a variety of shell orientations updip leaves doubt that oscillatory waves oriented shells, indicating that flow was unidirectional.

The coarse nature found within the alternating beds along with the preserved sedimentary

structures leads to the interpretation that this lithofacies was deposited by the effects of high energy waves (trough cross-bedding) and storm surge (alternating coarse to fine beds). Strong storms along coasts can produce powerful bottom return currents which erode, suspend, orient, and can even be the dominant sediment-transporting agent in storms (Mount 1982; Nelson 1982; Hobday and Morton 1984). Alternating coarser and finer grained beds are also common in storm systems affected by bottom return flow (Nelson 1982; Hobday and Morton 1984; Cheel and Leckie 1992). In summary, as the basin filled, periods of intense storms lowered storm wave-base and allowed for the reworking of sediments, creating the trough cross-beds. These cross-beds were then overlain by the interbedded gravel and sand deposits that originated from storm surge return flow

Bioclastic Rudstone Association

Description.---This lithofacies association consists of the Bryozoan-Coralline Algae Rudstone and Bivalve-Coralline Algae Rudstone (Fig. 11). These lithofacies are classified as a single association because of their coralline algae content 21-27% and a similar grain sizes of 12- 15mm (outcrop measurements).

The Bryozoan-Coralline Algae Rudstone (Table 1) is distributed primarily in distal regions of the clinothem with minor distribution in medial areas. Distribution is widespread throughout the entire clinothem; and it is the second most abundant lithofacies. Thicknesses range from 1-to-5.6m and beds are composed of 32% bryozoans and 21% coralline algae. Grains are fragmented and whole, with the majority being partially fragmented, but still retaining original skeletal textures. Bryozoans exhibit robust branching and globular morphologies. The majority of these facies have a low matrix content ($< 1\%$), however, a few scattered beds, less than 1m thick, contain up to 8% silty matrix. These beds are rare, and are mostly found in medial

settings.

The Coralline Algae-Bivalve Rudstone (Table 1) has a minor distribution in the distal parts of the clinotherm. Thickness ranges from 1.5-to-3m and it is composed of 27% coralline algae and 30% *Pecten* bivalves. Calcite cement makes up 13% of the rock volume, 1.5-2 times the amount found in other Pliocene facies

This association is entirely composed of massive beds with minor individual burrows. The Bryozoan-Coralline Algae Rudstone represents the medial-distal version of this association, and the Bivalve-Coralline Algae Rudstone represents the distal variant. The sharp decrease in bryozoans between these two facies from proximal to distal (32-9%) is a trend seen throughout the Pliocene and Miocene.

Fifty to sixty percent of bivalve shells are oriented concave up, a majority of which are whole valves, but disarticulated, whereas others are fragmented. There are a variety of grain sizes ranging from silts and fine sands to very coarse gravels. Whole rhodoliths and oysters are also present. The majority of the grains are gravel-sized, ~12-15mm. It is important to note that all rudstone facies are bimodal in their grain size.

Interpretation.---This association is the downdip equivalent to the Sand-Gravel Packstone Association and similar facies were interpreted to form at depths greater than 45m (Dillett et al. 2004). The decrease in sand-sized grains and the increase in gravel-sized grains (compared to the packstone facies) in these facies is due to the increased distance (compared to proximal facies) from the source of abraded grain production (Dillett et al. 2004). The concave up orientation for the majority of shells and the massive bedding support intense bioturbation of the facies within this association (e.g. Salazar et al. 1982).

Rhodolith-Bivalve Rudstone Association

Description.---This lithofacies association consists of *Pecten* Rudstone, Ostreid-Pectinid Rudstone, and a Rhodolith Rudstone. The *Pecten* Bivalve Rudstone (Table 1, Fig. 11C) has a limited distribution and is primarily found in medial regions, with a minor distribution in proximal and distal regions of the clinothem. Stratigraphically, it is found at the base and in the middle of the clinothem. Thicknesses range from 1-to-1.5m. Petrographic analyses indicate a *Pecten* bivalve composition of 37%, however, this is an under-representation of the actual amount in the outcrop, as seen in similar lithofacies in Figure 11C. Grains are whole, valves are disarticulated, and original shell textures are unaltered. Shells are primarily concave up within massive beds.

The Ostreid-Pectinid Rudstone (Table 1, Fig. 11E) has a distribution limited to distal parts of the basin. Stratigraphically it is primarily found in the top half of the clinothem. Thicknesses range from 1-to-5m and it is composed of 34% bivalves and 32% coralline algae in the form of rhodoliths. As with the *Pecten* Bivalve Rudstone, the high bivalve content is underrepresented in thin section measurements. Ostreids are the dominant bivalve in this facies and are highly bored. Pectinids are encrusted by bryozoans. Both bivalve types are whole with some fragmented grains, and a portion of them are fully articulated. Sixty percent of the shells are oriented concave up.

The Rhodolith Rudstone (Table 1, Fig. 12) has a widespread distribution ranging from proximal to distal regions of the clinothem, however, it is most concentrated in medial to distal regions. Thicknesses range from .4-to-7m and beds are composed of 52% coralline algae in the form of rhodoliths. Bivalves are also important grains in this facies, making up 17% of the total rock volume. Whole rhodoliths are distributed consistently throughout this lithofacies and

commonly weather out forming nodular spheres. Rhodoliths are all in physical contact with one another, are round, spherical, symmetrical, and range in size from 2-to-4cm. They have columnar (e.g. Bosence 1983a) or fructose (e.g. Farr et al. 2009) thalli that protrude a few millimeters. These can be classified as monospecific spherical columnar rhodoliths (e.g. Bosence 1983a).

Intermixed with rhodoliths are orange-colored, spherical, asymmetrical bryoliths (e.g. Moissette et al. 2010). The bryoliths range from 4cm-7cm. Nuclei consist of rhodoliths, bivalve shells, or the nucleus is entirely absent leaving a ~2cm pore within the bryolith (see Chapter 3). Bryozoans concentrically encrust to form 1-2mm layering to build multi-centimeter crusts around each nucleus. These facies are composed of the coarsest grains in the clinotherm, with grain sizes potentially greater than 10cm, and average grain sizes of ~4cm.

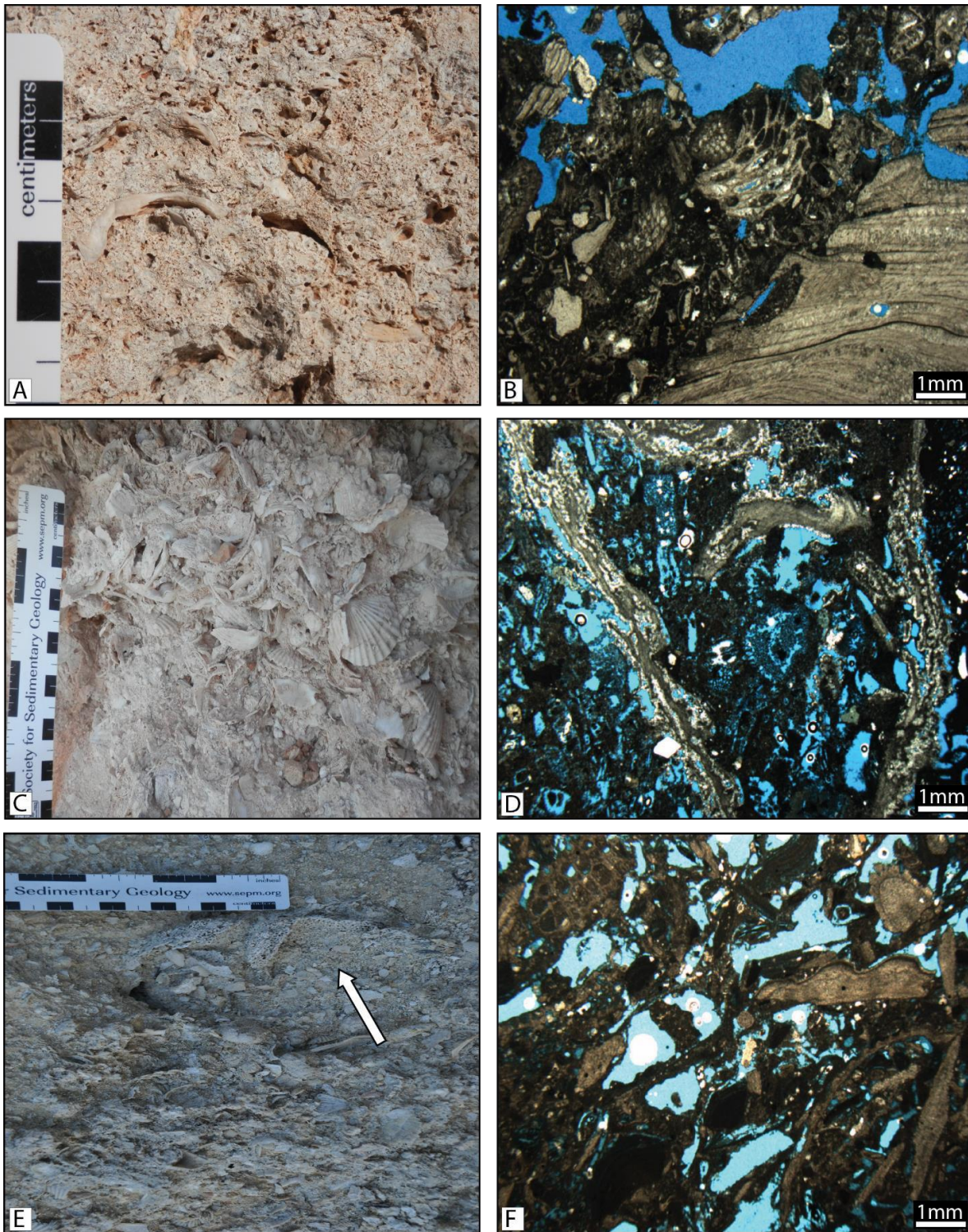


Figure 11: Photographs and photomicrograph of three rudstone facies from the Miocene and Pliocene. A) Bryozoan-Ostreid Rudstone from the Miocene. Centimeter sized oyster shells are widespread throughout this lithofacies, as well as robust and globular bryozoans and other bivalves. Note the centimeter-scale shelter porosity created by the oysters. B) Photomicrograph of the same lithofacies as image A. Lithofacies from this association are the most matrix-rich facies seen in the Miocene. Note the bimodal grain size of this rudstone. C) *Pecten* Rudstone lithofacies from the Miocene. Centimeter-scale, whole and crushed but unabraded bivalves are characteristic of this lithofacies. This is a calcitic example of this lithofacies; where it has been dolomitized, the bivalve shells are mainly only preserved as molds. D) Photomicrograph of the lithofacies from image C. Centimeter-scale whole bivalves with some bryozoans and scattered coralline algae fragments are characteristic of this facies. E) Ostreid-Pectinid Rudstone from distal parts of the Pliocene cliniothem. The white arrow points out a 9 cm oyster shell that is heavily bored. F)

Photomicrograph of the same lithofacies from image E. Centimeter-scale bivalves are the dominant grain with an array of other grain types shown in this image.

These systems are bi- modal in their grain size, as intergranular pore space between gravels are infilled with silt and sand of all sizes. Gravel-sized grains show no evidence for abrasion. Beds are massive with no individual burrows visible.

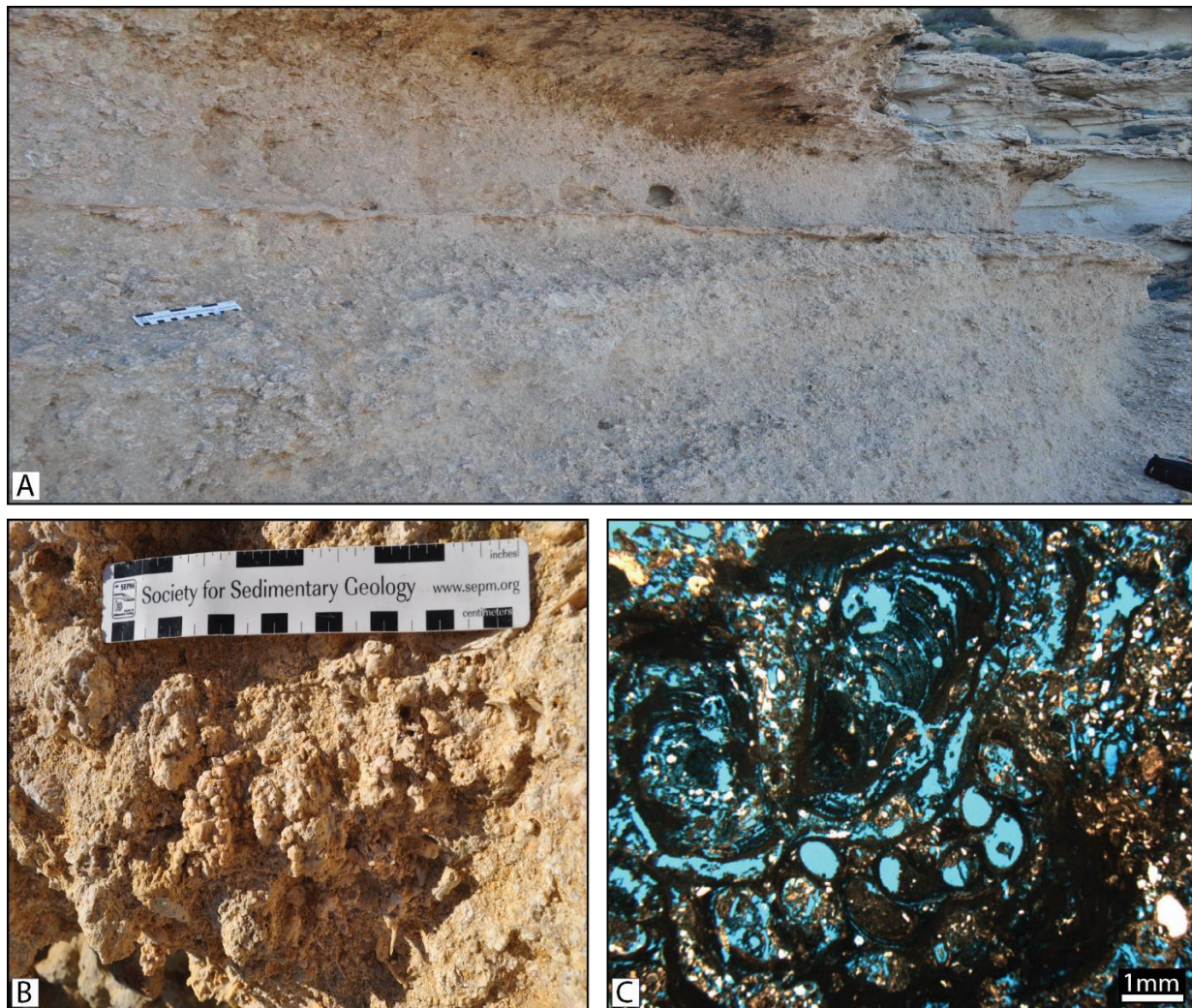


Figure 12: Photographs and photomicrographs of Rhodolith Rudstone from the Pliocene area. A) Outcrop of the Rhodolith Rudstone from a medial section of the Pliocene clinothem. The entire outcrop in the image has abundant 2-to-4cm spherical rhodoliths. Scale in the photo is 15cm. B) Up-close image of rhodoliths from the Pliocene. C) Photomicrograph of a Pliocene rhodolith. This sample has been partially dolomitized and contains framework pore space within the skeleton of the rhodolith. Note the grains that are encrusted by the coralline algae and the finer sand grains infilling around the rhodolith.

Interpretation.---This lithofacies association is the downdip equivalent to the Bioclastic Rudstone Association. It marks the most downdip transition into deeper water along the clinothem and is interpreted to form at depths of 65-100+m (Dillett et al., 2004). This is

consistent with its rhodolith morphologies, which form at depths of 30-80m in the modern Mediterranean Sea (Carannante and Simone 1996; Peres and Picard 1964). The coarse, unabraded, and whole nature of the organisms in the *Pecten* Bivalve Rudstone and the Ostreid-Pectinid Rudstone, leads to the interpretation that these facies formed in a low energy environment away from the effects of waves, and had less input of sediment from updip higher energy environments than other facies. The finer sediments in the interparticle porosity are likely the only sediments that were transported from updip, or perhaps were generated *in situ* by bioerosion. The concave-upward shell orientation of these lithofacies also supports a low energy system, as currents did not rotate shells to a more stable orientation. The mechanism for the concave up shells is interpreted to be extensive bioturbation, which also created the massive beds (Salazar-Jimenez et al. 1982).

The measurements collected from the rhodolith beds indicate that the rhodoliths formed in an environment that was conducive to consistent rotation, as they show symmetrical growth (e.g. Bosellini and Ginsburg 1971; Bosence 1983a, 1983b; Basso 1998). The energy regime, however, was not high enough to cause abrasion on rhodoliths or to allow for symmetrical growth of the coarser bryoliths. Bottom currents are a possible source of physical energy (Carannante et al. 1988; Carannante and Simone 1996; Basso 1998; Dillet et al. 2004), but rotation may also have been caused by organisms in the sediment (e.g. Prager and Ginsburg 1989).

MIocene STRATIGRAPHIC ARCHITECTURE

Draping and Onlapping Cyclothems

Data were collected systematically along the Miocene exposure to document how deposition differed from proximal-to-distal regions and to capture the 3-D exposure of the

outcrop (Figs. 13, 14). The carbonates were deposited on a volcanic substrate with a slope of 6.8° and have onlapping and draping geometries (Figs. 13, 14). Facies show proximal-to-distal textural patterns similar to those in the Pliocene yet lack the clinoform geometry. Paleoslopes on time-equivalent carbonate strata are 1° -to- 3° , with a consistent dip toward the southeast. Proximal-to-distal distribution of fossil constituents are similar to those in the Pliocene (Fig. 15).

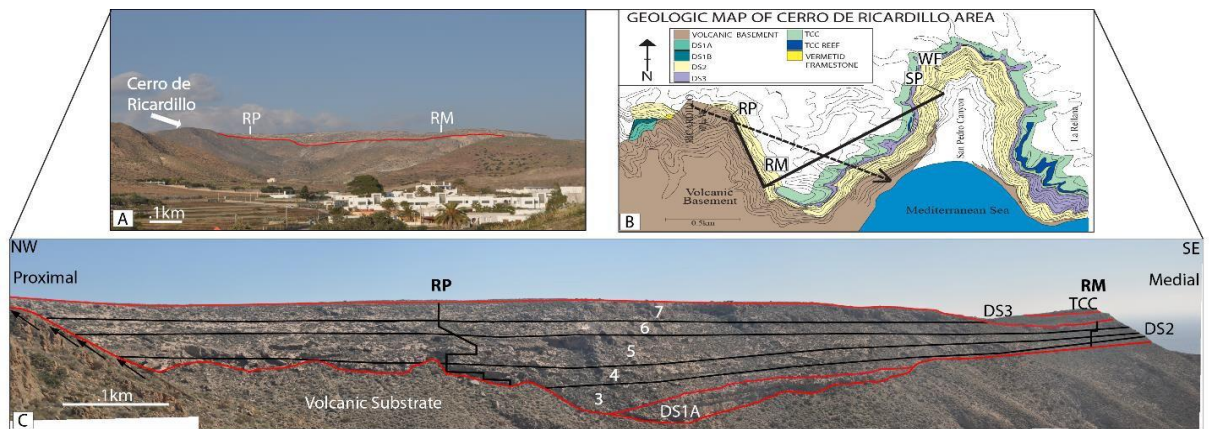


Figure 13: Field relationships of heterozoan carbonate cyclothem onlapping onto Cerro de Ricardillo. A) Volcanic highs create substrate on which Miocene carbonates developed and accumulated. This image shows the proximal-medial portion of the Ricardillo ramp. B) Geologic map showing the 5 regional sequences on the Ricardillo area and the Rellana Platform. A dashed arrow on image B shows the direction of true dip. Modified from Toomey et al. (2003). C) Photomosaic of the proximal to medial sections of the Ricardillo ramp and a close up of image A. This shows an oblique strike/dip cut of the outcrop. RM is .6km away from RP, the base of it is 35m in elevation lower than RP, and it is down depositional dip. The outcrop however is oblique and not along true dip. Black lines and numbers differentiate the 5 cycles along this part of the upper ramp. Dashed arrow indicates direction of true dip.

MIocene Lithofacies and Interpretations

Miocene deposits contain 13 lithofacies, composing five lithofacies associations. These lithofacies are similar to those in the Pliocene clinothem, but show enough variation from the Pliocene strata to warrant separate description. The lithofacies description table (Table 2) contains detailed measurements and results from microfacies analyses, and is referred to in the text for lithofacies specifics. Interpretations of depositional environments are guided by preserved clinoform geometries in the Pliocene analog and additional observations and analogs.

Grain constituents for these deposits are diverse and are composed of: cheilostome,

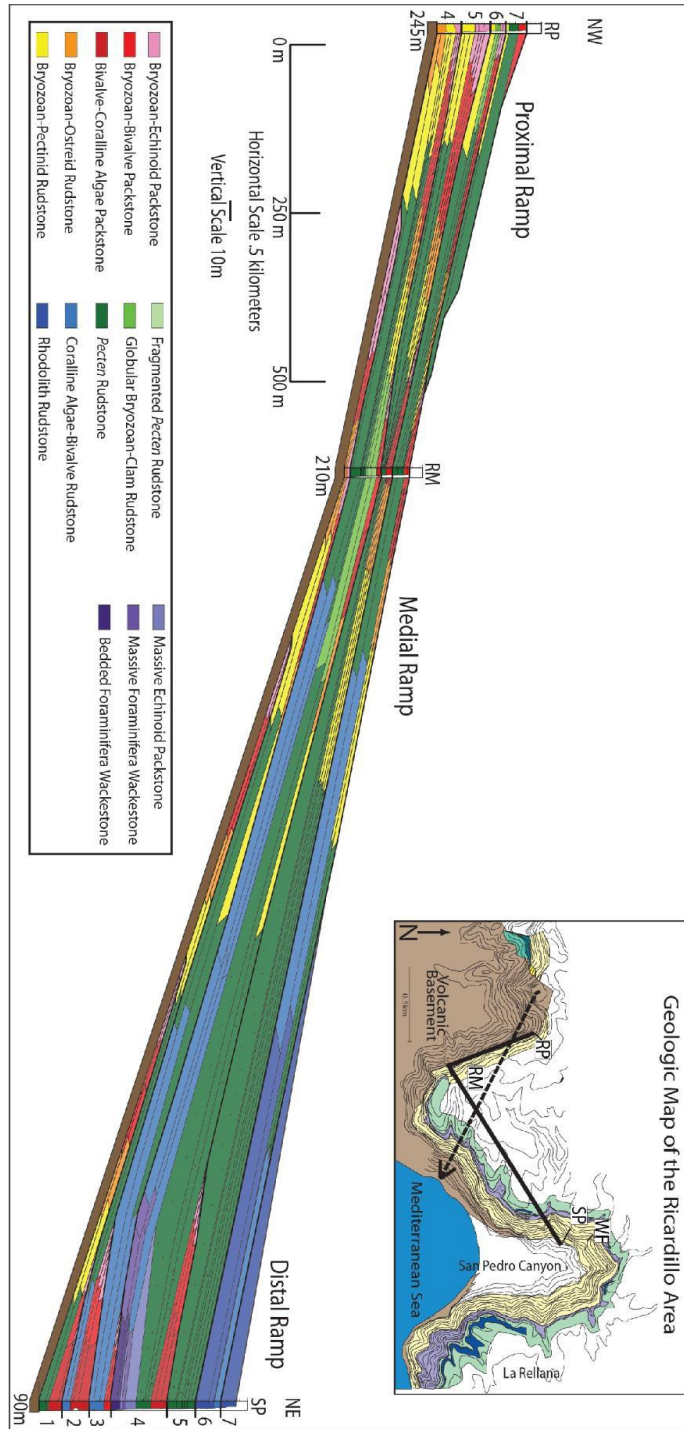


Figure 14: Cross section of Miocene carbonate sequences in the Ricardillo area. The cross section shows the seven measured cycles along the ramp. Proximal, medial, and distal sections are labeled. Overall 13 lithofacies have been identified and described. Note the elevation differences used to quantify relative sea-level amplitudes and facies depths. For interpretations of paleotopography, 7 m are subtracted from the elevations of the proximal and medial sections elevations to correct for tectonic tilt. Dislocated packstone facies are apparent throughout the cross section in all regions of the ramp. Measured sections are placed directly on the cross section. Dashed arrow indicates direction of true dip.

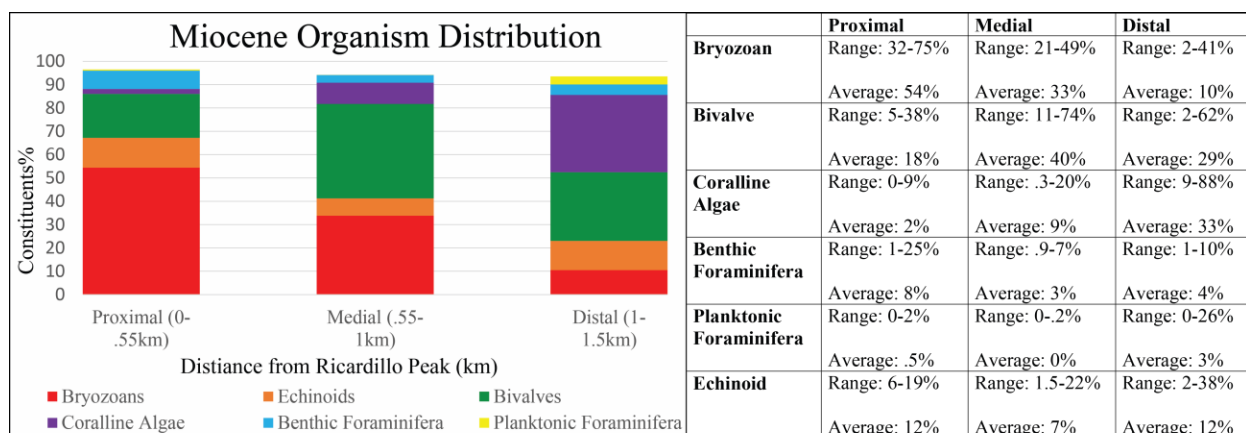


Figure 15: Paleotopographic distribution of organisms in the Miocene strata. Bryozoans have a peak abundance in proximal regions, bivalves in medial regions, and coralline algae in distal regions. These trends are similar between the two study areas. Tables show ranges and averages of organism distribution. These values were measured through point counting of 320 thin sections. Planktonic foraminifera play a significant role in grain composition in few facies in distal regions of San Pedro. Benthic foraminifera are most abundant in proximal and medial regions in both study areas. Grain constituent percentages came from lithofacies within the stated ranges (Appendix III). This data has been normalized for grain constituents only, pore space, cement, and matrix were removed. Columns don't reach 100% as there are other minor grains present in each sample.

cyclostome, and fenestrina bryozoans with globular, branching, and encrusting morphologies.

Thin, branching geniculate coralline algae and non-geniculate rhodoliths (*Mesolobus*, *Lithothamnion*), ostreids, pectinids, and other (various clams) bivalves, as well as echinoids (*Chlypeaster*). Less abundant organisms include: benthic (Rotaliacea, Milionacea, and Textularia) and planktonic (*Globigerina*) foraminifera, gastropods, serpulids, barnacles, minor lithoclasts, volcanics (<1%), and calcisilt matrix. These are grain-rich, matrix-poor packstone and rudstone facies and two silty wackestone facies.

Texturally, facies show an excellent correlation between sorting and grain size. As with the Pliocene facies, the packstone facies (coarse sand) have the best sorting (Fig. 16). With the exception of the Massive Echinoid Packstone, these fine-grained and well sorted facies are found updip on the most proximal parts of the cross section, whereas the coarse-grained and poorly sorted facies are found mostly downdip (Figs. 14, 15, 16).

Each of these facies associations include a paleobathymetric interpretation based off of facies distribution and corrected paleotopography. The paleobathymetric ranges are measured

by tracing lithofacies from their most distal position to most proximal, using a wave base depth of 8m. However, this methodology requires strata to be time-equivalent, not diachronous, to interpret paleobathymetric ranges. A few lines of evidence are used to support the assumption that these beds are in fact time-equivalent, and developed over the depth ranges stated in the subsequent sections

The first evidence comes from the analogous Pliocene deposits. The Pliocene exposure (Fig. 5) allows for tracing of individual beds from proximal to distal and observation of lateral facies changes along the same beds. The change seen from rudstones in distal regions and packstones in proximal regions along identical beds indicates that there are time-equivalent facies fluctuations from proximal to distal. Using this model for the Miocene allows for the comparison of paleobathymetric depths of similar deposits to the Pliocene. If similar lithofacies have similar depths, than this is evidence that the Miocene deposits also formed in a similar fashion. This assumption is further supported by evidence from the actual Miocene deposits. If diachronous deposition is the mechanism for the development of these facies, than evidence of facies shifting back and forth would be recorded and proximal facies would be found deposited stratigraphically below distal facies within individual cycles. Taking Cycle 5 of the medial section for example (Figure 14), the *Pecten* Rudstone directly overlies the Bryozoan-Bivalve Packstone of the underlying cycle (Cycle 4). This *Pecten* Rudstone is then directly overlain by the Bivalve- Coralline Algae Packstone. If facies were deposited diachronously, there would be deposition of facies that develop at depths between these packstones and rudstone, however there is not.

Lastly, time-equivalent beds between the medial and proximal regions of the Ricardillo ramp can be traced from proximal to medial regions in the field. An example of this comes from

Cycle 6 (Figs. 13 and 14). The dislocated packstone deposit that occur at the top of the cycle in the medial region pinches out further updip into the rudstone facies of this cycle. When followed further updip, the upper portion of the rudstone transitions into packstone facies, along the same time-equivalent bed. These lines of evidence support that these are time-equivalent strata and therefore their distribution across paleotopography allows for the quantification of paleobathymetric depth ranges.

Cross-Bedded Packstone Association

Description.---This lithofacies association consists of Bryozoan-Echinoid Packstone, Bryozoan-Bivalve Packstone, and Bivalve-Coralline Algae Packstone (Fig. 10). The Bryozoan-Echinoid Packstone (Table 2) is found at the top of cyclothems in the most proximal regions of the Ricardillo ramp and ranges from 1-5m in thickness. Branching, disarticulated, and abraded bryozoans make up 47% of the constituents in this lithofacies. Equant calcite cements are also abundant, reaching up to 12% of the overall rock composition.

Miocene Lithofacies Description						
Facies Association	Lithofacies	Grain Constituents	Sorting vs. Grain Size	Grain Size	Sedimentary Structures	Depositional Mechanism
Cross- Bedded Packstone Association	Bryozoan-Echinoid Packstone	Bryozoan: 49% Bivalve: 9% Coralline Algae: 4% Echinoid: 15% Benthic Foram: 4% Matrix: 3% Cement: 12% Other:4%	σ_i : .8-1.25 Well-Moderate $y = 6.6284x^4 - 8.8587x^3 + 1.4941x^2 + 1.1734x + 0.8594$ R = 0.6849	Thin Section: .9-1.3mm Outcrop: 1-3mm	- Cross-Beds - Massive?	- Moderately Abraded -Sediment transport by waves

	Bryozoan-Bivalve Packstone	Bryozoan: 25% Bivalve: 33% Coralline Algae: 4% Echinoid: 4% Benthic Foram: 7% Matrix: 2% Cement: 22% Other: 3%	σ_i : 1.7-1.4 Well-Moderate $y = 7.949x^4 - 1.8847x^3 - 2.5889x^2 + 0.0775x + 1.209$ R = 0.4301	Thin Section: .8-2.1mm Outcrop: 1-3mm	- Cross-Beds - Massive?	- Moderately Abraded - Sediment transport by waves
	Bivalve-Coralline Algae Packstone	Bryozoan: 13% Bivalve: 28% Coralline Algae: 30% Echinoid: 8% Benthic Foram: 4% Matrix: 1% Cement: 10% Other: 6%	σ_i : .9-1.2 Moderate No correlation	Thin Section: .8-1.3 Outcrop: 1-4mm	- Cross-Beds - Massive?	- Moderately Abraded - Sediment transport by waves
Bryozoan-Bivalve Rudstone Association	Bryozoan-Ostreid Rudstone	Bryozoan: 47% Bivalve: 8% Coralline Algae: 7% Echinoid: 8% Benthic Foram: 4% Matrix: 16% Cement: 9% Other: 1%	σ_i : 1.1-1.7 Moderate-Poor $y = -1.1013x^2 - 1.8362x + 0.9798$ R = 0.9327	Thin Section: 1.2-4.4mm Outcrop: 5-15mm, up to 5cm	- Massive Beds	- <i>In situ</i> deposition - Minor sediment transport
	Bryozoan-Pecten Rudstone	Bryozoan: 49% Bivalve: 20% Coralline Algae: 1% Echinoid: 13% Benthic Foram: 5% Planktonic Foram: 1% Matrix: 7% Cement: 3% Other: 1%	σ_i : 1.1-2 Moderate-Poor $y = 0.7442x^2 + 0.7476x + 1.4514$ R = 0.6095	Thin Section: 1.6-6.4mm Outcrop: 5-15mm	- Massive Beds	- <i>In situ</i> deposition - Minor sediment transport
Bivalve Rudstone Association	Fragmented Pecten Rudstone	Bryozoan: 21% Bivalve: 71% Echinoid: 1% Benthic Foram: 1% Matrix: 5% Cement: 1%	σ_i : 1.3-1.5 Moderate $y = -2.7249x^2 - 7.8345x - 3.987$ R = 0.9654	Thin Section: 2.5-4.5mm Outcrop: 6-15mm	- Massive Beds	- <i>In situ</i> deposition - Low Energy
	Pecten Rudstone	Bryozoan: 17% Bivalve: 46% Coralline Algae: 10% Echinoid: 8% Benthic Foram: 4% Matrix: 5% Cement: 6% Other: 4%	σ_i : 1.1-2.1 Moderate-Very Poor No correlation	Thin Section: 2-12mm Outcrop: 15-20mm	- Massive Beds - Horizontal Beds	- <i>In situ</i> deposition - Low Energy
	Globular Bryozoan-Clam Rudstone	Bryozoan: 49% Bivalve: 19% Coralline Algae: 3% Echinoid: 17% Benthic Foram: 8% Matrix: 2% Cement: 1% Other: 1%	σ_i : 1.5-1.9 Poor $y = -0.4803x + 1.3857$ R = 0.7298	Thin Section: 2.6-4.5mm Outcrop: 20+mm	- Massive Beds - Horizontal Beds	- <i>In situ</i> deposition - Low Energy
Coralline Algae	Coralline Algae-Bivalve Rudstone	Bryozoan: 18% Bivalve: 28% Coralline Algae: 38% Echinoid: 4% Benthic Foram: 4% Matrix: 2% Cement: 4%	σ_i : 1.1-1.9 Moderate-Poor No correlation	Thin Section: 1.7-5.8mm Outcrop: 5-15+mm	- Massive Beds	- <i>In situ</i> deposition - Low Energy

Rudstone Association		Other: 2%				
	Rhodolith Rudstone	Bryozoan: 4% Bivalve: 6% Coralline Algae: 76% Echinoid: 3% Benthic Foram: 3% Matrix: 3% Cement: 4%	σ_i : 1.5-2.2 Poor-Very Poor No correlation	Thin Section: 3-14mm Outcrop: 20-50+mm	- Massive Beds	- <i>In situ</i> deposition - Low Energy
Foraminifera Wackestone and Packstone Association	Massive Echinoid Packstone	Bryozoan: 3% Bivalve: 14% Coralline Algae: 25% Echinoid: 27% Benthic Foram: 3% Planktonic Foram: 1% Matrix: 6% Cement: 14%	σ_i : .7-.8 Well $y = 1.7408e^{-1.031x}$ R = 0.8365	Thin Section: .5-.8 Outcrop: 1-2mm	- Massive Beds	- Debris flow - Water depth:
	Massive Planktonic Foraminiferal Wackestone	Bryozoan: 2% Bivalve: 11% Coralline Algae: 9% Echinoid: 14% Benthic Foram: 3% Planktonic Foram: 12% Matrix: 35% Cement: 5% Other: 9%	$y = 2.6746x - 2.0645$ R = 1	Thin Section: silt- ~.5mm Outcrop: -----	- Massive Beds - Bioturbation	-Low density turbidite -Hemipelagic suspension -Bioturbation
	Massive Planktonic Foraminiferal Wackestone	Bryozoan: 3% Bivalve: 16% Coralline Algae: 6% Echinoid: 1% Benthic Foram: 8% Planktonic Foram: 18% Matrix: 28% Cement: 7% Other: 13%	$y = -76.794x^3 + 331.58x^2 - 475.83x + 227.66$ R = 0.6601	Thin Section: Silt- ~.3-.4 Outcrop: -----	- Horizontal laminations	-Low density turbidite -Hemipelagic suspension

Table 2: Miocene lithofacies descriptions. Summary table of diagnostic features for 13 lithofacies from the Ricardillo area of the Miocene. The equations of lines and R² values for sorting values are based on regression analyses from Figure 16.

Bivalve-Bryozoan Packstone (Table 2) is found at the top of cycles in medial regions of Ricardillo and in one locality in the San Pedro area. Thickness ranges from 2-to-3m and it is composed of crushed and disarticulated pectinid bivalves (33%) and branching bryozoans (24%). This lithofacies has abundant equant and bladed calcite cement, consisting of up to 32% of total rock composition in some locations. Coralline Algae-Bivalve Packstone (Table 2) is found at the top of cyclothems in distal regions of San Pedro. Thickness range from 2-7m and facies are composed of 30% geniculate and nongeniculate coralline algae fragments and 28% crushed pectinid bivalves. The majority of grains are less than 2mm in size, while a minor amount reach gravel size (~4mm; e.g. Udden 1914; Wentworth 1922).

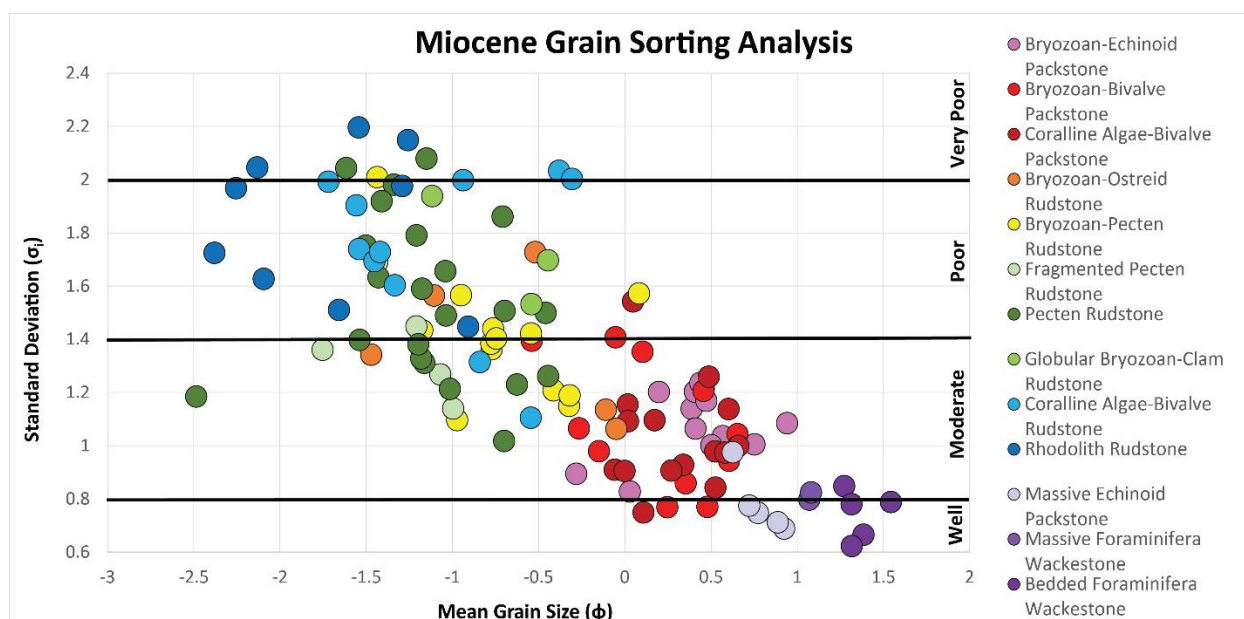


Figure 16: Quantitative sorting analysis of Miocene lithofacies. This is based on measurements of grain size from petrographic analyses. The x-axis shows the mean grain size in phi values and grain size increases towards more negative values. The y-axis shows the standard deviation and allows for the quantification of grain sorting. Higher values indicate poorer sorting and are classified on the right of the graph. Lithofacies generally plot closely together. Note that the wackestone lithofacies have 28-39% matrix, however the grain sorting analysis only measures grains. Therefore this analysis shows that the grains from these silty deposits are sorted, however they are deposited among high silt content, and the measurements of only grains, rather than grains and matrix, biases their sorting, providing lower standard deviations than they actually have. Equation of regression lines and R^2 values are found in Table 2. The equation for this entire dataset and R^2 value is as follows: $y = -0.009x^4 - 0.0096x^3 + 0.043x^2 - 0.31x + 1.1446$, $R = 0.6846$

Overall, matrix (calcsilt) content is low in these facies only reaching about 3% at a maximum with one exception in a 50cm bed at the base of Cycle 4 (Fig. 14) in the Bryozoan-Echinoid Packstone with a matrix up to 8%. All of the grains are fragmented, disarticulated, and original grain textures have been smoothed, truncated by fragmentation or rounded. Tabular (planar) cross-bedding is the most abundant bedding, although trough cross-bedding was also observed (Fig. 10c). Cross-beds are small to medium and are .5-2m in scale.

Interpretation.---The three packstone lithofacies are the updip equivalent of the Bryozoan-Bivalve Rudstone lithofacies association. Modern Mediterranean analogs record fairweather wave-base at 8-15m water depth (Hernández-Molina et al. 1995, 1998; Martin et al. 1996; Fornos and Ahr 1997). The tabular (planar) cross-beds indicate that these facies were deposited under a high energy regime (e.g. Burchette and Wright 1992; Boggs 1995; Wright and

Burchette 1996) and are interpreted to form at and near wave base (8-15m). The one 50cm bed with increased matrix is interpreted to be an area with *Posidonia oceanica* baffling. Overall, the facies association forms from the reworking of sediments with coarser original grain sizes; fragmenting, abrading, and sorting them, reflecting deposition in a high-energy environment, as wave base encroached upon these depositional environments. The composition of these facies is related to the underlying facies, which represents the downdip facies equivalent that has not been reworked extensively by currents. The Bryozoan-Echinoid Packstone is interpreted to be the most updip proximal facies and is the most abundant packstone on Ricardillo, followed downdip by the Bivalve-Bryozoan Packstone, followed by the Coralline Algae- Bivalve Packstone.

The Bryozoan-Echinoid Packstone is the only proximal Miocene lithofacies with consistently high echinoid content (Table 2). The proximal distribution and dominance of this lithofacies measured here is consistent with results from the modern echinoid *Clypeaster fervens* (Tsaparas et al. 2007). This modern echinoid lives in shallow water areas up to <1m (with a range of 1-50m) and is similar to *Clypeaster altus*, an echinoid found throughout the Mediterranean in the Miocene that lived in the shallowest water, high energy environments (Tsaparas et al. 2007), which is consistent with the conditions for the interpretation of the depositional environment for the Bryozoan-Echinoid Packstone. The abundance of test fragments and ossicles in this association likely originated from fragmentation of echinoids that lived in the environment. In addition, Betzler et al. (2000) also described a cross-bedded sand-sized bryozoan packstone abundant with echinoid test fragments in a different (but proximal) location on the western slope of Ricardillo. Using 8m as the depth of fairweather wave-base, and the Pliocene analog, Dilleott et al. (2004) interpreted similar Pliocene deposits (the Sand-

Gravel Packstone Association) to form in 8-30m water depth. The Miocene packstones probably represent the shallower end of this range as they are cross-bedded, whereas Pliocene equivalents lack these physical sedimentary structures and are interpreted to be transported and deposited below effective wave-base.

Bryozoan-Bivalve Rudstone Association

Description.---This lithofacies association consists of Bryozoan- Ostreid Rudstone and Bryozoan-*Pecten* Rudstone (Fig. 11A, B). The Bryozoan-Ostreid Rudstone (Table 2) is found at the base of cyclothems in proximal and medial regions of Ricardillo, always deposited directly on volcanic substrate. Beds range in thickness from 1-to-3.5m and are composed of 47% articulated branching (thin and robust) bryozoans and 8+% whole clams and oysters. The robust bryozoan grains are up to 10-to-20mm in branch diameter, 2-4 times the size of the thinly branching bryozoans. Clams and oysters are scattered among the abundant bryozoans and range in size from 3-to-5+cm. This facies has the highest matrix content (16%) of any of the grainy lithofacies in the Miocene.

The Bryozoan-*Pecten* Rudstone (Table 2) is found at the base and in the middle of cycles in the proximal regions of Ricardillo. Beds range in thickness from 1.5-to-4m and are composed of 48% articulated branching bryozoans and 20% whole valves of unabraded *Pectens*. This lithofacies does not contain the whole clams and oysters of the Bryozoan-Ostreid Rudstone, and instead consists of pectinids that are intermixed with the bryozoans. Matrix content decreases to 7% in this lithofacies compared to the 16% of the Bryozoan-Ostreid Rudstone

Globular bryozoans are scattered within this association and make up 10-15% of the bryozoans. They have a flat base and a dome shaped top, with 4-5mm hollow tubes at their base. None of the bivalve shells have a particular orientation, but are heavily bored and are encrusted

by bryozoans. All shells, bryozoans, and other fossils have preserved shell and body morphology and have undergone fragmentation but not extensive abrasion. These strata are massive with no original bedding preserved.

Overall the Bryozoan-*Pecten* Rudstone is the coarser of the two facies as there is an increase in robust branching and globular bryozoan in it compared to the Bryozoan-Ostreid Rudstone. Additionally, the coarse *Pectens* are a more common grain type and are not just scattered sparsely as with the oysters of the Bryozoan-Ostreid Rudstone. The Bryozoan-Ostreid Rudstone can be traced downdip ~12m from its most proximal position, and the Bryozoan-*Pecten* Rudstone can be traced about an additional 12m down dip from there.

Interpretation.---This lithofacies association is the updip equivalent to the Bivalve Rudstone facies association and downdip equivalent of Cross-Bedded Packstone Association. The lack of bedding and the unabraded, but heavily fragmented nature of the bryozoan grains leads to an interpretation that these formed beneath fairweather wave-base. Assuming the most updip Bryozoan-Ostreid Rudstone formed just downdip from the Cross-Bedded Packstone Association at 12-15m, the Bryozoan-Ostreid Rudstone formed on this ramp at depths of 12-24m, while the Bryozoan-*Pecten* Rudstone is interpreted to have formed at depths of 24-36m. The depths of these facies indicate that storm wave-base likely had an intermittent effect on grain fragmentation as the greatest extent of the lower limit of wave action in the Mediterranean is 25- 30m (Hernandez-Molina et al. 1995, 1998). An overall low energy system is consistent with past research showing that whole globular bryozoans are indicative of low energy environment (Bassi 2006), and that the preservation of delicate bryozoan skeletons adds further evidence that the grains accumulated *in situ*, and were only slightly reworked (Stockmann et al. 1967).

Burrowing in the sediment likely destroyed any original sedimentary structures, causing massive beds. The hollow cores in globular bryozoans are consistent with observations from Betzler et al. (2000) who compared the tubes with structures produced in bryozoans that were attached to *Poseidonia* sea grasses as described by Voigt (1981). It is also possible that the hollow cores have developed from attachment to sponges that have since decayed (e.g. Taylor and James 2013). However, these facies interpretations are still in the bathymetric range of *Poseidonia oceanica* grass beds (e.g. Moissette et al. 2007), which are known to thrive down to 30m in the modern Mediterranean. In association with bryozoan meadows, *Poseidonia* could have acted as baffles for silt-sized sediments produced from abrasion updip and subsequently transported downdip into this facies association. Since these facies are interpreted to be directly downdip of the zone of abrasion, it is a reasonable explanation for the high matrix content of these lithofacies.

Bivalve Rudstone Association

Description.---This lithofacies association consists of a Fragmented *Pecten* Rudstone, *Pecten* Rudstone, and Globular Bryozoan-Clam Rudstone (Fig. 11C, D). The Fragmented *Pecten* Rudstone (Table 2) has a limited distribution and is only found in one place, in the middle of Cycle 4 (Fig. 14) on the medial part of the ramp of Ricardillo. This facies is 4m thick and is composed of 70% *Pecten* bivalves. The majority of shells are fragmented with average grain size of ~8mm. Rarely, shells are whole and disarticulated. The shells do not have a preferred orientation, have minor boring, and exhibit original surface textures, indicating little abrasion.

Pecten Rudstone (Table 2) has the most widespread distribution of all Miocene lithofacies and is found at the base and in the middle of cycles and throughout all of the medial and distal regions of the ramp, and in the proximal section of Cycle 7 (Fig. 14). It is composed

of 47% *Pecten* bivalves. The only rhodoliths found in the medial ramp come from this lithofacies. This is the only rudstone facies in the Miocene to contain significant coralline algae (10%) in medial and proximal positions. Where this lithofacies is deposited in the distal ramp, coralline algae content increases up to 18%.

Globular Bryozoan-Clam Rudstone (Table 2) also has a limited distribution and is only found in the middle of Cycle 6 (Fig. 14) in the proximal section. It has a thickness of 2m and is composed of 19% clams and 49% bryozoans, the majority of which are multi-centimeter globular forms. This lithofacies contains whole articulated clams (both valves) up to 6cm in size and dome-shaped globular bryozoans up to 2cm in size that are deposited upright in life position. Globular bryozoans have a hollow cavity in their base as described above.

Beds in this association are primarily massive with some individual burrows visible. Where horizontal bedding is present, beds are up to 10cm thick with no internal bedding. Bivalve shells are well preserved, have original surface textures, and are heavily encrusted by bryozoans. Due to the bi-modal grain size in these beds, sorting ranges from moderate to very poor sorting. This facies association can be traced across 45m of elevation difference, where coralline algae content increases, it can be traced an additional 40m.

Interpretation.---This association is the downdip equivalent to the Bryozoan-Bivalve Rudstone Association. Assuming the most updip *Pecten* Rudstone formed just downdip from the Bryozoan-Bivalve Association at 35m, the *Pecten* Rudstone formed on this ramp at depths of 35-80m. The portion of this lithofacies that has an increase in coralline algae is interpreted to form at depth ranges from 80-120m. The increase in coralline algae content compared to more proximal *Pecten* Rudstones is significant enough to distinguish between the two.

Due to the partially fragmented, but unabraded nature of the Fragmented *Pecten* Rudstone,

it is interpreted to have formed near storm wave-base (~25m in the modern Mediterranean; Hernandez-Molina et al. 1995, 1998), as the wave energy produced from storms caused the fragmentation of the *Pectens*. The lack of abrasion indicates that this lithofacies did not develop in a consistently high energy environment where the grains would have been transported, abraded, and further fragmented. The development of this lithofacies at storm wave-base is necessary as if it were deposited at greater depths, the *Pectens* would have not undergone fragmentation.

The Globular Bryozoan-Clam Rudstone is interpreted to have formed beneath storm wave-base due to the unfragmented articulated bivalve shells and the preserved multi-centimeter globular bryozoans. The depositional environment was shallow enough to have abundant bryozoan content (49%), formed deeper than the Bryozoan-Bivalve Rudstone Association, and formed at a similar depth range to the *Pecten* Rudstone (as this a variant of the *Pecten* Rudstone). These observations have been used to estimate that the facies formed at depths of 30-40m, and does not have a wide depositional range, as only a few meters of it are observed in one location.

The paleobathymetric range for the *Pecten* Rudstone, although wide (85m), greatly constrains the potential depths at which *Pecten* deposits can occur (from intertidal zones to 6,000m deep; Brand 2006), depending on nutrients (Fr  chette et al. 1993). The lack of abrasion, sorting, cross-beds, as well as the paleotopographic downslope position provides strong evidence that the *Pecten* and the Globular Bryozoan-Clam Rudstones formed in a low energy environment. The preserved life position of many of the organisms is further evidence for *in situ* growth.

The massive structure of these beds is interpreted to form from intense bioturbation. The hollow tubules inside of globular bryozoans cannot be from attachment to grass beds as these

facies must have formed at depths greater than those of sea grass depths. Therefore the hollow cores have been interpreted as forming from attachment to sponges that have decayed (Taylor and James 2013).

Using similar Pliocene facies as an analog, Dillett et al. (2004) interpreted the *Pecten* Rudstone in the Pliocene to form at depths >50m. This interpretation is consistent with the data presented for the Miocene. However, the Miocene provides a more constrained range, indicating that depths were no greater than 120m.

Coralline Algae Rudstone Association

Description.---This facies association consists of Coralline Algae-Bivalve Rudstone and Rhodolith Rudstone (Fig. 12B, C). The Coralline Algae-Bivalve Rudstone (Table 2) is found at both the base and top of cyclothems in distal regions of the ramp. Thickness ranges from 3-6m and it is composed of 38% coralline algae and 28% *Pecten* bivalves. The coralline algae are geniculate and non-geniculate, with whole rhodoliths scattered throughout. The geniculate coralline algae are composed of thin and robust branching coralline algae that are broken, but articulated.

Rhodolith Rudstone (Table 2) is the coarsest facies in the Miocene. It contains rhodoliths that range from 2-10cm and have an average size of 4cm. It is distributed at the base of Cycles 6 and 7 in the distal regions of the ramp in San Pedro. Bed thicknesses range from 7-9m and are composed of 76% coralline algae, primarily in the form of rhodoliths. The rhodoliths have a elongate fructose-warty texture (Farr et al. 2009) and can be classified as monospecific discoidal columnar rhodoliths (Bosence 1983a). The geniculate coralline algae are thin and have long branching morphologies, multiple cases were observed where the algae were deposited with branches oriented upward, in life position. In between the individual rhodoliths, interparticle

pore space is filled by fine sand grains and calcisilt. Overall, deposits from both facies have beds that are massive with no sedimentary structures. The Coralline Algae-Bivalve Rudstone can be traced ~35m updip from its most distal location and can be traced along time-equivalent strata across 127m of elevation.

Interpretation.---This association is the downdip equivalent of the *Pecten* Rudstone Association. The distal distribution of these facies shows that coralline algae abundance increases basinward, with 1% average content in proximal regions and 25% average in distal regions. Assuming the most updip Coralline Algae-Bivalve Rudstone formed just downdip from the *Pecten* Rudstone at ~80m, the Coralline Algae-Bivalve Rudstone formed on this ramp at depths of 80-115m. As the Rhodolith Rudstone can be traced along 127m, and assuming it formed at depths beneath the Coralline Algae-Bivalve Rudstone, it is interpreted that the Rhodolith Rudstone therefore formed at depths of 115-135m.

Evidence for a low energy environment includes the lack of grain abrasion, poor sorting, the presence of articulated delicate coralline algae branches, and rhodolith morphology (Bosence 1983b). This low energy environment and depth estimate is consistent with similar modern rhodoliths, which are recorded to grow at depths between 35 -150m in the Mediterranean Sea (Bosence 1985; Basso 1998; Hall-Spencer and Moore 2000). Rhodolith and coralline algae morphology and paleotopographic position indicate that these rhodolith beds were deposited in the deeper end of the modern range. Using similar facies from the Pliocene as an analog, Dille et al. (2004) interpreted rhodolith beds from the Pliocene to form at depths of 65-100m, based on columnar, spherical morphologies, which indicate shallower water depths (Carannante and Simone 1996; Peres and Picard 1964), compared to the Miocene rhodolith beds (Bosence 1983b).

Planktonic Foraminifera Wackestone and Packstone Association

Description.---This lithofacies association consists of the Massive Echinoid Packstone, Massive Planktonic Foraminiferal Wackestone, and a Bedded Planktonic Foraminiferal Wackestone (Fig. 17).

The Massive Echinoid Packstone (Table 2) has a distribution limited to the distal parts of the ramp (San Pedro) and is only found interbedded with wackestone rich in planktonic foraminifera. Thickness of these massive beds ranges from 1-to-4m and they are composed of 27% fragmented echinoid tests and 25% coralline algae. This lithofacies also contains 14% equant calcite cement, and also includes 1% planktonic foraminifera.

The Massive Planktonic Foraminiferal Wackestone (Table 2) is only found in one bed in the distal part of the ramp in San Pedro. It is one meter thick and is composed of 39% matrix, and 8% planktonic foraminifera and planktonic foraminiferal molds. In addition to the foraminifera and calcisilts, other grains are sand-sized bioclast fragments. Rare nine to twelve centimeter, whole echinoids are found sparsely scattered in this bed. This bed contains no evidence of sedimentary structures other than burrows.

The Bedded Planktonic Foraminiferal Wackestone (Table 2) is only found in one bed in the distal part of the ramp in San Pedro. It is 4m thick and is composed of 28% matrix, and 14% planktonic foraminifera and planktonic foraminifera molds. Benthic foraminifera make up about 6% of the sediment. This facies has millimeter scale horizontal laminae that alternate between grainy laminae with minor amounts of calcisilt and calcisilt-rich laminae abundant in planktonic foraminifera, forming an interbedded pattern. The two wackestones are the only mud dominated textures in the Miocene and have the highest amounts of benthic and planktonic foraminifera. Strata that are time-equivalent with the base of the most distal position of the Massive Planktonic

Foraminifera Wackestone can be traced across 132m of elevation, while the bedded Planktonic Foraminifera Wackestone can be traced across 140m of elevation.

Interpretation.---This lithofacies association is found downdip of the Coralline Algae Rudstone Association. It is estimated that the Massive Planktonic Foraminifera Wackestone formed at maximum depths of 140m and the Bedded Planktonic Foraminifera Wackestone formed at depths of at least 148m. The Massive Echinoid Packstone deposited at depths between the two (140-148m). In support of this interpretation, sedimentary structures and textures indicate there are sediment gravity flow deposits interbedded with hemipelagic fallout. The high mud content and abundance of planktonic foraminifera are indicators of hemipelagic deposits, which occur at depths greater than 100m down to the Carbonate Compensation Depth of ~4,500m (e.g. Grimsdale & Van Morkhoven 1955; Smith 1955; Scholle et al. 1983; Gorsline 1984). In addition, Franseen et al. (1997) interpreted similar hemipelagic facies in the region at over 100m depth. The laminae-scale, sand-sized layers are interpreted as sediment gravity flows (e.g. Bouma 1962). These sand-sized layers are unaltered by bioturbation, whereas the massive beds are interpreted to be churned by organisms. The whole echinoids found in this bed are likely the source of bioturbation. The lack of bioturbation in the bedded hemipelagics is likely due to anoxic or hypoxic conditions (e.g. Clarke 1990).

The Massive Echinoid Packstone is interpreted as a debris flow deposit. The highly fragmented and fractured grains appear similar to grains found much farther updip that have undergone the effects of physical abrasion. In addition, echinoids and bryozoans are not common in distal settings, therefore the echinoid and bryozoan fragments of this facies appear to have been transported from updip sources where echinoids and bryozoans are abundant. As these are interbedded within the hemipelagic deposits, it is speculated that as shoaling began,

updip, proximal sediments may have become unstable and were transported downdip. This is consistent with a similar model for such facies in nearby time-equivalent rocks (Johnson et al. 2005).

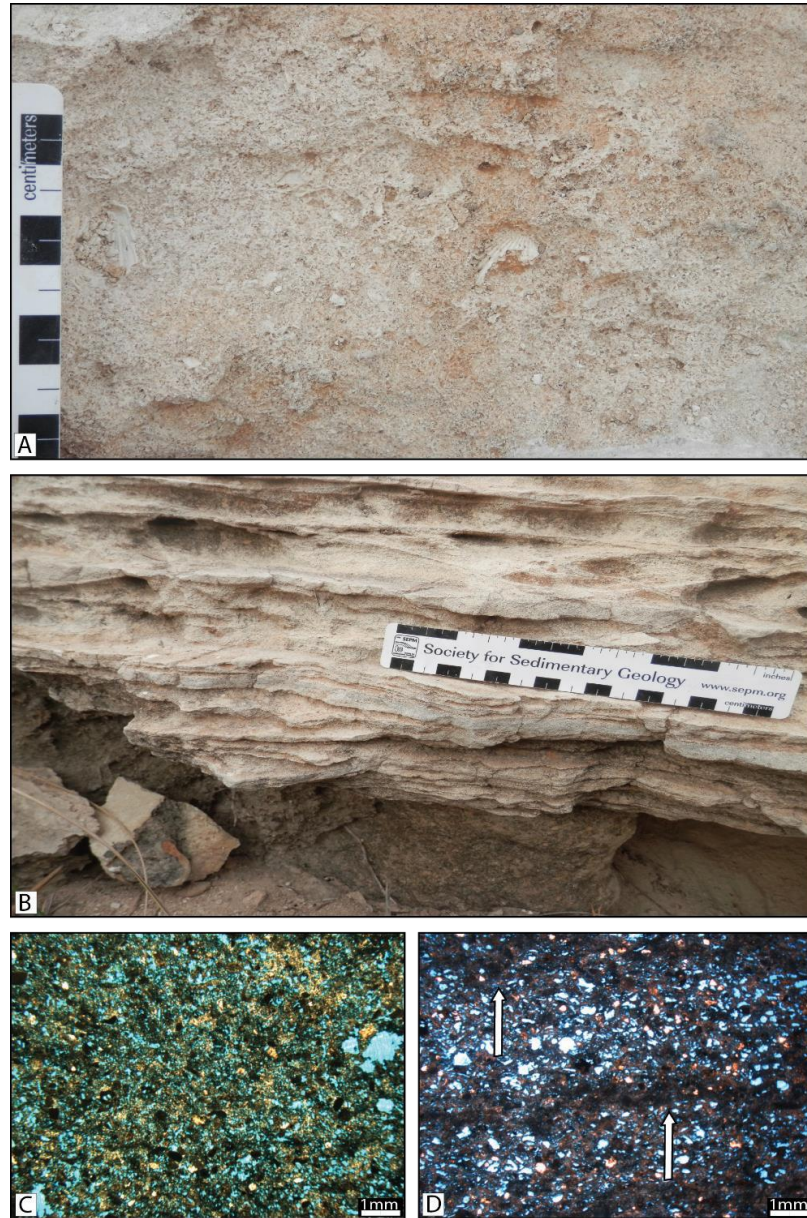


Figure 17: Photographs and photomicrographs of the Wackestone Association of the distal regions of the Miocene. A) Massive Foraminifera Wackestone. Coarse grains have a scattered distribution in this lithofacies and are intermixed with matrix and other fine grains with no preferred shell orientation or bedding. B) Bedded Foraminifera Wackestone. Interbedded millimeter-centimeter scale laminae can be differentiated by color variation between the beds. Darker laminae are more matrix-rich. C) Sample from the lithofacies from image A. Moldic porosity is extensive and matrix has been recrystallized to coarser dolomite crystals. Grains are composed of planktonic and benthic foraminifera, coralline algae, and bivalves. D) Sample from the lithofacies from image B. Planktonic foraminifera molds are common in this lithofacies. Note the laminations shown in thin section marked by the white arrows, darker layers are more mud-rich than the lighter more porous layers. All of these lithofacies have been 100% dolomitized.

MIOCENE CYCLOTHEMS

Miocene strata from this study consist of 7 onlapping and topography-draping cyclothems. Cyclothems are numbered as Cycles 1-7 (Figs. 13, 14). Each cyclothem shows predictable vertical lithofacies patterns that are dependent on paleotopographic position. In proximal positions, cyclothems coarsen upward at the base, and then fine upward at the top; in medial-distal areas, cyclothems fine upward; and in the most distal areas they coarsen upward at the base, and then fine upward at the top. Figure 14 shows the compilation of the vertical lithofacies patterns in a cross section from proximal regions on the ramp near Cerro de Ricardillo down to the paleovalley of San Pedro. Figure 18 shows the idealized vertical lithofacies pattern within cyclothems for each paleotopographic position.

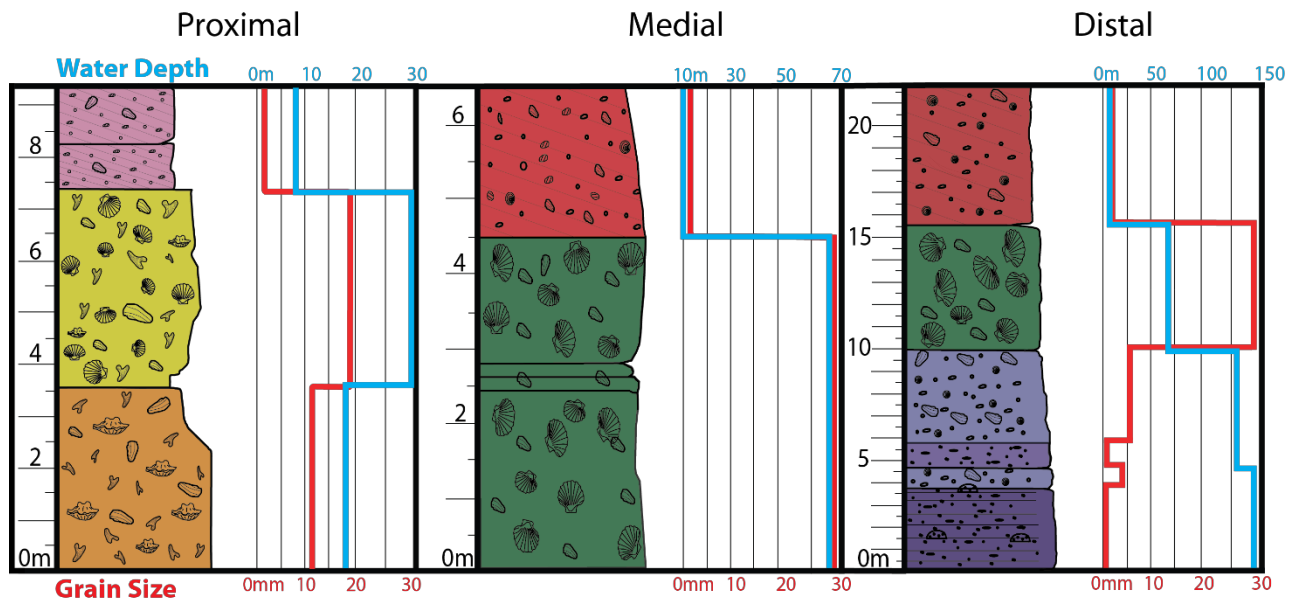


Figure 18: Idealized vertical lithofacies pattern within cyclothems tied to paleotopographic position on the Ricardillo ramp. Proximal cycles are composed of three lithofacies, medial and most of the distal cycles are composed of two lithofacies and have a similar vertical trend. The most distal cycles are composed of five lithofacies. With deep-water hemipelagic deposits forming the base of the cycle. This cycle pattern is unique and is only found in one (Cycle 4) with the deepest deposits. Grain size curves from outcrop measurements are shown in red and interpreted average water depths are shown in blue.

Proximal Cyclothems

Four cyclothems (Cycles 3-7) are preserved in the most proximal region of the ramp (Figs. 13, 14) and are 6m, 8m, 9m, and 11m thick in the most proximal region (Cycles 4,5,6, and 7 respectively). The base of the measured section comprising them is located at a present day elevation of 245m. Given corrections for Pliocene tilt, this position is 35m higher along the paleotopography than the medial section and 148 m higher than the distal section. The most common vertical facies pattern found in Cycles 4, 6, and 7, consists of a basal facies composed of the Bryozoan-Bivalve Rudstone Association with average grain sizes of 10-12+mm. These basal facies are 2-to-3.5m thick and have a gradational or sharp contact with overlying Bryozoan-Bivalve Rudstone and the Bivalve Rudstone Association. These middle beds range in thickness from 2-to-6m and have grain sizes that range from 15-20+m. Above these beds, a primarily sharp contact (Fig. 10B) marks the transition into the third and capping facies of the cyclothem, the Cross-Bedded Packstone Association. This marks an abrupt change from coarse gravel (15-20mm) grains to lithofacies dominated by very coarse sands (~2mm). Cycle 5 consists of Bryozoan-Pectinid Rudstone facies at its base, which are sharply overlain by the Bryozoan- Echinoid Packstone facies.

Medial Cyclothems

Four cyclothems (Cycles 3-6) are preserved in the medial region of the ramp (Figs. 13, 14) and are 2, 12, 4.5, and 7.5m thick (Cycles 3, 4, 5, and 6 respectively). The medial measured section is located at 210m elevation. This position is 35m lower along the paleotopography than the proximal section and 113m higher (after correction) than the distal section. Cyclic sequences (3, 5 and 6) consist of basal Bryozoan-Bivalve Rudstone or/and Bivalve Rudstone Association. These basal lithofacies range from 1-6m in thickness and are sharply overlain by Cross-Bedded

Packstone Association. These medial cycle patterns are also commonly found in more distal locations of the ramp that do not develop deep enough to be influenced by pelagic deposits. Cycle 4 is composed of a basal *Pecten* Rudstone, overlain gradationally by the Fragmented *Pecten* Rudstone, followed by a sharp contact into the Cross-Bedded Packstone Association, indicating shoaling. Overall, cyclothems are thinner in the medial region than in proximal areas.

Distal Cyclothems

The distal measured stratigraphic section spans from 90-166m elevation and the base of it is 113m lower than the medial measured stratigraphic section. The stratigraphically lowest three fining-upward cycles (Cycles 1, 2, and 3) are 9, 10, and 8.5m thick and follow the same vertical lithofacies patterns as seen in the medial deposits, but are greater in thickness. Cycles 4-7 (21, 11, 9.7, and 6.7m thick), however, show different depositional trends. The base of Cycle 4 consists of interbedded lithofacies from the Foraminiferal Wackestone and Packstone Association. These deposits make up the basal 10m of this cyclothem, which is sharply overlain by *Pecten* Rudstone. This is then overlain by the same fining-upward trend seen in the medial ramp and Cycles 1-3, creating a coarsening-upward and overlain by a fining-upward trend. Cycles 5 and 7 only record rudstone facies with no fining-upward component. Cycle 6 has a fining-upward transition, however, not from rudstone to packstones but from the Rhodolith Rudstone to Coralline Algae-Bivalve Rudstone (Fig. 14).

DISCUSSION AND CONTROLS

Paleotopography and Substrate

The effect of substrate paleotopographic slope on the geometry of the overlying carbonates is apparent from both field areas. The Miocene deposition on Ricardillo resulted from

interaction between sea-level fluctuations and the sloping substrate. The gradient of the volcanic substrate on the eastern flank of Ricardillo in the Miocene was 6.8° , and onlap and drape geometries are prevalent along the slope.

The Pliocene deposition in Carboneras resulted from intersection of shallow waters with an extensive low gradient surface during a lowstand. The Pliocene substrate paleotopography in this study area of the Carboneras Basin is variable, consisting of areas with flat to gently sloping ($<2^\circ$) substrates, substrates with moderate slope gradients ($4.3-6^\circ$), and steeper substrates with gradients $>6^\circ$. A broad shallow surface just updip from the Pliocene clinothem allowed for an expanse where organisms flourished and abundant carbonate grains developed. During sea-level lowstands, these grains were funneled downdip into the depression that distally flattens towards the southern end of the basin (Fig. 7). Draping geometries form along the steeper slopes ($\sim 6^\circ$), and clinoform geometries developed at the break-in-slope and downlap onto the lower-gradient strata in the depression, forming a wedge (Fig. 7).

The differences in paleotopographic gradient and the types of geometries that form highlights the effects that paleoslope has on the development of “loose-grained” heterozoan carbonate systems. Homoclinal slopes ($\sim 4-7^\circ$) resulted in onlapping and draping geometries. Gentle surfaces ($< 2^\circ$) allowed for either broad areas of sediment generations, or local basins onto which the clinothem downlapped.

Paleotopography also is an important control on the location of depositional environments as it governs bathymetry and the extent of facies distribution. *Posidionia oceanica* grass bed distribution is an example of this. These grasses form from .5-to-30 m (Procaccini et al. 2003; Moissette et al. 2007) along shallow shelves. The broad, shallow area with low slope in the Pliocene in the Carboneras Basin provides an area for the dispersion of high energy in

shallow water, therefore allowing for development of stable and abundant grass beds. This broad area in the Carboneras Basin is just updip of the clinothem and was within the range of water depths that support *Poseidonia oceanica* life. This flat area provides ample space for grains to be abraded by wave energy to form calcisilt, which is then baffled and trapped by grass beds; this effect is apparent as seen in two of the updip clinothem facies discussed earlier (5-10% matrix). This lack of a broad shallow area on the homoclinally sloping Ricardillo area (Miocene) likely prevents extensive development of grass banks; the high energy in shallow water destabilizes the grasses, similar to blowouts documented from Wanless (1981) and Patriquin (1975).

The correlation between organism distribution and paleotopographic position is similar in both study areas, except that there is abundant coralline algae in proximal Pliocene deposits (~16%) and almost none in the proximal setting of the Miocene (<5%). If the *Poseidonia* grass beds were mostly missing from the Miocene, but are present in the Pliocene because of its broad flat area in shallow water, this also explains the difference in coralline algal distribution. *Poseidonia* grass beds are prime areas for the development of coralline algae as an abundant encrusting organism (Procaccini et al. 2003; Moissette et al. 2007).

Lastly, substrate plays an important role in controlling the distribution of bivalves. The Pliocene clinothem allows for the testing of hypotheses on controls of the distribution of bivalves. This is important in the Pliocene deposits as the *Pecten* Rudstone and the Ostreid-Pectinid Rudstone are distinct facies, and understanding their distribution allows for increased facies prediction. *Pectens* are distributed through all facies in the Pliocene, even where oysters and other clams are present, however abundant oyster deposits are mostly limited to the Ostreid-Pectinid Rudstone, with minor amounts in the Rhodolith Rudstone. In addition, this lithofacies

is found immediately overlying other rudstone facies, predominantly Rhodolith Rudstone (Fig. 7), with one exception of oyster-rich facies are only deposited in one 80cm bed overlying packstone facies in the medial part of the upper clinothem (Fig. 7). Many oysters require a stable substrate to attach. Therefore, the coarse nature of rudstone facies, and especially rhodolith beds provide an appropriate substrate for attachment. Scallops, on the other hand, can swim and live unattached, only requiring a sand bed in which to burrow (Brand 2006). This explains why pectinids are deposited everywhere throughout the clinothem and oysters are only abundant immediately above an appropriately stable coarse substrate. In addition, the only place the Bryozoan-Ostreid Rudstone definitively forms in the Miocene is directly onto the volcanic substrate.

Energy regime

Energy regime not only plays an important role in the development of the cross-bedded packstone lithofacies, but also in the formation of rhodoliths. Miocene and Pliocene rhodoliths show fundamental differences in morphology, and rhodolith morphology is known to be correlated to differences in depositional environments (Bosence 1983b). The round, spherical, symmetrical, consistent, and tightly packed rhodoliths of the Pliocene show that energy was consistently high enough to rotate 2-4cm sized rhodoliths. Bryoliths are also widely distributed in the rhodolith beds of the Pliocene, but have different characteristics. The bryoliths are asymmetrical and grow from 4-7cm. This growth pattern indicates that the energy regime capable of rotating the rhodoliths was not forceful enough to consistently move the coarser bryoliths, resulting in asymmetric growth of bryoliths. Since there is at least some encrusting growth around the nucleus of the bryolith, it is interpreted that storm energy strong enough to penetrate to deep depths was able to episodically rotate the bryoliths. The moderate energy

normal bottom currents (10cm/s; Oceanography Center) were not capable of moving these coarser grains.

It is important to address the work done by Prager and Ginsburg (1989) and Littler et al. (1991), showing that spherical rhodoliths can form in low energy environments due to extensive bioturbation. Bioturbation likely influences the morphology of the Pliocene rhodoliths in conjunction with energy from bottom currents, however bioturbation is not a primary cause for rotation. Foster (2001) showed that modern rhodoliths from moderate energy environments form spherical shapes; irregularly shaped rhodoliths, such as those seen in the Miocene, are representative of low energy environments.

During the deposition of DP-1 in the Pliocene, rhodoliths consistently grew in the most distal regions of the clinothem (Fig. 7). However, during DP-2, rhodolith deposition shifted updip into shallower waters and deposition in the most distal regions of the clinothem was dominated by whole ostreid and pectinid facies (Fig. 7). It is apparent that during DP-2 the Ostreid-Pectinid Rudstone was not affected by significant currents, as grains are whole, <10cm, and they are unabraded. The progressive filling of accommodation throughout the clinothem was likely a cause of fluctuation (and overall decrease) of the bottom currents that governed rhodolith rotation. The lower the energy the less rhodoliths are capable of rotating, therefore causing the stagnation of rhodolith growth and allowing for bivalves to colonize the most distal substrate during DP-2, as rhodolith development shifted updip. It is possible that the progressive change in accommodation either redirected bottom currents further updip, providing sufficient energy for continued rhodolith growth updip. An additional hypothesis is that as accommodation changed, the distribution of nutrient input was altered. This could have increased water turbidity, therefore decreasing light penetration. This decreased the ability of rhodoliths to grow in deeper

waters, but allowed them to grow further updip, where light penetration would have been greater. Since there are still some rhodoliths in the distal beds of the Ostreid-Pectinid Rudstone, it is apparent that the conditions were not completely unfavorable for their growth; however updip was an area of more favorable growth.

Relative Sea Level

Development of Pliocene Clinotherm.--- The four primary depositional profiles within the Pliocene clinotherm are interpreted to form due to a decrease in accommodation, created by progressive filling of remaining space in distal areas. DP-1 and DP-2 are rich in deep-water facies in distal regions, whereas DP-3 has distal deposits that reflect storm wave-base influence, and DP-4 returns to extended grass beds and only minor deposition of the deepest water lithofacies association, the Rhodolith-Bivalve Association (Fig. 7). This facies trend is consistent with Dillett's et al. (2004) interpretation that this clinotherm is a lowstand wedge deposited in association with a single lowstand and that as the accommodation was progressively filled, water became shallower.

Development of Miocene Cyclothem.--- One of the primary hypotheses tested in this work is if the cyclic deposits of the Miocene developed under rises and falls of sea level, forming depositional sequences, or if they are simply built by sedimentation after flooding events, forming parasequences (e.g. Van Wagoner et al. 1988; Van Wagoner et al. 1990; Posamentier et al. 1992). The three-component vertical lithofacies pattern seen in the proximal ramp of Ricardillo (Fig. 18) reflects: 1) a deepening event as grains coarsen; and 2) an abrupt shift into finer abraded grains and cross-bedding (Fig. 18). This shows that facies that deposited at or near wave base directly overlie coarse *in situ* lithofacies that represent a low energy environment. The two hypotheses for the development of this pattern are: 1) that as sedimentation increased, the

packstone facies that formed the capping facies of the cyclothem began to prograde out onto underlying sediments. After progradation, sea level again rose, creating a flooding event and marking the development of the next stacked parasequence; or 2) that a drop in sea level was required to deposit the abraded packstone facies directly onto rudstone facies at multiple paleotopographic positions.

Preserved paleotopography allows for evaluation of which is incorrect. Between the proximal and medial sections on Ricardillo (Fig. 14), there is a 35m paleotopographic drop. The parasequence hypothesis would require 35 m of deposition in the cycles of the medial area to fill accommodation to reach wave base and begin to deposit the abraded packstone facies. As cycles only range from 2-12m and four instances occur where the packstone facies is deposited in the medial region, a relative fall in sea level is necessary, and therefore, the parasequence hypothesis is disproven. Relative falls in sea level are required to cause the fining-upward portion of each cyclothem. This causes a downdip shift in proximal facies forming a facies dislocation or stranded deposit at a lower elevation, interpreted as a forced regression (Figs. 14, 19) (e.g. Hunt and Tucker 1992; Posamentier et al. 1992). Figure 19 shows a schematic model of the development of these cyclothem with wave base and sea level as a guide. The characteristic sharp contact between rudstone and overlying packstone lithofacies (Fig.10B) provides evidence that there was subaqueous erosion during the downstepping of wave base. This allows for the physical effects of an encroaching wave base to rework, abrade, and transport previously deposited gravel sediments, to form the cross-bedded packstone association. Using tilt-corrected paleotopography, facies composition, and facies distribution; a quantitative sea-level curve can be derived for 7 cyclothem in the Ricardillo-San Pedro area (Fig. 20). Overall the region was experiencing a relative rise in sea level before the large drop in sea level towards the end of DS2, entering into a

mixed heterozoan-photozoan system and eventually into the photozoan reefs of DS3 (Franseen and Goldstein 1996; Franseen et al. 1998; Toomey et al. 2003). The five sequences of the region are third (1-10my) order sequences, with higher frequency sequences within them (Franseen et al. 1998). The cyclothem in this study is classified as part of DS2 of Toomey et al. (2003) which correlates to the regional sea-level history and dating to indicate a maximum duration of .8ma, from the beginning of DS2 (8.4ma) until the region-wide megabreccia (7.6ma; Franseen et al. 1998). Each of the 8 cyclothem (7 from this study and an eighth mapped by Toomey et al., (2003) that is outside of this study area and at the very base of DS2) deposited within this timeframe could at a maximum take 0.1ma (8 cycles divided by .8ma) to form this portion of the third order sequence. This timeframe however assumes each cyclothem required the same amount of time to develop. Paleomagnetic data (Franseen et al. 1998) indicates that time-equivalent strata (to DS2 of Ricardillo), located on La Molata of the Las Negras, area have cyclic deposits that range from 54ky/cycle in older cyclothem to 185-433ky/cycle in younger cyclothem. Indicating that it is possible that the cyclothem in this study (from Ricardillo) increase in time-duration from older-younger and that some of the younger cyclothem could potentially be 4th or 5th order sequences with the remaining cyclothem being 5th order sequences ranging from .01-.1my. Minimum sea-level amplitudes of the seven cyclothem are 47m, 64m, 98m, 118m, 28m, 51m, and 30m with averages for the smaller five “typical” amplitudes at 44m (Fig. 20). The highest amplitudes recorded on the ramp, composed of basal hemipelagics and debrites, has a sea-level rise of 118m and fall of approximately 110m. Incorporating this anomalous amplitude and the other higher amplitude (98m) into the average, the amplitudes average increases to 62m. Averages are made to aid in comparison with glacioeustatic sea-level amplitudes.

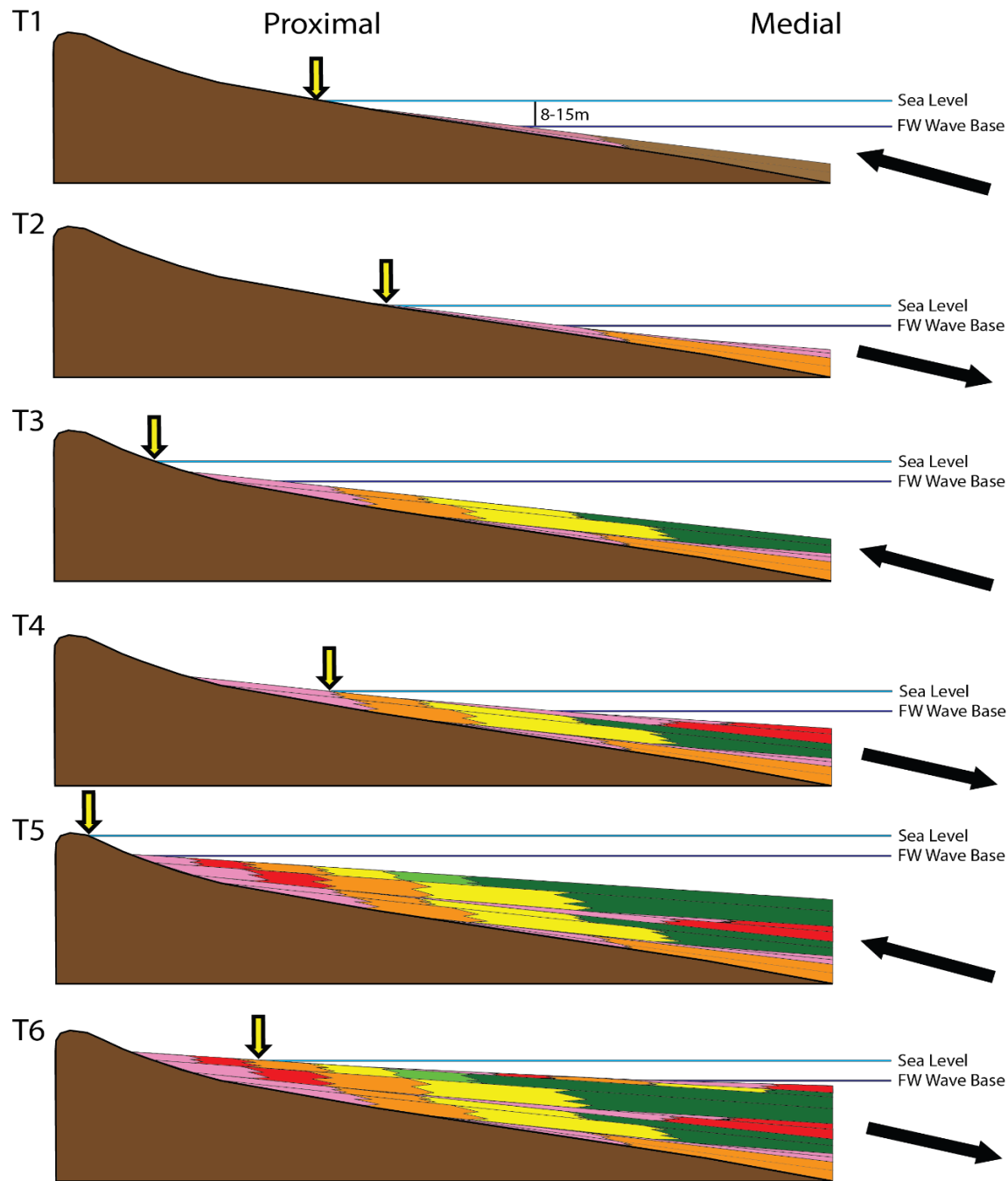


Figure 19: Schematic depositional model for the formation of the fining-upward cyclothems on Ricardillo. This model shows six time lines, each one showing a step in the formation of three cyclothems between medial and proximal areas of the ramp. Sea level and wave base are both shown as lines that move up and down; the model shows the effect these fluctuations have on deposition. Yellow arrows track the shoreline. Black arrows show the direction of facies migration during deposition at that particular timeline. **Time 1 (T1):** Onlapping deposition of facies from the Bryozoon-Bivalve Association, and further updip along time-equivalent strata, facies from the Cross-bedded Packstone Association are deposited near/at wave base. Sea level is rising during this time. **Time 2 (T2):** Sea level drops and causes a forced shift of facies downdip, displacing packstone facies directly above coarse rudstone facies. Showing that these packstone facies are detached and are not connected to packstone facies further updip. Updip areas above wave base are now undergoing a time of non-deposition and submarine erosion. Further updip bare volcanics remain subaerially exposed with no carbonate deposition. **Time 3 (T3):** Sea level rises to higher levels than that of Time 1. Proximal regions of Ricardillo are now flooded and the carbonate factory is turned on updip. Transgressive deposition occurs in proximal areas, depositing rudstone facies, as sea level continues to rise, coarser rudstone facies are deposited, creating a coarsening upward cycle that then fines as wave base encroaches on organisms and grain constituents. **Time 4 (T4):** A sea level drop exposes updip carbonates to subaerial exposure. All facies are shifted downdip and again displace packstone facies onto coarse rudstone facies. **Time 5 (T5):** Sea level rises to higher elevations than during Time 1 and Time 3. Packstone facies have more diverse fossil biota as more of a variety of sediments are now available.

to be reworked, sorted, abraded, and deposited. As deepening occurs, rudstones deposit onto the underlying packstone and surface of subaerial exposure, similar to during Time 3. **Time 6 (T6):** A drop in sea level causes subaerial exposure of proximal carbonates. A facies dislocation occurs again, displacing packstone facies above rudstone facies, allowing for and continuing the formation of fining-upward cyclothems.

For this time interval, the marine $\delta^{18}\text{O}$ isotope values from Miller et al. (2005) indicate that amplitudes of glacioeustatic sea-level fluctuations were between 20-60m and averaged between ~30-40m. The isotope data are consistent with the majority of sea-level amplitudes measured from the Ricardillo area, lending support that the cyclothems originate from glacioeustatic sea-level changes. Although the isotope data does not record amplitudes as high as Cycles 3 and 4, they likely developed from the glacioeustatic changes as well, as they are deposited among the smaller amplitude cyclothems.

Long-term trends are not easily comparable to the data in the Ricardillo-San Pedro area. During the end of the middle Miocene (Serravalian, 14ma) an abrupt drop in eustatic sea level occurred, followed by an overall decreasing trend in sea level through to the Pleistocene. During the late Miocene (Tortonian-Messinian), drastic fluctuations in sea level were initiated (Miller et al., 2005). This research contributes to documentation and quantification of amplitudes of relative sea-level changes associated with the Tortonian-Messinian stratigraphic sequences from various locations in the Cabo de Gata region to determine the local, regional, and global controls on deposition (e.g. Esteban 1979; Esteban and Giner 1980; Pomar et al. 1983; Franseen 1989; Martin, et al. 1989; Franseen and Mankiewicz 1991; Franseen et al. 1993; Martin and Braga 1994; Sun and Esteban 1994; Esteban 1996; Goldstein and Franseen 1995, 2002; Franseen and Goldstein 1996, 1997; Franseen et al. 1998; Pomar 2001; Toomey et al. 2003; Johnson 2005; Dvoretzky 2009; Lipinsky 2010).

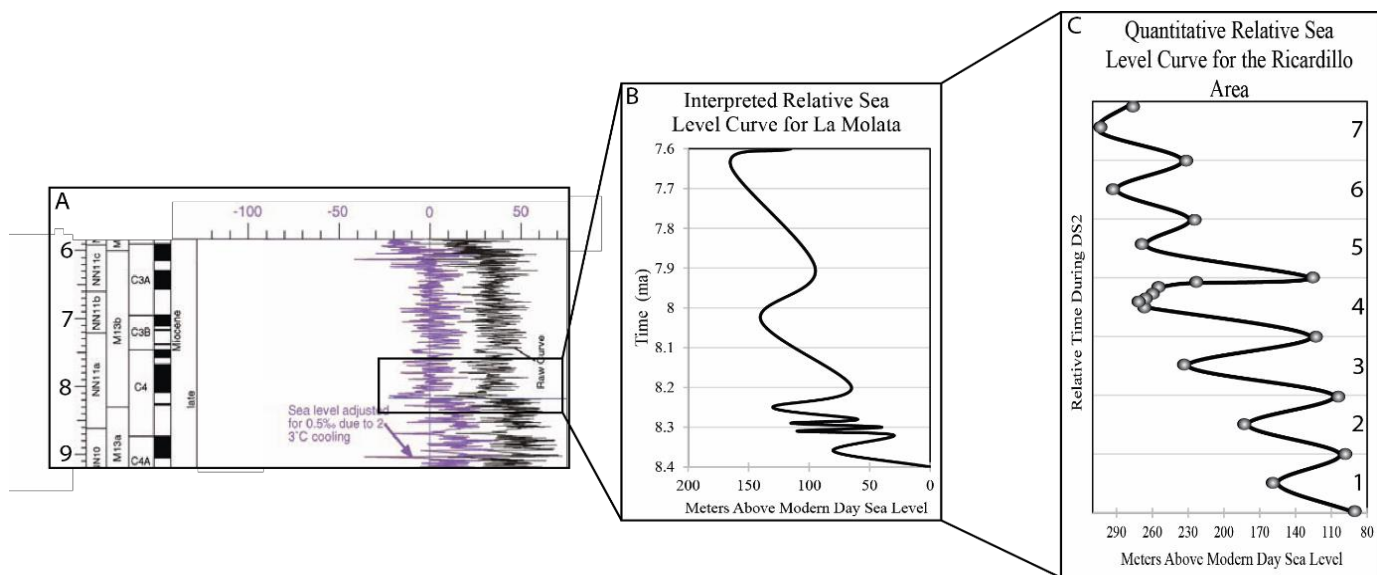


Figure 20: Miocene quantitative relative sea level curve for A) the Miocene, B) for the Las Negras area, and C) for the Ricardillo area. A) the isotope curve from Miller et al. (2005) with 8.6-7.6ma highlighted in the black box. B) Estimated relative sea level curve from Franseen et al.(1998) for DS1B in the Las Negras area, showing a regional relative sea level curve for strata at a lower elevation. Dates are based off of paleomagnetic data. C) Quantitative sea level curve for the Ricardillo area from this study. Overall the sea level curve shows a long term rise in relative sea level. Data point measurements are based off of tracing lithofacies across time equivalent, tilt-corrected, paleotopography from the most downdip outcrop position to the most proximal, and using 8m as a wave base depth. This method allowed for using quantitative lithofacies depth interpretations traced across paleotopography to determine fluctuations in sea level. All places packstones were deposited mark where depth was ~8m. Time is only represented in relative terms during DS2 from ~8.4-7.6ma.

Development of Proximal Miocene Cyclothem Trends--- Proximal paleotopographic positions are the only locations in which a three-component, genetic stratigraphic pattern is preserved in a cyclothem (Fig. 18). During sea-level rise onto proximal regions of Ricardillo, carbonate deposition initiated and the development of basal facies began. In proximal cyclothem, the basal facies is always composed of either the Bryozoan-Ostreid Rudstone or the Bryozoan-*Pecten* Rudstone, which form at depths between 12-36m. As transgression and flooding progressed, depositional conditions become appropriate for the development of either only the Bryozoan-Pectinid Rudstone or coarser-grained, deeper-water facies that have an increase in bivalve (14-45%) and coralline algae (4-10%) content, and a decrease in bryozoans (48-29%) and echinoids (11-8%) (Bivalve Rudstone Association). Lithofacies from the Bivalve Rudstone Association indicate that depths during time of deposition ranged from 35-80m.

However, with the presence of the Globular Bryozoan-Clam Rudstone and the proximal paleotopographic position on the ramp, it is estimated that depths during the time of deposition were approximately 30-40m. The capping lithofacies of these cyclothems at this elevation are primarily composed of the Bryozoan-Echinoid Packstone, and in one case, of the Bryozoan-Bivalve Packstone, indicating paleobathymetry of 8-15m.

Development of Medial Miocene Cyclothem Trends.--- The medial cyclothems and a portion of the distal cyclothems (Fig. 18) are composed of a two-part vertical lithofacies pattern, which record fining upward during shoaling, similar to the shoaling- and fining-upward trend seen in the Pliocene clinothem. Basal rudstones at this paleotopographic position is primarily composed of the *Pecten* Rudstone. Since the paleotopographic position of this stratigraphic section is 35m lower in elevation than the proximal section, it is estimated that this rudstone deposited at depths of 50-60m. Above these deposits, the abrupt change into abraded, cross-bedded packstones provides evidence of shoaling, causing abrasion, sorting, and transporting of sediments, even at this medial elevation on the ramp. Packstone lithofacies at this paleotopographic position are primarily composed of the Bivalve-Bryozoan Packstone and the Bivalve-Coralline Algae Packstone. This marks the most proximal significant increase of coralline algae (4-30%), and decrease in bryozoan (47-13%) and echinoid (13-9%) content deposited in a packstone lithofacies at this position on the ramp. Deposition of these facies indicates that wavebase was encroaching on sediments that were developing at a paleodepth of 8-15m. This medial-distal cyclothem pattern does not record the three-part component cycle that is preserved in proximal regions of Ricardillo. There are two hypotheses that could explain this variation. The mechanism for hypothesis 1 is the interaction between paleotopography and a constant sea-level rise. For hypothesis 2, the mechanism is a decrease in the rate of sea-level

rise. Hypothesis 1 is favored over the other, as there is more evidence in support of this hypothesis.

The first hypothesis is that as relative sea level rises and floods volcanic substrate, the productivity of the carbonate factory was delayed until organisms began to colonize the substrate. By the time the carbonate factory was effectively turned on, in the medial regions, sea level had risen high enough for the deposition of deeper water facies that have a broader depth range i.e. the *Pecten* Rudstone, and a second rudstone facies did not develop. However further updip, by the time relative sea level encroached upon the proximal part of the ramp, the higher elevation allowed for the deposition of shallower rudstone deposits, i.e. Bryozoan-Bivalve Association, that formed in a shallower depth range. Their distribution is more sensitive to sea-level fluctuations than other rudstone facies, therefore as sea level rose, that deepening event was recorded in the proximal region with a facies change to a coarser rudstone.

The second hypothesis is that the rate of sea-level rise is not constant. As sea level reaches its highstand position, the rate of rise begins to slow, allowing for an increased amount of time for the proximal carbonate factory to begin producing sediments. In contrast, sea-level rates of rise were higher in medial and distal parts of the ramp, which did not allow for extended periods of time in shallower waters. By the time the carbonate factory began producing sediment in distal and medial locations on the ramp, sea level had already risen high enough so that deeper water rudstone facies (*Pecten* Rudstone) were deposited in those locations.

Development of Distal Miocene Cyclothem Trends.--- The majority of distal cycles (Fig. 18) (see cyclothem description section) are composed of the same two-part vertical lithofacies pattern as is found in the medial region of Ricardillo. However distally, basal rudstone lithofacies have an increase in coralline algae and consist of either the Coralline Algae-

Bivalve Rudstone or the *Pecten* Rudstone, but with a <2- >10% increase in coralline algae content. These lithofacies indicate that the rudstones in distal region formed at depths of 80-120m, and are estimated to be closer to ~100m by tracing time-equivalent strata updip along preserved paleotopography. The Coralline Algae-Bivalve Packstone is the primary cycle-capping lithofacies, which is interpreted to indicate that sea level had lowered and distal regions of the ramp were at, or near, wave base (8-15 m water depths.) for reworking and abrasion of grains.

In Cycle 5 and Cycle 7 (distally; Fig. 14) no shoaling (packstone) deposits develop. During deposition, wave base did not drop low enough to abrade and transport sediments this far out into the basin. The last distal vertical lithofacies trend comes from Cycle 4 (Fig. 14). Deposition began to develop at the greatest depths in this study area as indicated by the hemipelagic/turbidites and grainy debrite deposits at the base of this cyclothem. Tracing these beds along time-equivalent strata across preserved paleotopography indicate that the bedded hemipelagic deposits formed at depths of approximately 150m. Evidence that shoaling began after the deposition of these bedded hemipelagics is found stratigraphically above them as the remaining hemipelagics become massive and bioturbated, and are interbedded with grainy debrites. As shoaling continued, the *Pecten* Rudstone, followed by the Bivalve-Coralline Algae Packstone, were deposited stratigraphically above the turbidites and debrites. Lateral tracing of this *Pecten* Rudstone unit and its elevated coralline algae content indicate that that this deposit formed at its greatest depth of ~120m only in this one cyclothem. The deposition of the Coralline Algae-Bivalve Packstone above indicates that shoaling continued to a depth where wave base impacted these deposits.

Sequence Boundaries and Systems Tracts in the Miocene.--- The drop in sea level

atop each cyclothem creates a surface of non-deposition from wave base to the shoreline, above which would be subaerial exposure. No petrographic or large-scale evidence of subaerial exposure surfaces were found, however Schlager (2003) discussed that the preservation of subaerial exposure surfaces in the cool water carbonate factory, or heterozoan carbonates, is highly variable and dependent on the rate of cementation during these events. Since abiotic cementation in heterozoan systems is low, this causes the process of lithification to proceed at a slower pace than photozoans, allowing for reworking of sediments (Schlager 2003). In addition, the majority of the grains in these deposits are made originally of low and high magnesium calcite, with the only aragonite derived from a portion of the bivalves (James 1997; Scholle, and Ulmer-Scholle 2003; Smith et al. 2006). The calcite grains are an unlikely mineral to dissolve rapidly during meteoric diagenesis and reprecipitate as cement at a sequence boundary. Magnesium calcite is known to recrystallize *in situ* and expel magnesium, forming stable calcite (Reeckmann and Gill 1981; James and Bone 1989; Knoerich and Mutti 2003). This leaves only the aragonite to provide adequate ions for the cementation of sequence boundaries, which is the primary mineral source for meteoric cementation (Nelson et al. 1988; James 1997).

Lastly, the climate in the Mediterranean could have reduced fresh ground water, and limited the extent of cementation during subaerial exposure events (Sun and Esteban 1994). Combine these features with high frequency sea-level fluctuations (Miller et al. 2005) of the Miocene and the chances of the preservation of obvious subaerial exposure surfaces are less than favorable.

Using the discussed observations for the three-component vertical lithofacies trend (proximal) and data combined with the onlapping geometries, it is interpreted that the rudstone facies in each cyclothem was deposited during transgression, at least until the deposition of the

2nd rudstone facies began (Fig. 18). The dislocated packstone facies were subsequently deposited during falling sea level (forming a forced regressive deposit). It is possible that a highstand/stillstand could have occurred sometime after that, and before the regression. However there is no strong evidence for placing a maximum flooding surface and highstand deposits within these cyclothems. If highstand deposits are present, they would be insignificant, as progradation of sediments will only happen if sediment outpaces sea-level rise (e.g. Tucker 1993). Since calcareous organisms precipitate skeleton and shells at such a slow rate in cool, eutrophic waters, it is possible that highstand deposits never developed significantly (Schlager 2000, 2003). Kendall and Schlager (1981) also pointed out that productive photozoan systems grow at a rate of 200-900 cm/ky and can keep up with sea level, causing progradation and forming the typical systems tracts of photozoan carbonates. However, using the time range from 8.4-7.6my, total carbonate accumulation in that portion of DS2 (the purely heterozoan portion, beneath the megabreccia) only show average depositional rates at of .01 cm/ky. This number is significantly less than the rate of optimal photozoan production, and it is unreasonable to conclude that typical systems tracts would fully develop under such a low sedimentation rate. These results are supported by the findings of Esteban (1996) in that rhodolagal deposits are mostly deposited during the transgression.

Sequence Architecture: Grainy fining- and shoaling-upward cyclothems and clinothems

The Pliocene clinothem shows conclusively that sandy, well-sorted sediments are generated in near-wave base settings, whereas sediments become coarser and more poorly sorted downdip. The origin of these trends are the combination of in place growth to create coarse sediment, and the abrasion and sorting of that material in shallow, high energy depths. Progradation of a clinothem produces a grainy, shoaling- and fining-upward sedimentary

succession. The same depth distribution of facies combined with rapid relative sea-level fluctuations across relatively steep topography, created the same transition expressed as grain-rich, fining- and shoaling-upward cyclothems of the Miocene. The Miocene cyclothems most similar to this shoaling- and fining-upward pattern of the Pliocene clinothem is the two-component vertical lithofacies pattern that is primarily present in the medial and distal regions of the ramp of Ricardillo and the upper part of the cyclothem in proximal areas.

Essentially, the progradational clinothem of the Pliocene represents one shoaling- and fining-upward cycle, whereas the Miocene provides an example of multiple, thin, stacked cyclothems. These two examples exhibit a similar grainy fining-upward trend, despite forming at different positions of sea level and in environments with different modes of deposition. This indicates that this fining-upward and fining-updip depositional trend is consistent, and is an important pattern developed during the deposition of shallow-water, temperate (as heterotrophic conditions need to be widespread), heterozoan carbonates. We propose that this depositional trend is a fundamental unit for heterozoan carbonate deposition that should be evaluated and tested in other heterozoan outcrops and in the subsurface.

APPLICATION TO THE SUBSURFACE

These analyses and proposed depositional models can be applied to all grainy heterozoan carbonates, however, direct application is best for Neogene deposits, especially those deposited during the Miocene. Sun and Esteban (1994) discussed the distribution of carbonates in the upper Miocene occurring mainly in the Mediterranean, the Gulf of Suez, the Caribbean, the Gulf of Mexico, and the South China Sea. These carbonates were deposited during times of global cooling and eutrophic waters alternating with times of global warming. The rhodalgal and heterozoan complexes formed ramps, whereas photozoans formed the rimmed shelves, reefs,

and ramps. Esteban (1996) further discussed the deep and extensive seaways that provided substrate along their flanks for heterotrophic organisms to colonize throughout the Mediterranean, Atlantic, Paratethys, and the Indo-Pacific, with primary heterozoan deposition in the Mediterranean and Mesopotamia (the Asmari and Euphrates Limestone). In addition, the Gulf of Suez has hydrocarbon production from heterozoan units as well as Middle Miocene deposits of the Hungarian Panonian Basin (Esteban 1996). Depositional models of the Gulf of Suez look strikingly similar to the deposits of the southeastern Spain, with heterozoan ramps capped by coral reefs with final deposition composed of ooids and stromatolites (TCC).

The South China Sea has extensive Neogene carbonate platforms that are dominated by benthic foraminifer and coralline algae deposits (Wilson 2002). Wilson (2002) provided an extensive look at Cenozoic carbonates in the South China Sea, claiming that warm water models are inadequate as the analogs for the majority of South China Sea carbonates. Wilson provides lists of hundreds of carbonate formations from this area, and from these lists, the authors found 22 of them to be similar in composition to the outcrops used in this study, as they are grainy carbonates composed of the Heterozoan Association. Of these 22, eight (Pugliano et al., 2015; Chapter 3) of them have been described as hydrocarbon reservoirs and/or freshwater aquifers including the, Pre-Parigi onshore, Cunda Limestone, and the Cibulukan Formation (Wilson 2002). In addition, Miocene formations of the Liuhau Platform and the Wonosari Formation of the South China and Java Seas contain heterozoan deposits on tropical shelves, due to temperature, salinity, and nutrient variations (Wilson 2002; James 1997).

Lastly, the late Oligocene-Miocene aged Perla Field of offshore Venezuela is a large-scale example of a heterozoan system (mainly rhodagal) that is a currently producing hydrocarbon reservoir (Fioretta et al. 2011) These are some examples of the wide distribution

of currently known Neogene and Mesozoic heterozoan carbonate complexes worldwide. This work can be used as an analog for the variety of depositional trends, lithofacies, lithofacies distribution, and depositional units of heterozoan carbonates. A companion study containing a petrophysical analysis, dataset, diagenetic study, and PetrelTM models for these outcrops can be further applied to hydrocarbon systems. These data provide very detailed insight into the stratigraphy and sedimentology of heterozoan carbonates, applicable at a broader scale.

CONCLUSIONS

- 1) Heterozoan carbonates from the Miocene and Pliocene of southeastern Spain provide outcrop analogs for the modeling of sedimentologic variables, stratigraphic architecture, and depositional patterns of heterozoan carbonates.
- 2) Heterozoan carbonates in a Pliocene clinothem form grain-dominated depositional trends that fine updip as energy from wave base abrades and fragments grains. As these facies prograde, they form a fining- and shoaling-upward, grain-rich succession
- 3) Pliocene strata comprise sets of prograding clinothem with six depositional profiles, reflecting four depositional environments in the basin. Proximal facies contain sorted bryozoan-coralline algae packstones, while time equivalent strata immediately downdip are composed of poorly-sorted rhodolith and bivalve-rich rudstones. Overall 10 heterozoan carbonate lithofacies have been described from the Pliocene strata.
- 4) Miocene strata are composed of stacked cyclothem; each cyclothem consists of basal transgressive coarse-gravel rudstones and an upper regressive cross-bedded mud-poor packstone Overall 13 heterozoan carbonate lithofacies have been described from the Miocene strata.
- 5) Packstone lithofacies are developed by the abrasion of coarser bioclastic grains as sea

level drops and wave base is lowered. Packstones are composed primarily of coarse sands and scattered gravel. The packstones are well- to moderately-sorted and are cross-bedded in the Miocene deposits. These lithofacies have a calcisilt content <3% except for two of the most proximal facies in the Pliocene that have <5% calcisilt, representing *Posidonia* grass beds. Pliocene packstones are massive, graded, or are cross-bedded.

- 6) Rudstone lithofacies form *in situ* deposits beneath the effects of wave base and are composed of whole and fragmented fossils, many of which are deposited in life position. Rudstones are primarily massive with scattered horizontal bedding and have poor to very poor sorting.
- 7) Grain type distribution is similar throughout both field areas as bryozoans dominate in the proximal ramp, bivalves in the middle ramp, and coralline algae and rhodoliths in the distal ramp. Variations between the two areas include that coralline algae are the primary grain type in the Pliocene clinothem whereas in the Miocene they are only a dominate grain component in distal portions of the ramp. In addition, hemipelagic sediment, turbidites and debrites mark the deepest water deposits of the Miocene.
- 8) The distribution of Miocene cyclothem form predictable stratigraphic trends dependent on paleotopographic position. Proximal areas of the ramp record three-part vertical trends composed of rudstones and a packstone that coarsen-upward at the bottom, and fine-upward at the top. Medial-distal parts of the ramp record only two-component vertical lithofacies trends composed of a rudstone and a packstone that fine upward. Most distal regions of the ramp have cyclothem that are composed of basal hemipelagic turbidites and debrites that transition vertically into a coarser rudstone that then fines-upward into a packstone. Vertical lithofacies trends occur in a predictable manner, depending on

paleotopographic position.

- 9) Each of the cyclothems of the Miocene are composed of transgressive- regressive 4th-5th order sequences. Rudstones are deposited during transgression and packstones form during forced regressions, as wave base is lowered, causing abrasion, sorting, and transportation. Forced regressions result in a dislocation and detachment of packstone lithofacies.
- 10) Preserved paleotopography, distribution of lithofacies, and using the Pliocene deposits as a calibration allows for the quantification of paleobathymetry for Miocene deposits. With typical sea-level fluctuations ranging from 28-65m and two higher amplitudes of 98m and 118m. These sea-level fluctuations are controlled by the glacioeustasy of the late Miocene.
- 11) The grain-rich, shoaling- and fining-upward trend in cyclothems forms in a variety of sea-level positions and different depositional environments. This consistency indicates that this depositional profile is an important, fundamental depositional unit developed during the deposition of grain-rich, shallow-water heterozoan carbonates.

REFERENCES CITED

- Aguirre, J., 1998, El Plioceno del SE de la Península Ibérica (provincia de Almería) Síntesis estratigráfica, sedimentaria, bioestratigráfica y paleogeográfica: *Rev. Soc.Geol., Esp.* 11, p. 297-315.
- Bassi, D., Carannante, G., Murru, M., Simone, L., Toscano, F., 2006, Rhodalgae/bryomol assemblages in temperate-type carbonate, channelized depositional systems: the Early Miocene of the Sarcidano area (Sardinia, Italy), *Journal: Geological Society, London, Special Publications*, vol. 255, no. 1, pp. 35-52, 2006
- Basso, D., 1998, Deep rhodolith distribution in the Potian Islands, Italy: a model for the paleoecology of a temperate sea: *Paleogeography, Paleoclimatology, Paleoecology*, v. 137, p. 173- 187.
- Betzler, C., Martin, J.M., and Braga, J.C., 2000, Non-tropical carbonates related to rocky submarine cliffs (Miocene, Almeria, southern Spain): *Sedimentary Geology*, v.131, p. 51-65.
- Björk, M., Mohammed, S.M., Björklund, M., and Semesi, A., 1995, Coralline algae, important reef-builders threatened by pollution: *Ambio*, v. 24, p. 502–505.
- Boggs, S., 1995, *Principles of Sedimentology and Stratigraphy*: Prentice Hall, 2nd edition, 774 pp
- Boreen, T. D., and James, N. P., 1993, Stratigraphic sedimentology of Tertiary cool-water limestones, SE Australia: *Journal of Sedimentary Research*, B65, n. 1, p. 142-159.
- Bosellini, A. and Ginsburg, R.N., 1971, Form and internal structure of recent algal nodules (rhodolites) from Bermuda: *Journal of Geology*, v. 79, p. 669- 682.
- Bosence, D. W. J., 1983a, Description and classification of rhodoliths (rhodoids, rhodolites), in Peryt, T.M. ed., *Coated Grains*, p. 217- 224.
- Bosence, D. W. J., 1983b, The occurrence and ecology of recent rhodoliths- a review, in Peryt, T.M. ed., *Coated Grains*, p. 225- 242.
- Bosence, D. W. J., 1985, The "coralligene" of the Mediterranean-a recent analog for Tertiary Coralline algal limestones, in Toomy, D.F., and Nitecki, M.H., eds., *Paleoalgology, Contemporary Research and Applications*: Springer-Verlag, p. 216- 225.
- Braga, J.C., Betzler, C., Martin, J.M., and Aguirre, J., 2003, Spit-platform temperate carbonates: the origin of landward-downlapping beds along a basin margin (Lower Pliocene, Carboneras Basin, SE Spain): *Sedimentology*, v. 50, p. 553-563.
- Brand, A.R., 2006, Scallop ecology: distributions and behavior: *Scallops: Biology, Ecology and Aquaculture*, v. 35, p. 651–744.
- Bouma, A.H., 1962, *Sedimentology of Some Flysch Deposits*: Elsevier, p. 168.
- Burchette, T. P., and Wright, V. P., 1992, Carbonate ramp depositional systems: *Sedimentary Geology*, v. 79, p. 3-57.
- Carannante, G., Simone, L., and Barbera, C., 1981, Calcari a briozoi e litotamni of Southern Apennines: Miocene analogs of Recent Mediterranean rhodolitic sediments (Abstract), in *International Association of Sedimentologists Abstracts*, 2nd European regional meeting, p. 17-20.
- Carannante, G., Esteban, M., Milliman, J.D., and Simone, L., 1988, Carbonate Lithofacies as paleolatitude indicators: problems and limitations: *Sedimentary Geology*, v. 60, p. 333-346.
- Carannante, G., and Simone, L., 1996, Rhodolith facies in the central-Southern

- Apennines Mountains, Italy, in Franseen, E.K., Esteban, M., Ward, W.C., and Rouchy, J.M., eds., *Models for Carbonate Stratigraphy from Miocene Reef Complexes of the Mediterranean Regions: SEPM Concepts in Sedimentology and Paleontology Series*, n. 5, p. 261- 275.
- Cheel, R.J., and Leckie, D.A., 1992, Coarse-grained storm beds of the Upper Cretaceous Chungo Member (Wapiabi Formation), Southern Alberta, Canada: *Journal of Sedimentary Petrology*, v. 62, p. 933-945.
- Clarke, J.D.A., 1990, Slope facies deposition and diagenesis of the Early Cambrian Parara Limestone, Wilkawillina Gorge, South Australia, in Jago J.B. & Moore P.S., eds., *The evolution of a Late Precambrian-Early Palaeozoic rift complex: Geological Society of Australia, Special Publication 16*, p. 230-246
- Dillett, P.M., Goldstein, R.H., Franseen, E.K., 2004, Paleotopographic and sea-level controls on the sequence stratigraphic character of a heterozoan carbonate succession: Pliocene, Carboneras Basin, southeast Spain: Master's Thesis, University of Kansas, Lawrence, 119 pp.
- Dunham, R. J., 1962, Classification of carbonate rocks according to depositional texture, in *Classification of carbonate rocks-a symposium: American Association of Petroleum Geologists, Memoir 1*, p. 108-121.
- Dvoretzky, R.A., 2009, Stratigraphy and reservoir-analog modeling of Upper Miocene shallow-water and deep-water carbonate deposits: Agua Amarga basin, Southeast Spain: Master's Thesis, University of Kansas, Lawrence, 138pp.
- Embry III, A.F., Klovan, J.E., 1971, A late Devonian reef tract on northeastern Banks Island: *N.W.T. Bull. Can. Petrol. Geol.* 19, p. 730–781.
- Esteban, M., 1979, Significance of the upper Miocene coral reefs of the western Mediterranean: *Paleogeography, Paleoclimatology, Paleoecology*, v. 29, p. 169-188.
- Esteban, M., and Giner, J., 1980, Messinian coral reefs and erosion surfaces in Cabo de Gata (Almeria, southeastern Spain): *Acta Geologica Hispanica*, v. 15, p. 97-104.
- Esteban, M., 1996, Overview of Miocene reefs from the Mediterranean area: General trends and facies models, in Franseen, E.K., Esteban, M., Ward, W.C., and Rouchy, J.M., eds., *Models for Carbonate Stratigraphy from Miocene Reef Complexes of the Mediterranean Regions: SEPM, Concepts in Sedimentology and Paleontology Series# 5*, p. 3-53.
- Farr, T., Broom, J., Hart, D., Neill, K., and Nelson, W., 2009, Common coralline algae of northern New Zealand: an identification guide: *NIWA Information Series*, No. 70.
- Fernandez-Soler, J.M., 1996, El volcanismo calco-alcalino de Cabo de Gata (Almeria), estudio volcanologico y petrologico.: *Sociedad Almeriense de Historia Natural*, 295 pp.
- Fioretta, A., Schioli, A., and Barletta, V., 2011, The Perla World-Class Giant Gas Field, Gulf of Venezuela: An Overview on a Successful Case History in a Virtually Unexplored Basin: *AAPG Search and Discovery*, article # 90135, AAPG International Conference and Exhibition, Milan, Italy, p. 23 26.
- Flos, J., 1985, The Driving Machine, in Margalef, R., ed., *Western Mediterranean: Oxford, Pergamon Press*, p. 60-99.
- Flügel, E., 2010, *Microfacies of carbonate rocks: Springer – Verlag*, 2nd edition, 984 pp.
- Folk, R.L., 1965, *Petrology of sedimentary rocks: Hemphill's Bookstore, Austin*, 170 pp.
- Folk, R.L., and Robles, R., 1964, Carbonate sands of Isla Perez, Alacran reef complex, Yucatan: *Journal of Geology*, v. 72, p. 255-292
- Fornos, J.J., and Ahr, W.M., 1997, Temperate carbonates on a modern, low-energy, isolated ramp; the Balearic Platform, Spain. *Journal of Sedimentary Research*, v. 67, p. 64-373.

- Foster, M.S., 2001, Rhodoliths: between rocks and soft places: *Journal of Phycol.*, v. 37, p. 659
- Franseen, E.K., 1989, Depositional Sequences and Correlation of Middle to Upper Miocene Carbonate Complexes, Las Negras Area, Southeastern Spain: Ph.D. dissertation, University of Wisconsin-Madison, 374 pp.
- Franseen, E.K., and Mankiewicz, C., 1991, Depositional sequences and correlation of middle to late Miocene carbonate complexes, Las Negras and Nijar areas, southeastern Spain: *Sedimentology*, v. 38, p. 871-898.
- Franseen, E.K., Goldstein, R.H., and Whitesell, T.E., 1993, Sequence stratigraphy of Miocene carbonate complexes, Las Negras area, southeastern Spain: Implications for quantification of changes in relative sea level, *in* Loucks, R.G. and Sarg, J.F., eds., *Carbonate Sequence Stratigraphy: Recent Developments and Applications: AAPG Memoir 57*, p. 409-434.
- Franseen, E.K., and Goldstein, R.H., 1996, Paleoslope, sea level, and climate controls on upper Miocene platform evolution, Las Negras area, southeastern Spain, *in* Franseen, E.K., Esteban, M., Ward, W.C., and Rouchy, J.M., eds., *Models for Carbonate Stratigraphy from Miocene Reef Complexes of the Mediterranean Regions: SEPM, Concepts in Sedimentology and Paleontology Series #5*, p. 159-176.
- Franseen, E.K., Goldstein, R.H., and Farr, M.R., 1997, Substrate-slope and temperature controls on carbonate ramps: Revelations from upper Miocene outcrops, SE Spain, *in* James, N.P. and Clarke, J., eds., *Cool-water Carbonates: SEPM, Special Publication 56*, p. 271-290.
- Franseen, E.K., Goldstein, R.H., and Farr, M.R., 1998, Quantitative controls on location and architecture of carbonate depositional sequences: upper Miocene, Cabo De Gata region, SE Spain: *Journal of Sedimentary Research*, v. 68, p. 283-298.
- Fréchette, M., Lefavre, D., and Butman, C. A., 1993, Bivalve feeding and the benthic boundary layer, *in* *Bivalve Filter Feeder: Springer Berlin Heidelberg*, p. 325-369.
- Friedman, G.M., 1962, Comparison of moment measures for sieving and thin-section data in sedimentary petrological studies: *Journal of Sedimentary Petrology*, v. 32, p. 15-35.
- Freiwald, A., 1998, Modern nearshore cold-temperate calcareous sediments in the Troms district, northern Norway: *Journal of Sedimentary Research*, v. 68, p. 763-776.
- Gibbons, W., and Moreno, M.T., EDS., 2003, *The Geology of Spain: Geological Society of London*, 649 pp.
- Goldstein, R.H., and Franseen, E.K., 1995, Pinning points: A method that provides quantitative constraints on relative sea-level history: *Sedimentary Geology*, v. 95, p. 1-10.
- Goldstein, R.H., and Franseen, E.K., 2000, Control of Original Basin Geomorphology on Sequences and Sediment Dispersal in Adjacent Basins: 2000 AAPG Annual Convention Official Program, New Orleans, LA, p. A5
- Goldstein, R.H., and Franseen, E.K., 2002, Point-Sourced Fill-and-Fan Sediment Gravity-Flow Deposits Along a Low-Relief Basin Margin, Miocene Carbonates, Agua Amarga Basin, SE Spain: 2002 AAPG Annual Convention Official Program, v. 11, Houston, TX, p. A65.
- Gorsline, D.S., 1984, A review of fine-grained sediment origins, characteristics, transport and deposition, *in* Stow, A.V., and Piper, J.W., *Fine- Grained Sediments: Deep-Water Processes and Facies: The Geological Society, Blackwell Scientific Publications, London*, p. 17-34.
- Grimsdale, T.F. and Van Morkhoven, F.P.C.M., 1955, The ratio between pelagic and benthonic foraminifera as a means of estimating depth of deposition of sedimentary rocks: *Proceedings – World Petroleum Congress*, 4th, sect. 1/D4, p. 473-491.
- Hall-Spencer, J.M. and Moore, P.G., 2000, Scallop dredging has profound, long-term impacts

- on maerl habitats: ICES Journal of Marine Science, v. 57, p. 1407-1415.
- Hernández-Molina, F.J.L., Somoza, L.M., Vazquez, J.T., and Rey, J., 1995, Estructuración de los prismas litorales del Cabo de Gata: Respuesta a los cambios climático-eustáticos holocenos: *Geogaceta*, v. 18, p. 79-82.
- Hernández-Molina, F.J.L., Somoza, L.M., Fernández-Salas, Lobo, L.M., and Llave, E., 1998, Late Holocene infralittoral wedge: A large-scale progradational lithosome in shallow marine environment: *15th International Sedimentological Congress*, Abstracts book, Alicante, p. 421-422.
- Hess, A.V., Goldstein, R.H., Franseen, E.K., 2011, Heterozoan carbonate lithofacies and sequence stratigraphy: a study of Pliocene strata of the Agua Amarga basin, southeastern Spain: Master's Thesis, University of Kansas, Lawrence, 119 pp.
- Hobday, D., K., and Morton, R., A., 1984. Lower Cretaceous Shelf Storm Deposits, North Texas: AAPG Bulletin, v. 64, p. 0149-1423.
- Hopkins, T. S., 1985, Physics of the sea, in Margalef, R., ed., Western Mediterranean: Oxford, Pergamon Press, p. 100-125.
- Hunt, D., Tucker, M.E., 1992, Stranded Parasequences and the forced regressive wedge *Systems* Tract: deposition during base-level fall: *Sedimentary Geology*, v. 81, p. 1-9.
- Instituto Geológico y Minero de España, 1981, Mapa Geológico de España: Servicio de Publicaciones, Ministerio de Industria, Spain.
- James, N. P., 1997, The cool-water carbonate depositional realm, in James, N.P. and Clarke, J.A.D., eds., Cool-water Carbonates: SEPM, Special Publication 56, p. 1-20.
- James, N.P., and Bone, Y., 1989, Petrogenesis of Cenozoic temperate water calcarenites, South Australia: a model for meteoric/shallow burial diagenesis of shallow water calcite sediments: *Journal of Sedimentary Petrology*, v. 59, p. 191-203.
- James, N.P., Bone, Y., Von Der Borch, C.C., and Gostin, V.A., 1992, Modern carbonate and terrigenous clastic sediments on a cool water, high energy, mid-latitude shelf: Lacepede, southern Australia: *Sedimentology*, v. 39: p. 877-903.
- James, N. P., Boreen, T. D., Bone, Y., and Feary, D. A., 1994, Holocene carbonate sedimentation on the west Eucla Shelf, Great Australian Bight: a shaved shelf: *Sedimentary Geology*, v. 90, p. 161-177.
- James, N. P., Collins, L. B., Bone, Y. and Hallock, P., 1999, Subtropical carbonates in a temperate realm: modern sediments on the southwest Australian shelf: *Journal of Sedimentary Research, Section B: Stratigraphy and Global Studies*, v. 69, p. 1297-1321.
- James, N. P., 1997, The cool-water carbonate depositional realm, in James, N.P. and Clarke, J.A.D., eds., Cool-water Carbonates: SEPM, Special Publication 56, p. 1-20.
- James, N. P., Collins, L. B., Bone, Y. and Hallock, P., 1999, Subtropical carbonates in a temperate realm: modern sediments on the southwest Australian shelf: *Journal of Sedimentary Research*, v. 69, p. 1297-1321.
- James, N.P., Feary, D.A., Surlyk, F., Simo, J.A.T., Betzler, C., Holbourn, A.E., Li, Q.Y., Matsuda, H., Machiyama, H., Brooks, G.R., Andres, M.S., Hine, A.C., Malone, M.J., and Ocean Drilling Program LEG 182 Scientific Party, 2000, Quaternary bryozoan reef mounds in cool-water, upper slope environments: Great Australian Bight: *Geology*, v. 28, p. 647-650.
- James, N.P., Bone, Y., Collins, L.B., Kyser, T.K., 2001, Surficial sediments of the Great Australian Bight: facies dynamics and oceanography on a vast cool-water carbonate

- shelf: *Journal of Sedimentary Research*, v. 71, p. 549–567.
- Johnson, C.L., Franseen, E.K., Goldstein, R.H., 2005, The effects of sea level and palaeotopography on lithofacies distribution and geometries in heterozoan carbonates, southeastern Spain: *Sedimentology*, 52: 513–536.
- Kendall, C. G. St. C., Schlager, W., 1981, Carbonates and relative changes in sea level: *Marine Geology*, v. 44, p. 181–212.
- Knoerich, A.C., and Mutti, 2003, Controls of facies and sediment composition on the diagenetic pathway of shallow-water heterozoan carbonates; the Oligocene of the Maltese Islands: *International Journal of Earth Sciences*, v. 92, p.494-510.
- Lees, A. and Buller, A.T., 1972, Modern temperate-water and warm-water shelf carbonate sediments contrasted: *Marine Geology*, v. 13, p. 67-73.
- Lees, A., 1975, Possible influence of salinity and temperature on modern shelf carbonate sedimentation: *Marine Geology*, v. 19, p. 159–198.
- Lindholm, R., and Finkelman, R., 1972, Clacite staining; semiquantitative determination of ferrous iron: *Journal of Sedimentary Research*, v. 42, p. 239-242.
- Littler, M.M., Littler, D.S., and Hanisak, M.D., 1991, Deep-water rhodolith distribution, productivity, and growth history at sites of formation and subsequent degradation: *Journal of Experimental Marine Biology and Ecology*, v. 150, p. 163–182.
- Lopez-Ruiz, and Rodgriguez-Badiola, E., 1980, La Region Volcanica Neogena del Sureste de Espana: *Estudios Geologicos*, v. 36, p. 5- 63.
- Martin, J.M., Braga, J.C. and Rivas, P., 1989, Coral successions in upper Tortonian reefs in SE Spain: *Lethia*, v. 22, p. 271-286.
- Martin, J.M., and Braga, J.C., 1994, Messinian events in the Sorbas Basin in southeastern Spain and their implications in the recent history of the Mediterranean: *Sedimentary Geology*, v. 90, p. 257-268.
- Martin, J.M., Braga, J.C., Betzler, C., and Brachert, T., 1996, Sedimentary model and high frequency cyclicity in a Mediterranean, shallow-shelf, temperate-carbonate environment (uppermost Miocene, Agua Amarga Basin, Southern Spain): *Sedimentology*, v. 43, p. 263-277.
- Martin, J.M., Braga, J.C., and Betzler, C., 2003, Late Neogene- Recent uplift of the Cabo de Gata volcanic province, Almeria, SE Spain: *Geomorphology*, v. 50, p. 27-42.
- Michel, J., Vicens, G. M. & Westphal, H., 2011, Modern Heterozoan Carbonates from eutrophical shelf (Mauritania): *Journal of Sedimentary Research*, v. 81, p. 641– 655.
- Middleton, A.P., Freestone, I.C., Leese, M.N., 1985, Textural analysis of ceramic thin sections: evaluation of grain sampling procedures: *Archaeometry*, v. 27, p. 64-74.
- Miller, K.G., Kominz, M.A., Browning, J., V., Wright, J., D., Mountain, G.S., Katz, M.E., Sugarman, P.J., Cramer, B.S., Christie-Blick, N., and Pekar, S.F., 2005, The Phanerozoic record of global sea-level change: *Science*, v. 310, p. 1293–1298.
- Moissette, P., Koskeridou, E., Cornee, J.J., Guillocheau, F., and Lecuyer, C., 2007, Spectacular preservation of seagrasses and seagrass-associated communities from the Pliocene of Rhodes, Greece: *Palaaios*, v. 22, p. 200–211.
- Moissette, P., Cornee, J.J., and Koskeridou, E., 2010, Pleistocene rolling stones or large bryozoan nodules in a mixed siliciclastic–carbonate environment (Rhodes, Greece): *Palaaios*, v. 25, p. 24–39.
- Montenat, C., Ott, D’Estevou, P., and Mase, P., 1987, Tectonic-sedimentary characters of the Betic Neogene basins evolving in a crustal transcurrent shear zone (SE Spain): *Bulletin Centres Rech. Explor.-Prod., Elf-Aquitaine*, v. 11, p. 1- 22.

- Montenat, C., Ott, D'Estevou, P., and La Chappelle, G., 1990, Le bassin de Nijar-Carboneras et le couloir de Bas-Andrax, in Montenat, C., ed., Les Bassins Néogènes du Domaine Betique Oriental (Espagne): Doc. Trav. Geol. Albert de Lapparent, 12-13, IGAL, Paris, p. 129- 164.
- Mount, J., F., 1982, Storm-surge-ebb origin of hummocky cross-stratified units of the Andrews Mountain Member, Campito Formation (Lower Cambrian), White-Inyo Mountains, Eastern California: *Journal of Sedimentary Petrology*, v. 52, p. 941-958.
- National Oceanography centre, <http://noc.ac.uk/science-technology/earth-ocean-system/seafloor/bottom-currents>.
- Nelson, C. H., 1982, Modern shallow-water graded sand layers from storm surges, Bering shelf: a mimic of Bouma sequences and turbidite systems: *Journal of Sedimentary Petrology*, v. 52, p. 537-545.
- Nelson, C. S., Keane, S. L., and Head, P. S., 1988, Non-tropical deposits on the modern New Zealand shelf, in Nelson, C. S ed., Non-tropical shelf carbonates-Modern and ancient: *Sedimentary Geology*, v. 60, p. 71-94.
- O'Connell, L.G., and James, N.P., 2015, Composition and Genesis of Temperate, Shallow Marine Carbonate Muds: Spencer Gulf, South Australia, *Journal of Sedimentary Research*, v. 85, p. 1275-1291.
- Patriquin, D. G., 1975, Migration" of blowouts in seagrass beds at Barbados and Carriacou, West Indies, and its ecological and geological implications: *Aquatic Botany*, v. 1, p. 163 189.
- Peres, J.M. and Picard, J., 1964, Nouveau manuel de bionomie benthique de la Mer Méditerranée: *Rec. Trav. Stn. March. Endoume-Marseille Bull.*, 31.
- Pevear, D. R., 1966, The estuarine formation of United States Atlantic Coastal Plain phosphorite: *Economic Geology*, v. 61, p. 251-256.
- Platt, J.P., and Vissers, R.L.M., 1989, Extensional collapse of thickened continental lithosphere: a working hypothesis for the Alboran sea and Gibraltar arc: *Geology*, v. 17, p. 540-543.
- Pomar, L., 2001, Ecological control of sedimentary accommodation: evolution from carbonate ramp to rimmed shelf, Upper Miocene, Balearic Islands: *Paleogeography, Paleoclimatology, Paleoecology*, v. 175, p. 249- 272.
- Pomar, L., Obrador, A., Fornos, J., Rodriguez-Perea, A., eds., 1983, El Tercenario de las Baleares (Mallorca-Menorca), Guia de las Excursiones del X Congreso Nacional De Sedimentología: Institut D'Estudis Balearics and Universitat de Palma de Mallorca, 233 pp.
- Posamentier, H.W., and Vail, P.R., 1988, Eustatic controls on clastic deposition II sequence and systems tract models, in Wilgus, C.K., Hastings, B.S., St. C. Kendall, C.G., Posamentier, H.W., Ross, C.A., and Van Wagoner, J.C., eds., *Sea Level Changes: An Integrated Approach*: SEPM, Special Publication No. 42, p. 125-154.
- Posamentier, H.W., Allen, G.P., James, D.P., and Tesson, M., 1992, Forced regressions in a sequence stratigraphic framework: concepts, examples, and exploration significance: *AAPG Bulletin*, v. 76, p. 1687-1709.
- Prager, E.J., and Ginsburg, R.N., 1989. Carbonate nodule growth on Florida's outer shelf and its implication for fossil interpretations, *Palaaios*, v. 4, p. 310-317.
- Procaccini, G., Buia, M.C., Gambi, M.C., Pergent, G., Pergent-Martini, C., Romero, J., 2003, The seagrasses of the western Mediterranean, in Green, E.P., et al. (ed.), *World atlas of seagrasses*, p. 48-58.
- Pugliano, T.M., Goldstein, R.H., Franseen, E.K., 2015, Petrophysical Character of Fining- Upward Cyclothems and Clinothems in Heterozoan Carbonates: Diagenetic and Depositional

- Controls, Masters Thesis, University of Kansas, Lawrence KS.
- Reeckmann, S.A., and Gill, E.D., 1981, Rates of vadose diagenesis in Quaternary dune and shallow marine calcarenites, Warrnambool, Victoria, Australia: *Sedimentary Geology*, v. 30, p. 157-172.
- Rehault, J.P., Boillot, G., and Mauffret, A., 1985, The western Mediterranean basin, in Stanley, D.J. and Wezel, F.C., eds., *Geologic Evolution of the Mediterranean Basin*: Springer-Verlag, p. 101-130.
- Salazar-Jimenez, A., Frey, R.W., and Howard, J.D., 1982, Concavity orientations of bivalve shells in estuarine and nearshore shelf sediments, Georgia: *Journal of Sedimentary Petrology*, v. 52, p. 565-586.
- Sanz de Galdeano, C., and Vera, J. A., 1992, Stratigraphic record and palaeogeographical context of the Neogene basins in the Betic Cordillera, Spain: *Basin Research*, n. 4, p. 21- 36.
- Schlager, W., 2000, Sedimentation rates and growth potential of tropical, cool-water and mud-mound carbonate systems: Geological Society, London, Special Publications 178, p. 217-227.
- Schlager, W., 2003, Benthic carbonate factories of the Phanerozoic: *International Journal of Earth Sciences*, v. 92, p. 445-464.
- Schlager, W., 2005, Carbonate Sedimentology and Sequence Stratigraphy: SEPM, Concepts in Sedimentology and Paleontology #8, 200pp.
- Scholle, P.A., Arthur, M.A., and Allan, E.A., 1983, Pelagic environments, in P.A. Scholle, Debout, D.G., and Moore, C.H., eds., *Carbonate Depositional Environments*: AAPG, Memoir 33, p. 619-691.
- Scholle, P., A., and Ulmer-Scholle, D., S., 2003, *Color Guide to Petrography of Carbonate Rocks*: AAPG, Memoir 77, 459pp.
- Scoffin, T. P., 1988, The environments of production and deposition of calcareous sediments on the shelf west of Scotland: *Sedimentary Geology*, v. 60, p. 107-124.
- Scoffin, T. P., and Bowes, G. E., 1988, The facies distribution of carbonate sediments on Porcupine Bank, Northeast Atlantic: *Sedimentary Geology*, v. 60, p. 125-134.
- Serrano, F., 1992, Biostratigraphic control of Neogene volcanism in Sierra de Gata (southeast Spain): *Geologie en Mijnbouw*, v. 71, p. 3- 14.
- Simone, L., and Carannante, G., 1988, The fate of forams (temperate-type) carbonate platforms: *Sedimentary Geology*, v. 60, p. 347-354.
- Smith, F.D. Jr, 1955, Planktonic foraminifera as indicators of depositional environment: *Micropaleontology*, v. 1, p. 147-151.
- Smith, A.M., Key, M.M., Jr., and Gordon, D.P., 2006, Skeletal mineralogy of bryozoans: Taxonomic and temporal patterns: *Earth-Science Reviews*, v. 78, p. 287-306.
- Stockman, K., Ginsburg, R., Shinn, E., 1967, The Production of Lime Mud by Algae in South Florida: *Journal of Sedimentary Petrology*, v. 37, p. 633-648.
- Sun, S.Q., Esteban, M., 1994, Paleoclimatic controls on sedimentation, diagenesis, and reservoir quality — lessons from Miocene carbonates: *AAPG Bulletin*, v. 78, p. 519-543.
- Sweeney, R., J., Goldstein, R.H., Franseen, E.K., 2015, Sequence stratigraphy and facies distribution in a Miocene carbonate platform; La Rellana Platform Area, Master's thesis, KICC, University of Kansas, Lawrence, KS, 129p.
- Taylor, P., and James, N.P., 2013, Secular changes in colony-forms and bryozoan carbonate sediments through geological history: *Sedimentology*, v. 60, p. 1184-1212.
- Toomey, N., Goldstein, R.H., Franseen, E.K., 2003, Controls on Sequence Stratigraphy in Upper

- Miocene Carbonates of Cerro De Ricardillo, Southeastern Spain: Master's Thesis, University of Kansas, 146 pp.
- Tsaparas, N., Drinia, H., Antonarakou, A., Marcopoulou Diakantoni, A., and Dermitzakis, M.D., 2007, Tortonian Clypeaster fauna (Echinoidea: Clypeasteroida) from Gavdos Island (Greece): Bulletin of the Geological Society of Greece, v. 40, p. 225–237.
- Tucker, M.E., 1993, Carbonate diagenesis and sequence stratigraphy, in Wright, W.P., (ed.): Sedimentology Review, v. 1, p. 51-72.
- Udden, J., 1914, Mechanical composition of clastic sediments: Geologic Society of America Bulletin, p. 25,655-25,744.
- Van Wagoner, J.C., Posamentier, H.W., Mitchum, R.M., Vail, P. R., Sarg, J.F., Louit, T.S., and Hardenbol, J., 1988, An overview of sequence stratigraphy and key definitions, in Wilgus et al., eds., Sea-level changes: an integrated approach: SEPM, Special Publication 42, 39-45
- Van Wagoner, J.C., R.M. Mitchum, K.M. Campion, and V.D. Rahmanian, 1990, Siliciclastic sequence stratigraphy in well logs, cores, and outcrops: concepts for high resolution correlation of time and facies: AAPG Methods in Exploration, Series 7, 55 pp.
- Voigt, Ehrhard, 1981, Upper Cretaceous Bryozoan-seagrass association in the Maastrichtian of the Netherlands, in: Larwood, G.P., and Nielsen, C., eds., Recent and Fossil Bryozoa: Olsen & Olsen, Fredensborg, p. 281-298
- Wanless, H.R., 1981, Fining-upwards sedimentary sequences generated in seagrass beds: Journal of Sedimentary Petrology, v. 51, p. 445–454.
- Wentworth, C., 1922, A scale of grade and class terms for clastic sediments: Journal of Geology, v. 30, p. 377-392.
- Wilson, M.E.J., 2002, Cenozoic carbonates in Southeast Asia: implication for equatorial carbonate development: Sedimentary Geology, v. 147, p. 295–428.
- Wright and Burchette, 1996, Shallow-water carbonate environments, in Reading, H. L., ed., Sedimentary Environments: processes, facies, and stratigraphy, 3rd edition.

Chapter 3:

Distribution of Petrophysical Character in Fining-Upward Cyclothem and Clinothem in Heterozoan Carbonates: Diagenetic and Depositional Controls

Tony M. Pugliano, Robert H. Goldstein, and Evan K. Franseen

*Department of Geology, the University of Kansas, 1475 Jayhawk Boulevard, 120 Lindley Hall,
Lawrence, KS, 66045, USA*

ABSTRACT

Outcrops from Pliocene and Miocene carbonate complexes of the Cabo de Gata region of SE Spain provide analogs for determining controls and modeling reservoir properties of heterozoan systems. Pliocene strata are composed of grain-rich, fining-updip, prograding clinothem. Miocene strata show similar facies distributed mostly as fining-upward cyclothem. Miocene strata are partially dolomitized and cemented with calcite, whereas Pliocene strata have minor diagenetic alteration, allowing for analysis of the petrophysical impact of diagenesis. Pliocene sorted packstones have the highest average porosity and permeability at 51% and 7,503md. Rudstone lithofacies have higher variability and averages of 42% and 4,200md. Miocene rudstones with only minor diagenetic alteration have 40% porosity and 1,888md permeability, whereas diagenetically altered rudstones have averages of 34% and 1,307md. Packstones with only minor diagenetic alteration have average porosity of 43% and permeability of 5,131md, whereas diagenetically altered packstones have drastically lower averages of 30% and 690md. Diagenetic alteration has a more profound effect on porosity and permeability on packstones than it does on rudstones. Where extensive dolomite cement is absent, dolomite amount and moldic porosity have a positive correlation, indicating dolomitization and dissolution are related processes. The facies distribution of the shoaling- and fining-upward

cycle creates vertical petrophysical trends that increase upward from rudstones to packstones, packstones having the highest values. In diagenetically altered cycles, packstones are highly variable, and diagenesis commonly leads to lower porosity and permeability at tops of cycles rather than the high values typical of cycle tops without major diagenetic alteration. Grain-rich fining-updip clinothems and fining-upward cyclothems construct a predictable architecture of lithofacies that contain sedimentologic and diagenetic variables that govern the distribution of petrophysical values.

INTRODUCTION

The distribution of petrophysical properties in carbonate systems is primarily dependent on depositional controls and diagenesis. In heterozoan systems, there is a need for the fundamental understanding of the controls that govern porosity and permeability to model predictable patterns in heterozoan carbonate reservoirs. Petrophysical parameters have been studied in photozoan carbonates, but little has been done in heterozoan carbonate systems. One might expect the controls on heterozoan carbonates would be fundamentally different from those in photozoans as organisms, source of mud, water chemistry, original mineralogy, and platform morphology are all expected to differ (James, 1997). The stratigraphic architecture of shallow-water heterozoans results in grainy fining-upward clinothems and cyclothems as shown in a Miocene system and Pliocene system of southeastern Spain (Pugliano et al., 2015; Chapter 2). Population of this stratigraphic architecture with porosity and permeability values allows for the visualization and development of reservoir-analog models for heterozoans. Reservoir models based on outcrop analogs are applicable for prediction of lithofacies and reservoir character in the subsurface (e.g. Borgomano et al., 2002, 2008; Adams et al., 2005; Dutton et al., 2005; Janson et al., 2007; Pranter et al., 2007).

The Miocene and Pliocene carbonate complexes of the Cabo de Gata region of southeastern Spain provide excellent outcrops for modeling sedimentologic variables, stratigraphic architecture, and for petrophysical characterization of heterozoan carbonates. In particular, Pliocene heterozoans of the Carboneras Basin were deposited in association with a shaved-shelf system (e.g. James et al., 1994) dominated by prograding clinothems that contain grainy, fining-updip depositional profiles (Dillett et al., 2004). Miocene heterozoans of the Ricardillo area contain stacked, laterally extensive packages of partially dolomitized cycles that: 1) shoal- and fine-upward (Toomey et al., 2003); or 2) deepen- and coarsen-upward and then shoal- and fine-upward, depending on paleotopographic position (Chapter 2; Pugliano et al., 2015).

These grain-dominated, fining-updip and fining-upward trends are distinctly different depositional patterns from photozoan carbonate systems. Analyzing the petrologic and petrophysical properties of these systems allows for testing of hypotheses related to sedimentologic, stratigraphic, and diagenetic controls that govern porosity and permeability in heterozoan carbonates.

GEOLOGIC SETTING

The Carboneras Basin and Cerro de Ricardillo area (Figure 1) contain heterozoan carbonate complexes deposited in the Cabo de Gata volcanic province of southeastern Spain. During the mid-late Miocene (Serravallian-Tortonian), compressional stress shifted to the northwest, creating a shear zone with strike-slip faults and pull apart basins in southeastern Spain, and eruption of calc-alkaline dacite and rhyolite in the Cabo de Gata province. These volcanics and older metamorphic basement to the north were subsequently eroded, faulted, and highly fractured forming an archipelago system with interconnected basins and straits (Franseen,

1989, Lopez- Ruiz et al., 1980; Rehault et al. 1985; Montenat et al., 1987; Platt and Vissers, 1989; Montenat et al., 1990; Sanz de Galdeano and Vera, 1992; Esteban, 1979; Esteban and Giner, 1980; Sanz de Galdeano and Vera, 1992; Esteban, 1996; Franseen and Goldstein, 1996; Franseen et al., 1998).

Around the time that volcanism ceased, a temperate climate (Franseen et al., 1998) allowed for the deposition of heterozoan carbonates on the flanks of the volcanic highs in the Betic basins (Franseen et al., 1998). One of these volcanic highs was Cerro de Ricardillo. Currently at 309 meters elevation (Fernandez-Soler, 1996), this peak is the highest in the area that is flanked by upper Miocene carbonates (Figure 2), the oldest of which correlate to strata with ages of 8.5 ± 0.1 Ma (Argon/Argon dating) (Franseen et al., 1997; Franseen et al., 1998, Hess et al., 2011).

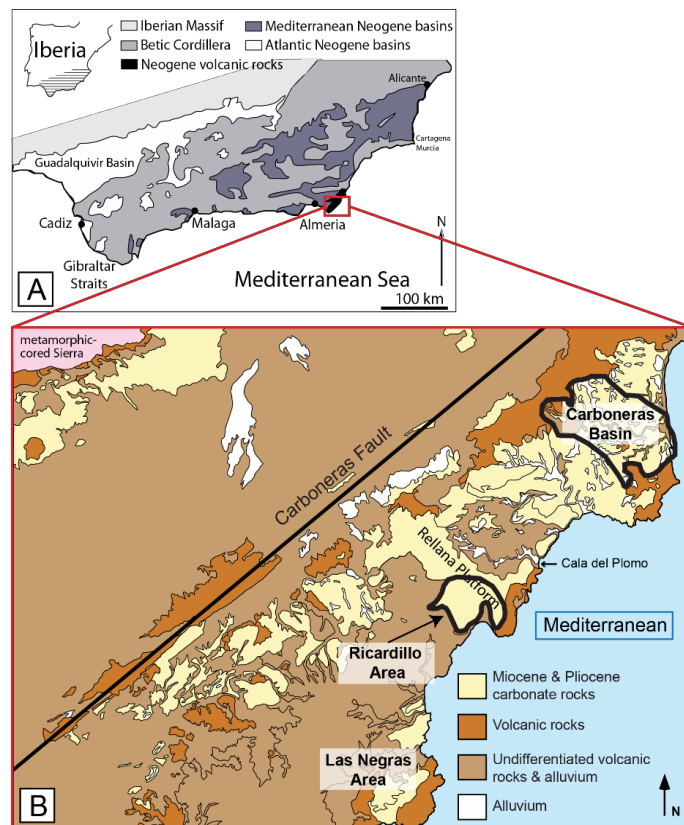


Figure 1: A) Location map of Neogene basins in the Betic Cordillera of southern Spain. The red box outlines the Cabo de Gata volcanic province. Modified from Gibbons and Moreno (2003). B) Generalized geologic map of the Cabo de Gata region and location of the Ricardillo area and the Carboneras Basin. Modified from Instituto Geologico y Minero de Espana (1981).

Dolomitization, dissolution, and calcite cementation then altered these strata (Franseen, 1989; Oswald, 1992; Meyers et al., 1997; Lu and Meyers, 1998; Li et al., 2013; 2014).

Pliocene relative sea-level rise during the Zanclean (5.2-3.5 Ma) stage, created accommodation in the low-lying Carboneras Basin (Figure 1) allowing for the deposition of heterozoan carbonates, comparable to those in the Miocene (Montenat et al., 1990; Franseen et al., 1993; Aguirre, 1998). The southern part of the basin consists of downlapping, prograding clinothems formed below a shaved shelf system, deposited during a lowstand (Dillett et al., 2004). The Pliocene strata lack dolomite, abundant calcite cement, and extensive dissolution common in the Miocene deposits. Therefore, the Pliocene strata better preserve a record of primary petrophysical properties in heterozoan facies, before major diagenetic alteration.

Post depositional deformation is minor in the Cabo de Gata. The area is characterized by broad regional uplift and only minor tilting and faulting. For the most part, paleotopography is preserved (Esteban and Giner, 1980; Franseen and Mankiewicz, 1991; Franseen et al., 1993, 1997, 1998; Franseen and Goldstein, 1996; Toomey et al., 2003; Dillett et al., 2004; Johnson et al., 2005; Hess et al., 2011; Sweeney et al., 2015).

This research focuses on two areas with outcrops of heterozoan carbonates: Miocene (Tortonian)-aged DS2 cyclical sequences of Cerro de Ricardillo (Toomey et al., 2003; Chapter 2); and a Pliocene (Zanclean)-aged, lowstand, prograding clinothem, in the southern portion of the Carboneras Basin (Figure 3).

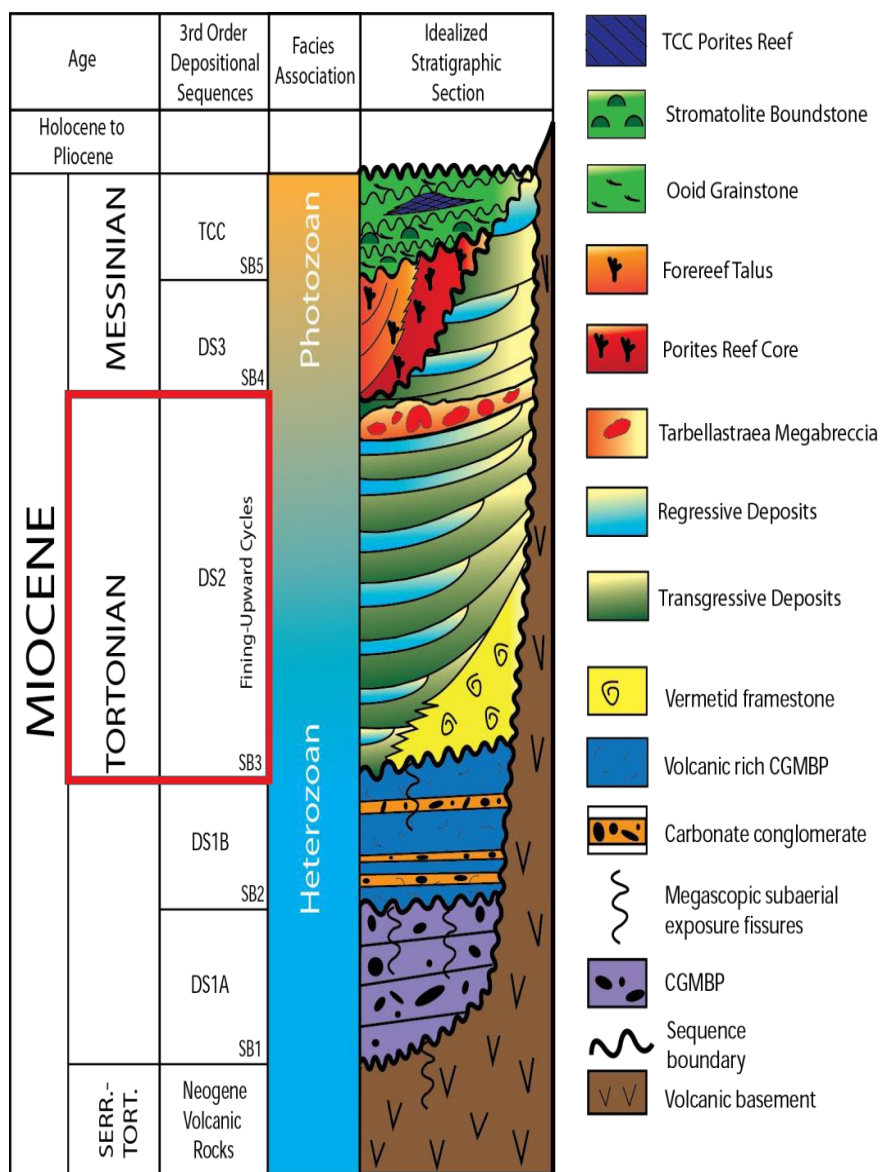


Figure 2: Generalized stratigraphic section for the Miocene-aged Cerro de Ricardillo area. The 3rd order sequence (DS2) containing the cyclic heterozoan deposits for this study is boxed in red. Five third-order depositional sequences are recognized throughout the region with multiple 5th order sequences in DS2 and the TCC. Modified from Toomey et al. (2003) and Franseen et al. (1998).

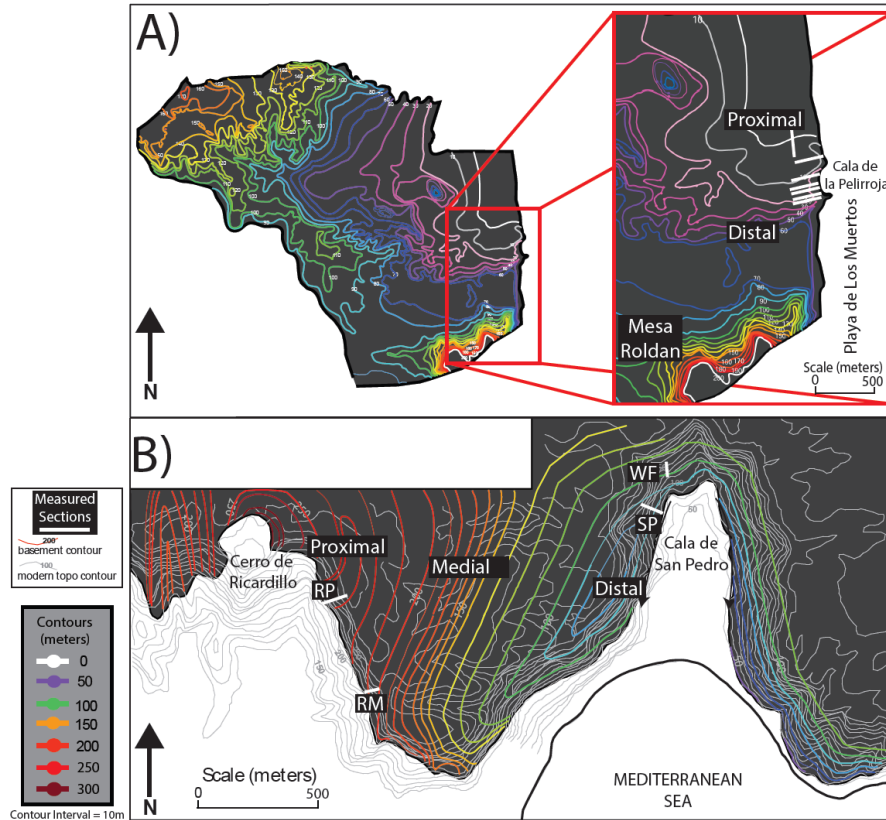


Figure 3: A) Map for the Carboneras Basin showing contours of modern-day elevation at the base of Pliocene strata. This basin is 5.5 x 4.75 km across. This research only focused on the clinotherms in the southeastern part of the basin just northeast of Mesa Roldan, outlined in the red box. Topography within the box is 10-20m above modern day sea level. Modified from Dillett et al. (2004). B) Map of the Ricardillo area showing contours of modern-day elevation at the contact between Miocene carbonate strata and underlying volcanics. The area is 1.5km long and 0.93 wide. The most proximal carbonate section was measured at 245m, medially at 210m, and distally at 90m elevation. The eleven measured sections from this study are marked on both maps by white lines. Modified from Toomey et al. (2003)

METHODOLOGY

Fieldwork was conducted at the northern end of Playa de Los Muertos, Cala de la Pelirroja in the Carboneras Basin, and at Cerro de Ricardillo and Cala de San Pedro in the Ricardillo Area (Figure 3). A total of 11 stratigraphic sections were measured and described at centimeter scale, four from the Miocene of the Ricardillo area, and seven from the Pliocene of the southern part of the Carboneras Basin.

A total of 333 thin sections were used for transmitted light and UV petrography to point count grain constituents, point count and measure relative grain size, categorize cements, categorize pore type, and to determine and quantify mineralogy. Miocene samples were stained using Alzarin Red-S and Potassium Ferricyanide (e.g. Lindholm and Finkelman, 1972) to

distinguish calcite from dolomite. Background extraction micro-imaging analysis was used to quantify dolomite content for Miocene samples. The dolomite percentages represents the total percent dolomite of the minerals in the rock with pore space removed, it is expressed as: dolomite/ (calcite + dolomite). Three hundred sixty-one core plugs were taken parallel to bedding for petrophysical analyses. Core plugs were cored from hand samples at the Kansas Geological Survey and are 2.45cm in diameter and 1.27 to 5cm in length. One hundred eighty-six of the plugs were taken from Miocene deposits, and 175 from Pliocene deposits. Helium porosity, air permeability (K_{air}), and grain density measurements were taken on each core plug by Weatherford Labs. A total of 4 outliers were removed from the Pliocene dataset and 6 from the Miocene dataset, these outliers fell outside of 2.5 standard deviations from the mean and are thought to represent errors in the measurements.

Facies and petrophysical models were created in Petrel™ to use as analogs for facies prediction and petrophysical distribution in heterozoan carbonate reservoirs. Altogether, a total of 8 distinct models were constructed with the following characteristics: (1) all Miocene deposits along Ricardillo; (2) entire Pliocene clinothem from Carboneras; and (3-8) six end-member, lateral depositional profiles forming clinothem in the Pliocene. Each model includes a facies model, porosity model, permeability model, and predictive distribution models for individual lithofacies.

LITHOFACIES AND STRATIGRAPHY

The detailed stratigraphic architecture, lithofacies characteristics and distribution, sedimentologic features, and controls on heterozoan carbonate deposition from both the Ricardillo area and the Carboneras Basin are documented in Pugliano et al. (2015) and Chapter 2. The Pliocene clinothem (Figure 4A) contains 10 lithofacies, grouped into four lithofacies

associations, whereas the Miocene deposits contain 13 lithofacies grouped into five lithofacies associations. The Pliocene clinotherm is composed of individual prograding clinotherms that developed during relative sea-level lowstands. The clinotherm downlaps onto underlying Miocene deposits (Dillett et al., 2004) and show toplap and truncation updip. Six patterns of proximal to distal facies changes have been documented along the clinotherm (Pugliano et al., 2015, Chapter 2). Altogether, these stacked, laterally changing facies trends form a grain-rich, fining-upward depositional pattern. Proximal facies contain sorted bryozoan- coralline algae packstones, which change laterally downdip along time equivalent strata into poorly sorted, rhodolith and bivalve rudstones.

Miocene strata (Figure 4B) are composed of partially dolomitized stacked cyclothem that onlap and drape paleotopography. Each cyclothem is composed of basal transgressive coarse rudstone lithofacies and an upper regressive cross-bedded packstone lithofacies. As shoaling occurred during relative sea-level fall, waves reworked coarse sediments into sorted, abraded sands, creating a fining-upward trend.

Vertical depositional cyclic trends vary depending on paleotopographic position, and form predictable trends downslope. Strata from both areas are composed primarily of bryozoans, ostreids, pectinids, coralline algae and rhodoliths, benthic and planktonic foraminifera, echinoids; and to a lesser extent serpulids, barnacles, ahermatypic corals, gastropods, and calcisilt.

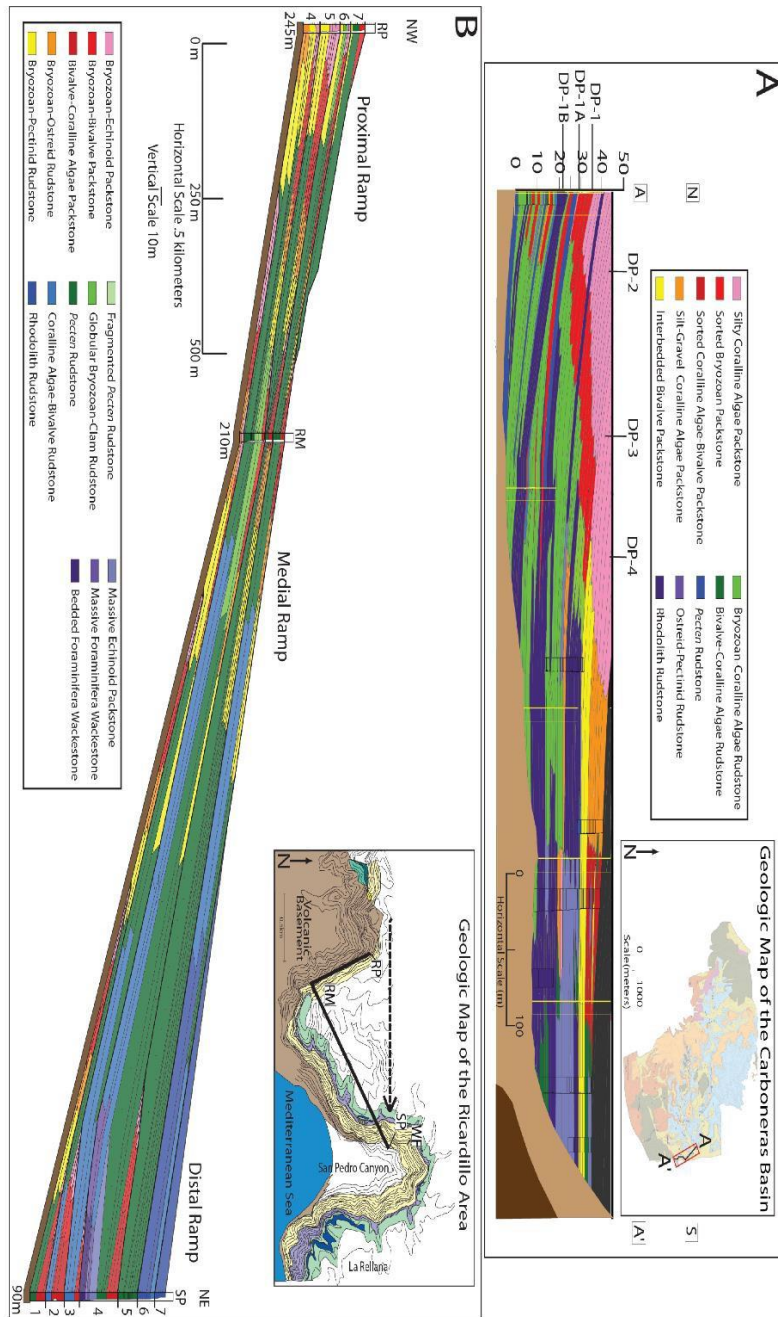


Figure 4: Cross sections of strata from both field areas. A) Cross section of the Pliocene clinothem at the southern end of the Carboneras basin. Measured sections from this research are located on the cross section. Measured sections described by Dillett et al. (2004) are marked in yellow boxes. Depositional profiles (DP) are labeled along the time-equivalent strata from which they are extracted. Note the fining-upward and fining updip depositional trends. B) Cross section of the Miocene cycles of the Ricardillo area. The cross section shows the seven measured cycles of the ramp. Each cycle is capped by a fining upward trend that is caused by increased abrasion during shoaling. In addition, note the fining updip trend of the ramp that represents a preponderance of shallower water, high abrasion conditions in the updip areas. Vertical scale is 2x exaggerated.

DIAGENESIS

Miocene lithofacies in the Ricardillo area have been separated into five diagenetic facies and the entire Pliocene clinotherm has been designated as one diagenetic facies forming a sixth diagenetic facies. These facies (Table 1, Figure 5) are classified on the basis of amount of dolomitization, dolomite cement, calcite cement, and dissolution. There is a wide range of diagenetic alteration, from a minor alteration to extensive dolomitization, dissolution, and calcite cementation. Dissolution mostly created moldic porosity and is shown as percent rock volume that is moldic porosity. Understanding the effects and distribution of diagenetic variables is highly important as it directly relates to pore space and has not been extensively studied for heterozoan carbonates (Knoerich and Mutti, 2003; Li et al., 2013).

Pliocene

Work by Li et al. (2013; 2014) demonstrated that dolomitization, dissolution and calcite cementation alter Miocene deposits in this region, and that the Pliocene deposits are undolomitized and have experienced less dissolution and calcite cementation. Much of the diagenetic alteration predated Pliocene deposition, and the Pliocene strata can be considered less affected by diagenetic alteration.

Results

Pliocene diagenetic alteration (Table 1; Figure 5A) consists of minor amounts (1-6%) of syntaxial and bladed calcite cement, and up to .5-12% moldic porosity. The few samples (Appendix III) where cement content is greater than 5% (up to 18%), directly overlie the Miocene sequence boundary. Immediately above that boundary, cement content decreases upward from an average of 12 to 1% within a 1.5m stratigraphic interval. Moldic porosity reaches up to 4% in proximal areas and rarely up to 9.5% at the distal end of the clinotherm, but

overall moldic porosity is less than 5%. Due to this low amount of alteration, Pliocene samples fit within the “least altered” diagenetic facies (DF-1).

Diagenetic Facies	Mineralogy	Cement	Moldic Porosity	Lateral Distribution
DF-1 n= 158	0% dolomite	<5%	<5%	Throughout clinothem
DF-2 n=59	0-30% dolomite	< 10%	<10%	Proximal: 46.6% Medial: 12% Distal: 21.2%
DF-3 n=9	0-30% dolomite	> 10%	>10%	Proximal: 20.6% Medial: 4% Distal: 0%
DF-4 N=44	50-100% dolomite	<10%	>10%	Proximal: 9.6% Medial: 36% Distal: 47.5%
DF-5 N=9	50-100% dolomite	> 10%	>10%	Proximal: 14.5% Medial: 4% Distal: 6.6%
DF-6 N=35	50-100% dolomite	Varying cement %	<10%	Proximal: 8.7% Medial: 44% Distal: 24.7%

Table 1: Diagenetic facies description. Summary table of diagnostic features for six diagenetic facies from the Pliocene and Miocene. The table gives the ranges and parameters that were used to distinguish between facies. The far right column quantifies the percentage of the paleotopographic position that the diagenetic facies compose. These percentages were calculated by summing the thickness of each diagenetic facies from measured sections

.Miocene

The origin of dolomite and its associated moldic porosity in this region (Choquette and Pray 1970), was determined by Li et al. (2013) on the nearby platform of La Molata. Li et al. (2013) developed the ascending freshwater-mesohaline mixing idea, a mechanism for dolomitization resulting from an underlying freshwater aquifer that leaked upward into the overlying seawater-saturated platform. The injection of the freshwater from below allowed for a decrease in pressure and outgassing, and induced mixing and fluid flow. This resulted in rapid and simultaneous dissolution and dolomitization at the end of the Miocene. In this scenario, dolomitization is practically absent in proximal areas and increases in abundance basinward. In carbonate reservoirs, dolomite most commonly replaces original calcite or aragonite grains, and forms cement where overdolomitization occurred (e.g. Lucia, 2004; Saller and Henderson, 1998). Both types of dolomitization have an impact on reservoir quality. Calcite cementation

from meteoric waters also had a major impact on extant porosity in Miocene strata of this region (Li et al. 2014). For a thorough discussion of the diagenetic history and paragenesis, see Li et al. (2013; 2014).

Results

All of the grain types observed in the Miocene show evidence of dolomitization, depending on location. Coralline algae grains are the least likely to be dolomitized, as these grains commonly remain calcite where other grains have been replaced. Dolomite crystals (Appendix V) are 10-30 μ m in size and are sub-rhombohedral to rhombohedral (rare) in shape. The dolomite is mostly fabric-destructive, making depositional fabrics difficult to discern.

Calcite cements (Figure 5C, 5E) are abundant and have six different morphologies: equant, syntaxial, bladed, fibrous, rhombohedral, and poikilotopic (e.g. Folk, 1965; James and Choquette, 1984). Equant and syntaxial cements are the most abundant, whereas the other cements are only found in 24 of the 147 samples. Poikilotopic cements form 1.2 to 3.2cm crystals that only develop in strata that have been entirely dolomitized and have undergone extensive later dissolution, such as in DF-5. Equant and syntaxial calcite cements range in size from 25-100 μ m. Some cements are isopachous (e.g. James and Choquette, 1984) and reduce depositional porosity, molds, and solution-enlarged pores (Figure 5C, 5E).

Dissolution is widespread and 44% of samples studied have greater than 10% moldic porosity. In many of these, moldic porosity is the dominant pore type. Bivalves and foraminifera are the most common grains to have undergone dissolution, and coralline algae are the most resilient. Dissolution either entirely removes the original grain, or as is more common, removes the majority of the grain, leaving a portion of the grain behind, or only the rim (Figure 5D, 5E).

Point counting and image analysis of the Miocene samples is used to define five diagenetic

facies (Table 1; Figure 5). DF-2 (Table 1; Figure 1B) is the least altered Miocene diagenetic facies and is most similar to the Pliocene diagenetic facies. Where dolomite is present, it is less than 30% of the total rock volume, and DF-2 has minor calcite cementation and moldic pores. Original textures and pores are preserved. This facies is found in the most proximal areas updip, and in some distal rhodolith beds. DF-3 (Table 1; Figure 5C) is defined on the basis of low dolomite content (<30%) and extensive calcite cementation. The cement occludes nearly all pore space, with the only preserved pores being moldic, primarily bivalves. Distribution of this facies decreases downdip. DF-4 (Table 3; Figure 5D) is entirely dolomitized and is destructive to original depositional grains and textures. This facies has >10% moldic porosity. Distribution of this facies increases downdip. DF-5 (Table 3; Figure 5E) is destructive to depositional fabrics as all grains have been dolomitized and dissolved. This facies is similar to DF-4 and has the greatest amount of moldic porosity, however some of these pores are occluded by both dolomite cement and poikilotopic calcite cement. The poikilotopic cement has grown around grains and is only found in this diagenetic facies. Distribution of this facies decreases downdip. Lastly, DF-6 (Table 3; Figure 5F) consists primarily of replacement dolomite and dolomite cement. This facies has undergone little dissolution, and porosity is primarily depositional, within dolomitized grains. This diagenetic facies is most abundant in distal regions.

Figure 6 shows the dolomite distribution by elevation along Ricardillo. Dolomite is prominent (nearly 100%) in distal deposits and decreases inconsistently as elevation increases. In distal and medial areas, dolomite is more abundant at the base of the sections than at the tops, as dolomite amount decreases abruptly from 77% in underlying facies to 43% upon crossing the contact into rhodolith beds, with dolomite percentages decreasing down to 3% upward. Few samples have 100% dolomite in medial and proximal regions, and at 265m elevation and higher,

dolomite content abruptly decreases to nearly 0%. This distribution is consistent with the findings of Li et al. (2013, 2014).

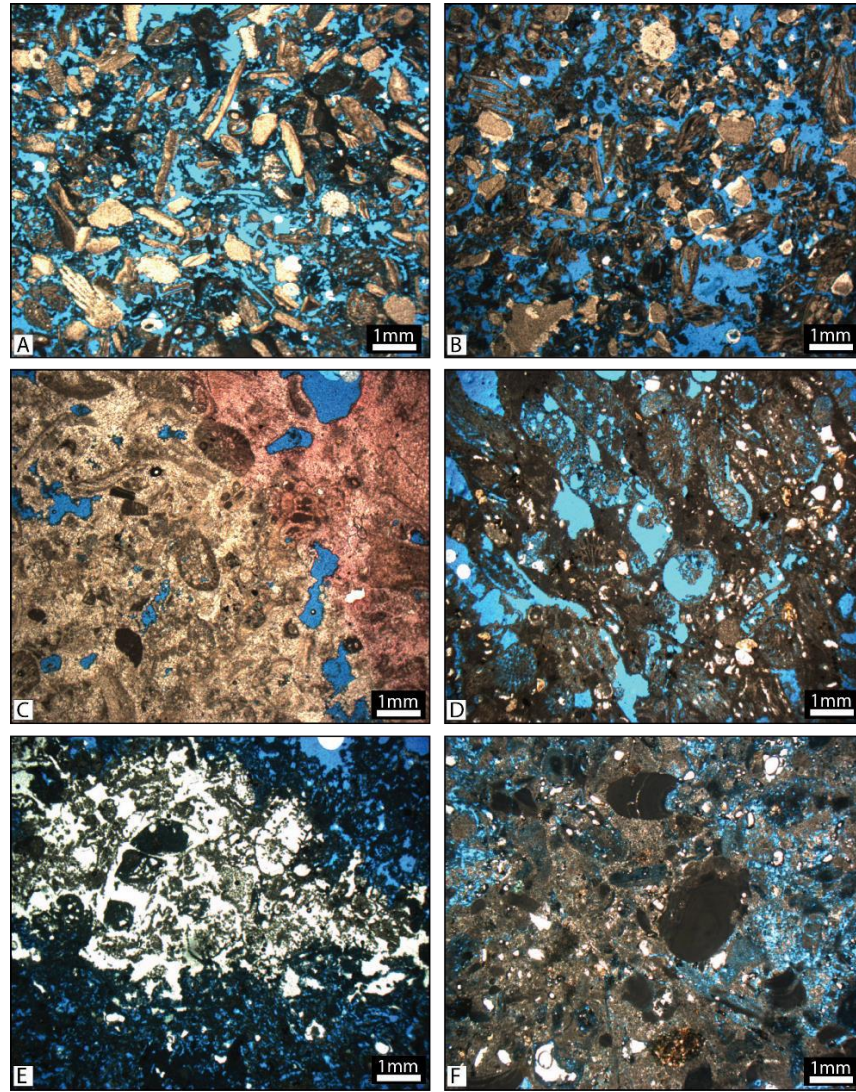


Figure 5: Photomicrographs of the six diagenetic facies. Details of these facies are located in Table 1. A) **DF-1** represents the primarily unaltered deposits of the Pliocene. B) **DF-2** represents the primarily unaltered facies of the Miocene deposits. C) **DF-3** consists of all calcite grains and extensive calcite cementation. D) **DF-4** has been dolomitized and has undergone extensive dissolution, creating moldic porosity. E) **DF-5** shows the extensive dolomitization, dissolution, and poikilotopic cement. F) **DF-6** consists of grains that have been dolomitized, dolomite cement, and primarily depositional porosity.

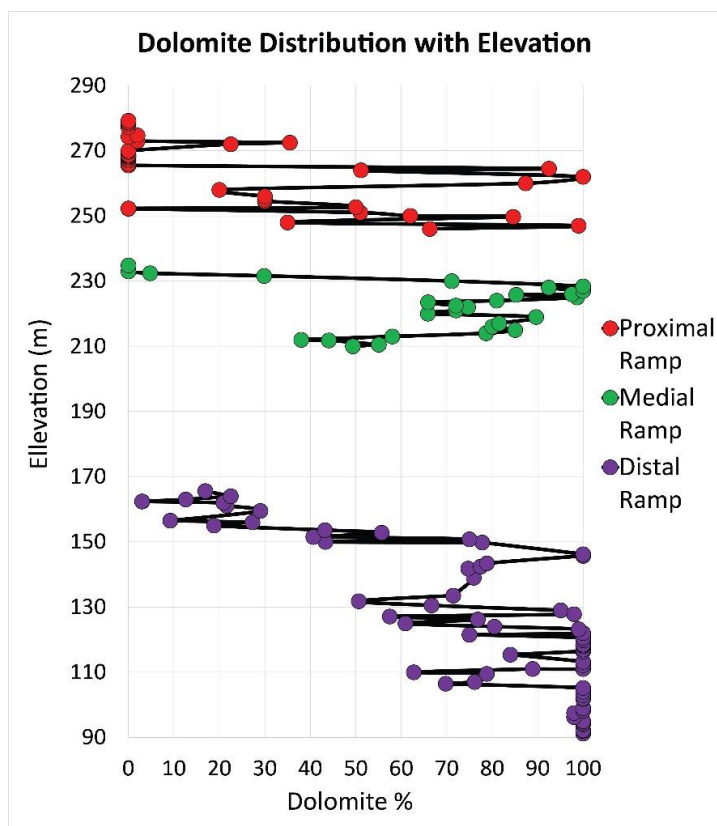


Figure 6: Distribution of dolomite with modern day elevation in the Ricardillo area. Elevations without data are areas where no stratigraphic sections were measured. Dolomite content greatly increases in distal regions of the slope in increases toward the base of the section. In addition to elevation, other controls include, grain size ratios, matrix, and rhodolith content.

PORE TYPE DISTRIBUTION AND CLASSIFICATION

The most common pore types found in both Miocene and Pliocene datasets are interparticle, intraparticle, and moldic porosity with framework, shelter, vug, intercrystalline, fracture, and channel pores present to a lesser extent (Figure 5, 7; e.g. Choquette & Pray, 1970). Bryozoan grains have the most abundant intraparticle pore space (Figure 7C, D, and E). Encrusting morphologies have the largest pores followed by globular and branching morphologies. Abundant intraparticle porosity within individual zooecia is present in all three morphologies as well as framework pore space within encrusting nodules or bryoliths (Figure 7C). Bryoliths are only found abundantly in the Rhodolith Rudstone in the Pliocene. They show a nucleus composed of a bivalve shell, rhodolith, or an internal void that was likely originally a sponge, in most cases creating a pore up to 2cm in diameter.

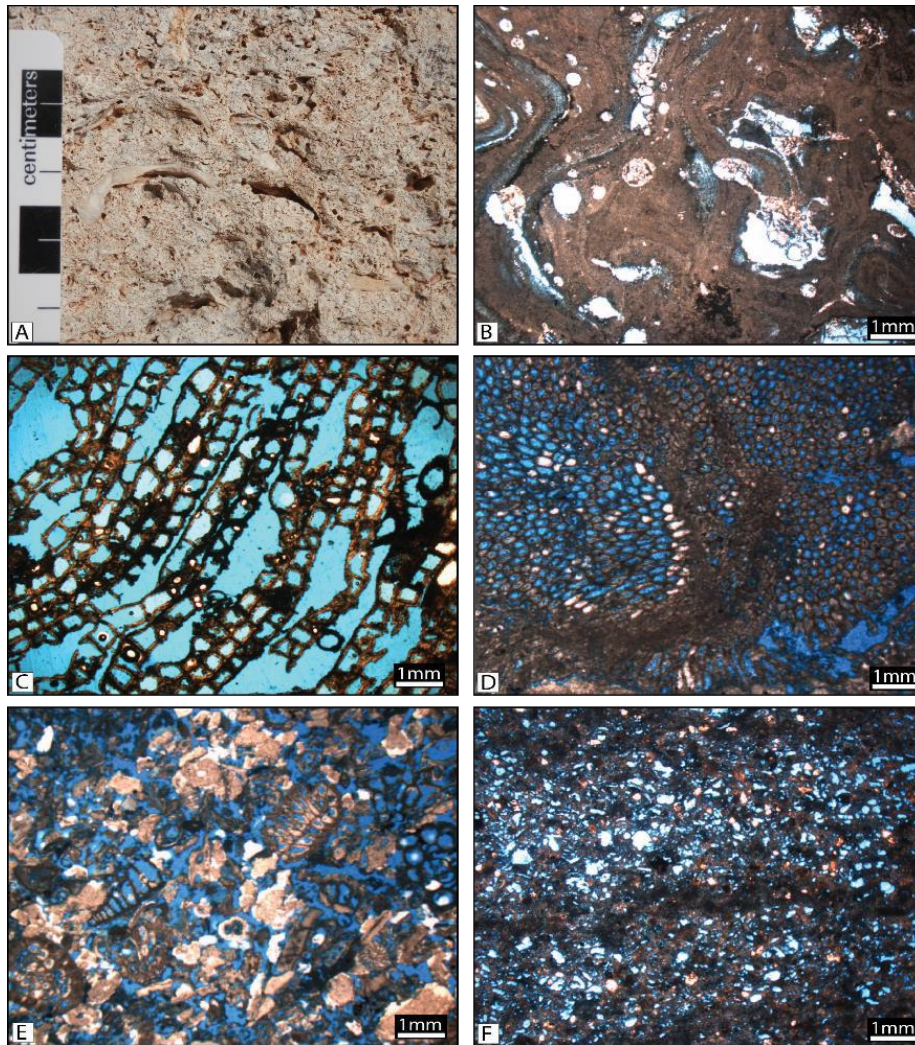


Figure 7: Photomicrographs and a photograph showing pore distribution and grain constituents. A) Photograph of Bryozoan-Ostreid Rudstone from the Miocene. This image shows the centimeter scale shelter porosity located under concave down bivalves. B) Photomicrograph of the Rhodolith Rudstone from the Miocene. Individual rhodoliths contain extensive framework porosity, however these pores are not likely well connected to one another. C) Photomicrograph of a bryolith from the Pliocene Rhodolith Rudstone beds. Bryoliths form thick encrustations around a nucleus creating millimeter-scale framework pores in addition to intraparticle pore space within zooecia. Individual bryoliths range from 4-7cm with ~2cm pore inside of the bryozoan nodule. D) Photomicrograph of a globular bryozoan from the Globular bryozoan-Clam Rudstone from the Miocene. This globular morphology forms extensive intraparticle porosity within individual zooecia. Both of the bryozoans in C and D are at the same scale, but note the difference in grain and pore size between encrusting and globular morphologies. E) Photomicrograph of sand- sized grains from the Miocene showing the abundant interparticle and intraparticle porosity within benthic foraminifera, bivalves, branching bryozoans, and echinoids. F) Photomicrograph of the dolomitized Bedded Foraminifera Wackestone from the Miocene. The calcisilts have been replaced by dolomite and many of the planktonic and benthic foraminifera are dissolved out.

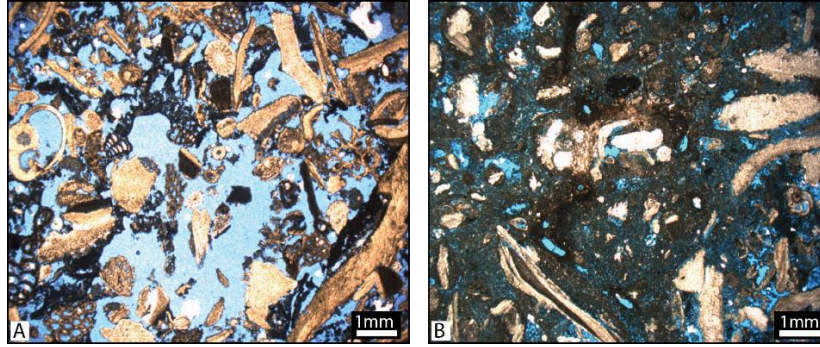


Figure 8: Photomicrographs comparing porosity between packstone lithofacies from the Pliocene. A) Interbedded Bivalve Packstone. This packstone is sorted and clean of matrix, creating abundant interparticle and intraparticle porosity. This lithofacies represents storm deposits that have been reworked by high energy waves and surges. B) Silt-Gravel Coralline Algae Packstone. This lithofacies is poorly sorted and has abundant matrix dispersed throughout it, occluding pore space. This lithofacies is interpreted to form from abraded sediment transported into *Poseidonia oceanica* grass beds that baffled and entrapped calcisilts.

Framework pores are abundant in coralline algae, especially within rhodoliths (Figure 7B). Although the pores within rhodoliths are up to 3mm, they occur within a skeletal framework, thereby leaving the pores disconnected. Finer-grained sands and calcisilts reduce interparticle porosity between rhodoliths and exhibit minor interparticle porosity (Appendix III). Bivalve fragments are primarily found associated with interparticle porosity (Figures 7E and 7A). At a larger scale, multiple centimeter-sized whole oysters and scallops create mm-cm scale shelter pores (Figure 5A) and are primarily found in the Bryozoan-Ostreid Rudstone and the Globular Bryozoan-Clam Rudstone in the Miocene, and the Ostreid-Pectinid Rudstone from the Pliocene.

Echinoids contain no intraparticle porosity but are found within lithofacies with extensive interparticle porosity (Figure 7A, 7E). Along with bivalves, benthic and planktonic foraminifera are the only other grains that are consistently dissolved, creating moldic porosity (Figure 7F). The only macroporosity in wackestone facies is developed through moldic foraminifera and intercrystalline porosity from the dolomitization of calcisilts.

Lastly, calcisilt reduces pore space (Figure 8) but is only a major factor in the Silty Coralline Algae Packstone, Silt-Gravel Coralline Algae Packstone from the Pliocene and lithofacies from the Bryozoan-Bivalve Rudstone Association from the Miocene. Overall, Pliocene deposits retain primary pores along with additional minor moldic porosity (Figure 5A, 7E).

PETROPHYSICAL DATASET

Descriptive Statistics

Porosity

Figure 9 shows the distribution of porosity values from both datasets. Pliocene mean values range from 29 to 53% among all lithofacies, whereas Miocene mean values range from 25 to 39%. In the Pliocene dataset, sorted packstones consistently contain the highest porosity values. Of these sorted packstones, the primary differences among them are the grain constituents. Packstones rich in bryozoans plot the highest, then coralline algae and bivalve-rich packstones, and lastly bivalve-only dominated packstones. This high porosity content within bryozoan-rich facies is consistent with the abundant intraparticle pores found within bryozoan skeletons (Figure 7C, D). This trend is also observed between the lithofacies of the Bioclastic Rudstone Association, as the Bryozoan-Coralline Algae Rudstone has a median porosity of 43% and the Bivalve-Coralline Algae Rudstone has a median porosity of 39%. Among the three most distal Pliocene rudstones, as coralline algae content increases, porosity increases (Figure 9A). Calcisilt-rich packstones have the lowest porosity. With the exception of the calcisilt-rich facies, porosity decreases from proximal to distal facies.

The Miocene porosity dataset (Figure 9B) appears to have a different trend than the Pliocene dataset, as porosity values are more variable, overall lower, and porosity does not show a decrease from proximal to distal facies. Median porosity values for packstones are highly variable (unlike the Pliocene) and packstone facies have some of the widest ranges of porosity. In addition, whole bivalve dominated rudstones have some of the highest values and lowest ranges, and rhodolith-rich facies have some of the lowest median values. The wackestones have high porosity, with median values greater than those of five of the packstone and rudstone facies.

Porosity distribution in diagenetic facies (Figure 10) shows that the low alteration of the Pliocene deposits results in retention of the highest porosity, mostly representing primary porosity. DF-2, 4, 5, and 6 have median values consistent with one another, all averaging at 36% porosity. DF-3 has the highest variance and lowest median and quartile values.

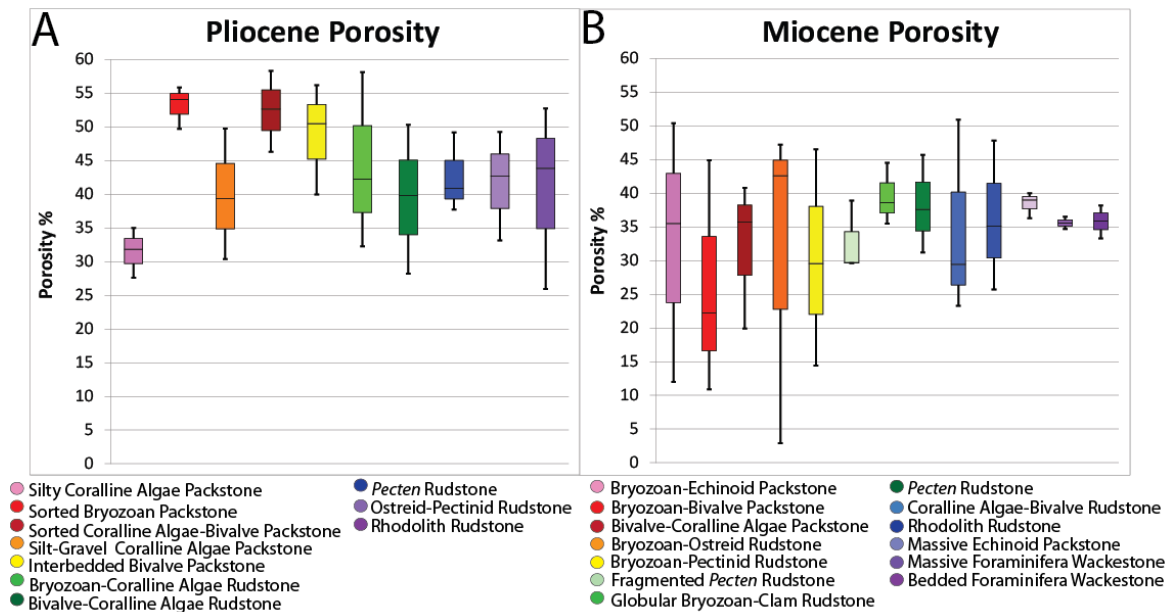


Figure 9: Box and whiskers plot of porosity distribution for both A) Pliocene and B) Miocene datasets. The first and third quartiles are the tops and bottoms of the boxes and the median is represented by the black line within each box. The maximum values and minimum values are represented by the top and bottom extensions. Facies are ordered from most proximal facies to the left of each chart to most distal facies on the right. Note that lithofacies colors do not correlate to the same lithofacies between the two datasets.

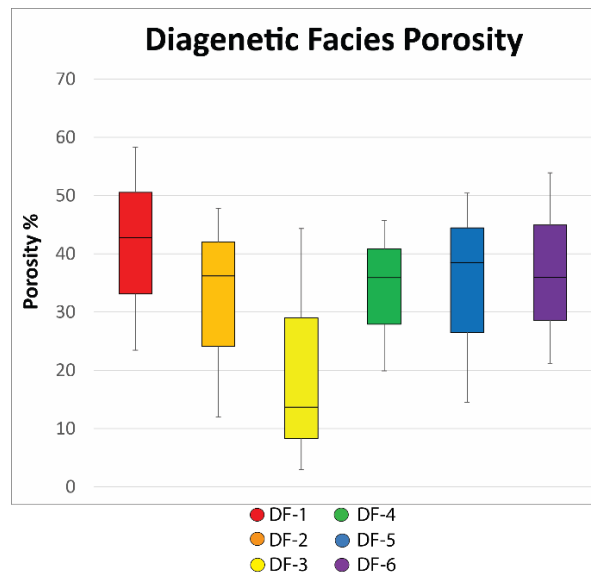


Figure 10: Box and whisker plots of porosity distribution of each of the six diagenetic facies. The first and third quartiles are the tops and bottom of the boxes and the median is represented by the black line within each box. The maximum values and minimum values are represented by the top and bottom extensions.

Permeability

Figure 11 shows the distribution of permeability values from both Pliocene and Miocene datasets. In the Pliocene, median permeability ranges from 186 to 11,881md, and in the Miocene, median permeability ranges from 54 to 1,496md. In the Pliocene, sorted packstones follow similar trends to their porosity distribution and consistently have the highest permeability values within a small range. The Bryozoan-Coralline Algae Rudstone and the *Pecten* Rudstone permeability values also reach those of the sorted packstones and have outliers that exceed them. Porosity values of the three most distal rudstones increase with rhodolith content whereas, their permeability values increase with a higher bivalve content (~17 to 60%) and decrease with increased rhodoliths. Both calcisilt-rich packstones have low median permeability values with the Silt-Gravel Coralline Algae Packstone on the higher end. With the exception of the silty packstone, permeability decreases from proximal to distal facies.

Permeability values of the Miocene are highly variable with greatest ranges within the five most proximal facies, especially the Bryozoan-Ostreid and Bryozoan-*Pecten* Rudstones. Although median permeability values of packstones are close to the average for the entire dataset, they have some of the highest first quartiles and ranges. The Globular Bryozoan-Clam Rudstone and the *Pecten* Rudstone have the highest and most consistent values, similar to porosity. Coralline algae-rich facies and the Bedded Foraminifera Wackestone plot amongst some of the lowest median values.

In addition to lithofacies and constituents, sedimentary structures such as massive beds, horizontal beds, and cross-beds have an effect on permeability values from both datasets. Examples include trough cross-beds and massive beds in the Interbedded Bivalve Packstone in the Pliocene, and horizontal and massive beds in both Miocene rudstones and wackestones.

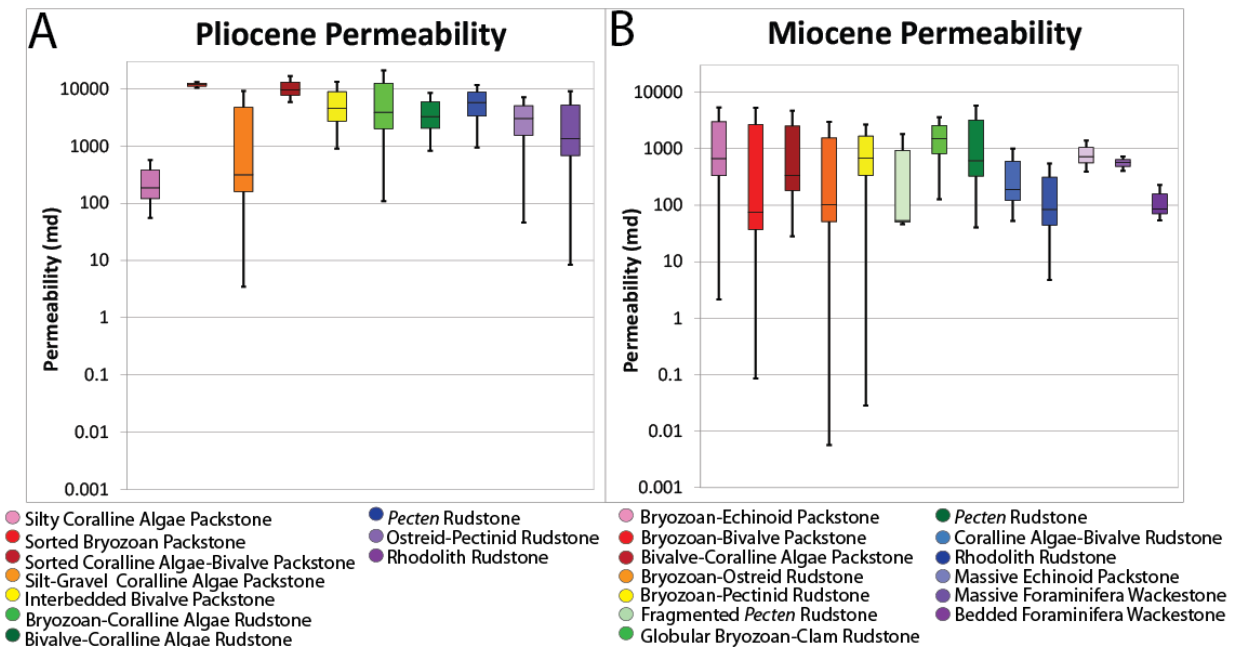


Figure 11: Box and whiskers plot of permeability distribution for both A) Pliocene and B) Miocene datasets. The first and third quartiles are the tops and bottom of the boxes and the median is represented by the black line within each box. The maximum values and minimum values are represented by the top and bottom extensions. Facies are ordered from most proximal facies to the left of each chart to most distal facies on the right. Note that lithofacies colors do not correlate to the same lithofacies between the two datasets.

The variation in the permeability within these bedding types is summarized in Table 2. Student t-tests (e.g. Student, 1908) were run to determine if variation in permeability values is random or due to the variations in bedding type. Student t-tests were only run for permeability, as porosity among the facies is identical or nearly identical (i.e. unaffected; Table 2). The differences of mean permeability values among bedding types in the Miocene rudstone lithofacies could not reject the null hypothesis, indicating there is not as statistically significant

Examples	Massive	Horizontal/Cross-Bedding	Alpha Value (p)
Miocene Rudstone	41%, 691md	39%, 878md	.8
Pliocene Packstone	51%, 7,551md	51%, 5,517md	.01
Miocene Wackestone	36%, 564md	36%, 109md	.00

Table 2: Results of the t tests. Student t-tests were run to determine if the differences between massive units and bedding create a statistically significant difference in petrophysical values. Porosity values are shown in percentage and permeability values are shown in millidarcies.

difference in permeability values between horizontal and massive beds in rudstone lithofacies at the 95% confidence level. The mean permeability values of the packstone and wackestone facies

showed statistically significant differences for different types of bedding. In both instances, permeability is higher in massive beds, indicating that bedding style makes a difference in packstone and wackestone lithofacies.

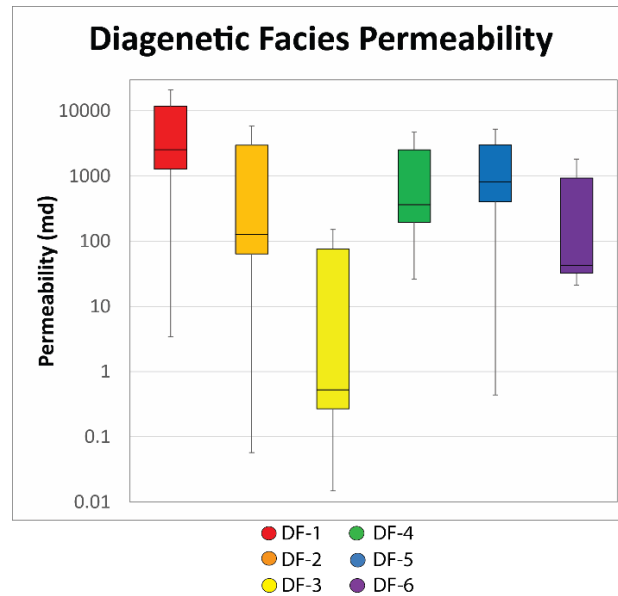


Figure 12: Box and whisker plots of permeability distribution of each of the six diagenetic facies. The first and third quartiles are the tops and bottoms of the boxes and the median is represented by the black line within each box. The maximum values and minimum values are represented by the top and bottom extensions.

Permeability by diagenetic facies (Figure 12) shows that the low alteration of the Pliocene facies have the highest permeability, which relates to preservation much of the primary pore system. In relation to porosity, DF-2, 4, 5, and 6 have about the same median porosity values, but in regards to permeability, these facies have different (tested at the 95% confidence level) median values and diverse ranges. The two dolomitized facies with high moldic porosity, DF-4 and DF-5, have the highest median values of the Miocene diagenetic facies. The least altered (DF-1) deposits and the uncemented 100% dolomite (DF-4, 5) deposits retain the highest permeability values.

Porosity and Permeability

Tables 3 and 4 show descriptive statistics for all petrophysical data from lithofacies of both datasets. Descriptive statistics for petrophysical data by diagenetic facies are summarized in (Table 5).

Pliocene Lithofacies Petrophysical Dataset Summary							
Lithofacies Association	Lithofacies	Range	Mean: ϕ Median: k	Standard Deviation	Coefficient of Variation	Equation of Line and R²: $x=\phi$ & $y=k$	Primary Pore Types
Silty Packstone Association	Silty Coralline Algae Packstone	ϕ : 27-35 k: 56-400	ϕ : 29 k: 186	ϕ : 3.45 k: 157.27	ϕ : .12 k: .76	$y = -1.5443x^3 + 153.98x^2 - 5024.1x + 53896$ polynomial R = 1	Interparticle Moldic Intraparticle
Sand-Gravel Packstone Association	Sorted Bryozoan Packstone	ϕ : 50-56 k: 10,447-13,137	ϕ : 53 k: 11,8882	ϕ : 2.7 k: 1,335	ϕ : .05 k: .11	$y = 251.28x^2 - 26565x + 712493$ polynomial R = 0.7251	Interparticle Intraparticle Moldic
	Silt-Gravel Coralline Algae Packstone	ϕ : 30-50 k: 3-9,229	ϕ : 40 k: 315	ϕ : 4.45 k: 2,082	ϕ : .14 k: 1.66	$y = 0.01e^{0.2643x}$ expon. R = 0.6676	Interparticle Intraparticle Moldic
	Sorted Coralline Algae-Bivalve Packstone	ϕ : 46-58 k: 5,871-16,636	ϕ : 52 k: 9,589	ϕ : 5.63 k: 4,160	ϕ : .09 k: .41	$y = 794.79x - 31164$ linear R = 0.721	Interparticle Intraparticle Moldic
	Interbedded Bivalve Packstone	ϕ : 40-56 k: 903-13,226	ϕ : 50 k: 4,506	ϕ : 5.24 k: 2,827	ϕ : .11 k: .57	$y = 7.497e^{0.1258x}$ expon. R = 0.7204	Interparticle Moldic Intraparticle
Bioclastic Rudstone Association	Bryozoan-Coralline Algae Rudstone	ϕ : 23-58 k: 14-21,039	ϕ : 43 k: 3,776	ϕ : 7.34 k: 5,463	ϕ : .17 k: 1.07	$y = 1E-08x^{6.9929}$ power R = 0.5569	Interparticle Intraparticle Moldic
	Bivalve-Coralline Algae Rudstone	ϕ : 28-50 k: 823-8,561	ϕ : 40 k: 3,277	ϕ : 6.55 k: 2,419	ϕ : .17 k: .61	$y = -2.7442x^3 + 324.12x^2 - 12337x + 154679$ polynomial R = 0.2535	Interparticle Moldic Framework
Rhodolith-Bivalve Rudstone Association	<i>Pecten</i> Rudstone	ϕ : 38-49 k: 939-10,957	ϕ : 43 k: 5,767	ϕ : 4.18 k: 8,408	ϕ : .1 k: .95	$y = -13.887x^4 + 2465.6x^3 - 163517x^2 + 5E+06x - 5E+07$ polynomial R = 0.5881	Interparticle Moldic Shelter
	Ostreid-Pectinid Rudstone	ϕ : 33-49 k: 91-7,111	ϕ : 43 k: 3,866	ϕ : 5.82 k: 2,539	ϕ : .14 k: .81	$y = 2E-12x^{9.2349}$ power R = 0.739	Interparticle Moldic Framework
	Rhodolith Rudstone	ϕ : 26-53 k: 8-9,042	ϕ : 42 k: 1,350	ϕ : 6.99 k: 2,328	ϕ : .17 k: .90	$y = 1.7205e^{0.1516x}$ expon. R = 0.4936	Framework Intraparticle Interparticle

Table 3: Petrophysical summary chart of the Pliocene dataset. Ranges, means, medians, and standard deviations were used as input parameters in the Petrel™ models. Coefficients of variation are calculated by dividing the standard deviation by the mean of each value. Coefficients of variation <1 show low variation and values >1 show high variation. Equations of line and R² values are the results of regressions from Figure 14A. Primary pore types are ordered from most abundant to least abundant.

Miocene Lithofacies Petrophysical Dataset Summary							
Lithofacies Association	Lithofacies	Range	Mean: ϕ Median: k	Standard Deviation	Coefficient of Variation	Equation of Line and R ² :	Pore Type
Cross- Bedded Packstone Association	Bryozoan-Echinoid Packstone	ϕ : 33-50 k: 2-5,354	ϕ : 33 k: 667	ϕ : 11.8 k: 2,256	ϕ : .35 k: 1.3	$y = 0.4568e^{0.1891x}$ expon. R = 0.6	Moldic Interparticle Intraparticle
	Bryozoan-Bivalve Packstone	ϕ : 11-45 k: .1-5,253	ϕ : 25 k: 74	ϕ : 12.6 k: 1,405	ϕ : .51 k: 2.51	$y = 5E-08x^{6.3823}$ power R = 0.8648	Interparticle Moldic Intraparticle
	Bivalve-Coralline Algae Packstone	ϕ : 20-41 k: 28-4,679	ϕ : 34 k: 335	ϕ : 6 k: 1,268	ϕ : 17 k: 1.46	$y = 31.292e^{0.074x}$ expon R = 0.1058	Moldic Interparticle Intraparticle
Bryozoan-Bivalve Rudstone Association	Bryozoan-Clam Rudstone	ϕ : 3-47 k: .01-2995	ϕ : 35 k: 102	ϕ : 15.7 k: 1,186	ϕ : .45 k: 1.67	$y = 0.0068e^{0.2505x}$ expon R = 0.9428	Moldic Interparticle Vug
	Bryozoan- <i>Pecten</i> Rudstone	ϕ : 15-47 k: .1-2,655	ϕ : 31 k: 950	ϕ : 12 k: 961	ϕ : .38 k: .98	$y = 1823.5\ln(x) - 5094.5$ logarithmic R = 0.6545	Interparticle Intraparticle Moldic
Bivalve Rudstone Association	Fragmented <i>Pecten</i> Rudstone	ϕ : 30-39 k: 46-1,817	ϕ : 33 k: 53	ϕ : 5.3 k: 1,020	ϕ : .16 k: .16	$y = 0.0005e^{0.389x}$ expon. R = 0.9994	Interparticle Moldic Intraparticle
	Globular Bryozoan-Clam Rudstone	ϕ : 36-45 k: 128-3,611	ϕ : 39 k: 1,496	ϕ : 3.1 k: 1,070	ϕ : .08 k: .74	$y = 1E-14x^{10.574}$ power R = 0.6998	Interparticle Intraparticle Moldic
	<i>Pecten</i> Rudstone	ϕ : 31-46 k: 41-5,814	ϕ : 38 k: 656	ϕ : 3.5 k: 1,418	ϕ : .09 k: 1.27	$y = 198.73x - 6444.3$ linear R = 0.2359	Moldic Interparticle Intraparticle
Coralline Algae Rudstone Association	Coralline Algae-Bivalve Rudstone	ϕ : 26-54 k: 53-1006	ϕ : 34 k: 209	ϕ : 7.8 k: 311	ϕ : .23 k: 1.08	$y = 0.3229x^2 + 8.6x - 380.23$ polynomial R = 0.7732	Moldic Interparticle Intraparticle
	Rhodolith Rudstone	ϕ : 26-48 k: 26-544	ϕ : 35 k: 84	ϕ : 5.3 k: 120	ϕ : .15 k: .97	$y = 0.0003x^{3.5094}$ power R = 0.2502	Framework Interparticle Intraparticle
Foraminifera Wackestone and Packstone Association	Massive Echinoid Packstone	ϕ : 36-40 k: 394-1,383	ϕ : 39 k: 722	ϕ : 1.5 k: 392	ϕ : .04 k: .5	$y = 148.97x - 4958$ linear R = 0.3257	Interparticle Moldic
	Massive Foraminifera Wackestone	ϕ : 35-37 k: 407-721	ϕ : 36 k: 564	ϕ : 1.3 k: 222	ϕ : .04 k: .39	$y = 174.44x - 5646.2$ linear R = 1	Moldic Intercrystalline Interparticle
	Bedded Foraminifera Wackestone	ϕ : 33-38 k: 54-228	ϕ : 36 k: 87	ϕ : 1.8 k: 60.6	ϕ : .05 k: .56	$y = 19.315x^2 - 1360.6x + 24012$ polynomial R = 0.8416	Moldic Intercrystalline Interparticle

Table 4: Petrophysical summary chart of the Miocene dataset. Ranges, means, medians, and standard deviations were used as input parameters in the Petrel™ models. Coefficients of variation <1 show low variation of each dataset within lithofacies and values >1 show high variation. Equations of line and R² values are the results from regressions from Figure 14B. Primary pore types are ordered from most abundant to least abundant.

Overall, Pliocene rudstone facies have lower petrophysical values than sorted Pliocene packstones, while Miocene packstones have a wide distribution of petrophysical values and in only some instances yield higher petrophysical values than Micoene rudstone facies (Figures 9 and 11). The amount of variation within lithofacies and diagenetic facies is quantified by the

coefficient of variation and is displayed in Tables 3, 4, and 5. Coefficient of variation averages for porosity from both field areas are .22; averages are .79 for permeability in the Pliocene and 1.2 for the Miocene, highlighting the enhanced variation to permeability caused by diagenesis.

Diagenesis Petrophysical Dataset Summary					
Diagenetic Facies	Range	Mean: ϕ Median: k	Standard Deviation	Coefficient of Variation	Pore Type
DF-1: Pliocene	ϕ : 23-58 k: 3-21,039	ϕ : 43 k: 2,439	ϕ : 7.38 k: 4,125	ϕ : .27 k: 1.69	Interparticle Intraparticle Framework
DF-2: Calcite Low Cement Low Moldic Porosity	ϕ : 12-48 k: .06-5,814	ϕ : 35 k: 1,101	ϕ : 8.4 k: 1,595	ϕ : .24 k: 1.45	Interparticle Intraparticle Moldic
DF-3: Calcite High Cement Moldic Porosity	ϕ : 3-44 k: .01-152	ϕ : 18 k: 21	ϕ : 13.48 k: 48.7	ϕ : .75 k: 2.31	Moldic Intraparticle Interparticle
DF-4: Dolomitized Low Cement Moldic Porosity	ϕ : 20-46 k: 26-4,679	ϕ : 36 k: 838	ϕ : 4.14 k: 1,177.12	ϕ : .12 k: 1.4	Moldic Interparticle Intraparticle
DF-5: Dolomitized High Cement Moldic Porosity	ϕ : 26-50 k: 13-5,253	ϕ : 40 k: 1,102	ϕ : 7.53 k: 1,606.38	ϕ : .19 k: 1.18	Moldic Interparticle Intraparticle
DF-6: Overdolomitized and/or Low Moldic Porosity	ϕ : 21-54 k: 28-1,817	ϕ : 34 k: 478	ϕ : 6.52 k: 542.1	ϕ : .19 k: 1.14	Interparticle Moldic

Table 5: Petrophysical summary chart of the diagenetic facies dataset in the Pliocene and the Miocene.

Table 6 shows a direct comparison of petrophysical values of lithofacies equivalents from the Pliocene (DF-1), less altered Miocene (DF-2), and diagenetically altered Miocene (DF-3, 4, 5, and 6). This table highlights the abrupt decrease in petrophysical values, especially permeability, as diagenetic alteration increases. The abruptly decreasing trend is most apparent in packstone facies.

Lithofacies	Pliocene (DF-1)	Less Altered Miocene (DF-2)	Altered Miocene (DF-3, 4, 5, and 6)
Bryozoan-Echinoid Packstone (similar)	53% 11,881md	43% 5,279md	30% 141md
Bryozoan (branching)- <i>Pecten</i> Rudstone	-----	40% 1,908md	21% 77md
<i>Pecten</i> Rudstone	43% 4,371md	40% 851md	38% 594md
Rhodolith Rudstone	42% 1,350md	35% 84md	-----

Table 6: Diagenetic variations in porosity and permeability from three lithofacies. Permeability values for each lithofacies are represented by median values. There is no Bryozoan-Echinoid Packstone in the Pliocene, however the Sorted Bryozoan Packstone is similar and is used as a proxy in this table. There is no Pliocene equivalent of the Bryozoan-*Pecten* Rudstone, and therefore, it is left blank.

Lastly, Table 7 shows the results of t-test and F-tests (e.g. Fisher, 1921; Snedecor and Cochran, 1989) for porosity and permeability based on rock texture. This table also includes a summary of mean porosity and mean and median permeability values grouped by textures and diagenetic facies. This summary is included to highlight the differences between the textures and alteration from both datasets. The t-tests were run to determine whether or not mean values of lithofacies textures are significantly different or are not statistically distinguishable. Results from the Pliocene deposits show that means of each textural group are statistically distinct based on an alpha of .05. For porosity values of the Miocene deposits, however, only a comparison between the packstones and rudstones allow rejection of the null hypothesis. For permeability, rudstones, packstones, and wackestone all fail to show statistically distinctive means. It is apparent however, from Figures 9 and 11 that permeability values for the Miocene rudstones, packstones, and wackestones have visible differences. For this reason, F-tests were run to test the statistical significance of variance of ranges between textures. In all instances, the null hypothesis was rejected, showing statistically significant differences in variance amongst all textures (Table 7).

Strata	Lithofacies	Mean: ϕ	Mean: k Median: k	Student-t test: P Values for Porosity	Student-t test: P Values for Permeability	F-test: P Values for Porosity	F-test: P Values for Permeability
Pliocene Clinothem	DF-1 Rudstone	42.3%	4,200md 2,538md	P< .00	P< .00	P< .00	P< .00
	DF-1 Silty Packstone	38.3%	1,129md 350md	P< .00	P< .00	P< .00	P< .00
	DF-1 Sorted Packstone	51.3%	7,503md 6,230md	P< .00	P< .00	P< .00	P< .00
Miocene Ricardillo Area	DF-2 Rudstone	40%	1,888md- no distal rhodoliths (mean) 1,383md- no distal rhodoliths (mean) 379md- with distal rhodoliths (median value)	To PS=.02 To WS=.87	To PS=.44 To WS=.24	To PS=.00 To WS=.00	To PS=.01 To WS=.02
	DF-3-6 Rudstone	34%	693md 252md				
	DF-2 Packstone	43%	5,131md 5,279 md	To RS=.02 To WS=.01	To RS=.44 To WS=.84	To RS=.00 To WS=.00	To RS=.01 To WS=.00
	DF-3-6 Packstone	32%	700md 313 md				
	DF-4 Wackestone	36%	210md 115md	To RS=.87 To PS=.01	To RS=.44 To PS=.84	To RS=.00 To PS=.00	To RS=.02 To PS=.00

Table 7: Averages of porosity and permeability categorized by rock texture and diagenesis. Results of t- and F-tests for each textural groups are also displayed and were only analyzed for rock textures. Student-t and F-test results are displayed for both porosity and permeability. An alpha (P) value of $\leq .05$ was set to indicate a statistically significant difference (95%). Student-t tests test the mean value of each group while F-tests test the variance of each group. PS represents packstone, RS represents rudstone, and WS represents wackestone.

Petrophysical Correlations

Diagenesis and Petrophysics

Porosity and permeability trends show a positive relationship and are plotted with power-law, exponential, and linear regression models for each dataset (Figure 13), each to achieve the best fit to the data. As porosity increases permeability increases in each diagenetic facies with the exception of DF-3. Of the Miocene facies, DF-4 and DF-5's trendlines plot the highest and run nearly parallel to the trendlines of DF-1 and DF-2. DF-6 has a shallower slope than the others, indicating that for DF-6, permeability does not increase at the same rate as porosity. The extensively cemented (calcite) samples of DF-3 have the lowest values, and show a negative

correlation between porosity and permeability: i.e. as porosity increases, permeability decreases.

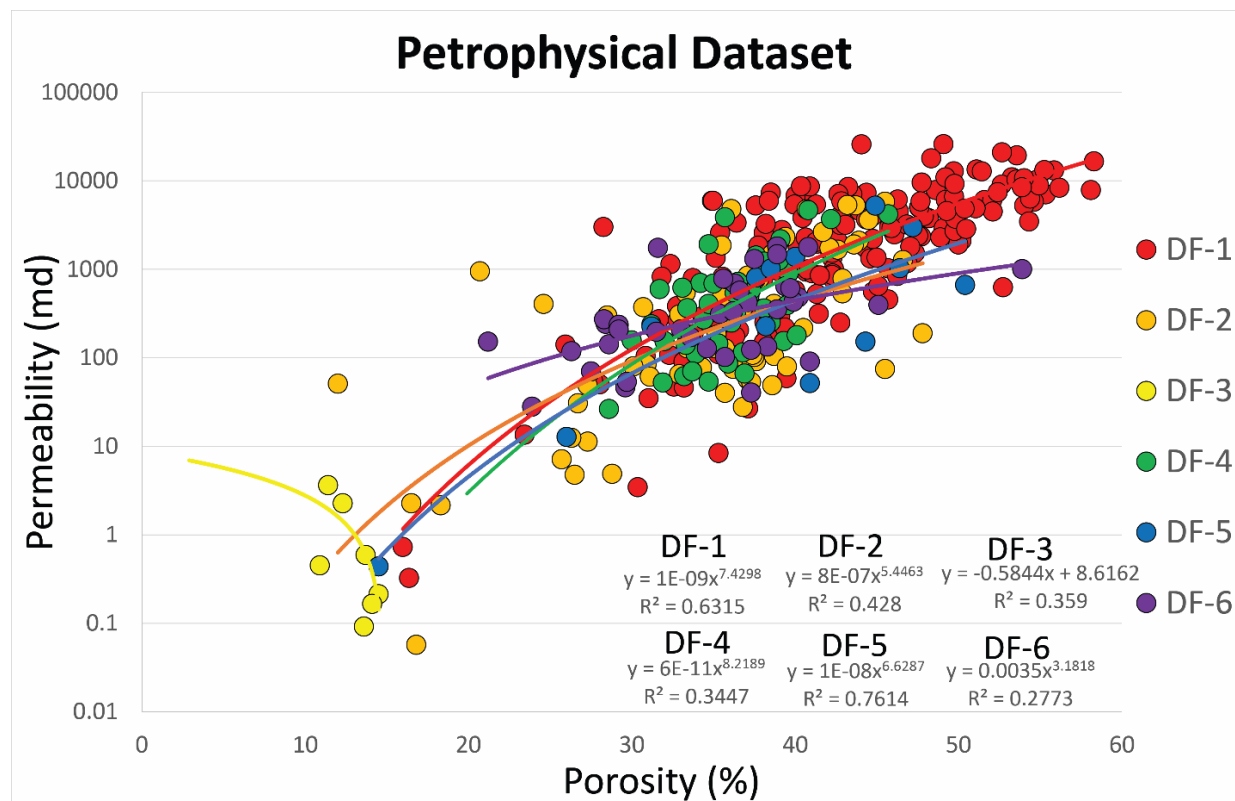


Figure 13: Petrophysical dataset for each field area. The data are grouped by diagenetic facies. Note how the Pliocene (DF-1) samples plot at higher magnitudes than the altered Miocene samples. Regressions were run on each dataset and equations of each line and their associated R² values are included on the graph.

Figure 14 shows the correlation between percent moldic porosity and percent of the mineral in the rock that is dolomite rather than calcite. Strata that have undergone dolomitization show a positive correlation with percent moldic porosity; this is consistent with the Li et al. (2013) diagenetic model. Greater than 49% dolomite content, moldic porosity values increase from about 5% to 20%, showing high variance at the highest dolomite contents. The majority of the entirely dolomitized samples, however, have moldic porosity >15%.

There is a somewhat predictable effect of diagenesis on certain components of the cyclothems in the Miocene. In 77% of the examples, the capping packstone facies is diagenetically altered to a greater extent than the underlying, rudstone facies, whether by dolomitization, calcite cementation, or dissolution.

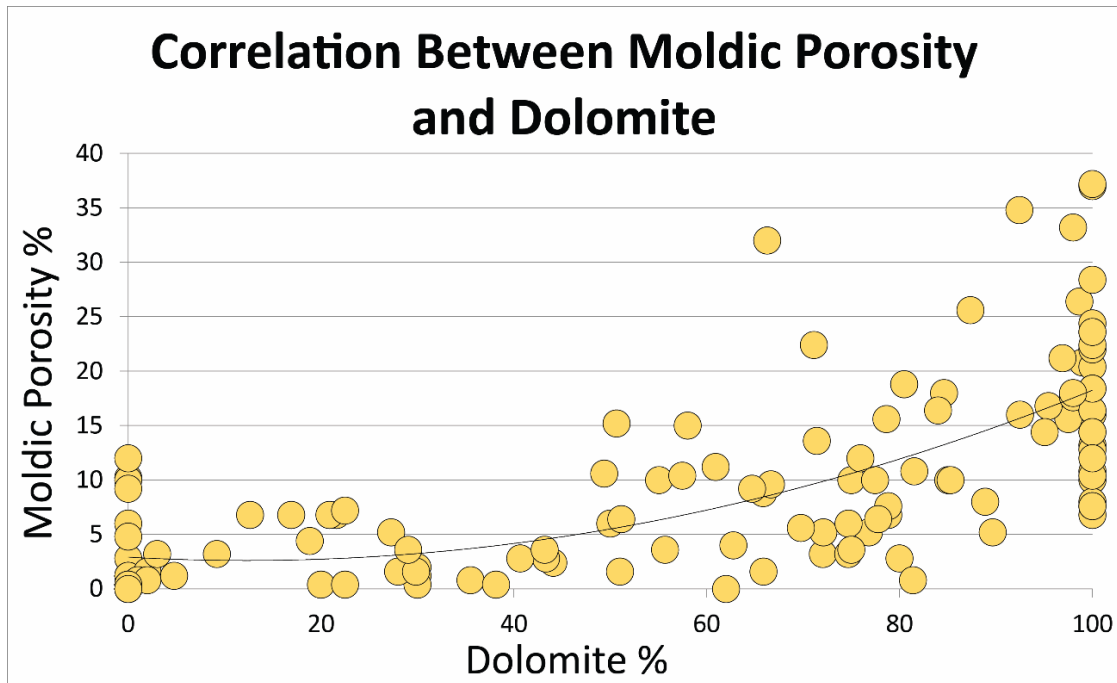


Figure 14: Correlation between moldic porosity and dolomite amount. Overall, as dolomite content increases, moldic porosity increases. Equation of the line and R^2 values are as follows: $y = 0.002x^2 - 0.0499x + 2.9077$, $R^2 = 0.5039$. The dolomite content here represents the total percent dolomite of the minerals in the rock. It is similar to: $\text{dolomite}/(\text{calcite} + \text{dolomite})$, but expressed as percent.

This increased alteration and diverse types of alteration cause enhanced variability in the distribution of petrophysical values in Miocene packstones. This enhanced alteration can lead to either lower or higher porosity and permeability values, depending on the diagenetic facies. For example, DF- 5 (Tables 1 and 5E) deposits have been entirely dolomitized and have undergone extensive dissolution. Where late-stage poikilotopic cement has not reduced those pore spaces, permeability and porosity average 734md and 44% respectively. Where poikilotopic cementation has reduced pore space, (DF-5) these values decrease to 13md and 26% porosity. In DF-6 (Tables 1 and 5F) overdolomitization and minor dissolution create permeability and porosity values of 324md and 33.8% respectively. Lastly, pores from DF-3 (Tables 1 and 5C) have been occluded by extensive calcite cementation, and petrophysical values only average 1.06md permeability and 12.9% porosity, highlighting the diversity of petrophysical values of diagenetically altered packstone facies.

Dolomitization also appears to exert a major control on the petrophysical values of

calcsilt-rich facies, and this is related to the paleotopographic position and increased likelihood for dolomitization in distal settings. The distal facies, Bedded Foraminifera Wackestone, contains 22% calcsilt. This lithofacies has been 100% dolomitized, and the calcsilt is replaced by coarse dolomite. Porosity averages 36% and median permeability values are 87md in this lithofacies. In contrast, a 50cm thick bed in the proximal facies, Bryozoan-Echinoid Packstone, contains only 7% calcsilt matrix, is 100% calcite. The calcsilts have not been replaced by coarser crystals. Average porosity is 14% and median permeability is 5md in this thin bed. Calcsilts that are replaced by dolomite have high porosity and permeability, and calcsilts that remain calcite have lower porosity and permeability.

Lithofacies and Petrophysics

Correlations of porosity to permeability by lithofacies are shown in Figure 15. Many of these trends show high (close to 1) R^2 values (Tables 3 and 4), indicating strong correlation between porosity and permeability by lithofacies. For the Pliocene dataset (Figure 15A), rudstones have the lowest R^2 values, in some instances indicating little to no correlation. Petrophysical values of sorted packstones have the highest correlations (>0.7). With the exception of the two calcsilt-rich packstones and the *Pecten* Rudstone, all correlations show an increase of permeability as porosity increases and generally parallel one another with similar slopes. The calcsilt-rich packstones, however, have inconsistent trends and wide distributions. The *Pecten* Rudstone has a nonlinear (4th order polynomial) distribution and although it has some of the highest permeability values, its porosity peaks at 49%; other lithofacies with similar permeability have porosity values that reach up to nearly 60%.

Petrophysical correlations by lithofacies in the Miocene (Figure 15B) show a different distribution than those of the Pliocene (Figure 15A). All lithofacies (rudstones, wackestones,

and the Massive Echinoid Packstone) with the exception of lithofacies from the Cross-Bedded Packstone Association show a positive correlation between porosity and permeability. The Bryozoan-*Pecten* Rudstone is the only lithofacies with a logarithmic distribution and samples from this lithofacies plot in three distinct groups, from some of the highest to some of the lowest values. In coralline algae-rich rudstones, the Rhodolith Rudstone has a low gradient slope where porosity values increase at a greater rate than permeability values. The Coralline Algae-Bivalve Rudstone, which is abundant with coralline algae but not rhodoliths, has higher permeability, lower porosity, and a steeper slope than the Rhodolith Rudstone.

Grain Sorting, Grain Size, and Petrophysics

Figure 16 displays the correlations between lithological textures and petrophysical correlations. The Pliocene plot (Figure 16A) shows that all packstones plot along a narrow and linear distribution with sorted packstones consistently plotting higher and calcisilt-rich facies plotting lower. Rudstones have a scattered distribution with no specific correlation.

The Miocene textural lithofacies data (Figure 16B) do not directly compare to the Pliocene data. For the Miocene, packstones do not show the highest petrophysical values and rudstones fit along a more consistent linear correlation. The primary observation from this figure is the petrophysical differences between systems that are controlled by deposition (Pliocene) and systems controlled by both deposition and diagenesis (Miocene).

Figure 17 shows the distribution of porosity and permeability plotted against grain size, and classified by grain sorting. These grain size determinations do not include calcisilt matrix, only measurements of sand and coarser components. The scattered distribution and lack of a correlation indicates that grain size has no direct control on petrophysical values.

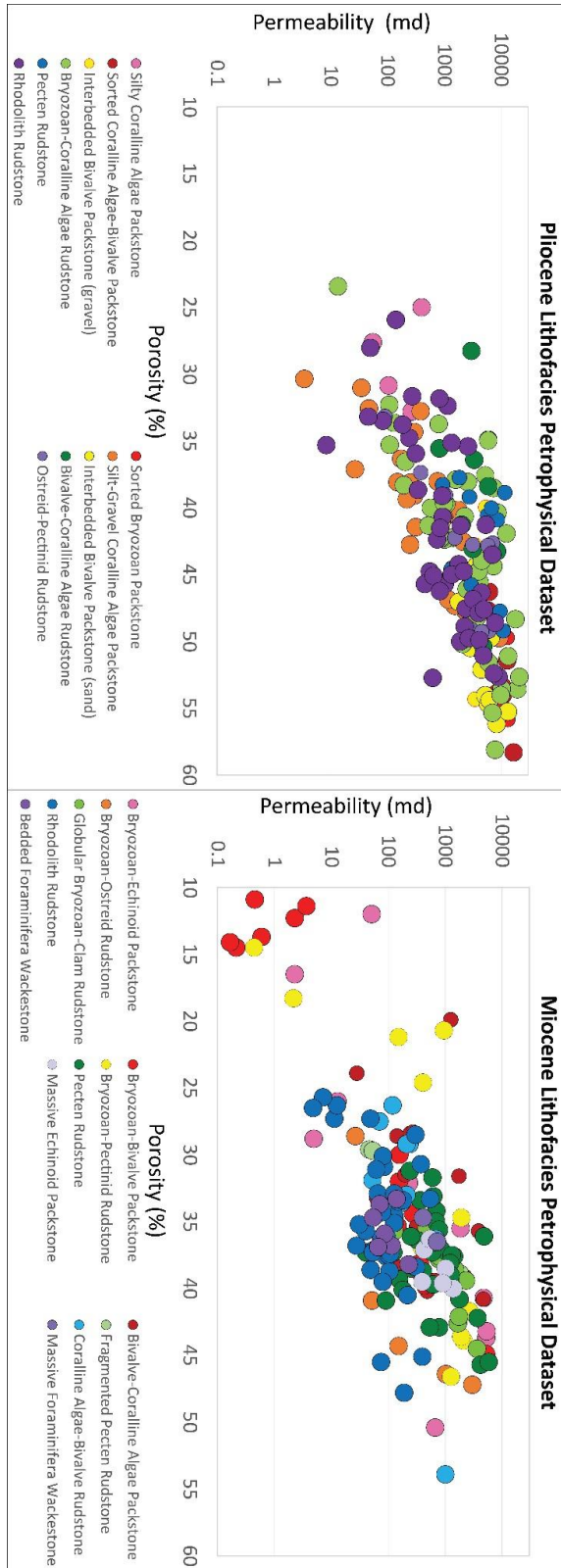


Figure 15: Petrophysical distribution of the Pliocene and Miocene datasets grouped by lithofacies. Equations of line and R^2 values are displayed in Tables 3 and 4.

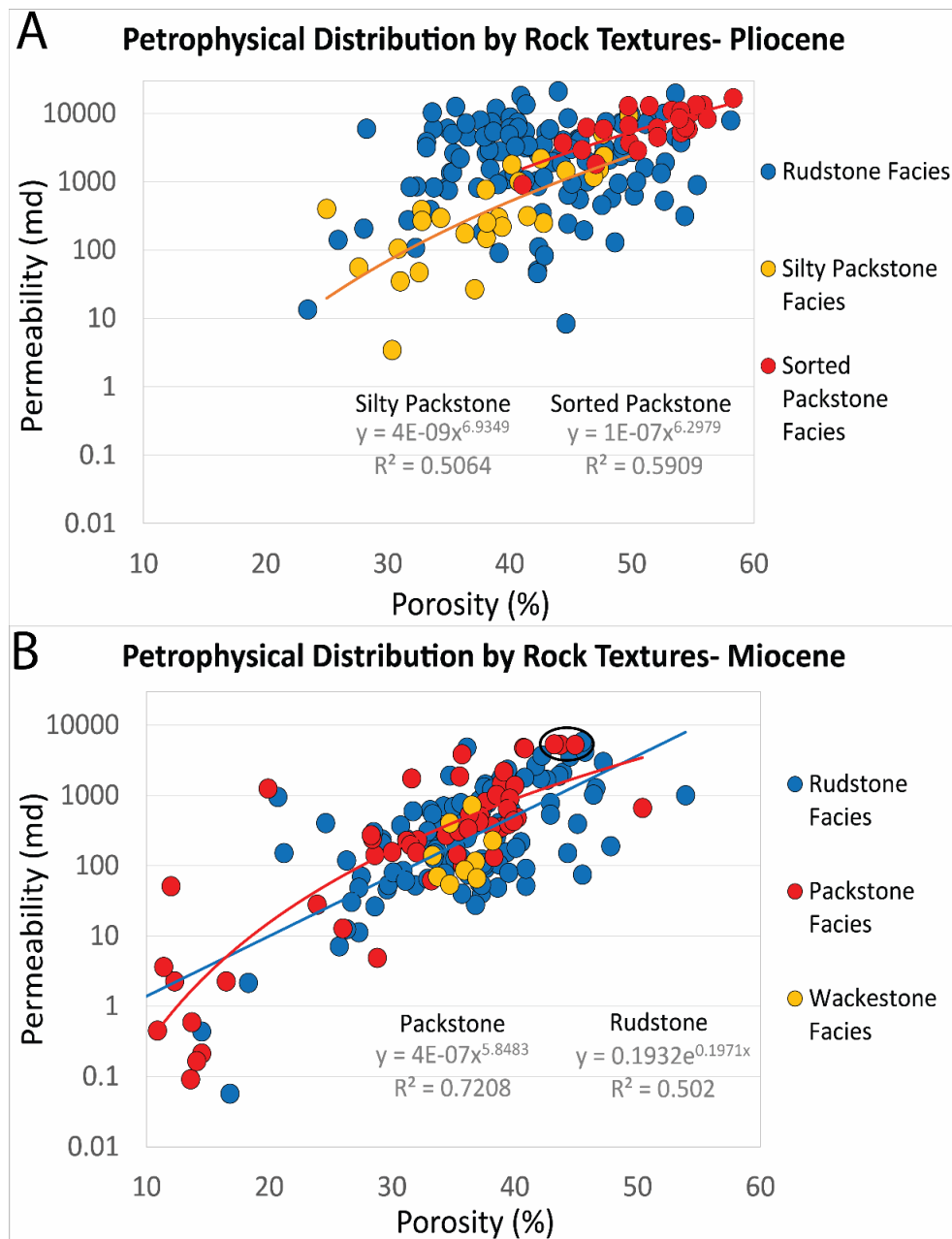


Figure 16: Petrophysical distribution by rock texture for the A) Pliocene and B) Miocene deposits. No trendlines were developed for the rudstone facies or the wackestone facies due to low correlation. The other regression equations and R^2 values are displayed on the plot. Note the difference in distribution and correlation by rock texture between the two datasets. The sorted packstones from DF-2 are circled on the Miocene graph (B).

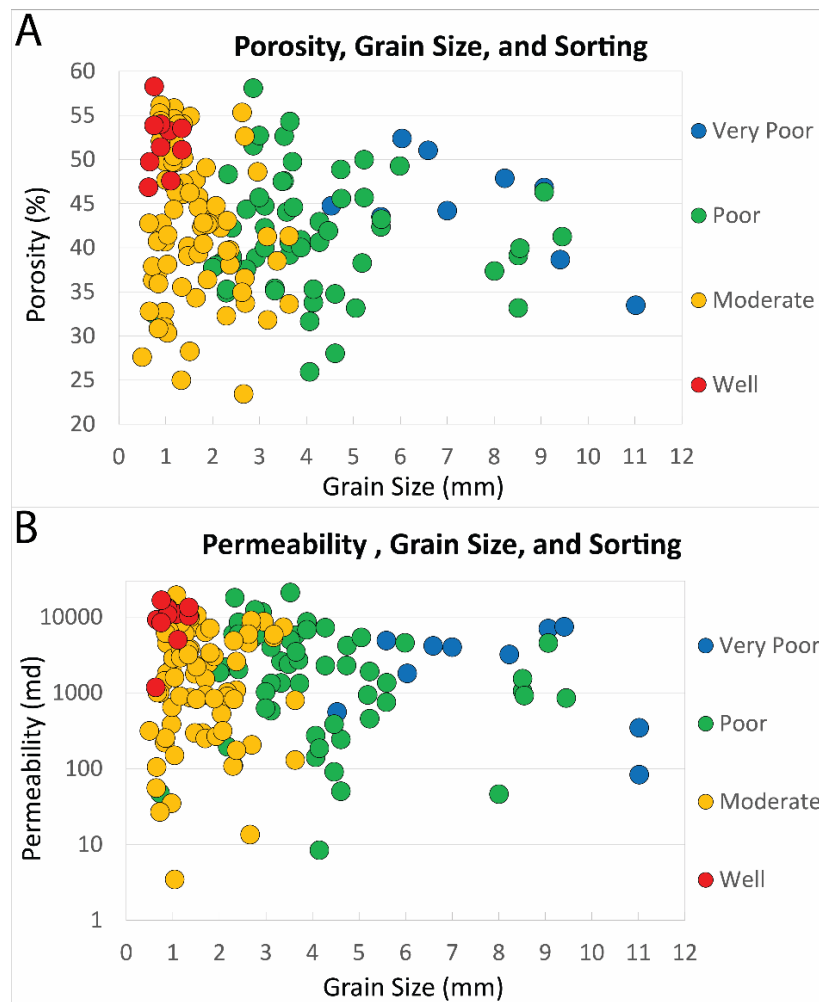


Figure 17: A) Porosity plotted against grain size, and grouped by sorting classification sorting grouped for the Pliocene. A) Permeability plotted against grain size, and grouped by sorting classification sorting grouped for the Pliocene. Note that the scattered data show no direct correlation between petrophysical values and grain size. However grain size and sorting do develop distinct groups.

Lastly, Figure 18 shows the correlation between porosity and permeability classified by grain sorting for the Pliocene deposits. All classifications show positive trends and all correlations are similar. The correlations for poor and moderate sorting are nearly identical. The correlation for well sorted samples is the only one that does not fit a power log model and has a polynomial distribution. It has an abrupt decrease in permeability ($\sim 4,000$ md) with only a minor decrease in porosity (2%). Indicating higher variation in permeability than porosity. Although moderately sorted samples show some of the highest petrophysical values, a portion of these samples have lower petrophysical ranges than those of their main grouping.

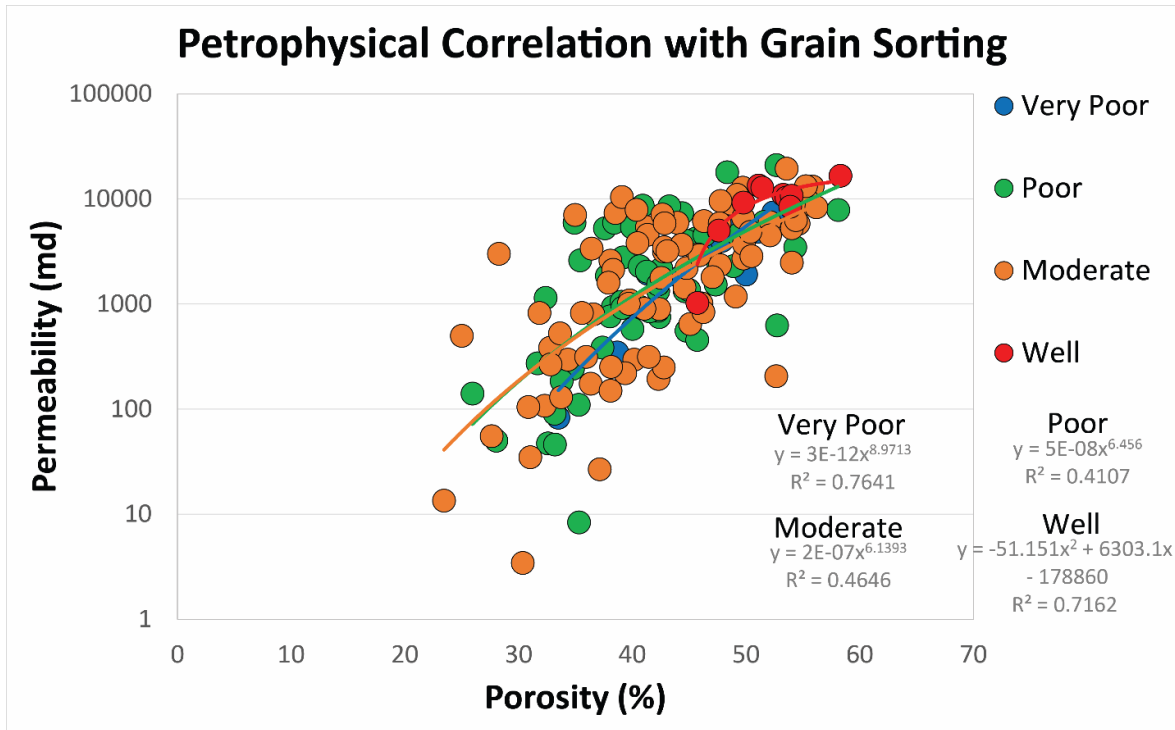


Figure 18: Correlation of porosity, permeability, and grain sorting classification. Trendlines and R^2 values for each line are displayed on the plot. The well and very poorly sorted classifications have the best fit lines. The petrophysical correlation between the moderate and poorly sorted samples are nearly identical.

Petrophysical Distribution in Fining-Upward Trends

Pliocene

Porosity and permeability curves for each of the six depositional profiles (DP) found in the Pliocene clinothem (Pugliano, et al., 2015; Chapter 2) are displayed in Figure 19. These curves represent stacked, lateral lithofacies depositional profiles that have prograded, depositing finer-grained proximal deposits stratigraphically above coarser, more distal deposits. As these lateral trends prograde, they form a shoaling- and fining-upward cycle. Vertical trends produced by progradation of DP-1, DP-1a, DP-1b, and DP-2 (Figure 19A, 19B, 19C, and 19D) show a general increase in both porosity and permeability upward with minor fluctuation. DP-1 and DP-2 are capped by the Silty Coralline Algae Packstone, causing an abrupt decrease in petrophysical values at the tops of the upward-increasing porosity and permeability trends.

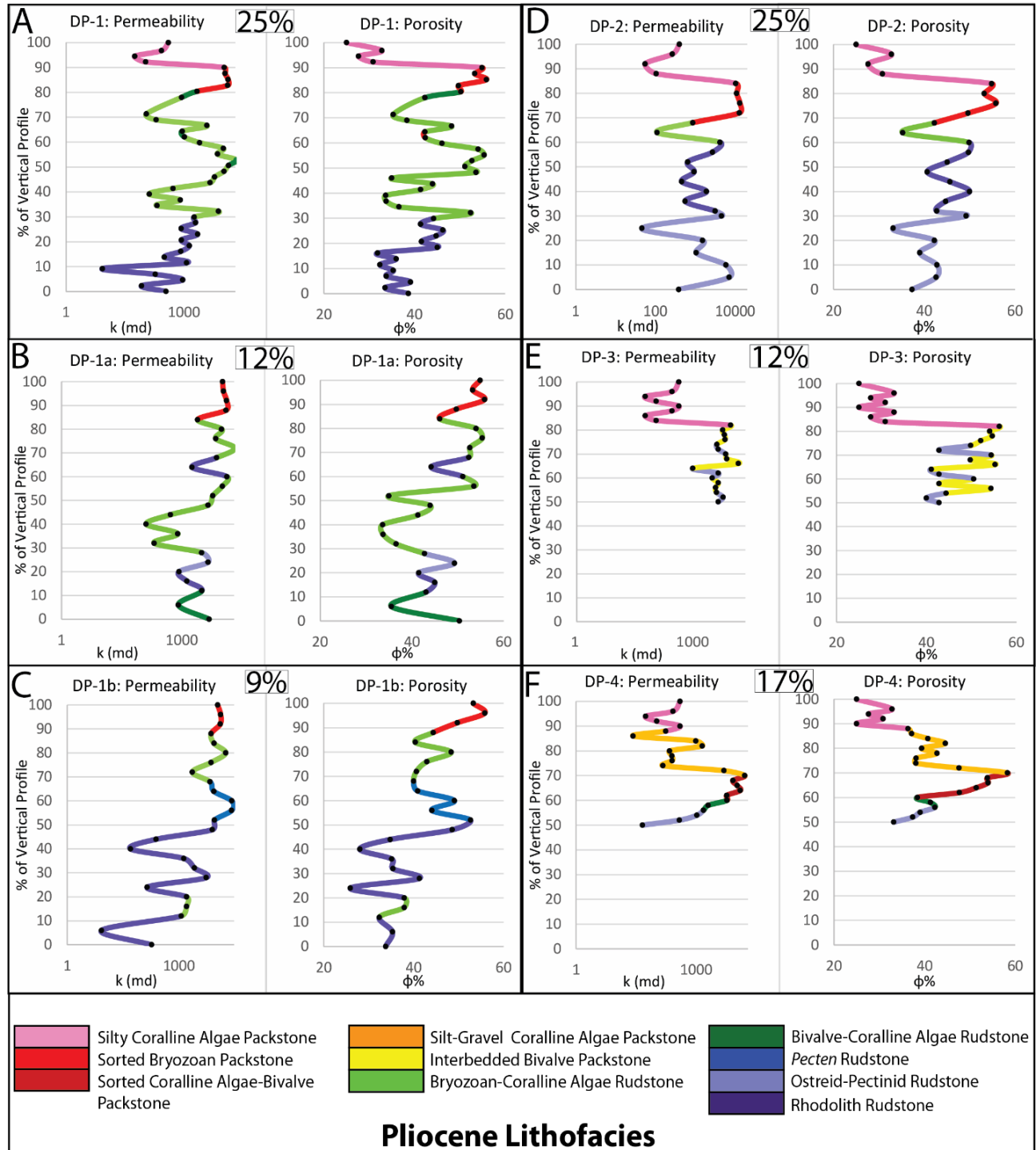


Figure 19: Vertical petrophysical curves produced by synthesizing progradation of each of the six depositional profiles from the Pliocene clinothem. Each curve is colored based on the lithofacies from which petrophysical data originates. The y-axis represents the percentage of the clinothem that each lithofacies takes up for that particular profile. These are generated by stacking progradational facies from time-equivalent transects onto one another. These are pseudo-petrophysical logs and may be similar to wireline logs measured from subsurface data. Percentages reflect abundance of the particular depositional profile.

This lower porosity and permeability cap is found in 66% of the cycles. DP-1a and DP-1b do not include this low-permeability capping facies and show an increase in petrophysical character upward, throughout the entire cycle. DP-3 and DP-4 (Figure 19E and F) represent shallower-water facies (compared to the other cycles) of clinothem deposits (Pugliano et al., 2015; Chapter 2). These profiles can be thought of as incomplete cycles that develop towards the top of the clinothem. They do not show as great a change in water depth as the other profiles, and therefore do not show the same vertical petrophysical trend as the other cycles do. The upward petrophysical trends found in these two cycles ends more abruptly and is capped with calcisilt-rich packstones. DP-3 contains interbedded rudstones and packstones, the rudstones have lower petrophysical values, creating major variability. DP-4 is the only profile to contain the Silt-Gravel Coralline Algae Packstone in addition to the Silty Coralline Algae Packstone. This increases the total thickness of the calcisilt-rich packstone portion of the cycle, decreasing petrophysical values in a high percentage of the vertical profile.

Miocene

The Miocene deposits along Ricardillo preserve grain-rich cyclothem that fine upward in association with shoaling. Less common deepening-upward trends at the base of some of the cyclothem (proximal and most distal locations) show coarsening-upward trends that are overlain by a fining-upward trend.

Figure 20 shows the petrophysical distribution in cycles plotted along measured sections from proximal, medial, and distal paleotopographic positions of Ricardillo. Out of the thirteen, fining-upward cycle patterns (cycles with both packstones and rudstones), only six (46%) of them show petrophysical values that increase vertically from rudstone to packstone P (proximal section)-Cycle 5, P-Cycle 6, M (medial section)-Cycle 4, M-Cycle-5, D (distal section)-Cycle

1, D-Cycle 2; Figure 20). The stratigraphically uppermost cycles in the proximal (Cycle 7) and medial sections (Cycle 6) show the greatest vertical decrease in petrophysical values from rudstones to packstones. In coarsening-upward trends at the bases of proximal cycles, petrophysical values generally increase upward, except in the less altered (DF-1) Cycle 6. The proximal position of Cycle 6 is the only cycle where both the rudstone and packstone facies are entirely composed of DF-2 in the Miocene deposits, and it has an increasing upward petrophysical trend, similar to the Pliocene trends.

The entire distal section of the ramp has relatively homogeneous porosity values, whereas permeability values are variable. At the base of Cycle 4 in the distal location (Figure 20), debrites (the Massive Echinoid Packstone) create zones of high permeability interbedded between low permeability hemipelagic/turbidites.

Overall, these vertical petrophysical trends are much different than the predictable petrophysical trends created by shoaling-upward heterozoans in Pliocene strata and highlight the inversion of the distribution of petrophysical values caused by a diagenetic overprint onto depositional features.

DISCUSSION - CONTROLS ON PETROPHYSICAL HETEROGENEITY

Understanding controls on the distribution of petrophysical values allows for predicting the development of these variables. As the strata from the Pliocene dataset has not undergone extensive diagenesis, this dataset (and DF-2 from the Miocene) are applicable for understanding the distribution and controls on heterozoan systems that are governed by depositional controls. The remainder, of the dataset from the Miocene strata are useful for understanding the controls and distribution of petrophysical character in systems that are governed by a combination of depositional and diagenetic controls, and for dolomitized heterozoan systems.

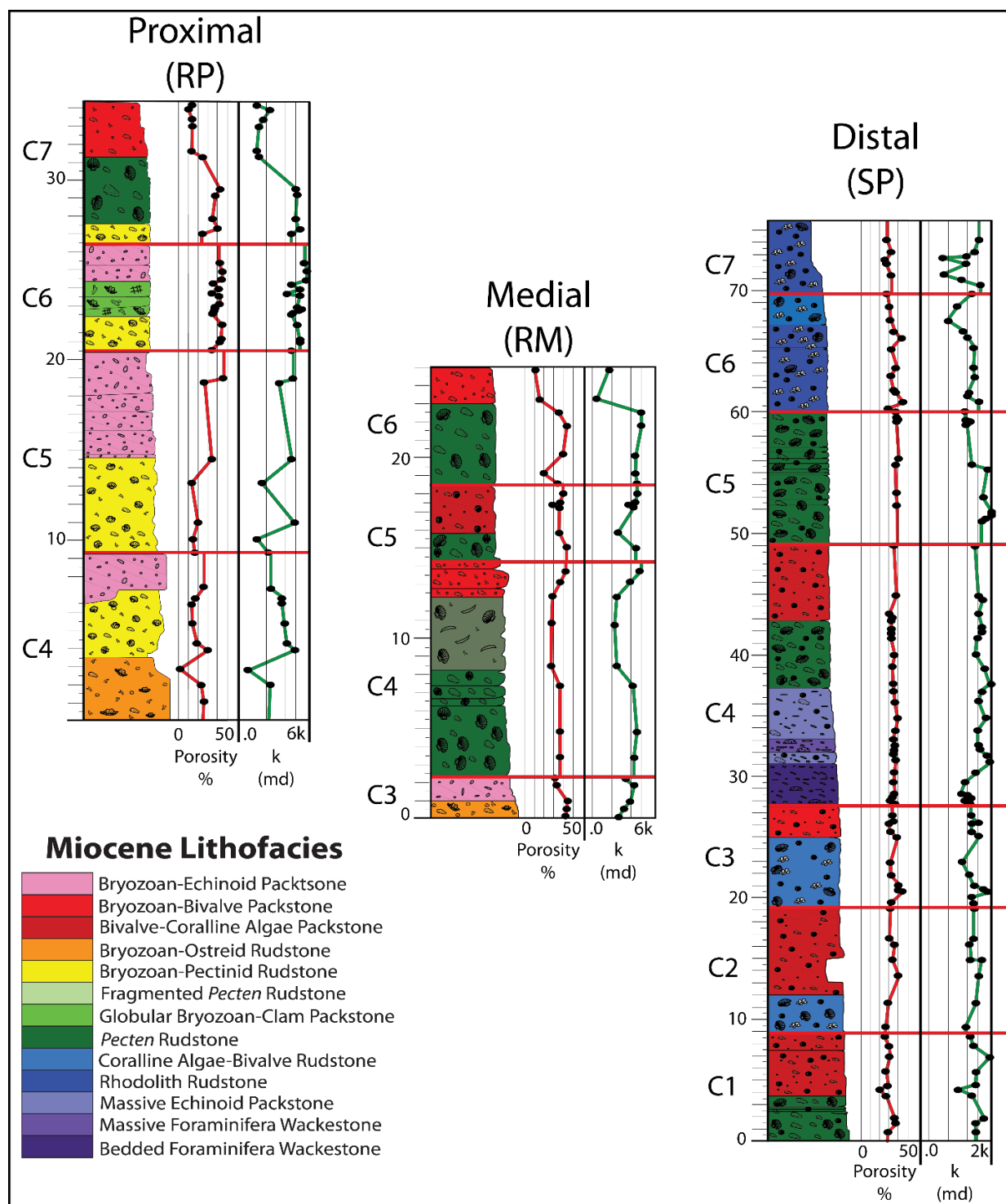


Figure 20: Vertical petrophysical curves for proximal, medial, and distal cycles for the Miocene deposits plotted with lithofacies and grain size curves. These are pseudo-petrophysical logs and may be similar to wireline logs measured from subsurface data. Note porosity values become less variable in the distal region. Red lines represent the breaks in cycles, i.e. sequence boundaries. Cycles are labeled by their correlations from outcrop data. The scale is in meters.

Grain Constituents

The variety of skeletal constituents in heterozoan carbonates creates an array of pore types and geometries. Data in Figures 7, 9, and 11 indicate that as bryozoan content increases, petrophysical values increase in packstones and rudstones. An example of this comes from the three sorted packstone facies of the Pliocene. These packstones are nearly identical in all variables except grain constituents, and show an increase in petrophysical values (Figures 9 and 11) with bryozoan content. The two rudstones from the Bioclastic Rudstone Association show this same trend. In Miocene packstones that have not been extensively cemented, this same trend again is present. Although pores within all bryozoan morphologies are primarily intraparticle and framework, it is apparent that the thin walls of zooecia contain micropores that allow for connectivity between the intraparticle skeletal pores, as these samples also have high permeability. With burial, it is possible that some micropores will not be preserved, creating isolated pores, and potentially decreasing permeability (Hanken et al., 2010). In both the Miocene and Pliocene systems, bryozoans are located predominantly in proximal regions. The low permeability and high porosity of rhodolith beds from both systems originate from millimeter scale framework pores that are separated by multiple millimeter-thick encrusting coralline algae, which results in disconnected pores and decreased permeability. In addition, the poorly sorted grainy- and calcisilt-rich matrix between rhodoliths decreases permeability.

In both the Pliocene and Miocene systems, rudstone facies primarily composed of whole *Pecten* and other bivalves consistently have high petrophysical values, whereas rudstones consisting of fragmented bivalves have significantly lower values (Figure 9, 11). Using a specific example from the Miocene, the Fragmented *Pecten* Rudstone has 33% average porosity and 53md median permeability, whereas the *Pecten* Rudstone, which is identical, except that

Pectens are whole, has average porosity of 38% and median permeability of 656md. This variation results from whole shells creating abundant connected interparticle and shelter pores (Figures 5A and 7A). Fragmented shells are closer packed, thereby decreasing pore size and connectivity. The *Pecten* Rudstone shows a variety of diagenetic alteration and textures including fully preserved calcite and dolomite shells, molds, infilled molds, and infilled borings in shells. In each of these occurrences, the *Pecten* Rudstone retains consistently high porosity and permeability, which is interpreted to result from the chemical instability of their original mixed calcite/aragonite (e.g. Taylor et al., 1969; Carter et al., 1998) shells, leading to ready dissolution and diagenetic alteration. These diagenetically altered *Pecten*-rich facies will likely retain their high petrophysical values with compaction and eventual burial as the dominance of interparticle pores associated with bivalves have some of the highest preservation potential with compaction (e.g. Budd, 2001), and the dolomitized bivalves will likely retain porosity with depth (e.g. Lucia, 2004).

Rock Texture and Grain Sorting

Data (Figures 9, 11, and 13) from the less altered Pliocene and Miocene (DF-1, 2) facies indicate that sorted, finer-grained packstone textures have the highest petrophysical values. This idea is in contrast to common belief, coming from photozoan systems, that the coarser the grain size, the higher the porosity and permeability. The multiple samples that lie significantly lower than the primary grouping for moderately sorted samples (Figure 17, 18) is due to calcisilt-rich packstones classifying as moderately sorted, with σ_i values close to that of poor sorting (1.5). This occurrence is caused as grain size analyses do not include calcisilts in their measurements, and therefore bias the sorting classification of calcisilt-rich samples.

Although the well to moderate sorted samples have the highest petrophysical values,

many samples with poor and very poor sorting also have similarly high petrophysical values (Figures 17 and 18). An example of this comes from data produced in samples with grains \leq 1mm (Figure 17A). Samples that are well sorted at this grain size, range in porosity from 46-58%, whereas many samples of identical mean size (\leq 1mm), are moderately sorted and have porosity values ranging from 28-43%. In addition, the majority of poorly sorted gravel-sized samples have porosity values $>40\%$. This observation can be explained by the relationship between grain size and sorting (Figure 17; Pugliano et al., 2015; Chapter 2); the coarser the grain size, the less of an impact poor sorting has on decreasing petrophysical values, allowing for high petrophysical values in some gravel-sized samples that are poorly and very poorly sorted.

Well to moderate sorting is associated with packstones as they are commonly abraded and sorted by wave energy in shallow waters at or near wave base, and therefore are concentrated in shallow depositional environments or transported distally by sediment gravity flows (generally less than 2m thick). It is concluded that well to moderate sorting is a primary control on consistently high petrophysical values, and that these two sorting classifications are primarily distributed in packstone lithofacies.

Sedimentary Structures

Pugliano et al. 2015 (Chapter 2) interpreted massive beds in both the Miocene and Pliocene systems to have formed from extensive bioturbation. The t-test run for sedimentary structures indicates that permeability is statistically different in packstones and wackestones with massive beds compared to those with horizontal and cross bedding. As porosity is also higher in massive beds (Table 2), this indicates that as bioturbation increases, permeability in packstones and wackestones also increases. Bioturbation in rudstones, however, does not appear to alter permeability. In the Pliocene deposits, extensive bioturbation takes place most

abundantly in the Sorted Bryozoan Packstone and the Bivalve-Coralline Algae Packstone (Pugliano et al., 2015; Chapter 2), and includes centimeter-meter scale vertical burrows. Although large-scale petrophysical values could not be measured from these “pipe” like burrows, they are infilled with sand-sized grains, which has the potential to greatly improve permeability within strata (Tonkin et al., 2010)

The Miocene Bedded Foraminiferal Wackestone consists of vertically alternating laminae of high permeability (turbidites) and low permeability, calcisilt-rich deposits (hemipelagics) (Figure 7F). Permeability values for these facies are higher where it occurs as massive (bioturbated) beds. The higher permeability likely results from sediments from the higher permeability laminae (which are more abundant) being mixed with sediments from the lower permeability laminae. This is consistent with data from Flügel (2004), stating that permeability in hemipelagic deposits has been reported to be reduced within silty interbedded laminae.

Diagenesis

Overall, diagenesis and dolomitization lower petrophysical values in Miocene strata in comparison to the Pliocene (Figures 10, 12, and 13). This is due to pore space reduction and decrease in pore throat size from dolomitization and overdolomitization primarily in distal regions, and calcite cements that form primarily in proximal regions. Although diagenetic alteration has overprinted onto all depositional textures, packstone facies have been altered the most, causing increased petrophysical variability. This variability causes both positive and negative effects on petrophysical character, however as variability increases, predictability decreases. Here, we speculate that the increased diagenetic alteration in packstones is due to higher original permeability (prior to diagenesis) in packstones compared to rudstones. Evidence

for this is found in the less altered facies of Cycles 6 and 7 (Tables 6, 7; Figure 20) in the proximal region of Ricardillo. These cycles are calcite and retain primary pores and textures. The Bryozoan-Echinoid Packstone in Cycle 6 in this location has permeability values ranging from 4,761-5,354md. Compared to unaltered rudstone lithofacies from the same cycle (and same stratigraphic section), permeability ranges from 128-3,600md. In addition, sorted packstone facies from the Pliocene consistently have higher permeability values than those of rudstones (Table 7, Figure 11). These higher permeability values in the less altered Miocene packstones (DF-2) and Pliocene packstones (DF-1) indicate that originally, all sorted packstones on Ricardillo likely had similar (high) permeability, prior to diagenetic alteration. It is hypothesized that the original higher permeability made the packstones better conduits for diagenetic fluid flow, allowing more fluids to flow through them than through rudstones, and causing increased diagenetic alteration in packstone facies.

Petrophysical values in wackestones perhaps benefits the most from diagenesis, as their extant pore space is in direct relation to moldic bivalve and foraminifera grains as well as intercrystalline porosity. Intercrystalline pore space was developed from the replacement of calcisilt with dolomite which increased permeability (e.g. Lucia, 2004). Using subsurface core data from Indonesia as an analog, a dolomitized, bedded foraminiferal wackestone at depths of 770m is reported to have porosity ranges from 6-40%, with most values ranging from 26-38%. (Bukhari, 2006). Using this as an analog for the dolomitized hemipelagic wackestone in this study, it appears that with depth, porosity in a similar facies has not decreased compared to outcrop values (33-38%). Permeability from the core ranges from .6-304md, whereas permeability in the dolomitized hemipelagic facies in this study range from 54-228md. Indicating that even after burial, petrophysical values were maintained when compared with an outcrop

analog. This effect is likely due to dolomitization and would likely be common to the majority of the dolomitized facies as dolomite resists compaction greater than limestone (Lucia, 2004).

The negative correlation between porosity and permeability in DF-3 (Figure 13) can be explained by dissolution and cementation. This diagenetic facies contains up to 32% calcite cement, and porosity is developed through dissolution of bivalves. These molds create porosity of 18%, however they are partially surrounded by impermeable interparticle pores filled with calcite cement. This creates median permeability values of 21md, and in some cases lower than .1md, the lowest permeability measured from all of the diagenetic facies. This dissolution and cementation diagenetic pattern creating high porosity and low permeability is a trend similar to patterns observed in photozoan oolitic systems with oomoldic pores and calcite cement filling all original interparticle porosity between the ooids, such as in the Smackover formation. In the Smackover formation oomoldic grainstones range in porosity from 25-35%, but have permeability values less than 4md, and do not show a positive correlation (Mitchell, 1983).

Dolomite distribution on Ricardillo is primarily controlled by paleotopographic position, however the dolomite content variation in Figure 6 indicates that there are additional controls. Original permeability of lithofacies prior to dolomitization appears to be the main control on dolomite distribution on Ricardillo. The main factors that influence original permeability are 1) a high sand: gravel ratio (good sorting in packstones), 2) matrix, 3) and rhodolith facies. The first and second factors have already been discussed, as better sorting creates higher permeability through which diagenetic fluids can flow, and calcisilts greater than 5% in these facies greatly reduce permeability. In distal regions where dolomite is ubiquitous, calcisilt amount does not alter dolomite content. In contrast, in proximal regions (in the few locations where abundant calcisilt is present) dolomite content decreases compared to surrounding strata with less calcisilt.

The third factor, rhodoliths and rhodolith facies, bears some further discussion. Rhodolith facies have some of the lowest permeability values (Tables 3 and 4; Figure 15). In the distal region of the Ricardillo area, dolomitization is ubiquitous and most deposits are dolomitized. As mentioned previously, at the sharp contact between underlying *Pecten* Rudstone and overlying Rhodolith Rudstones in the distal section of Ricardillo (Figures 6 and 20), there is an abrupt decrease in dolomite content from 77% in *Pecten* Rudstone facies to 43% in the Rhodolith Rudstone, with dolomite percentages decreasing down to 3% further upward throughout the stratigraphic section. The lower permeability values in this rhodolith facies is correlative with low diagenetic alteration, implying that low, original permeability created a barrier for later diagenetic fluids. Since there was a barrier to fluid flow, less of the upward-flowing fluids were available to dolomitize the rhodolith facies in the distal ramp. In addition to paleotopographic position, these lines of evidence provide support that original permeability of facies is correlated to dolomite distribution.

Overall, diagenetic overprint increases porosity and permeability variation within each lithofacies. Petrophysical values within rock textures are also altered as petrophysical variability in packstones increases and in rudstones decreases (Tables 3, 4; Figure 16). Where extensive dolomitization has taken place, i.e. the distal regions of Ricardillo, porosity variation between textures also decrease. This is apparent from the distal stratigraphic section of Ricardillo (Figure 20) where porosity is similar for packstones, wackestones, and rudstones, but permeability remains highly variable between textures. As the Pliocene rudstones and packstones have statistically different mean permeability values, it is assumed that the Miocene textures also originally had statistically differing mean permeability values, which have been altered by diagenesis. However, even with the diagenetic overprint, mean petrophysical values of rock

textures retain a statistically different variance (f-test results; Table 7).

Grain-Rich Shoaling- and Fining-Upward Cycles

The Pliocene system allows for correlating depositional controls with petrophysical values within the stratigraphic framework of the shoaling- and fining-upward cycle. The upward increase in petrophysical values in packstones in the Pliocene cycles (Figure 19) is controlled by the progradation of updip facies. Updip, proximal facies, are abraded by wave energy at or near wave base, creating sorted packstones. As accommodation in the basin fills, facies prograde, creating a vertical cycle that is coarser (gravel- cobble) at the base and finer (sand-gravel) at the top. Therefore, during shoaling, individual clinothem fine upward, remain grain-rich, and petrophysical values increase upward. During final progradation, the shallowest water facies prograde out across the top of the clinothem. In some cases, the shallowest-water facies are calcisilt-rich packstones interpreted to be the remnant of *Posidonia oceanica* grass beds (Pugliano et al., 2015; Chapter 2). These capping facies are calcisilt-rich (>5%) and decrease petrophysical values, permeability more so than porosity. Cycles that don't have calcisilt-rich packstones at the top show a consistent increase in petrophysical values upward. Overall, progradation results in a vertical cycle that shows a consistent upward increase of petrophysical values, except where calcisilt-rich packstones cap a cycle. Their presence results in lower permeability at the tops of cycles.

Using the Pliocene as an analog, one would predict that Miocene vertical cycle trends would also show an upward increase in petrophysical values from rudstones to packstones. The low permeability calcisilt-rich packstone facies does not occur in Miocene deposits, so a sharp decrease in permeability at the top of Miocene deposits is not predicted. The predicted upward increasing petrophysical trend is found at the proximal location of the less altered (DF-2) Cycle

6 on Ricardillo (Figure 20). This occurrence supports the hypothesis that in various depositional settings, porosity and permeability increase in updip, sand-sized facies that develop during shoaling. This petrophysical trend is governed by the architecture of the shoaling- and fining-upward cycle and should be found in other temperate, shallow-water, grain-rich heterozoan carbonate systems that preserve primary pore characteristics.

Out of the diagenetically altered Miocene cyclothem, only 46% show the upward increasing trend of petrophysical values. Where this trend is present, it primarily forms due to extensive dissolution of the capping packstone facies, such as in the proximal location of Cycle 5 (Figure 20). This indicates that diagenetic alteration decreases, and in some instances reverses, the predictable trend found in heterozoan carbonates that contain primary pores. Meaning that this trend cannot be consistently used as a predictive method in heterozoan systems that are governed by diagenetic controls and secondary pores. As rudstones are less diagenetically altered and less petrophysically variable than associated packstones, they may have a more consistent and predictable petrophysical distribution after diagenesis than packstones (Figure 16). These data and results can be used as geologic and petrophysical models for predicting the distribution of reservoir character in similar deposits in the subsurface.

SUBSURFACE IMPLICATIONS

The lack of extensive tectonism, burial, or compaction of the studied Miocene and Pliocene systems (Esteban and Giner, 1980; Franseen and Mankiewicz, 1991; Franseen et al., 1993, 1997, 1998; Franseen and Goldstein, 1996) results in the preservation of high petrophysical values that are near that of modern carbonate sediments (45-70%; Enos & Sawatsky, 1981). Simulation of porosity at reservoir depths was completed by applying compaction algorithms down to 2,000m depth using a modified version of the Athy's equation (e.g. Athy, 1930, Schmoker and Halley,

1982) for calcitic, grain-rich carbonates (e.g. Goldhammer, 1997). All calcitic samples in both the Pliocene and Miocene datasets were used (Figure 21). Since the majority of Miocene deposits have been dolomitized, their porosity reduction would not decrease as markedly as calcitic deposits do with depth (e.g. Schmoker and Halley, 1982).

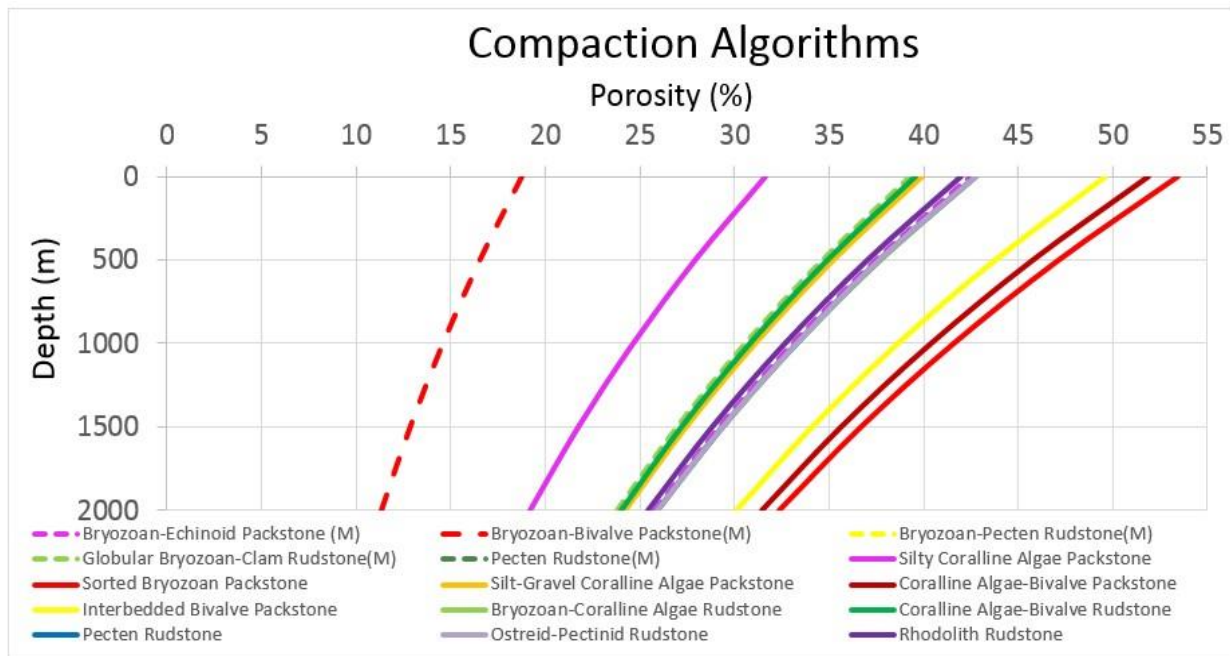


Figure 21: Compaction algorithms for calcite samples grouped by their lithofacies. At 2,000m depth, these lithofacies still retain porosity from 12-33%.

Although the compaction algorithms are only an estimate of burial compaction, the results indicate that the outcrops of this study would likely preserve porosity at depth and could yield highly economic reservoirs. The high amounts of interparticle porosity in these deposits adds to their potential to preserve reservoir quality (e.g. Budd, 2001). In addition, the original calcite mineralogy and dolomite content of the Miocene deposits indicate that similar deposits would have a lower chance of further diagenetic alteration in the subsurface (e.g. Ehrenberg and Nadeau, 2005).

RESERVOIR MODELING

Eight static 3-D reservoir analog models of heterozoan carbonates were constructed in

Petrel™ using field and petrophysical data collected in this study. Visual 3-D distribution of petrophysical values allows for application to potential plays in similar subsurface reservoirs, assuming a source rock for hydrocarbons and a seal are present.

One model represents the entire clinothem of the Carboneras Basin (Appendices XI and XII) and six models represent end-members of the six described lateral depositional profiles from the clinothem (Figure 22), the same profiles as in Figure 19. These proximal to distal lateral trends have been stacked as if prograding to show the same clinothem stratal geometries and 3D areal distribution as seen in outcrop. The last model is representative of the cyclothem deposited on Ricardillo (Figures 23, 4) and shows the same areal distribution of Ricardillo as seen in outcrop. Each of the eight models includes a lithofacies model, a probability distribution model for individual lithofacies, a porosity model, and a permeability model (Appendix XI, XII).

Data input

Lithofacies distinguished from fieldwork and lab work, as well as their stratigraphic distribution were imported into Petrel™. Measured stratigraphic sections were used to create pseudosections which are direct representation of the measured stratigraphic sections and placed in their exact geographical location. Pseudowells were also developed and simulated based off of observed and predicated facies distributions for particular elevations throughout the ramps. The pseudowells were used to help constrain and guide lithofacies distribution during population of the 3-D grid. Three of the Miocene measured sections were converted into pseudosections and from those an additional 22 pseudowells were created. For the Pliocene clinothem, data from all seven of the stratigraphic sections were used to recreate the six lateral depositional profiles as observed and described in the field. In addition, eighteen pseudowells were placed in each model. Each of the six end-member clinothem models reflect downlapping clinoform geometries downdip and pinching out geometries updip.

Each pseudowell and pseudosection contains lithofacies, elevation, and petrophysical data assigned by integer values, kelly bushing depths, total thicknesses, lithofacies thicknesses, ranges, means, and standard deviations of porosity and permeability values. Thickness (depths) for each lithofacies were used from outcrop data measurements and range from centimeters to meters. Clinotherm models for DP-1, DP-1A, DP-1B, and DP-2 are set to the same scale, while models for DP-3 and DP-4 are set at a smaller scale as they represent shallower-water, thinner deposits than the previous four models, this style is consistent with outcrop measurements. The consistent thickness of all the Pliocene models allows for a comparison of pore volume between reservoirs at the same scale. Porosity and permeability measurements were entered into the models at their corresponding depths based on collection location. Pseudowells and pseudosections were input into the X and Y model based on UTM coordinates converted from measurements from topographic maps and GPS.

A full model construction workflow and the details on facies and petrophysical modeling are included in Appendix X. Sequential indicator simulation (e.g. Deutsch and Journel, 1998) was used to populate the facies models and the sequential Gaussian simulation (e.g. Corvi et al., 1992; Deutsch and Journel, 1998) was used for populating petrophysical values in the models.

Model Results and Discussion-Pliocene

The six end-member depositional profiles of the prograding clinotherm were successfully reproduced as facies (Figure 22, Column A) and petrophysical models (Figure 22, Column B; Appendix XII) as well as models for the entire clinotherm (Appendices XI and XII). Only permeability models (Figure 22, Column B) are pictured here as they display the most interesting variations, showing the diversity of the end-member depositional profiles.

The DP-1 clinotherm contains 2.68M m³ (22.4M barrels) of pore space. It is capped by

updip facies that are low in permeability and would act as baffles or stratigraphic traps for fluid flow. The best quality reservoir would be from the Sorted Bryozoan Packstone and the Bryozoan- Coralline Algae Rudstone directly beneath the low permeability cap, especially in areas where the Sorted Bryozoan Packstone is the most widespread.

The DP-1a clinothem contains 2.65M m³ (22.3M barrels) of pore space. The updip Sorted Bryozoan packstone has the highest permeability and would be the primary reservoir target. Reservoir facies could also potentially extend downdip into the Bryozoan- Coralline Algae Rudstone.

The DP-1b clinothem contains 2.62M m³ (22.0M barrels) of pore space. Similar to DP-1a, the updip facies have the highest permeability. The clinothem contains significantly more, low permeability Rhodolith Rudstone than the previous DP-1, and DP-1A, which in comparison, reduces the overall reservoir volume.

The DP-2 clinothem contains 2.60M m³ (21.8M barrels) of pore space. Low permeability facies cap the clinothem and as seen in the previous clinothem models, the Rhodolith Rudstone facies decrease permeability values throughout the majority of the medial-distal region. The target reservoir is juxtaposed between these two low permeability zones within the Sorted Bryozoan Packstone.

The DP-3 clinothem contains 1.24Mm³ (10.4M barrels) of pore space. Proximal regions of this clinothem are capped by the low permeability, Silty Coralline Algae Packstone. Medial to distal regions of this clinothem consist of interbedded higher permeability Bivalve Packstones and lower permeability Ostreid-Pectinid Rudstones. Further basinward, the high permeability bivalve packstone beds decrease into beds <10cm in thickness. Therefore the primary reservoir target is located in the medial region of the clinothem, within the packstone. However within

this lithofacies, the lower permeability, interbedded rudstones would act as potential inhibitors to fluid flow, creating internal reservoir baffles, decreasing fluid flow.

The DP-4 clinothem contains 1.25M m³ (10.5M barrels) of pore space. This clinothem contains the Silty Coralline Algae Packstone and the Silt-Gravel Coralline Algae Packstone throughout proximal and into medial regions of the clinothem. Both of these facies have the lowest permeability values in the clinothem and together create a 2-component updip baffle. The primary target reservoir of this play would be the Bivalve-Coralline Algae Packstone that is juxtaposed between the low permeability cap and the most distal bivalve-rich rudstone facies. This creates a downdip play in the medial/distal region of the clinothem.

The Silty Coralline Algae Packstone, the Silt-Gravel Coralline Algae Packstone, and the Rhodolith Rudstones are baffle facies in each play. The Sorted Bryozoan Packstone, Sorted Bivalve-Coralline Algae Packstone, Interbedded Bivalve Packstone, and the Bryozoan-Coralline Algae Rudstone are the targets in each play based off of permeability, porosity, and lateral distribution. Compared to these reservoir facies, neither the *Pecten* Rudstone nor the Ostreid- Pectinid Rudstone have enough pore space or a wide enough lateral distribution to be target reservoirs in any of the clinothems.

Model Results and Discussion-Miocene

Lithofacies distribution in the Miocene model (Figure 23A) closely matches the distribution documented in outcrop (compare with Figure 4). The model calculates 26.5M m³ (166.7M barrels) of pore space for the entire system. In the petrophysical models (Figure 23B, C), thin layers with lower permeability are seen in the uppermost parts of the model in proximal areas, reflecting the extensive calcite cementation of those lithofacies. However, directly beneath these cemented layers, the facies consist of permeability >1,000md. Figure 23B shows scattered

and disconnected areas of high porosity in distal and medial regions of the model. This represents scattered areas of high moldic porosity that form in extensively dolomitized deposits.

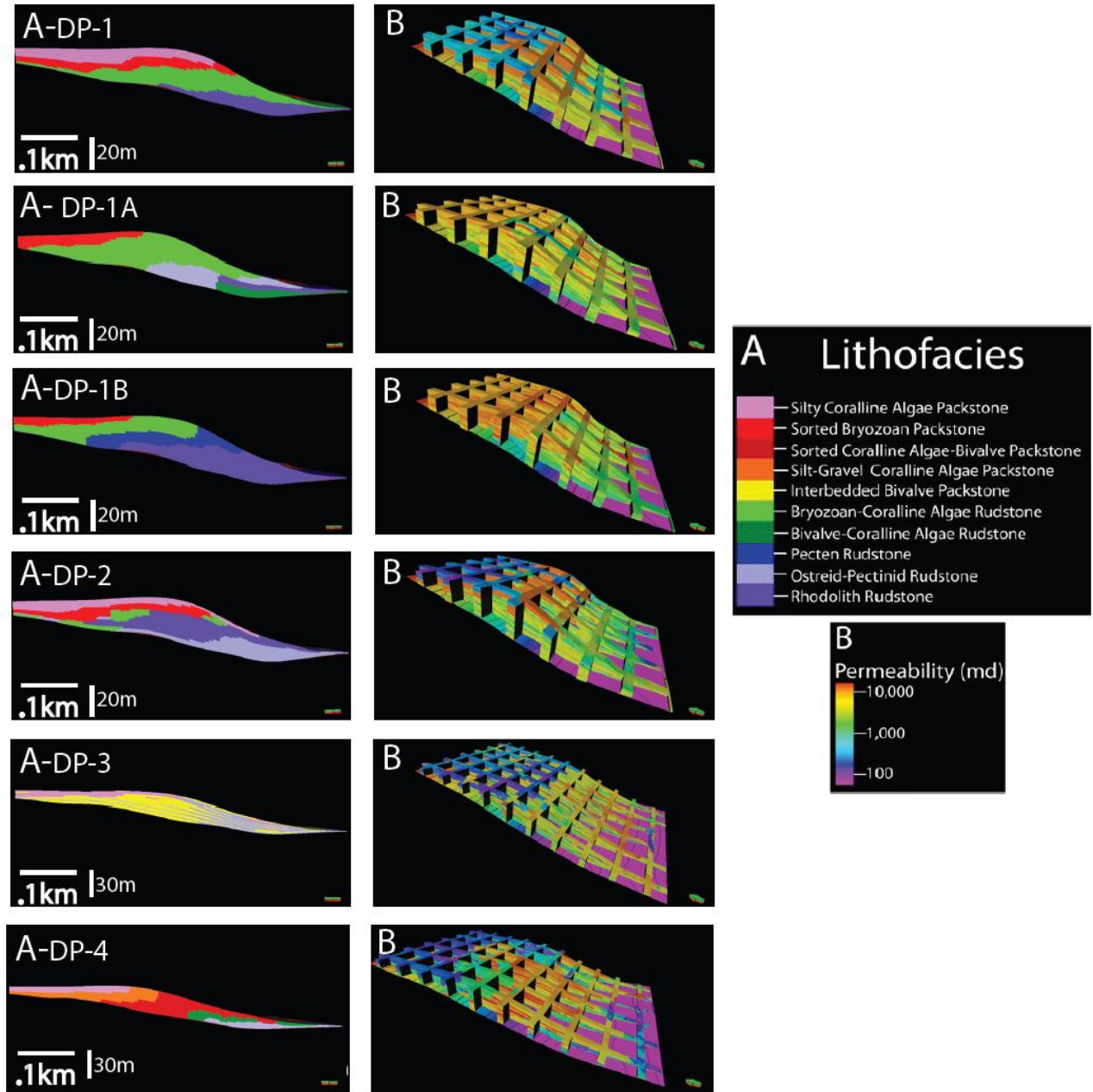


Figure 22: Property models of the Pliocene deposits from the Carboneras Basin. A) Lithofacies models of the six end-member depositional profiles from proximal to distal along the clinothem. Each model progrades, reflecting geometries of the clinothem. B) Fence diagrams of permeability models for each end-member depositional profile from the Pliocene. Areas where calcisilt-rich lithofacies are present show the lowest permeability values and are concentrated in proximal parts of the clinothem. These represent the distribution of facies generated by *Posedonia oceanica* grass beds (Pugliano, et al., 2015; Chapter 2). Higher permeability values generally match the distribution of sorted packstone deposits. Note the interbedded fluctuations of permeability within DP-3. This represents deposition from storm surge return flow.

Reservoir targets occur in proximal and distal regions. In distal regions, baffle facies are found at the base of the pseudosection in both Coralline Algae-Bivalve Rudstones and Packstones where extensive dolomitization has occurred at its greatest extent. However, stratigraphically above the hemipelagic wackestone deposits, these baffles transition into reservoir units composed of the *Pecten* Rudstone and the Coralline Algae-Bivalve Packstone. The Rhodolith Rudstone and the Coralline Algae-Bivalve Rudstone act as low permeability baffles to the reservoir units (*Pecten* Rudstone and the Coralline Algae-Bivalve Packstone) and along with the wackestone facies, are the only deposits that can be consistently classified as baffle facies. However, if permeability can be enhanced by hydraulic mechanisms, rhodolith beds could become volumetrically significant reservoirs due to high porosity values. The *Pecten* Rudstone reservoir continues updip into medial regions of the ramp where stratigraphically higher lithofacies (near label RM; Figure 23A) consist of alternating packstones and rudstones that contain a variety of diagenetic alteration. Some of these include extensive calcite cementation, creating a baffle/barrier for fluid flow, potentially forming a trap, creating a downdip target that is laterally extensive. A potential drilling location for this downdip target (Figure 23A) is recommended to be placed in the medial region of the ramp, just downdip of pseudosection RM, and perforated within the *Pecten* Rudstone (shown in green) due, to its extensive lateral distribution and consistently high petrophysical values. Placing a well in this location will target the hydrocarbons within the *Pecten* Rudstone that are trapped/baffled directly beneath the low permeability, and cemented facies at location RM (Figure 23A).

Further updip (RP), facies composed of the Bryozoan-Echinoid Packstone, Bryozoan-Ostreid Rudstone, Globular Bryozoan-Clam Rudstone, and the *Pecten* Rudstone, and represent DF-2, DF-4, and DF-5, create a proximal reservoir that is comprised of high permeability

dolomite and calcite facies starting with the base of Cycle 5, and through the top of Cycle 7 (Figure 20, RP; the stratigraphic sections of Figure 20 are identical to the labeled pseudosections of Figure 23A).

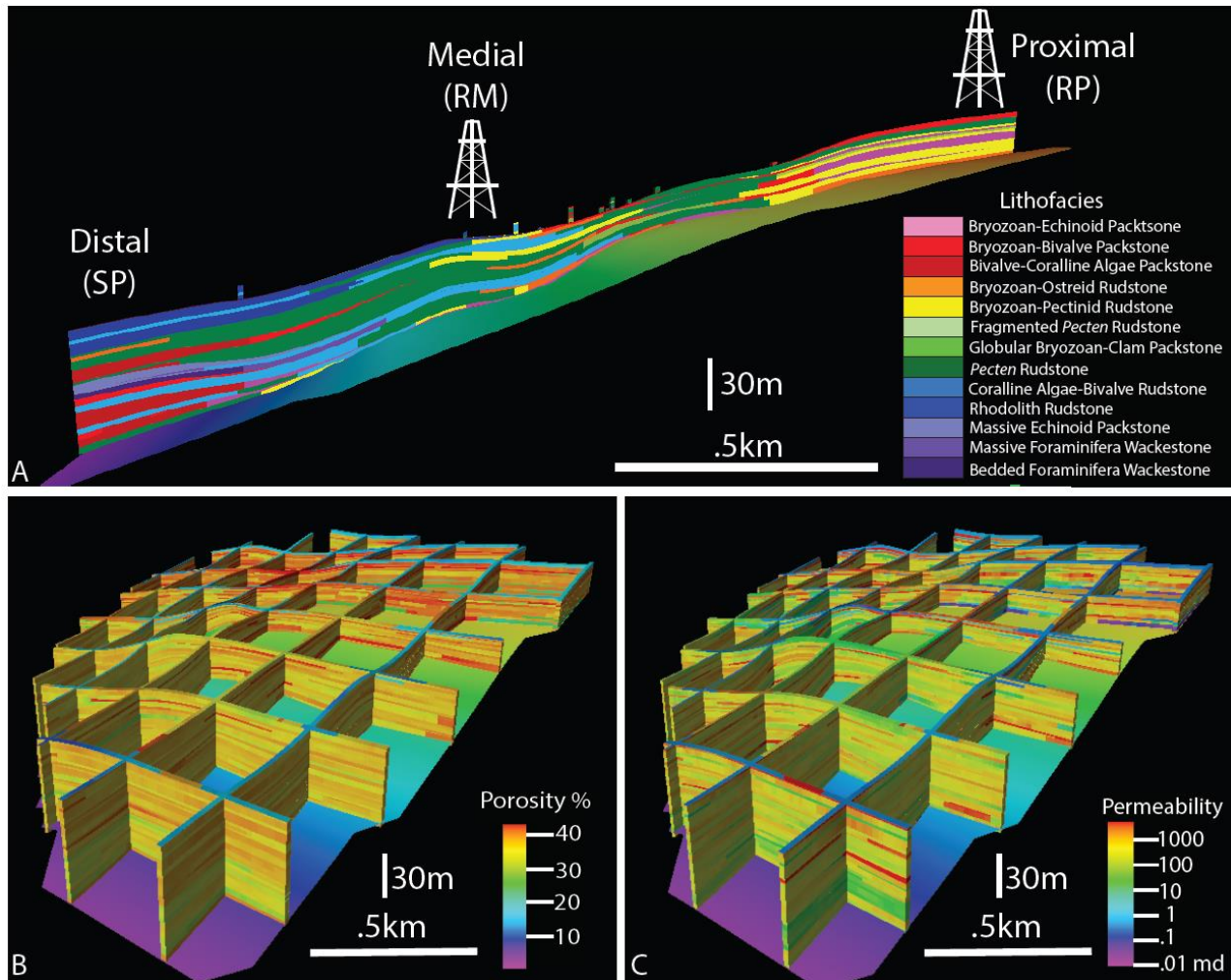


Figure 23: Property models of the Miocene deposits from the Ricardillo area. A) Cross section from the Lithofacies model depicting lateral facies changes from proximal to distal. Note the discontinuous packstone lithofacies from other packstone lithofacies further updip. Oil derricks represent locations of potential drill location in this reservoir model. B) Fence diagram of the porosity model. Highest values are concentrated in proximal region where diagenesis has not altered lithofacies. The lowest porosity streaks are also found at the top of proximal and medial regions where calcite cement has occluded pore space. C) Fence diagram of the permeability model. Highest values are concentrated in proximal regions. There is much more diversity in permeability distribution in the model than porosity. The vertical scale is exaggerated x2.5.

This proximal play contains a combination of diagenetic and depositional controls from facies that have porosity values >30% and permeability up to 1,000s of millidarcies, with 16m of vertical reservoir column, and is capped by a packstone containing 32% calcite cement with .09-2.27md permeability. In addition, these strata onlap underlying deposits in their most proximal

position, allowing for the development of an updip stratigraphic trap. These strata are the target for the second recommended drilling location as these stacked reservoir units allow for a well with multiple zones of perforation, in the most proximal position of the Miocene system.

Overall, diagenetic alteration creates the most abundant baffles throughout this reservoir analog, and the diagenetic effects on packstone facies greatly reduces predictability of reservoir quality (Table 4 and 7). Due to this decreased predictability, rudstone lithofacies may be a more viable option for exploration in diagenetically altered deposits. If packstone lithofacies are considered as potential plays, it is important to note their detached geometries as they pinch out updip and are not connected to further updip packstone facies (Figure 23A; Pugliano et al., 2015; Chapter 2).

RESERVOIR ANALOGS

The results of this research have application to grain-dominated heterozoan carbonate systems, especially those deposited during high-amplitude glacioeustasy. However, they are most applicable to Miocene heterozoan carbonates systems deposited throughout the Mediterranean, the Gulf of Suez, the Caribbean, and in the South China Sea (Sun and Esteban 1994; Esteban, 1996; Wilson et al., 2002). Interestingly, the Gulf of Suez, a hydrocarbon-producing, ramp-reef profile, has a strikingly similar depositional trend to the Cabo de Gata region (e.g. Esteban, 1996).

Wilson (2002) provides an extensive list of Cenozoic carbonate formations in the South China Sea. Twenty-two formations to be similar in organism composition and grain size to the outcrops used in this study. Of these 22, nine are described as hydrocarbon reservoirs and/or freshwater aquifers including the following: the Bojonglompang Member- Cimandri Formation, Cunda Limestone, Main Limestone Member- Cibulukan Formation, Ngimbang Carbonates,

Parigi Limestone, Pre-Parigi Onshore Limestone, Wonosari/Punung Formation, Balambangan /Tigapapan Limestone, and the Tonasa Formation. Lastly, the late Oligocene-Miocene Perla Field of offshore Venezuela is an example of a currently producing, heterozoan (primarily rhodagal) hydrocarbon reservoir (Fioretta et al., 2011).

CONCLUSIONS

- 1) Heterozoan carbonates from the Miocene and Pliocene of southeastern Spain provide outcrop analogs for the modeling of sedimentologic variables, stratigraphic architecture, and reservoir character. Pliocene deposits and Miocene deposits that are less altered by diagenesis represent heterozoan systems governed by depositional controls, whereas the remaining Miocene deposits represent a system governed by diagenetic and depositional controls.
- 2) Six diagenetic facies are identified for these heterozoan systems including: facies that have little diagenetic alteration (DF-1), are 100% calcite and have <5% moldic porosity and calcite cement (DF-2), facies that range from 50-100% dolomite and have undergone extensive dissolution (DF-4, DF-5) with upwards of 35% moldic porosity, facies with a similarly high dolomite content but have undergone overdolomitization and dolomite cement occludes portions of both primary and secondary pores (DF-6), and facies that are 100% calcite and have up to 35% calcite cement and abundant bivalve molds (DF-3).
- 3) Strata in distal regions of the Miocene system, are extensively dolomitized (50-100%). Dolomite amount decreases updip and most proximal strata become entirely calcite above 265m elevation. In addition, dolomitized strata have a positive correlation with moldic porosity.
- 4) For both the Pliocene and Miocene systems, sorted (well-moderate) packstones with little

diagenetic alteration (DF-1, 2), have the highest average porosity at 51% and median permeability of 6,099md. Calcisilt content greater than 5% causes decreases in petrophysical measurements, primarily permeability, and calcisilt-rich packstones have average porosity of 38% and median permeability of 296md. Rudstone lithofacies with little diagenetic alteration (DF-1, 2) have a wide range of petrophysical values, average porosity of 42% and median permeability of 2,537md.

- 5) Diagenetically altered deposits include packstones with average porosity of 32% and median permeability of 313md. Altered rudstones have average porosity of 35% and median permeability of 154md, and altered wackestones have 36% porosity and median permeability of 115md.
- 6) In the Pliocene deposits, lithofacies with the highest petrophysical values are sorted bryozoan- and coralline algae-rich packstones. In the Miocene, *Pecten* Rudstones consistently have the highest petrophysical values.
- 7) Diagenetic facies with the highest petrophysical values include those that are 100% calcite and have little alteration (DF-1, 2), and those that are 100% dolomite and have undergone extensive dissolution (DF-4, 5).
- 8) In both the Pliocene and Miocene heterozoan systems in this study, facies that are governed by depositional controls, have porosity to permeability power log correlations in packstones and plot the highest petrophysical values, whereas rudstones have no definitive correlation. In the diagenetically altered deposits (compared to those with little alteration), petrophysical values in packstones become highly variable and rudstones decrease in variability.
- 9) Abundant bioturbation (massive bedding) increases permeability in wackestones and packstones, however, it has no effect on the permeability of rudstones.

- 10) In both packstones and rudstones, as bryozoan content increases, porosity and permeability increase. Bryozoans contain abundant intraparticle and framework porosity. Bivalves, especially *Pectens*, retain high petrophysical values in a variety of diagenetic settings, i.e. from deposits with 100% calcite and low diagenetic alteration to 100% dolomite with extensive dissolution. Rhodoliths have millimeter sized framework pores, creating abundant porosity. The structure of the rhodoliths, however, causes isolation of pores, and along with the poorly sorted matrix, grains, and calcisilts surrounding rhodoliths, permeability values are some of the lowest in the dataset. Moldic foraminifera and replacement of calcisilts by coarser dolomite crystals increases petrophysical values in hemipelagic/turbidite deposits.
- 11) As sorting decreases, permeability and porosity also decrease. The finer the grain size, the better the sorting is required for high petrophysical values. This relationship allows for poor and very poorly sorted rudstone lithofacies to retain high petrophysical values in some instances.
- 12) Packstone facies are more prone to extensive diagenetic alteration and 77% of packstones that cap fining-upward cycles are more highly altered than underlying rudstones. This increased alteration causes increased variability in packstones. Increased alteration is due to original higher permeability of packstone facies, allowing for enhanced diagenetic fluid flow through these conduits, causing the increased diagenetic alteration. Extensive dolomitization decreases variation in petrophysical values between rock textures.
- 13) As accommodation filled in the Carboneras Basin (Pliocene) sand-sized facies prograded over coarser *in situ* deposits forming a grain-rich fining- and shoaling-upward cycle within the clinothem. Six-end member lateral lithofacies profiles develop within this clinothem, and when stacked, each form a cycle with petrophysical properties that increase upward as grain size decreases from gravel to sand during shoaling. If the clinothem is capped by shallow

water calcisilt-rich deposits, then petrophysical values abruptly decrease in the top <15% of the cycle, due to the calcisilt- rich nature of the beds. In Miocene deposits that are not extensively diagenetically altered, shoaling upward leads to increased porosity and permeability upward.

- 14) In diagenetically altered and dolomitized cycles of the Miocene, only 46% of the cycles retain this predictable trend of increasing-upward petrophysical character. Cycles that do preserve this pattern have cycle-capping packstones that have undergone extensive dissolution. Diagenesis therefore decreases and in some cases reverses the predictable petrophysical trend found in depositional controlled heterozoan systems. As rudstones are less altered and less variable in diagenetic systems, they retain a more predictable petrophysical distribution.
- 15) These data show that heterozoan systems that retain depositional pores and textures form specific petrophysical trends that are predictable based on the stratigraphic architecture and facies distribution of the shoaling- and fining-upward cycle. This trend has been developed into 3D PetrelTM reservoir-analog models and facies models to aid in predicting the distribution of reservoir character in similar deposits in the subsurface. They yield reservoir analog models capable of storing 26-166 barrels of fluid. Some with stratigraphic trapping mechanisms.

REFERENCES CITED

- Adams, E. W., Grotzinger, J.P., Watters, W.A., Schroder, S., McCormick D.S., and Al Siyabi, H.A., 2005, Digital characterization of thrombolite stromatolite reef distribution in a carbonate ramp system [terminal Proterozoic, Nama Group, Namibia]: AAPG Bulletin, v. 89, p. 1293-1318, doi:10.1306/06160505005.
- Aguirre, J., 1998, El Plioceno del SE de la Península Ibérica (provincia de Almería). Síntesis estratigráfica, sedimentaria, bioestratigráfica y paleogeográfica: Rev. Soc. Geol. Esp., v. 11, p. 297-315.
- Athy, L.F., 1930, Density, porosity and compaction of sedimentary rocks, AAPG Bulletin, v. 14, p. 1-24.
- Borgomano, J., J. P. Masse, and S. Al Maskiry, 2002, The lower Aptian Shuaiba carbonate outcrops in Jebel Akhdar, northern Oman: Impact on static modeling for Shuaiba petroleum reservoirs: AAPG Bulletin, v. 86, p. 1513–1529.
- Borgomano, J., F. Fournier, S. Viseur, and L. Rijkels, 2008, Stratigraphic well correlations for 3-D static modeling of carbonate reservoirs: AAPG Bulletin, v. 92, p.789–824, doi:10.1306 /02210807078.
- Budd, D.A., 2001, Permeability variation with depth in the Cenozoic carbonate platform of west-central Florida, USA: AAPG Bulletin, v. 85, p.1253-1272, doi: 10.1306/8626CAAF-173B-11D7-8645000102C1865D.
- Bukhari, T., Kaldi, J. G., Yaman, F., Kakung, H. P., & Williams, D. O. (1992). Parigi carbonate build-ups: northwest Java sea. In C. T. Siemers, M. W. Longman, R. K. Park, & J. G. Kaldi (Eds.), Carbonate rocks and reservoirs of Indonesia. Indonesian Petroleum Association Core Workshop Notes 1, Chap. 6. Indonesian Petroleum Association, Jakarta
- Carter, J.G., Barrera, E., Tevesz, M.J.S., 1998. Thermal potentiation and mineralogical evolution in the Bivalvia (Mollusca). Journal of Paleontology 72, 991–1010
- Choquette, P.W., and Pray, L.C., 1970, Geologic nomenclature and classification of porosity in sedimentary carbonates: AAPG Bulletin, v. 54, p. 207- 244.
- Corvi, P., K. Heffer, P., King, Tyson, and G. Verly, 1992, Reservoir Character using expert knowledge, data, and statistics: Schlumberger, Oilfield Reviews, v.4, p. 25 – 39.
- Deutsch, C.V., and A. G., Journel, 1998, GSLIB Geostatistical software library and user's guide: Oxford University Press, 2nd edition, 369 pp.
- Dickson, J. A. D., 1965, A modified technique for carbonates in thin section: Nature, v. 205, p. 587.
- Dillett, P.M., Goldstein, R.H., Franseen, E.K., 2004, Paleotopographic and sea-level controls on the sequence stratigraphic character of a heterozoan carbonate succession: Pliocene, Carboneras Basin, southeast Spain, Master's thesis, University of Kansas, Lawrence, Kansas, 119 p.
- Dutton, S. P., Kim, E.M., Broadhead, R.F., Raatz, W.D., Breton, C.L., Ruppel, S.C., and Kerans, C., 2005, Play analysis and leading edge oil-reservoir development methods in the Permian Basin: Increased recovery through advance technologies: AAPG Bulletin, v. 89, p. 553–576, doi:10.1306/12070404093.
- Ehrenberg, S. N., and P. H. Nadeau, 2005, Sandstone vs. carbonate petroleum reservoirs: A global perspective on porosity-depth and porosity-permeability relationships: AAPG Bulletin, v. 89, no. 4, p. 435–445.

- Enos, P., AND Sawatsky, L.H., 1981, Pore networks in Holocene carbonate sediments: *Journal of Sedimentary Petrology*, v. 51, p. 961–986.
- Esteban, M., 1979, Significance of the upper Miocene coral reefs of the western Mediterranean: *Paleogeography, Paleoclimatology, Paleoecology*, v. 29, p. 169-188.
- Esteban, M., and Giner, J., 1980, Messinian coral reefs and erosion surfaces in Cabo de Gata (Almeria, southeastern Spain): *Acta Geologica Hispanica*, v. 15, p. 97-104.
- Esteban, M., 1996, Overview of Miocene reefs from the Mediterranean area: General trends and facies models, in Franseen, E.K., Esteban, M., Ward, W.C., and Rouchy, J.M., eds., *Models for Carbonate Stratigraphy from Miocene Reef Complexes of the Mediterranean Regions: SEPM Concepts in Sedimentology and Paleontology Series #5*, p. 3-53.
- Fernandez-Soler, J.M., 1996, El volcanismo calco-alcalino de Cabo de Gata (Almeria), estudio volcanológico y petrológico.: *Sociedad Almeriense de Historia Natural*, 295 pp.
- Fernandez-Soler, J.M., 1996, El volcanismo calco-alcalino de Cabo de Gata (Almeria), estudio volcanológico y petrológico.: *Sociedad Almeriense de Historia Natural*, 295 pp.
- Fioretta, A., Schiroli, A., and Barletta, V., 2011, The Perla World-Class Giant Gas Field, Gulf of Venezuela: An Overview on a Successful Case History in a Virtually Unexplored Basin: *AAPG Search and Discovery*, article # 90135, AAPG International Conference and Exhibition, Milan, Italy, p. 23-26.
- Fisher, R., A., 1921, On the Probable Error of a Coefficient of Correlation Deduced from a Small Sample: *Metron*, v. 1, p. 3-32.
- Flügel, E., 2004, *Microfacies of carbonate rocks*: Springer – Verlag, 2nd edition, pp. 984.
- Folk, R.L., 1965, *Petrology of sedimentary rocks*: Hemphill's Bookstore, Austin, 170 pp.
- Franseen, E.K., 1989, *Depositional Sequences and Correlation of Middle to Upper Miocene Carbonate Complexes, Las Negras Area, Southeastern Spain*, Ph.D. dissertation, University of Wisconsin-Madison, Wisconsin, 374 p.
- Franseen, E.K., Goldstein, R.H., and Whitesell, T.E., 1993, Sequence stratigraphy of Miocene carbonate complexes, Las Negras area, southeastern Spain: Implications for quantification of changes in relative sea level, in Loucks, R.G. and Sarg, J.F., eds., *Carbonate Sequence Stratigraphy: Recent Developments and Applications: AAPG Memoir 57*, p. 409-434.
- Franseen, E.K., and Goldstein, R.H., 1996, Paleoslope, sea level, and climate controls on upper Miocene platform evolution, Las Negras area, southeastern Spain, in Franseen, E.K., Esteban, M., Ward, W.C., and Rouchy, J.M., eds., *Models for Carbonate Stratigraphy from Miocene Reef Complexes of the Mediterranean Regions: SEPM Concepts in Sedimentology and Paleontology Series #5*, p. 159-176.
- Franseen, E.K., Goldstein, R.H., and Farr, M.R., 1997, Substrate-slope and temperature controls on carbonate ramps: Revelations from upper Miocene outcrops, SE Spain, in James, N.P. and Clarke, J., eds., *Cool-water Carbonates: SEPM Special Publication 56*, p. 271-290.
- Franseen, E.K., Goldstein, R.H., and Farr, M.R., 1998, Quantitative controls on location and architecture of carbonate depositional sequences: upper Miocene, Cabo De Gata region, SE Spain: *Journal of Sedimentary Research*, v. 68, p. 283-298.
- Franseen, E.K., and Mankiewicz, C., 1991, Depositional sequences and correlation of middle to late Miocene carbonate complexes, Las Negras and Nijar areas, southeastern Spain: *Sedimentology*, v. 38, p. 871-898.
- Goldhammer, R.K. 1997, *Compaction and decompaction algorithms for sedimentary*

- carbonates: *Journal of Sedimentary Research*, v. 67, p. 26-56.
- Hanken, N., Bjørlykke, K., and Jesper, K. N., 2010, Carbonate Sediments in ed. Bjørlykke, K. Petroleum Geoscience, from Sedimentary Environments to Rock Physics, 2010. SpringerVerlag, Berlin.
- Hess, A., V., Goldstein, R.H., Franseen, E.K., 2011, Heterozoan carbonate lithofacies and sequence stratigraphy: a study of Pliocene strata of the Agua Amarga basin, southeastern Spain, Master's thesis, University of Kansas, Lawrence, Kansas, 119 p.
- James, N. P., and Choquette, P.W., 1984, Diagenesis 9. Limestones — the meteoric diagenetic environment: *Geoscience Canada*, v. 11, p. 161-194.
- James, N. P., Boreen, T. D., Bone, Y., and Feary, D. A., 1994, Holocene carbonate sedimentation on the west Eucla Shelf, Great Australian Bight: a shaved shelf: *Sedimentary Geology*, v. 90, p. 161–177.
- James, N. P., 1997, The cool-water carbonate depositional realm, in James, N.P. and Clarke, J.A.D., eds., *Cool-water Carbonates: SEPM, Special Publication 56*, p. 1-20.
- Janson, X., Kerans, C., Bellian, J.A., and Fitchen, W., 2007, Three- dimensional geological and synthetic seismic model of Early Permian redeposited basinal carbonate deposits, Victorio Canyon, west Texas: *AAPG Bulletin*, v. 91, p. 1405–1436.
- Johnson, C. L., Franseen, E.K., and Goldstein, R.H., 2005, The effects of sea level and paleotopography on lithofacies distribution and geometries in heterozoan carbonates, south-eastern Spain: *Sedimentology*, v. 52, p. 513–536, doi:10.1111/j.1365-3091.2005.00708.x.
- Katz, A., Friedman, G.M., 1965, The preparation of stained acetate peels for the study of carbonate rocks *Journal of Sedimentary Petrology*, v. 35, p. 248-249.
- Knoerich, A.C. & Mutti, M., 2003, Controls on facies and sediment composition on the diagenetic pathway of shallow-water heterozoan carbonates: the Oligocene of the Maltese Islands: *International Journal of Earth Sciences*, v. 92, p. 494-510.
- Li, Z., Goldstein, R.H., and Franseen, E.K., 2013, Ascending Freshwater Mesohaline Mixing: A New Scenario for Dolomitization: *Journal of Sedimentary Research*, v. 83, p. 277-283.
- Li, Z., Goldstein, R.H., and Franseen, E.K., 2014, Climate, duration, and mineralogy controls on meteoric diagenesis, La Molata, southeast Spain: Interpretation, *Journal of SEG/AAPG*, v. 2, p. SF111-SF123 doi: 10.1190/INT-20140060.1
- Lindholm, R., and Finkelman, R., 1972, Calcite staining; semiquantitative determination of ferrous iron: *Journal of Sedimentary Research*, v.42, p. 239-242.
- Lopez-Ruiz, and Rodriguez-Badiola, E., 1980, La Region Volcanica Neogena del Sureste de Espana: *Estudios Geologicos*, v. 36, p. 5- 63.
- Lu, F.H., and Meyers, W.J., 1998, Massive dolomitization of a late Miocene carbonate platform: a case of mixed evaporative brines with meteoric water, Nijar, Spain: *Sedimentology*, v. 45, p. 263-277.
- Lucia, F.J., 2004, Origin and petrophysics of dolostone porespace, In, Braithwaite, C.J.R., Rizzi, G., and Darke, G. (eds.), *The Geometry and Petrogenesis of Dolomite Hydrocarbon Reservoirs: Geological Society of London, Special Publications*, v. 235, p. 141-155.
- Mitchell, H. J. (1983, July 1). *Petrophysical Evaluation of the Smackover Oomoldic Porosity of East Texas and Southern Arkansas*. Society of Petrophysicists and Well-Log Analysts.

- Meyers, W.J., Lu, F.H., and Zachariah, J.K., 1997, Dolomitization by mixed evaporative brines and freshwater, Upper Miocene carbonates, Nijar, Spain: *Journal of Sedimentary Research*, v. 67, p. 898-912.
- Montenat, C., Ott, D'Estevou, P., and Mase, P., 1987, Tectonic-sedimentary characters of the Betic Neogene basins evolving in a crustal transcurrent shear zone (SE Spain): *Bulletin Centres Rech. Explor.-Prod., Elf-Aquitaine*, v. 11, p. 1- 22.
- Montenat, C., Ott, D'Estevou, P., and La Chappelle, G., 1990, Le bassin de Nijar-Carboneras et le couloir de Bas-Andrax, in Montenat, C., ed., *Les Bassins Néogènes du Domaine Betique Oriental (Espagne): Doc. Trav. Geol. Albert de Lapparent*, 12-13, IGAL, Paris, p. 129- 164.
- Oswald, E.J., 1992, Dolomitization of an upper Miocene reef complex, Mallorca, Spain, PhD dissertation, State University of New York, Stony Brook, N.Y., 424 p.
- Platt, J.P., and Vissers, R.L.M., 1989, Extensional collapse of thickened continental lithosphere: a working hypothesis for the Alboran sea and Gibraltar arc: *Geology*, v. 17, p. 540-543.
- Pranter, M. J., Ellison, A.I., Cole, R.D., and Patterson, P.E., 2007, Analysis and modeling of intermediate-scale reservoir heterogeneity based on a fluvial point bar outcrop analog, Williams Fork Formation, Piceance Basin, Colorado: *AAPG Bulletin*, v. 91, p. 1025– 1051, doi:10.1306/02010706102.
- Pugliano, T.M., Goldstein, R.H., Franseen, E.K., 2015, Fundamental Elements of Stratigraphic Architecture in Heterozoan Carbonates: Grain-Rich Fining-and Shoaling-Upward Cyclothems and Clinothems, Master's thesis, KICC, University of Kansas, Lawrence, KS, 75p.
- Rehault, J.P., Boillot, G. and Mauffret, A., 1985, The western Mediterranean basin, in Stanley, D.J. and Wezel, F.C., eds., *Geologic Evolution of the Mediterranean Basin*: Springer-Verlag, New York, p. 101- 130.
- Saller, A.H, and Henderson, N., 1998, Distribution of porosity and permeability in platform dolomites, insight from the Permian of west Texas: *AAPG Bulletin*, v. 82, p. 1528-1550.
- Sanz de Galdeano, C., and Vera, J. A., 1992, Stratigraphic record and palaeogeographical context of the Neogene basins in the Betic Cordillera, Spain: *Basin Research*, n. 4, p. 21- 36.
- Schlumberger, 2013, *Petrel Fundamentals Guide Book*.
- Schmoker, J. W., and Halley, R.B., 1982, Carbonate porosity versus depth: a predictable relation for south Florida: *AAPG Bull.*, v. 66, p. 2561-2570.
- Schmoker, J. W., Krystink, K. B., and Halley, R. B., 1985, Selected characteristics of limestone and dolomite reservoirs in the United States: *AAPG Bulletin*, v. 69, p. 733-741.
- Snedecor, G. W., and Cochran, W.G., 1989. *Statistical methods*: Blackwell Publishing Professional, 8th edition. 503 p.
- Student, 1908, The Probable Error of a Mean: *Biometrika*, v. 6, p. 1–25.
- Sun, S.Q., Esteban, M., 1994, Paleoclimatic controls on sedimentation, diagenesis, and reservoir quality — lessons from Miocene carbonates: *AAPG, Bulletin*, v. 78, p. 519-543.
- Sweeney, R., J., Goldstein, R.H., Franseen, E.K., 2015, Sequence stratigraphy and facies distribution in a Miocene carbonate platform; La Rellana Platform Area, Master's thesis, KICC, University of Kansas, Lawrence, KS, 129p.
- Taylor, J.D., Kennedy, W.J., and Hall, A., 1969. The shell structure and mineralogy of the

- Bivalvia: Introduction: Nuculacea-Trigonacea. Bull. Br. Mus. Nat. Hist. Zool. Suppl. 3, 1 125.
- Tonkin, N.S., D. McIlroy, R. Meyer and A. Moore-Turpin, 2010. Bioturbation influence on reservoir quality: A case study from the Cretaceous Ben Nevis Formation, Jeanne d'Arc Basin, offshore Newfoundland, Canada. AAPG Bull., 94: 1059-1078.
- Toomey, N., Goldstein, R.H., Franseen, E.K, 2003, Controls on Sequence Stratigraphy in Upper Miocene Carbonates of Cerro De Ricardillo, Southeastern Spain, Master's thesis, KICC, University of Kansas, Lawrence, KS, 146p.
- Wilson, M.E.J., 2002, Cenozoic carbonates in Southeast Asia: implication for equatorial carbonate development: Sedimentary Geology, v. 147, p. 295–428.

APPENDICES

Appendix I

Measured Stratigraphic Sections

A total of 11 stratigraphic sections were measured and described, 4 from the Miocene and 7 from the Pliocene. Google Earth™ images and photographs indicate where stratigraphic sections were measured that are not shown in the text are included below. UTM coordinates, thicknesses, and elevations are provided for each section as well as digitized versions of the sections. An additional lateral section was measured in the medial portion of the clinothem, a few samples were collected along that section. These samples are labeled PL.



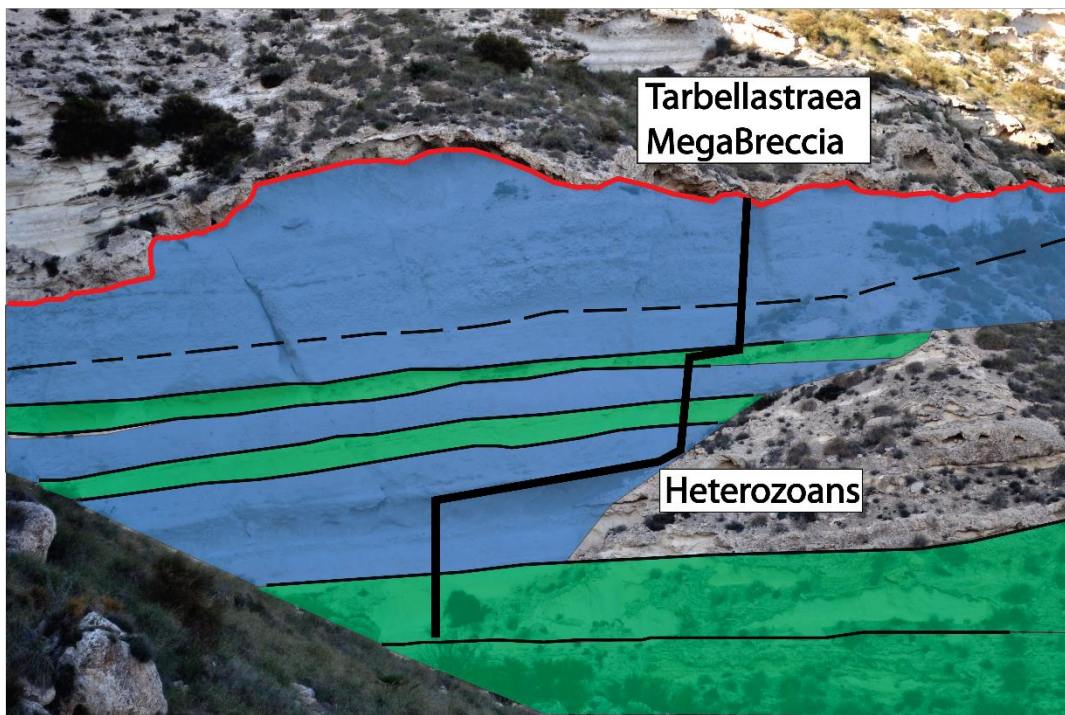
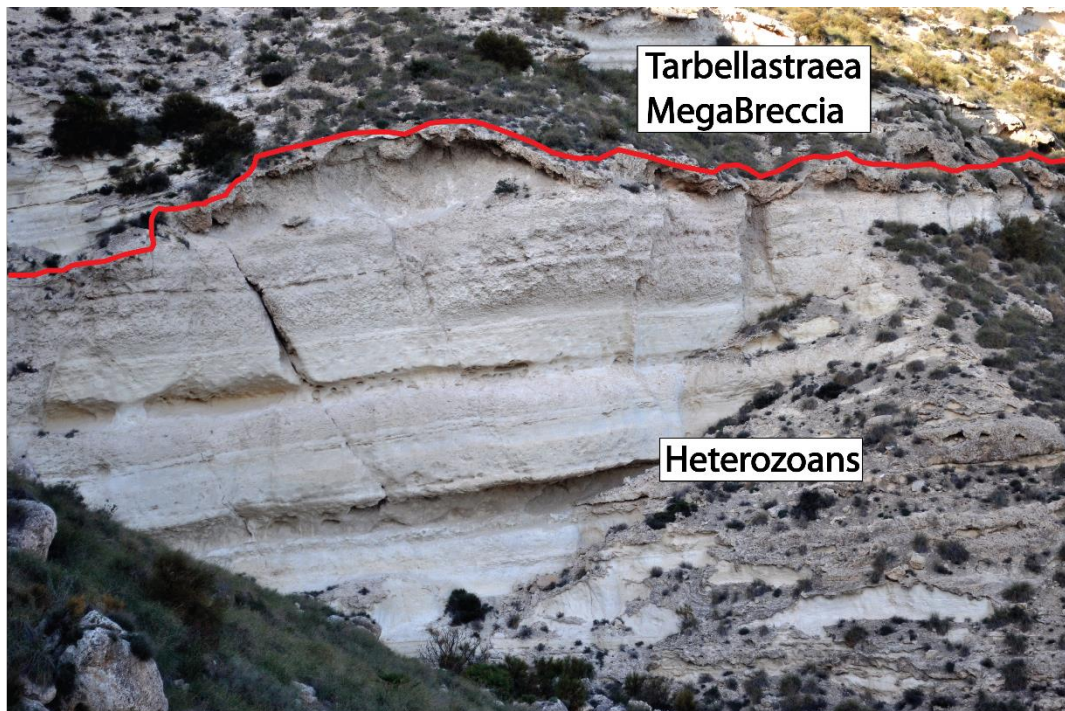
Google Earth™ image of the Miocene deposits from the Ricardillo area. Image shows the location of all measured sections from this area.

Section	Easting	Northing	Thickness	Elevation
RP- Cerro de Ricardillo	589615	4084950	34.3m	245m
RM- Cerro de Ricardillo	589821	4084344	25m	210m
SP- San Pedro	590857	4085263	75.6m	90m
WF- San Pedro			21.4m	148m

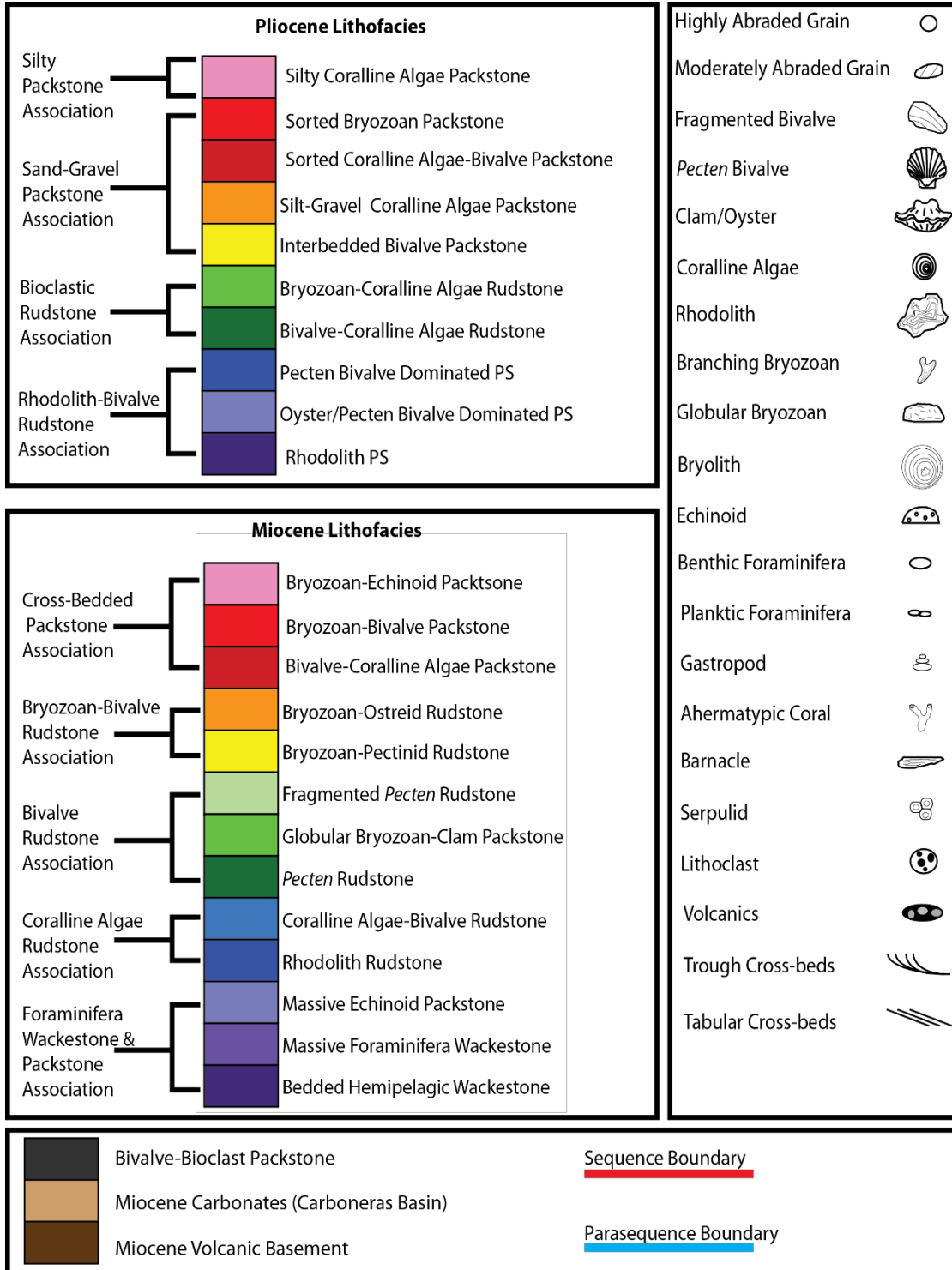
Miocene measured section data.



Location of distal measured sections of the Miocene deposits in San Pedro Canyon.

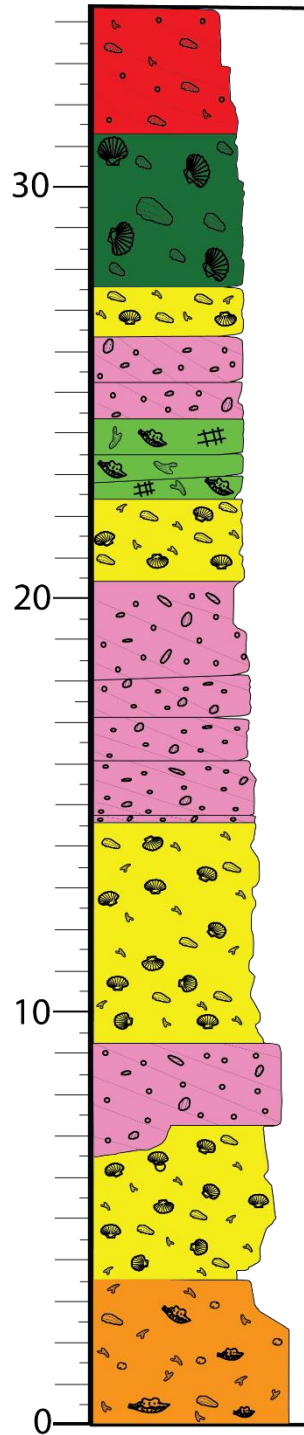


Interpreted photo of the WF (Miocene) measured section. Green represents the *Pecten* Rudstone and Blue represents the Rhodolith Rudstone.



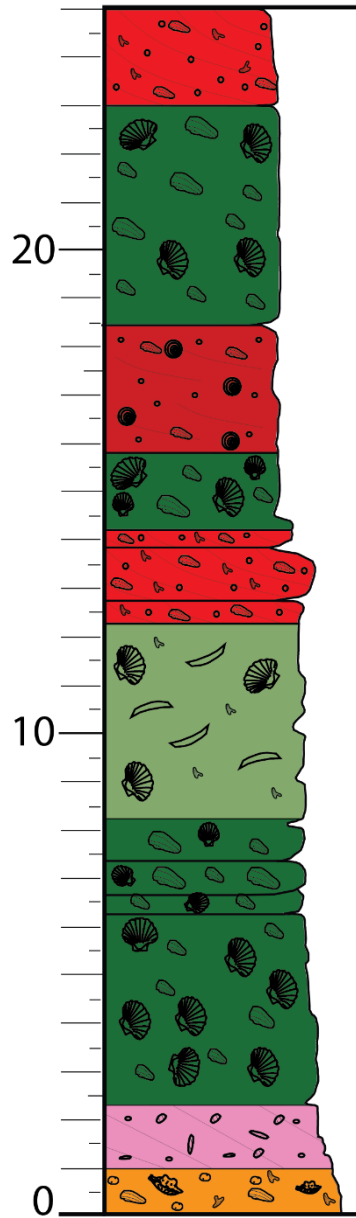
Key

Proximal (RP)



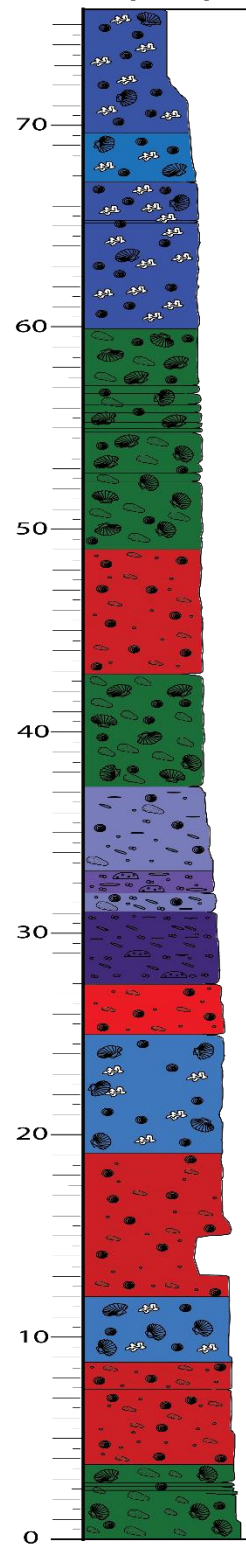
Proximal measured section from the Miocene.

Medial (RM)

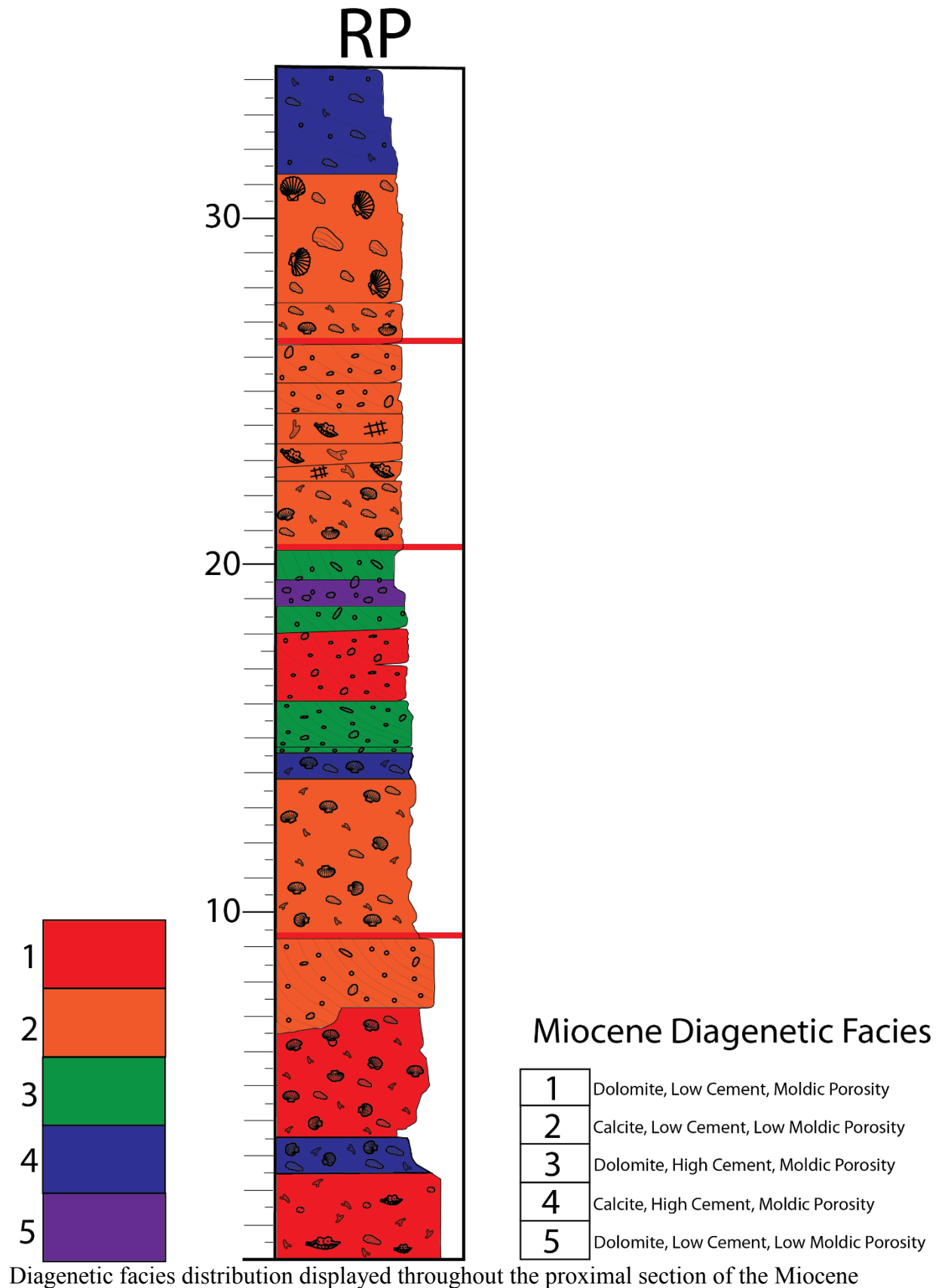


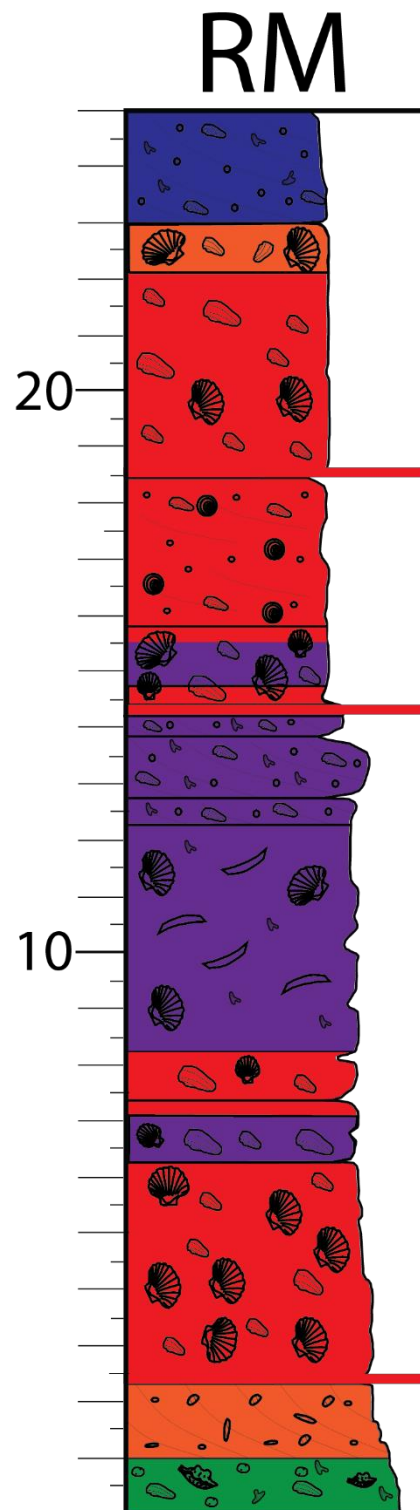
Medial measured section from the Miocene

Distal (SP)

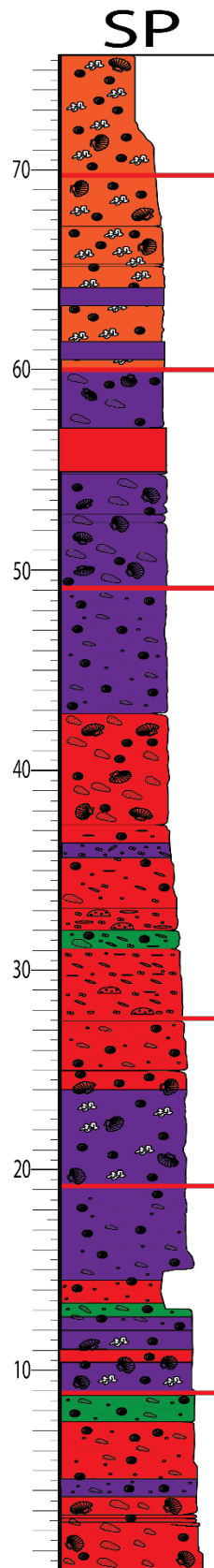


Distal measured section from the Miocene





Diagenetic facies distribution displayed throughout the medial section of the Miocene



Diagenetic facies distribution displayed throughout the distal section of the Miocene



Google Earth™ image of the Pliocene deposits from the Carboneras Basin. Image shows the location of all measured sections from this area.

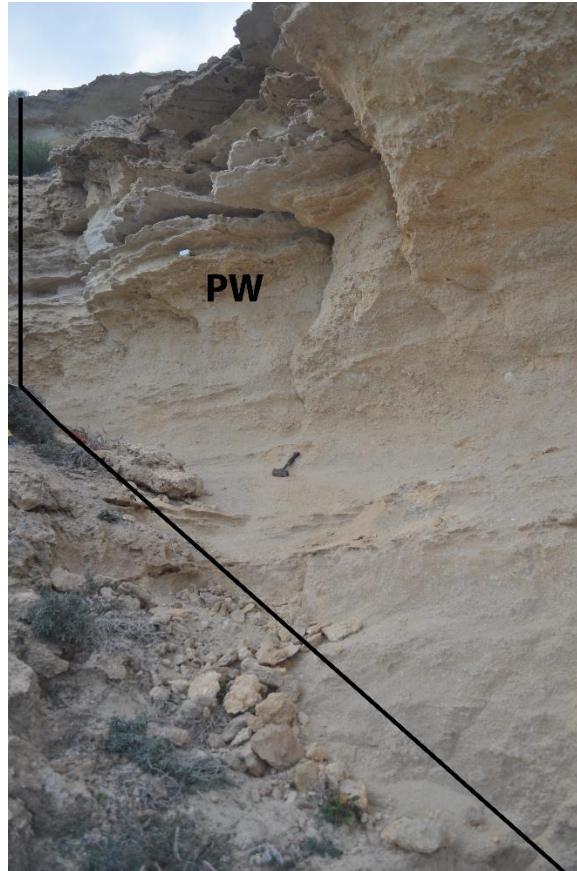
Section	Easting	Northing	Thickness	Elevation
PR- North of Cala de la Pelirroja	597688	4091341	22.8m	10m
PW- North of Cala de la Pelirroja	597900	4091075	14.8m	24m
PT- Cala de la Pelirroja	597929	4090994	6.3m	38m
PM- Cala de la Pelirroja	597925	4090908	27.3m	15m
PB- Cala de la Pelirroja	597926	4090862	6.4m	18m
PD- Cala de la Pelirroja	597912	4090821	16m	22m

PV- Cala de la Pelirroja	597899	4090806	20.5m	31.2m
--------------------------	--------	---------	-------	-------

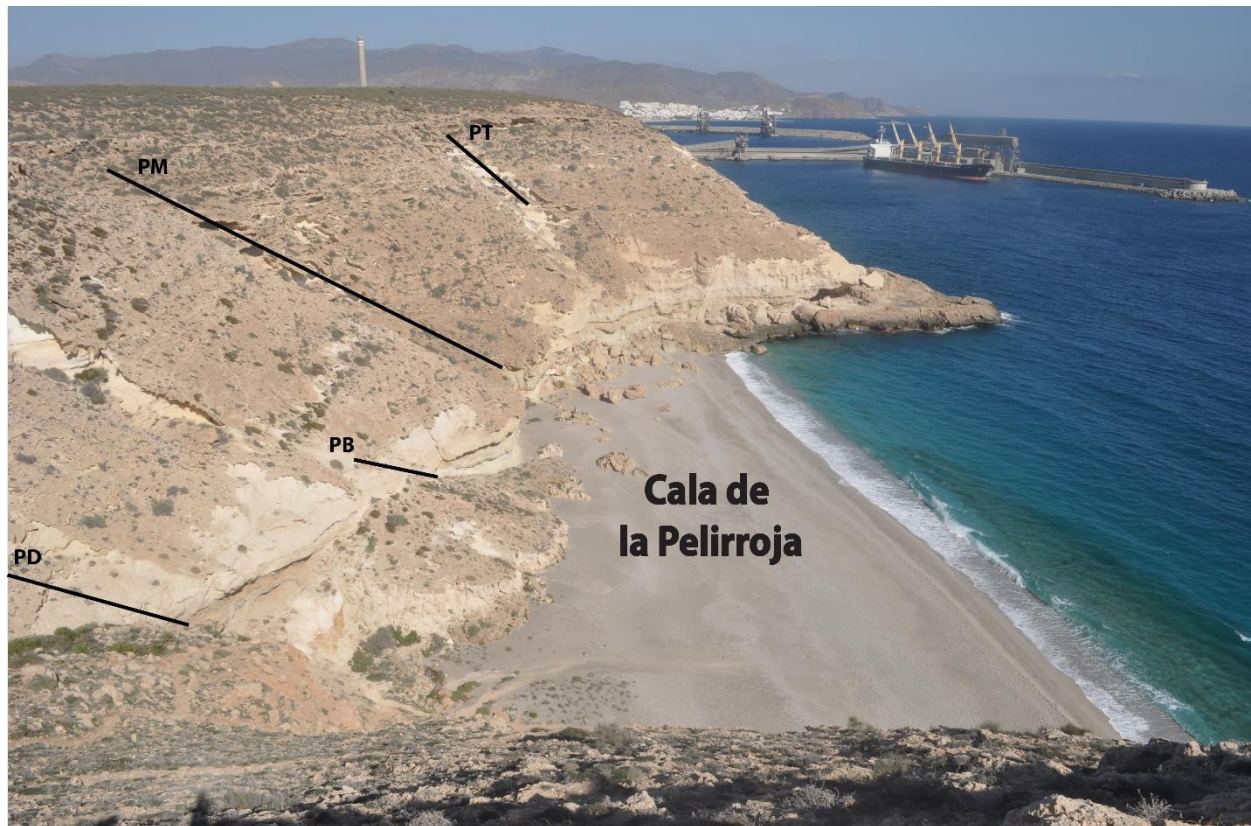
Pliocene measured section data.



Location of most proximal measured section (PR) of the Pliocene deposits, Carboneras Basin

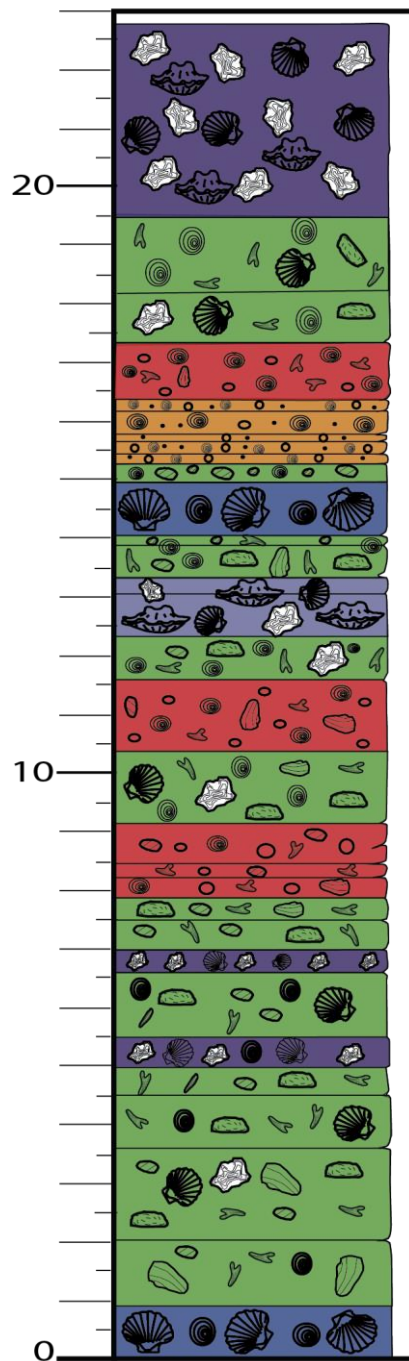


Location of proximal-medial measured section (PW) of the Pliocene deposits, Carboneras Basin



Location of medial-distal measured sections of the Pliocene deposits in Cala de la Pelirroja, Carboneras Basin.

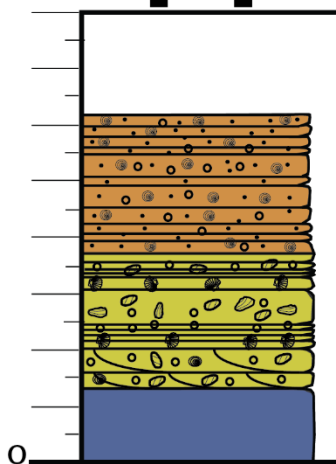
PR



PR measured section from the Miocene

A vertical stratigraphic column showing 15 layers of fossil distribution. The layers are color-coded: yellow (top), purple, orange, green, and blue (bottom). Fossils include brachiopods, bryozoans, and other marine organisms. A scale on the left indicates depth in meters (0 to 10).

PT

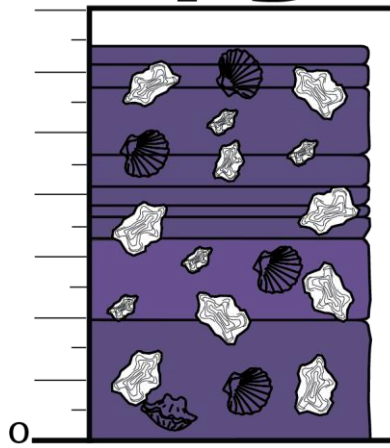


169

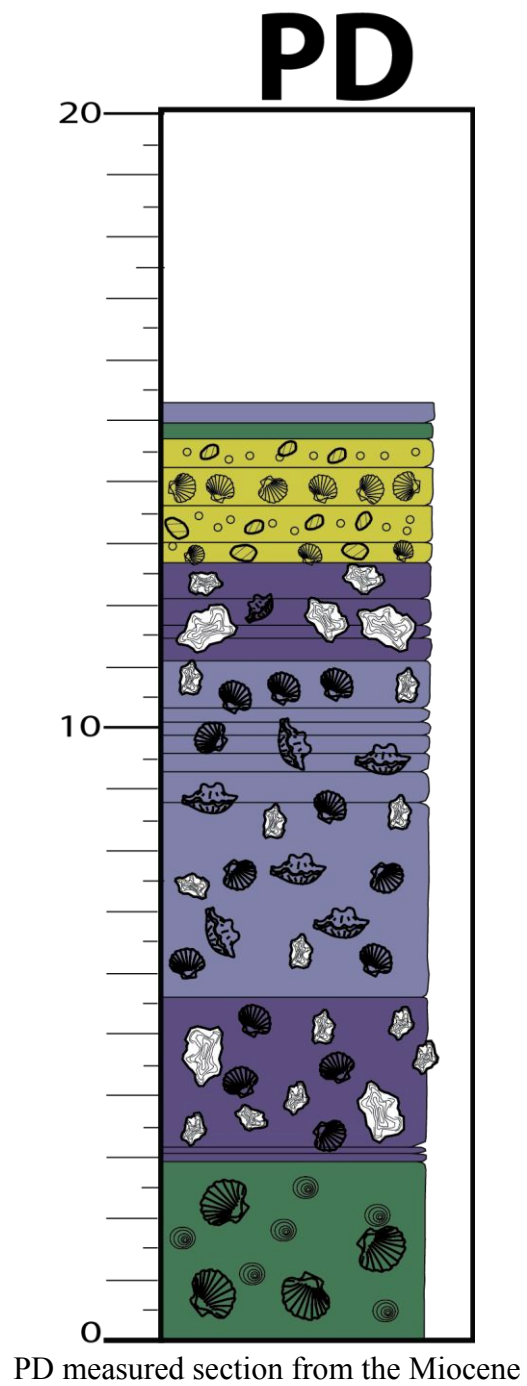
A vertical stratigraphic column representing 30 numbered layers (0 to 30). The column is divided into colored bands: red (layers 1-10), yellow (11-15), blue (16-18), green (19-21), orange (22-24), and purple (25-30). Fossils are illustrated within these layers, including various shells, brachiopods, and other marine organisms. The fossils are distributed across the layers, with some layers containing multiple types of fossils.

170

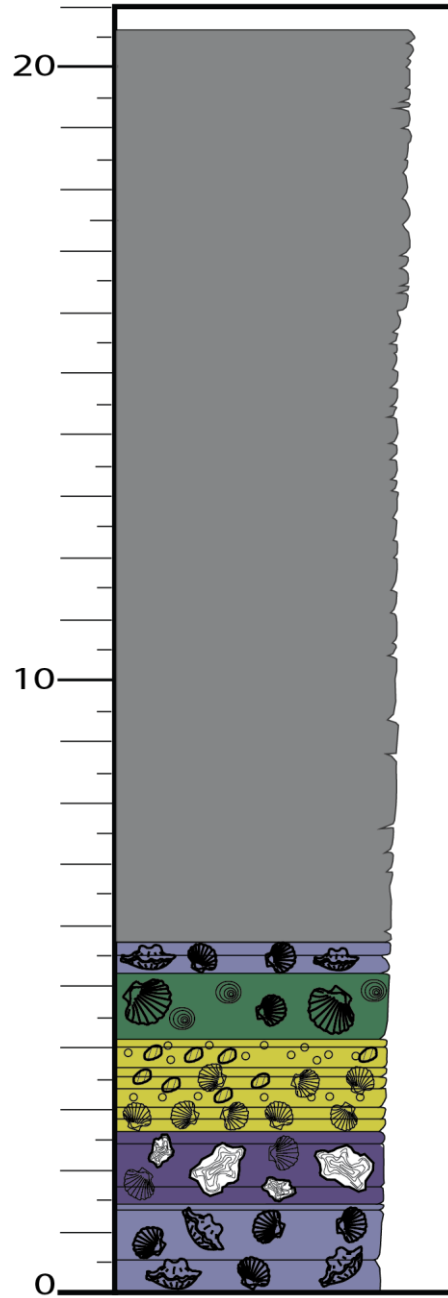
PB



PB measured section from the Miocene



PV



PV measured section from the Miocene

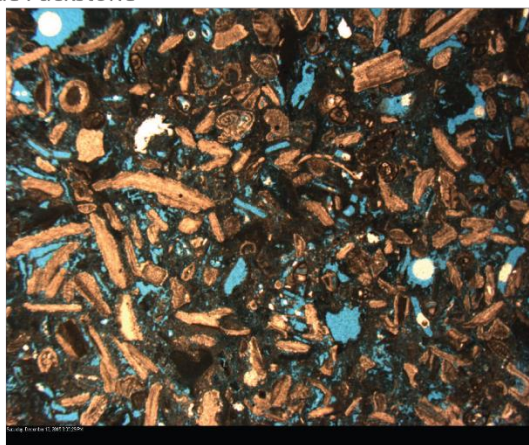
Appendix II

Lithofacies

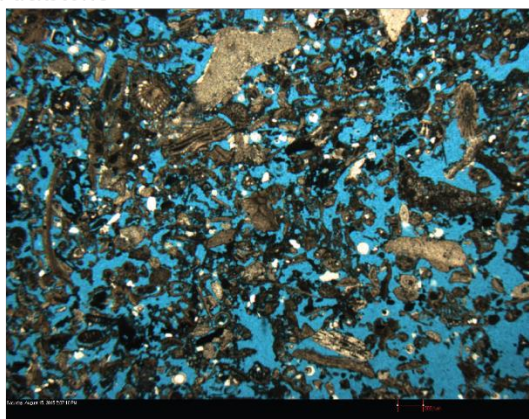
This appendix contains outcrop images and photomicrographs representing each of the 10 Pliocene and 13 Miocene lithofacies.

Pliocene Lithofacies

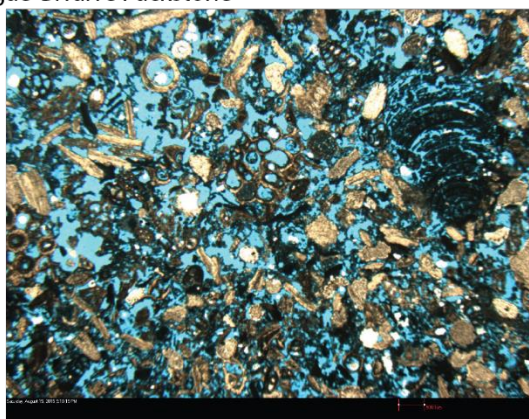
Silty Coralline Algae Packstone



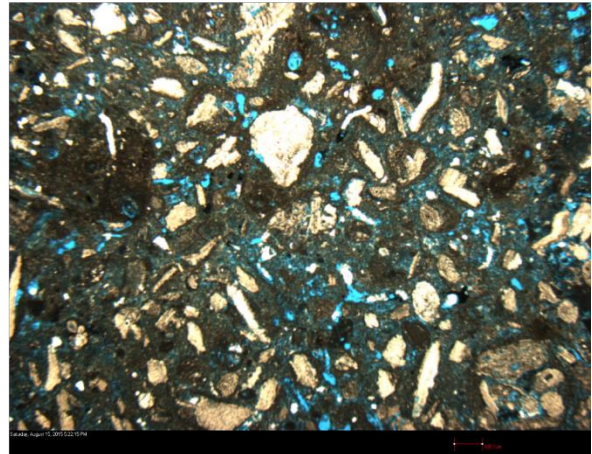
Sorted Bryozoan Packstone



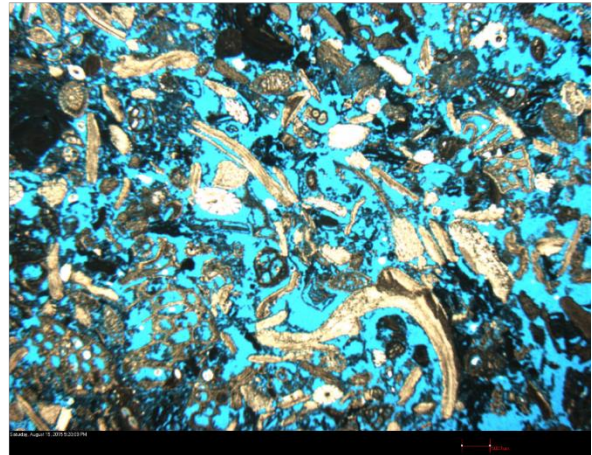
Sorted Coralline Algae-Bivalve Packstone



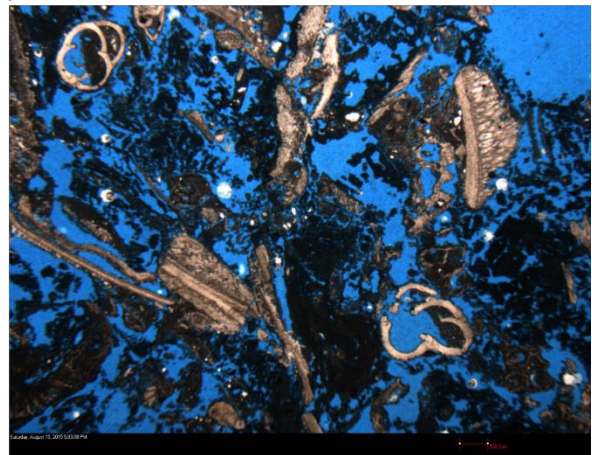
Silt-Gravel Coralline Algae Packstone



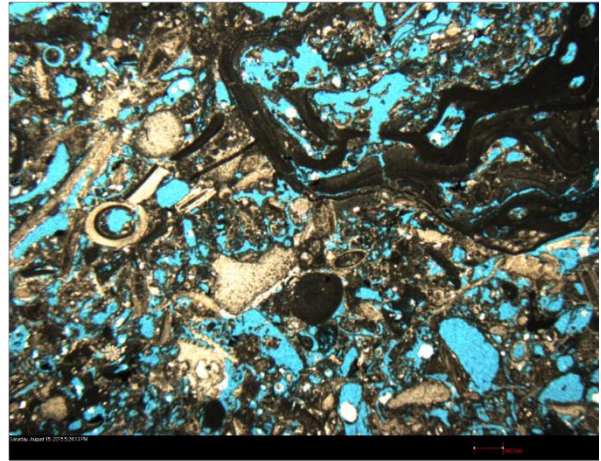
Interbedded Bivalve Packstone



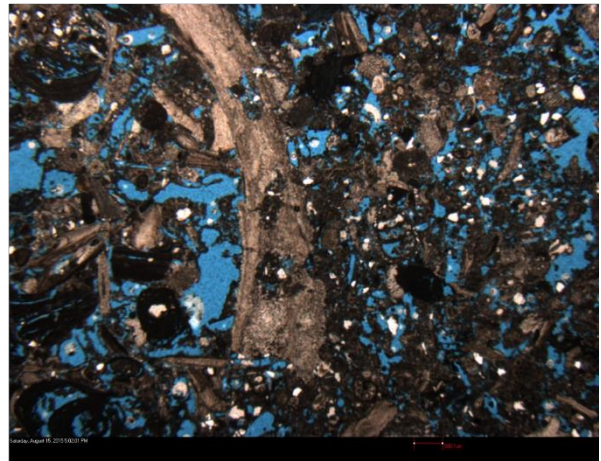
Bryozoan-Coralline Algae Rudstone



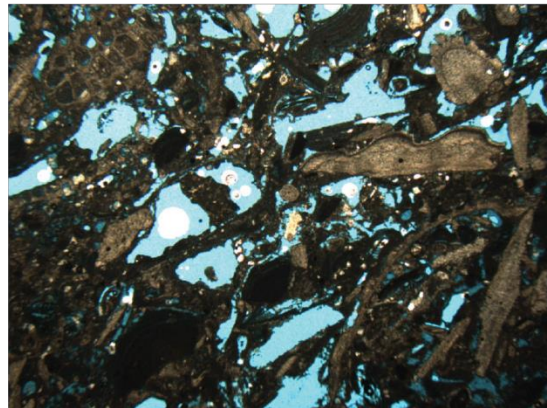
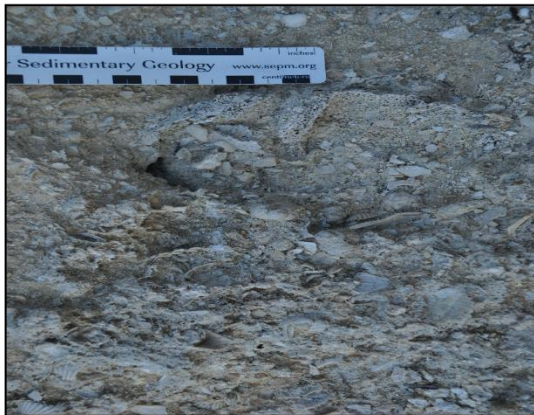
Coralline Algae-Bivalve Rudstone



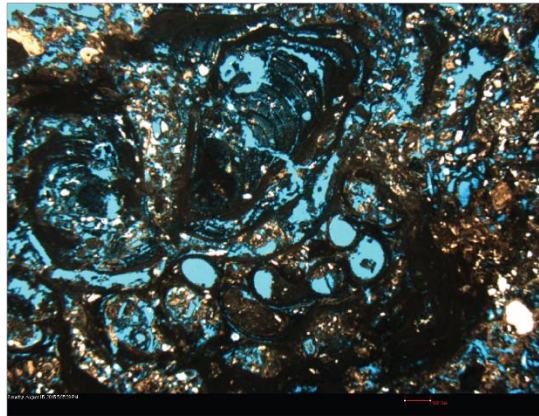
Pecten Rudstone



Ostreid-Pectinid Rudstone

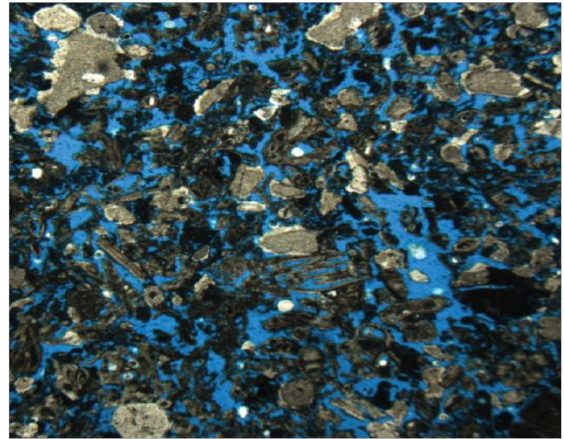
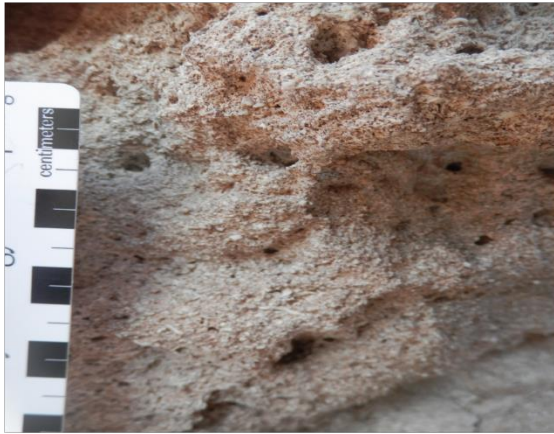


Rhodolith Rudstone

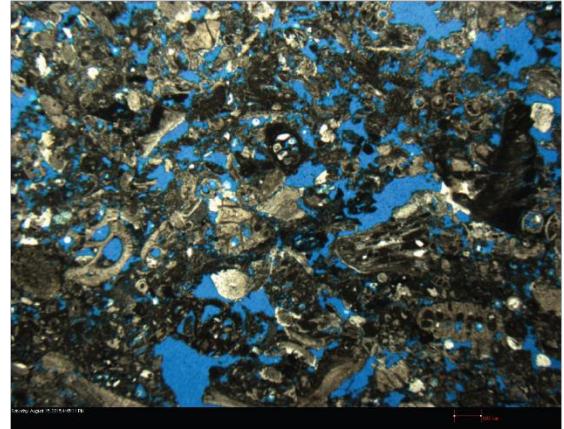


Miocene Lithofacies

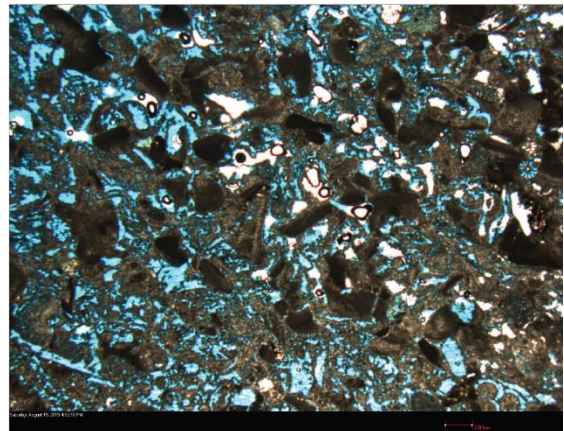
Bryozoan-Echinoid Packstone



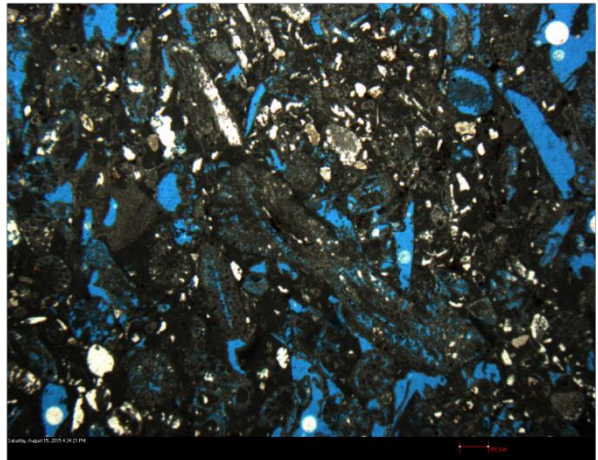
Bryozoan-Bivalve Packstone



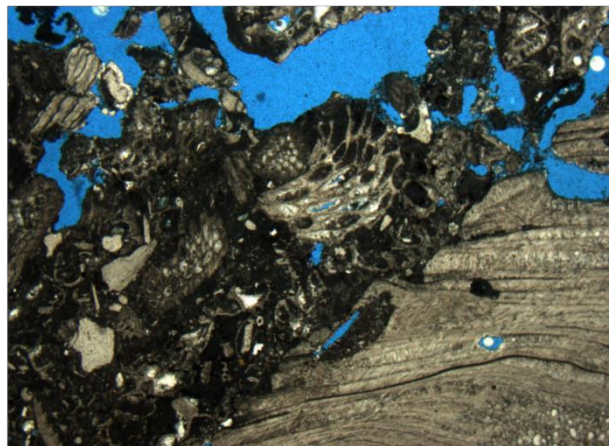
Bivalve-Coralline Algae Packstone



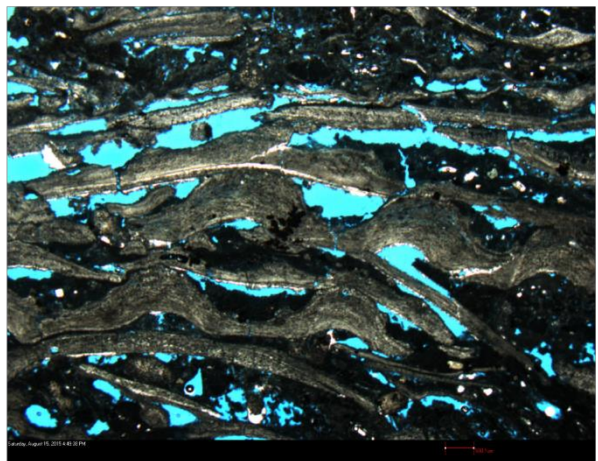
Bryozoan-Ostreid Rudstone



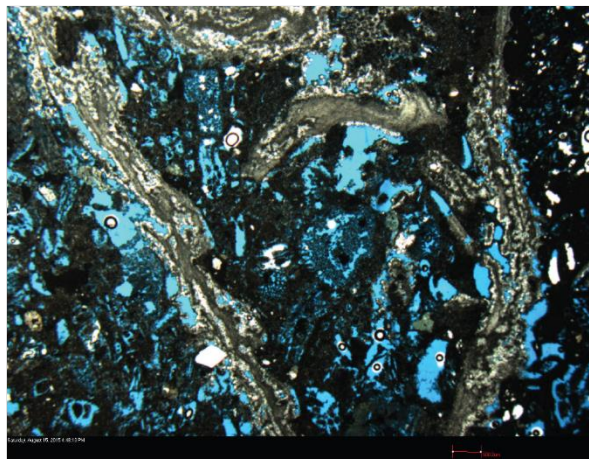
Bryozoan-Pectinid Rudstone



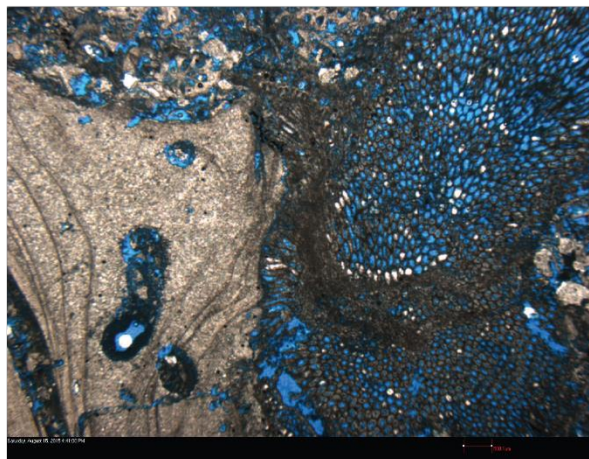
Fragmented Bivalve Rudstone



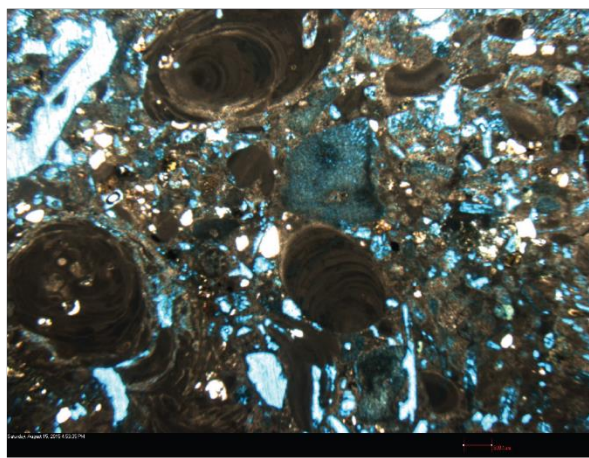
Pecten Rudstone



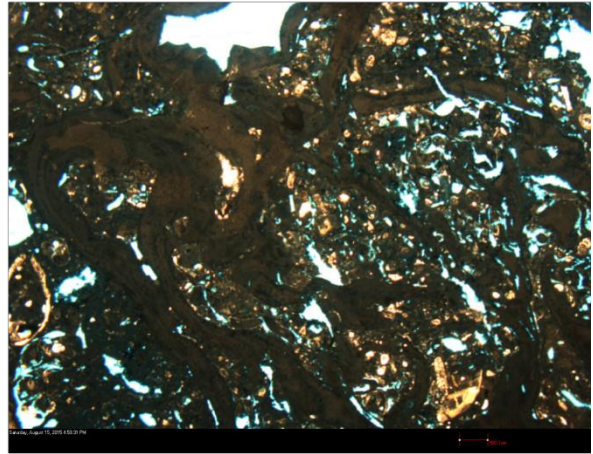
Globular Bryozoan-Clam Rudstone



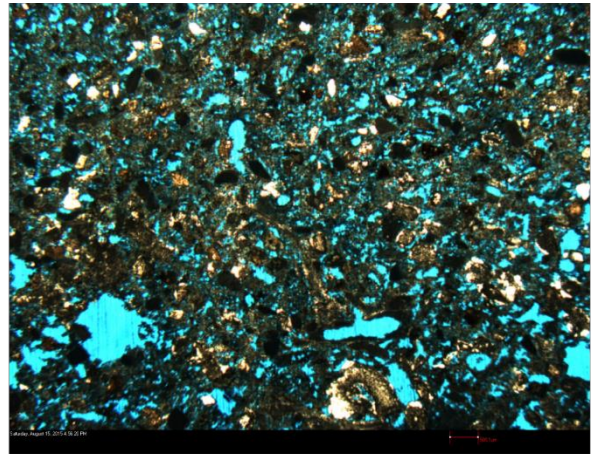
Coralline Algae-Bivalve Rudstone



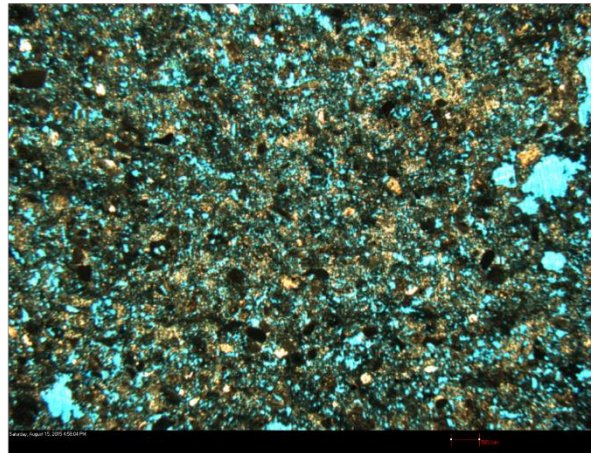
Rhodolith Rudstone



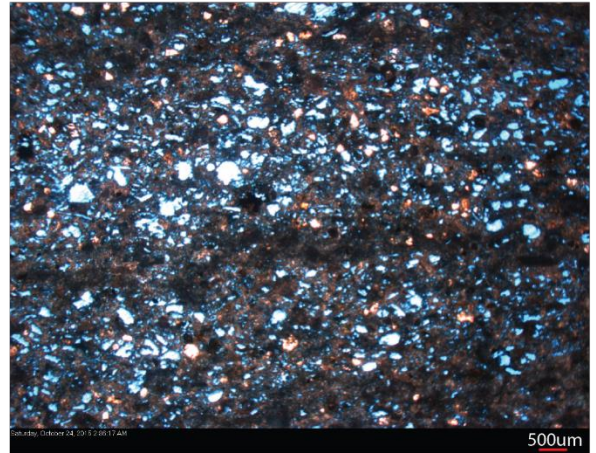
Massive Echinoid Packstone



Massive Foraminifera Wackestone



Bedded Planktonic Foraminiferal Wackestone



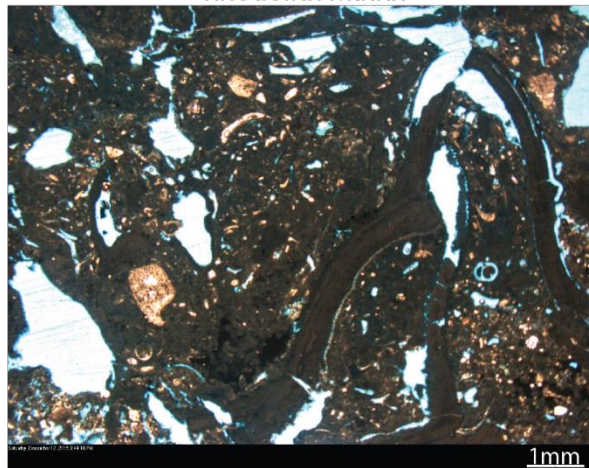
Globular Bryozoans



Bryolith- Encrusting Bryozoan



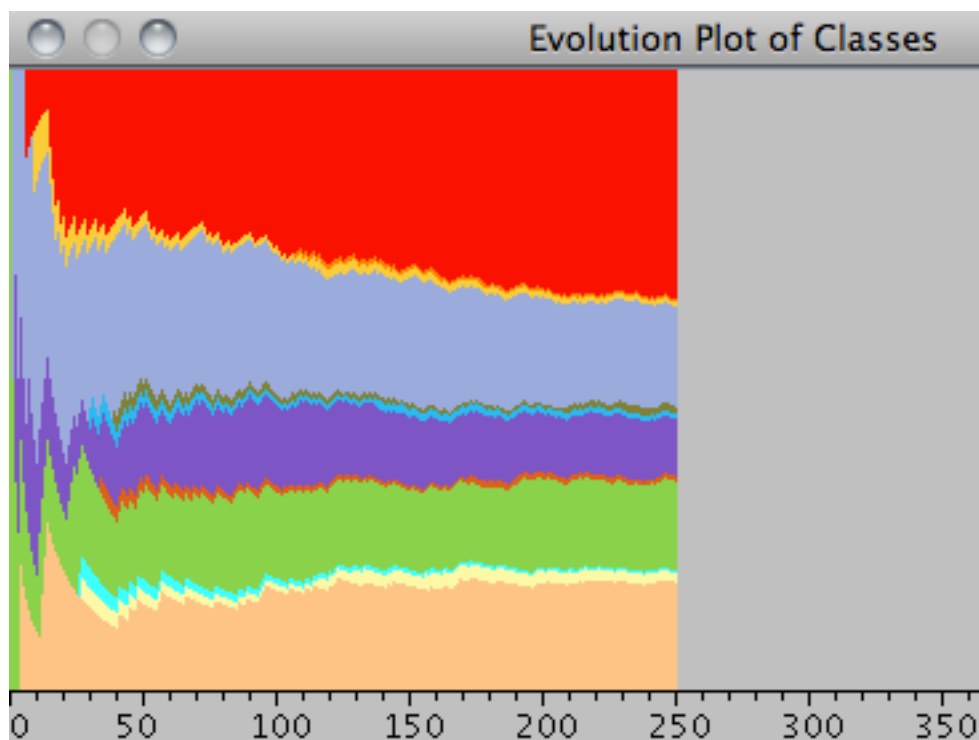
Rhodolith Matrix



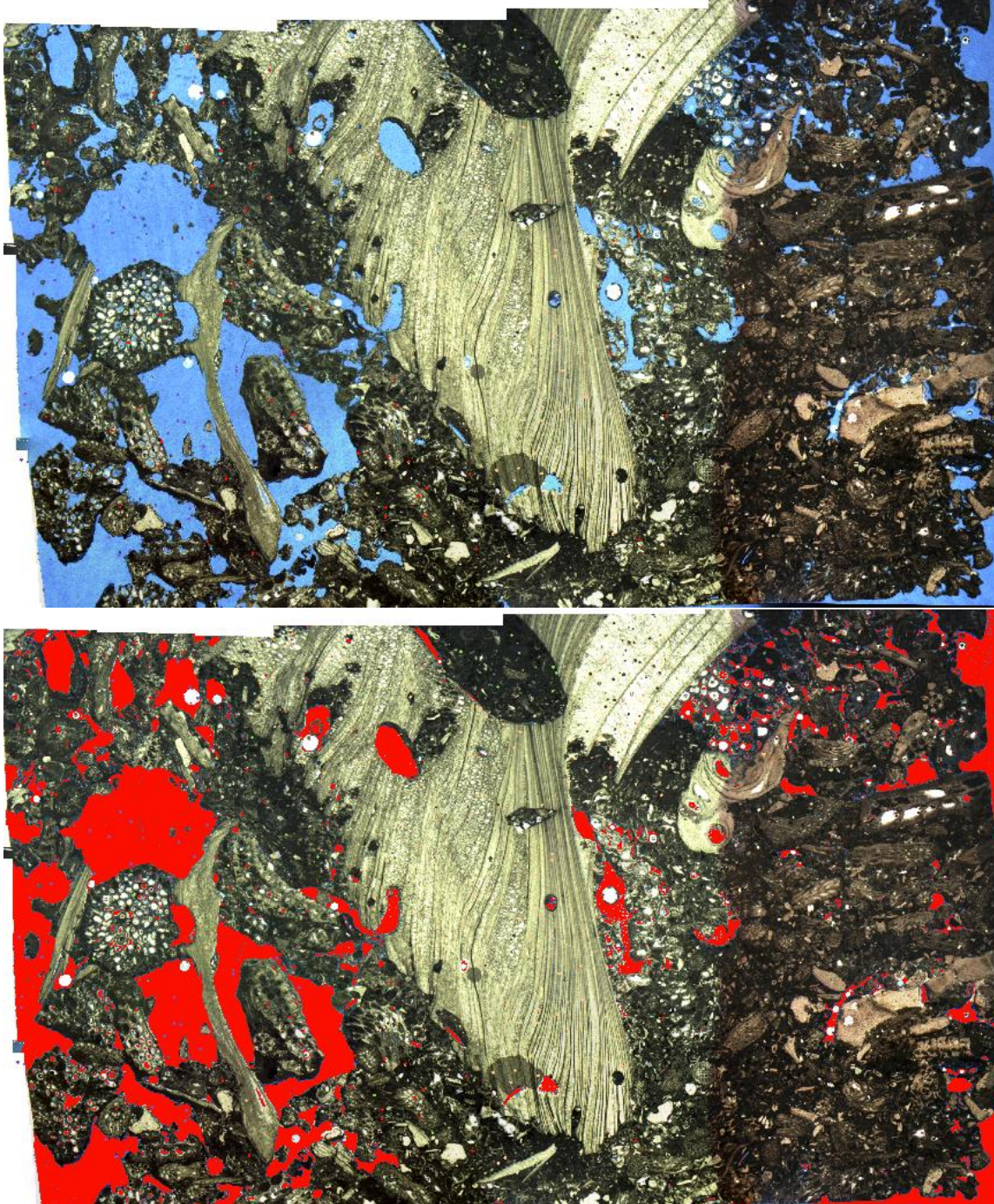
Appendix III

Petrography

Three hundred and thirty-three thin sections were prepared for petrographic analysis for each lithofacies from the Pliocene and Miocene. Point counting was used to measure grain composition and macroporosity. The grid methodology on an electronic stepping stage was used for measurements. Values in the spreadsheets below represent volumes of grain constituents in percentage from each individual sample. Tables in Chapter 2 that contain grain constituent data have been normalized to represent only grain constituents in the rock, with porosity removed. Below the tables include macroporosity values measured through point counting. Background extraction was utilized on a few samples to compare the amounts of macroporosity.



Evolution plot from JMicroVision™. This shows the statistical analysis of constituents as they are point counted. This image shows high fluctuations in constituent percentage when low amount of counts have been recorded, as more point counts are collected, the constituents on the plot flatten out, indicating that a statistically significant amount of point counts have been collected. In this example, the constituents flattened out near 200 counts, and another 50 counts were measured to ensure correct constituent percentages. Point counts taken for each sample ranged from 250-300, based on this evolution plot for the facies.



Photomicrograph showing how background extraction in JMicro Vision™ can be utilized to quantify macroporosity in thin sections and calculate the percentages of macroporosity in thin sections. The top photomicrograph is the normal thin section where blue epoxy has impregnated the sample. The bottom photomicrograph shows the same thin section but the impregnated porosity has been highlighted red and shows how closely background extraction can match and quantify macroporosity in a thin section.

Table including the type of pore space and cement found in each sample.

Section	Type of Pore Space	Cement type
RP		
RP-F1-S2	moldic, intra	equant
RP-F1-S3	moldic	equant
RP-F1-S4	moldic, inter, channel	equant
RP-F2-S1	moldic, intra	equant
RP-F2-S2	moldic, vug	equant
RP-F2-S3	minor moldic, intr, inter	equant
RP-F2-S4	intra, inter, fracture, shelter, minor moldic	equant, syntax overgrowth
RP-F3-S1	intra, minor moldic, inter	equant
RP-F3-S2	inter, minor moldic	equant
RP-F3-S3	moldic, inter, intra	equant, syntax
RP-F4-S1	inter, intra, minor moldic	equant
RP-F4-S2	inter, intra, minor moldic	equant
RP-F4-S3	inter, intra, minor moldic	equant
RP-F4-S4	inter, minor moldic	equant, poikilotopic
RP-F5-S1	moldic, minor vug	poikilotopic
RP-F5-S2a	moldic, minor vug	poikilotopic
RP-F5-S2b	moldic	poikilotopic
RP-F5-S4	moldic, intra	poikilotopic, equant
RP-F5-S5	moldic, intra	poikilotopic, equant
RP-F6-S1	intra, inter, minor moldic	syntaxial, equant
RP-F6-S2	inter, intra, minor moldic	equant, syntaxial
RP-F6-S3	inter, intra, minor moldic	equant, syntaxial
RP-F7-S1a	inter, intra, minor moldic	syntaxial, equant
RP-F7-S1b	inter, intra, minor moldic	syntaxial, equant
RP-F7-S2	inter, intra, minor moldic	syntaxial, equant
RP-F8-S1	inter, intra, minor moldic, shelter	syntaxial, equant
RP-F8-S2	inter, intra, minor moldic	equant, syntaxial
RP-F8-S3	inter, moldic	equant, syntaxial
RP-F9-S2a	inter, shelter, intra, minor moldic	equant, syntaxial
RP-F9-S2b	inter, intra, minor moldic	equant, syntax
RP-F9-S3	inter, intra, moldic	equant, syntax, some bladed
RP-F10-S1	inter, intra, minor moldic	equant
RP-F10-S2	inter, intra, shelter, moldic	equant, syntax

RP-F10-S3a	inter, intra, minor moldic	equant
RP-F10-S3b	inter, intra, minor moldic	equant
RP-F10-S4	intra, inter, vug, shelter	equant
RP-F10-S5	intra, inter, vug, shelter	equant
RP-F11-S1	intra, inter, vug, moldic	equant, bladed
RP-F11-S2	moldic, vug	equant, fibrous
RP-F11-S4a	modlic, intra	equant, blocky
RP-F11-S4b	moldic, intra	equant, blocky
RP-F11-S5	moldic	equant
RM		
RM-F1-S1	inter, moldic, vug	equant-blocky, some drusy
RM-F1-S2	moldic, inter, inter cryst, minor intra	syntax, blocky, drusy,
RM-F1-S4	moldic, vug	equant, minor bladed
RM-F2-S1a	inter, moldic, minor intra	equant, drusy/blocky
RM-F2-S1b	inter, moldic	equant, drusy
RM-F3-S1	intra, moldic, vug	equant, bladed
RM-F3-S3	intra, moldic, vug, inter	equant, bladed
RM-F3-S4	moldic, intra	equant, bladed
RM-F3-S5	moldic, vug, intra	poikilitopic, equant, bladed
RM-F3-S6	moldic, intra, inter	equant, drusy
RM-F4-S1	intra, moldic, inter	bladed, equant
RM-F4-S3	inter, intra, shelter, moldic	equant
RM-F4-S4	inter, shelter, moldic	equant, syntax
RM-F4-S6	inter, intra, moldic	equant
RM-F4-S7	inter, moldic	equant
RM-F5-S2	inter, shelter, intra, moldic	poikilitopic.
RM-F5-S4	inter, intra, moldic	equant, bladed, poikilitopic
RM-F6-S1	moldic, vug, intra	equant
RM-F6-S2	moldic, vug, intra	equant
RM-F6-S3	moldic, vug, intra	equant, fibrous
RM-F7-S2	moldic, vug, intra, inter	equant, other
RM-F7-S3	moldic, intra, inter	dolo rhombs
RM-F7-S4	moldic, intra, inter, vug	equant, rhombs
RM-F8-S1	moldic, intra, inter, vug	rhombs
RM-F8-S2	moldic, vug, intra	-
RM-F8-S3	inter, intra, shelter	syntax, bladed, equant
RM-F8-S4	inter, intra, shelter	syntax, bladed, equant
RM-F9-S1	inter, moldic	syntax, equant, some bladed

RM-F9-S3	inter, modlic, fracture	syntax, equant, some bladed
SP		
SP-F1-S1	modlic, inter	dolo rhombs
SP-F1-S3	modlic, inter	dolo rhombs
SP-F2-S2	modlic, inter, minor intra	dolo rhombs
SP-F2-S3	modlic, inter	dolo rhombs
SP-F2-S4	modlic, inter, vug,	dolo rhombs
SP-F2-S5	modlic, inter, vug, fracture	dolo rhombs
SP-F2-S6	modlic, inter, some intra	dolo rhombs
SP-F2-S7	modlic, inter	dolo rhombs
SP-F2-S8	modlic, inter	dolo rhombs
SP-F3-S1	modlic, inter	dolo rhombs
SP-F3-S2	modlic, inter, intra	dolo rhombs
SP-F3-S3	modlic, inter	dolo rhombs
SP-F4-S1	modlic, intra, inter	dolo rhombs
SP-F4-S3	modlic, intra, vug inter	dolo rhombs, poikl.
SP-F4-S4	modlic, intra, inter	equant,dolo rhombs, poikl.
SP-F4-S5	inter,modlic, intra	equant,dolo rhombs, poikl.
SP-F4-S7	modlic, intra	equant,dolo rhombs
SP-F5-S1	modlic, inter, intra	equant,dolo rhombs, poikl.
SP-F5-S2	inter, modlic, intra	equant, syntax, dolo-rhom
SP-F5-S3	modlic, inter, intra	equant,dolo rhombs, poikl.
SP-F5-S4	modlic, inter, intra	equant,dolo rhombs
SP-F5-S6	modlic, inter, intra	dolo rhombs, poikl.
SP-F5-S7	modlic, inter, intra	dolo rhombs
SP-F6-S1	modlic, inter, vug	dolo rhombs, equant. fibrous
SP-F6-S2	modlic, inter, vug	dolo rhombs
SP-F6-S3	modlic, inter, vug	dolo rhombs
SP-F7-S1	modlic, inter	dolo rhombs
SP-F7-S2	modlic, inter	dolo rhombs
SP-F7-S3	modlic, inter	dolo rhombs
SP-F7-S4	modlic, inter	dolo rhombs
SP-F7-S5	modlic, inter	dolo rhombs
SP-F8-S1	inter, modlic	equant, syntax
SP-F9-S1	modlic, inter	dolo rhombs
SP-F9-S2	modlic, inter	dolo rhombs, poikilotopic
SP-F10-S1	modlic, inter, vug	equant, dolo rhombs
SP-F10-S2	inter, modlic	equant, syntax, dolo rhombs

SP-F10-S3	inter, moldic	equant, syntax, dolo rhombs
SP-F10-S4	inter, moldic	equant, dolo rhombs
SP-F11-S1	moldic, inter	dolo rhombs
SP-F11-S2	moldic inter vug	dolo rhombs
SP-F11-S3	inter, moldic	equant, dolo rhombs
SP-F11-S4	inter, moldic	equant, dolo rhombs
SP-F11-S5	inter, moldic	equant, dolo rhombs
SP-F13-S1	moldic, inter	dolo rhombs
SP-F13-S2	moldic, inter	equant, dolo rhombs
SP-F13-S3	moldic, inter, minor intra	dolo rhombs
SP-F13-S4	moldic, inter	equant, syntax, dolo rhombs
SP-F13-S5	moldic, inter, vug	dolo rhombs, syntax, fibrous
SP-F13-S6	mostly moldic, some inter	dolo rhombs
SP-F13-S8	mostly moldic, vug, some inter	dolo rhombs
SP-F13-S9	moldic, inter, intra	dolo rhombs, equant
SP-F14-S1	inter, moldic, intra	dolo rhombs, equant, syntax, fibrous
SP-F14-S2	inter, intra, moldic	dolo rhomb, poikilitic, syntax, bladed
SP-F14-S3	inter, moldic, intra	dolo rhomb, equant, poikilitic
SP-F14-S4	inter, moldic, intra	dolo rhomb, equant, syntax
SP-F14-S5	inter, moldic, intra	dolo rhomb, equant, syntax
SP-F14-S6	inter, intra, minor moldic	equant, bladed
SP-F14-S7	inter, intra, minor moldic	equant, syntax,
SP-F14-S8	inter, intra, minor moldic	equant, syntax
SP-F16-S1	inter, intra, minor moldic	bladed, equant
SP-F16-S2	intra, inter, minor moldic	bladed, equant, syntax
SP-F16-S3	inter, intra, moldic	bladed, some equant, syntax
SP-F16-S5	intra, inter, moldic	equant, bladed
SP-F16-S6	intra, inter, moldic, fracture	equant, calcite rhombs
SP-F16-S7	inter, intra, moldic	equant, dolo rhombs
SP-F16-S10	inter, intra, moldic	equant, bladed, syntax
WF		
WF-F1-S1	inter, intra, framework, moldic	equant, syntax
WF-F2-S1	framework, intra, some moldic	equant, syntax
WF-F4-S1	framework, moldic, minor inter	equant, bladed, syntax
WF-F5-S1	intra, moldic, minor inter	equant, bladed, syntax
WF-F5-S2	inter, moldic, minor intra	equant, bladed, syntax
WF-F6-S1	framework, moldic	equant

WF-F6-S3	framework, moldic	equant
WF-F6-S4	framework, moldic	equant
WF-F6-S5	framework, moldic	equant
WF-F6-S6	framework, moldic	equant
PR		
PR-F1-S1	inter, moldic, intra and frame	bladed, syntax
PR-F1-S2	inter, moldic, intra and frame	bladed, syntax
PR-F1-S3	inter, moldic, intra and frame	bladed, syntax
PR-F2-S2	inter, moldic, intra, minor shelter and frame	bladed, syntax
PR-F2-S4	inter, moldic, intra, minor shelter and frame	bladed, syntax
PR-F2-S5	inter, moldic, intra, minor shelter and frame	bladed, syntax
PR-F2-S6	inter, moldic, intra, minor shelter and frame	bladed, syntax
PR-F2-S7	inter, moldic, intra, minor shelter and frame	bladed, syntax
PR-F2-S8	inter, moldic, intra, minor shelter and frame	bladed, syntax
PR-F3-S1	inter, framework, minor intra	bladed, syntax, equant
PR-F3-S2	inter, framework, minor intra	bladed, syntax, equant
PR-F3-S3	inter, framework, minor intra	bladed, syntax, equant
PR-F4-S1	inter, intra, moldic	bladed, syntax
PR-F5-S1	inter, intra, moldic	bladed, syntax
PR-F5-S2	intra, moldic, minor inter	bladed, syntax
PR-F5-S3	intra, moldic, minor inter	bladed, syntax
PR-F6-S1	inter, intra	bladed, syntax
PR-F7-S1	inter, intra, minor moldic	bladed, syntax
PR-F7-S2	inter, intra, minor moldic	bladed, syntax
PR-F7-S3	inter, intra, minor moldic	bladed, syntax
PR-F8-S1	inter, intra, shelter	bladed, syntax
PR-F11-S1	inter, moldic, intra, framework	bladed, syntax
PR-F11-S2	inter, moldic, intra, framework	bladed, syntax
PR-F11-S4	inter, moldic, intra, framework	bladed, syntax
PR-F13-S1	inter, intra, minor moldic	bladed, syntax
PR-F13-S2	intra, moldic, minor inter	bladed, syntax
PR-F13-S3	inter, intra, moldic- all about the same	bladed, syntax
PR-F14-S1	inter, intra, moldic	bladed, syntax
PR-F14-S2	inter, intra, shelter, moldic framework	bladed, syntax

PR-F14-S3	inte, moldic, intra	bladed, syntax
PR-F14-S4	inter, intra	bladed, syntax
PR-F14-S5	inter, intra	bladed, syntax
PR-F14-S6	inter, intra, shelter, moldic	bladed, syntax
PR-F14-S7	intra, moldic	bladed, syntax
PR-F14-S8	inter, intra, moldic, shelter	bladed, syntax
PR-F14-S9	inter, intra, minor moldic	bladed, syntax
PR-F15-S1	intra, frame, moldic	bladed, syntax
PR-F15-S2	inter, modlic, frame	bladed, syntax
02-114	inter, moldic, intra	bladed
PW		
PW-F1-S4	mostly inter, some intra	bladed, fibrious, syntaxial
PW-F1-S5	mostly inter, some intra, minor moldic	bladed, minor syntax
PW-F1-S6	inter, intra, minor moldic	bladed, equant
PW-F2-S1	intra, inter	bladed, equant
PW-F3-S2	inter, intra, shelter, minor moldic	bladed, syntax
PW-F3-S4	mostly intra, inter, minor modlic	
PW-F4-S1	mostly all inter, minor intra and moldic	bladed, syntax
PW-F4-S2	inter, moldic, intra	
PW-F5-S1	inter, moldic	bladed, syntax
PW-F6-S3	intra, inter, moldic	bladed
PW-F6-S4	inter, intra	syntax, bladed
PW-F6-S7	inter, intra, moldic	bladed, syntax
PW-F6-S9	inter, intra, moldic	bladed, syntax
PT		
PT-F1-S2	inter, intra, shelter, minor moldic	bladed, syntax
PT-F1-S4	inter, moldic, intra	bladed, syntax
PT-F1-S1-lat 10	inter, minor intra and minor moldic	syntax, bladed
PT-F2-S1	inter, minor intra and minor moldic	bladed
PT-F2-S4	inter, intra, minor moldic	bladed rind, syntax
PT-F2-S6	inter, minor intra	bladed, syntax
PT-F3*-S1	intra, inter, moldic	bladed, syntax
PT-Trunc.-F3*-S3	intra, inter, moldic	bladed
PT-Trunc.-F3*-S4	intra, inter, moldic	bladed, syntax
PM		

PM-F1-S1	inter, intra, moldic	bladed, equant
PM-F5-S1	inter, intra, shelter, moldic	bladed
PM-F5-S2	inter, moldic, intra	bladed, rhombs
PM-F5-S3	inter, moldic, intra	bladedm equant
PM-F5-S4	inter, moldic, intra	bladed
PM-F6-S1	intra, moldic, inter	bladed
PM-F6-S4	inter, moldic, intra	bladed
PM-F7-S1	inter, moldic, intra	bladed
PM-F7-S2	inter, moldic	bladed
PM-F7-S4	inter, moldic, minor intra	bladed
PM-F7-S6	inter, moldic	bladed
PM-F8-S1	inter, moldic, intra	bladed, syntax
PM-F8-S2	inter, moldic, intra	bladed, syntax
PM-F10-S1	intra, moldic	
PM-F10-S3	inter, moldic, intra, shelter,	bladed, syntax
PM-F11-S1	inter, moldic, intra	bladed
PM-F11-S3	inter, moldic, minor shelter	bladed
PM-F11-S5	inter, moldic, minor shelter	bladed, equant
PM-F11-S6	inter, moldic, minor intra	bladed, fibrious
PM-F12-S1	intra, moldic, inter	bladed, equant
PM-F12-S2	inter, moldic, minor intra	bladed, minor syntax
PM-F12-S3	inter, moldic, minor intra	bladed, minor syntax
PM-F13-S1	inter, intra, moldic	bladed, minor syntax
PM-F13-S2	inter, intra, moldic	bladed, minor syntax
PM-F16-S2	inter, minor moldic	bladed, syntax
PM-F17-S1	inter, minor intra	bladed, syntax
PB		
PB-F1-S1	inter, moldic, intra, framework	bladed, equant
PB-F1-S4	inter, moldic, intra, framework	bladed, equant
PB-F2-S1	framework, moldic, inter, intra	bladed
PB-F3-S1	inter, moldic, framework, intra	bladed, syntax
PB-F3-S2	inter, framework, moldic, intra	bladed, equant
PB-F3-S3	framework, moldic, intra, inter, shelter	bladed, equant
PB-F3-S4	framework, moldic, inter, intra	bladed
PD		
PD-F1-S1	inter, moldic, framework	bladed, syntax
PD-F1-S4	moldic, inter, framework	bladed, syntax

PD-F2-S1	framework, minor moldic	bladed, equant
PD-F3-S4	moldic, inter, framework	bladed, syntax
PD-F3-S7	inter, moldic, framework	bladed
PD-F4-S1	framework, moldic, inter	bladed, equant
PD-F4-S3	framework, inter, moldic	bladed
PD-F4-S4	framework, moldic, inter	bladed and rhombs, syntax
PD-F5-S2	inter, moldic, framework	bladed
PV		
PV-F1-S3	moldic, framework, shelter	bladed, equant
PV-F2-S1	framework, minor inter and moldic	bladed
PV-F2-S3	framework, minor inter and moldic	minor bladed and syntax
PV-F3-S4	inter, moldic, minor framework and shelter	bladed, syntax
PV-F4-S1	inter, moldic minor intra	bladed
PV-F4-S2	inter, moldic, framework	bladed
PV-F5-S4	shelter, moldic, inter, minor framework	bladed, syntax
PV(PB)-F3-S5	inter, moldic	bladed, syntax

Table of percentages of constituents in each sample.

RP			RM	
Class	Percentage		Class	Percentage
RP-F1-S2			RM-F1-S1	
Bryozoan (b)	29.25		Bryozoan	30.00
Matrix	18.58		Echinoid	9.60
Bryozoan (g)	14.62		Benthic Foram	3.00
Echinoid	2.37		Macro ϕ	11.00
Benthic Foram	1.58		Unknown	0.80
Macro ϕ	1.00		Matrix	7.60
Moldic ϕ	32.00		Mold-Bivalve	2.40
			Bivalve	8.40
RP-F1-S3			Cement	10.00
Bryozoan	54.80		Coralline Algae (b)	9.20
Coralline Algae (b)	1.60		Mold- B. Foram	0.40
Echinoid	2.40		Cement- Bryozoan	1.60
Benthic Foram	2.00		Cement- Foram	0.40
Cement	0.40		Mold-Bryozoan	0.40

Macro ϕ	4.40		Mold-Bivalve	2.40
Unknown	0.40			
Matrix	12.80		RM-F1-S2	
Moldic ϕ	20.80		Bryozoan	23.00
			Macro ϕ	9.00
RP-F1-S4			Echinoid	12.00
Bryozoan	27.60		Moldic ϕ	10.00
Bivalve	14.4		Cement-Bryozoan	5.00
Gastropod	0.40		Bivalve	6.00
Coralline Algae	6.00		Cement	16.00
Echinoid	8.00		Coralline Algae	6.40
Benthic Foram	2.00		Unknown	0.80
Cement	10.00		Benthic Foram	3.60
Macro ϕ	7.20		Matrix	5.20
Matrix	24.00		Cement- Foram	0.40
			Cement- Bivalve	0.40
RP-F2-S1				
Bryozoan (b)	41.20			
Bryozoan (g)	16.80		RM-F1-S4	
Bivalve	4.40		Bivalve	6.43
Cement	0.80		Moldic ϕ	17.60
Moldic ϕ	27.20		Bryozoan	35.70
Unknown	0.40		Echinoid	4.00
Matrix	2.00		Matrix	6.40
Macro ϕ	6.80		Mold-Bivalve	1.60
			Benthic Foram	5.22
RP-F2-S2			Macro ϕ	8.83
Bryozoan (b)	46.00		Coralline Algae	8.43
Bryozoan (g)	0.80		Mold- B. Foram	0.80
Bivalve	6.00		Cement	3.61
Echinoid	1.60		Mold- Bryozoan	0.40
Benthic Foram	6.00		Unknown	0.80
Cement	2.80			
Macro ϕ	9.60		RM-F2-S1a	
Unknown	0.80		Echinoid	20.4
Matrix	7.20		Macro ϕ	10.8
Mold-Bryozoan	0.80		Bivalve	6.8

Cement-Bryozoan	1.20		Cement	10
Moldic ϕ	17.20		Gastropod	0.4
			Cement- Bivalve	0.8
RP-F2-S3			Bryozoan	22.8
Bryozoan (b)	34.00		Coralline Algae	6.4
Bryozoan (g)	14.80		Unknown	8.4
Echinoid	6.40			
Benthic Foram	1.60		Benthic Foram	0.4
Cement	3.20		Moldic ϕ	1.6
Macro ϕ	14.80		Coralline Algae (e)	9.2
Unknown	1.60		Cement- Echinoid	0.4
Matrix	4.40		Matrix	0.8
Bivalve	18.40		Mold-Bivalve	0.8
RP-F2-S4			RM-F2-S1b	
Bryozoan (b)	45.42		Echinoid	14.1
Bryozoan (g)	1.99		Macro ϕ	12
Coralline Algae	0.40		Bryozoan	43
Echinoid	8.37		Coralline Algae (b)	2
Benthic Foram	1.59		Cement	8.7
Cement	6.37		Matrix	1.2
Macro ϕ	9.56		Benthic Foram	0.4
Unknown	0.40		Bivalve	6.2
Matrix	7.57		Coralline Algae (e)	10.4
Moldic ϕ	1.59		Unknown	0.8
Bivalve	16.73		Moldic ϕ	0.4
RP-F3-S1			RM-F2-S2	
Bryozoan	62.40		Echinoid	12.4
Echinoid	15.60		Macro ϕ	10.4
Matrix	4.80		Cement	28.4
Bivalve	6.00		Bryozoan	14
Macro ϕ	5.20		Benthic Foram	1.2
Unknown	0.40		Bivalve	16.8
Benthic Foram	1.60		Volcanics	4.8
Moldic ϕ	1.20		Moldic ϕ	1.6
Barnacle	0.80		Unknown	1.6

Cement	1.60		Coralline Algae (e)	8.4
Planktonic Foram	0.40		Matrix	0.4
			RM-F3-S1	
RP-F3-S2			Matrix	8
Bryozoan (b)	65.60		Bivalve	11.2
Bryozoan (g)	0.40		Bryozoan	40
Barnacle	0.40		Moldic ϕ	19.2
Echinoid	9.20		Benthic Foram	1.6
Benthic Foram	2.80		Mold-Foram	1.6
Cement	0.40		Cement	3.2
Macro ϕ	2.40		Mold-Bivalve	1.2
Unknown	1.60		Echinoid	0.4
Matrix	8.00		Unknown	2.4
Mold-Bivalve	0.80		Coralline Algae (e)	0.8
Moldic ϕ	0.40		Coralline Algae	0.4
Bivalve	8.00			
			RM-F3-S3	
RP-F3-S3			Mold-Bivalve	1.2
Bryozoan	41.20		Bivalve	30
Serpulid	0.40		Bryozoan	32.4
Gastropod	1.20		Benthic Foram	2.4
Echinoid	13.60		Moldic ϕ	13.2
Benthic Foram	5.60		Echinoid	3.2
Cement	4.80		Mold-Bryozoan	0.4
Macro ϕ	14.00		Matrix	10
Unknown	2.40		Macro ϕ	1.6
Matrix	3.60		Coralline Algae	1.2
Mold-Bivalve	0.40		Unknown	1.2
Moldic ϕ	6.00		Mold- B. Foram	1.2
Bivalve	5.60		Cement	0.4
Scaphopod	0.40		Mold- Bryozoan	1.2
			Planktonic Foram	0.4
RP-F4-S1				
Bryozoan	37.05		RM-F3-S4	
Serpulid	0.40		Bivalve	27.6
Barnacle	0.80		Macro ϕ	8
Echinoid	16.33		Bryozoan	33.6
Benthic Foram	1.20		Echinoid	2.8

Cement	0.80		Unknown	5.2
Macro ϕ	9.16		Mold- Echinoid	0.8
Unknown	0.80		Mold-Bivalve	2.4
Matrix	14.34		Benthic Foram	3.6
Mold-Bivalve	0.40		Matrix	3.6
Moldic ϕ	1.59		Coralline Algae	0.8
Bivalve	17.13		Moldic ϕ	5.2
			Planktonic Foram	0.4
RP-F4-S2			Cement	2
Bryozoan	46.00		Mold- B. Foram	0.8
Barnacle	0.40		Coralline Algae (e)	2.4
Echinoid	9.20		Mold- Bryozoan	0.8
Benthic Foram	0.40			
Cement	2.80		RM-F3-S5	
Macro ϕ	0.80		Bivalve	40.8
Unknown	0.40		Bryozoan	31.2
Matrix	21.20		Cement- Bryozoan	~5.6
Mold-Bivalve	0.40		Mold Coralline Algae	1.2
Cement- Bryozoan	3.20		Mold-Bivalve	1.6
Cement- B. Foram	0.40		Matrix	2.8
Cement- Echinoid	0.40		Cement- Bivalve	1.2
Moldic ϕ	0.80		Serpulid	0.4
Bivalve	13.60		Macro ϕ	4
			Cement	3.2
RP-F4-S3			Echinoid	0.8
Bryozoan	22.40		Unknown	2
Echinoid	3.20		Coralline Algae	0.4
Benthic Foram	1.20		Coralline Algae (e)	0.8
Cement	0.80			
Macro ϕ	18.40		RM-F3-S6	
Unknown	0.40		Bivalve	54.4
Matrix	8.00		Bryozoan	19.2
Moldic ϕ	0.40		Moldic ϕ	6.4
Bivalve	45.20		Mold-Bivalve	2
			Macro ϕ	6
RP-F4-S4			Mold- Bryozoan	1.2

Bryozoan	53.88		Matrix	4.8
Serpulid	0.39		Benthic Foram	0.8
Echinoid	5.81		Mold- B. Foram	1.2
Benthic Foram	0.78		Echinoid	1.2
Cement	19.77		Cement- Bryozoan	0.4
Macro ϕ	2.71		Cement- B. Foram	0.4
Unknown	0.39		Cement	1.2
Matrix	7.75			
Cement- Bivalve	0.39		RM-F4-S1	
Cement- Bryozoan	1.55		Bryozoan	34
Moldic ϕ	0.39		Macro ϕ	7.6
Bivalve	5.81		Bivalve	46
			Benthic Foram	0.8
RP-F5-S1			Moldic ϕ	3.6
Bryozoan	33.20		Matrix	2.4
Echinoid	5.60		Cement	1.6
Benthic Foram	2.40		Mold- Bryozoan	0.4
Cement	18.00		Cement- Bryozoan	0.8
Macro ϕ	5.20		Echinoid	1.6
Unknown	6.00		Mold- Bivalve	0.8
Matrix	3.60		Mold- B. Foram	0.4
Mold-Bivalve	0.40			
Mold- B. Foram	0.40		RM-F4-S3	
Moldic ϕ	24.80		Matrix	2.4
Bivalve	0.40		Mold-Bivalve	7.2
			Bivalve	79.2
RP-F5-S2a			Moldic ϕ	1.6
Bryozoan	34.40		Bryozoan	5.2
Echinoid	2.80		Macro ϕ	2.4
Benthic Foram	4.40		Benthic Foram	0.8
Macro ϕ	6.40		Echinoid	0.8
Unknown	9.60		Unknown	0.4
Matrix	1.60			
Mold-Bivalve	0.80		RM-F4-S4	
Mold- B. Foram	0.40		Bivalve	74.4
Moldic ϕ	36.80		Macro ϕ	8.4

Bivalve	2.80		Moldic ϕ	1.2
Cement	2.00		Matrix	6.4
			Benthic Foram	2
RP-F5-S4			Bryozoan	4.8
Bryozoan	44.80		Mold-Bivalve	2
Cement	28.80		Echinoid	0.8
Echinoid	5.60			
Mold- B. Foram	0.40		RM-F4-S6	
Moldic ϕ	6.40		Bivalve	50
Matrix	4.40		Macro ϕ	9.6
Bivalve	1.20		Bryozoan	25.2
Cement- B. Foram	0.80		Matrix	6
Macro ϕ	1.20		Moldic ϕ	2
Benthic Foram	1.60		Coralline Algae	0.8
Unknown	1.20		Echinoid	2
Barnacle	3.20		Moldic- B. Foram	0.4
Cement- Bivalve	0.40		Cement	2
			Coralline Algae (e)	0.4
RP-F5-S5			Mold-Bivalve	0.8
Bryozoan	44.00		Benthic Foram	0.8
Moldic ϕ	16.00			
Cement	18.80		RM-F4-S7	
Matrix	2.80		Bryozoan	23.2
Echinoid	4.80		Moldic ϕ	2.4
Bivalve	6.40		Bivalve	58.4
Unknown	0.80		Matrix	3.6
Benthic Foram	2.00		Macro ϕ	4.8
Macro ϕ	4.00		Mold-Bivalve	2.4
			Benthic Foram	2
RP-F6-S1			Mold- B. Foram	0.4
Bryozoan	49.20		Serpulid	0.4
Echinoid	13.20		Cement	0.8
Planktonic Foram	1.60		Echinoid	1.2
Benthic Foram	5.60			
Macro ϕ	19.20		RM-F5-S2	
Unknown	1.20		Bryozoan	23.6

Matrix	4.00		Macro ϕ	14
Mold-Bivalve	0.40		Bivalve	51.2
Bivalve	5.60		Moldic ϕ	1.6
Cement	1.00		Echinoid	6
			Benthic Foram	0.8
RP-F6-S2			Matrix	1.6
Bivalve	18.40		Cement	0.4
Benthic Foram	7.60			
Bryozoan	38.00		RM-F5-S3	
Macro ϕ	9.60		Macro ϕ	16
Echinoid	18.40		Bryozoan	29.6
Moldic ϕ	2.80		Bivalve	28.8
Barnacle	0.80		Benthic Foram	2
Planktonic Foram	0.80		Echinoid	3.6
Matrix	2.40		Coralline Algae	1.6
Coralline Algae	0.80		Matrix	5.2
Gastropod	0.40		Cement	5.6
			Mold- Bivalve	1.6
RP-F6-S3			Serpulid	0.4
Benthic Foram	11.20		Unknown	1.6
Macro ϕ	10.80		Coralline Algae (e)	1.2
Bryozoan	47.20		Moldic ϕ	0.4
Coralline Algae	1.20		Mold- B. Foram	0.4
Echinoid	16.40		Volcanic	0.4
Planktonic Foram	0.80			
Bivalve	8.80		RM-F5-S4	
Matrix	1.60		cement	18.8
Unknown	0.40		Bivalve	28.8
Moldic ϕ	1.20		Macro ϕ	12.8
Serpulid	0.40		Bryozoan	26.8
Cement	0.02		Echinoid	1.2
			Moldic ϕ	0.4
RP-F7-S1a			Cement- Bryozoan	0.8
Benthic Foram	11.20		Matrix	3.2
Macro ϕ	10.80		Coralline Algae	0.4
Bryozoan	47.20		Peloid	0.4

Coralline Algae	1.20		Coralline Algae (e)	4.4
Echinoid	16.40		Unknown	1.2
Planktonic Foram	0.80		Mold-Bivalve	0.4
Bivalve	8.80		Serpulid	0.4
Matrix	1.60			
Unknown	0.40		RM-F6-S1	
Moldic ϕ	1.20		Benthic Foram	1.6
Serpulid	0.40		Bivalve	38.8
Cement	0.02		Moldic ϕ	24.4
			Mold-Bivalve	0.8
RP-F7-S1b			Bryozoan	23.2
Bryozoan	36.00		Matrix	2.4
Benthic Foram	9.20		Macro ϕ	6
Macro ϕ	11.20		Mold- B. Foram	1.2
Echinoid	22.00		Cement	0.4
Bivalve	14.80		Echinoid	0.8
Coralline Algae	3.60			
Matrix	1.60		RM-F6-S2	
Planktonic Foram	0.40		Bryozoan	9.6
Cement	0.80		Bivalve	63.2
Serpulid	0.40		Echinoid	5.6
			Matrix	6
RP-F7-S2			Moldic ϕ	8.8
Macro ϕ	9.20		Mold- B. Foram	1.2
Benthic Foram	3.60		Coralline Algae (e)	5.2
Echinoid	13.20		Benthic Foram	0.4
Bivalve	21.20			
Serpulids	0.80		RM-F6-S3	
Cement	2.00		Bryozoan	14.8
Coralline Algae (e)	0.80		Bivalve	55.2
Moldic ϕ	0.40		Moldic ϕ	15.2
Matrix	0.80		Echinoid	2.4
Bryozoan	48.00		Coralline Algae (e)	2
			Benthic Foram	2.4
RP-F7-S9			Macro ϕ	1.6
Bryozoan (g)	18.00		Cement	2

Coralline Algae	4.00		Matrix	4
Echinoid	10.80		Mold- B. Foram	0.4
Bryozoan (b)	26.40			
Macro ϕ	6.40		RM-F7-S2	
Bivalve	24.40		Bivalve	29.2
Mold-Bivalve	0.80		Echinoid	3.2
Benthic Foram	4.00		Bryozoan	26.4
Serpulid	0.40		Moldic ϕ	16
Unknown	0.40		Benthic Foram	2.4
Matrix	4.40		Matrix	2.8
			Coralline Algae (b)	4.4
RP-F8-S1			Coralline Algae (e)	6.8
Bryozoan	41.60		cement	4.8
Macro ϕ	23.20		Macro ϕ	1.6
Echinoid	13.60		Unknown	1.2
Matrix	2.40		Mold- B. Foram	0.4
Benthic Foram	4.80		Gastropod	0.4
Bivalve	11.20		Volcanic	0.4
Cement	1.60			
Serpulid	0.40		RM-F7-S3	
Coralline Algae (b)	1.2		Mold- Bivalve	0.4
			Moldic ϕ	34.4
RP-F8-S2			Echinoid	2.8
bivalve	13.60		Bivalve	21.6
Benthic Foram	6.80		Cement	1.6
Echinoid	9.60		Bryozoan	16.4
Bryozoan	41.20		Unknown	13.6
Macro ϕ	22.00		Coralline Algae (b)	1.2
Cement	1.60		Benthic Foram	1.6
Matrix	2.80		Coralline Algae (e)	4
Barnacle	0.40		Matrix	0.4
Unknown	0.40		Macro ϕ	2
Coralline Algae	0.80			
Planktonic Foram	0.40		RM-F7-S4	
Gastropod	0.40		Unknown	14.4

			Bivalve	22.4
RP-F8-S3			Moldic ϕ	19.6
Cement	10.80		Bryozoan	18
Bivalve	12.00		Coralline Algae (e)	15.6
Bryozoan	42.00		Matrix	0.8
Moldic ϕ	6.20		Cement	4
Echinoid	8.40		Benthic Foram	2.8
Benthic Foram	4.00		Mold- B. Foram	0.8
Macro ϕ	15.00		Echinoid	0.4
Matrix	0.40		Coralline Algae	0.8
Coralline Algae	0.80		Serpulid	0.4
Gastropod	0.40			
			RM-F8-S1	
RP-F9-S2a			Macro ϕ	3.2
Bryozoan	34.00		Bivalve	15.2
Echinoid	12.80		Bryozoan	24
Bivalve	22.40		Coralline Algae (e)	11.6
Macro ϕ	15.20		Benthic Foram	0.8
Matrix	5.20		Moldic ϕ	16.4
Benthic Foram	6.80		Coralline Algae (b)	0.4
Moldic ϕ	1.60		Unknown	23.6
Cement	0.80		Matrix	1.2
Coralline Algae	1.20		Cement	1.6
			Echinoid	1.6
RP-F9-S2b			Mold- B. Foram	0.4
Bryozoan	28.80			
Benthic Foram	5.20		RM-F8-S2	
Echinoid	12.00		Bivalve	22.4
Coralline Algae (b)	1.20		Moldic ϕ	22
Bivalve	25.20		Cement	8
Macro ϕ	18.80		Bryozoan	8.8
Matrix	4.00		Coralline Algae (e)	6.8
Cement	0.40		Unknown	26
Planktonic Foram	1.20		Echinoid	3.2
Moldic ϕ	0.40		Coralline Algae (b)	0.4

Serpulid	1.60		Benthic Foram	1.2
Coralline Algae (e)	0.40		Mold- B. Foram	0.4
			Matrix	0.4
RP-F9-S3			Serpulid	0.4
Bivalve	20.80			
Macro ϕ	27.20		RM-F8-S3	
Echinoid	16.40		Matrix	4.8
Coralline Algae (b)	3.60		Macro ϕ	12
Coralline Algae (e)	0.40		Bivalve	25.2
Benthic Foram	8.00		Bryozoan (b)	23.6
Bryozoan	15.20		Benthic Foram	4.4
Barnacle	0.40		Cement	1.6
Planktonic Foram	1.20		Moldic ϕ	1.6
Moldic ϕ	0.80		Bryozoan (g)	4
Cement	3.20		Coralline Algae	2.4
Matrix	1.60		Echinoid	5.6
Serpulid	0.40		Coralline Algae (e)	10.8
Unknown	0.80			
			RM-F8-S4	
RP-F10-S1			Benthic Foram	6.4
Bryozoan	25.60		Bivalve	28.8
Bivalve	36.40		Coralline Algae	0.4
Benthic Foram	4.80		Matrix	2
Echinoid	8.80		Moldic ϕ	1.2
Macro ϕ	14.80		Echinoid	6.8
Unknown	0.40		Bryozoan	24
Matrix	4.80		Macro ϕ	10.8
Coralline Algae	0.40		Coralline Algae (e)	13.2
Serpulid	2.00		Cement	5.6
Moldic ϕ	1.60		Bryozoan (g)	0.8
Cement	0.40			
			RM-F9-S1	
RP-F10-S2			Cement	39.6
Bryozoan	16.00		Bryozoan	15.2
Benthic Foram	8.00		Unknown	3.2
Macro ϕ	22.00		Bivalve	26

Bivalve	30.40		Echinoid	3.2
Matrix	8.00		Macro ϕ	3.6
Serpulid	2.00		Coralline Algae (e)	2
Echinoid	8.40		Benthic Foram	4.8
Planktonic Foram	2.80		Coralline Algae	0.8
Moldic ϕ	0.80		Moldic ϕ	0.4
Coralline Algae	1.20		Volcanic	0.8
Unknown	0.40		Matrix	0.4
RP-F10-S3a			RM-F9-S3	
Bryozoan	28.80		Cement	42.4
Benthic Foram	7.60		Echinoid	6.4
Bivalve	33.20		Unknown	10.4
Macro ϕ	14.40		Bivalve	11.2
Echinoid	7.20		Bryozoan	24.4
Matrix	4.40		Macro ϕ	1.6
Planktonic Foram	1.20		Benthic Foram	3.2
Serpulid	0.80			
Barnacle	0.40			
Coralline Algae (b)	0.40			
Coralline Algae (e)	1.20			
Unknown	0.40			
RP-F10-S3b				
Bryozoan	25.60			
Benthic Foram	8.80			
Planktonic Foram	2.00			
Bivalve	22.40			
Echinoid	11.20			
Macro ϕ	18.00			
Matrix	4.80			
Serpulid	2.00			
Coralline Algae (e)	2.00			
Cement	0.80			

Unknown	1.60			
Gastropod	0.80			
RP-F10-S4				
Bryozoan	25.20			
Bivalve	21.20			
Benthic Foram	10.00			
Echinoid	7.60			
Macro ϕ	26.80			
Serpulid	0.80			
Planktonic Foram	3.20			
Moldic ϕ	0.80			
Matrix	1.60			
Coralline Algae (e)	0.40			
Unknown	2.40			
RP-F10-S5				
Bivalve	32.40			
Bryozoan	27.20			
Matrix	6.40			
Macro ϕ	16.80			
Benthic Foram	9.60			
Echinoid	3.20			
Unknown	0.80			
Serpulid	1.60			
Coralline Algae	0.80			
Planktonic Foram	0.80			
Moldic ϕ	0.40			
RP-F11-S1				
Unknown	1.20			
Bivalve	14.80			
Bryozoan	35.20			
Echinoid	7.20			
Benthic Foram	6.40			
Moldic ϕ	3.60			

Macro ϕ	8.00			
Mold- Bryozoan	0.40			
Serpulid	0.40			
Mold- Bivalve	0.80			
Matrix	0.80			
Planktonic Foram	0.40			
Cement- Bivalve	1.20			
RP-F11-S2				
Benthic Foram	4.00			
Cement	34.40			
Matrix	1.60			
Echinoid	3.20			
Bryozoan	22.00			
Macro ϕ	2.00			
Moldic ϕ	9.20			
Bivalve	20.80			
Cement- Bryozoan	0.80			
Mold- Bivalve	0.40			
Unknown	0.40			
Coralline Algae	0.80			
RP-F11-S4a				
Echinoid	3.20			
Bivalve	5.20			
Bryozoan	17.60			
Benthic Foram	17.20			
Cement	39.20			
Moldic ϕ	9.60			
Coralline Algae	6.80			
Mold- B. Foram	0.40			
Unknown	0.80			

RP-F11-S4b				
Coralline Algae	7.60			
Benthic Foram	23.60			
Mold- B. Foram	0.80			
Cement	45.60			
Moldic ϕ	8.40			
Bivalve	2.80			
Bryozoan	9.20			
Macro ϕ	0.40			
Echinoid	0.80			
Unknown	0.80			
RP-F11-S5				
Bryozoan	13.20			
Bivalve	11.60			
Moldic ϕ	12.00			
Cement	34.40			
Coralline Algae	9.60			
Benthic Foram	14.40			
Unknown	2.80			
Echinoid	0.40			
Bryozoan (g)	1.20			
Matrix	0.40			

SP				
Class	Percentage		Class	Percentage
SP-F1-S1	11.60		SP-F10-S3	11.60
Coralline Algae (b)	11.60		Bivalve	31.20
Benthic Foram	3.20		Coralline Algae (e)	14.00
Bivalve	50.40		Macro ϕ	0.40

Bryozoan	10.80		foram mold	22.80
Moldic ϕ	10.00		Echinoid	4.40
Mold-Bivalve	0.80		Unknown	3.60
Matrix	2.00		Moldic ϕ	3.20
Unknown	2.40		Benthic Foram	4.00
Cement	2.00		Matrix	3.20
Echinoid	3.60		Cement	0.80
Coralline Algae (e)	2.40		Bryozoan	0.80
Macro ϕ	0.40		Mold-Bivalve	0.40
SP-F1-S3				
Bivalve	51.60		SP-F10-S4	
Mold-Bivalve	1.20		Echinoid	27.20
Bryozoan	10.00		Moldic ϕ	6.80
Moldic ϕ	14.80		Coralline Algae (e)	17.60
Coralline Algae (e)	2.80		Cement	8.00
Benthic Foram	3.20		Macro ϕ	11.60
Unknown	4.80		Bivalve	10.80
Echinoid	3.20		Unknown	5.20
Mold- Bryozoan	0.40		Bryozoan	1.20
Coralline Algae (b)	2.80		Matrix	4.00
Cement	0.80		Mold-Bivalve	2.40
Gastropod	0.40		Mold- B. Foram	5.2
Mold- B. Foram	2.00		Volcanic	0.40
Macro ϕ	1.20			
Serpulid	0.40			
Matrix	0.40		SP-F11-S1	
			Bivalve	38.00
SP-F2-S2			Macro ϕ	4.00
Coralline Algae (e)	42.40		Mold-Bivalve	4.40
Echinoid	4.00		Moldic ϕ	13.20
Benthic Foram	2.00		Bryozoan	9.60
Coralline Algae (b)	10.00		Echinoid	6.00
Moldic ϕ	6.80		Coralline Algae (e)	9.60
Bivalve	13.20		Benthic Foram	2.00
Unknown	7.60		Matrix	5.20
Macro ϕ	0.80		Unknown	6.40
Cement	2.80		Mold- P. Foram	0.40

Bryozoan	10.40		volcanic	0.40
			Cement	0.40
SP-F2-S3				
Moldic ϕ	8.40		SP-F11-S2	
Echinoid	2.40		Bivalve	50.00
Mold- B. Foram	0.80		Mold-Bivalve	4.00
Bryozoan	8.40		Matrix	7.20
Coralline Algae (b)	11.60		Coralline Algae (e)	4.80
Bivalve	28.40		Macro ϕ	9.60
ca mold	0.80		Unknown	7.60
Unknown	10.40		Moldic ϕ	10.00
Coralline Algae (e)	23.20		Echinoid	3.20
Cement	3.20		Benthic Foram	1.20
Benthic Foram	1.20		Bryozoan	1.20
Matrix	1.20		Mold- B. Foram	0.40
			Cement	0.80
SP-F2-S4				
Moldic ϕ	18.40		SP-F11-S3	
Bivalve	26.00		Bivalve	36.80
Bryozoan	15.20		Moldic ϕ	8.80
Coralline Algae (b)	4.40		Echinoid	28.00
Cement	8.80		Matrix	6.40
Benthic Foram	4.80		Unknown	6.80
Unknown	10.00		Cement	0.80
Coralline Algae (e)	7.20		Benthic Foram	2
Macro ϕ	3.20		Bryozoan	1.20
Matrix	0.40		Macro ϕ	5.20
Echinoid	1.20		Coralline Algae (e)	3.60
			Mold-Bivalve	0.40
SP-F2-S5				
Bivalve	27.20			
Unknown	12.00		SP-F11-S4	
Coralline Algae (b)	19.60		Bivalve	28.40
Moldic ϕ	20.80		Coralline Algae (e)	8.40
Bryozoan	6.40		Echinoid	31.60
Echinoid	0.40		Matrix	5.60
Macro ϕ	0.40		Mold-Bivalve	2.80

Coralline Algae (e)	2.40		Planktonic Foram	0.40
Benthic Foram	3.60		Unknown	5.20
Cement	6.80		Moldic ϕ	12.00
Mold- B. Foram	0.40		Benthic Foram	1.2
			Macro ϕ	2.00
SP-F2-S6			Cement	1.20
Moldic ϕ	15.20		Volcanic	0.40
Bivalve	22.40		Bryozoan	0.40
Coralline Algae (e)	12.40			
Benthic Foram	5.20			
Coralline Algae (b)	10.00		SP-F11-S5	
Bryozoan	8.00		Coralline Algae (e)	16.00
Cement	16.00		Bivalve	24.40
Echinoid	1.60		Moldic ϕ	10.80
Unknown	5.20		Echinoid	20.40
Serpulid	0.40		Macro ϕ	9.20
Gastropod	0.40		Cement	1.60
Macro ϕ	0.80		Mold- B. Foram	0.80
Mold-Bivalve	1.60		Mold-Bivalve	2.00
Mold- Echinoid	0.40		Matrix	8.80
Mold- Coralline Algae	0.40		Unknown	5.60
SP-F2-S7				
Moldic ϕ	31.20		SP-F12-S1	
Bryozoan	5.60		Bivalve	20.00
Coralline Algae (b)	6.80		Bryozoan	5.60
Bivalve	8.40		Echinoid	21.60
Unknown	0.80		Unknown	2.40
Cement	7.20		Macro ϕ	8.00
Echinoid	4.40		Benthic Foram	4.00
Coralline Algae (e)	30.40		Coralline Algae (e)	26.40
Mold- B. Foram	1.20		Moldic ϕ	7.20
Benthic Foram	2.80		Matrix	1.20
Volcanic	0.40		Cement	3.60
Mold-Bivalve	0.80			
			SP-F12-S2	
SP-F2-S8			Moldic ϕ	10.80

Bryozoan	15.20		Cement	4.80
Moldic ϕ	23.20		Macro ϕ	10.40
Coralline Algae (b)	4.00		Bivalve	18.40
Bivalve	11.60		Coralline Algae (e)	17.20
Benthic Foram	3.60		Echinoid	24.80
Cement	10.80		Lithoclast	2.00
Coralline Algae (e)	20.00		Bryozoan	4.80
Unknown	5.60		Benthic Foram	2.40
Echinoid	4.00			4.40
Macro ϕ	0.40			
Mold- B. Foram	0.40		SP-F13-S1	
Mold- Bivalve	0.80		Bivalve	50.80
Matrix	0.40		Bryozoan	6.00
			Moldic ϕ	10.40
SP-F3-S1			Cement	4.40
Coralline Algae (e)	19.20		Coralline Algae (e)	14.80
Bivalve	24.00		Echinoid	5.60
Bryozoan	5.60		volcanic	0.40
Coralline Algae (b)	36.80		Macro ϕ	1.60
Matrix	2.00		Matrix	1.60
Echinoid	1.60		Benthic Foram	2.40
Moldic ϕ	7.20		Mold-Bivalve	1.60
Mold- B. Foram	0.80		Serpulid	0.40
Mold-Bivalve	0.80			
Cement	1.20		SP-F13-S2	
Benthic Foram	0.40		Bivalve	63.60
Planktonic Foram	0.40		Bryozoan	5.20
			Coralline Algae (e)	3.60
SP-F3-S2			Moldic ϕ	6.00
Bivalve	29.60		Echinoid	9.60
Coralline Algae (e)	20.00		Benthic Foram	1.20
Echinoid	1.60		Cement	6.40
Coralline Algae (b)	12.80		Macro ϕ	2.80
Moldic ϕ	11.60		Matrix	1.20
Benthic Foram	6.00			
Mold-Bivalve	3.60		SP-F13-S3	
Mold- B. Foram	1.20		Bivalve	46.00

Bryozoan	8.00		Coralline Algae (e)	11.20
Cement	3.60		Bryozoan	10.40
Matrix	1.60		Echinoid	14.00
Macro ϕ	0.40		Moldic ϕ	10.00
			Macro ϕ	3.20
SP-F3-S3			Cement	4.80
Bivalve	37.20		Unknown	0.40
Bryozoan	7.60			
Moldic ϕ	7.20		SP-F13-S4	
Coralline Algae (e)	20.80		Bivalve	24.40
Coralline Algae (b)	13.60		Bryozoan	3.60
Matrix	1.20		Echinoid	15.60
Cement	2.80		Coralline Algae (b)	0.80
Unknown	2.40		Coralline Algae (e)	30.00
Macro ϕ	0.40		Moldic ϕ	6.80
Benthic Foram	4.00		Serpulid	2.00
Echinoid	1.60		Cement	4.80
Mold- B. Foram	0.40		Benthic Foram	4.80
			Macro ϕ	5.20
SP-F4-S1			Matrix	0.80
Bivalve	20.80		Mold- B. Foram	0.40
Moldic ϕ	18.80		Unknown	0.40
Coralline Algae (e)	12.00		Mold-Bivalve	0.40
Coralline Algae (b)	18.80			
Cement	11.20		SP-F13-S5	
Unknown	1.20		Bivalve	38.80
Benthic Foram	3.20		Moldic ϕ	9.20
Mold- Bryozoan	0.80		Bryozoan	4.00
Echinoid	3.20		Echinoid	10.00
Bryozoan	6.00		Benthic Foram	0.80
Mold- B. Foram	2.40		Cement	4.00
Macro ϕ	0.40		Coralline Algae (e)	22.80
			Macro ϕ	6.80
SP-F4-S3			Serpulid	0.80
Bivalve	24.80		Unknown	1.20
Coralline Algae (e)	20.00		Matrix	1.20

Mold- B. Foram	2.00		Coralline Algae (b)	0.40
Coralline Algae (b)	12.00			
Macro ϕ	0.40		SP-F13-S6	
Benthic Foram	3.20		Bivalve	57.60
Bryozoan	7.60		Mold-Bivalve	0.40
Mold-Bivalve	3.60		Moldic ϕ	14.00
Echinoid	2.00		Bryozoan	6.00
Cement	8.80		Echinoid	0.40
Matrix	0.80		Cement	6.00
Unknown	2.00		Coralline Algae (e)	12.80
Moldic ϕ	12.80		Macro ϕ	1.60
			Benthic Foram	0.80
SP-F4-S4			Unknown	0.40
Coralline Algae (b)	14.40			
Bivalve	38.40		SP-F13-S8	
Cement	8.40		Coralline Algae (e)	22.80
Benthic Foram	4.00		Moldic ϕ	11.60
Unknown	2.40		Bivalve	48.40
Coralline Algae (e)	15.60		Macro ϕ	1.20
Moldic ϕ	4.80		Benthic Foram	1.60
Bryozoan	7.20		Bryozoan	8.00
Matrix	1.60		Unknown	2.80
Echinoid	1.20		Cement	2.80
Macro ϕ	1.20		Echinoid	0.40
Mold-Bivalve	0.40		Mold-Bivalve	0.40
Mold- Coralline Algae	0.40			
			SP-F13-S9	
SP-F5-S1			Bivalve	34.00
Echinoid	6.40		Coralline Algae (e)	28.80
Bivalve	18.40		Cement	8.40
Bryozoan	20.40		Volcanic	1.60
Coralline Algae (b)	35.60		Moldic ϕ	6.40
Moldic ϕ	5.20		Macro ϕ	2.40
Cement	5.60		Bryozoan	5.60
Matrix	2.00		Serpulid	0.40
Volcanic	1.60		Benthic Foram	3.60

Macro ϕ	0.80		Unknown	2.00
Benthic Foram	1.60		Matrix	1.60
Unknown	1.20		Gastropod	0.40
Mold-Bivalve	1.20		Echinoid	3.20
			Cement- B. Foram	0.40
SP-F5-S2			Planktonic Foram	0.40
Coralline Algae (b)	27.60		Coralline Algae (b)	0.80
Bivalve	20.80			
Matrix	3.20		SP-F14-S1	
Echinoid	16.80		Coralline Algae (e)	70.80
Cement	2.80		Bivalve	7.60
Moldic ϕ	3.60		Bryozoan	0.40
Benthic Foram	2.40		Moldic ϕ	2.80
Macro ϕ	3.20		Macro ϕ	3.60
Bryozoan	16.40		Benthic Foram	3.60
Volcanic	0.80		Barnacle	1.60
Unknown	2.00		Cement	4.80
Mold- Bivalve	0.40		Echinoid	3.20
			Unknown	0.40
SP-F5-S3				
Bivalve	20.80		SP-F14-S2	
Bryozoan	13.60		Bryozoan	4.80
Coralline Algae (b)	34.40		Coralline Algae (e)	39.20
Echinoid	3.20		Bivalve	21.60
Moldic ϕ	8.00		Moldic ϕ	3.60
Coralline Algae (e)	2.40		Serpulid	0.80
Cement	6.40		Cement	4.40
Unknown	2.80		Macro ϕ	12.00
Mold- B. Foram	1.20		Benthic Foram	5.20
Macro ϕ	3.20		Matrix	3.20
Matrix	0.40		Coralline Algae (b)	0.40
Volcanic	0.80		Echinoid	3.20
Benthic Foram	2.80		Planktonic Foram	0.80
			Unknown	0.40
SP-F5-S4				
Coralline Algae (b)	30.40		SP-F14-S3	

Benthic Foram	4.80		Matrix	2.00
Bivalve	19.20		Coralline Algae (e)	65.20
Bryozoan	22.40		Bryozoan	2.40
Echinoid	3.20		Echinoid	2.80
Matrix	2.00		Bivalve	9.20
Coralline Algae (e)	1.60		Macro ϕ	7.60
Unknown	2.00		Cement	4.80
Moldic ϕ	6.40		biv mold	0.80
Cement	3.20		Unknown	0.80
Macro ϕ	1.20		Coralline Algae (b)	1.60
Volcanic	2.00		Moldic ϕ	2.00
Mold-Bivalve	0.40		Benthic Foram	0.40
Moldic ϕ	0.40		Volcanic	0.40
Mold- Foram	0.80			
			SP-F14-S4	
SP-F5-S6			Coralline Algae (e)	55.20
Bivalve	24.80		Macro ϕ	10.40
Benthic Foram	3.60		Bivalve	10.40
Moldic ϕ	9.20		Planktonic Foram	0.40
Coralline Algae (e)	2.00		Bryozoan	4
Bryozoan	28.80		Coralline Algae (b)	2.40
Mold- Bryozoan	1.20		Echinoid	2.00
Mold- Foram	2.00		Matrix	6.00
Cement	3.20		Unknown	1.20
Matrix	5.60		Benthic Foram	2.80
Coralline Algae (b)	14.00		Moldic ϕ	3.20
Volcanic	0.80		Cement	2.00
Serpulid	1.60			
Macro ϕ	1.60			
Mold-Bivalve	0.80		SP-F14-S5	
Unknown	0.40		Bivalve	10.80
Echinoid	0.40		Coralline Algae (e)	60.80
			Matrix	2.40
SP-F5-S7			Moldic ϕ	3.20
Bryozoan	46.80		Macro ϕ	5.20
Bivalve	15.60		Benthic Foram	6,8

Benthic Foram	4.80		Unknown	1.20
Coralline Algae (e)	0.80		Cement	3.20
Mold-Bivalve	1.20		Coralline Algae (b)	0.40
Macro ϕ	1.20		Bryozoan	3.60
Moldic ϕ	9.20		Volcanic	0.40
Coralline Algae (b)	11.20		Echinoid	1.20
Cement	2.40		Mold- Foram	0.40
Unknown	2.40			
	2.00			
			SP-F14-S6	
SP-F6-S1			Planktonic Foram	0.40
Bryozoan	30.40		Coralline Algae (e)	70.40
Moldic ϕ	14.40		Bryozoan	6.00
Bivalve	29.20		Bivalve	2.80
Macro ϕ	5.20		Macro ϕ	10.80
Unknown	2.00		Echinoid	1.20
Benthic Foram	4.80		Serpulid	0.40
Cement	3.60		Mold- Coralline Algae	1.20
Echinoid	2.00		Moldic ϕ	2.40
Matrix	1.20		Mold- Bivalve	0.80
Coralline Algae (e)	1.6		Benthic Foram	2.00
Coralline Algae (b)	3.20			1.60
Mold- Bryozoan	1.20			
Mold- B. Foram	0.80		SP-F14-S7	
Cement- Foram	0.40		Coralline Algae (e)	61.60
			Benthic Foram	3.60
SP-F6-S2			Bryozoan	5.60
Bivalve	27.20		Echinoid	8.00
Moldic ϕ	12.00		Mold- Bivalve	2.40
Macro ϕ	2.40		Planktonic Foram	1.20
Bryozoan	26.00		Macro ϕ	5.20
Benthic Foram	8.00		Cement	1.60
Coralline Algae (b)	3.60		Matrix	0.80
Echinoid	4.00		Bivalve	5.20
Cement	4.40		Moldic ϕ	2.80
Matrix	0.80		Unknown	0.40

Unknown	3.60			
Coralline Algae (e)	5.60		SP-F14-S8	
Mold-Bryozoan	0.40		Coralline Algae (e)	74.00
Mold- B. Foram	2.00		Echinoid	5.60
			Bivalve	1.20
SP-F6-S3			Macro ϕ	10.40
Bryozoan	39.60		Moldic ϕ	3.20
Moldic ϕ	12.80		Bryozoan	1.60
Cement	6.40		Cement	2.00
Echinoid	0.80		Benthic Foram	1.20
Mold- Bivalve	0.40			0.80
Bivalve	26.00			
Coralline Algae (e)	4.00		SP-F16-S1	
Planktonic Foram	0.40		Coralline Algae (e)	54.40
Unknown	2.80		Bryozoan	16.00
Volcanic	0.80		Matrix	1.60
Matrix	0.40		Bivalve	6.00
Benthic Foram	4.80		Echinoid	2.80
Coralline Algae (b)	0.40		Moldic ϕ	2.80
Macro ϕ	0.40		Macro ϕ	8.00
			Benthic Foram	5.2
SP-F7-S1			Coralline Algae (b)	0.40
Bivalve	13.20		Cement	1.20
Benthic Foram	9.20		Planktonic Foram	0.80
Mold-Bivalve	6.80		Unknown	0.80
Matrix	24.80			
Coralline Algae (e)	7.20			
Mold- P. Foram	9.60		SP-F16-S2	
Moldic ϕ	10.80		Bivalve	2.00
Cement	0.80		Coralline Algae (e)	72.00
Planktonic Foram	0.80		Macro ϕ	11.60
Unkown	7.60		Moldic ϕ	6.00
Bryozoan	0.80		Echinoid	1.60
Volcanic	2.80		Benthic Foram	3.20
Mold- B. Foram	4.80		Bryozoan	1.60
Mold-Echinoid	0.40		Mold-Bivalve	0.40

Macro ϕ	0.40		Mold- Coralline Algae	0.40
			Matrix	0.80
SP-F7-S2			Cement	0.40
Volcanic	3.20			
Matrix	26.40		SP-F16-S3	
Bivalve	10		Benthic Foram	4.80
Mold-Bivalve	3.60		Moldic ϕ	5.20
Coralline Algae (e)	7.60		Coralline Algae (e)	70.80
Unknown	7.20		Mold-Coralline Algae	0.40
Mold-P. Foram	8.80		Mold-Bivalve	1.20
Mold-B. Foram	2.80		Bivalve	2.80
Moldic ϕ	7.20		Matrix	2.80
Benthic Foram	7.60		Echinoid	2.40
Bryozoan	2.40		Macro ϕ	5.20
Planktonic Foram	4.00		Cement	3.60
Cement	4.00		Coralline Algae (b)	0.40
Echinoid	1.20		Bryozoan	0.40
Macro ϕ	4.00			
			SP-F16-S5	
SP-F7-S3			Coralline Algae (e)	68.40
Planktonic Foram	4.40		Matrix	8.40
Matrix	32.80		Macro ϕ	11.60
Benthic Foram	4.80		Cement	2.80
Bivalve	11.60		Bivalve	1.20
Unknown	6.00		Echinoid	2.00
Coralline Algae (e)	5.20		Moldic ϕ	3.20
Mold- P. Foram	7.20		Bryozoan	0.40
Moldic ϕ	9.20		Benthic Foram	1.60
Echinoid	1.20		Unknown	0.40
biv mold	4.00			
Macro ϕ	6.40		SP-F16-S6	
Mold-B. Foram	2.80		Coralline Algae (e)	78.40
Bryozoan	1.20		Macro ϕ	6.80
Cement	0.80		Cement	2.80
Mold-Echinoid	0.40		Moldic ϕ	6.00

Volcanic	2.00		Benthic Foram	2.40
			Matrix	1.60
SP-F7-S4			Unknown	0.40
Moldic ϕ	17.20		Mold-Bivalve	0.80
Benthic Foram	4.00		Echinoid	0.40
Bivalve	12.40		Bivalve	0.40
Coralline Algae (e)	2.00			
Mold- P. Foram	16.00		SP-F16-S7	
Mold-Bivalve	7.20		Coralline Algae (e)	74.80
Matrix	11.20		Matrix	1.60
Unknown	8.00		Benthic Foram	2.40
Bryozoan	3.20		Mold- B. Foram	0.40
Planktonic Foram	4.80		Bryozoan	0.80
Echinoid	1.20		Moldic ϕ	6.40
Cement	7.20		Bivalve	0.40
Mold- Echinoid	0.40		Macro ϕ	6.00
Macro ϕ	0.80		Cement	4.40
Mold- B. Foram	3.60		Echinoid	2.40
Volcanic	0.40		Mold- Bryozoan	0.40
Cement- Coralline Algae	0.40			
			SP-F16-S10	
SP-F7-S5			Bivalve	1.20
Moldic ϕ	11.20		Coralline Algae (e)	76.00
Benthic Foram	2.00		Cement	8.00
Mold- B. Foram	2.80		Moldic ϕ	6.80
Unknown	9.20		Macro ϕ	6.00
Planktonic Foram	3.60		Matrix	0.40
Bivalve	12.80		Bryozoan	0.40
Cement	12.80		Serpulid	0.40
Mold- P. Foram	9.20		Benthic Foram	0.40
Bryozoan	4.00		Coralline Algae (b)	0.40
Macro ϕ	5.60			
Matrix	16.80			
Mold-Bivalve	4.00			
Mold- Echinoid	1.20			
Volcanic	3.60			

Echinoid	0.80			
Coralline Algae (e)	0.40			
SP-F8-S1				
Cement	15.60			
Macro ϕ	17.20			
Mold-Bivalve	3.20			
Echinoid	19.20			
Coralline Algae (e)	16.80			
Mold- P. Foram	0.40			
Planktonic Foram	0.80			
Bivalve	6.00			
Moldic ϕ	5.60			
Benthic Foram	0.80			
Matrix	6.80			
Unknown	4.40			
Bryozoan	1.20			
Mold- B. Foram	0.80			
Volcanic	1.20			
SP-F9-S1				
Unknown	4.40			
Macro ϕ	11.60			
Matrix	30.00			
Coralline Algae (e)	6.80			
Bivalve	8.40			
volcanic	2.40			
Moldic ϕ	5.60			
Mold- P. Foram	4.40			
Bryozoan	1.60			
Cement	3.60			
Planktonic Foram	4.80			
Mold- Bryozoan	0.40			
Echinoid	10.80			
Mold- Bivalve	2.00			
Benthic Foram	2.40			
Mold- B. Foram	0.40			
SP-F10-S1				

Coralline Algae (e)	24.80			
Macro ϕ	4.40			
Bryozoan	6.80			
Bivalve	23.20			
Moldic ϕ	18.80			
Coralline Algae (b)	0.40			
Echinoid	11.60			
Matrix	1.60			
Benthic Foram	0.80			
Planktonic Foram	0.40			
Cement	6.40			
Unknown	0.80			
SP-F10-S2				
Macro ϕ	10.00			
Cement	7.60			
Moldic ϕ	6.80			
Echinoid	24.40			
Mold- B. Foram	1.60			
Mold-Bivalve	2.00			
Bivalve	16.00			
Benthic Foram	6.00			
Coralline Algae (e)	10.00			
Matrix	1.60			
Unknown	6.40			
Planktonic Foram	1.60			
Bryozoan	4.00			
Mold- Echinoid	0.40			
Volcanic	0.80			
Mold- P. Foram	0.40			
Cement- B. Foram	0.40			

WF	
Class	Percentage
WF-F1-S1	
Coralline Algae	22.40
Bryozoan	15.20
Cement	5.20
Bivalve	28.80
Benthic Foram	6.80
Macro ϕ	8.40
Echinoid	5.20
Unknown	3.20
Moldic Porosity	4.00
Matrix	0.40
Planktonic Foram	0.40
WF-F5-S1	
Bivalve	33.20
Coralline Algae	10.80
Macro ϕ	14.00
Benthic Foram	2.40
Bryozoan	11.20
Cement	6.80
Echinoid	10.40
Matrix	2.00
Moldic Porosity	4.40
Unknown	2.40
Volcanic	1.60
Planktonic Foram	0.80
WF-F5-S2	
Bivalve	38.00
Echinoid	10.00
Coralline Algae	14.00
Bryozoan	10.00
Macro ϕ	11.60
Volcanic	0.40
Moldic Porosity	4.80
Benthic Foram	6.40

Matrix	0.80
Unknown	0.40
Cement	3.20
Calcishpere thing	0.40
WF-F5-S3	
Benthic Foram	5.60
Moldic Porosity	5.60
Bryozoan	8.00
Coralline Algae	18.00
Macro ϕ	16.00
Echinoid	10.80
Volcanic	1.20
Bivalve	22.80
Matrix	1.60
Cement	9.20
Unknown	0.80
Planktonic Foram	0.40

Pliocene

PR			PW	
Class	Percentage		Class	Percentage
PR-F1-S1			PW-F1-S1	
Coralline Algae	43.20		Echinoid	20.8
Bivalve	11.20		Macro Porosity	10
Macro Porosity	14.40		Coralline Algae	28.4
Echinoid	8.00		Bryozoan	10.4
Bryozoan	4.40		Bivalve	15.2
Cement	4.00		Matrix	3.2
Benthic Foram	4.80		Moldic Porosity	3.2
Moldic Porosity	6.40		Benthic Foram	4.8
Matrix	2.00		Cement	1.6

Lithoclasts	0.80		Barnacle	0.4
Serpulid	0.40		Unknown	0.8
			Bivalve Mold	0.4
PR-F1-S2			Planktonic Foram	0.8
Bivalve	20.40			
Macro Porosity	13.60		PW-F1-S2	
Bryozoan	16.40		Macro Porosity	8
Echinoid	10.80		Echinoid	10
Coralline Algae	21.20		Bryozoan	22
Moldic Porosity	7.20		Bivalve	27.6
Planktonic Foram	0.80		Coralline Algae	24.8
Cement	3.20		Matrix	2.8
Gastropod	0.40		Moldic Porosity	2.4
Benthic Foram	4.40		Benthic Foram	2
Matrix	0.40		Bivalve Mold	0.4
Lithoclasts	1.20			
			PW-F1-S3	
PR-F1-S3			Bryozoan	17.6
Cement	2.00		Bivalve	24.4
Echinoid	4.80		Matrix	9.2
Coralline Algae	42.40		Coralline Algae	13.6
Lithoclasts	0.40		Macro Porosity	16
Moldic Porosity	4.80		Echinoid	10.4
Bivalve	20.00		Benthic Foram	5.2
Macro Porosity	12.80		Unknown	1.2
Bryozoan	8.40		Moldic Porosity	1.6
Benthic Foram	3.20		Planktonic Foram	0.8
Volcanic	0.40			
Matrix	0.40		PW-F1-S4	
Planktonic Foram	0.40		Bryozoan	16.8
			Coralline Algae	29.2
			Macro Porosity	21.6
			Echinoid	6.8
			Bivalve	14.8
PR-F2-S4			Bivalve mold	1.2
Bivalve	12.00		Foram Benthic	2
Coralline Algae	46.40		Matrix	2.4
Bryozoan	12.80		Barnacle	0.8

Cement	4.00		Moldic Porosity	2.4
Moldic Porosity	2.80		Cement	2
Echinoid	5.60			
Macro Porosity	11.20		PW-F1-S5	
Matrix	1.60		Bivalve	11.6
Benthic Foram	1.60		Macro Porosity	23.2
Serpulid	0.40		Matrix	4
Barnacle	0.80		Foram Benthic	6.4
Gastropod	0.40		Coralline Algae	16.4
Lithoclasts	0.40		Echinoid	10.8
			Bryozoan	17.2
PR-F2-S5			Bivalve mold	1.2
Echinoid	11.60		Cement	4.4
Bryozoan	18.40		Barnacle	1.6
Coralline Algae	14.80		Moldic Porosity	2.8
Barnacle	2.40		Benthic Foram Mold	0.4
Macro Porosity	16.80			
Bivalve	22.00		PW-F1-S6	
Moldic Porosity	6.80		Coralline Algae	26.4
Benthic Foram	4.80		Echinoid	4.8
Cement	0.40		Bryozoan	17.2
Matrix	0.80		Bivalve	16
Planktonic Foram	0.40		Macro Porosity	23.2
Serpulid	0.80		Foram Benthic	1.6
			Moldic Porosity	1.6
PR-F2-S6			Matrix	3.6
Coralline Algae	32.40		Barnacle	2.8
Bivalve	12.80		Foram Planktonic	0.4
Macro Porosity	12.80		Cement	2
Echinoid	10.00		Unknown	0.4
Moldic Porosity	6.80			
Bryozoan	17.20		PW-F2-S1	
Cement	1.60		Coralline Algae	40.8
Serpulid	1.60		Macro Porosity	10
Matrix	1.60		Bryozoan	30.4
Barnacle	1.20		Bivalve	6.4
Benthic Foram	2.00		Moldic Porosity	1.2
			Echinoid	4

PR-F2-S7			Foram Benthic	2.4
Macro Porosity	20.00		Cement	3.6
Bryozoan	19.20		Matrix	0.8
Benthic Foram	5.20			
Bivalve	14.80		PW-F2-S2	
Coralline Algae	19.60		Coralline Algae	48
Echinoid	11.20		Echinoid	2.4
Matrix	3.60		Macro Porosity	11.2
Cement	2.00		Matrix	5.2
Moldic Porosity	4.00		Cement	4
Planktonic Foram	0.40		Bivalve	12
			Foram Benthic	1.6
PR-F3-S0			serpulid	0.4
Coralline Algae	44.40		Bryozoan	14
Macro Porosity	12.00		benthic Foram Mold	0.4
Echinoid	4.80		Barnacle	0.8
Bivalve	13.20			
Moldic Porosity	5.20		PW-F3-S1	
Benthic Foram	2.00		Bryozoan	24.8
Matrix	2.80		Coralline Algae	16
Cement	7.60		Bivalve	14
Bryozoan	8.00		Macro Porosity	13.2
			Matrix	9.2
PR-F3-S1			Echinoid	13.6
Coralline Algae	30.00		Foram Benthic	4.8
Macro Porosity	13.20		Cement	2.4
Moldic Porosity	5.60		Barnacle	1.6
Bivalve	20.00		Moldic Porosity	0.4
Benthic Foram	2.80			
Bryozoan	15.60		PW-F3-S2	
Echinoid	6.80		Echinoid	8.4
Matrix	1.60		Coralline Algae	20.4
Unknown	0.40		Foram Benthic	6
Barnacle	1.60		Macro Porosity	23.2
Gastropod	0.40		Bivalve	14.4
Planktonic Foram	0.40		Bryozoan	24
Cement	0.80		Matrix	3.2

Serpulid	0.80		Cement	0.4
PR-F3-S2			PW-F3-S3	
Bryozoan	17.20		Bryozoan	20.4
Macro Porosity	12.00		Coralline Algae	33.2
Bivalve	7.20		Echinoid	9.6
Coralline Algae	48.80		Macro Porosity	14.4
Moldic Porosity	3.60		Bivalve	8.8
Cement	2.80		Cement	4.8
Echinoid	3.20		Matrix	1.2
Benthic Foram	3.20		Bivalve mold	0.4
Matrix	1.20		Foram Benthic	4
Barnacle	0.40		Moldic Porosity	0.8
Gastropod	0.40		Unknown	0.8
			PW-F3-S4	
			Coralline Algae	61.6
PR-F4-S1			Bivalve	4
Moldic Porosity	3.20		Foram Benthic	0.8
Macro Porosity	14.00		Cement	2.8
Bryozoan	29.20		Bryozoan	12
Cement	3.60		Macro Porosity	12.4
Bivalve	12.80		Echinoid	3.6
Benthic Foram	1.60		Moldic Porosity	1.2
Coralline Algae	23.60		Serpulid	0.4
Echinoid	8.00		Matrix	1.2
Matrix	3.60			
Lithoclasts	0.40		PW-F3-S5	
			Coralline Algae	54.8
PR-F5-S1			Bivalve	4.4
Bivalve	18.40		Echinoid	6
Macro Porosity	12.40		Matrix	7.2
Echinoid	16.00		Bryozoan	14.4
Coralline Algae	20.00		Foram Benthic	1.2
Benthic Foram	3.20		foram planktonic	0.8
Bryozoan	24.40		Macro Porosity	6.8
Matrix	1.20		Cement	1.6
Barnacle	0.40		Moldic Porosity	1.6
Cement	1.60		Gastropod	1.2

Moldic Porosity	1.20			
Planktonic Foram	0.40		PW-F3-S6	
Unknown	0.40		Coralline Algae	37.2
Gastropod	0.40		Macro Porosity	12.4
			Echinoid	10.8
PR-F5-S2			Matrix	5.6
Bryozoan	26.80		Bryozoan	13.6
Coralline Algae	33.20		Bivalve	8.8
Echinoid	10.00		Foram Benthic	3.6
Benthic Foram	2.80		Cement	1.6
Bivalve	14.00		Moldic Porosity	0.8
Macro Porosity	6.40		Serpulid	5.2
Calcisphere	0.40		Volcanic	0.4
Cement	0.80			
Moldic Porosity	3.60		PW-F3-S7	
Lithoclasts	0.40		Bryozoan	10
Matrix	1.20		Macro Porosity	14.4
Volcanic	0.40		Coralline Algae	34.4
			Foram Benthic	5.2
PR-F5-S3			Echinoid	18.8
Bivalve	19.60		Bivalve	8.8
Bryozoan	34.00		Matrix	4.4
Matrix	8.80		Cement	1.2
Echinoid	12.40		Serpulid	1.2
Coralline Algae	11.60		Unknown	1.2
Serpulid	0.80		Moldic Porosity	0.4
Macro Porosity	3.60			
Lithoclasts	1.20		PW-F4-S1	
Benthic Foram	3.20		Bivalve	21.6
Planktonic Foram	0.80		Bryozoan	12.4
Barnacle	1.60		Matrix	4
Moldic Porosity	1.20		Macro Porosity	25.2
Cement	0.80		Foram Benthic	6.4
Unknown	0.40		Cement	1.2
			Echinoid	13.6
PR-F6-S1			Barnacle	0.8
Coralline Algae	16.80		Moldic Porosity	2.4
Bryozoan	18.80		Coralline Algae	9.6

Macro Porosity	23.60		Bivalve mold	0.8
Benthic Foram	6.00		Unknown	0.4
Bivalve	15.60		Serpulid	0.8
Echinoid	9.60		Benthic foram mold	0.4
Moldic Porosity	5.20		Foram Planktonic	0.4
Matrix	1.20			
Lithoclasts	0.40		PW-F4-S2	
Cement	1.60		Foram Benthic	9.2
Planktonic Foram	0.80		Macro Porosity	18
Volcanic	0.40		Bivalve	20.4
			Echinoid	10.4
			Bryozoan	10.4
PR-F7-S1			Coralline Algae	24.4
Echinoid	10.40		Cement	0.8
Macro Porosity	30.00		Gastropod	0.8
Bivalve	15.20		Matrix	2.4
Bryozoan	24.80		Moldic Porosity	2.4
Calcisphere things	0.80		Unknown	0.4
Coralline Algae	6.80		Bivalve mold	0.4
Benthic Foram	4.40			
Cement	2.40		PW-F5-S1	
Moldic Porosity	3.20		Foram Benthic	5.2
Barnacle	0.80		Bivalve	12.4
Planktonic Foram	0.80		Macro Porosity	30.8
Matrix	0.40		Bryozoan	5.2
			Echinoid	6.8
PR-F7-S2			Coralline Algae	23.2
Macro Porosity			Cement	0.8
Coralline Algae	36.00		Moldic Porosity	12.4
Bivalve	5.60		Benthic Foram mold	0.4
Bryozoan	14.40		Unknown	0.8
Serpulid	22.80		Bivalve mold	0.4
Benthic Foram	0.40		Matrix	1.2
Moldic Porosity	5.20		Serpulid	0.4
Matrix	1.60			
Cement	1.60		PW-F5-S2	

Echinoid	5.20		Coralline Algae	24
Unknown	5.60		Echinoid	11.6
Planktonic Foram	0.80		Macro Porosity	16.4
	0.80		Bivalve	21.2
PR-F7-S3a			Moldic Porosity	2.8
Bryozoan			Bryozoan	10
Bivalve	33.20		Foram Benthic	6.4
Benthic Foram	19.60		Cement	2.8
Echinoid	3.20		Matrix	1.6
Macro Porosity	10.40		Unknown	2.8
Coralline Algae	21.20		Serpulid	0.4
Cement	4.80			
Matrix	7.20		PW-F6-S1	
	0.40		Coralline Algae	39.6
PR-F7-S3b			Macro Porosity	19.2
Macro Porosity	40.40		Bryozoan	8
Bivalve	11.60		Moldic Porosity	4.8
Gastropod	0.40		Bivalve	16.4
Moldic Porosity	1.20		Echinoid	5.2
Bryozoan	18.40		Cement	0.8
Coralline Algae	6.00		Benthic foram Mold	0.4
Echinoid	9.20		Foram Benthic	3.2
Benthic Foram	4.80		Unknown	0.4
Matrix	2.40		Matrix	1.6
Cement	4.80		Gastropod	0.4
Planktonic Foram	0.80			
			PW-F6-S2	
PR-F8-S1			Moldic Porosity	2.8
Bryozoan			Bryozoan	11.2
Planktonic Foram	28.00		Coralline Algae	43.2
Macro Porosity	0.80		Macro Porosity	18.8
Coralline Algae	30.00		Bivalve	12.8
Echinoid	8.00		Benthic Foram	2.4
Cement	10.40		Echinoid	7.2
Bivalve	3.20		Foram Planktonic	0.4
Benthic Foram	11.20		Serpulid	0.8

Matrix	5.20		Gastropod	0.4
Moldic Porosity	1.20			
Gastropod	0.80		PW-F6-S3	
Unknown	0.80		Coralline Algae	54.4
	0.40		Bryozoan	10.8
PR-F11-S1			Macro Porosity	16.4
Echinoid	9.60		Moldic Porosity	0.8
Macro Porosity	19.60		Bivalve	6.8
Coralline Algae	21.20		Unknown	0.4
Benthic Foram	3.20		Matrix	3.6
Bivalve	14.80		Cement	1.2
Cement	10.00		Benthic Foram	2
Bryozoan	16.00		Gastropod	0.4
Matrix	1.20		Echinoid	2
Planktonic Foram	0.40		Foram Planktonic	0.4
Moldic Porosity	4.00		Benthic Foram Mold	0.4
			Bivalve Mold	0.4
PR-F11-S2				
Macro Porosity	24.40		PW-F6-S4	
Matrix	1.60		Bivalve	18.4
Bivalve	18.40		Macro Porosity	20.4
Coralline Algae	20.80		Echinoid	5.2
Echinoid	4.80		Coralline Algae	42
Bryozoan	13.20		Bryozoan	8.8
Moldic Porosity	5.20		Cement	0.8
Benthic Foram	5.20		Benthic Foram	1.6
Cement	4.80		Foram Planktonic	1.2
Barnacle	0.40		Moldic Porosity	0.8
Planktonic Foram	0.80		Unknown	0.8
Unknown	0.40			
			PW-F6-S5	
PR-F11-S4			Echinoid	6
Coralline Algae	33.20		Macro Porosity	18
Bivalve	15.20		Coralline Algae	49.6
Macro Porosity	15.20		Moldic Porosity	1.2
Benthic Foram	8.80		Bivalve	13.6
Bryozoan	8.00		Benthic Foram	1.2

Moldic Porosity	5.60		Bryozoan	8.4
Lithoclast	0.40		Unknown	0.4
Cement	2.80		Foram Planktonic	0.4
Serpulid	1.20		Cement	0.8
Echinoid	8.40		Matrix	0.4
Matrix	0.80			
Planktonic Foram	0.40		PW-F6-S6	
			Coralline Algae	43.6
PR-F13-S1			Echinoid	8.4
Bryozoan	26.80		Benthic Foram	2.8
Bivalve	20.00		Macro Porosity	12.4
Macro Porosity	17.60		Bivalve	18
Benthic Foram	11.20		Unknown	0.8
Coralline Algae	7.20		Cement	3.6
Echinoid	2.80		Moldic Porosity	1.6
Planktonic Foram	0.80		Bryozoan	4
Matrix	6.00		Bivalve Mold	0.4
Cement	2.40		Matrix	4
Moldic Porosity	4.00		Calcifers	0.4
Barnacle	0.80			
Serpulid	0.40		PW-F6-S7	
			Coralline Algae	45.2
PR-F13-S2			Bryozoan	6
Bryozoan	28.00		Macro Porosity	15.6
Macro Porosity	9.60		Bivalve Mold	0.4
Coralline Algae	10.40		Bivalve	16
Echinoid	5.60		Benthic Foram	4.4
Benthic Foram	6.00		Echinoid	4
Bivalve	24.40		Cement	4
Moldic Porosity	4.00		Matrix	2
Matrix	8.00		Moldic Porosity	2
Cement	3.60		Unknown	0.4
Unknown	0.40			
			PW-F6-S9	
PR-F13-S3			Bivalve	12.4
Macro Porosity	22.40		Coralline Algae	48.8
Bivalve	9.60		Macro Porosity	14.4
Coralline Algae	10.40		Bryozoan	12

Bryozoan	38.00		Unknown	0.4
Benthic Foram	5.60		Echinoid	3.2
Moldic Porosity	3.60		Moldic Porosity	4
Serpulid	2.00		Benthic Foram	2.4
Matrix	2.40		Cement	0.8
Echinoid	3.60		Matrix	1.6
Cement	2.40			
			PB	
PR-F14-S1			PB-F1-S1	
Bryozoan	27.20		Coralline Algae	32.8
Moldic Porosity	2.80		Cement	10
Coralline Algae	26.00		Macro Porosity	8.4
Macro Porosity	11.20		Matrix	0.8
Bivalve	16.00		Bryozoan	4.4
Echinoid	6.40		Bivalve	31.6
Benthic Foram	4.00		Echinoid	6
Matrix	3.20		Serpulid	1.6
Barnacle	0.80		Moldic Porosity	3.6
Cement	2.00		Benthic Foram	0.8
Serpulid	0.40			
			PB-F1-S2	
PR-F14-S2			Moldic Porosity	3.6
Bryozoan	27.20		Bivalve	16.4
Macro Porosity	20.40		Serpulid	0.4
Bivalve	18.80		Coralline Algae	27.6
Cement	2.40		Cement	10
Matrix	2.80		Benthic Foram	4
Echinoid	7.20		Macro Porosity	10.8
Calcisphere things	0.40		Calcisphere Thing	14.8
Moldic Porosity	4.40		Bryozoan	1.6
Benthic Foram	8.80		Echinoid	6.8
Coralline Algae	6.80		Barnacle	0.8
Serpulid	0.40		Matrix	3.2
Planktonic Foram	0.40			
			PB-F1-S4	
PR-F14-S3			Echinoid	3.98
Bryozoan	18.00		Moldic Porosity	9.453
Macro Porosity	24.40		Bivalve	29.851

Bivalve	15.20		Macro Porosity	5.97
Benthic Foram	4.80		Coralline Algae	33.831
Coralline Algae	16.80		Barnacle	1.493
Moldic Porosity	5.20		Benthic Foram	1.493
Matrix	1.60		Cement	2.985
Barnacle	2.40		Unknown	0.995
Echinoid	9.60		Serpulid	2.488
Cement	1.20		Matrix	4.478
Volcanic	0.40		Bryozoan	2.985
Unknown	0.40			
			PB-F2-S1	
PR-F14-S4			Moldic Porosity	12.4
Bryozoan	26.00		Coralline Algae	20.4
Macro Porosity	25.60		Echinoid	13.2
Coralline Algae	11.20		Bivalve	19.2
Echinoid	5.20		Barnacle	0.4
Bivalve	15.20		Benthic Foram	7.6
Matrix	1.60		Cement	13.2
Moldic Porosity	3.20		Macro Porosity	6.8
Cement	4.00		Bryozoan	3.2
Serpulid	0.40		Matrix	1.2
Barnacle	4.80		Gastropod	0.4
Benthic Foram	2.80		Calcisphere	1.2
			Serpulid	0.4
PR-F14-S5			Volcanics	0.4
Bryozoan	31.20			
Macro Porosity	31.60		PB-F3-S1	
Echinoid	9.20		Bryozoan	4.4
Bivalve	11.20		Coralline Algae	34.8
Coralline Algae	7.20		Bivalve	22
Cement	2.80		Moldic Porosity	7.6
Benthic Foram	4.00		Echinoid	12.4
Moldic Porosity	1.20		Matrix	2
Barnacle	1.20		Cement	3.2
Matrix	0.40		Benthic Foram	1.6
			Calcisphere Thing	2.8
PR-F14-S6			Gastropod	0.4
Bryozoan	32.40		Serpulid	0.8
Coralline Algae	12.80		Macro Porosity	8

Bivalve	15.20			
Benthic Foram	6.00		PB-F3-S2	
Macro Porosity	16.00		Coralline Algae	47.2
Echinoid	8.00		Macro Porosity	12.8
Cement	4.00		Bivalve	15.2
Matrix	3.60		Moldic Porosity	8.4
Serpulid	0.80		Cement	0.8
Moldic Porosity	0.40		Bryozoan	2.8
Barnacle	0.80		Echinoid	8.4
			Benthic Foram	2.8
PR-F14-S7			Matrix	0.8
Bryozoan	36.00		Serpulid	0.4
Echinoid	7.20		Calcsphere Thing	0.4
Bivalve	13.20			
Macro Porosity	11.60		PB-F3-S3	
Benthic Foram	5.20		Coralline Algae	51.2
Coralline Algae	8.40		Bivalve	8.8
Matrix	11.60		Macro Porosity	14
Moldic Porosity	3.20		Bryozoan	10.8
Unknown	0.40		Moldic Porosity	5.2
Cement	2.00		Echinoid	2
Barnacle	1.20		Matrix	1.6
			Cement	4.4
			Benthic Foram	1.2
PR-F14-S8			Barnacle	0.8
Bryozoan	30.00			
Bivalve	14.40			
Coralline Algae	13.20			
Macro Porosity	22.80			
Echinoid	4.80			
Moldic Porosity	4.40			
Matrix	5.60			
Benthic Foram	2.80			
Lithoclast	0.40			
Cement	1.20			
Serpulid	0.00			
Planktonic Foram	0.40			
PR-F14-S9				

Echinoid	9.60			
Bryozoan	27.60			
Moldic Porosity	2.40			
Bivalve	19.20			
Coralline Algae	18.80			
Macro Porosity	11.60			
Barnacle	0.40			
Matrix	4.80			
Cement	3.60			
Benthic Foram	2.00			
PR-F15-S1				
Coralline Algae	47.60			
Bivalve	11.20			
Matrix	5.60			
Macro Porosity	7.60			
Bryozoan	16.00			
Moldic Porosity	4.80			
Echinoid	5.20			
Benthic Foram	1.60			
Cement	0.40			
PR-F15-S2				
Moldic Porosity	4.80			
Macro Porosity	10.80			
Bryozoan	18.40			
Echinoid	4.40			
Coralline Algae	40.40			
Cement	1.60			
Barnacle	0.80			
Serpulid	0.40			
Matrix	6.00			
Bivalve	7.60			
Benthic Foram	3.20			
Lithoclasts	1.60			
02-114				
Coralline Algae	17.40			
Benthic Foram	8.40			

Bivalve	13.40			
Macro Porosity	17.60			
Matrix	6.00			
Cement	4.00			
Echinoid	11.20			
Moldic Porosity	4.00			
Bryozoan	17.60			

Class	Percentage	Class	Percentage
PM		PT	
PM-F1-S1		PT-F1-S1	
Coralline Algae	9.6	Coralline Algae	35.6
Lithoclasts	2.4	Bivalve	15.2
Matrix	4	Bryozoan	15.2
Bryozoan	22.8	Macro Porosity	16
Barnacle	2	Moldic Porosity	6
Moldic Porosity	8	Matrix	4
Macro Porosity	20	Lithoclast	2
Cement	7.2	Echinoid	2.8
Echinoid	10.8	Benthic Foram	2.8
Bivalve	9.6	Unknown	0.4
Benthic Foram	1.6		
Gastropod	0.4	PT-F1-S2	
Unknown	1.6	Macro Porosity	20.4
		Benthic Foram	9.6
PM-F5-S1		Echinoid	10
Unknown	1.11	Bryozoan	6.8
Benthic Foram	1.11	Bivalve	27.2
Cement	1.11	Coralline Algae	19.2
Matrix	1.67	Moldic Porosity	2.4
Moldic Porosity	3.33	Cement	2.8
Bryozoan	3.89	Matrix	0.8
Echinoid	5.56	Bivalve Mold	0.4
Macro Porosity	8.33	Foram Planktonic	0.4
Bivalve	27.78		

Coralline Algae	46.11	PT-F1-S3	
		Bivalve	10
PM-F5-S2		Macro Porosity	19.2
Bryozoan	4	Coralline Algae	64.8
Bivalve	65.6	Bryozoan	2.8
Moldic Porosity	3.2	Cement	1.2
Coralline Algae	12.4	Bivalve Mold	0.4
Echinoid	4.4	Moldic Porosity	1.2
Benthic Foram	2	Benthic Foram	0.4
Cement	1.6		
Matrix	1.2	PT-F1-S4	
Macro Porosity	4.4	Coralline Algae	16
Serpulid	1.2	Bivalve	30.4
		Macro Porosity	22.4
PM-F5-S3		Bryozoan	9.6
Macro Porosity	16	Benthic Foram	8
Coralline Algae	50	Echinoid	8.4
Bivalve	10.8	Moldic Porosity	2.4
Bryozoan	6	Foram Planktonic	0.4
Benthic Foram	3.6	Cement	1.6
Matrix	3.2	Benthic Foram Mold	0.4
Echinoid	4.8	Matrix	0.4
Cement	2.4		
Moldic Porosity	2	PT-F1-S1-lat10	
Lithoclasts	0.8	Benthic Foram	10.4
Unknown	0.4	Macro Porosity	24.8
		Bivalve	30.4
PM-F5-S4		Matrix	2
Bivalve	28	Bryozoan	8.4
Coralline Algae	36.4	Coralline Algae	12
Macro Porosity	10	Moldic Porosity	2
Benthic Foram	2.8	Echinoid	8
Bryozoan	4	Foram Planktonic	0.4
Moldic Porosity	8.4	Benthic Foram Mold	0.4

Echinoid	6.4	Bivalve Mold	0.4
Barnacle	0.4	Cement	0.8
Matrix	2		
Cement	1.6	PT-F1-S3-lat10	
		Echinoid	8.4
PM-F6-S1		Bivalve	28.4
Matrix	2	Coralline Algae	8.4
Macro Porosity	12.8	Bryozoan	13.2
Coralline Algae	48.8	Macro Porosity	29.2
Cement	2.4	Moldic Porosity	2
Benthic Foram	2.8	Benthic Foram	7.2
Moldic Porosity	5.6	Cement	0.8
Bivalve	14	Matrix	1.6
Bryozoan	3.2	Foram Planktonic	0.4
Echinoid	8	Bivalve Mold	0.4
Barnacle	0.4		
		PT-F1-S4-lat10	
PM-F6-S2		Macro Porosity	30
Bivalve	17.6	Echinoid	10
Benthic Foram	2.4	Bivalve	25.6
Bryozoan	4	Moldic Porosity	3.2
Macro Porosity	15.2	Benthic Foram	7.2
Coralline Algae	37.2	Coralline Algae	8.4
Echinoid	13.2	Serpulid	0.4
Matrix	2.4	Bryozoan	8.8
Moldic Porosity	7.2	Cement	3.2
Cement	0.4	Matrix	2
Unknown	0.4	Unknown	0.8
		Calcifers	0.4
PM-F6-S3			
Benthic Foram	6.4	PT-F1-S5-lat10	
Macro Porosity	15.2	Matrix	6.8
Echinoid	6.8	Echinoid	13.6
Bivalve	16.8	Bryozoan	12.4
Coralline Algae	28.8	Bivalve	24.8
Matrix	5.6	Macro Porosity	24.4

Moldic Porosity	10.8	Moldic Porosity	2.4
Bryozoan	7.6	Coralline Algae	7.2
Cement	1.2	Benthic Foram	6.8
Unknown	0.8	Cement	1.2
PM-F6-S4		PT-F2-S1	
Coralline Algae	74.4	Cement	4
Macro Porosity	3.2	Macro Porosity	17.2
Echinoid	1.6	Bryozoan	20
Benthic Foram	3.6	Bivalve	31.6
Moldic Porosity	4	Echinoid	11.6
Cement	1.6	Benthic Foram	6.8
Bryozoan	3.2	Matrix	1.6
Bivalve	6.4	Coralline Algae	3.6
Matrix	1.6	Barnacle	1.2
Serpulid	0.4	Moldic Porosity	1.2
		Unknown	1.2
PM-F7-S0			
Bivalve	14.8	PT-F2-S2	
Cement	9.6	Serpulid	0.4
Moldic Porosity	4	Macro Porosity	35.2
Coralline Algae	27.6	Bivalve	13.2
Bryozoan	12.4	Bryozoan	18.4
Echinoid	10	Coralline Algae	9.6
Benthic Foram	7.2	Echinoid	11.2
Macro Porosity	11.6	Benthic Foram	8.8
Barnacle	0.4	Cement	2
Matrix	2	Moldic Porosity	0.8
		Barnacle	0.4
PM-F7-S1			
Moldic Porosity	4.8	PT-F2-S3	
Coralline Algae	17.6	Macro Porosity	27.6
Bivalve	22.4	Echinoid	17.2
Echinoid	17.2	Bryozoan	9.6

Benthic Foram	10.4	Benthic Foram	8
Macro Porosity	7.2	Bivalve	22.4
Matrix	4.8	Coralline Algae	10.8
Bryozoan	11.6	Cement	4
Cement	3.2	Moldic Porosity	0.4
Gastropod	0.4		
Unknown	0.4	PT-F2-S4	
		Macro Porosity	27.2
PM-F7-S2		Bivalve	19.2
		Coralline Algae	17.2
PM-F7-S3		Moldic Porosity	1.6
Bivalve	18	Bryozoan	13.2
Macro Porosity	6	Echinoid	15.2
Matrix	5.2	Benthic Foram	4.4
Coralline Algae	40.4	Unknown	0.8
Benthic Foram	5.6	Gastropod	0.4
Echinoid	10	Cement	0.8
Bryozoan	10.8		
Moldic Porosity	2.4	PT-F2-S5	
Cement	1.6	Coralline Algae	22
		Bivalve	32
PM-F7-S4		Echinoid	9.6
Moldic Porosity	4	Bryozoan	8.4
Bivalve	18	Macro Porosity	15.6
Macro Porosity	21.2	Benthic Foram	4.8
Coralline Algae	20.4	Matrix	4.4
Matrix	4.8	Unknown	2.8
Benthic Foram	9.2	Moldic Porosity	0.4
Bryozoan	11.2		
Echinoid	8	PT-F2-S6	
Cement	2	Echinoid	11.6
Planktonic Foram	0.4	Benthic Foram	6.4
Lithoclasts	0.4	Macro Porosity	17.6
Unknown	0.4	Bryozoan	14.4
		Bivalve	26
PM-F7-S5		Coralline Algae	15.6

Lithoclasts	21.2	Serpulid	0.4
Coralline Algae	27.2	Gastropod	0.4
Macro Porosity	11.2	Matrix	5.6
Benthic Foram	6.8	Cement	0.4
Echinoid	8.4	Unknown	0.8
Moldic Porosity	8	Moldic Porosity	0.4
Bryozoan	1.6	Barnacle	0.4
Bivalve	10.4		
Matrix	4	PT-F2-S7	
Cement	1.2	Echinoid	3.6
		Coralline Algae	72.4
PM-F7-S6		Bryozoan	8
Bryozoan	12.4	Bivalve	3.6
Matrix	16.4	Macro Porosity	11.2
Bivalve	31.2	Matrix	1.2
Echinoid	10.8		
Coralline Algae	13.2	PT-F2-S8	
Benthic Foram	8	Coralline Algae	30.4
Macro Porosity	2	Bryozoan	8
Moldic Porosity	3.2	Cement	1.6
Cement	2.4	Bivalve	19.2
Unknown	0.4	Macro Porosity	21.6
		Echinoid	10
PM-F7-S7		Benthic Foram	5.2
Coralline Algae	29.6	Moldic Porosity	0.8
Bivalve	14.4	Matrix	2
Benthic Foram	5.2	Unknown	0.8
Macro Porosity	13.2	Barnacle	0.4
Cement	5.2		
Moldic Porosity	7.6	PD	
Echinoid	11.2	PD-F1-S1	
Bryozoan	8.8	Bivalve	13.2
Matrix	4	Coralline Algae	24.8
Unknown	0.4	Cement	18
Lithoclasts	0.4	Echinoid	8.8

		Bryozoan	9.6
PM-F8-S1		Macro Porosity	12
Echinoid	15.6	Benthic Foram	5.6
Coralline Algae	19.6	Moldic Porosity	4.8
Bryozoan	11.2	Gastropod	0.4
Cement	7.6	Unknown	1.2
Macro Porosity	5.6	Serpulid	0.4
Bivalve	14	Matrix	0.8
Benthic Foram	6.4		
Moldic Porosity	6.8	PD-F1-S4	
Matrix	12	Coralline Algae	36.8
Lithoclasts	0.4	Bryozoan	4.4
Barnacle	0.4	Macro Porosity	14.4
Unknown	0.4	Bivalve	10.4
		Echinoid	6
PM-F8-S2		Benthic Foram	3.6
Benthic Foram	4.8	Cement	5.2
Echinoid	14	Moldic Porosity	14.8
Macro Porosity	7.6	Matrix	1.6
Bivalve	24.8	Serpulid	2.4
Coralline Algae	22.8	Calcisphere	0.4
Bryozoan	6		
Matrix	10.4	PD-F2-S1	
Cement	4	Coralline Algae	62
Moldic Porosity	3.6	Macro Porosity	8.8
Serpulid	0.4	Bivalve	5.6
Unknown	1.6	Moldic Porosity	2.4
		Bryozoan	9.2
PM-F8-S3		Matrix	2.8
Bivalve	22	Echinoid	4
Macro Porosity	8.4	Cement	2.8
Matrix	10.4	Serpulid	2
Coralline Algae	25.2	Benthic Foram	0.4
Echinoid	8.4		
Benthic Foram	5.6	PD-F3-S4	
Unknown	1.6	Serpulid	1.6

Moldic Porosity	3.6	Bivalve	17.6
Cement	7.6	Echinoid	12.4
Bryozoan	7.2	Moldic Porosity	9.6
		Benthic Foram	5.6
PM-F10-S1		Cement	7.2
Bryozoan	13.2	Macro Porosity	13.2
Bivalve	8	Coralline Algae	20.8
Macro Porosity	16	Matrix	3.2
Coralline Algae	51.2	Bryozoan	5.2
Lithoclasts	0.8	Gastropod	0.8
Moldic Porosity	1.6	Lithoclast	0.8
Benthic Foram	2.8	Barnacle	0.8
Echinoid	2	Calcisphere	0.8
Cement	1.2		
Matrix	2.8	PD-F3-S7	
Unknown	0.4	Matrix	2.4
		Bryozoan	7.6
PM-F10-S2		Bivalve	18
Coralline Algae	42.4	Coralline Algae	31.6
Bivalve	18.4	Moldic Porosity	9.2
Macro Porosity	14.8	Echinoid	9.2
Echinoid	4	Macro Porosity	12.4
Moldic Porosity	3.6	Benthic Foram	5.6
Matrix	5.6	Serpulid	2.4
Benthic Foram	2.4	Cement	0.8
Bryozoan	6.4	Unknown	0.4
Cement	0.4	Lithoclasts	0.4
Barnacle	0.4		
Unknown	1.2	PD-F4-S1	
Planktonic Foram	0.4	Coralline Algae	59.6
		Bivalve	8
PM-F10-S3		Bryozoan	4.8
Coralline Algae	22.8	Macro Porosity	7.6
Macro Porosity	17.2	Cement	4.8

Bivalve	30.4	Moldic Porosity	8
Benthic Foram	5.6	Benthic Foram	0.8
Moldic Porosity	3.6	Matrix	0.4
Bryozoan	5.6	Serpulid	3.2
Echinoid	6.4	Echinoid	2
Cement	5.6	Gastropod	0.4
Barnacle	0.4	Barnacle	0.4
Matrix	2		
Unknown	0.4	PD-F4-S3	
		Coralline Algae	53.6
PM-F11-S1		Bryozoan	10
Bryozoan	11.2	Macro Porosity	10
Bivalve	28.8	Cement	1.2
Moldic Porosity	4.4	Bivalve	13.2
Serpulid	0.4	Barnacle	0.4
Macro Porosity	12.4	Matrix	2
Coralline Algae	30.8	Moldic Porosity	5.2
Echinoid	1.6	Benthic Foram	2
Matrix	6	Echinoid	2
Lithoclasts	0.4	Planktonic Foram	0.4
Benthic Foram	2.4		
Cement	0.8	PD-F4-S4	
		Bryozoan	5.2
PM-F11-S3		Macro Porosity	11.2
Bivalve	35.2	Cement	2.4
Macro Porosity	15.6	Bivalve	23.6
Coralline Algae	15.2	Coralline Algae	41.6
Echinoid	5.2	Echinoid	6.8
Matrix	7.6	Moldic Porosity	3.6
Benthic Foram	4.4	Benthic Foram	4.4
Moldic Porosity	7.6	Planktonic Foram	0.4
Bryozoan	5.2	Matrix	0.8
Unknown	2.4		
Cement	0.4	PD-F5-S2	
Gastropod	0.8	Bivalve	42

Planktonic Foram	0.4	Moldic Porosity	12.4
		Coralline Algae	8.8
PM-F11-S5		Matrix	2.8
Bryozoan	6	Echinoid	6.8
Macro Porosity	8.4	Macro Porosity	16.4
Bivalve	43.6	Benthic Foram	1.2
Matrix	4.8	Serpulid	1.2
Moldic Porosity	5.2	Bryozoan	5.8
Echinoid	3.6	Planktonic Foram	1.2
Coralline Algae	17.6	Lithoclast	0.4
Benthic Foram	6		
Unknown	0.8	PV-F1-S3	
Planktonic Foram	0.4	Bivalve	30.4
Lithoclasts	3.2	Moldic Porosity	14
Cement	0.4	Bryozoan	12
		Coralline Algae	16
PM-F11-S6		Matrix	5.2
Bivalve	39.6	Macro Porosity	10.4
Coralline Algae	21.6	Echinoid	6
Echinoid	4.4	Benthic Foram	5.2
Macro Porosity	11.2	Cement	0.8
Bryozoan	10.8		
Matrix	2.8	PV	
Moldic Porosity	5.6	PV-F2-S1	
Benthic Foram	1.6	Coralline Algae	64.4
Serpulid	0.4	Macro Porosity	10.4
Lithoclasts	0.4	Bivalve	8.4
Barnacle	0.4	Bryozoan	6
Unknown	0.8	Cement	0.4
		Echinoid	3.2
PM-F12-S1		Moldic Porosity	3.6
Coralline Algae	56.8	Matrix	2
Bryozoan	6	Benthic Foram	1.6
Lithoclasts	6.8		

Macro Porosity	10.8	PV-F2-S2	
Bivalve	10.8	Coralline Algae	31.6
Matrix	3.6	Bivalve	20
Benthic Foram	0.8	Matrix	3.6
Serpulid	4	Macro Porosity	13.2
Unknown	0.4	Cement	4.4
		Bryozoan	9.2
PM-F12-S2		Echinoid	8
Coralline Algae	9.2	Moldic Porosity	5.2
Bivalve	26	Benthic Foram	4
Moldic Porosity	8	Gastropod	0.4
Bryozoan	13.2	Barnacle	0.4
Echinoid	8		
Macro Porosity	20.4	PV-F3-S4	
Volcanic	0.4	Bivalve	26.4
Benthic Foram	6.8	Benthic Foram	6
Cement	3.2	Echinoid	9.6
Serpulid	0.8	Cement	8
Matrix	3.6	Bryozoan	6
Planktonic Foram	0.4	Matrix	1.6
		Macro Porosity	19.2
PM-F12-S3		Coralline Algae	10.8
Bivalve	29.2	Moldic Porosity	11.2
Moldic Porosity	6.4	Gastropod	1.2
Macro Porosity	19.6		
Bryozoan	11.2	PV-F3-S5	
Echinoid	10	Macro Porosity	24
Coralline Algae	13.6	Bivalve	21.6
Benthic Foram	2.4	Echinoid	8.4
Matrix	2	Bryozoan	9.6
Serpulid	0.8	Coralline Algae	15.2
Lithoclasts	3.6	Cement	6.8
Unknown	1.2	Benthic Foram	7.2
		Moldic Porosity	5.6
PM-F13-S1		Barnacle	0.4
Echinoid	15.2	Gastropod	0.8

Macro Porosity	22.4	Matrix	0.4
Cement	7.2		
Bivalve	18.8	PV-F4-S1	
Benthic Foram	4.4	Moldic Porosity	10.8
Coralline Algae	16.8	Macro Porosity	17.2
Bryozoan	11.2	Echinoid	10.8
Matrix	1.2	Bivalve	34.8
Gastropod	0.4	Gastropod	1.6
Planktonic Foram	0.4	Coralline Algae	10.4
Barnacle	0.4	Cement	2.8
Moldic Porosity	1.6	Bryozoan	6.8
		Benthic Foram	2
PM-F13-S2		Matrix	1.6
Moldic Porosity	2	Serpulid	0.4
Coralline Algae	16.8		
Cement	4	PV-F4-S2	
Bivalve	18	Bivalve	32.8
Macro Porosity	18.4	Matrix	1.6
Echinoid	17.6	Benthic Foram	2.4
Benthic Foram	6	Coralline Algae	8
Bryozoan	12.8	Macro Porosity	20.4
Matrix	3.2	Moldic Porosity	5.6
Barnacle	0.8	Echinoid	8.4
Gastropod	0.4	Cement	12.4
		Bryozoan	5.6
PM-F13-S3		Serpulid	0.4
Bivalve	15.2	Barnacle	2.4
Coralline Algae	15.2		
Macro Porosity	31.2	PV-F5-S4	
Echinoid	13.6	Bivalve	37.2
Matrix	1.2	Bryozoan	1.6
Bryozoan	10	Matrix	4.4
Moldic Porosity	1.6	Macro Porosity	12.8
Benthic Foram	6.4	Coralline Algae	13.2

Barnacle	0.8	Moldic Porosity	12.8
Cement	4.8	Echinoid	6
		Cement	1.2
PM-F16-S2		Benthic Foram	2
Coralline Algae	26.4	Gastropod	0.8
Bivalve	18.4	Serpulid	1.6
Macro Porosity	20	Barnacle	6.4
Echinoid	13.2		
Matrix	2		
Bryozoan	7.2		
Benthic Foram	6		
Moldic Porosity	2.8		
Cement	3.6		
Barnacle	0.4		
PM-F17-S1			
Coralline Algae	23.2		
Macro Porosity	25.2		
Echinoid	9.6		
Bryozoan	7.6		
Benthic Foram	10		
Bivalve	15.6		
Cement	2.4		
Serpulid	0.4		
Planktonic Foram	0.4		
Matrix	1.6		
Moldic Porosity	3.6		
Gastropod	0.4		

Grain Size Measurements and Sorting Quantification

One hundred grain size measurements were taken from ~325 thin sections to obtain relative grain sizes and sorting quantification. Grains were measured along their longest axis. Silt and smaller sediments were not measured in this analysis. Grain were selected based on a random point counting method through JMicroVision™ and 100 grains were measured per sample. The spreadsheet below contains measurements converted from mm to ϕ units along with mean values. Of the measurements for each sample as well as the mean values of the 1st and 3rd quartile. These values were used for calculating mean ϕ values for grain size and σ_i values for sorting.

RP

[illegible]

252

RP-F5-52b				rp-f5-54				rp-f5-55				RP-F6-51				rp-f6-52				rp-f6-53				rp-f6-54				RP-F7-51a				RP-F7-52					
Grain Size (mm)	phi	Results		Grain Size (mm)	phi	Results		Grain Size (mm)	phi	Results		Grain Size (mm)	phi	Results		Grain Size (mm)	phi	Results		Grain Size (mm)	phi	Results		Grain Size (mm)	phi	Results		Grain Size (mm)	phi	Results							
0.135	2.8889425	84	0.1753	2.5120085	84	0.2129	2.3918813	84	0.1399	1.8584632	84	0.2545	1.9186415	84	0.1348	2.35991446	84	0.2792	1.8457906	84	0.2392	1.8457906	84	0.2392	1.8457906	84	0.2392	1.8457906	84	0.2392	1.8457906	84					
0.1684	2.7002422	1.9189609	0.0185	2.41272063	1.62151207	0.205	2.8628485	1.47577787	0.338	1.5743555	0.70772162	0.3088	1.695241	0.84078135	0.2103	2.24946022	0.78517294	0.2848	1.81103632	1.2254823	0.26	1.94340004	0.84547621	0.26	1.94340004	0.84547621	0.26	1.94340004	0.84547621	0.26	1.94340004	0.84547621					
0.1706	2.5512887	50	0.2107	2.24808085	50	0.3239	1.53087848	50	0.3396	1.53087848	50	0.3311	1.68451345	50	0.3229	1.63028086	50	0.2962	1.7534161	50	0.2962	1.7534161	50	0.2962	1.7534161	50	0.2962	1.7534161	50	0.2962	1.7534161	50	0.2962	1.7534161			
0.1766	2.5014216	1.0384904	0.2132	2.2297818	0.52999862	0.241	2.0527879	0.45594892	0.3481	1.5234161	-0.72759118	0.3114	1.6310615	-0.42474753	0.3274	1.6310615	-0.28756415	0.3369	1.56859439	-0.0727279	0.3425	1.4839472	-0.7820605	0.3425	1.4839472	-0.7820605	0.3425	1.4839472	-0.7820605	0.3425	1.4839472	-0.7820605					
0.1888	2.4050489	16	0.2138	2.1857322	16	0.2678	1.9007566	16	0.4171	1.2612431	16	0.3384	1.5810311	16	0.3664	1.44849634	16	0.3515	1.5083905	16	0.3731	1.42158056	16	0.3731	1.42158056	16	0.3731	1.42158056	16	0.3731	1.42158056	16	0.3731	1.42158056			
0.1932	2.37181294	-0.10430483	0.2264	2.14303001	-0.7777221	0.2796	1.8385481	-0.42815859	0.4317	1.1283887	-2.278851	0.3778	1.40505743	-0.04827605	0.4093	1.2887553	-1.47823099	0.3604	1.47211663	-2.91288959	0.3908	1.35548616	-2.09512701	0.3908	1.35548616	-2.09512701	0.3908	1.35548616	-2.09512701	0.3908	1.35548616	-2.09512701					
0.1976	2.23925256	Mz	0.2272	2.13794718	Mz	0.2972	1.75047917	Mz	0.4389	1.13461489	Mz	0.3802	1.3951573	Mz	0.4684	1.09417777	Mz	0.3927	1.34848909	Mz	0.4565	1.13113067	Mz	0.4565	1.13113067	Mz	0.4565	1.13113067	Mz	0.4565	1.13113067	Mz	0.4565	1.13113067			
0.2125	2.13940418	0.94304886	0.2465	2.0800702	0.45792953	0.308	1.69893197	0.50112207	0.4424	1.17626679	0.76423755	0.3907	1.35535137	0.54408803	0.4421	1.02256679	0.32007487	0.4069	1.29724284	0.44617176	0.4309	1.35535137	0.54408803	0.4309	1.35535137	0.54408803	0.4309	1.35535137	0.54408803	0.4309	1.35535137	0.54408803					
0.2323	2.0552113		0.2775	1.84942468		0.3189	1.64881005		0.4641	1.10748303		0.4056	1.3015543		0.5105	0.9700093		0.4091	1.2894635		0.5074	0.9767963		0.5074	0.9767963		0.5074	0.9767963		0.5074	0.9767963		0.5074	0.9767963			
0.2440	2.02971815	95	0.2861	1.80539333	95	0.3397	1.5576517	95	0.4712	1.0857937	95	0.4155	1.2670889	95	0.5319	0.96746775	95	0.4182	1.2577244	95	0.5099	0.97170554	95	0.5099	0.97170554	95	0.5099	0.97170554	95	0.5099	0.97170554	95	0.5099	0.97170554	95	0.5099	0.97170554
0.2483	2.00982084	2.58334359	0.2943	1.78462363	2.71630007	0.3471	1.5266382	2.15239383	0.5126	0.9566677	1.52018655	0.4402	1.20057313	1.70859016	0.5359	0.89595667	1.85951161	0.4251	1.23445481	1.69821607	0.5191	0.94592761	1.70316017	0.5191	0.94592761	1.70316017	0.5191	0.94592761	1.70316017	0.5191	0.94592761	1.70316017	0.5191	0.94592761	1.70316017		
0.2486	2.00982082	5	0.2943	1.78462363	5	0.3471	1.5266382	5	0.5126	0.9566677	5	0.4402	1.20057313	5	0.5359	0.89595667	5	0.4251	1.23445481	5	0.5191	0.94592761	5	0.5191	0.94592761	5	0.5191	0.94592761	5	0.5191	0.94592761	5	0.5191	0.94592761	5	0.5191	0.94592761
0.2559	1.9663112	-1.24052829	0.316	1.66198048	-1.73105067	0.3613	1.46871842	-1.3180153	0.5385	0.8829242	-3.07036336	0.511	0.9685961	-2.90995061	0.5918	0.756812	-2.25755415	0.4303	1.21657497	-3.70004082	0.5617	0.83212125	-3.56068484	0.5617	0.83212125	-3.56068484	0.5617	0.83212125	-3.56068484	0.5617	0.83212125	-3.56068484	0.5617	0.83212125	-3.56068484		
0.2559	1.9663112	Q	0.316	1.66198048	Q	0.3613	1.46871842	Q	0.5385	0.8829242	Q	0.511	0.9685961	Q	0.5918	0.756812	Q	0.4303	1.21657497	Q	0.5617	0.83212125	Q	0.5617	0.83212125	Q	0.5617	0.83212125	Q	0.5617	0.83212125	Q	0.5617	0.83212125			
0.2749	1.86305043	1.08525159	0.3351	1.57732307	1.21325038	0.3732	1.42196708	1.0019355	0.5787	0.78910578	1.48088955	0.5345	0.7502449	1.42210516	0.6213	0.68663223	1.18909943	0.4531	1.16714061	1.69716138	0.5758	0.7963537	1.53207038	0.5758	0.7963537	1.53207038	0.5758	0.7963537	1.53207038	0.5758	0.7963537	1.53207038	0.5758	0.7963537	1.53207038		
0.2797	1.8382131		0.3352	1.5769891		0.3828	1.3813255		0.5923	0.7510655		0.6123	0.6111328		0.6128	0.66017291		0.4767	1.09849625		0.5868	0.7643409		0.5868	0.7643409		0.5868	0.7643409		0.5868	0.7643409		0.5868	0.7643409			
0.2808	1.8323696		0.3608	1.47071632		0.3829	1.38494872		0.6217	0.60570372		0.6573	0.60570372		0.6584	0.60295866		0.4713	1.08527323		0.5917	0.7575505		0.5917	0.7575505		0.5917	0.7575505		0.5917	0.7575505		0.5917	0.7575505			
0.285	1.81095086		0.3824	1.46433275		0.3846	1.37855767		0.6255	0.67091429		0.6948	0.5251259		0.6748	0.54763132		0.4823	1.05188917		0.625	0.7806617		0.625	0.7806617		0.625	0.7806617		0.625	0.7806617		0.625	0.7806617			
0.2921	1.77540572		0.3977	1.44338071		0.3867	1.37070134		0.6781	0.56468667		0.7273	0.49377013		0.6771	0.5252442		0.4943	1.01832329		0.6354	0.64524747		0.6354	0.64524747		0.6354	0.64524747		0.6354	0.64524747		0.6354	0.64524747			
0.2938	1.7719755		0.4326	1.1860795		0.3896	1.3592322		0.6791	0.55823994		0.7358	0.4426108		0.6895	0.53817301		0.4962	1.01097981		0.638	0.64838619		0.638	0.64838619		0.638	0.64838619		0.638	0.64838619		0.638	0.64838619			
0.3057	1.7097978		0.3902	1.35585537		0.3996	1.32136032		0.7693	0.17817859		0.7457	0.42312517		0.7299	0.45422543		0.5043	0.96783752		0.6586	0.60253409		0.6586	0.60253409		0.6586	0.60253409		0.6586	0.60253409		0.6586	0.60253409			
0.3072	1.70273548		0.3937	1.33933382		0.4111	1.28242788		0.7757	0.17407719		0.7527	0.40849686		0.7329	0.44830794		0.5131	0.94590761		0.672	0.73746031		0.672	0.73746031		0.672	0.73746031		0.672	0.73746031		0.672	0.73746031			
0.3288	1.60479422		0.3953	1.33896862		0.4205	1.22917136		0.8157	0.2398806		0.7549	0.40561932		0.746	0.4274889		0.5341	0.94063677		0.6805	0.60312616		0.6805	0.60312616		0.6805	0.60312616		0.6805	0.60312616		0.6805	0.60312616			
0.3322	1.5986428		0.4153	1.1077835		0.4411	1.23422996		0.8176	0.29035044		0.7821	0.37194466		0.7656	0.38313401		0.5409	0.8881599		0.6994	0.51380294		0.6994	0.51380294		0.6994	0.51380294		0.6994	0.51380294		0.6994	0.51380294			
0.3332	1.58552628		0.4271	1.22743382		0.4348	1.20156599		0.908	0.1302462		0.7721	0.37117233		0.7667	0.38126267		0.5449	0.8792952		0.7065	0.5048226		0.7065	0.5048226		0.7065	0.5048226		0.7065	0.5048226		0.7065	0.5048226			
0.3436	1.54118502		0.4348	1.20156599		0.4458	1.16552162		0.913	0.1311212		0.7843	0.3405355		0.8039	0.31409398		0.5494	0.8640638		0.7291	0.55880754		0.7291	0.55880754		0.7291	0.55880754		0.7291	0.55880754		0.7291	0.55880754			
0.3443	1.5382489		0.4437	1.1733593		0.4627	1.11418159		0.9432	0.0463766		0.7898	0.3405355		0.815	0.2912524		0.5784	0.9305328		0.749	0.44457619		0.749	0.44457619		0.749	0.44457619		0.749	0.44457619		0.749	0.44457619			
0																																					

254

RP-F10-S5			RP-F11-S1			RP-F11-S2			RP-F11-S4			RP-F11-S5		
Grain Size (mm)	phi	Results	Grain Size (mm)	phi	Results	Grain Size (mm)	phi	Results	Grain Size (mm)	phi	Results	Grain Size (mm)	phi	Results
0.2632	1.92575322	84	0.2272	2.13794718	84	0.3126	1.67759613	84	0.2045	2.28980789	84	0.1893	2.40123338	84
0.332	1.5907314	0.62403625	0.2553	1.9697179	1.22516324	0.3174	1.65561196	1.13214274	0.2392	2.06369325	1.5038555	0.285	1.81095086	1.51578393
0.3419	1.54834058	50	0.289	1.79084346	50	0.3352	1.57689261	50	0.255	1.97141417	50	0.2857	1.80741177	50
0.3751	1.41464087	-1.37876225	0.3096	1.69150832	0.39436456	0.3419	1.54834058	0.2506551	0.2591	1.9484026	0.67393874	0.2946	1.76315575	0.87980191
0.4043	1.30649084	16	0.3204	1.64204006	16	0.3505	1.51250086	16	0.2855	1.80842205	16	0.2976	1.74853878	16
0.4202	1.25084135	-3.47716846	0.3265	1.61483145	-1.31099831	0.3564	1.48841817	-1.54324255	0.2862	1.80488916	-0.81076621	0.2993	1.7403211	-0.43458646
0.4396	1.18572668	Mz	0.3369	1.56959439	Mz	0.3684	1.44064285	Mz	0.2994	1.73983916	Mz	0.3011	1.73167074	Mz
0.4415	1.17950468	-1.41063149	0.3448	1.53615533	0.10284316	0.3835	1.36268982	-0.05348157	0.3021	1.72688731	0.45567601	0.3135	1.6734485	0.65366646
0.527	0.92411732		0.3465	1.52905981		0.3938	1.34445361		0.309	1.69430693		0.3206	1.64113979	
0.5512	0.85934494	95	0.3513	1.50921175	95	0.3952	1.33933382	95	0.3217	1.63619832	95	0.3212	1.63844234	95
0.5659	0.82137401	1.5571912	0.3684	1.44064285	1.84641138	0.4024	1.31328668	1.59418843	0.3279	1.60865859	2.01634799	0.3281	1.6077789	1.90625811
0.5807	0.78412843	5	0.3953	1.33896882	5	0.4097	1.28734931	5	0.3284	1.60646038	5	0.3351	1.57732307	5
0.5853	0.77274528	-4.34315567	0.4275	1.22599331	-2.90161132	0.4104	1.2848865	-3.28294561	0.3338	1.58293075	-2.126699	0.3475	1.52490222	-1.76330569
0.5892	0.76316421	Qi	0.4427	1.1758878	Qi	0.4195	1.25324668	Qi	0.3369	1.56959439	Qi	0.3509	1.51085537	Qi
0.5934	0.7529168	1.91929313	0.4446	1.16941026	1.35343777	0.4354	1.19957654	1.40780602	0.3534	1.50661336	1.20638982	0.3525	1.50429211	1.04358711
0.6139	0.70391847		0.4479	1.15874163		0.4562	1.13225207		0.3615	1.46792003		0.3569	1.48639562	
0.6672	0.58380387		0.4695	1.09079371		0.4639	1.10810488		0.3647	1.45520559		0.3577	1.48316543	
0.6692	0.57948575		0.4712	1.08557937		0.4734	1.07885926		0.3675	1.44417163		0.358	1.48195597	
0.7773	0.3634535		0.4931	1.02003922		0.475	1.0739915		0.368	1.44221013		0.3586	1.47954009	
0.7912	0.33788281		0.4972	1.00809327		0.4926	1.02150283		0.3718	1.42738925		0.3651	1.45362413	
0.7957	0.32970071		0.5201	0.94313108		0.5225	0.93648914		0.3908	1.35548616		0.383	1.38457199	
0.8654	0.20855921		0.5235	0.93373066		0.5257	0.92768051		0.3908	1.35548616		0.3841	1.38043446	
0.8698	0.20124268		0.5295	0.91728965		0.5259	0.92713176		0.4076	1.29476309		0.39	1.35844248	
0.9178	0.12374724		0.5317	0.91130792		0.5419	0.88389397		0.4136	1.27368114		0.3944	1.34225719	
0.9435	0.08390487		0.5329	0.90805558		0.5512	0.85934494		0.4267	1.22869559		0.4042	1.30684772	
0.9633	0.05394247		0.5431	0.88070278		0.5634	0.82776153		0.4441	1.17103362		0.4067	1.29795213	
0.9948	0.00752152		0.5443	0.87751864		0.5692	0.81298556		0.4557	1.13383413		0.4078	1.29405538	
1.0213	-0.03040645		0.5606	0.83494929		0.6016	0.73311733		0.4574	1.12846219		0.4091	1.28946365	
1.0271	-0.03857633		0.5613	0.83314899		0.6264	0.67483817		0.4579	1.126886		0.4238	1.23853403	
1.1159	-0.15820641		0.5619	0.83160766		0.6376	0.64927097		0.4634	1.10960667		0.4335	1.20586859	
1.1617	-0.21623572		0.5674	0.81755503		0.6382	0.64791401		0.4684	1.09417777		0.4417	1.17885129	
1.1846	-0.24439792		0.5698	0.81146561		0.6468	0.6286031		0.4789	1.06219468		0.447	1.16164344	
1.2894	-0.36669679		0.5741	0.80061927		0.6476	0.62681981		0.4798	1.05948598		0.4471	1.16132073	
1.3673	-0.451326		0.5751	0.79810851		0.6591	0.60142564		0.4826	1.05109129		0.4482	1.15777565	
1.3758	-0.46026687		0.5767	0.79410036		0.6647	0.58921976		0.4827	1.05079238		0.4491	1.15488813	
1.4124	-0.49814451		0.6108	0.71122202		0.6694	0.57905465		0.4847	1.04482718		0.45	1.15199335	
1.4644	-0.55030502		0.6211	0.68709672		0.6837	0.54856003		0.4855	1.04244798		0.4517	1.14655348	
1.5319	-0.61531692		0.6434	0.63620678		0.687	0.54161342		0.5047	0.98649367		0.4653	1.10375757	
1.5846	-0.66411309		0.6487	0.62437138		0.6898	0.53574544		0.5089	0.97453766		0.4774	1.06672051	
1.5895	-0.66856736		0.6547	0.61108895		0.7012	0.51209777		0.5183	0.94813268		0.4899	1.0294321	
1.6437	-0.71694095		0.672	0.57346201		0.7155	0.48297224		0.54	0.88896117		0.491	1.02619639	
1.9223	-0.94282553		0.6783	0.55999987		0.7224	0.46912623		0.5559	0.84709555		0.5019	0.99451974	
1.9471	-0.96131885		0.679	0.5585118		0.7438	0.42700974		0.5592	0.83855664		0.5029	0.99164815	
2	-0.99999154		0.6797	0.55702526		0.7586	0.39858535		0.56	0.83649419		0.5063	0.98192731	
2	-0.99999154		0.6831	0.54982665		0.7973	0.32680266		0.5795	0.78711278		0.5063	0.98192731	
2.1369	-1.09551013		0.6877	0.54014418		0.8075	0.30846323		0.5811	0.78313502		0.518	0.94896797	
2.3647	-1.24164667		0.6957	0.52345835		0.8189	0.28823837		0.5881	0.76580613		0.5193	0.94535187	
2.409	-1.26842367		0.7042	0.50593859		0.8214	0.28384075		0.6009	0.73479696		0.5223	0.93704147	
2.491	-1.31671389		0.7063	0.50164276		0.8323	0.26482222		0.6011	0.73431686		0.5223	0.93704147	
2.5057	-1.32520249		0.7083	0.49756334		0.8336	0.2625706		0.6125	0.70721227		0.5229	0.93538511	
2.9371	-1.55437924		0.7562	0.40315684		0.8612	0.21557795		0.6165	0.6978213		0.5297	0.91674483	
2.9847	-1.57757259		0.7725	0.37239001		0.8673	0.20539525		0.6181	0.69408196		0.5497	0.86327631	
3.1268	-1.64467303		0.7882	0.34336344		0.8674	0.20522892		0.6248	0.6785279		0.553	0.85464139	
3.1879	-1.67259223		0.8054	0.31221998		0.876	0.19099561		0.6957	0.52345835		0.566	0.8221191	
3.212	-1.68345766		0.8133	0.29813796		0.9475	0.07780149		0.6965	0.52180033		0.5737	0.8016248	
3.3358	-1.73801809		0.8173	0.2910599		0.9496	0.07460753		0.6989	0.51683768		0.5868	0.76905272	
3.3656	-1.75084892		0.842	0.24810576		0.9741	0.03785789		0.7001	0.51436274		0.61	0.71311282	
3.6332	-1.86122504		0.8576	0.22162131		0.9761	0.03489884		0.708	0.49817452		0.611	0.7107497	
3.6694	-1.87552832		0.8756	0.19165452		0.9779	0.03224088		0.7099	0.4943081		0.6249	0.67829702	
3.6845	-1.88145294		0.8927	0.16375128		0.9886	0.01654105		0.7326	0.4488986		0.6337	0.65812251	
3.8067	-1.92852457		0.929	0.1062486		0.9904	0.01391666		0.736	0.44221859		0.6372	0.65017633	
3.9815	-1.9932952		0.9537	0.068392		0.9953	0.00679659		0.7684	0.38006736		0.6425	0.63822624	
4.1715	-2.06054882		0.9709	0.04260502		1.0188	0.02687064		0.8129	0.29884768		0.6439	0.63508607	
4.1944	-2.06844696		1.0186	-0.0265874		1.0504	-0.07093822		0.8329	0.26378225		0.6512	0.61882216	
4.4492	-2.15352774		1.0319	-0.04530278		1.0571	-0.08011118		0.8447	0.24348698		0.6547	0.61108895	
7.0524	-2.81809047		1.068	-0.09491084		1.0705	-0.09828396		0.8716	0.19826022		0.6562	0.60778736	
7.2161	-2.85119522		1.0894	-0.12353273		1.079	-0.10969394		0.9385	0.09157058		0.6631	0.59269663	
7.3033	-2.86852423		1.0965	-0.13290469		1.0812	-0.11263246		0.9457	0.08054482		0.6658	0.58683426	
7.333	-2.87437923		1.1179	-0.16078978		1.1735	-0.23081589		0.9656	0.05050199		0.7295	0.45501627	
7.3837	-2.88431954		1.1449	-0.19521994		1.1842	-0.2439107		0.9703	0.04349685		0.7343	0.44555473	
7.5516	-2.91675768		1.2341	-0.30345674		1.1927	-0.25422906		1.0002	-0.00028851		0.7602	0.39554572	
8.633	-3.10983569		1.2502	-0.32215618		1.2741	-0.34947556		1.001	-0.0014196		0.8217	0.28331393	
8.633	-3.10983569		1.2995	-0.37795344		1.2762	-0.35185146		1.0379	-0.053667		0.8635	0.21173013	
8.633	-3.10983569		1.4559	-0.54190668		1.3329	-0.41456504		1.070					

RM-F1-52	phi	results	RM-F1-52	phi	results	RM-F2-51a	phi	results	RM-F2-51b	phi	results	RM-F3-51	phi	results	RM-F3-53	phi	results	RM-F3-55	phi	results	RM-F3-56	phi	results
0.268	1.8996703	0	0.5194	0.9450749	0.341491	0.3827	1.4631398	84	0.2627	1.5249358	84	0.2902	1.7261658	84	0.3627	2.5820815	84	0.4424	1.1571203	84	0.2486	2.0011379	84
0.028	0.1210228	-0.076584	0.74	0.5252	0.9229246	0.144192	0.342	1.0966116	0.3787	0.4371	0.6791666	0.8378021	0.1387	0.21021	0.5110453	0.3139	0.1716095	0.4654573	0.5138	0.32	0.03282	0.0372946	0.2017056
0.4528	1.1430447	50	0.6773	0.5621204	50	0.3907	1.3555337	50	0.431	0.1130084	50	0.4958	0.1278024	50	0.1165	0.8970856	50	0.0423	0.7114395	50	0.6801	1.0694284	50
0.5314	0.9042703	-1.5329687	0.6911	0.5302911	-0.7454948	0.4141	1.2719381	-0.3348914	0.429	1.2294042	-0.0154379	0.5462	0.8203195	-0.5230704	0.7397	1.3970528	-1.5500165	0.6623	0.9548381	-1.0528719	0.4965	1.0101283	-0.9464539
0.6312	0.6638258	16	0.7009	0.5127513	16	0.4407	1.182122	16	0.4309	1.2259417	16	0.6738	0.5700314	16	0.4397	0.7091889	16	0.6678	0.5542807	16	0.6877	0.9375316	16
0.6787	0.5591493	-2.8033212	0.7086	0.4969524	-2.7177282	0.4447	1.1693858	-1.1132992	0.4351	1.2005792	-0.7324595	0.4703	0.5083991	-2.7167739	0.5462	0.4512485	-2.942323	0.7533	0.4087011	-2.9453578	0.6283	0.6845718	-2.9854301
0.7814	0.3816479	-1.4095718	0.8111	0.3717184	-1.4095718	0.4447	1.1693858	-1.1132992	0.4351	1.2005792	-0.7324595	0.4703	0.5083991	-2.7167739	0.5462	0.4512485	-2.942323	0.7533	0.4087011	-2.9453578	0.6283	0.6845718	-2.9854301
0.8211	0.3816479	-1.4095718	0.8111	0.3717184	-1.4095718	0.4447	1.1693858	-1.1132992	0.4351	1.2005792	-0.7324595	0.4703	0.5083991	-2.7167739	0.5462	0.4512485	-2.942323	0.7533	0.4087011	-2.9453578	0.6283	0.6845718	-2.9854301
0.963	0.0359427	0	0.8063	0.3120504	0	0.4877	1.0664139	0	0.4877	1.0664139	0	0.7913	0.3770048	0	0.5987	0.7619406	0	0.8032	0.3161651	0	0.7601	0.3937551	0
1.021	0.0299821	95	0.8129	0.2887648	95	0.5399	0.89822836	95	0.4698	1.0254266	95	0.8292	0.2700059	95	0.5927	0.5600885	95	0.8034	0.3158066	95	0.8071	0.3937551	95
1.0367	0.0271262	1.165349	0.8606	0.2165842	0.6962332	0.5377	0.8423417	1.3327303	0.4931	0.2389132	1.445399	0.8323	0.2684282	1.1326993	0.6404	0.6396624	1.7326706	0.8851	0.2095942	0.8524601	0.816	0.2933466	1.2993808
1.1561	0.0146832	0.12181	0.8758	0.1648678	0.0146832	0.5377	0.8423417	1.3327303	0.4931	0.2389132	1.445399	0.8323	0.2684282	1.1326993	0.6404	0.6396624	1.7326706	0.8851	0.2095942	0.8524601	0.816	0.2933466	1.2993808
1.1936	0.1847206	0.055895	0.8701	0.2027158	-4.9608491	0.6261	0.9575299	-1.7463852	0.5295	0.9172895	-1.4287304	0.639	0.2517024	-2.8102189	0.7411	0.4123655	-4.7322412	0.9368	0.0941622	-3.9776692	0.9053	0.2424259	-3.425555
1.1937	0.18865252	0	0.9261	0.1104755	0	0.6356	0.8538044	0	0.5729	0.8038													

RM-F4-S1				RM-F4-S2				RM-F4-S3				RM-F4-S4				RM-F4-S5				RM-F4-S6				RM-F4-S7				RM-F4-S8				RM-F4-S9				RM-F4-S10				RM-F4-S11				RM-F4-S12				RM-F4-S13				RM-F4-S14				RM-F4-S15				RM-F4-S16				RM-F4-S17				RM-F4-S18				RM-F4-S19				RM-F4-S20				RM-F4-S21				RM-F4-S22				RM-F4-S23				RM-F4-S24				RM-F4-S25				RM-F4-S26				RM-F4-S27				RM-F4-S28				RM-F4-S29				RM-F4-S30				RM-F4-S31				RM-F4-S32				RM-F4-S33				RM-F4-S34				RM-F4-S35				RM-F4-S36				RM-F4-S37				RM-F4-S38				RM-F4-S39				RM-F4-S40				RM-F4-S41				RM-F4-S42				RM-F4-S43				RM-F4-S44				RM-F4-S45				RM-F4-S46				RM-F4-S47				RM-F4-S48				RM-F4-S49				RM-F4-S50				RM-F4-S51				RM-F4-S52				RM-F4-S53				RM-F4-S54				RM-F4-S55				RM-F4-S56				RM-F4-S57				RM-F4-S58				RM-F4-S59				RM-F4-S60				RM-F4-S61				RM-F4-S62				RM-F4-S63				RM-F4-S64				RM-F4-S65				RM-F4-S66				RM-F4-S67				RM-F4-S68				RM-F4-S69				RM-F4-S70				RM-F4-S71				RM-F4-S72				RM-F4-S73				RM-F4-S74				RM-F4-S75				RM-F4-S76				RM-F4-S77				RM-F4-S78				RM-F4-S79				RM-F4-S80				RM-F4-S81				RM-F4-S82				RM-F4-S83				RM-F4-S84				RM-F4-S85				RM-F4-S86				RM-F4-S87				RM-F4-S88				RM-F4-S89				RM-F4-S90				RM-F4-S91				RM-F4-S92				RM-F4-S93				RM-F4-S94				RM-F4-S95				RM-F4-S96				RM-F4-S97				RM-F4-S98				RM-F4-S99				RM-F4-S100				RM-F4-S101				RM-F4-S102				RM-F4-S103				RM-F4-S104				RM-F4-S105				RM-F4-S106				RM-F4-S107				RM-F4-S108				RM-F4-S109				RM-F4-S110				RM-F4-S111				RM-F4-S112				RM-F4-S113				RM-F4-S114				RM-F4-S115				RM-F4-S116				RM-F4-S117				RM-F4-S118				RM-F4-S119				RM-F4-S120				RM-F4-S121				RM-F4-S122				RM-F4-S123				RM-F4-S124				RM-F4-S125				RM-F4-S126				RM-F4-S127				RM-F4-S128				RM-F4-S129				RM-F4-S130				RM-F4-S131				RM-F4-S132				RM-F4-S133				RM-F4-S134				RM-F4-S135				RM-F4-S136				RM-F4-S137				RM-F4-S138				RM-F4-S139				RM-F4-S140				RM-F4-S141				RM-F4-S142				RM-F4-S143				RM-F4-S144				RM-F4-S145				RM-F4-S146				RM-F4-S147				RM-F4-S148				RM-F4-S149				RM-F4-S150				RM-F4-S151				RM-F4-S152				RM-F4-S153				RM-F4-S154				RM-F4-S155				RM-F4-S156				RM-F4-S157				RM-F4-S158				RM-F4-S159				RM-F4-S160				RM-F4-S161				RM-F4-S162				RM-F4-S163				RM-F4-S164				RM-F4-S165				RM-F4-S166				RM-F4-S167				RM-F4-S168				RM-F4-S169				RM-F4-S170				RM-F4-S171				RM-F4-S172				RM-F4-S173				RM-F4-S174				RM-F4-S175				RM-F4-S176				RM-F4-S177				RM-F4-S178				RM-F4-S179				RM-F4-S180				RM-F4-S181				RM-F4-S182				RM-F4-S183				RM-F4-S184				RM-F4-S185				RM-F4-S186				RM-F4-S187				RM-F4-S188				RM-F4-S189				RM-F4-S190				RM-F4-S191				RM-F4-S192				RM-F4-S193				RM-F4-S194				RM-F4-S195				RM-F4-S196				RM-F4-S197				RM-F4-S198				RM-F4-S199				RM-F4-S200				RM-F4-S201				RM-F4-S202				RM-F4-S203				RM-F4-S204				RM-F4-S205				RM-F4-S206				RM-F4-S207				RM-F4-S208				RM-F4-S209				RM-F4-S210				RM-F4-S211				RM-F4-S212				RM-F4-S213				RM-F4-S214				RM-F4-S215				RM-F4-S216				RM-F4-S217				RM-F4-S218				RM-F4-S219				RM-F4-S220				RM-F4-S221				RM-F4-S222				RM-F4-S223				RM-F4-S224				RM-F4-S225				RM-F4-S226				RM-F4-S227				RM-F4-S228				RM-F4-S229				RM-F4-S230				RM-F4-S231				RM-F4-S232				RM-F4-S233				RM-F4-S234				RM-F4-S235				RM-F4-S236				RM-F4-S237				RM-F4-S238				RM-F4-S239				RM-F4-S240				RM-F4-S241				RM-F4-S242				RM-F4-S243				RM-F4-S244				RM-F4-S245				RM-F4-S246				RM-F4-S247				RM-F4-S248				RM-F4-S249				RM-F4-S250				RM-F4-S251				RM-F4-S252				RM-F4-S253				RM-F4-S254				RM-F4-S255				RM-F4-S256				RM-F4-S257				RM-F4-S258				RM-F4-S259				RM-F4-S260				RM-F4-S261				RM-F4-S262				RM-F4-S263				RM-F4-S264				RM-F4-S265				RM-F4-S266				RM-F4-S267				RM-F4-S268				RM-F4-S269				RM-F4-S270				RM-F4-S271				RM-F4-S272				RM-F4-S273				RM-F4-S274				RM-F4-S275				RM-F4-S276				RM-F4-S277				RM-F4-S278				RM-F4-S279				RM-F4-S280				RM-F4-S281				RM-F4-S282				RM-F4-S283				RM-F4-S284				RM-F4-S285				RM-F4-S286				RM-F4-S287				RM-F4-S288				RM-F4-S289				RM-F4-S290				RM-F4-S291				RM-F4-S292				RM-F4-S293				RM-F4-S294				RM-F4-S295				RM-F4-S296				RM-F4-S297				RM-F4-S298				RM-F4-S299				RM-F4-S300				RM-F4-S301				RM-F4-S302				RM-F4-S303				RM-F4-S304				RM-F4-S305				RM-F4-S306				RM-F4-S307				RM-F4-S308				RM-F4-S309				RM-F4-S310				RM-F4-S311				RM-F4-S312				RM-F4-S313				RM-F4-S314				RM-F4-S315				RM-F4-S316				RM-F4-S317				RM-F4-S318				RM-F4-S319				RM-F4-S320				RM-F4-S321				RM-F4-S322				RM-F4-S323				RM-F4-S324				RM-F4-S325				RM-F4-S326				RM-F4-S327				RM-F4-S328				RM-F4-S329				RM-F4-S330				RM-F4-S331				RM-F4-S332				RM-F4-S333				RM-F4-S334				RM-F4-S335				RM-F4-S336				RM-F4-S337				RM-F4-S338				RM-F4-S339				RM-F4-S340				RM-F4-S341				RM-F4-S342				RM-F4-S343				RM-F4-S344				RM-F4-S345				RM-F4-S346				RM-F4-S347				RM-F4-S348				RM-F4-S349				RM-F4-S350				RM-F4-S351				RM-F4-S352				RM-F4-S353				RM-F4-S354				RM-F4-S355				RM-F4-S356				RM-F4-S357				RM-F4-S358				RM-F4-S359				RM-F4-S360				RM-F4-S361				RM-F4-S362				RM-F4-S363				RM-F4-S364				RM-F4-S365				RM-F4-S366				RM-F4-S367				RM-F4-S368				RM-F4-S369				RM-F4-S370				RM-F4-S371				RM-F4-S372				RM-F4-S373				RM-F4-S374				RM-F4-S375				RM-F4-S376				RM-F4-S377				RM-F4-S378				RM-F4-S379				RM-F4-S380				RM-F4-S381				RM-F4-S382				RM-F4-S383				RM-F4-S384				RM-F4-S385				RM-F4-S386				RM-F4-S387				RM-F4-S388				RM-F4-S389				RM-F4-S390				RM-F4-S391				RM-F4-S392				RM-F4-S393				RM-F4-S394				RM-F4-S395				RM-F4-S396				RM-F4-S397				RM-F4-S398				RM-F4-S399				RM-F4-S400				RM-F4-S401				RM-F4-S402				RM-F4-S403				RM-F4-S404				RM-F4-S405				RM-F4-S406				RM-F4-S407				RM-F4-S408				RM-F4-S409				RM-F4-S410				RM-F4-S411				RM-F4-S412				RM-F4-S413				RM-F4-S414				RM-F4-S415				RM-F4-S416				RM-F4-S417				RM-F4-S418				RM-F4-S419				RM-F4-S420				RM-F4-S421				RM-F4-S422				RM-F4-S423				RM-F4-S424				RM-F4-S425				RM-F4-S426				RM-F4-S427				RM-F4-S428				RM-F4-S429				RM-F4-S430				RM-F4-S431				RM-F4-S432				RM-F4-S433				RM-F4-S434				RM-F4-S435				RM-F4-S436				RM-F4-S437				RM-F4-S438				RM-F4-S439				RM-F4-S440				RM-F4-S441				RM-F4-S442				RM-F4-S443				RM-F4-S444				RM-F4-S445				RM-F4-S446				RM-F4-S447				RM-F4-S448				RM-F4-S449				RM-F4-S450				RM-F4-S451				RM-F4-S452				RM-F4-S453				RM-F4-S454				RM-F4-S455				RM-F4-S456				RM-F4-S457				RM-F4-S458				RM-F4-S459				RM-F4-S460				RM-F4-S461				RM-F4-S462				RM-F4-S463				RM-F4-S464				RM-F4-S465				RM-F4-S466				RM-F4-S467				RM-F4-S468				RM-F4-S469				RM-F4-S470				RM-F4-S471				RM-F4-S472				RM-F4-S473				RM-F4-S474				RM-F4-S475				RM-F4-S476				RM-F4-S477				RM-F4-S478				RM-F4-S479				RM-F4-S480				RM-F4-S481				RM-F4-S482				RM-F4-S483				RM-F4-S484				RM-F4-S485				RM-F4-S486				RM-F4-S487				RM-F4-S488				RM-F4-S489				RM-F4-S490				RM-F4-S491				RM-F4-S492				RM-F4-S493				RM-F4-S494				RM-F4-S495				RM-F4-S496				RM-F4-S497				RM-F4-S498				RM-F4-S499				RM-F4-S500				RM-F4-S501				RM-F4-S502				RM-F4-S503				RM-F4-S504				RM-F4-S505				RM-F4-S506				RM-F4-S507				RM-F4-S508				RM-F4-S509				RM-F4-S510				RM-F4-S511				RM-F4-S512				RM-F4-S513				RM-F4-S514				RM-F4-S515				RM-F4-S516				RM-F4-S517				RM-F4-S518				RM-F4-S519				RM-F4-S520				RM-F4-S521				RM-F4-S522				RM-F4-S523				RM-F4-S524				RM-F4-S525				RM-F4-S526				RM-F4-S527				RM-F4-S528				RM-F4-S529				RM-F4-S530				RM-F4-S531				RM-F4-S532				RM-F4-S533				RM-F4-S534				RM-F4-S535				RM-F4-S536				RM-F4-S537				RM-F4-S538				RM-F4-S539				RM-F4-S540				RM-F4-S541				RM-F4-S542				RM-F4-S543				RM-F4-S544				RM-F4-S545				RM-F4-S546				RM-F4-S547				RM-F4-S548				RM-F4-S549				RM-F4-S550				RM-F4-S551				RM-F4-S552				RM-F4-S553				RM-F4-S554				RM-F4-S555				RM-F4-S556				RM-F4-S557				RM-F4-S558				RM-F4-S559				RM-F4-S560				RM-F4-S561				RM-F4-S562				RM-F4-S563				RM-F4-S564				RM-F4-S565				RM-F4-S566				RM-F4-S567				RM-F4-S568				RM-F4-S569				RM-F4-S570				RM-F4-S571				RM-F4-S572				RM-F4-S573				RM-F4-S574				RM-F4-S575				RM-F4-S576				RM-F4-S577				RM-F4-S578				RM-F4-S579				RM-F4-S580				RM-F4-S581				RM-F4-S582				RM-F4-S583				RM-F4-S584				RM-F4-S585				RM-F4-S586				RM-F4-S587				RM-F4-S588				RM-F4-S589				RM-F4-S590				RM-F4-S591				RM-F4-S592				RM-F4-S593				RM-F4-S594				RM-F4-S595				RM-F4-S596				RM-F4-S597				RM-F4-S598				RM-F4-S599				RM-F4-S600				RM-F4-S601				RM-F4-S602				RM-F4-S603				RM-F4-S604				RM-F4-S605				RM-F4-S606				RM-F4-S607				RM-F4-S608				RM-F4-S609				RM-F4-S610				RM-F4-S611				RM-F4-S612				RM-F4-S613				RM-F4-S614				RM-F4-S615				RM-F4-S616				RM-F4-S617				RM-F4-S618				RM-F4-S619				RM-F4-S620				RM-F4-S621				RM-F4-S622				RM-F4-S623				RM-F4-S624				RM-F4-S625				RM-F4-S626				RM-F4-S627				RM-F4-S628				RM-F4-S629				RM-F4-S630				RM-F4-S631				RM-F4-S632				RM-F4-S633				RM-F4-S634				RM-F4-S635				RM-F4-S636				RM-F4-S637				RM-F4-S638				RM-F4-S639				RM-F4-S640				RM-F4-S641				RM-F4-S642				RM-F4-S643				RM-F4-S644				RM-F4-S645				RM-F4-S646				RM-F4-S647				RM-F4-S648				RM-F4-S649				RM-F4-S650				RM-F4-S651				RM-F4-S652				RM-F4-S653				RM-F4-S654				RM-F4-S655				RM-F4-S656				RM-F4-S657				RM-F4-S658				RM-F4-S659				RM-F4-S660				RM-F4-S661				RM-F4-S662				RM-F4-S663				RM-F4-S664				RM-F4-S665				RM-F4-S666				RM-F4-S667				RM-F4-S668				RM-F4-S669				RM-F4-S670				RM-F4-S671				RM-F4-S672				RM-F4-S673				RM-F4-S674				RM-F4-S675				RM-F4-S676				RM-F4-S677				RM-F4-S678				RM-F4-S679				RM-F4-S680				RM-F4-S681				RM-F4-S682				RM-F4-S683				RM-F4-S684				RM-F4-S685				RM-F4-S686				RM-F4-S687				RM-F4-S688				RM-F4-S689				RM-F4-S690				RM-F4-S691				RM-F4-S692				RM-F4-S693				RM-F4-S694				RM-F4-S695				RM-F4-S696				RM-F4-S697				RM-F4-S698				RM-F4-S699				RM-F4-S700				RM-F4-S701				RM-F4-S702				RM-F4-S703				RM-F4-S704				RM-F4-S705				RM-F4-S706				RM-F4-S707				RM-F4-S708				RM-F4-S709				RM-F4-S710				RM-F4-S711				RM-F4-S712				RM-F4-S713				RM-F4-S714				RM-F4-S715				RM-F4-S716				RM-F4-S717				RM-F4-S718				RM-F4-S719				RM-F4-S720				RM-F4-S721				RM-F4-S722				RM-F4-S723				RM-F4-S724				RM-F4-S725				RM-F4-S726				RM-F4-S727				RM-F4-S728				RM-F4-S729				RM-F4-S730				RM-F4-S731				RM-F4-S732				RM-F4-S733				RM-F4-S734				RM-F4-S735				RM-F4-S736				RM-F4-S737				RM-F4-S738				RM-F4-S739				RM-F4-S740				RM-F4-S741				RM-F4-S742				RM-F4-S743				RM-F4-S744				RM-F4-S745				RM-F4-S746				RM-F4-S747				RM-F4-S748				RM-F4-S749				RM-F4-S750				RM-F4-S751				RM-F4-S752				RM-F4-S753				RM-F4-S754				RM-F4-S755				RM-F4-S756				RM-F4-S757				RM-F4-S758				RM-F4-S759				RM-F4-S760				RM-F4-S761				RM-F4-S762				RM-F4-S763				RM-F4-S764				RM-F4-S765				RM-F4-S766				RM-F4-S767				RM-F4-S768				RM-F4-S769				RM-F4-S770				RM-F4-S771				RM-F4-S772				RM-F4-S773				RM-F4-S774				RM-F4-S775				RM-F4-S776				RM-F4-S777				RM-F4-S778				RM-F4-S779				RM-F4-S780				RM-F4-S781				RM-F4-S782				RM-F4-S783				RM-F4-S784				RM-F4-S785				RM-F4-S786				RM-F4-S787				RM-F4-S788				RM-F4-S789				RM-F4-S790				RM-F4-S791				RM-F4-S792				RM-F4-S793				RM-F4-S794				RM-F4-S795				RM-F4-S796				RM-F4-S797				RM-F4-S798				RM-F4-S799				RM-F4-S800				RM-F4-S801				RM-F4-S802				RM-F4-S803				RM-F4-S804				RM-F4-S805				RM-F4-S806				RM-F4-S807				RM-F4-S808				RM-F4-S809				RM-F4-S810				RM-F4-S811				RM-F4-S812				RM-F4-S813				RM-F4-S814				RM-F4-S815				RM-F4-S816				RM-F4-S817				RM-F4-S818				RM-F4-S819				RM-F4-S820				RM-F4-S821				RM-F4-S822				RM-F4-S823				RM-F4-S824				RM-F4-S825				RM-F4-S826				RM-F4-S827				RM-F4-S828				RM-F4-S829				RM-F4-S830				RM-F4-S831				RM-F4-S832				RM-F4			
----------	--	--	--	----------	--	--	--	----------	--	--	--	----------	--	--	--	----------	--	--	--	----------	--	--	--	----------	--	--	--	----------	--	--	--	----------	--	--	--	-----------	--	--	--	-----------	--	--	--	-----------	--	--	--	-----------	--	--	--	-----------	--	--	--	-----------	--	--	--	-----------	--	--	--	-----------	--	--	--	-----------	--	--	--	-----------	--	--	--	-----------	--	--	--	-----------	--	--	--	-----------	--	--	--	-----------	--	--	--	-----------	--	--	--	-----------	--	--	--	-----------	--	--	--	-----------	--	--	--	-----------	--	--	--	-----------	--	--	--	-----------	--	--	--	-----------	--	--	--	-----------	--	--	--	-----------	--	--	--	-----------	--	--	--	-----------	--	--	--	-----------	--	--	--	-----------	--	--	--	-----------	--	--	--	-----------	--	--	--	-----------	--	--	--	-----------	--	--	--	-----------	--	--	--	-----------	--	--	--	-----------	--	--	--	-----------	--	--	--	-----------	--	--	--	-----------	--	--	--	-----------	--	--	--	-----------	--	--	--	-----------	--	--	--	-----------	--	--	--	-----------	--	--	--	-----------	--	--	--	-----------	--	--	--	-----------	--	--	--	-----------	--	--	--	-----------	--	--	--	-----------	--	--	--	-----------	--	--	--	-----------	--	--	--	-----------	--	--	--	-----------	--	--	--	-----------	--	--	--	-----------	--	--	--	-----------	--	--	--	-----------	--	--	--	-----------	--	--	--	-----------	--	--	--	-----------	--	--	--	-----------	--	--	--	-----------	--	--	--	-----------	--	--	--	-----------	--	--	--	-----------	--	--	--	-----------	--	--	--	-----------	--	--	--	-----------	--	--	--	-----------	--	--	--	-----------	--	--	--	-----------	--	--	--	-----------	--	--	--	-----------	--	--	--	-----------	--	--	--	-----------	--	--	--	-----------	--	--	--	-----------	--	--	--	-----------	--	--	--	-----------	--	--	--	-----------	--	--	--	-----------	--	--	--	-----------	--	--	--	-----------	--	--	--	-----------	--	--	--	-----------	--	--	--	-----------	--	--	--	-----------	--	--	--	-----------	--	--	--	-----------	--	--	--	-----------	--	--	--	------------	--	--	--	------------	--	--	--	------------	--	--	--	------------	--	--	--	------------	--	--	--	------------	--	--	--	------------	--	--	--	------------	--	--	--	------------	--	--	--	------------	--	--	--	------------	--	--	--	------------	--	--	--	------------	--	--	--	------------	--	--	--	------------	--	--	--	------------	--	--	--	------------	--	--	--	------------	--	--	--	------------	--	--	--	------------	--	--	--	------------	--	--	--	------------	--	--	--	------------	--	--	--	------------	--	--	--	------------	--	--	--	------------	--	--	--	------------	--	--	--	------------	--	--	--	------------	--	--	--	------------	--	--	--	------------	--	--	--	------------	--	--	--	------------	--	--	--	------------	--	--	--	------------	--	--	--	------------	--	--	--	------------	--	--	--	------------	--	--	--	------------	--	--	--	------------	--	--	--	------------	--	--	--	------------	--	--	--	------------	--	--	--	------------	--	--	--	------------	--	--	--	------------	--	--	--	------------	--	--	--	------------	--	--	--	------------	--	--	--	------------	--	--	--	------------	--	--	--	------------	--	--	--	------------	--	--	--	------------	--	--	--	------------	--	--	--	------------	--	--	--	------------	--	--	--	------------	--	--	--	------------	--	--	--	------------	--	--	--	------------	--	--	--	------------	--	--	--	------------	--	--	--	------------	--	--	--	------------	--	--	--	------------	--	--	--	------------	--	--	--	------------	--	--	--	------------	--	--	--	------------	--	--	--	------------	--	--	--	------------	--	--	--	------------	--	--	--	------------	--	--	--	------------	--	--	--	------------	--	--	--	------------	--	--	--	------------	--	--	--	------------	--	--	--	------------	--	--	--	------------	--	--	--	------------	--	--	--	------------	--	--	--	------------	--	--	--	------------	--	--	--	------------	--	--	--	------------	--	--	--	------------	--	--	--	------------	--	--	--	------------	--	--	--	------------	--	--	--	------------	--	--	--	------------	--	--	--	------------	--	--	--	------------	--	--	--	------------	--	--	--	------------	--	--	--	------------	--	--	--	------------	--	--	--	------------	--	--	--	------------	--	--	--	------------	--	--	--	------------	--	--	--	------------	--	--	--	------------	--	--	--	------------	--	--	--	------------	--	--	--	------------	--	--	--	------------	--	--	--	------------	--	--	--	------------	--	--	--	------------	--	--	--	------------	--	--	--	------------	--	--	--	------------	--	--	--	------------	--	--	--	------------	--	--	--	------------	--	--	--	------------	--	--	--	------------	--	--	--	------------	--	--	--	------------	--	--	--	------------	--	--	--	------------	--	--	--	------------	--	--	--	------------	--	--	--	------------	--	--	--	------------	--	--	--	------------	--	--	--	------------	--	--	--	------------	--	--	--	------------	--	--	--	------------	--	--	--	------------	--	--	--	------------	--	--	--	------------	--	--	--	------------	--	--	--	------------	--	--	--	------------	--	--	--	------------	--	--	--	------------	--	--	--	------------	--	--	--	------------	--	--	--	------------	--	--	--	------------	--	--	--	------------	--	--	--	------------	--	--	--	------------	--	--	--	------------	--	--	--	------------	--	--	--	------------	--	--	--	------------	--	--	--	------------	--	--	--	------------	--	--	--	------------	--	--	--	------------	--	--	--	------------	--	--	--	------------	--	--	--	------------	--	--	--	------------	--	--	--	------------	--	--	--	------------	--	--	--	------------	--	--	--	------------	--	--	--	------------	--	--	--	------------	--	--	--	------------	--	--	--	------------	--	--	--	------------	--	--	--	------------	--	--	--	------------	--	--	--	------------	--	--	--	------------	--	--	--	------------	--	--	--	------------	--	--	--	------------	--	--	--	------------	--	--	--	------------	--	--	--	------------	--	--	--	------------	--	--	--	------------	--	--	--	------------	--	--	--	------------	--	--	--	------------	--	--	--	------------	--	--	--	------------	--	--	--	------------	--	--	--	------------	--	--	--	------------	--	--	--	------------	--	--	--	------------	--	--	--	------------	--	--	--	------------	--	--	--	------------	--	--	--	------------	--	--	--	------------	--	--	--	------------	--	--	--	------------	--	--	--	------------	--	--	--	------------	--	--	--	------------	--	--	--	------------	--	--	--	------------	--	--	--	------------	--	--	--	------------	--	--	--	------------	--	--	--	------------	--	--	--	------------	--	--	--	------------	--	--	--	------------	--	--	--	------------	--	--	--	------------	--	--	--	------------	--	--	--	------------	--	--	--	------------	--	--	--	------------	--	--	--	------------	--	--	--	------------	--	--	--	------------	--	--	--	------------	--	--	--	------------	--	--	--	------------	--	--	--	------------	--	--	--	------------	--	--	--	------------	--	--	--	------------	--	--	--	------------	--	--	--	------------	--	--	--	------------	--	--	--	------------	--	--	--	------------	--	--	--	------------	--	--	--	------------	--	--	--	------------	--	--	--	------------	--	--	--	------------	--	--	--	------------	--	--	--	------------	--	--	--	------------	--	--	--	------------	--	--	--	------------	--	--	--	------------	--	--	--	------------	--	--	--	------------	--	--	--	------------	--	--	--	------------	--	--	--	------------	--	--	--	------------	--	--	--	------------	--	--	--	------------	--	--	--	------------	--	--	--	------------	--	--	--	------------	--	--	--	------------	--	--	--	------------	--	--	--	------------	--	--	--	------------	--	--	--	------------	--	--	--	------------	--	--	--	------------	--	--	--	------------	--	--	--	------------	--	--	--	------------	--	--	--	------------	--	--	--	------------	--	--	--	------------	--	--	--	------------	--	--	--	------------	--	--	--	------------	--	--	--	------------	--	--	--	------------	--	--	--	------------	--	--	--	------------	--	--	--	------------	--	--	--	------------	--	--	--	------------	--	--	--	------------	--	--	--	------------	--	--	--	------------	--	--	--	------------	--	--	--	------------	--	--	--	------------	--	--	--	------------	--	--	--	------------	--	--	--	------------	--	--	--	------------	--	--	--	------------	--	--	--	------------	--	--	--	------------	--	--	--	------------	--	--	--	------------	--	--	--	------------	--	--	--	------------	--	--	--	------------	--	--	--	------------	--	--	--	------------	--	--	--	------------	--	--	--	------------	--	--	--	------------	--	--	--	------------	--	--	--	------------	--	--	--	------------	--	--	--	------------	--	--	--	------------	--	--	--	------------	--	--	--	------------	--	--	--	------------	--	--	--	------------	--	--	--	------------	--	--	--	------------	--	--	--	------------	--	--	--	------------	--	--	--	------------	--	--	--	------------	--	--	--	------------	--	--	--	------------	--	--	--	------------	--	--	--	------------	--	--	--	------------	--	--	--	------------	--	--	--	------------	--	--	--	------------	--	--	--	------------	--	--	--	------------	--	--	--	------------	--	--	--	------------	--	--	--	------------	--	--	--	------------	--	--	--	------------	--	--	--	------------	--	--	--	------------	--	--	--	------------	--	--	--	------------	--	--	--	------------	--	--	--	------------	--	--	--	------------	--	--	--	------------	--	--	--	------------	--	--	--	------------	--	--	--	------------	--	--	--	------------	--	--	--	------------	--	--	--	------------	--	--	--	------------	--	--	--	------------	--	--	--	------------	--	--	--	------------	--	--	--	------------	--	--	--	------------	--	--	--	------------	--	--	--	------------	--	--	--	------------	--	--	--	------------	--	--	--	------------	--	--	--	------------	--	--	--	------------	--	--	--	------------	--	--	--	------------	--	--	--	------------	--	--	--	------------	--	--	--	------------	--	--	--	------------	--	--	--	------------	--	--	--	------------	--	--	--	------------	--	--	--	------------	--	--	--	------------	--	--	--	------------	--	--	--	------------	--	--	--	------------	--	--	--	------------	--	--	--	------------	--	--	--	------------	--	--	--	------------	--	--	--	------------	--	--	--	------------	--	--	--	------------	--	--	--	------------	--	--	--	------------	--	--	--	------------	--	--	--	------------	--	--	--	------------	--	--	--	------------	--	--	--	------------	--	--	--	------------	--	--	--	------------	--	--	--	------------	--	--	--	------------	--	--	--	------------	--	--	--	------------	--	--	--	------------	--	--	--	------------	--	--	--	------------	--	--	--	------------	--	--	--	------------	--	--	--	------------	--	--	--	------------	--	--	--	------------	--	--	--	------------	--	--	--	------------	--	--	--	------------	--	--	--	------------	--	--	--	------------	--	--	--	------------	--	--	--	------------	--	--	--	------------	--	--	--	------------	--	--	--	------------	--	--	--	------------	--	--	--	------------	--	--	--	------------	--	--	--	------------	--	--	--	------------	--	--	--	------------	--	--	--	------------	--	--	--	------------	--	--	--	------------	--	--	--	------------	--	--	--	------------	--	--	--	------------	--	--	--	------------	--	--	--	------------	--	--	--	------------	--	--	--	------------	--	--	--	------------	--	--	--	------------	--	--	--	------------	--	--	--	------------	--	--	--	------------	--	--	--	------------	--	--	--	------------	--	--	--	------------	--	--	--	------------	--	--	--	------------	--	--	--	------------	--	--	--	------------	--	--	--	------------	--	--	--	------------	--	--	--	------------	--	--	--	------------	--	--	--	------------	--	--	--	------------	--	--	--	------------	--	--	--	------------	--	--	--	------------	--	--	--	------------	--	--	--	------------	--	--	--	------------	--	--	--	------------	--	--	--	------------	--	--	--	------------	--	--	--	------------	--	--	--	------------	--	--	--	------------	--	--	--	------------	--	--	--	------------	--	--	--	------------	--	--	--	------------	--	--	--	------------	--	--	--	------------	--	--	--	------------	--	--	--	------------	--	--	--	------------	--	--	--	------------	--	--	--	------------	--	--	--	------------	--	--	--	------------	--	--	--	------------	--	--	--	------------	--	--	--	------------	--	--	--	------------	--	--	--	------------	--	--	--	------------	--	--	--	------------	--	--	--	------------	--	--	--	------------	--	--	--	------------	--	--	--	------------	--	--	--	------------	--	--	--	------------	--	--	--	------------	--	--	--	------------	--	--	--	------------	--	--	--	------------	--	--	--	------------	--	--	--	------------	--	--	--	------------	--	--	--	------------	--	--	--	------------	--	--	--	------------	--	--	--	------------	--	--	--	------------	--	--	--	------------	--	--	--	------------	--	--	--	------------	--	--	--	------------	--	--	--	------------	--	--	--	------------	--	--	--	------------	--	--	--	------------	--	--	--	------------	--	--	--	------------	--	--	--	------------	--	--	--	------------	--	--	--	------------	--	--	--	------------	--	--	--	------------	--	--	--	------------	--	--	--	------------	--	--	--	------------	--	--	--	------------	--	--	--	------------	--	--	--	------------	--	--	--	------------	--	--	--	------------	--	--	--	------------	--	--	--	------------	--	--	--	------------	--	--	--	------------	--	--	--	------------	--	--	--	------------	--	--	--	------------	--	--	--	------------	--	--	--	------------	--	--	--	------------	--	--	--	------------	--	--	--	------------	--	--	--	------------	--	--	--	------------	--	--	--	------------	--	--	--	------------	--	--	--	------------	--	--	--	------------	--	--	--	------------	--	--	--	------------	--	--	--	------------	--	--	--	------------	--	--	--	------------	--	--	--	------------	--	--	--	------------	--	--	--	------------	--	--	--	------------	--	--	--	------------	--	--	--	------------	--	--	--	------------	--	--	--	------------	--	--	--	------------	--	--	--	------------	--	--	--	------------	--	--	--	------------	--	--	--	------------	--	--	--	------------	--	--	--	------------	--	--	--	------------	--	--	--	------------	--	--	--	------------	--	--	--	------------	--	--	--	------------	--	--	--	------------	--	--	--	------------	--	--	--	------------	--	--	--	------------	--	--	--	------------	--	--	--	------------	--	--	--	------------	--	--	--	------------	--	--	--	------------	--	--	--	------------	--	--	--	------------	--	--	--	------------	--	--	--	------------	--	--	--	------------	--	--	--	------------	--	--	--	------------	--	--	--	------------	--	--	--	------------	--	--	--	------------	--	--	--	------------	--	--	--	------------	--	--	--	------------	--	--	--	------------	--	--	--	------------	--	--	--	------------	--	--	--	------------	--	--	--	------------	--	--	--	------------	--	--	--	------------	--	--	--	------------	--	--	--	------------	--	--	--	------------	--	--	--	------------	--	--	--	------------	--	--	--	------------	--	--	--	------------	--	--	--	------------	--	--	--	------------	--	--	--	------------	--	--	--	------------	--	--	--	------------	--	--	--	------------	--	--	--	------------	--	--	--	------------	--	--	--	------------	--	--	--	------------	--	--	--	------------	--	--	--	------------	--	--	--	------------	--	--	--	------------	--	--	--	------------	--	--	--	------------	--	--	--	------------	--	--	--	------------	--	--	--	------------	--	--	--	------------	--	--	--	------------	--	--	--	------------	--	--	--	------------	--	--	--	------------	--	--	--	------------	--	--	--	------------	--	--	--	------------	--	--	--	------------	--	--	--	------------	--	--	--	------------	--	--	--	------------	--	--	--	------------	--	--	--	------------	--	--	--	------------	--	--	--	------------	--	--	--	------------	--	--	--	------------	--	--	--	------------	--	--	--	------------	--	--	--	------------	--	--	--	------------	--	--	--	------------	--	--	--	------------	--	--	--	------------	--	--	--	------------	--	--	--	------------	--	--	--	------------	--	--	--	------------	--	--	--	------------	--	--	--	------------	--	--	--	------------	--	--	--	------------	--	--	--	------------	--	--	--	------------	--	--	--	------------	--	--	--	------------	--	--	--	------------	--	--	--	------------	--	--	--	------------	--	--	--	------------	--	--	--	------------	--	--	--	------------	--	--	--	------------	--	--	--	------------	--	--	--	------------	--	--	--	------------	--	--	--	------------	--	--	--	------------	--	--	--	------------	--	--	--	------------	--	--	--	------------	--	--	--	------------	--	--	--	------------	--	--	--	------------	--	--	--	------------	--	--	--	------------	--	--	--	------------	--	--	--	------------	--	--	--	------------	--	--	--	------------	--	--	--	------------	--	--	--	------------	--	--	--	------------	--	--	--	------------	--	--	--	------------	--	--	--	------------	--	--	--	------------	--	--	--	------------	--	--	--	------------	--	--	--	------------	--	--	--	------------	--	--	--	------------	--	--	--	------------	--	--	--	------------	--	--	--	------------	--	--	--	------------	--	--	--	------------	--	--	--	------------	--	--	--	------------	--	--	--	------------	--	--	--	------------	--	--	--	------------	--	--	--	------------	--	--	--	------------	--	--	--	------------	--	--	--	------------	--	--	--	------------	--	--	--	------------	--	--	--	------------	--	--	--	------------	--	--	--	------------	--	--	--	------------	--	--	--	------------	--	--	--	------------	--	--	--	------------	--	--	--	------------	--	--	--	------------	--	--	--	------------	--	--	--	------------	--	--	--	------------	--	--	--	------------	--	--	--	------------	--	--	--	------------	--	--	--	------------	--	--	--	------------	--	--	--	------------	--	--	--	------------	--	--	--	------------	--	--	--	------------	--	--	--	------------	--	--	--	------------	--	--	--	------------	--	--	--	------------	--	--	--	------------	--	--	--	------------	--	--	--	------------	--	--	--	------------	--	--	--	------------	--	--	--	------------	--	--	--	-------	--	--	--

RM-F6-S2				RM-F7-S2				RM-F7-S3				RM-F7-S4				RM-F8-S4				RM-F8-S5				RM-F9-S1				RM-F9-S3			
mm	phi	results	#	mm	phi	results	#	mm	phi	results	#	mm	phi	results	#	mm	phi	results	#	mm	phi	results	#	mm	phi	results	#	mm	phi	results	#
0.4823	1.05198839		84	0.4354	1.19957654		84	0.3266	1.64113979		84	0.0856	3.54622154		84	0.5613	0.83263503		84	0.5256	0.85566853		84	0.2483	2.00982684		84	0.2027	3.20256233		84
0.5627	0.82555512		84	0.4407	1.1821212	0.83355623	0.3626	1.46153679	0.79776948	0.3075	1.7013273	0.99676053	0.6284	0.67023925	0.06309736	0.5773	0.79260017	0.00338033	0.2567	1.9612821	0.135650762	0.2544	1.97481272	1.21388766							
0.6258	0.67622072	50	0.4535	1.1408159	50	0.3798	1.39667638	0.454	1.19226116	0.06639699	0.3882	1.36531641	0.14907273	0.7376	0.43905783	0.81742675	0.7074	0.49939705	0.84829064	0.2962	1.75334161	0.09789921	0.3146	1.6683951	0.40957928						
0.6378	0.64881851	2.13256908	0.4561	1.1252685	0.15691148	0.454	1.19226116	0.06639699	0.3882	1.36531641	0.14907273	0.7376	0.43905783	0.81742675	0.7074	0.49939705	0.84829064	0.2962	1.75334161	0.09789921	0.3146	1.6683951	0.40957928								
0.6944	0.52618367	16	0.4715	1.08466115	16	0.4367	1.12807174	16	0.4025	1.13129281	16	0.4025	1.13129281	16	0.7216	0.41607232	16	0.2975	1.7902361	16	0.2975	1.7902361	16	0.3193	1.64770161	16					
0.808	0.3075792	4.84473846	0.4893	1.03120009	0.66743318	0.4699	1.08956511	0.56863233	0.4443	1.17963481	1.08925242	0.7051	0.3862785	2.36733881	0.8227	0.28155927	3.3277095	0.303	1.72259573	0.34148193	0.3375	1.56070274	0.18774818								
0.8202	0.2854939	Mz	0.4962	1.01099781	Mz	0.509	0.9742542	Mz	0.4554	1.13478421	Mz	0.4554	1.13478421	Mz	0.8226	0.28246313	Mz	0.8231	0.28085181	Mz	0.3192	1.64745351	Mz	0.3591	1.53144823	Mz					
1.0135	-0.01694593	2.48627617	0.5138	0.96073038	0.10781151	0.5151	0.95706746	0.00148862	0.4601	1.11997117	0.01886028	0.8496	0.23514234	1.0404894	0.9327	1.69533881	0.60424164	0.3786	1.40124183	0.47870625											
1.0197	-0.02814543		0.5166	0.95287239		0.5196	0.94451868		0.462	1.11402282		0.8755	0.1918299		0.935	0.09696091		0.3491	1.5182749		0.3853	1.3793427									
1.0838	-0.11609757	95	0.5293	0.91783468	95	0.5478	0.88827149	95	0.505	0.98563637	95	0.8771	0.18918516	95	0.5272	0.04067462	95	0.3516	1.50780027	95	0.3883	1.3260138	95								
1.0946	-0.13940266	0.74854789	0.5294	0.91756214	1.14794883	0.5509	0.88013036	1.35425017	0.5115	0.96155569	1.8775067	0.879	0.16812134	0.58295136	0.973	0.0949796	0.62833178	0.3573	1.48477962	1.87869763	0.4605	1.30095516	1.87983488								
1.476	-0.56188797	5	0.5397	0.88976286	5	0.5601	0.85624059	5	0.527	0.92411732	5	1.1991	0.16294347	5	0.742	0.0777029	5	0.3596	1.47552259	5	0.4056	1.20335943	5								
1.5102	-0.59473459	-5.78131082	0.5433	0.8801716	-1.3189053	0.5671	0.81183182	-1.87183249	0.5399	0.83995657	-1.89031961	0.9225	-0.1163782	-2.2898947	0.9892	0.05166572	-4.80731426	0.3751	1.41464807	-1.74448194	0.434	1.27228657	-0.89179544								
1.5751	-0.65543783	Q1	0.549	0.86511463	Q1	0.5701	0.81070624	Q1	0.5375	0.89565577	Q1	0.9513	0.07202711	Q1	1.0081	-0.01163866	Q1	0.3923	1.34959394	Q1	0.4306	1.21556949	Q1								
1.5808	-0.6604926	2.07987187	0.5511	0.8596067	0.74911131	0.5841	0.77570615	0.90540086	0.5426	0.88201159	1.09238601	0.9742	0.0770979	1.18525008	1.06635519	0.10839	-0.11623088	1.65635519	0.3923	1.34959394	0.604126	0.4315	1.21255728	0.77035295							
1.6032	-0.68094885		0.5527	0.85542425		0.5946	0.75000229		0.5489	0.87604367		0.9854	0.02121844		1.0957	0.11381573		0.3944	1.34225719		0.445	1.18811288									
1.6195	-0.69554239		0.5593	0.83219637		0.6118	0.78086199		0.5475	0.86295983		1.0116	-0.01949226		1.0954	-0.13540239		0.4274	1.22630802		0.7907	1.07890295									
1.6196	-0.69588981		0.5594	0.83104075		0.6177	0.69501589		0.5517	0.85216136		1.0252	-0.03950508		1.0998	-0.1374003		0.4309	1.21456472		0.4815	1.0543138									
1.717	-0.77988341		0.5662	0.82060941		0.625	0.67806617		0.5559	0.84799555		1.0568	-0.0797017		1.1241	-0.16876899		0.4319	1.2112053		0.483	1.0489693									
1.7481	-0.80429462		0.5679	0.81628428		0.6259	0.6759902		0.5625	0.8308798		1.0666	-0.09301845		1.1242	-0.16889729		0.4437	1.2133363		0.4844	1.04572039									
1.7524	-0.84185551		0.5799	0.78611731		0.6273	0.67276684		0.5694	0.81247873		1.0692	-0.09633093		1.1329	-0.180019		0.4443	1.17038406		0.4913	1.02325138									
1.809	-0.89174234		0.5886	0.78463609		0.6404	0.6384508		0.5751	0.79831083		1.0925	-0.12763622		1.1592	-0.19932328		0.4483	1.15785181		0.5011	0.95917852									
1.9175	-0.93521863		0.6004	0.7559789		0.6429	0.6373235		0.5986	0.67525955		1.1034	-0.13937374		1.1608	-0.21511761		0.4568	1.12677174		0.5277	0.91581725									
1.9931	-0.99515044		0.6067	0.72093869		0.6704	0.5769037		0.6114	0.7080554		1.1067	-0.14626296		1.1666	-0.2223081		0.4636	1.10903815		0.5295	0.91728965									
2.0839	-1.05227709		0.6376	0.64927057		0.6787	0.56340694		0.6196	0.69585811		1.1318	-0.17861753		1.1814	-0.2404548		0.479	1.06813946		0.5442	0.87778371									
2.0991	-1.06978185		0.6493	0.63237602		0.6773	0.56212834		0.6172	0.68865405		1.1396	-0.18852593		1.1843	-0.24403252		0.4816	1.0548379		0.5483	0.8722273									
2.1859	-1.12821786		0.6541	0.6124117		0.6854	0.54497729		0.6242	0.67991399		1.1415	-0.19143487		1.1916	-0.25287899		0.4843	1.04601825		0.5476	0.8689783									
2.2589	-1.17541004		0.6581	0.59880182		0.6879	0.53474046		0.6273	0.64924944		1.1479	-0.20101164		1.1981	-0.26131485		0.4846	1.04512485		0.551	0.87131266									
2.2675	-1.18109256		0.6914	0.51240269		0.7452	0.42425683		0.6438	0.63531014		1.2029	-0.26651446		1.2262	-0.29413182		0.486	1.0496298		0.5547	0.85023118									
2.3727	-1.24651916		0.7092	0.49573137		0.7547	0.40602139		0.6594	0.60678913		1.2254	-0.29325028		1.2392	-0.3000626		0.4938	1.07179265		0.5571	0.84988464									
2.5991	-1.37800499		0.712	0.49004671		0.7549	0.40563912		0.6681	0.58185911		1.2468	-0.3122737		1.2582	-0.3082417		0.5026	1.09250903		0.5831	0.7781819									
2.6454	-1.40347403		0.7155	0.48297224		0.7584	0.39896376		0.6784	0.56917469		1.2605	-0.32250213		1.2763	-0.3511645		0.5175	1.05306119		0.5929	0.75413292									
2.6564	-1.40940046		0.7162	0.4815615		0.7645	0.3747406		0.6973	0.52014421		1.2775	-0.35132823		1.2961	-0.38108817		0.526	1.02685746		0.5963	0.74388345									
2.6847	-1.42474883		0.7172	0.47945805		0.796	0.32915488		0.7012	0.51209777		1.2861	-0.36299975		1.3133	-0.41499792		0.527	0.92411732		0.6026	0.73072124									
2.7218	-1.44454884		0.7206	0.47272545		0.7982	0.32517507		0.702	0.51054275		1.3478	-0.43060279		1.3336	-0.4153225		0.5306	0.91425969		0.6119	0.7086282									
2.7635	-1.46648421		0.7351	0.44983832		0.8095	0.30489444		0.7033	0.50778358		1.3639	-0.44734048		1.3728	-0.45711759		0.5362	0.8914927		0.6218	0.68547168									
2.8034	-1.48714503		0.7432	0.42817397		0.8288	0.2709018		0.7061	0.50520513		1.3809	-0.46564041		1.3757	-0.460162		0.5394	0.8956504		0.6307	0.59139182									
2.8496	-1.50862151		0.7602	0.39554572		0.8306	0.25777796		0.709	0.49431827		1.4466	-0.53266195		1.384	-0.4688399		0.5426	0.88203159		0.6494	0.52687611									
2.8752	-1.52849483		0.7693	0.32118827		0.8465	0.25101384		0.7139	0.49349544		1.5112	-0.59578503		1.3958	-0.48108817		0.5499	0.86570151		0.6997	0.53187125									
2.9594	-1.58231851		0.8105	0.30311335		0.8461	0.24109787		0.7248	0.46434121		1.5202	-0.59604391		1.4097	-0.58358398		0.5508	0.8426919		0.7061	0.50505133									
3.0045	-1.5871115		0.8406	0.25050652		0.8514	0.23108904		0.751	0.41111169		1.5207	-0.60473046		1.5268	-0.61050593		0.5517	0.85203686		0.7116	0.4908574									

SP

SP-F1-S1				SP-F1-S2				SP-F1-S3				SP-F2-S2				SP-F2-S3				SP-F2-S4				SP-F2-S5				SP-F2-S6				
mm	phi	results		mm	phi	results		mm	phi	results		mm	phi	results		mm	phi	results		mm	phi	results		mm	phi	results		mm	phi	results		
0.3056	1.71020909	84	0.3279	1.60085859	84	0.3511	0.95700746	84	0.2084	2.26255386	84	147.9	0.1479	2.73728272	84	0.2678	1.90075606			0.2788	1.75944947	84	0.2541	1.976515			0.3948	1.34079477	84			
0.4198	1.25215134	3192573	0.3777	1.42189123	0.3250581	0.5756	0.7901357	0.14754431	0.2409	1.6003449	148277158	246.4	0.2446	2.26088482	1.2032559	0.292	1.7794947	1.36781463	0.2788	1.85114479	1.4847544	0.2741	1.42171695	1.4847544	0.2788	1.85114479	1.4847544	0.2741	1.42171695	1.4847544		
0.5452	0.87513513	50	0.4413	1.18015817	50	0.5847	0.77422496	50	0.2653	1.9157523	50	262.6	0.2626	1.92094486	50	0.2959	1.75860154			0.2959	1.84780587	50	0.2344	1.23645408			0.4304	1.23645408	50			
0.5877	0.76684717	-1.11660022	0.5128	0.96532368	-0.76114856	0.5917	0.750558	-1.11374038	0.287	1.80086213	0.76613563	288.1	0.2881	1.79343125	0.30992924	0.3048	1.7140507	0.73678075	0.2951	1.76079598	0.82593475	0.4309	1.21454647	0.40741681	0.4309	1.21454647	0.40741681	0.4309	1.21454647	0.40741681		
0.6219	0.68523968	16	0.5205	0.94021096	16	0.621	0.68729091	16	0.287	1.80086213	16	317.1	0.3171	1.16569762	16	0.3152	1.66564647	16	0.2978	1.74756956	16	0.4357	1.1958284	16	0.4357	1.1958284	16	0.4357	1.1958284	16		
0.6261	0.67525292	-0.5183047	0.5401	0.88894943	-2.67731562	0.6281	0.67092815	-2.52387181	0.2915	1.77847117	0.44490534	324.3	0.3241	1.63405833	1.37169749	0.3185	1.65978086	-0.5319829	0.2978	1.74756956	-0.33550034	0.4461	1.1645511	-0.87117781	0.4461	1.1645511	-0.87117781	0.4461	1.1645511	-0.87117781		
0.6515	0.61815790	Me	0.5709	0.80868159	Me	0.651	0.65462047	Me	0.3073	1.7023059	Me	331.4	0.3314	1.59134102	Me	0.3241	1.6547532	Me	0.3023	1.72592322	Me	0.4357	1.1958284	Me	0.4357	1.1958284	Me	0.4357	1.1958284	Me		
0.6545	0.61152979	-1.61639265	0.6766	0.56362015	-1.03780179	0.6334	0.56880566	-1.63355955	0.3109	1.68543622	0.04716255	337	0.337	1.56916623	0.04716255	0.3438	1.54034552	0.65839627	0.3106	1.668586	0.65839627	0.4592	1.12725996	0.17288482	0.4592	1.12725996	0.17288482	0.4592	1.12725996	0.17288482		
0.6619	0.59530979		0.7183	0.4773754		0.6366	0.65153543		0.3135	1.6774485		390.4	0.3904	1.35696357		0.3494	1.51703566		0.3181	1.65243375		0.4765	1.06944284		0.4765	1.06944284		0.4765	1.06944284			
0.7325	0.44909534	95	0.7287	0.46056429	95	0.691	0.53323787	95	0.3148	1.66747845	95	408.6	0.4086	1.29122757	95	0.3542	1.48735122	95	0.3183	1.65152897	95	0.4781	1.06460669	95	0.4781	1.06460669	95	0.4781	1.06460669	95		
0.7362	0.44120661	1.05794109	0.7419	0.43409971	1.22365377	0.6979	0.51896337	0.94480616	0.3171	1.65097362	1.95719961	425.5	0.4255	1.21075854	2.02934657	0.5592	1.40112659	1.76264029	0.3224	1.63062618	1.8375629	0.4816	1.0408379	1.25240502	0.4816	1.0408379	1.25240502	0.4816	1.0408379	1.25240502		
0.7392	0.43549963	5	0.7602	0.39554572	5	0.7188	0.47631366	5	0.3274	1.61086015	5	437.4	0.4374	1.19256479	5	0.3626	1.46533679	5	0.3265	1.61481345	5	0.4885	1.03356679	5	0.4885	1.03356679	5	0.4885	1.03356679	5		
0.7589	0.39801493	-5.21896932	0.7628	0.35128135	-3.65532091	0.7294	0.45521405	-3.45769225	0.3468	1.52781127	-2.37201984	438.2	0.4382	1.19032854	-3.90301622	0.3667	1.44731559	-1.56545339	0.3534	1.50061316	-1.75551094	0.4826	1.02130281	-2.92311801	0.4826	1.02130281	-2.92311801	0.4826	1.02130281	-2.92311801		
0.7615	0.39308071	Q	0.7997	0.32246648	Q	0.9483	0.23751513	Q	0.3776	1.40505745	Q	438.9	0.4389	1.18802578	Q	0.3729	1.43212726	Q	0.3575	1.48397231	Q	0.5063	0.96192731	Q	0.5063	0.96192731	Q	0.5063	0.96192731	Q		
0.8109	0.30401512	2.04181877	0.8015	0.31922287	1.48981204	0.9179	0.21293906	1.31211137	0.3625	1.38645662	1.13786207	448.2	0.4482	1.13777565	1.54558116	0.3841	1.38043446	0.879206	0.3613	1.46877182	0.99946881	0.5183	0.94813268	1.09608162	0.5183	0.94813268	1.09608162	0.5183	0.94813268	1.09608162		
0.8119	0.30063521		0.8425	0.24724932		0.9194	0.1212144		0.3835	1.38268962		470	0.47	1.08912833		0.3875	1.36772022		0.3631	1.4615488		0.5195	0.94679636		0.5195	0.94679636		0.5195	0.94679636			
0.8344	0.27858123		0.8521	0.23090339		0.9272	0.10904661		0.3875	1.36772022		478.4	0.4784	1.06170171		0.41	1.28629311		0.3653	1.45238405		0.5198	0.94396348		0.5198	0.94396348		0.5198	0.94396348			
0.8271	0.27886401		0.8728	0.19627533		1.0097	-0.0192859		0.3928	1.4821276		519.7	0.5197	0.94242105		0.4144	1.27089334		0.3684	1.44042485		0.5245	0.93097745		0.5245	0.93097745		0.5245	0.93097745			
0.8321	0.26516893		0.9311	0.1029911		1.0121	-0.0179517		0.3998	1.3288484		526	0.526	0.92485746		0.4145	1.27054525		0.3851	1.37668313		0.5316	0.90618176		0.5316	0.90618176		0.5316	0.90618176			
0.842	0.24814076		0.9469	0.07551937		1.0803	-0.0408411		0.4007	1.31039443		635.4	0.6354	0.93429569		0.4227	1.3422348		0.3961	1.35607261		0.5349	0.90265126		0.5349	0.90265126		0.5349	0.90265126			
0.9017	0.14527931		1.0137	0.01361059		1.0852	-0.11795996		0.4039	1.30771889		535.5	0.5355	0.9010339		0.4389	1.18802578		0.3928	1.34812176		0.5387	0.89243488		0.5387	0.89243488		0.5387	0.89243488			
0.9211	0.1185693		1.0391	0.05533403		1.1801	-0.21424736		0.4138	1.2728368		536.7	0.5367	0.89780461		0.4447	1.1690858		0.3964	1.33495984		0.5414	0.88525272		0.5414	0.88525272		0.5414	0.88525272			
0.9481	0.07688821		1.0458	0.06466043		1.1801	-0.289071		0.4144	1.2709334		538.3	0.5383	0.89351011		0.4463	1.16390444		0.3967	1.33338842		0.5419	0.88389397		0.5419	0.88389397		0.5419	0.88389397			
0.9722	0.04067462		1.0663	0.09261261		1.2243	-0.29195465		0.4161	1.2642394		539.9	0.5399	0.88922836		0.4466	1.16293501		0.3995	1.3237234		0.5463	0.87222373		0.5463	0.87222373		0.5463	0.87222373			
1.0097	-0.01302659		1.0907	0.12235318		1.2873	-0.34175210		0.4209	1.2456472		583.1	0.5831	0.77187819		0.4466	1.16220806		0.4008	1.38689515		0.549	0.86111843		0.549	0.86111843		0.549	0.86111843			
1.0212	-0.04036129		1.0987	0.13379636		1.2996	-0.37806445		0.4252	1.2377606		556.6	0.5566	0.84538004		0.4532	1.14177058		0.4184	1.26027303		0.5613	0.83226303		0.5613	0.83226303		0.5613	0.83226303			
1.0777	-0.10795472		1.1074	0.14717518		1.3013	-0.37995038		0.4256	1.2324152		556.8	0.5568	0.84476174		0.4607	1.1880914		0.4209	1.2444003		0.5732	0.80282869		0.5732	0.80282869		0.5732	0.80282869			
1.1304	-0.17683188		1.1079	0.14726842		1.3021	-0.38083703		0.4289	1.22127645		559.7	0.5597	0.83728727		0.4627	1.11841359		0.4213	1.2470963		0.5759	0.7961004		0.5759	0.7961004		0.5759	0.7961004			
1.1347	-0.25664602		1.1245	0.13692323		1.3138	-0.41533884		0.4305	1.21891028		572.4	0.5724	0.84889716		0.4763	1.0795408		0.4242	1.23771943		0.5775	0.79310403		0.5775	0.79310403		0.5775	0.79310403			
1.2501	-0.32208077		1.1273	0.17287004		1.414	-0.52040603		0.4309	1.2456472		583.1	0.5831	0.77187819		0.4466	1.16220806		0.4008	1.38689515		0.549	0.86111843		0							

SP-F2-S7	mm	results	SP-F2-S8	mm	results	SP-F3-S1	mm	results	SP-F3-S2	mm	results	SP-F3-S3	mm	results	SP-F4-S1	mm	results	SP-F4-S4	mm	results	SP-F4-S7	mm	results
0.2393	2.03009020	84	0.2394	1.766097	84	0.3183	1.65155997	2.05530219	84	0.3485	1.51910165	84	0.2456	2.0256004	84	0.2585	1.93174731	84	0.3555	1.49120692	84	0.3355	1.49120692
0.2486	2.00804842	1.24680242	0.3207	1.64608987	1.1729447	0.389	1.36214642	0.50253219	480	0.404	1.05808473	0.2045016	0.3938	1.34845361	0.31397175	0.2124	2.23512451	1.07063855	0.3025	1.74897836	1.07576427	0.4317	1.27331237
0.2746	1.8645807	50	0.3267	1.44967806	50	0.4562	1.13225207	50	507.4	0.5074	0.9787963	50	0.4468	1.16329808	50	0.319	1.64835773	50	0.3215	1.63709551	0.07707744	0.4494	1.15391821
0.3099	1.7041504	0.56392337	0.3789	1.40009911	0.50423828	0.5566	0.94528004	1.33371528	526	0.528	0.92682746	1.25564699	0.4942	1.01682448	1.43679935	0.3749	1.41541031	0.33857118	0.3215	1.63709551	0.07707744	0.4494	1.15391821
0.3121	1.6799053	16	0.3879	1.36623176	16	0.5762	0.81806493	16	594.1	0.5641	0.82597037	16	0.5453	0.87407954	16	0.3879	1.41541031	16	0.3215	1.63709551	0.07707744	0.4494	1.15391821
0.322	1.54303358	0.23377289	0.3894	1.34066137	0.6048171	0.598	0.741771634	3.54679808	617	0.617	0.69651171	3.30781291	0.5802	0.78531716	3.54326113	0.4227	1.24260349	0.5978983	0.3228	1.63709551	0.07707744	0.4494	1.15391821
0.3344	1.58031988	Mr	0.3908	1.35548616	Mr	0.6863	0.54308415	Mr	628.7	0.6287	0.6695067	Mr	0.615	0.70133575	Mr	0.4274	1.2263302	Mr	0.3411	1.5517022	Mr	0.4644	1.10555676
0.3447	1.5365738	0.52565063	0.4053	1.30529269	0.33915115	0.6925	0.53010954	1.54127765	676.6	0.6766	0.56362015	1.4520861	0.6195	0.69081797	1.55736298	0.4307	1.21523493	0.27043997	0.3685	1.44025219	0.01628453	0.4623	1.05198339
0.3492	1.5178617	0.4059	1.30079275	0.7102	0.49369856	0.9118	0.6911	0.53158589	691.8	0.6911	0.53158589	0.6818	0.54834903	0.6818	0.54834903	0.4334	1.26021874	0.3937	1.34482001	0.5153	0.95560741		
0.3636	1.30211369	95	0.4456	1.19759683	95	0.7303	0.54345303	95	714.5	0.7149	0.48438255	95	0.7452	0.42429683	95	0.4424	1.17656676	95	0.4044	1.30613405	95	0.5554	0.9255404
0.3859	1.17768931	1.86396127	0.4185	1.1894119	1.52455916	0.7569	0.40182199	1.16185383	730.7	0.7307	0.45284506	1.06192206	0.7518	0.4151757	1.28480762	0.4604	1.11903008	1.80321869	0.445	1.16811288	1.71724368	0.5452	0.87515313
0.4006	1.21556949	5	0.4438	1.17200852	5	0.7682	0.38044291	5	755.1	0.7551	0.40525695	5	0.8059	0.31124643	5	0.4614	1.11590065	5	0.4479	1.15874163	5	0.5613	0.83314899
0.4325	1.20921774	1.25440782	0.4441	1.17103362	1.76160047	0.7729	0.37164319	4.04435991	761.2	0.7612	0.33949492	4.32189154	0.8228	0.28138192	4.9068491	0.4691	1.09022336	1.42982054	0.4554	1.13478421	2.21091401	0.565	0.82367026
0.4436	1.1720581	Q	0.4464	1.16581123	Q	0.8532	0.22904219	Q	841.6	0.8416	0.24871929	Q	0.891	0.18605125	Q	0.5062	0.86221228	Q	0.4741	1.07767276	Q	0.5758	0.79625157
0.4463	1.16304044	0.84262399	0.4534	1.14431949	0.92827342	0.9141	0.129575	1.73931828	841.7	0.8417	0.24861987	1.69380796	0.8919	0.16504474	1.90393808	0.5082	0.79823496	0.90688654	0.4744	1.07514499	1.15526502	0.5758	0.79625157
0.4567	1.13067174	0.458	1.1265707	0.915	0.12815527	0.915	0.12815527	0.915	918.6	0.9186	0.128249028	0.915	0.9186	0.128249028	0.915	0.509	0.9742542	0.4946	1.01565727	0.4991	1.02539071	0.6445	0.64494726
0.4596	1.1231981	0.4587	1.12496768	0.9297	0.10516185	917.4	0.9374	0.09326251	917.4	0.9374	0.09326251	917.4	0.9374	0.09326251	917.4	0.5134	0.96183666	0.4991	1.02539071	0.6445	0.64494726		
0.4612	1.11652634	0.476	1.0795766	0.957	0.06340863	966.3	0.9663	0.04945652	966.3	0.9663	0.04945652	966.3	0.9663	0.04945652	966.3	0.5295	0.91728905	0.5298	0.91419069	0.6445	0.64494726		
0.4625	1.11240312	0.4996	1.00114615	0.9787	0.04796429	1003.8	1.0038	0.03044718	1003.8	1.0038	0.03044718	1003.8	1.0038	0.03044718	1003.8	0.5297	0.91403382	0.5298	0.91403382	0.6445	0.64494726		
0.4754	1.07277712	0.5043	0.98367552	0.9697	0.04381924	1012.4	1.0124	0.01777926	1012.4	1.0124	0.01777926	1012.4	1.0124	0.01777926	1012.4	0.5329	0.90505558	0.5329	0.90505558	0.6445	0.64494726		
0.4766	1.0691401	0.5061	0.98249731	1.0087	0.01249706	1133.8	1.1338	0.01194166	1133.8	1.1338	0.01194166	1133.8	1.1338	0.01194166	1133.8	0.5596	0.83752505	0.5596	0.83752505	0.6445	0.64494726		
0.4833	1.04900231	0.5107	0.96944384	1.031	0.00440436	1136.2	1.1362	0.18425125	1136.2	1.1362	0.18425125	1136.2	1.1362	0.18425125	1136.2	0.5985	0.80216565	0.5985	0.80216565	0.6445	0.64494726		
0.4854	1.04717017	0.5107	0.96944384	1.031	0.00440436	1136.2	1.1362	0.18425125	1136.2	1.1362	0.18425125	1136.2	1.1362	0.18425125	1136.2	0.5985	0.80216565	0.5985	0.80216565	0.6445	0.64494726		
0.4998	1.00505677	0.5107	0.96944384	1.031	0.00440436	1136.2	1.1362	0.18425125	1136.2	1.1362	0.18425125	1136.2	1.1362	0.18425125	1136.2	0.5985	0.80216565	0.5985	0.80216565	0.6445	0.64494726		
0.5295	0.91728965	0.5403	0.8881599	1.1159	0.13820641	1180.9	1.1809	0.23980477	1180.9	1.1809	0.23980477	1180.9	1.1809	0.23980477	1180.9	0.6062	0.78459318	0.6062	0.78459318	0.6445	0.64494726		
0.5383	0.9351011	0.5499	0.86275151	1.2203	0.16388713	1236	1.236	0.30567616	1236	1.236	0.30567616	1236	1.236	0.30567616	1236	0.6062	0.78459318	0.6062	0.78459318	0.6445	0.64494726		
0.5402	0.88842894	0.5537	0.85281836	1.1842	0.21933707	1250.4	1.2504	0.32238966	1250.4	1.2504	0.32238966	1250.4	1.2504	0.32238966	1250.4	0.6062	0.78459318	0.6062	0.78459318	0.6445	0.64494726		
0.5427	0.88176573	0.5552	0.84891335	1.1706	0.22774626	1265.9	1.2659	0.34016057	1265.9	1.2659	0.34016057	1265.9	1.2659	0.34016057	1265.9	0.6062	0.78459318	0.6062	0.78459318	0.6445	0.64494726		
0.5449	0.8759292	0.5552	0.84891335	1.1706	0.22774626	1265.9	1.2659	0.34016057	1265.9	1.2659	0.34016057	1265.9	1.2659	0.34016057	1265.9	0.6062	0.78459318	0.6062	0.78459318	0.6445	0.64494726		
0.5454	0.8748066	0.5799	0.78811731	1.238	0.30808071	1317.1	1.238	0.30808071	1317.1	1.238	0.30808071	1317.1	1.238	0.30808071	1317.1	0.6111	0.7105136	0.6111	0.7105136	0.6445	0.64494726		
0.5463	0.8722273	0.5823	0.78015888	1.2338	0.32630448	1362.3	1.3623	0.44604067	1362.3	1.3623	0.44604067	1362.3	1.3623	0.44604067	1362.3	0.6138	0.70415493	0.6138	0.70415493	0.6445	0.64494726		
0.5465	0.87199223	0.5914	0.7577874	1.2919	0.30949128	1392	1.392	0.47715518	1392	1.392	0.47715518	1392	1.392	0.47715518	1392	0.6138	0.70415493	0.6138	0.70415493	0.6445	0.64494726		
0.5519	0.78135024	0.6015	0.71333716	1.3435	0.42599172	1441.2	1.4412	0.49589559	1441.2	1.4412	0.49589559	1441.2	1.4412	0.49589559	1441.2	0.6138	0.70415493	0.6138	0.70415493	0.6445	0.64494726		
0.5585	0.7729233	0.6077	0.72800314	1.3673	0.451326	1558.7	1.5587	0.64031737	1558.7	1.5587	0.64031737	1558.7	1.5587	0.64031737	1558.7	0.6138	0.70415493	0.6138	0.70415493	0.6445	0.64494726		
0.5921	0.7560805	0.6158	0.69447081	1.4091	0.49478081	1596	1.596	0.67445591	1596	1.596	0.67445591	1596	1.596	0.67445591	1596	0.6138	0.70415493	0.6138	0.70415493	0.6445	0.64494726		
0.6003	0.7382382	0.6174	0.69571873	1.4687	0.55453505	1606.4	1.6064	0.68832539	1606.4	1.6064	0.68832539	1606.4	1.6064	0.68832539	1606.4	0.6138	0.70415493	0.6138	0.70415493	0.6445	0.64494726		
0.6027	0.73048185	0.6278	0.67517739	1.5072	0.59186586	1679.1	1.6791	0.74788183	1679.1	1.6791	0.74788183	1679.1	1.6791	0.74788183	1679.1	0.6138	0.70415493	0.6138	0.70415493	0.6445	0.64494726		
0.6105	0.71193078	0.6358	0.64836619	1.6029	0.68067987	1691.7	1.6917	0.75846773	1691.7	1.6917	0.75846773	1691.7	1.6917	0.75846773	1691.7	0.6138	0.70415493	0.6138	0.70415493	0.6445	0.64494726		
0.6145	0.70209154	0.6394	0.64520389	1.6331	0.70760715	1706.1	1.7061	0.77089569	1706.1	1.7061	0.77089569	1706.1	1.7061	0.77089569	1706.1	0.6138	0.70415493	0.6138	0.70415493	0.6445	0.64494726		
0.6186	0.6923514	0.644	0.63486204	1.6667	0.73698821	1710.6	1.7106	0.77466564	1710.6	1.7106	0.77466564	1710.6	1.7106	0.77466564	1710.6	0.6138	0.70415493	0.6138	0.70415493	0.6445	0.64494726		
0.6279	0.6713676	0.6465	0.6292724	1.7753	0.82052584	1730.2	1.7302	0.79593212	1730.2	1.7302	0.79593212	1730.2	1.7302	0.79593212	1730.2	0.6138	0.70415493	0.6138	0.70415493	0.6445	0.64494726		
0.6391	0.64580894	0.6515	0.63757609	1.829	0.87104771	1743.9	1.7439	0.80216565	1743.9	1.7439	0.80216565	1743.9	1.7439	0.80216565									

SP-F5-S1				SP-F5-S2				SP-F5-S3				SP-F5-S4				SP-F5-S5				SP-F5-S6				SP-F5-S7				SP-F5-S8				SP-F5-S9				SP-F5-S10				SP-F5-S11				SP-F5-S12				SP-F5-S13				SP-F5-S14				SP-F5-S15				SP-F5-S16				SP-F5-S17				SP-F5-S18				SP-F5-S19				SP-F5-S20				SP-F5-S21				SP-F5-S22				SP-F5-S23				SP-F5-S24				SP-F5-S25				SP-F5-S26				SP-F5-S27				SP-F5-S28				SP-F5-S29				SP-F5-S30				SP-F5-S31				SP-F5-S32				SP-F5-S33				SP-F5-S34				SP-F5-S35				SP-F5-S36				SP-F5-S37				SP-F5-S38				SP-F5-S39				SP-F5-S40				SP-F5-S41				SP-F5-S42				SP-F5-S43				SP-F5-S44				SP-F5-S45				SP-F5-S46				SP-F5-S47				SP-F5-S48				SP-F5-S49				SP-F5-S50				SP-F5-S51				SP-F5-S52				SP-F5-S53				SP-F5-S54				SP-F5-S55				SP-F5-S56				SP-F5-S57				SP-F5-S58				SP-F5-S59				SP-F5-S60				SP-F5-S61				SP-F5-S62				SP-F5-S63				SP-F5-S64				SP-F5-S65				SP-F5-S66				SP-F5-S67				SP-F5-S68				SP-F5-S69				SP-F5-S70				SP-F5-S71				SP-F5-S72				SP-F5-S73				SP-F5-S74				SP-F5-S75				SP-F5-S76				SP-F5-S77				SP-F5-S78				SP-F5-S79				SP-F5-S80				SP-F5-S81				SP-F5-S82				SP-F5-S83				SP-F5-S84				SP-F5-S85				SP-F5-S86				SP-F5-S87				SP-F5-S88				SP-F5-S89				SP-F5-S90				SP-F5-S91				SP-F5-S92				SP-F5-S93				SP-F5-S94				SP-F5-S95				SP-F5-S96				SP-F5-S97				SP-F5-S98				SP-F5-S99				SP-F5-S100				SP-F5-S101				SP-F5-S102				SP-F5-S103				SP-F5-S104				SP-F5-S105				SP-F5-S106				SP-F5-S107				SP-F5-S108				SP-F5-S109				SP-F5-S110				SP-F5-S111				SP-F5-S112				SP-F5-S113				SP-F5-S114				SP-F5-S115				SP-F5-S116				SP-F5-S117				SP-F5-S118				SP-F5-S119				SP-F5-S120				SP-F5-S121				SP-F5-S122				SP-F5-S123				SP-F5-S124				SP-F5-S125				SP-F5-S126				SP-F5-S127				SP-F5-S128				SP-F5-S129				SP-F5-S130				SP-F5-S131				SP-F5-S132				SP-F5-S133				SP-F5-S134				SP-F5-S135				SP-F5-S136				SP-F5-S137				SP-F5-S138				SP-F5-S139				SP-F5-S140				SP-F5-S141				SP-F5-S142				SP-F5-S143				SP-F5-S144				SP-F5-S145				SP-F5-S146				SP-F5-S147				SP-F5-S148				SP-F5-S149				SP-F5-S150				SP-F5-S151				SP-F5-S152				SP-F5-S153				SP-F5-S154				SP-F5-S155				SP-F5-S156				SP-F5-S157				SP-F5-S158				SP-F5-S159				SP-F5-S160				SP-F5-S161				SP-F5-S162				SP-F5-S163				SP-F5-S164				SP-F5-S165				SP-F5-S166				SP-F5-S167				SP-F5-S168				SP-F5-S169				SP-F5-S170				SP-F5-S171				SP-F5-S172				SP-F5-S173				SP-F5-S174				SP-F5-S175				SP-F5-S176				SP-F5-S177				SP-F5-S178				SP-F5-S179				SP-F5-S180				SP-F5-S181				SP-F5-S182				SP-F5-S183				SP-F5-S184				SP-F5-S185				SP-F5-S186				SP-F5-S187				SP-F5-S188				SP-F5-S189				SP-F5-S190				SP-F5-S191				SP-F5-S192				SP-F5-S193				SP-F5-S194				SP-F5-S195				SP-F5-S196				SP-F5-S197				SP-F5-S198				SP-F5-S199				SP-F5-S200				SP-F5-S201				SP-F5-S202				SP-F5-S203				SP-F5-S204				SP-F5-S205				SP-F5-S206				SP-F5-S207				SP-F5-S208				SP-F5-S209				SP-F5-S210				SP-F5-S211				SP-F5-S212				SP-F5-S213				SP-F5-S214				SP-F5-S215				SP-F5-S216				SP-F5-S217				SP-F5-S218				SP-F5-S219				SP-F5-S220				SP-F5-S221				SP-F5-S222				SP-F5-S223				SP-F5-S224				SP-F5-S225				SP-F5-S226				SP-F5-S227				SP-F5-S228				SP-F5-S229				SP-F5-S230				SP-F5-S231				SP-F5-S232				SP-F5-S233				SP-F5-S234				SP-F5-S235				SP-F5-S236				SP-F5-S237				SP-F5-S238				SP-F5-S239				SP-F5-S240				SP-F5-S241				SP-F5-S242				SP-F5-S243				SP-F5-S244				SP-F5-S245				SP-F5-S246				SP-F5-S247				SP-F5-S248				SP-F5-S249				SP-F5-S250				SP-F5-S251				SP-F5-S252				SP-F5-S253				SP-F5-S254				SP-F5-S255				SP-F5-S256				SP-F5-S257				SP-F5-S258				SP-F5-S259				SP-F5-S260				SP-F5-S261				SP-F5-S262				SP-F5-S263				SP-F5-S264				SP-F5-S265				SP-F5-S266				SP-F5-S267				SP-F5-S268				SP-F5-S269				SP-F5-S270				SP-F5-S271		
----------	--	--	--	----------	--	--	--	----------	--	--	--	----------	--	--	--	----------	--	--	--	----------	--	--	--	----------	--	--	--	----------	--	--	--	----------	--	--	--	-----------	--	--	--	-----------	--	--	--	-----------	--	--	--	-----------	--	--	--	-----------	--	--	--	-----------	--	--	--	-----------	--	--	--	-----------	--	--	--	-----------	--	--	--	-----------	--	--	--	-----------	--	--	--	-----------	--	--	--	-----------	--	--	--	-----------	--	--	--	-----------	--	--	--	-----------	--	--	--	-----------	--	--	--	-----------	--	--	--	-----------	--	--	--	-----------	--	--	--	-----------	--	--	--	-----------	--	--	--	-----------	--	--	--	-----------	--	--	--	-----------	--	--	--	-----------	--	--	--	-----------	--	--	--	-----------	--	--	--	-----------	--	--	--	-----------	--	--	--	-----------	--	--	--	-----------	--	--	--	-----------	--	--	--	-----------	--	--	--	-----------	--	--	--	-----------	--	--	--	-----------	--	--	--	-----------	--	--	--	-----------	--	--	--	-----------	--	--	--	-----------	--	--	--	-----------	--	--	--	-----------	--	--	--	-----------	--	--	--	-----------	--	--	--	-----------	--	--	--	-----------	--	--	--	-----------	--	--	--	-----------	--	--	--	-----------	--	--	--	-----------	--	--	--	-----------	--	--	--	-----------	--	--	--	-----------	--	--	--	-----------	--	--	--	-----------	--	--	--	-----------	--	--	--	-----------	--	--	--	-----------	--	--	--	-----------	--	--	--	-----------	--	--	--	-----------	--	--	--	-----------	--	--	--	-----------	--	--	--	-----------	--	--	--	-----------	--	--	--	-----------	--	--	--	-----------	--	--	--	-----------	--	--	--	-----------	--	--	--	-----------	--	--	--	-----------	--	--	--	-----------	--	--	--	-----------	--	--	--	-----------	--	--	--	-----------	--	--	--	-----------	--	--	--	-----------	--	--	--	-----------	--	--	--	-----------	--	--	--	-----------	--	--	--	-----------	--	--	--	-----------	--	--	--	-----------	--	--	--	-----------	--	--	--	-----------	--	--	--	-----------	--	--	--	-----------	--	--	--	-----------	--	--	--	-----------	--	--	--	------------	--	--	--	------------	--	--	--	------------	--	--	--	------------	--	--	--	------------	--	--	--	------------	--	--	--	------------	--	--	--	------------	--	--	--	------------	--	--	--	------------	--	--	--	------------	--	--	--	------------	--	--	--	------------	--	--	--	------------	--	--	--	------------	--	--	--	------------	--	--	--	------------	--	--	--	------------	--	--	--	------------	--	--	--	------------	--	--	--	------------	--	--	--	------------	--	--	--	------------	--	--	--	------------	--	--	--	------------	--	--	--	------------	--	--	--	------------	--	--	--	------------	--	--	--	------------	--	--	--	------------	--	--	--	------------	--	--	--	------------	--	--	--	------------	--	--	--	------------	--	--	--	------------	--	--	--	------------	--	--	--	------------	--	--	--	------------	--	--	--	------------	--	--	--	------------	--	--	--	------------	--	--	--	------------	--	--	--	------------	--	--	--	------------	--	--	--	------------	--	--	--	------------	--	--	--	------------	--	--	--	------------	--	--	--	------------	--	--	--	------------	--	--	--	------------	--	--	--	------------	--	--	--	------------	--	--	--	------------	--	--	--	------------	--	--	--	------------	--	--	--	------------	--	--	--	------------	--	--	--	------------	--	--	--	------------	--	--	--	------------	--	--	--	------------	--	--	--	------------	--	--	--	------------	--	--	--	------------	--	--	--	------------	--	--	--	------------	--	--	--	------------	--	--	--	------------	--	--	--	------------	--	--	--	------------	--	--	--	------------	--	--	--	------------	--	--	--	------------	--	--	--	------------	--	--	--	------------	--	--	--	------------	--	--	--	------------	--	--	--	------------	--	--	--	------------	--	--	--	------------	--	--	--	------------	--	--	--	------------	--	--	--	------------	--	--	--	------------	--	--	--	------------	--	--	--	------------	--	--	--	------------	--	--	--	------------	--	--	--	------------	--	--	--	------------	--	--	--	------------	--	--	--	------------	--	--	--	------------	--	--	--	------------	--	--	--	------------	--	--	--	------------	--	--	--	------------	--	--	--	------------	--	--	--	------------	--	--	--	------------	--	--	--	------------	--	--	--	------------	--	--	--	------------	--	--	--	------------	--	--	--	------------	--	--	--	------------	--	--	--	------------	--	--	--	------------	--	--	--	------------	--	--	--	------------	--	--	--	------------	--	--	--	------------	--	--	--	------------	--	--	--	------------	--	--	--	------------	--	--	--	------------	--	--	--	------------	--	--	--	------------	--	--	--	------------	--	--	--	------------	--	--	--	------------	--	--	--	------------	--	--	--	------------	--	--	--	------------	--	--	--	------------	--	--	--	------------	--	--	--	------------	--	--	--	------------	--	--	--	------------	--	--	--	------------	--	--	--	------------	--	--	--	------------	--	--	--	------------	--	--	--	------------	--	--	--	------------	--	--	--	------------	--	--	--	------------	--	--	--	------------	--	--	--	------------	--	--	--	------------	--	--	--	------------	--	--	--	------------	--	--	--	------------	--	--	--	------------	--	--	--	------------	--	--	--	------------	--	--	--	------------	--	--	--	------------	--	--	--	------------	--	--	--	------------	--	--	--	------------	--	--	--	------------	--	--	--	------------	--	--	--	------------	--	--	--	------------	--	--	--	------------	--	--	--	------------	--	--	--	------------	--	--	--	------------	--	--	--	------------	--	--	--	------------	--	--	--	------------	--	--	--	------------	--	--	--	------------	--	--	--	------------	--	--	--	------------	--	--	--	------------	--	--	--	------------	--	--	--	------------	--	--	--	------------	--	--	--	------------	--	--

262

263

SP-F13-52				SP-F13-54				SP-F13-55				SP-F13-59				SP-F14-51				SP-F14-53				SP-F14-54				SP-F14-55						
mm	phi	results	mm	phi	results	mm	phi	results	mm	phi	results	mm	phi	results	mm	phi	results	mm	phi	results	mm	phi	results	mm	phi	results	mm	phi	results	mm	phi	results		
0.7279	1.47733985		84	0.4015	1.11651897	84	0.4143	1.27124152	84	0.3672	1.300399198	84	0.3109	1.46546832	84	0.3916	1.35253589	84	0.1987	2.31131651	84	0.2556	1.36802061	84	0.2556	1.36802061	84	0.2556	1.36802061	84	0.2556	1.36802061		
0.1139	1.67160893	0.44817652	0.4043	1.30649084	0.69324169	0.4466	1.16295001	0.56533381	0.3604	1.47221663	0.70178443	0.3904	1.35693657	0.48260604	0.4119	1.27263508	0.28788237	0.1987	2.31131651	0.8021841	0.2593	1.94728942	0.82280914	0.2593	1.94728942	0.82280914	0.2593	1.94728942	0.82280914	0.2593	1.94728942			
0.3531	1.04438357	50	0.4561	1.12526833	50	0.4842	1.10717221	50	0.3689	1.18886814	50	0.3942	1.34280896	50	0.4289	1.22127645	50	0.2009	2.31134095	50	0.2722	1.87724513	50	0.2722	1.87724513	50	0.2722	1.87724513	50	0.2722	1.87724513	50	0.2722	1.87724513
0.3673	1.04456686	-1.0055944	0.4689	1.09263857	-0.17569634	0.4682	1.0947399	-0.56148831	0.3729	1.42212726	-0.47059776	0.4068	1.29759794	-0.74030034	0.4354	1.19957654	-2.34652385	0.2797	1.18302321	-1.40381204	0.3474	1.52531744	-0.86446312	0.3474	1.52531744	-0.86446312	0.3474	1.52531744	-0.86446312	0.3474	1.52531744			
0.5132	0.95678741	16	0.474	1.07703191	16	0.4736	1.07628789	16	0.4301	1.21724567	16	0.5131	0.96287993	16	0.4605	1.11871743	16	0.2902	1.74886458	16	0.3702	1.48116343	16	0.3702	1.48116343	16	0.3702	1.48116343	16	0.3702	1.48116343	16	0.3702	1.48116343
0.5215	0.93952929	-2.97138064	0.4804	1.03856513	-1.85276662	0.4802	1.05828374	-1.88011284	0.4549	1.20123923	-2.32240065	0.5462	0.8724914	-4.63676596	0.5093	0.97949413	-4.33588417	0.3122	1.79844335	-4.02890766	0.3914	1.35327289	-3.73360417	0.3914	1.35327289	-3.73360417	0.3914	1.35327289	-3.73360417	0.3914	1.35327289	-3.73360417		
0.5598	0.83709263	Mz	0.4927	1.02120999	Mz	0.5126	0.90886798	Mz	0.4404	1.18103162	Mz	0.4357	0.63576408	Mz	0.5175	0.95061013	Mz	0.3788	1.39677638	Mz	0.4	1.32151891	Mz	0.4	1.32151891	Mz	0.4	1.32151891	Mz	0.4	1.32151891	Mz	0.4	1.32151891
0.5678	0.8163834	-1.17626617	0.5227	0.93595702	-0.46507372	0.5681	0.82086423	-0.62542245	0.4581	1.12625061	-0.69707132	0.6655	0.58531827	-1.29148863	0.5296	0.91701702	-2.13150855	0.4099	1.28664522	-1.54531187	0.4354	1.19567654	-1.25841938	0.4354	1.19567654	-1.25841938	0.4354	1.19567654	-1.25841938	0.4354	1.19567654	-1.25841938		
0.5923	0.75539362		0.5558	0.84735509		0.5679	0.81628428		0.4605	1.11871748		0.6731	0.57110241		0.5402	0.88842964		0.5026	0.99250903		0.436	1.19758983		0.436	1.19758983		0.436	1.19758983		0.436	1.19758983		0.436	1.19758983
0.6074	0.7192751	95	0.5066	0.83494929	95	0.5751	0.78810851	95	0.5001	0.99970303	95	0.6748	0.56746332	95	0.5059	0.86013636	95	0.5091	0.97937079	95	0.523	0.93510294	95	0.523	0.93510294	95	0.523	0.93510294	95	0.523	0.93510294	95	0.523	0.93510294
0.6206	0.68825858	1.48974635	0.5727	0.80414169	1.18504933	0.5824	0.77991114	1.14287851	0.5079	0.97779735	1.49107354	0.6931	0.5288661	1.32913862	0.6	0.73695936	1.23294829	0.525	0.92962081	2.12019235	0.5274	0.92920272	1.76020621	0.5274	0.92920272	1.76020621	0.5274	0.92920272	1.76020621	0.5274	0.92920272	1.76020621		
0.6340	0.65602028	5	0.5925	0.75510053	5	0.5838	0.77447752	5	0.558	0.89431436	5	0.7201	0.47727062	5	0.602	0.72215842	5	0.5545	0.85075344	5	0.5524	0.85020753	5	0.5524	0.85020753	5	0.5524	0.85020753	5	0.5524	0.85020753	5	0.5524	0.85020753
0.7703	0.17600449	-3.36454398	0.6009	0.79476966	-2.94178232	0.6045	0.72617961	-2.94211519	0.5874	0.76757834	-3.46273625	0.7418	0.4112832	-4.95415441	0.6321	0.66176968	-6.64381691	0.5626	0.82981152	-4.4059551	0.5885	0.76487921	-4.9068491	0.5885	0.76487921	-4.9068491	0.5885	0.76487921	-4.9068491	0.5885	0.76487921	-4.9068491		
0.7762	0.36549657	Qj	0.6029	0.73003193	Qj	0.6065	0.72141433	Qj	0.6096	0.71405915	Qj	0.7593	0.39725477	Qj	0.6425	0.63822624	Qj	0.5907	0.75949606	Qj	0.5911	0.75851946	Qj	0.5911	0.75851946	Qj	0.5911	0.75851946	Qj	0.5911	0.75851946	Qj	0.5911	0.75851946
0.7871	0.34537823	-1.59083782	0.6206	0.68825858	-1.2617796	0.6346	0.65607502	-1.2303001	0.6311	0.66428247	-1.50662351	0.7944	0.33205996	-1.87085569	0.6668	0.58466905	-2.04618061	0.5952	0.74854724	-2.19658136	0.6118	0.70886199	-2.149226353	0.6118	0.70886199	-2.149226353	0.6118	0.70886199	-2.149226353	0.6118	0.70886199	-2.149226353		
0.8057	0.3118827		0.6716	0.57432101		0.6359	0.68044707		0.6443	0.63419014		0.7889	0.3420876		0.7088	0.50062182		0.6007	0.73527721		0.6175	0.69948308		0.6175	0.69948308		0.6175	0.69948308		0.6175	0.69948308		0.6175	0.69948308
0.8301	0.38612564		0.6725	0.57238999		0.693	0.52960827		0.6477	0.626859705		0.7944	0.33205996		0.7096	0.34080322		0.6056	0.73308004		0.6176	0.69948308		0.6176	0.69948308		0.6176	0.69948308		0.6176	0.69948308		0.6176	0.69948308
0.854	0.2276901		0.6735	0.57024533		0.7319	0.45027774		0.6823	0.65315721		0.8112	0.31067879		1.0434	-0.06129182		0.8611	0.59705453		0.6388	0.65108225		0.6388	0.65108225		0.6388	0.65108225		0.6388	0.65108225		0.6388	0.65108225
0.8742	0.19393608		0.6821	0.55194016		0.763	0.39024174		0.7254	0.46314743		0.8116	0.30115668		1.0449	-0.06336434		0.6746	0.56789097		0.6433	0.63843102		0.6433	0.63843102		0.6433	0.63843102		0.6433	0.63843102		0.6433	0.63843102
0.8901	0.16759325		0.6964	0.52200748		0.7743	0.36903233		0.7807	0.45246506		0.8174	0.25088339		1.0711	-0.0990234		0.7187	0.47539878		0.6515	0.61851759		0.6515	0.61851759		0.6515	0.61851759		0.6515	0.61851759		0.6515	0.61851759
0.9088	0.14114251		0.7017	0.51106941		0.7919	0.33666099		0.7382	0.43712905		0.853	0.22938041		1.1134	-0.15497068		0.7413	0.43225621		0.6616	0.59596382		0.6616	0.59596382		0.6616	0.59596382		0.6616	0.59596382		0.6616	0.59596382
0.917	0.1250053		0.7041	0.50814347		0.8048	0.29468083		0.7482	0.41850009		0.8617	0.17240209		1.2807	-0.2838765		0.7581	0.3991566		0.6469	0.57991698		0.6469	0.57991698		0.6469	0.57991698		0.6469	0.57991698		0.6469	0.57991698
0.9386	0.09141696		0.7081	0.49797077		0.824	0.2792814		0.7618	0.42596452		0.8626	0.21234548		1.2142	-0.28003749		0.8295	0.3266383		0.7123	0.4384897		0.7123	0.4384897		0.7123	0.4384897		0.7123	0.4384897		0.7123	0.4384897
0.996	0.0057823		0.7166	0.48075599		0.8451	0.24280398		0.7775	0.36308235		0.869	0.205702		1.2287	-0.2971302		0.8548	0.2263397		0.7248	0.4644121		0.7248	0.4644121		0.7248	0.4644121		0.7248	0.4644121		0.7248	0.4644121
1.004	-0.00057696		0.7259	0.46215337		0.8306	0.23445527		0.8076	0.30824858		0.8765	0.1901724		1.2605	-0.3339929		0.861	0.21913503		0.7513	0.4125355		0.7513	0.4125355		0.7513	0.4125355		0.7513	0.4125355		0.7513	0.4125355
1.0396	-0.05602807		0.7275	0.45897697		0.8974	0.15617539		0.8214	0.28184075		0.8978	0.15553268		1.3316	-0.41131758		0.8682	0.20889895		0.753	0.40297427		0.753	0.40297427		0.753	0.40297427		0.753	0.40297427		0.753	0.40297427
1.0552	-0.07751581		0.7311	0.46183552		0.9157	0.127502		0.8471	0.23939378		0.904	0.14560409		1.3393	-0.44280015		0.9106	0.13510949		0.7688	0.37931605		0.7688	0.37931605		0.7688	0.37931605		0.7688	0.37931605		0.7688	0.37931605
1.0681	-0.08202088		0.7339	0.46332917		0.9345	0.11418492		0.8623	0.20625512		0.9002	0.14207802		1.3427	-0.45037812		0.9122	0.1325766		0.8062	0.35227689		0.8062	0.35227689		0.8062	0.35227689		0.8062	0.35227689		0.8062	0.35227689
1.1572	-0.21063645		0.7786	0.3610427		0.9383	0.09187805		0.9633	0.05394247		0.9348	0.09726954		1.5541	-0.83607396		1.058	-0.01133894		0.836	0.29335646		0.836	0.29335646		0.836	0.29335646		0.836	0.29335646		0.836	0.29335646
1.1641	-0.21921314		0.7839	0.3512555		0.9379	0.09194432		0.9379	0.09194432		0.9379	0.09194432		1.5961	-0.8745434		1.0804	-0.1155661		0.9125	0.13121042		0.9125	0.13121042		0.9125	0.13121042		0.9125	0.13121042		0.9125	0.13121042
1.1826	-0.24196014		0.8134	0.29756058		0.9596	0.05949443		0.9794	0.03466661		0.934	0.08466661		1.6184	-0.6945623		1.096	-0.1324668		0.9236	0.11465895		0.9236	0.11465895									

265

WF

WF-F1-S1				WF-F5-S1				WF-F5-S2				WF-F5-S3			
mm	phi	results		mm	phi	results		mm	phi	results		mm	phi	results	
0.2865	1.8033777		84	0.2789	1.84216458		84	0.2577	1.95621901		84	0.2466	2.01973821		84
0.3351	1.57723207	0.5826014		0.2871	1.80035954	1.27495783		0.262	1.93234494	1.36030912		0.2611	1.93730925	1.32202471	
0.4457	1.16584527		50	0.2875	1.79835093		50	0.3175	1.6551575		50	0.2693	1.89269786		50
0.4461	1.1645511	-1.82490365		0.3057	1.70979708	-0.79094732		0.3224	1.6306254	0.58405486		0.2822	1.82519467	0.35208312	
0.4552	1.13541793		16	0.3136	1.67298839		16	0.3275	1.61041957		16	0.2942	1.76511592		16
0.4561	1.13256835	-3.91784211		0.314	1.6711494	-3.29850988		0.3293	1.60251203	-3.08841402		0.3069	1.70414504	-2.59160319	
0.4596	1.12153981	Mz		0.3191	1.64790555	Mz		0.3457	1.53239453	Mz		0.312	1.68036785	Mz	
0.491	1.02619639	-1.72004812		0.3281	1.60777789	-0.93816646		0.3512	1.50962248	-0.38135001		0.3241	1.62547533	-0.30583179	
0.4931	1.02003922			0.3328	1.58725924			0.3513	1.50921175			0.3378	1.56574552		
0.5193	0.94535187		95	0.3433	1.54244519		95	0.3532	1.50143005		95	0.3501	1.51414823		95
0.526	0.92685746	1.36930302		0.3476	1.52448712	1.7647321		0.3642	1.45718485	1.75744071		0.3531	1.50183857	1.88801118	
0.5353	0.90157282		5	0.3539	1.49857366		5	0.373	1.42274043		5	0.3632	1.46115153		5
0.5481	0.86748162	-4.35751515		0.3811	1.39174672	-3.87957494		0.3755	1.41310324	-4.32189154		0.3652	1.45322904	-4.87278755	
0.5854	0.77249882	Qi		0.4078	1.29405538	Qi		0.3796	1.39743628	Qi		0.3792	1.3989573	Qi	
0.5913	0.75803141	1.9928106		0.4154	1.26741616	1.99856497		0.3819	1.38872143	2.03329173		0.4182	1.2577244	2.00277042	
0.6089	0.71571673			0.419	1.25496724			0.3929	1.34775453			0.4225	1.24296624		
0.6268	0.67391722			0.4257	1.23208058			0.3945	1.34189145			0.4248	1.23513388		
0.6417	0.6400237			0.4392	1.18704			0.3978	1.32987357			0.4484	1.15713203		
0.7188	0.47633366			0.4401	1.18408671			0.4021	1.31436264			0.4533	1.14145228		
0.7265	0.4609614			0.4708	1.08680458			0.4111	1.28242788			0.4658	1.10220813		
0.7514	0.41234349			0.4782	1.06430496			0.4113	1.28172618			0.4669	1.09880521		
0.85	0.23446327			0.4811	1.05558237			0.4301	1.21724567			0.4729	1.08038382		
0.8803	0.18393127			0.4987	1.0037474			0.4304	1.21623973			0.479	1.06189346		
0.9212	0.11841268			0.5009	0.99739705			0.4335	1.2058859			0.4832	1.04929877		
1.0368	-0.05213718			0.5107	0.96944384			0.4574	1.12846219			0.4931	1.02003922		
1.0503	-0.07080087			0.5112	0.96803207			0.4606	1.11840422			0.4969	1.00896402		
1.0761	-0.10581126			0.5248	0.93015251			0.4691	1.09202336			0.5139	0.96043232		
1.1687	-0.22490274			0.5488	0.86564029			0.4801	1.05858421			0.5143	0.95930983		
1.1911	-0.25229241			0.5535	0.85333756			0.486	1.04096298			0.5235	0.93373066		
1.1973	-0.25978249			0.5813	0.78263857			0.4904	1.02796042			0.5376	0.89538738		
1.2229	-0.29030398			0.588	0.76610546			0.4932	1.01974667			0.5414	0.88522572		
1.2618	-0.33548042			0.5984	0.74081165			0.5053	0.98477959			0.5473	0.86958888		
1.2822	-0.35861828			0.6145	0.70250914			0.5101	0.97113978			0.5669	0.8188269		
1.4762	-0.56188344			0.6254	0.67714315			0.5143	0.95930983			0.5692	0.81298556		
1.658	-0.72943784			0.7046	0.50511935			0.5183	0.94813268			0.5719	0.80615837		
1.6743	-0.74355176			0.7226	0.46872688			0.5226	0.93621305			0.5841	0.77570615		
1.6884	-0.75565034			0.7454	0.42390969			0.5278	0.92192895			0.5902	0.76071774		
1.7194	-0.7818986			0.7508	0.41349595			0.5394	0.89056504			0.6	0.73695936		
1.8322	-0.87356961			0.7663	0.38401554			0.544	0.87831402			0.6075	0.7190376		
1.9448	-0.95961368			0.8307	0.26759828			0.5482	0.86721843			0.6287	0.66955067		
2.0836	-1.05906939			0.8537	0.22819699			0.559	0.83907272			0.6401	0.64362534		
2.3628	-1.24048703			0.8551	0.22583304			0.5592	0.83855664			0.6469	0.62838007		
2.747	-1.45784458			0.9849	0.02195066			0.5744	0.79986558			0.6529	0.61506085		
2.9075	-1.53976617			1.0442	-0.06239754			0.5758	0.79633357			0.6585	0.60273956		
2.912	-1.54199731			1.1391	-0.18789282			0.5782	0.7903528			0.6666	0.58510183		
2.92	-1.54595529			1.2938	-0.37161147			0.6038	0.72785118			0.6967	0.52138612		
3.0011	-1.58547798			1.4041	-0.48964155			0.6062	0.72212814			0.6987	0.51725058		
3.2216	-1.6877631			1.435	-0.52104633			0.6109	0.71098584			0.7066	0.50103011		
3.3095	-1.72659867			1.4512	-0.53724182			0.6132	0.70556443			0.7831	0.35272856		
3.3532	-1.74552377			1.4565	-0.54250111			0.6181	0.69408196			0.7915	0.33733589		
3.416	-1.77229299			1.6926	-0.75923465			0.6275	0.67230695			0.8085	0.30667773		
3.4254	-1.77625745			1.7092	-0.77331468			0.6449	0.63284727			0.812	0.30044583		
3.8417	-1.94172844			1.8737	-0.90588232			0.6474	0.62726542			0.8138	0.2972513		
3.9019	-1.96416019			1.902	-0.9275094			0.6589	0.60186348			0.8306	0.26777196		
3.9986	-1.99947806			2.1221	-1.08548346			0.6918	0.53156859			0.8309	0.26725098		
4.3041	-2.10569379			2.3586	-1.2379203			0.7171	0.47974972			0.8755	0.19181929		
4.5354	-2.18121135			3.4604	-1.79092367			0.7219	0.47012511			0.8771	0.18918516		
5.3553	-2.42094692			3.4673	-1.7937975			0.7312	0.4516582			0.891	0.16650125		
7.123	-2.83246103			3.4974	-1.80626753			0.7413	0.43186693			0.9712	0.04215932		
7.123	-2.83246103			3.5685	-1.83530225			0.8051	0.31275746			1.0004	-0.00057696		
7.7741	-2.95865064			4.1442	-2.05107628			0.8467	0.24007518			1.0056	-0.00805649		
7.8292	-2.96883979			4.462754	-2.15791603			0.8596	0.21826077			1.0564	-0.07915554		
7.8611	-2.97470604			5.4	-2.43293883			0.8639	0.21106199			1.0606	-0.08487994		
7.925	-2.98638568			5.4	-2.43293883			0.9519	0.07111747			1.092	-0.12697178		
8.4925	-3.08616321			5.4	-2.43293883			1.0838	-0.11609757			1.1464	-0.19710885		
8.5	-3.08743673			5.4	-2.43293883			1.1288	-0.17478841			1.2199	-0.28676046		
8.5036	-3.08804762			5.4	-2.43293883			1.1626	-0.21735298			1.2546	-0.3272247		
8.5163	-3.09020064			5.4	-2.43293883			1.58	-0.65991898			1.453	-0.53903014		
8.6455	-3.11192308			5.4	-2.43293883			1.7114	-0.77517044			1.6512	-0.72350876		
8.748	-3.12892676			5.4	-2.43293883			1.957	-0.96863556			1.8375	-0.87773683		
11.3	-3.49822128			5.4	-2.43293883			2.0438	-1.0312453			1.8782	-0.90934301		
11.3	-3.49822128			5.4	-2.43293883			2.1915	-1.13190911			1.9738	-0.98096752		
11.3	-3.49822128			5.4	-2.43293883			2.22	-1.15054995			2.0099	-1.00711521		
11.3	-3.49822128			5.4	-2.43293883			2.2452	-1.1668341			2.0303	-1.02168428		
11.3	-3.49822128			5.4472	-2.44549416			3.5359	-1.82206206			2.2979	-1.20030586		
11.3	-3.49822128			10.5	-3.39228873			4.417199	-2.1431137			2.3335	-1.22248513		
11.3	-3.49822128			10.5	-3.39228873			4.9591	-2.31005878			2.6769	-1.42055123		
11.3	-3.49822128			10.5	-3.39228873			6.8054	-2.76665656			3.3049	-1.72459203		
11.3	-3.49822128			10.5	-3.39228873			6.8112	-2.76788559			3.7486	-1.90633577		
11.3	-3.49822128			10.5	-3.39228873			6.8144	-2.76856322			3.9065	-1.96585999		
11.3	-3.49822128			10.5	-3.39228873			6.8308	-2.77203111			4.124736	-2.04428449		
19	-4.24789159			10.6	-3.40596355			6.8375	-2.77344547			4.2592	-2.0905648		
19	-4.24789159			10.6	-3.40596355			12	-3.58493218			4.3514	-2.1214617		
19	-4.24789159			10.6	-3.40596355			12.177	-3.60605634			4.5894	-2.19828696		
19	-4.24789159			10.6	-3.40596355			12.17							

PR

PR-F1-51				PR-F1-52				PR-F1-53				PR-F2-52				PR-F2-55				PR-Q2-114				PR-F2-56					
mm	phi	results	mm	phi	results	mm	phi	results	mm	phi	results	mm	phi	results	mm	phi	results	mm	phi	results	mm	phi	results	mm	phi	results	mm		
0.4699	1.08956311	84	0.2409	2.05347633	84	0.4007	1.11939443		84	0.232	1.2844061	84	0.2943	1.76462563	84	0.3274	1.61086015	84	0.1712	2.54623386	84	0.3565	1.48803143	84	0.3545	1.48803143	84		
0.5475	0.8096178	0.2252956	0.5758	1.95592929	0.43893487	0.4484	1.15711203	0.16952217		0.2314	2.09910578	0.86845181	0.3696	1.43510519	0.2512379	0.3629	1.46234367	0.44908865	0.2057	2.28136701	1.71257758	0.4715	1.08466115	0.02678668	0.5359	0.86013056	90		
0.5961	0.7463674	0.78595529	0.4274	1.22633082	0.94724838	0.5039	0.98487828	-1.1902589		0.3239	1.62636587	-0.42580034	0.5091	0.97397079	0.84828997	0.4153	1.2677635	-0.60850566	0.2428	2.0421424	0.98267435	0.6335	0.66131975	-1.5814832	0.5961	0.7463674	16		
0.6046	0.7239408	16	0.4998	1.00056873	16	0.6149	0.70157035	16	0.3569	1.48839562	16	0.8165	0.8978213	16	0.4158	1.26602763	16	0.2439	2.02238924	16	0.6332	0.61439811	16	0.6332	0.61439811	16	0.6332	0.61439811	16
0.6491	0.62348027	-2.35302945	0.5118	0.9663977	-2.68542514	0.6459	0.63061194	-2.84943455		0.3751	1.41464087	-2.15208086	0.6882	0.54750536	-2.2325105	0.422	1.24467457	-2.10047034	0.2476	2.01389975	-0.14393414	0.7375	0.43928133	-2.46234253	0.6755	0.50396754	Mz		
0.7001	0.51406274	0.97225173	0.6933	0.4602954	-1.06457949	0.7597	0.43949414	-1.29005709		0.4158	1.25221534	Mz	0.6594	0.52698796	0.94316752	0.5284	0.90208984	-0.75329579	0.2581	1.95398143	0.85028595	0.7021	0.52572856	-1.5687147	0.7021	0.52572856	-1.5687147		
0.7413	0.43186693		0.6459	0.83061194		0.7955	0.33068317			0.4236	1.3291502		0.7152	0.48083148		0.555	0.84943314		0.2789	1.84214658		0.7942	0.33242392		0.7942	0.33242392			
0.7715	0.37425877		0.672	0.57346201	95	0.8014	0.31940208	95	0.4317	1.21188875	95	0.7520	0.40506059	95	0.6	0.73695936	95	0.2821	1.82570599	95	0.8575	0.27316647	95	0.8575	0.27316647	95	0.8575	0.27316647	95
0.7763	0.36531077	0.85821313	0.6897	0.5359546	1.50264173	0.8634	0.21189721	1.05073673		0.4599	1.12098842	1.8579425	0.7522	0.40125029	1.23300198	0.6448	0.633071	1.37943281	0.2849	1.81145715	2.2235742	0.8478	0.23820211	0.91181489	0.7942	0.33242392	0.91181489		
0.7946	0.3318965	5	0.6848	0.52532959	5	0.8916	0.16530058	5	0.4666	1.11804422	5	0.8281	0.2721208	5	0.6054	0.60594727	5	0.3048	1.7140507	5	0.834	0.2276901	5	0.834	0.2276901	5	0.834	0.2276901	5
0.7979	0.32571739	-3.58602299	0.6967	0.53138612	-3.3219	0.8949	0.16502026	-3.40596355		0.4607	1.13051789	-3.09083989	0.8801	0.35125908	-3.40596355	0.6459	0.53664959	-1.1867344	0.3075	1.7013279	-1.04952443	0.8541	0.27257118	-3.0076941	0.7979	0.32571739	-3.58602299		
0.8101	0.30382532	Q	0.7158	0.48236747	Q	0.9051	0.14348968	Q		0.552	0.87252534	Q	0.9114	0.1338429	Q	0.7675	0.56383339	Q	0.3102	1.68871513	Q	0.8789	0.18953144	Q	0.8789	0.18953144	Q		
0.85	0.23446327	1.309681	0.7217	0.47052486	1.5120832	0.9271	0.10920221	1.4299968		0.6059	0.92728428	1.50492622	0.9288	0.10655922	1.32183066	0.7181	0.4381081	1.118921	0.3102	1.68871513	1.90616696	0.9534	0.07187546	1.20275346	0.9534	0.07187546	1.20275346		
0.8601	0.21742185		0.7539	0.40755148		0.9295	0.10547234			0.6076	0.71880015		0.9398	0.08957357		0.8154	0.29441765		0.3106	1.688656		1.006	0.00863023		0.8601	0.21742185			
0.8711	0.19908807		0.7699	0.37275383		0.9878	0.01770898			0.6175	0.69348583		0.9457	0.08054482		0.8346	0.26084097		0.316	1.68398948		1.0112	0.01006823		0.8711	0.19908807			
0.8788	0.18619185		0.8831	0.17934976		1.0147	-0.02105307			0.6227	0.68318504		0.9461	0.07993474		0.8526	0.2305709		0.3248	1.62336274		1.1379	-0.1363722		0.8788	0.18619185			
0.9124	0.13226053		0.884	0.17780022		1.0377	-0.0533897			0.6257	0.67945127		0.9544	0.06733348		0.8499	0.07871536		0.3254	1.61572738		1.2186	-0.2825252		0.9124	0.13226053			
0.9344	0.09788699		0.9102	0.15734336		1.0476	-0.0670874			0.6277	0.6745696		0.9706	0.04305087		0.9706	0.06899721		0.3278	1.60997912		1.2803	-0.3546789		0.9344	0.09788699			
0.9563	0.06446427		0.9109	0.13463427		1.0568	-0.0797017			0.6711	0.57359547		0.974	0.038006		0.9776	0.03268353		0.3281	1.6077789		1.3294	-0.4017778		0.9563	0.06446427			
1.0154	-0.02204798		0.9782	0.03179836		1.0597	-0.08355319			0.7247	0.46454027		1.012	-0.07120914		0.9876	0.01800111		0.3312	1.59421194		1.3433	-0.42577794		1.0154	-0.02204798			
1.0195	-0.02847366		0.9854	0.02112844		1.1008	-0.1385512			0.7261	0.46175594		1.0597	-0.08355319		1.0147	-0.02103507		0.3371	1.5687382		1.3608	-0.44445129		1.0195	-0.02847366			
1.0386	-0.05211718		0.9961	0.00274137		1.1079	-0.14782462			0.7441	0.4734413		1.078	-0.1054489		1.0217	-0.03097188		0.3401	1.5241341		1.381	-0.44466131		1.0386	-0.05211718			
1.0925	-0.1726332		1.0294	-0.04180333		1.1238	-0.16838388			0.7862	0.34180338		1.0959	-0.1373712		1.0223	-0.03181386		0.3637	1.45916683		1.4406	-0.52666536		1.0925	-0.1726332			
1.1111	-0.15198788		1.0416	-0.05880086		1.1239	-0.16851225			0.8346	0.27875624		1.1478	-0.18861839		1.0476	-0.0670874		0.3673	1.44495698		1.5072	-0.95186586		1.1111	-0.15198788			
1.1416	-0.10915562		1.0564	-0.07915554		1.1737	-0.23106175			0.8426	0.26040997		1.1749	-0.232536		1.0751	-0.10446997		0.382	1.38834371		1.5399	-0.6228314		1.1416	-0.10915562			
1.1787	-0.2373457		1.0661	-0.09234199		1.2	-0.28303218			0.8432	0.24605115		1.1945	-0.25640489		1.0845	-0.11702906		0.3923	1.38770222		1.5742	-0.65461331		1.1787	-0.2373457			
1.2125	-0.30885142		1.1189	-0.14077973		1.257	-0.32998166			0.8461	0.22752118		1.1470	-0.26170912		1.0896	-0.1263499394		0.3928	1.376078776		1.6255	-0.78087768		1.2125	-0.30885142			
1.2483	-0.32019311		1.1375	-0.18584607		1.2674	-0.34189693			0.863	0.21265774		1.2012	-0.26474124		0.9447	-0.17287054		0.3947	1.34116203		1.7099	-0.77395041		1.2483	-0.32019311			
1.2811	-0.35738007		1.1492	-0.2006282		1.3436	-0.4261001			0.9097	0.13636089		1.2131	-0.27896932		1.1286	-0.17453378		0.3985	1.32737314		1.8324	-0.8773728		1.2811	-0.35738007			
1.2851	-0.36187757		1.186	-0.26410193		1.3512	-0.43423756			0.9251	0.12312782		1.2256	-0.2834572		1.1439	-0.1935993		0.4019	1.31580084		1.8372	-0.87750127		1.2851	-0.36187757			
1.2877	-0.36479344		1.2428	-0.31359149		1.4301	-0.51611167			0.947	0.078563		1.2501	-0.32227157		1.1553	-0.20826577		0.4029	1.3114952		1.9067	-0.93109999		1.2877	-0.36479344			
1.3353	-0.41710638		1.2929	-0.37060756		1.4344	-0.52044299			0.9565	0.06416258		1.2688	-0.34361077		1.1579	-0.21150887		0.4113	1.28170218		2.0197	-1.04313244		1.3353	-0.41710638			
1.3598	-0.44239072		1.3325	-0.41521421		1.5847	-0.66420413			1.0224	-0.04002166		1.3064	-0.38570386		1.158	-0.21163346		0.4155	1.28767089		2.197	-1.13559993		1.3598	-0.44239072			
1.3599	-0.44349682		1.3355	-0.41737645		1.6077	-0.68499243			1.0582	-0.0861163		1.3139	-0.39358215		1.1604	-0.21462039		0.4164	1.26394734		2.21	-1.14403669		1.3599	-0.44349682			
1.3624	-0.44614657		1.3481	-0.43092387		1.6722	-0.74174114			1.0809	-0.11223211		1.3222	-0.40293701		1.169	-0.22527302		0.4274	1.22633082		2.2117	-1.14540627		1.3624	-0.44614657			
1.4008	-0.48624688		1.3853	-0.47019446		1.767	-0.7820901			1.1029	-0.14330079		1.3313	-0.41283222		1.1816	-0.2407397		0.4283	1.22329607		2.2632	-1.17835412		1.4008	-0.48624688			
1.4221	-0.50081862		1.4168	-0.50261187		1.7625	-0.76764831			1.1158	-0.16276481		1.3659	-0.46948486		1.1864	-0.24658842		0.4304	1.216231973		2.3778	-1.24697996		1.4221	-0.50081862			
1.4346	-0.5204523		1.4508	-0.51681763		1.7795	-0.82541987			1.1185	-0.16156389		1.3757	-0.460162		1.1973	-0.25973829		0.4483	1.15745381		2.4077	-1.26764452		1.4346	-0.5204523			
1.4459	-0.53193828		1.4407	-0.5267655		1.8942	-0.92158087			1.1418	-0.19130835		1.3892	-0.46487341		1.266	-0.34027453		0.4525	1.14400093		2.447	-1.29100118		1.4459	-0.53193828			
1.4481																													

PR-F2-51	mm	phi	results	PR-F3-50	mm	phi	results	PR-F3-51	mm	phi	results	PR-F3-52	mm	phi	results	PR-F4-51	mm	phi	results	PR-F5-50	mm	phi	results	PR-F5-51	mm	phi	results	PR-F5-52	mm	phi	results	PR-F5-53	mm	phi	results	PR-F5-54	mm	phi	results																																																																																																																																																																																																																																																																																																																																																																																																																																																																																																																																																																																																																																																																																																																																																																																																																																																																																																																																																																																																																																																																
0.4441	1.17503362	84	0.3792	1.1989571	84	0.3421	1.5474969	84	0.3011	1.7436704	84	0.2722	1.87734513	84	0.2025	2.3039867	84	0.1595	2.64834927	84	0.1193	2.87779919	84	0.0824	3.17779919	84	0.0524	3.48834927	84	0.0324	3.79934927	84	0.0124	4.10934927	84	0.0024	4.41934927	84	0.0004	4.72934927	84	0.0004	5.03934927	84	0.0004	5.34934927	84	0.0004	5.65934927	84	0.0004	5.96934927	84	0.0004	6.27934927	84	0.0004	6.58934927	84	0.0004	6.89934927	84	0.0004	7.20934927	84	0.0004	7.51934927	84	0.0004	7.82934927	84	0.0004	8.13934927	84	0.0004	8.44934927	84	0.0004	8.75934927	84	0.0004	9.06934927	84	0.0004	9.37934927	84	0.0004	9.68934927	84	0.0004	9.99934927	84	0.0004	10.30934927	84	0.0004	10.61934927	84	0.0004	10.92934927	84	0.0004	11.23934927	84	0.0004	11.54934927	84	0.0004	11.85934927	84	0.0004	12.16934927	84	0.0004	12.47934927	84	0.0004	12.78934927	84	0.0004	13.09934927	84	0.0004	13.40934927	84	0.0004	13.71934927	84	0.0004	14.02934927	84	0.0004	14.33934927	84	0.0004	14.64934927	84	0.0004	14.95934927	84	0.0004	15.26934927	84	0.0004	15.57934927	84	0.0004	15.88934927	84	0.0004	16.19934927	84	0.0004	16.50934927	84	0.0004	16.81934927	84	0.0004	17.12934927	84	0.0004	17.43934927	84	0.0004	17.74934927	84	0.0004	18.05934927	84	0.0004	18.36934927	84	0.0004	18.67934927	84	0.0004	18.98934927	84	0.0004	19.29934927	84	0.0004	19.60934927	84	0.0004	19.91934927	84	0.0004	20.22934927	84	0.0004	20.53934927	84	0.0004	20.84934927	84	0.0004	21.15934927	84	0.0004	21.46934927	84	0.0004	21.77934927	84	0.0004	22.08934927	84	0.0004	22.39934927	84	0.0004	22.70934927	84	0.0004	23.01934927	84	0.0004	23.32934927	84	0.0004	23.63934927	84	0.0004	23.94934927	84	0.0004	24.25934927	84	0.0004	24.56934927	84	0.0004	24.87934927	84	0.0004	25.18934927	84	0.0004	25.49934927	84	0.0004	25.80934927	84	0.0004	26.11934927	84	0.0004	26.42934927	84	0.0004	26.73934927	84	0.0004	27.04934927	84	0.0004	27.35934927	84	0.0004	27.66934927	84	0.0004	27.97934927	84	0.0004	28.28934927	84	0.0004	28.59934927	84	0.0004	28.90934927	84	0.0004	29.21934927	84	0.0004	29.52934927	84	0.0004	29.83934927	84	0.0004	30.14934927	84	0.0004	30.45934927	84	0.0004	30.76934927	84	0.0004	31.07934927	84	0.0004	31.38934927	84	0.0004	31.69934927	84	0.0004	32.00934927	84	0.0004	32.31934927	84	0.0004	32.62934927	84	0.0004	32.93934927	84	0.0004	33.24934927	84	0.0004	33.55934927	84	0.0004	33.86934927	84	0.0004	34.17934927	84	0.0004	34.48934927	84	0.0004	34.79934927	84	0.0004	35.10934927	84	0.0004	35.41934927	84	0.0004	35.72934927	84	0.0004	36.03934927	84	0.0004	36.34934927	84	0.0004	36.65934927	84	0.0004	36.96934927	84	0.0004	37.27934927	84	0.0004	37.58934927	84	0.0004	37.89934927	84	0.0004	38.20934927	84	0.0004	38.51934927	84	0.0004	38.82934927	84	0.0004	39.13934927	84	0.0004	39.44934927	84	0.0004	39.75934927	84	0.0004	40.06934927	84	0.0004	40.37934927	84	0.0004	40.68934927	84	0.0004	40.99934927	84	0.0004	41.30934927	84	0.0004	41.61934927	84	0.0004	41.92934927	84	0.0004	42.23934927	84	0.0004	42.54934927	84	0.0004	42.85934927	84	0.0004	43.16934927	84	0.0004	43.47934927	84	0.0004	43.78934927	84	0.0004	44.09934927	84	0.0004	44.40934927	84	0.0004	44.71934927	84	0.0004	45.02934927	84	0.0004	45.33934927	84	0.0004	45.64934927	84	0.0004	45.95934927	84	0.0004	46.26934927	84	0.0004	46.57934927	84	0.0004	46.88934927	84	0.0004	47.19934927	84	0.0004	47.50934927	84	0.0004	47.81934927	84	0.0004	48.12934927	84	0.0004	48.43934927	84	0.0004	48.74934927	84	0.0004	49.05934927	84	0.0004	49.36934927	84	0.0004	49.67934927	84	0.0004	49.98934927	84	0.0004	50.29934927	84	0.0004	50.60934927	84	0.0004	50.91934927	84	0.0004	51.22934927	84	0.0004	51.53934927	84	0.0004	51.84934927	84	0.0004	52.15934927	84	0.0004	52.46934927	84	0.0004	52.77934927	84	0.0004	53.08934927	84	0.0004	53.39934927	84	0.0004	53.70934927	84	0.0004	54.01934927	84	0.0004	54.32934927	84	0.0004	54.63934927	84	0.0004	54.94934927	84	0.0004	55.25934927	84	0.0004	55.56934927	84	0.0004	55.87934927	84	0.0004	56.18934927	84	0.0004	56.49934927	84	0.0004	56.80934927	84	0.0004	57.11934927	84	0.0004	57.42934927	84	0.0004	57.73934927	84	0.0004	58.04934927	84	0.0004	58.35934927	84	0.0004	58.66934927	84	0.0004	58.97934927	84	0.0004	59.28934927	84	0.0004	59.59934927	84	0.0004	59.90934927	84	0.0004	60.21934927	84	0.0004	60.52934927	84	0.0004	60.83934927	84	0.0004	61.14934927	84	0.0004	61.45934927	84	0.0004	61.76934927	84	0.0004	62.07934927	84	0.0004	62.38934927	84	0.0004	62.69934927	84	0.0004	63.00934927	84	0.0004	63.31934927	84	0.0004	63.62934927	84	0.0004	63.93934927	84	0.0004	64.24934927	84	0.0004	64.55934927	84	0.0004	64.86934927	84	0.0004	65.17934927	84	0.0004	65.48934927	84	0.0004	65.79934927	84	0.0004	66.10934927	84	0.0004	66.41934927	84	0.0004	66.72934927	84	0.0004	67.03934927	84	0.0004	67.34934927	84	0.0004	67.65934927	84	0.0004	67.96934927	84	0.0004	68.27934927	84	0.0004	68.58934927	84	0.0004	68.89934927	84	0.0004	69.20934927	84	0.0004	69.51934927	84	0.0004	69.82934927	84	0.0004	70.13934927	84	0.0004	70.44934927	84	0.0004	70.75934927	84	0.0004	71.06934927	84	0.0004	71.37934927	84	0.0004	71.68934927	84	0.0004	71.99934927	84	0.0004	72.30934927	84	0.0004	72.61934927	84	0.0004	72.92934927	84	0.0004	73.23934927	84	0.0004	73.54934927	84	0.0004	73.85934927	84	0.0004	74.16934927	84	0.0004	74.47934927	84	0.0004	74.78934927	84	0.0004	75.09934927	84	0.0004	75.40934927	84	0.0004	75.71934927	84	0.0004	76.02934927	84	0.0004	76.33934927	84	0.0004	76.64934927	84	0.0004	76.95934927	84	0.0004	77.26934927	84	0.0004	77.57934927	84	0.0004	77.88934927	84	0.0004	78.19934927	84	0.0004	78.50934927	84	0.0004	78.81934927	84	0.0004	79.12934927	84	0.0004	79.43934927	84	0.0004	79.74934927	84	0.0004	80.05934927	84	0.0004	80.36934927	84	0.0004	80.67934927	84	0.0004	80.98934927	84	0.0004	81.29934927	84	0.0004	81.60934927	84	0.0004	81.91934927	84	0.0004	82.22934927	84	0.0004	82.53934927	84	0.0004	82.84934927	84	0.0004	83.15934927	84	0.0004	83.46934927	84	0.0004	83.77934927	84	0.0004	84.08934927	84	0.0004	84.39934927	84	0.0004	84.70934927	84	0.0004	85.01934927	84	0.0004	85.32934927	84	0.0004	85.63934927	84	0.0004	85.94934927	84	0.0004	86.25934927	84	0.0004	86.56934927	84	0.0004	86.87934927	84	0.0004	87.18934927	84	0.0004	87.49934927	84	0.0004	87.80934927	84	0.0004	88.11934927	84	0.0004	88.42934927	84	0.0004	88.73934927	84	0.0004	89.04934927	84	0.0004	89.35934927	84	0.0004	89.66934927	84	0.0004	89.97934927	84	0.0004	90.28934927	84	0.0004	90.59934927	84	0.0004	90.90934927	84	0.0004	91.21934927	84	0.0004	91.52934927	84	0.0004	91.83934927	84	0.0004	92.14934927	84	0.0004	92.45934927	84	0.0004	92.76934927	84	0.0004	93.07934927	84	0.0004	93.38934927	84	0.0004	93.69934927	84	0.0004	94.00934927	84	0.0004	94.31934927	84	0.0004	94.62934927	84	0.0004	94.93934927	84	0.0004	95.24934927	84	0.0004	95.55934927	84	0.0004	95.86934927	84	0.0004	96.17934927	84	0.0004	96.48934927	84	0.0004	96.79934927	84	0.0004	97.10934927	84	0.0004	97.41934927	84	0.0004	97.72934927	84	0.0004	98.03934927	84	0.0004	98.34934927	84	0.0004	98.65934927	84	0.0004	98.96934927	84	0.0004	99.27934927	84	0.0004	99.58934927	84	0.0004	99.89934927	84	0.0004	100.20934927	84	0.0004	100.51934927	84	0.0004	100.82934927	84	0.0004	101.13934927	84	0.0004	101.44934927	84	0.0004	101.75934927	84	0.0004	102.06934927	84	0.0004	102.37934927	84	0.0004	102.68934927	84	0.0004	102.99934927	84	0.0004	103.30934927	84	0.0004	103.61934927	84	0.0004	103.92934927	84	0.0004	104.23934927	84	0.0004	104.54934927	84	0.0004	104.85934927	84	0.0004	105.16934927	84	0.0004	105.47934927	84	0.0004	105.78934927	84	0.0004	106.09934927	84	0.0004	106.40934927	84	0.0004	106.71934927	84	0.0004	107.02934927	84	0.0004	107.33934927	84	0.0004	107.64934927	84	0.0004	107.95934927	84	0.0004	108.26934927	84	0.0004	108.57934927	84	0.0004	108.88934927	84	0.0004	109.19934927	84	0.0004	109.50934927	84	0.0004	109.81934927	84	0.0004	110.12934927	84	0.0004	110.439349

269

PR-F11-54				PR-F13-51				PR-F13-52				PR-F13-53				PR-F14-51				PR-F14-52				PR-F14-53				PR-F14-54						
mm	results	mm	results	mm	results	mm	results	mm	results	mm	results	mm	results	mm	results	mm	results	mm	results	mm	results	mm	results	mm	results	mm	results	mm	results	mm	results			
0.3034	1.72832067	84	0.5858	1.95007398	84	0.1136	2.71251019	84	0.1136	2.71251019	84	0.2157	2.2128832	84	0.3577	1.48316543	84	0.2648	1.81196362	84	0.3507	1.51167788	84	0.4608	1.31177792	84	0.4608	1.31177792	84	0.4608	1.31177792			
0.3037	1.71926605		0.3067	1.70508511	1.12965864	0.2209	2.17851625	1.15243972	0.2413	2.05108283	0.85577129	0.378	1.4111815	0.37830043	0.3761	1.41079986	0.81182938	0.42	1.25152818	0.50401081	0.4875	1.03651711	0.17322242	0.4875	1.03651711	0.17322242	0.4875	1.03651711	0.17322242	0.4875	1.03651711			
0.3288	1.80470422	50	0.3175	1.6551575	50	0.2882	1.79484258	50	0.3904	1.35969357	50	0.3904	1.35969357	50	0.4413	1.25566063	50	0.543	0.88968485	50	0.543	0.88968485	50	0.543	0.88968485	50	0.543	0.88968485	50	0.543	0.88968485			
0.502	0.99423232	-1.00201216	0.3197	1.65159544	-0.03309487	0.2986	1.74369918	-0.04584304	0.3975	1.33096138	0.04900177	0.4798	1.05948585	-1.26882663	0.4424	1.17656676	-0.30878955	0.5668	0.81908141	-0.54282912	0.5135	0.96155949	-0.99052933	0.5135	0.96155949	-0.99052933	0.5135	0.96155949	-0.99052933	0.5135	0.96155949			
0.5482	0.87249314	16	0.3266	1.61438995	16	0.3421	1.5474989	16	0.4093	1.28878583	16	0.4093	1.28878583	16	0.463	1.11090631	16	0.5718	0.88041063	16	0.5718	0.88041063	16	0.5718	0.88041063	16	0.5718	0.88041063	16	0.5718	0.88041063			
0.5531	0.85430653	2.63702959	0.3527	1.5034798	-1.82295488	0.3582	1.48115023	-1.19679862	0.4261	1.23072543	1.33951949	0.5868	0.76952572	-1.03939552	0.4818	1.05349479	-2.08367085	0.5868	0.76351116	-1.45104496	0.5868	0.76351116	-1.45104496	0.5868	0.76351116	-1.45104496	0.5868	0.76351116	-1.45104496	0.5868	0.76351116			
0.6018	0.95925777	Mz	0.3875	1.64117163	Mz	0.3867	1.44731559	Mz	0.4547	1.17031447	Mz	0.6081	0.71713144	Mz	0.4851	1.04363709	Mz	0.6033	0.77946335	Mz	0.6033	0.77946335	Mz	0.6033	0.77946335	Mz	0.6033	0.77946335	Mz	0.6033	0.77946335			
0.6687	0.58056407	-1.10313889	0.3777	1.40467543	-0.24214431	0.3798	1.39667638	-0.09673398	0.4665	1.0004711	-1.14491548	0.6173	0.69550042	-1.32810667	0.4892	1.03149497	-0.52704367	0.6073	0.71951264	-0.56328576	0.6346	0.65067502	-1.05804258	0.6346	0.65067502	-1.05804258	0.6346	0.65067502	-1.05804258	0.6346	0.65067502			
0.7021	0.51024725		0.3908	1.35548616		0.3851	1.37668333		0.4898	1.02796278		0.625	0.67806617		0.5312	0.91266532		0.6159	0.69922605		0.6159	0.69922605		0.6159	0.69922605		0.6159	0.69922605		0.6159	0.69922605			
0.7158	0.48236747	95	0.3913	1.35364154	95	0.3917	1.35216753	95	0.4054	1.02796042	95	0.4471	0.62793411	95	0.533	0.90778488	95	0.6187	0.69282822	95	0.6187	0.69282822	95	0.6187	0.69282822	95	0.6187	0.69282822	95	0.6187	0.69282822	95	0.6187	0.69282822
0.7398	0.39830535	1.38380305	0.3944	1.34225719	1.71398042	0.3991	1.35216661	0.3991	1.35216661	0.5029	0.99164815	1.64813002	0.6505	0.60273779	1.21803874	0.5363	0.98888024	1.33807902	0.6378	0.64881851	1.05393331	0.6918	0.53156809	1.00312447	0.6918	0.53156809	1.00312447	0.6918	0.53156809	1.00312447	0.6918	0.53156809		
0.7675	0.38176812	5	0.4823	1.24262482	5	0.4827	1.31496264	5	0.5419	0.83039597	-2.4111583	0.5419	0.83039597	-2.4111583	0.7145	0.48489998	-3.80732272	0.6455	0.6110566	-2.54079572	0.6455	0.6110566	-2.54079572	0.6455	0.6110566	-2.54079572	0.6455	0.6110566	-2.54079572	0.6455	0.6110566	-2.54079572		
0.8183	0.2892958	4.28256793	0.4596	1.12153981	-1.54840661	0.411	1.28277885	-2.033591	0.5916	0.75729964	0.5916	0.75729964	0.7413	0.41386973	0.7413	0.41386973	0.5414	0.88522572	0.6522	0.61660844	0.6522	0.61660844	0.6522	0.61660844	0.6522	0.61660844	0.6522	0.61660844	0.6522	0.61660844	0.6522	0.61660844		
0.8206	0.28524653	Qj	0.461	1.11715913	Qj	0.4646	1.10592599	Qj	0.5925	0.75106055	1.16186638	0.7413	0.41386973	1.16186638	0.7413	0.41386973	0.5414	0.88522572	0.6522	0.61660844	0.6522	0.61660844	0.6522	0.61660844	0.6522	0.61660844	0.6522	0.61660844	0.6522	0.61660844	0.6522	0.61660844		
0.8666	0.26056011	1.6002085	0.4664	1.100351	1.53154943	0.4907	1.02707814	1.24775383	0.5925	0.75106055	1.16186638	0.7413	0.41386973	1.16186638	0.7413	0.41386973	0.5414	0.88522572	0.6522	0.61660844	0.6522	0.61660844	0.6522	0.61660844	0.6522	0.61660844	0.6522	0.61660844	0.6522	0.61660844	0.6522	0.61660844		
0.8741	0.19412811		0.4677	1.0963359		0.4993	1.02001271		0.5929	0.75106055		0.7413	0.41386973		0.7413	0.41386973	0.5414	0.88522572	0.6522	0.61660844	0.6522	0.61660844	0.6522	0.61660844	0.6522	0.61660844	0.6522	0.61660844	0.6522	0.61660844	0.6522	0.61660844		
0.8746	0.19310311		0.472	1.08133077		0.5029	0.91646015		0.6151	0.66465136		0.7413	0.41386973		0.7413	0.41386973	0.5414	0.88522572	0.6522	0.61660844	0.6522	0.61660844	0.6522	0.61660844	0.6522	0.61660844	0.6522	0.61660844	0.6522	0.61660844	0.6522	0.61660844		
0.8995	0.15280352		0.4826	1.05109129		0.5035	0.98992794		0.6358	0.65134955		0.7413	0.41386973		0.7413	0.41386973	0.5414	0.88522572	0.6522	0.61660844	0.6522	0.61660844	0.6522	0.61660844	0.6522	0.61660844	0.6522	0.61660844	0.6522	0.61660844	0.6522	0.61660844		
0.9501	0.07354444		0.5174	0.95064		0.5107	0.96944384		0.65	0.62148312		0.7413	0.41386973		0.7413	0.41386973	0.5414	0.88522572	0.6522	0.61660844	0.6522	0.61660844	0.6522	0.61660844	0.6522	0.61660844	0.6522	0.61660844	0.6522	0.61660844	0.6522	0.61660844		
0.9539	0.06808949		0.5303	0.91511161		0.5241	0.9320781		0.6574	0.60551552		0.7413	0.41386973		0.7413	0.41386973	0.5414	0.88522572	0.6522	0.61660844	0.6522	0.61660844	0.6522	0.61660844	0.6522	0.61660844	0.6522	0.61660844	0.6522	0.61660844	0.6522	0.61660844		
0.9929	0.01027958		0.5366	0.89807344		0.5278	0.95129285		0.658	0.60838354		0.7413	0.41386973		0.7413	0.41386973	0.5414	0.88522572	0.6522	0.61660844	0.6522	0.61660844	0.6522	0.61660844	0.6522	0.61660844	0.6522	0.61660844	0.6522	0.61660844	0.6522	0.61660844		
0.9941	0.00849642		0.5429	0.88124145		0.5405	0.87006798		0.6584	0.60329986		0.7413	0.41386973		0.7413	0.41386973	0.5414	0.88522572	0.6522	0.61660844	0.6522	0.61660844	0.6522	0.61660844	0.6522	0.61660844	0.6522	0.61660844	0.6522	0.61660844	0.6522	0.61660844		
1.0057	-0.00881994		0.5579	0.84114442		0.5656	0.82213982		0.6805	0.55124424		0.7413	0.41386973		0.7413	0.41386973	0.5414	0.88522572	0.6522	0.61660844	0.6522	0.61660844	0.6522	0.61660844	0.6522	0.61660844	0.6522	0.61660844	0.6522	0.61660844	0.6522	0.61660844		
1.0278	-0.03955922		0.5615	0.81263503		0.5661	0.82086423		0.6931	0.53088061		0.7413	0.41386973		0.7413	0.41386973	0.5414	0.88522572	0.6522	0.61660844	0.6522	0.61660844	0.6522	0.61660844	0.6522	0.61660844	0.6522	0.61660844	0.6522	0.61660844	0.6522	0.61660844		
1.0413	-0.08583828		0.5688	0.81399975		0.5742	0.800368		0.6948	0.55252529		0.7413	0.41386973		0.7413	0.41386973	0.5414	0.88522572	0.6522	0.61660844	0.6522	0.61660844	0.6522	0.61660844	0.6522	0.61660844	0.6522	0.61660844	0.6522	0.61660844	0.6522	0.61660844		
1.0849	-0.11756107		0.5718	0.80641065		0.5967	0.74491602		0.706	0.50255566		0.7413	0.41386973		0.7413	0.41386973	0.5414	0.88522572	0.6522	0.61660844	0.6522	0.61660844	0.6522	0.61660844	0.6522	0.61660844	0.6522	0.61660844	0.6522	0.61660844	0.6522	0.61660844		
1.111	-0.15187673		0.5752	0.79785797		0.6221	0.6847758		0.7067	0.50829582		0.7413	0.41386973		0.7413	0.41386973	0.5414	0.88522572	0.6522	0.61660844	0.6522	0.61660844	0.6522	0.61660844	0.6522	0.61660844	0.6522	0.61660844	0.6522	0.61660844	0.6522	0.61660844		
1.1368	-0.18487789		0.6134	0.68723358		0.6713	0.57496559		0.7451	0.42449844		0.7413	0.41386973		0.7413	0.41386973	0.5414	0.88522572	0.6522	0.61660844	0.6522	0.61660844	0.6522	0.61660844	0.6522	0.61660844	0.6522	0.61660844	0.6522	0.61660844	0.6522	0.61660844		
1.1552	-0.20814089		0.5923	0.75559362		0.6243	0.67968288		0.7203	0.47312619		0.7413	0.41386973		0.7413	0.41386973	0.5414	0.88522572	0.6522	0.61660844	0.6522	0.61660844	0.6522	0.61660844	0.6522	0.61660844	0.6522	0.61660844	0.6522	0.61660844	0.6522	0.61660844		
1.1788	-0.23731696		0.6006	0.7355174		0.625	0.67806617		0.7281	0.45778761		0.7413	0.41386973		0.7413	0.41386973	0.5414	0.88522572	0.6522	0.61660844	0.6522	0.61660844	0											

PR-F14-S5	phi	results	PR-F14-S6	phi	results	PR-F14-S7	phi	results	PR-F14-S8	phi	results	PR-F14-S9	phi	results	PR-F15-S1	phi	results	PR-F15-S2	phi	results	
mm			mm			mm			mm			mm			mm			mm			
0.3375	1.56702734		0.2953	1.75973186		0.2632	1.92575232		0.2334	2.09910578		0.3569	1.48639562		0.3065	1.70602659		0.3293	1.60251203		
0.4136	1.27368114	84	0.43910202	0.34	1.55638019	0.58753031	0.2649	1.91646404	0.94547489	0.2745	1.86510617	0.87556811	0.3815	1.39023328	0.58161469	0.3475	1.52490222	0.2342847	0.3531	1.50183857	0.46389836
0.429	1.22094012	50	0.3901	1.35807281	50	0.3025	1.72497836	50	0.316	1.66198948	50	0.4512	1.14815132	50	0.4213	1.24706963	50	0.388	1.36585989	50	
0.475	1.0779915	-0.71683445	0.4102	1.38588973	-0.75711587	0.3248	1.62236274	-0.71455634	0.3474	1.52531744	-0.73794416	0.4565	1.13130867	-1.11372581	0.4463	1.16393444	-1.62979924	0.4452	1.16746463	-0.92320439	
0.5242	0.93180286	16	0.4239	1.28193866	16	0.3389	1.56105526	16	0.3487	1.51926888	16	0.4377	1.12751827	16	0.4696	0.72620419	16	0.4509	1.14811087	16	
0.5342	0.90454047	-2.28803604	0.4873	1.0371091	2.25570371	0.3661	1.44967806	2.39995777	0.399	1.32552814	-2.40449061	0.4602	1.11934419	-2.40584659	0.6093	0.71476931	-3.15271297	0.4689	1.09263857	-2.20520202	
0.5619	0.83160766	Mz	0.4873	1.0371091	Mz	0.3666	1.44779097	Mz	0.4047	1.30506421	Mz	0.492	1.02326113	Mz	0.6657	0.58705096	Mz	0.4871	1.03770134	Mz	
0.6002	0.73647855	-0.85525616	0.4597	1.02120999	-0.80842976	0.3973	1.33168804	-0.72301907	0.4475	1.19263499	-0.75562222	0.5075	0.978512	-0.97931924	0.6725	0.57238899	-1.51607584	0.5847	0.77422496	-0.88816935	
0.6159	0.69922605		0.5037	0.989355		0.4017	1.31579851		0.4474	1.16035302		0.5324	0.90940983		0.6806	0.55511625		0.665	0.58858678		
0.6196	0.69058511	95	0.5057	0.983638	95	0.4381	1.19065781	95	0.495	1.01490999	95	0.5494	0.86406388	95	0.7096	0.4949179	95	0.6828	0.55046038	95	
0.6467	0.62882617	1.21348859	0.5299	0.91620022	1.43959361	0.439	1.18769711	1.75012254	0.5262	0.9263091	1.73428955	0.593	0.75388961	1.25672003	0.7313	0.45146091	1.27290142	0.7067	0.50082595	1.3573572	
0.6558	0.60866705	5	0.5535	0.85333756	5	0.4532	1.14177058	5	0.5341	0.90481056	5	0.6173	0.69595042	5	0.733	0.44811111	5	0.7073	0.49960161	5	
0.6787	0.55914935	-2.98947361	0.6043	0.7665701	-3.3219	0.4613	1.11621336	-3.7655029	0.5456	0.87407077	-3.6030914	0.6298	0.6670287	-2.8067146	0.7429	0.42875644	-3.80732272	0.7184	0.47713671	-3.22250146	
0.6986	0.51745708	Qi	0.6147	0.70203967	Qi	0.4847	1.04482718	Qi	0.5469	0.87064367	Qi	0.6305	0.6654261	Qi	0.7477	0.41946501	Qi	0.7265	0.46096164	Qi	
0.7174	0.4791463	1.31859697	0.6424	0.6384508	1.433224693	0.4862	1.0403694	1.67206349	0.5565	0.84553926	1.62870876	0.6308	0.66473981	1.36253723	0.7882	0.34336344	1.61648035	0.7397	0.43498414	1.361191907	
0.7368	0.44065131		0.6967	0.52138612		0.5113	0.96774988		0.5799	0.78611731		0.6402	0.64339998		0.7927	0.33515028		0.7419	0.43069971		
0.7392	0.43599685		0.7389	0.43654527		0.5902	0.76071774		0.581	0.78338831		0.6534	0.61359645		0.9251	0.11231782		0.7813	0.35604847		
0.7554	0.40468389		0.7773	0.3634535		0.5934	0.7529168		0.5901	0.76709627		0.6868	0.54201347		0.9357	0.09588123		0.7871	0.34537823		
0.764	0.38835217		0.7815	0.35567921		0.5989	0.73966071		0.6038	0.72785118		0.6931	0.5208601		1.051	0.67176206		0.8191	0.28788607		
0.7899	0.3402552		0.8294	0.26985777		0.6087	0.71619067		0.6103	0.7134948		0.7303	0.45343509		1.0569	0.07983821		0.8406	0.25016331		
0.8282	0.27194659		0.832	0.2653242		0.631	0.66428247		0.6385	0.647226		0.7313	0.45146091		1.0905	0.12498871		0.8479	0.23803196		
0.9233	0.11512762		0.9139	0.1299068		0.6501	0.62126119		0.6452	0.63217631		0.7421	0.43031085		1.1182	0.16117689		0.8632	0.21223144		
0.9328	0.10035946		0.9159	0.12673693		0.6552	0.60989758		0.6471	0.62793411		0.7469	0.42100944		1.1264	0.17171779		0.8886	0.17039251		
1.0004	-0.00057696		0.9212	0.11841268		0.669	0.57991698		0.6632	0.59247908		0.8111	0.30204575		1.1719	0.22884753		0.9179	0.12359006		
1.0201	-0.02871034		0.9514	0.07187546		0.6965	0.52180033		0.6757	0.56554046		0.8545	0.22684568		1.1807	0.23964042		0.9357	0.09588123		
1.0552	-0.07751581		0.9569	0.06355939		0.7094	0.49373363		0.7273	0.45937363		0.877	0.18934965		1.1994	0.26231066		0.9776	0.03268353		
1.0653	-0.09125899		0.9673	0.04796429		0.729	0.45600521		0.7277	0.45885804		0.9145	0.12894383		1.2589	0.33216088		1.0319	0.01706658		
1.0682	-0.0951808		0.9762	0.03475105		0.7815	0.35567921		0.7671	0.3252102		0.9511	0.07232045		1.2907	0.3681506		1.0448	0.04935154		
1.1375	-0.18586497		0.9928	0.01042489		0.7992	0.32336878		0.8012	0.31976297		1.1187	0.16182183		1.3267	0.40783873		1.1289	0.17491622		
1.169	-0.22527302		0.9952	0.00694155		0.8437	0.24519592		0.8813	0.18229335		1.1318	0.17861753		1.5514	0.63356535		1.1504	0.20213387		
1.1718	-0.22872442		1.0297	-0.0422372		0.8621	0.21407106		0.8835	0.17869645		1.2587	0.33193166		1.5695	0.65029953		1.1565	0.20976349		
1.1778	-0.23609258		1.059	-0.08270189		0.8633	0.21206431		0.9266	0.10989848		1.2703	0.34516633		1.6176	0.69384903		1.1883	0.2488977		
1.2119	-0.28605072		1.0755	-0.10506664		0.8964	0.15778411		0.9665	0.04515791		1.3329	0.41456504		1.6748	0.743831024		1.2059	0.27010799		
1.2219	-0.28912277		1.1063	-0.14574143		0.9128	0.13162819		0.9794	0.0375586		1.3754	0.45984796		1.7696	0.82341633		1.2512	0.32330968		
1.2534	-0.32584414		1.2608	-0.3343661		0.9219	0.11731684		1.0363	-0.05144128		1.3988	0.48418561		1.814	0.85916719		1.253	0.32538366		
1.2599	-0.33330641		1.2702	-0.34505276		0.9328	0.10035946		1.0452	-0.06377849		1.4174	-0.5032427		1.8988	0.95208031		1.3217	0.40239135		
1.2986	-0.37695393		1.2728	-0.34800028		0.9316	0.01216972		1.067	-0.09355938		1.4329	-0.51893354		1.9195	-0.9407226		1.3601	0.44370898		
1.3367	-0.41862717		1.3136	-0.3935227		1.0299	-0.0425039		1.0869	-0.12021819		1.4418	-0.52786659		1.9479	0.96191148		1.38	0.46466434		
1.3489	-0.43177975		1.3704	-0.45439321		1.1262	-0.17146161		1.107	-0.14665398		1.5296	-0.61314924		1.9656	0.97496152		1.459	0.54497527		
1.3767	-0.46121031		1.3755	-0.45995225		1.1357	-0.18358024		1.1146	-0.15625473		1.5942	-0.67282694		2.0217	-0.10156034		1.6238	0.69938603		
1.4529	-0.53893085		1.3993	-0.4847012		1.2391	-0.3139397		1.1972	-0.25966199		1.6017	-0.67959821		2.0598	-0.10429455		1.6655	0.73594913		
1.4747	-0.56041676		1.407	-0.49261816		1.2897	-0.36703241		1.2397	-0.30998842		1.6536	-0.72560416		2.5013	-0.32266691		1.6801	0.74854077		
1.5137	-0.59807425		1.4245	-0.51905133		1.3413	-0.42362837		1.2665	-0.34084419		1.7135	-0.77693962		2.5991	-0.37800049		1.7118	0.77550759		
1.5309	-0.61437485		1.4311	-0.51712011		1.3976	-0.4829474		1.2805	-0.35670424		1.7447	-0.8029722		2.6177	-0.38828803		1.7552	0.81162857		
1.5364	-0.61954583		1.5022	-0.58079194		1.4445	-0.53056572		1.2925	-0.37016115		1.75	-0.80734809		2.8264	-0.45895298		1.7626	0.81798819		
1.5817	-0.6614704		1.5234	-0.60728966		1.4503	-0.53634682		1.3068	-0.3860151		1.7811	-0.83276148		2.9332	-0.55246231		1.8239	-0.8670193		
1.6055	-0.68031689		1.5509	-0.63310031		1.5178	-0.60197661		1.4671	-0.52566253		1.8165	-0.86115408		3.0073	-0.58845536		1.852	0.88907658		
1.622	-0.69776792		1.5525	-0.6345879		1.5621	-0.64348137		1.5148	-0.59951226		1.8914	-0.91944673		3.069	-0.61775496		1.992	0.99420934		
1.6359	-0.71007856		1.5898	-0.66883616		1.5782	-0.65827448		1.6315	-0.70619031		2.0062	-1.00445694		3.3951	-1.7634931		2.0155	-0.1112923		
1.6835	-0.75145737		1.682	-0.75017136		1.5841	-0.6636578		1.8296	-0.8715209		2.0444	-1.03166877		3.4753	-1.79712232		2.0166	-0.10191639		
1.684	-0.75188578		1.7186	-0.78127219		1.6261	-0.70141005		1.9503	-0.96368791		2.0501	-1.03568552		3.5833	-1.84127322		2.0559	-0.10397613		
1.7156	-0.77870664		1.7556	-0.81155731		1.7749	-0.84389633		2.0677	-1.04801802		2.3653	-1.24021267		3.6084	-1.85134362		2.0793	-0.10560899		
1.7886	-0.83882369		1.8601	-0.95537261		1.843	-0.8204861		2.1398	-1.09746668		2.3965	-1.26091828		3.7059	-1.88890737		2.0993	-0.10698997		
1.7994	-0.84750876		1.9259	-0.9455428		1.8796	-0.91041797		2.1913	-1.13177744		2.5056	-								

PW

PW-F1-51	phi	results	PW-F1-52	phi	results	PW-F1-53	phi	results	PW-F1-54	phi	results	PW-F1-55	phi	results	PW-F1-56	phi	results	PW-F2-51	phi	results	PW-F2-52	phi	results
0.3558	1.49048898	84	0.4961	1.01128858	84	0.2934	1.78904426	84	0.4203	1.25049806	84	0.4283	1.22329607	84	0.4678	1.09602696	84	0.2675	1.90237311	84	0.3599	1.47433192	84
0.4171	1.2612411	0.39000636	0.4991	1.00259071	0.01332264	0.3878	1.44294441	0.73196504	0.4606	1.11844124	-0.11746064	0.4401	1.18341124	0.49923317	0.491	1.02619319	0.35274557	0.4215	1.24638492	0.16546816	0.4154	1.28741616	-0.14145063
0.4353	1.19924523	90	0.534	0.905807	60	0.382	1.38834371	90	0.398	0.79293185	90	0.4903	1.03766627	90	0.5402	0.88842691	90	0.4666	1.11840422	90	0.4413	1.17364481	90
0.5198	0.94369648	-0.7856691	0.5978	0.74225892	-1.31218045	0.403	1.31131717	-0.24660647	0.6279	0.67138761	-1.17907283	0.5191	0.94590761	-0.25526407	0.5347	0.87910983	-0.42215511	0.6153	0.70632188	-1.62450287	0.558	0.76610546	-2.66610579
0.5414	0.8852272	16	0.6558	0.60866705	16	0.4044	1.30613405	16	0.6895	0.5367781	16	0.5402	0.88842694	16	0.5369	0.84450266	16	0.6406	0.64249886	16	0.6773	0.56212384	16
0.5504	0.8614034	-2.37794205	0.6898	0.53574544	-2.72192886	0.4179	1.25875969	-1.75490544	0.6907	0.53386436	-2.06971431	0.5721	0.79936314	-1.02102216	0.5066	0.83494529	-2.62559432	0.6836	0.54877106	-3.53129406	0.6817	0.55278644	-4.20423519
0.5885	0.76487921	Mz	0.703	0.50839911	Mz	0.4425	1.17624809	Mz	0.6988	0.51704411	Mz	0.5748	0.79936314	Mz	0.406	0.72260419	Mz	0.7081	0.49797707	Mz	0.6881	0.53930529	Mz
0.5980	0.7594762	-0.92453493	0.7094	0.49532458	-1.34026156	0.4538	1.15980185	-0.42318229	0.7201	0.47372682	-1.220426	0.5359	0.74903229	-0.25601762	0.6113	0.70880159	-1.07366662	0.7875	0.34466526	-1.66344292	0.7094	0.49532458	-2.33726387
0.6096	0.71405933		0.7334	0.48028083		0.4627	1.11184159		0.7529	0.40946637		0.6232	0.67760493		0.6358	0.65334955		0.7935	0.33169505		0.7736	0.73037177	
0.6179	0.69454885	95	0.5931	1.02371746	95	0.4833	1.04900023	95	0.9325	1.0082352	95	0.6328	0.67622072	95	0.6532	0.61438911	95	0.8308	0.26742462	95	0.7791	0.36011653	95
0.6301	0.66616415	1.1561615	0.5343	0.0980414	0.85397719	0.5009	0.99739705	1.44353072	0.9439	0.08829393	0.86718295	0.6484	0.62503872	1.05374563	0.6876	0.58293921	0.94685256	0.8549	0.28217051	1.12205866	0.8341	0.26170532	1.04872086
0.6413	0.64092327	5	0.5368	0.06418622	5	0.5544	0.85099364	5	0.9402	-0.09653093	5	0.638	0.61307533	5	0.6725	0.57238899	5	0.8621	0.21407106	5	0.9658	0.05020321	5
0.6564	0.60734772	-2.92746664	0.9807	0.0511642	-1.7344425	0.7964	0.23827711	-3.3219	1.0794	-0.20323866	-2.7935556	0.9729	0.57024313	-1.70141647	0.6731	0.5704959	-4.01788793	0.8847	0.19787498	-4.10430195	1.0191	-0.02799539	-4.4593919
0.7905	0.33915973	QI	1.6024	-0.00345629	QI	0.6086	0.7164277	QI	1.1119	-0.13022705	QI	0.6903	0.53470007	QI	0.7097	0.4047146	QI	0.8983	0.15472945	QI	1.0821	-0.11249902	QI
0.8041	0.3145505	1.0023	-0.01200571	1.17872472	0.6284	0.67483817	1.34175258	1.1365	-0.1849612	1.04279628	0.9597	0.52345835	0.79526269	1.09681838	0.7164	0.48115869	1.49681838	0.9057	0.14249363	1.71066337	1.0961	0.13273831	1.85025808
0.8347	0.26068812	1.046	-0.064823	1.046	-0.064823	0.6445	0.63374238	1.1393	-0.181461	1.1393	-0.181461	0.7454	0.42339069	0.7734	0.3707102	0.9164	0.12594957	0.9164	0.12594957	1.1366	0.18472306		
0.8372	0.25635362	1.0877	-0.1217967	1.0877	-0.1217967	0.6529	0.61506085	1.2722	-0.34732255	1.2722	-0.34732255	0.7691	0.3787537	0.7839	0.3512555	0.9365	0.0946483	0.9365	0.0946483	1.2359	0.30559493		
0.8381	0.25405931	1.0996	-0.11897765	1.0996	-0.11897765	0.6665	0.58531327	1.292	-0.39660294	1.292	-0.39660294	0.7788	0.37031717	0.877	0.39148979	0.9644	0.0483702	0.9644	0.0483702	1.2884	0.36133624		
0.894	0.2325675	1.116	-0.21412299	1.116	-0.21412299	0.6732	0.5708809	1.3221	-0.4032379	1.3221	-0.4032379	0.7797	0.35905592	0.8779	0.37876909	0.9818	0.0284987	0.9818	0.0284987	1.315	0.35905594		
0.8877	0.17185444	1.1807	-0.2396402	1.1807	-0.2396402	0.7134	0.48721276	1.326	-0.40707733	1.326	-0.40707733	0.7788	0.37031717	0.877	0.39148979	0.9818	0.0284987	0.9818	0.0284987	1.315	0.35905594		
0.8913	0.16601558	1.1867	-0.24695318	1.1867	-0.24695318	0.7166	0.48075599	1.3512	-0.43423756	1.3512	-0.43423756	0.8132	0.28831536	0.9031	0.14704111	1.0168	0.02403573	1.0168	0.02403573	1.3642	0.44085138		
0.8931	0.16310499	1.2086	-0.2733454	1.2086	-0.2733454	0.7466	0.42158902	1.3763	-0.46079108	1.3763	-0.46079108	0.8198	0.28665368	0.9102	0.14704111	1.0168	0.02403573	1.0168	0.02403573	1.3642	0.44085138		
0.9209	0.11882929	1.2208	-0.2878423	1.2208	-0.2878423	0.7549	0.40563912	1.3876	-0.47258775	1.3876	-0.47258775	0.8314	0.26638309	0.9313	0.10268125	1.081	0.01123657	1.081	0.01123657	1.4479	0.53595745		
1.0071	-0.0102686	1.29931871	-0.0102686	1.29931871	-0.0102686	0.7964	0.40777313	1.4412	-0.51728461	1.4412	-0.51728461	0.8634	0.26638309	0.9313	0.10268125	1.081	0.01123657	1.081	0.01123657	1.4479	0.53595745		
1.0325	-0.04614139	1.3464	-0.44447433	1.3464	-0.44447433	0.7958	0.32551941	1.5364	-0.61945462	1.5364	-0.61945462	0.8634	0.26638309	0.9313	0.10268125	1.081	0.01123657	1.081	0.01123657	1.4479	0.53595745		
1.0517	-0.0727262	1.3862	-0.45227531	1.3862	-0.45227531	0.8226	0.28173464	1.6451	-0.71816921	1.6451	-0.71816921	0.8707	0.19975088	0.9893	0.01551989	1.2197	-0.8652392	1.2197	-0.8652392	1.8635	-0.89600722		
1.0887	-0.12260543	1.3734	-0.457748	1.3734	-0.457748	0.8362	0.25807787	1.6635	-0.7421556	1.6635	-0.7421556	0.8861	0.17413151	1.0215	-0.0306894	1.2367	-0.36049298	1.2367	-0.36049298	1.9477	-0.96176335		
1.1101	-0.15094826	1.4192	-0.50507384	1.4192	-0.50507384	0.8363	0.25790353	1.6778	-0.74606444	1.6778	-0.74606444	0.887	0.17299233	1.1513	-0.20328029	1.2993	-0.37773118	1.2993	-0.37773118	2.0016	-1.00114523		
1.1459	-0.19647869	1.4594	-0.54537075	1.4594	-0.54537075	0.84319	0.24827711	1.7603	-0.76781727	1.7603	-0.76781727	0.8934	0.13784665	1.1715	-0.78357575	1.3553	-0.44880482	1.3553	-0.44880482	2.1004	-0.78050525		
1.1649	-0.2202425	1.468	-0.55384728	1.468	-0.55384728	0.8682	0.20389985	1.7621	-0.81172889	1.7621	-0.81172889	0.9157	0.12051177	1.1881	-0.24865417	1.3575	-0.44049487	1.3575	-0.44049487	2.1563	-1.10545053		
1.1672	-0.2230499	1.5009	-0.5858229	1.5009	-0.5858229	0.9051	0.18438968	1.7626	-0.81172889	1.7626	-0.81172889	0.9449	0.08176575	1.2591	-0.31239006	1.4248	-0.5107551	1.4248	-0.5107551	2.2806	-1.18903137		
1.1853	-0.24525018	1.555	-0.63690919	1.555	-0.63690919	0.9139	0.12898908	1.782	-0.83349029	1.782	-0.83349029	0.9585	0.06149155	1.2995	-0.37795354	1.4329	-0.51933454	1.4329	-0.51933454	2.6819	-1.42324341		
1.2081	-0.2727375	1.6225	-0.69821257	1.6225	-0.69821257	0.9173	0.1245334	1.7883	-0.83967732	1.7883	-0.83967732	0.9731	0.04082302	1.3276	-0.4088078	1.4747	-0.56041768	1.4747	-0.56041768	2.7011	-1.4333493		
1.2411	-0.31161673	1.6922	-0.76889367	1.6922	-0.76889367	0.9174	0.12437614	1.8007	-0.84505067	1.8007	-0.84505067	0.9747	0.03969594	1.3285	-0.40979476	1.5239	-0.60778309	1.5239	-0.60778309	2.7991	-1.48053035		
1.2451	-0.31624894	1.7186	-0.78121279	1.7186	-0.78121279	0.9205	0.11590836	1.8199	-0.86035187	1.8199	-0.86035187	1.0209	-0.0236413	1.3961	-0.41319821	1.6312	-0.7069549	1.6312	-0.7069549	3.02	-1.59930427		
1.2779	-0.35377195	1.749	-0.80652437	1.749	-0.80652437	0.9402	0.08895966	1.8464	-0.88462951	1.8464	-0.88462951	1.033	-0.0460396	1.4495	-0.5355508	1.647	-0.71983447	1.647	-0.71983447	3.03	-1.59930427		
1.2915	-0.36904452	1.7674	-0.82162164	1.7674	-0.82162164	0.9702	0.04364555	1.8693	-0.90256767	1.8693	-0.90256767	1.0358	-0.05074503	1.5372	-0.62029944	1.6621	-0.7300098	1.6621	-0.7300098	3.2563	-1.7021291		
1.3277	-0.40892574	1.7956	-0.84448886	1.7956	-0.84448886	0.9775	0.03785932	1.9345	-0.95152368	1.9345	-0.95152368	1.0398	-0.0563056	1.5765	-0.65671962	1.6728	-0.74225869	1.6728	-0.74225869	3.5672	-1.83477609		
1.3482	-0.43103088	1.8039	-0.85727108	1.8039	-0.85727108	0.9775	0.03281111	1.9419	-0.9574081	1.9419	-0.9574081	1.0516	-0.07523661	1.5846	-0.66411309	1.6794	-0.74360312	1.6794	-0.74360312	3.7631	-1.93170954		
1.3539	-0.46077639	1.7197	-0.12041337	1.7197	-0.12041337	1.0072	-0.1035051	1.9402	-0.96037296	1.9402	-0.96037296	1.056	-0.07606917	1.6029	-0.68067867	1.726	-0.7874258	1.726	-0.7874258	4.784	-2.45373385		
1.4058	-0.4138712	2.0305	-1.02182639	2.0305	-1.02182639	1.0314	-0.04460357	2.0098	-1.00488834	2.0098	-1.00488834	1.075	-0.10433378	1.6059	-0.68317628	2.0431	-1.0307511	2.0431	-1.0307511	5.5167	-2.46178469		

PW-F3-S1				PW-F3-S2				PW-F3-S3				PW-F3-S4				PW-F3-S5				PW-F3-S6				PW-F3-S7				PW-F3-S8				PW-F3-S9				PW-F3-S10				PW-F3-S11				PW-F3-S12				PW-F3-S13				PW-F3-S14				PW-F3-S15				PW-F3-S16				PW-F3-S17				PW-F3-S18				PW-F3-S19				PW-F3-S20				PW-F3-S21				PW-F3-S22				PW-F3-S23				PW-F3-S24				PW-F3-S25				PW-F3-S26				PW-F3-S27				PW-F3-S28				PW-F3-S29				PW-F3-S30				PW-F3-S31				PW-F3-S32				PW-F3-S33				PW-F3-S34				PW-F3-S35				PW-F3-S36				PW-F3-S37				PW-F3-S38				PW-F3-S39				PW-F3-S40				PW-F3-S41				PW-F3-S42				PW-F3-S43				PW-F3-S44				PW-F3-S45				PW-F3-S46				PW-F3-S47				PW-F3-S48				PW-F3-S49				PW-F3-S50				PW-F3-S51				PW-F3-S52				PW-F3-S53				PW-F3-S54				PW-F3-S55				PW-F3-S56				PW-F3-S57				PW-F3-S58				PW-F3-S59				PW-F3-S60				PW-F3-S61				PW-F3-S62				PW-F3-S63				PW-F3-S64				PW-F3-S65				PW-F3-S66				PW-F3-S67				PW-F3-S68				PW-F3-S69				PW-F3-S70				PW-F3-S71				PW-F3-S72				PW-F3-S73				PW-F3-S74				PW-F3-S75				PW-F3-S76				PW-F3-S77				PW-F3-S78				PW-F3-S79				PW-F3-S80				PW-F3-S81				PW-F3-S82				PW-F3-S83				PW-F3-S84				PW-F3-S85				PW-F3-S86				PW-F3-S87				PW-F3-S88				PW-F3-S89				PW-F3-S90				PW-F3-S91				PW-F3-S92				PW-F3-S93				PW-F3-S94				PW-F3-S95				PW-F3-S96				PW-F3-S97				PW-F3-S98				PW-F3-S99				PW-F3-S100				PW-F3-S101				PW-F3-S102				PW-F3-S103				PW-F3-S104				PW-F3-S105				PW-F3-S106				PW-F3-S107				PW-F3-S108				PW-F3-S109				PW-F3-S110				PW-F3-S111				PW-F3-S112				PW-F3-S113				PW-F3-S114				PW-F3-S115				PW-F3-S116				PW-F3-S117				PW-F3-S118				PW-F3-S119				PW-F3-S120				PW-F3-S121				PW-F3-S122				PW-F3-S123				PW-F3-S124				PW-F3-S125				PW-F3-S126				PW-F3-S127				PW-F3-S128				PW-F3-S129				PW-F3-S130				PW-F3-S131				PW-F3-S132				PW-F3-S133				PW-F3-S134				PW-F3-S135				PW-F3-S136				PW-F3-S137				PW-F3-S138				PW-F3-S139				PW-F3-S140				PW-F3-S141				PW-F3-S142				PW-F3-S143				PW-F3-S144				PW-F3-S145				PW-F3-S146				PW-F3-S147				PW-F3-S148				PW-F3-S149				PW-F3-S150				PW-F3-S151				PW-F3-S152				PW-F3-S153				PW-F3-S154				PW-F3-S155				PW-F3-S156				PW-F3-S157				PW-F3-S158				PW-F3-S159				PW-F3-S160				PW-F3-S161				PW-F3-S162				PW-F3-S163				PW-F3-S164				PW-F3-S165				PW-F3-S166				PW-F3-S167				PW-F3-S168				PW-F3-S169				PW-F3-S170				PW-F3-S171				PW-F3-S172				PW-F3-S173				PW-F3-S174				PW-F3-S175				PW-F3-S176				PW-F3-S177				PW-F3-S178				PW-F3-S179				PW-F3-S180				PW-F3-S181				PW-F3-S182				PW-F3-S183				PW-F3-S184				PW-F3-S185				PW-F3-S186				PW-F3-S187				PW-F3-S188				PW-F3-S189				PW-F3-S190				PW-F3-S191				PW-F3-S192				PW-F3-S193				PW-F3-S194				PW-F3-S195				PW-F3-S196				PW-F3-S197				PW-F3-S198				PW-F3-S199				PW-F3-S200				PW-F3-S201				PW-F3-S202				PW-F3-S203				PW-F3-S204				PW-F3-S205				PW-F3-S206				PW-F3-S207				PW-F3-S208				PW-F3-S209				PW-F3-S210				PW-F3-S211				PW-F3-S212				PW-F3-S213				PW-F3-S214				PW-F3-S215				PW-F3-S216				PW-F3-S217				PW-F3-S218				PW-F3-S219				PW-F3-S220				PW-F3-S221				PW-F3-S222				PW-F3-S223				PW-F3-S224				PW-F3-S225				PW-F3-S226				PW-F3-S227				PW-F3-S228				PW-F3-S229				PW-F3-S230				PW-F3-S231				PW-F3-S232				PW-F3-S233				PW-F3-S234				PW-F3-S235				PW-F3-S236				PW-F3-S237				PW-F3-S238				PW-F3-S239				PW-F3-S240				PW-F3-S241				PW-F3-S242				PW-F3-S243				PW-F3-S244				PW-F3-S245				PW-F3-S246				PW-F3-S247				PW-F3-S248				PW-F3-S249				PW-F3-S250				PW-F3-S251				PW-F3-S252				PW-F3-S253				PW-F3-S254				PW-F3-S255				PW-F3-S256				PW-F3-S257				PW-F3-S258				PW-F3-S259				PW-F3-S260				PW-F3-S261				PW-F3-S262				PW-F3-S263				PW-F3-S264				PW-F3-S265				PW-F3-S266				PW-F3-S267				PW-F3-S268				PW-F3-S269				PW-F3-S270				PW-F3-S271		
----------	--	--	--	----------	--	--	--	----------	--	--	--	----------	--	--	--	----------	--	--	--	----------	--	--	--	----------	--	--	--	----------	--	--	--	----------	--	--	--	-----------	--	--	--	-----------	--	--	--	-----------	--	--	--	-----------	--	--	--	-----------	--	--	--	-----------	--	--	--	-----------	--	--	--	-----------	--	--	--	-----------	--	--	--	-----------	--	--	--	-----------	--	--	--	-----------	--	--	--	-----------	--	--	--	-----------	--	--	--	-----------	--	--	--	-----------	--	--	--	-----------	--	--	--	-----------	--	--	--	-----------	--	--	--	-----------	--	--	--	-----------	--	--	--	-----------	--	--	--	-----------	--	--	--	-----------	--	--	--	-----------	--	--	--	-----------	--	--	--	-----------	--	--	--	-----------	--	--	--	-----------	--	--	--	-----------	--	--	--	-----------	--	--	--	-----------	--	--	--	-----------	--	--	--	-----------	--	--	--	-----------	--	--	--	-----------	--	--	--	-----------	--	--	--	-----------	--	--	--	-----------	--	--	--	-----------	--	--	--	-----------	--	--	--	-----------	--	--	--	-----------	--	--	--	-----------	--	--	--	-----------	--	--	--	-----------	--	--	--	-----------	--	--	--	-----------	--	--	--	-----------	--	--	--	-----------	--	--	--	-----------	--	--	--	-----------	--	--	--	-----------	--	--	--	-----------	--	--	--	-----------	--	--	--	-----------	--	--	--	-----------	--	--	--	-----------	--	--	--	-----------	--	--	--	-----------	--	--	--	-----------	--	--	--	-----------	--	--	--	-----------	--	--	--	-----------	--	--	--	-----------	--	--	--	-----------	--	--	--	-----------	--	--	--	-----------	--	--	--	-----------	--	--	--	-----------	--	--	--	-----------	--	--	--	-----------	--	--	--	-----------	--	--	--	-----------	--	--	--	-----------	--	--	--	-----------	--	--	--	-----------	--	--	--	-----------	--	--	--	-----------	--	--	--	-----------	--	--	--	-----------	--	--	--	-----------	--	--	--	-----------	--	--	--	-----------	--	--	--	-----------	--	--	--	-----------	--	--	--	-----------	--	--	--	-----------	--	--	--	-----------	--	--	--	-----------	--	--	--	------------	--	--	--	------------	--	--	--	------------	--	--	--	------------	--	--	--	------------	--	--	--	------------	--	--	--	------------	--	--	--	------------	--	--	--	------------	--	--	--	------------	--	--	--	------------	--	--	--	------------	--	--	--	------------	--	--	--	------------	--	--	--	------------	--	--	--	------------	--	--	--	------------	--	--	--	------------	--	--	--	------------	--	--	--	------------	--	--	--	------------	--	--	--	------------	--	--	--	------------	--	--	--	------------	--	--	--	------------	--	--	--	------------	--	--	--	------------	--	--	--	------------	--	--	--	------------	--	--	--	------------	--	--	--	------------	--	--	--	------------	--	--	--	------------	--	--	--	------------	--	--	--	------------	--	--	--	------------	--	--	--	------------	--	--	--	------------	--	--	--	------------	--	--	--	------------	--	--	--	------------	--	--	--	------------	--	--	--	------------	--	--	--	------------	--	--	--	------------	--	--	--	------------	--	--	--	------------	--	--	--	------------	--	--	--	------------	--	--	--	------------	--	--	--	------------	--	--	--	------------	--	--	--	------------	--	--	--	------------	--	--	--	------------	--	--	--	------------	--	--	--	------------	--	--	--	------------	--	--	--	------------	--	--	--	------------	--	--	--	------------	--	--	--	------------	--	--	--	------------	--	--	--	------------	--	--	--	------------	--	--	--	------------	--	--	--	------------	--	--	--	------------	--	--	--	------------	--	--	--	------------	--	--	--	------------	--	--	--	------------	--	--	--	------------	--	--	--	------------	--	--	--	------------	--	--	--	------------	--	--	--	------------	--	--	--	------------	--	--	--	------------	--	--	--	------------	--	--	--	------------	--	--	--	------------	--	--	--	------------	--	--	--	------------	--	--	--	------------	--	--	--	------------	--	--	--	------------	--	--	--	------------	--	--	--	------------	--	--	--	------------	--	--	--	------------	--	--	--	------------	--	--	--	------------	--	--	--	------------	--	--	--	------------	--	--	--	------------	--	--	--	------------	--	--	--	------------	--	--	--	------------	--	--	--	------------	--	--	--	------------	--	--	--	------------	--	--	--	------------	--	--	--	------------	--	--	--	------------	--	--	--	------------	--	--	--	------------	--	--	--	------------	--	--	--	------------	--	--	--	------------	--	--	--	------------	--	--	--	------------	--	--	--	------------	--	--	--	------------	--	--	--	------------	--	--	--	------------	--	--	--	------------	--	--	--	------------	--	--	--	------------	--	--	--	------------	--	--	--	------------	--	--	--	------------	--	--	--	------------	--	--	--	------------	--	--	--	------------	--	--	--	------------	--	--	--	------------	--	--	--	------------	--	--	--	------------	--	--	--	------------	--	--	--	------------	--	--	--	------------	--	--	--	------------	--	--	--	------------	--	--	--	------------	--	--	--	------------	--	--	--	------------	--	--	--	------------	--	--	--	------------	--	--	--	------------	--	--	--	------------	--	--	--	------------	--	--	--	------------	--	--	--	------------	--	--	--	------------	--	--	--	------------	--	--	--	------------	--	--	--	------------	--	--	--	------------	--	--	--	------------	--	--	--	------------	--	--	--	------------	--	--	--	------------	--	--	--	------------	--	--	--	------------	--	--	--	------------	--	--	--	------------	--	--	--	------------	--	--	--	------------	--	--	--	------------	--	--	--	------------	--	--	--	------------	--	--	--	------------	--	--	--	------------	--	--	--	------------	--	--	--	------------	--	--	--	------------	--	--	--	------------	--	--	--	------------	--	--	--	------------	--	--	--	------------	--	--	--	------------	--	--

274

PT

PT-F1-51				PT-F1-52				PT-F1-54				PT-F1-53-lat10				PT-F1-53-lat10				PT-F1-54-lat10				PT-F1-55-lat10				PT-F2-51										
mm	phi	results	mm	phi	results	mm	phi	results	mm	phi	results	mm	phi	results	mm	phi	results	mm	phi	results	mm	phi	results	mm	phi	results	mm	phi	results	mm	phi	results						
0.3097	1.69104241	84	0.3106	1.686856	84	0.2885	1.79334161	84	0.2526	1.98505667	84	0.2599	1.99479875	84	0.2544	1.97481272	84	0.2996	1.71887576	84	0.2456	2.02560004	84	0.2596	1.71887576	84	0.2456	2.02560004	84	0.2596	1.71887576	84						
0.4344	1.20289382	0.79159026	0.3151	1.57772307	0.8822984	0.3139	1.56249862	0.3233	1.77446126	1.25423002	0.2038	1.71974176	1.16746307	0.271	1.88186193	1.32205144	0.3065	1.70026209	1.0819462	0.2504	1.99796764	1.29757264	0.3131	1.6704081	0.298	0.298	1.73155175	0.298	0.298	1.73155175	0.298							
0.4519	1.14591485	90	0.3871	1.36921021	60	0.3436	1.54118902	60	0.2945	1.78046544	90	0.3165	1.65976864	90	0.2862	1.80488916	90	0.3213	1.6704081	0.298	0.298	1.73155175	0.298	0.298	1.73155175	0.298	0.298	1.73155175	0.298	0.298	1.73155175	0.298						
0.4639	1.10810488	-0.91187786	0.3878	1.36660733	0.1154204	0.3531	1.50183857	0.39449121	0.2959	1.76085504	0.42040467	0.3211	1.63891517	0.38495106	0.3215	1.63709551	0.60078386	0.3574	1.48437591	0.40055661	0.3007	1.73155857	0.55531145	0.3007	1.73155857	0.55531145	0.3007	1.73155857	0.55531145	0.3007	1.73155857	0.55531145						
0.4714	1.08496716	16	0.4093	1.28875853	16	0.3634	1.48603572	16	0.3217	1.62725697	16	0.3318	1.59160075	16	0.3264	1.61275318	16	0.4068	1.29759744	16	0.3268	1.60582804	16	0.3268	1.60582804	16	0.3268	1.60582804	16	0.3268	1.60582804	16	0.3268	1.60582804	16			
0.4745	1.07551091	-3.3901372	0.41	1.28623931	-0.96905393	0.3729	1.42312726	-0.64761347	0.3315	1.59290575	-0.96434246	0.3531	1.50183857	-0.89497771	0.3303	1.59813761	-0.51116036	0.4093	1.28875853	-0.86883196	0.3337	1.58336302	-0.4436305	0.3337	1.58336302	-0.4436305	0.3337	1.58336302	-0.4436305	0.3337	1.58336302	-0.4436305	0.3337	1.58336302	-0.4436305			
0.486	1.04096298	Mz	0.4238	1.23853401	Mz	0.3809	1.37768893	Mz	0.3178	1.56574552	Mz	0.3589	1.47833367	Mz	0.3403	1.55510779	Mz	0.4168	1.26256214	Mz	0.3402	1.55510779	Mz	0.4168	1.26256214	Mz	0.3402	1.55510779	Mz	0.4168	1.26256214	Mz	0.3402	1.55510779	Mz			
0.4863	1.04007271	-1.1701416	0.4234	1.20555124	0.00955616	0.4215	1.24638492	0.26098269	0.3701	1.45400083	0.23676408	0.3727	1.42590123	0.21914547	0.3537	1.45516683	0.47055898	0.4235	1.22626255	0.20422361	0.3511	1.51003253	0.4697512	0.3511	1.51003253	0.4697512	0.3511	1.51003253	0.4697512	0.3511	1.51003253	0.4697512	0.3511	1.51003253	0.4697512			
0.5069	0.98021864	0.4447	1.1690858	0.4447	1.1690858	0.4275	1.2259931	0.3952	1.33931882	0.3701	1.45400083	0.23676408	0.3727	1.42590123	0.21914547	0.3537	1.45516683	0.47055898	0.4235	1.22626255	0.20422361	0.3511	1.51003253	0.4697512	0.3511	1.51003253	0.4697512	0.3511	1.51003253	0.4697512	0.3511	1.51003253	0.4697512	0.3511	1.51003253	0.4697512		
0.5074	0.9797963	95	0.4474	1.10335302	95	0.4317	1.21188875	95	0.3953	1.33896882	95	0.3814	1.39061149	95	0.3689	1.43868614	95	0.4575	1.12041861	95	0.358	1.48155557	95	0.358	1.48155557	95	0.358	1.48155557	95	0.358	1.48155557	95	0.358	1.48155557	95	0.358	1.48155557	95
0.5131	0.96267993	1.24658462	0.4718	1.08374351	1.45775011	0.4657	1.10251789	1.57584423	0.3998	1.32168844	1.7814452	0.3952	1.33931882	1.72094828	0.3734	1.42141515	1.78118802	0.4605	1.1371748	1.5711833	0.3802	1.39315776	1.82512068	0.3802	1.39315776	1.82512068	0.3802	1.39315776	1.82512068	0.3802	1.39315776	1.82512068	0.3802	1.39315776	1.82512068	0.3802	1.39315776	1.82512068
0.519	0.9463555	5	0.499	1.0028798	5	0.4657	1.10251789	5	0.4039	1.30791889	5	0.4166	1.2625457	5	0.3781	1.40314838	5	0.4609	1.09880521	5	0.3802	1.39315776	5	0.3802	1.39315776	5	0.3802	1.39315776	5	0.3802	1.39315776	5	0.3802	1.39315776	5	0.3802	1.39315776	5
0.5314	0.9647026	-4.39228028	0.5101	0.97119378	-1.77584879	0.4654	1.10251789	-1.5118009	0.4096	1.2928697	-2.29124568	0.4322	1.21021379	-2.87909478	0.3998	1.39661038	-1.72722665	0.4742	1.07642333	-2.55200965	0.4045	1.3657775	-1.5634271	0.4045	1.3657775	-1.5634271	0.4045	1.3657775	-1.5634271	0.4045	1.3657775	-1.5634271	0.4045	1.3657775	-1.5634271	0.4045	1.3657775	-1.5634271
0.5398	0.8894958	Q	0.5596	0.81572505	Q	0.482	1.05288604	Q	0.4146	1.27197124	Q	0.4313	1.20651885	Q	0.4119	1.27962315	Q	0.4808	1.05648226	Q	0.4113	1.2726118	Q	0.4113	1.2726118	Q	0.4113	1.2726118	Q	0.4113	1.2726118	Q	0.4113	1.2726118	Q	0.4113	1.2726118	Q
0.55	0.86248918	1.89980533	0.5637	0.82699353	0.95277734	0.488	1.05301819	0.88874597	0.437	1.19438471	1.1717175	0.4639	1.10810488	1.21258642	0.4314	1.26741616	0.9901779	0.4877	1.03592536	1.11267074	0.4113	1.2670689	0.94871712	0.4113	1.2670689	0.94871712	0.4113	1.2670689	0.94871712	0.4113	1.2670689	0.94871712	0.4113	1.2670689	0.94871712	0.4113	1.2670689	0.94871712
0.5706	0.8094415	0.584	0.77595316	0.4921	1.02296793	0.4461	1.1645531	0.4645	1.10624014	0.418	1.25841451	0.4891	1.0317899	0.4185	1.25841451	0.4891	1.0317899	0.4185	1.25841451	0.4891	1.0317899	0.4185	1.25841451	0.4891	1.0317899	0.4185	1.25841451	0.4891	1.0317899	0.4185	1.25841451	0.4891	1.0317899	0.4185	1.25841451	0.4891	1.0317899	0.4185
0.571	0.80843051	0.5888	0.76414396	0.5003	0.99912619	0.4711	1.08588538	0.4711	1.08588538	0.4711	1.08588538	0.4711	1.08588538	0.4711	1.08588538	0.4711	1.08588538	0.4711	1.08588538	0.4711	1.08588538	0.4711	1.08588538	0.4711	1.08588538	0.4711	1.08588538	0.4711	1.08588538	0.4711	1.08588538	0.4711	1.08588538	0.4711	1.08588538	0.4711	1.08588538	0.4711
0.5724	0.80489762	0.6217	0.6857032	0.5089	0.97453766	0.485	1.12773417	0.485	1.12773417	0.485	1.12773417	0.485	1.12773417	0.485	1.12773417	0.485	1.12773417	0.485	1.12773417	0.485	1.12773417	0.485	1.12773417	0.485	1.12773417	0.485	1.12773417	0.485	1.12773417	0.485	1.12773417	0.485	1.12773417	0.485	1.12773417	0.485	1.12773417	0.485
0.6117	0.66288292	0.6111	0.66405386	0.5166	0.95872329	0.4605	1.11871748	0.4605	1.11871748	0.4605	1.11871748	0.4605	1.11871748	0.4605	1.11871748	0.4605	1.11871748	0.4605	1.11871748	0.4605	1.11871748	0.4605	1.11871748	0.4605	1.11871748	0.4605	1.11871748	0.4605	1.11871748	0.4605	1.11871748	0.4605	1.11871748	0.4605	1.11871748	0.4605	1.11871748	0.4605
0.631	0.65971702	0.6414	0.64069832	0.532	0.91045415	0.4669	1.09805221	0.5123	0.96493104	0.4304	1.21623973	0.5185	0.94757609	0.4524	1.1431349	0.5185	0.94757609	0.4524	1.1431349	0.5185	0.94757609	0.4524	1.1431349	0.5185	0.94757609	0.4524	1.1431349	0.5185	0.94757609	0.4524	1.1431349	0.5185	0.94757609	0.4524	1.1431349	0.5185	0.94757609	0.4524
0.6354	0.65425477	0.6511	0.61904372	0.5659	0.82137401	0.467	1.09849625	0.5202	0.94285372	0.4352	1.20023939	0.5252	0.92505332	0.4644	1.10655076	0.5252	0.92505332	0.4644	1.10655076	0.5252	0.92505332	0.4644	1.10655076	0.5252	0.92505332	0.4644	1.10655076	0.5252	0.92505332	0.4644	1.10655076	0.5252	0.92505332	0.4644	1.10655076	0.5252	0.92505332	0.4644
0.6424	0.6384508	0.6599	0.59967561	0.5772	0.78285009	0.4802	1.05828374	0.5259	0.92713176	0.4436	1.17268581	0.5288	0.91918184	0.467	1.09849625	0.5288	0.91918184	0.467	1.09849625	0.5288	0.91918184	0.467	1.09849625	0.5288	0.91918184	0.467	1.09849625	0.5288	0.91918184	0.467	1.09849625	0.5288	0.91918184	0.467	1.09849625	0.5288	0.91918184	0.467
0.6538	0.61307353	0.6	0.6599457	0.5778	0.7913512	0.4818	1.05248479	0.535	0.90238157	0.4481	1.15809757	0.53	0.91592799	0.4725	1.08106462	0.53	0.91592799	0.4725	1.08106462	0.53	0.91592799	0.4725	1.08106462	0.53	0.91592799	0.4725	1.08106462	0.53	0.91592799	0.4725	1.08106462	0.53	0.91592799	0.4725	1.08106462	0.53	0.91592799	0.4725
0.6812	0.5338488	0.6812	0.5338488	0.6812	0.5338488	0.6812	0.5338488	0.6812	0.5338488	0.6812	0.5338488	0.6812	0.5338488	0.6812	0.5338488	0.6812	0.5338488	0.6812	0.5338488	0.6812	0.5338488	0.6812	0.5338488	0.6812	0.5338488	0.6812	0.5338488	0.6812	0.5338488	0.6812	0.5338488	0.6812	0.5338488	0.6812	0.5338488	0.6812	0.5338488	0.6812
0.6962	0.51870316	0.6806	0.5511625	0.6172	0.69618415	0.4946	1.01565727	0.5491	0.8642649	0.4711	1.08588538	0.5498	0.8801389	0.4929	1.0260448	0.5498	0.8801389	0.4929	1.0260448	0.5498	0.8801389	0.4929	1.0260448	0.5498	0.8801389	0.4929	1.0260448	0.5498	0.8801389	0.4929	1.0260448	0.5498	0.8801389	0.4929	1.0260448	0.5498	0.8801389	0.4929
0.7487	0.41753681	0.6837	0.548560																																			

PT-F2-52	mm	phi	results	PT-F2-53	mm	phi	results	PT-F2-54	mm	phi	results	PT-F2-55	mm	phi	results	PT-F2-56	mm	phi	results	PT-F2-58	mm	phi	results	PT-F2-59	mm	phi	results	
0.2954	1.75924339			0.2544	1.97481272			0.2191	2.19032009			0.121	3.04689528			0.1089	3.19889709			0.1476	2.76021203			0.126	2.98847909			
0.3253	1.62014357		84	0.2581	1.95398143			0.2575	1.95733911			0.1561	2.6794349			0.1635	2.61261536			0.1574	2.66746999		84	0.1846	2.43750493		84	
0.3501	1.51414823			0.3152	1.66564647		50	0.2986	1.74369918		50	0.1948	2.35991446		50	0.1814	2.46273281		50	0.2091	2.25771594		50	0.1893	2.40123138		50	
0.3829	1.38494872		0.14760607	0.3311	1.5946476		0.4422784	0.3055	1.69966426		0.51020703	0.2057	2.28136701		0.75639492	0.1191	2.37109718		0.71065779	0.2559	1.96631132		0.78024814		0.2077	2.2674077		1.02895102
0.4269	1.22801955		16	0.3383	1.56361149		16	0.3372	1.61174172		16	0.2287	2.12345173		16	0.2384	2.06853673		16	0.2636	1.92904486		16	0.2118	2.23926657		16	
0.4391	1.18756852		-0.857926	0.3387	1.5619069		-0.49006172	0.3558	1.49084898		-0.57354566	0.2377	2.07276866		-1.26425998	0.2799	1.83700107		-0.40810361	0.2699	1.88948714		-0.07283549		0.2228	2.16616054		-0.23613781
0.4414	1.17983149		Mz	0.3472	1.52614824		Mz	0.3589	1.47833367		Mz	0.2393	2.06309025		Mz	0.2835	1.81856398		Mz	0.2722	1.87724515		Mz	0.2305	2.11714344		Mz	
0.4592	1.12279596		0.05409938	0.3531	1.50183587		0.40478394	0.3704	1.43283188		0.39237953	0.2593	1.94728942		0.37659125	0.2876	1.79784921		0.63310502	0.2912	1.77990269		0.77648195		0.2463	2.02145437		0.85773136
0.4846	1.04512485			0.3577	1.48316543			0.3714	1.42894219			0.2648	1.91700876			0.3001	1.73647008			0.2953	1.75973186			0.2472	2.0162323			
0.4972	1.00809327		95	0.3586	1.47954009		95	0.3802	1.39515776		95	0.2943	1.76462563		95	0.3053	1.71168603		95	0.3059	1.70885354		95	0.26	1.94340004		95	
0.508	0.97709133		1.50130069	0.3604	1.47231163		1.75053998	0.3913	1.35364154		1.83994867	0.2949	1.76168737		2.49921307	0.3207	1.64068987		2.54321576	0.31	1.68964559		2.31615483		0.2687	1.85991574		2.46676633
0.5135	0.96155569		5	0.3699	1.43478066		5	0.4059	1.30079275		5	0.3001	1.73647009		5	0.3253	1.62014357		5	0.3287	1.60514306		5	0.2785	1.84423517		5	
0.5173	0.95091886		-2.01435467	0.3807	1.39326174		-1.50043867	0.4219	1.24501648		-1.62014961	0.3095	1.69197438		-3.56068484	0.3337	1.58336302		-1.62051987	0.3311	1.5946476		-0.65060834		0.2934	1.76904426		-1.44812626
0.5307	0.91402382		Qi	0.393	1.34738739		Qi	0.4307	1.21523449		Qi	0.3173	1.65066657		Qi	0.3473	1.52573278		Qi	0.3327	1.5876928		Qi	0.3033	1.72118804		Qi	
0.5498	0.86301389		0.96531107	0.4021	1.31436264		0.93062174	0.4357	1.19858284		0.97776304	0.3174	1.65561196		1.64364105	0.3476	1.52448712		1.13208515	0.3371	1.5687382		0.87322674		0.305	1.71310436		1.09729521
0.5554	0.84839374			0.4025	1.31292821			0.4424	1.17656644			0.3489	1.51910165			0.3512	1.50962248			0.3416	1.54969701			0.312	1.68036785			
0.5775	0.79210045			0.439	1.18769711			0.4463	1.16390444			0.3514	1.50880114			0.3702	1.43361107			0.3435	1.54361049			0.3269	1.61306508			
0.5925	0.75510655			0.441	1.18113945			0.4667	1.09942333			0.3632	1.46115153			0.3774	1.42894219			0.3469	1.52739934			0.3293	1.60251203			
0.6185	0.69314084			0.45	1.15199335			0.4698	1.08987216			0.3833	1.38344024			0.3726	1.42428837			0.3513	1.50921175			0.3295	1.60163608			
0.6196	0.69058511			0.4599	1.12059869			0.4924	1.02208869			0.3853	1.37594927			0.3784	1.40200415			0.3583	1.48074753			0.3312	1.59421194			
0.6221	0.6847758			0.4926	1.02150283			0.4942	1.01682448			0.3944	1.34252719			0.3848	1.37780764			0.3652	1.45322904			0.3318	1.59160075			
0.6361	0.65266899			0.4971	1.00838346			0.4958	1.01216126			0.4047	1.30506421			0.3989	1.35918251			0.3656	1.45164975			0.3397	1.5576537			
0.6449	0.63284727			0.4998	1.0005867			0.498	1.00577385			0.4047	1.30506421			0.391	1.35474803			0.3825	1.38645662			0.3564	1.48841817			
0.6838	0.54834903			0.503	0.99136131			0.5067	0.98078797			0.4167	1.26290831			0.4069	1.29724284			0.3862	1.37256832			0.3612	1.46911778			
0.6938	0.52740379			0.5135	0.96155569			0.5087	0.97510475			0.4245	1.23615309			0.4317	1.21188875			0.3952	1.33933382			0.3704	1.43283188			
0.6962	0.52242186			0.5143	0.95930983			0.5143	0.96493104			0.4342	1.20355819			0.4394	1.18638319			0.3952	1.33933382			0.372	1.42661341			
0.6973	0.52014421			0.5312	0.91266523			0.5143	0.95930983			0.4466	1.16293501			0.461	1.1171519			0.4044	1.30613405			0.3723	1.42545402			
0.701	0.51250923			0.534	0.9058007			0.5188	0.94674161			0.4468	1.16228908			0.4645	1.10624014			0.4145	1.27054525			0.3733	1.42158056			
0.718	0.47794021			0.5377	0.89511905			0.5295	0.91728965			0.4482	1.15777565			0.4652	1.10406766			0.4145	1.27054525			0.3787	1.40086083			
0.7225	0.46892654			0.5462	0.8724914			0.537	0.89699842			0.4517	1.14655348			0.4657	1.10251789			0.4395	1.1860549			0.3795	1.39781639			
0.7354	0.43439517			0.553	0.85921006			0.5392	0.89110006			0.4794	1.06089922			0.4664	1.100351			0.4526	1.13181084			0.3841	1.38043446			
0.7388	0.43674005			0.5808	0.78388001			0.5597	0.83726727			0.4836	1.04810499			0.4769	1.06823228			0.4553	1.13501604			0.3933	1.34628652			
0.7408	0.43284034			0.5845	0.77471852			0.5645	0.79660415			0.4827	1.02120999			0.4779	1.06521032			0.4575	1.13314661			0.3959	1.33678072			
0.7518	0.4115757			0.5923	0.75539692			0.5802	0.78537116			0.4943	1.01653259			0.4835	1.04840334			0.4613	1.11621336			0.4017	1.31579851			
0.7577	0.40029796			0.5959	0.74685153			0.5847	0.77422496			0.4979	1.00606357			0.4871	1.03770134			0.4715	1.08466115			0.4037	1.30863444			
0.7614	0.3932702			0.5961	0.74636741			0.5886	0.76463409			0.4981	1.00548418			0.4885	1.03356079			0.4741	1.0767272			0.4067	1.29595213			
0.7691	0.3787537			0.6018	0.73283779			0.5943	0.75073036			0.513	0.96296112			0.5061	0.98249731			0.4754	1.07277712			0.4103	1.28523807			
0.7743	0.36903233			0.602	0.7215842			0.6117	0.70909782			0.5135	0.96155569			0.5236	0.9334551			0.4772	1.06732502			0.4116	1.28067428			
0.7747	0.36828724			0.6069	0.72046318			0.6322	0.66154146			0.5135	0.96155569			0.5278	0.92192895			0.478	1.06490847			0.413	1.27577552			
0.7749	0.36791484			0.6187	0.6928822			0.6352	0.65471165			0.524	0.9323534			0.5331	0.90751424			0.492	1.0236113			0.4136	1.27368114			
0.7772	0.36363912			0.6208	0.68779372			0.6423	0.6386754			0.527	0.92411731			0.5332	0.85411971			0.4947	1.01536561			0.4206	1.24946868			
0.7943	0.33224122			0.6267	0.6714474			0.6425	0.63822624			0.5392	0.89110006			0.5559	0.84709555			0.5042	0.98792362			0.4215	1.24683492			
0.8174	0.29083839			0.6422	0.63890003			0.6658	0.58683426			0.5414	0.88522572			0.5568	0.84476174			0.5112	0.96803207			0.4414	1.17983149			
0.8175	0.29070691			0.6496	0.6223712			0.6701	0.57754688			0.5582	0.84113886			0.5753	0.79760688			0.5353	0.90157282			0.4516	1.14687291			
0.827	0.27403845			0.6561	0.60800723			0.6716	0.57432101			0.5682	0.81552237			0.5802	0.78537116			0.5476	0.8687983			0.4535	1.1408159			
0.8412	0.24947713			0.658	0.6038354			0.6758	0.56532696			0.5702	0.8104552			0.5804	0.78487494			0.5605	0.83520666			0.4682	1.0947399			
0.8453	0.24246259			0.689	0.53741957			0.6827	0.55067169			0.571	0.80844051			0.5811	0.78263857			0.5622	0.83083761			0.4714	1.08494716			
0.8482	0.237521			0.6902	0.5349091			0.6838	0.54834903			0.5853	0.77274528			0.5946	0.75900229			0.5602	0.82069041							

PM

PM-F5-1	pmi	results	PM-F5-1	pmi	results	PM-F5-2	pmi	results	PM-F5-3	pmi	results	PM-F5-4	pmi	results	PM-F5-6	pmi	results	PM-F5-6	pmi	results		
0.3516	1.50798027		0.4	0.316	1.6618948	84	0.7353	1.41387185	84	6.2103	2.4372022	84	0.3175	1.60531575	84	0.1464	2.7718891	84	0.239	2.60490001		
0.3517	0.427396	0.35483273	0.3911	0.432	0.35678414	0.2681846	0.461	1.645511	0.45397252	0.3911	0.3564154	0.2681846	0.461	1.645511	0.45397252	0.3911	0.3564154	0.2681846	0.461	1.645511		
0.5186	0.95287239	50	0.4552	1.13541791	50	0.4565	1.13510367	50	0.4412	1.27902294	50	0.3352	1.50043654	50	0.3507	1.51677885	50	0.2382	1.29257232	50	0.4835	1.18943119
0.5217	0.95175756	-0.88455459	0.6586	0.60252049	-2.559483	0.4066	1.1180422	-1.1169364	0.4438	1.19825176	-2.8217566	0.4269	1.22801955	-0.53228079	0.3512	1.50962248	-2.0097785	0.383	1.38457199	-0.63809699	0.4828	1.05049353
0.5105	0.94202196	16	0.6901	0.95311814	16	0.4816	1.054008379	16	0.5901	1.7069226	16	0.3866	1.42008884	16	0.3666	1.44770907	16	0.4171	1.62152111	16	0.4846	1.05142485
0.5325	0.90913888	-2.02447545	0.8307	0.62759828	-4.5003127	0.5235	0.97128965	-4.9721295	0.6047	0.72738944	-4.5045332	0.5036	0.98964144	-2.11982378	0.4007	1.35178851	-3.79125484	0.4242	1.2428348	-2.9514854	0.4855	1.0442748
0.5325	0.90913888	-2.02447545	0.8307	0.62759828	-4.5003127	0.5235	0.97128965	-4.9721295	0.6047	0.72738944	-4.5045332	0.5036	0.98964144	-2.11982378	0.4007	1.35178851	-3.79125484	0.4242	1.2428348	-2.9514854	0.4855	1.0442748
0.5325	0.90913888	-2.02447545	0.8307	0.62759828	-4.5003127	0.5235	0.97128965	-4.9721295	0.6047	0.72738944	-4.5045332	0.5036	0.98964144	-2.11982378	0.4007	1.35178851	-3.79125484	0.4242	1.2428348	-2.9514854	0.4855	1.0442748
0.5325	0.90913888	-2.02447545	0.8307	0.62759828	-4.5003127	0.5235	0.97128965	-4.9721295	0.6047	0.72738944	-4.5045332	0.5036	0.98964144	-2.11982378	0.4007	1.35178851	-3.79125484	0.4242	1.2428348	-2.9514854	0.4855	1.0442748
0.5325	0.90913888	-2.02447545	0.8307	0.62759828	-4.5003127	0.5235	0.97128965	-4.9721295	0.6047	0.72738944	-4.5045332	0.5036	0.98964144	-2.11982378	0.4007	1.35178851	-3.79125484	0.4242	1.2428348	-2.9514854	0.4855	1.0442748
0.5325	0.90913888	-2.02447545	0.8307	0.62759828	-4.5003127	0.5235	0.97128965	-4.9721295	0.6047	0.72738944	-4.5045332	0.5036	0.98964144	-2.11982378	0.4007	1.35178851	-3.79125484	0.4242	1.2428348	-2.9514854	0.4855	1.0442748
0.5325	0.90913888	-2.02447545	0.8307	0.62759828	-4.5003127	0.5235	0.97128965	-4.9721295	0.6047	0.72738944	-4.5045332	0.5036	0.98964144	-2.11982378	0.4007	1.35178851	-3.79125484	0.4242	1.2428348	-2.9514854	0.4855	1.0442748
0.5325	0.90913888	-2.02447545	0.8307	0.62759828	-4.5003127	0.5235	0.97128965	-4.9721295	0.6047	0.72738944	-4.5045332	0.5036	0.98964144	-2.11982378	0.4007	1.35178851	-3.79125484	0.4242	1.2428348	-2.9514854	0.4855	1.0442748
0.5325	0.90913888	-2.02447545	0.8307	0.62759828	-4.5003127	0.5235	0.97128965	-														

PM-F7-50	mm	PM-F7-51	mm	PM-F7-52	mm	PM-F7-53	mm	PM-F7-54	mm	PM-F7-55	mm	PM-F7-56	mm	PM-F7-57	mm	PM-F7-58	mm	PM-F7-59	mm	PM-F7-60	mm		
results	results	results	results	results	results	results	results	results	results	results	results	results	results	results	results	results	results	results	results	results			
0.3841	1.38034346	84	0.3358	2.08434675	84	0.1248	8.05238477	84	0.2645	1.91646415	84	0.1764	2.50305618	84	0.0616	3.61525646	84	0.1966	2.34666493	84	0.1032	3.23645741	84
0.4015	1.31651697	0.8258493	0.2447	2.03089682	1.03519309	0.1684	2.57001422	1.81293993	0.2852	1.80993881	1.43357736	0.2331	2.10096132	1.11016839	0.0855	3.54790176	2.45319348	0.2405	2.05587781	1.53249137	0.1089	3.1889709	2.04392591
0.4068	1.2983008	50	0.3215	1.8709551	50	0.1716	2.54285704	50	0.2881	1.7934325	50	0.2821	1.97891516	50	0.0855	3.54790176	50	0.2597	1.94065063	50	0.1124	3.15225939	50
0.4374	1.19296479	0.17809966	0.3312	1.59421194	0.27671553	0.213	2.2310558	0.85014514	0.2985	1.74418241	0.81636897	0.2544	1.97481272	0.12784094	0.0903	3.46910086	0.90052225	0.262	1.93234494	0.60845611	0.1252	2.97966818	1.22193156
0.448	1.16487453	16	0.3617	1.46712209	16	0.2137	2.26832236	16	0.4202	1.68873113	16	0.403	1.71472147	16	0.0985	3.34377019	16	0.2642	1.93028139	16	0.1724	3.54283704	16
0.4994	1.017238	0.81381258	0.4118	1.38097428	0.72446057	0.2340	2.18395977	0.56813723	0.3215	1.63795951	0.2407017	0.4047	1.35056421	1.69215658	0.1046	3.2570177	0.3680206	0.2685	1.89898996	0.33077301	0.1831	2.44927559	0.38053695
0.5002	0.99961452	Mz	0.43	1.21758114	Mz	0.2424	2.0445211	Mz	0.3288	1.61150047	Mz	0.4048	1.30470757	Mz	0.1149	3.1215257	Mz	0.2997	1.89355658	Mz	0.1917	2.83850746	Mz
0.5019	0.94651974	0.06338789	0.4657	1.10251785	0.19581602	0.2458	2.0244206	0.6981595	0.3285	1.60022114	0.7580055	0.4079	1.29370165	0.55138242	0.12	3.05886782	0.99523105	0.2923	1.74463236	0.60340579	0.1987	2.33131851	1.21546481
0.5089	0.97453766	0.4664	1.100351	0.2489	2.0063449	0.3318	1.59140075	0.3318	1.59140075	0.4209	1.24844005	0.1284	2.96125785	0.2978	1.74765956	0.2978	1.74765956	0.2075	2.26879757	0.2075	2.26879757	0.2075	2.26879757
0.5222	0.93731771	95	0.4734	1.70885926	95	0.2518	1.5896328	95	0.3389	1.56959439	95	0.4267	1.22565588	95	0.1395	2.84616384	95	0.3021	1.97355661	95	0.2091	2.25771594	95
0.5385	0.83929742	1.27061953	0.4754	1.07277712	1.76273462	0.2518	1.5896328	2.51450684	0.3384	1.56185131	1.79136475	0.4529	1.20788408	1.97629341	0.1399	2.83750813	3.50477301	0.3183	1.65352697	2.04004214	0.2184	2.19493608	3.03827872
0.5527	0.85542425	5	0.4787	1.0627973	5	0.2606	1.9400746	5	0.3423	1.54663372	5	0.4402	1.18578094	5	0.1387	2.65560351	5	0.3207	1.64608987	5	0.2195	2.35768885	5
0.5549	0.84993111	1.64769856	0.4913	1.02531518	1.68873391	0.2722	1.8774255	0.7374072	0.3434	1.54020051	0.75374072	0.4528	1.14304447	1.70040842	0.1676	2.57688415	1.42252469	0.3213	1.61799326	1.8052353	0.2346	2.09170739	0.38032769
0.5552	0.84891335	Qj	0.5027	0.92222201	Qj	0.2767	1.85358977	Qj	0.3599	1.47431952	Qj	0.4539	1.13954937	Qj	0.1685	2.56915777	Qj	0.3226	1.63216785	Qj	0.2419	2.04750001	Qj
0.5652	0.83215967	0.85208488	0.5077	0.97794356	0.96286319	0.2781	1.84630874	1.39667943	0.3617	1.4516683	0.73799884	0.4554	1.13478421	1.56068758	0.1733	2.52863055	1.45186328	0.3311	1.5946476	1.04842316	0.2537	1.97355661	1.0314353
0.5739	0.80121295	0.5234	0.93400627	0.2923	1.77446326	0.3684	1.44604285	0.3684	1.44604285	0.4628	1.05109129	0.1913	2.18607704	0.3475	1.52490222	0.3475	1.52490222	0.2714	1.88149146	0.2714	1.88149146	0.2714	1.88149146
0.5991	0.76349099	0.5374	0.9123367	0.2954	1.79523939	0.4056	1.40831168	0.4056	1.40831168	0.5060	0.99824958	0.1979	2.37913572	0.3476	1.53446712	0.3476	1.53446712	0.2728	1.8746066	0.2728	1.8746066	0.2728	1.8746066
0.6015	0.73133716	0.5343	0.90427043	0.3096	1.69150832	0.3861	1.37294193	0.3861	1.37294193	0.4504	0.98763752	0.2074	2.26494901	0.3504	1.52121252	0.3504	1.52121252	0.2689	1.83185598	0.2689	1.83185598	0.2689	1.83185598
0.6163	0.6982894	0.5451	0.87339977	0.3121	1.67990553	0.4043	1.30649084	0.4043	1.30649084	0.5441	0.87751864	0.2187	2.19255631	0.3613	1.46871842	0.3613	1.46871842	0.2933	1.76953606	0.2933	1.76953606	0.2933	1.76953606
0.6177	0.69501589	0.5492	0.86458916	0.3148	1.66747845	0.4043	1.30649084	0.4043	1.30649084	0.559	0.89077272	0.2279	2.1335913	0.382	1.3883431	0.382	1.3883431	0.3106	1.688856	0.3106	1.688856	0.3106	1.688856
0.6222	0.68493191	0.5506	0.8609162	0.3256	1.6188137	0.4104	1.2484885	0.4104	1.2484885	0.595	0.89077272	0.2382	2.06913164	0.3998	1.3226384	0.3998	1.3226384	0.3169	1.6578941	0.3169	1.6578941	0.3169	1.6578941
0.6389	0.65796728	0.5654	0.82262955	0.3276	1.6099716	0.4145	1.2705425	0.4145	1.2705425	0.596	0.89077272	0.239	1.94898951	0.401	1.31811471	0.401	1.31811471	0.317	1.6578941	0.317	1.6578941	0.317	1.6578941
0.637	0.65062522	0.5662	0.8206941	0.3281	1.60775858	0.4145	1.2705425	0.4145	1.2705425	0.596	0.89077272	0.239	1.94898951	0.401	1.31811471	0.401	1.31811471	0.317	1.6578941	0.317	1.6578941	0.317	1.6578941
0.641	0.63710397	0.5896	0.76218512	0.3804	1.47231663	0.4171	1.26152411	0.4171	1.26152411	0.5721	0.80565394	0.2783	1.84527519	0.4148	1.26950446	0.4148	1.26950446	0.3284	1.61532738	0.3284	1.61532738	0.3284	1.61532738
0.6466	0.62904927	0.5958	0.74709365	0.3626	1.46353679	0.4202	1.2504135	0.4202	1.2504135	0.582	0.78092034	0.2819	1.82672917	0.427	1.28768164	0.427	1.28768164	0.3298	1.60932316	0.3298	1.60932316	0.3298	1.60932316
0.6602	0.59901989	0.5971	0.74394923	0.3642	1.45718485	0.4234	1.23789634	0.4234	1.23789634	0.5929	0.75132992	0.285	1.81910598	0.4385	1.18943119	0.4385	1.18943119	0.3314	1.59134102	0.3314	1.59134102	0.3314	1.59134102
0.6618	0.59527727	0.6092	0.71500611	0.3704	1.45283188	0.43	1.27193813	0.43	1.27193813	0.5933	0.75132992	0.2913	1.79407374	0.4431	1.17428584	0.4431	1.17428584	0.3318	1.59160075	0.3318	1.59160075	0.3318	1.59160075
0.6621	0.59448211	0.6102	0.71001153	0.3704	1.45283188	0.43	1.27193813	0.43	1.27193813	0.5933	0.75132992	0.2913	1.79407374	0.4431	1.17428584	0.4431	1.17428584	0.3318	1.59160075	0.3318	1.59160075	0.3318	1.59160075
0.6805	0.55532624	0.6133	0.70532918	0.3963	1.35523283	0.4488	1.15504564	0.4488	1.15504564	0.6372	0.65017633	0.3071	1.70320518	0.4613	1.1621336	0.4613	1.1621336	0.3372	1.56810239	0.3372	1.56810239	0.3372	1.56810239
0.6842	0.54750536	0.6158	0.69946031	0.399	1.32552814	0.4564	1.16131973	0.4564	1.16131973	0.6385	0.647236	0.3214	1.67354432	0.4669	1.09880521	0.4669	1.09880521	0.3474	1.52317144	0.3474	1.52317144	0.3474	1.52317144
0.6928	0.52948849	0.6293	0.682175	0.4054	1.30257099	0.4617	1.1146293	0.4617	1.1146293	0.6484	0.62503712	0.3357	1.49124551	0.4844	1.0572039	0.4844	1.0572039	0.3582	1.48115023	0.3582	1.48115023	0.3582	1.48115023
0.695	0.52491068	0.6349	0.65539117	0.4141	1.27193813	0.4625	1.1146293	0.4625	1.1146293	0.6484	0.62503712	0.3357	1.49124551	0.4844	1.0572039	0.4844	1.0572039	0.3582	1.48115023	0.3582	1.48115023	0.3582	1.48115023
0.708	0.49645245	0.6374	0.64972358	0.423	1.24125993	0.4636	1.1084159	0.4636	1.1084159	0.6506	0.62503712	0.3357	1.49124551	0.4844	1.0572039	0.4844	1.0572039	0.3582	1.48115023	0.3582	1.48115023	0.3582	1.48115023
0.7109	0.49122773	0.644	0.64486204	0.4257	1.23208058	0.4682	1.03444705	0.4682	1.03444705	0.7005	0.5135387	0.3821	1.3879661	0.519	0.94618555	0.519	0.94618555	0.3722	1.4253778	0.3722	1.4253778	0.3722	1.4253778
0.7163	0.48136008	0.6546	0.61130932	0.4289	1.2217645	0.4708	1.0120849	0.4708	1.0120849	0.7006	0.5135387	0.3821	1.3879661	0.519	0.94618555	0.519	0.94618555	0.3722	1.4253778	0.3722	1.4253778	0.3722	1.4253778
0.7259	0.46215337	0.6736	0.57003114	0.4559	1.1332011	0.4904	0.70296042	0.4904	0.70296042	0.704	0.50614347	0.3917	1.35216753	0.5335	0.90434292	0.5335	0.90434292	0.3764	1.40964954	0.3764	1.40964954	0.3764	1.40964954
0.7305	0.45303999	0.6789	0.55872428	0.4599	1.12059842	0.491	0.70296042	0.491	0.70296042	0.704	0.50614347	0.3917	1.35216753	0.5335	0.90434292	0.5335	0.90434292	0.3764	1.40964954	0.3764	1.40964954	0.3764	1.40964954
0.7323	0.44480805	0.6896	0.53616739	0.4612	1.11852014	0.5026	0.69205903	0.5026	0.69205903	0.7163	0.48136008	0.4079	1.29370165	0.5547	0.85021138	0.5547	0.85021138	0.3791	1.39657089	0.3791	1.39657089	0.3791	1.39657089
0.7467	0.4213958	0.6941	0.52678011	0.4752	1.07738418	0.5143	0.65930983	0.5143	0.65930983	0.7286	0.47272545	0.4286	1.23921502	0.5652	0.81658102	0.5652	0.81658102	0.3797	1.39705628	0.3797	1.39705628	0.3797	1.39705628
0.7488	0.41																						

PM-F10-S2				PM-F10-S1				PM-F11-S2				PM-F11-S1				PM-F12-S2				PM-F12-S1				PM-F13-S2				PM-F13-S1						
mm	phi	results	mm	phi	results	mm	phi	results	mm	phi	results	mm	phi	results	mm	phi	results	mm	phi	results	mm	phi	results	mm	phi	results	mm	phi	results	mm	phi	results		
0.1807	2.46831071		84	0.107	3.22429001	84	0.2861	1.80539333		84	0.4806	1.29122797	84	0.329	1.62147466	84	0.0207	5.59417811		84	0.2098	2.25289436	84	0.2442	2.03384749		84	0.2098	2.25289436	84	0.2442	2.03384749		
0.1848	2.43594274	1.55935483		0.1325	2.71309591	1.92807616	0.4486	1.15648889	0.33952097	0.4171	1.26152411	0.54686175	0.5449	1.20123423	0.54696262	0.3258	1.61792781	0.25615001	0.2249	2.12526263	0.94540817	0.3176	1.65470319	0.80198799		0.3176	1.65470319	0.80198799		0.3176	1.65470319			
0.2272	2.13794718		50	0.1693	2.56232443		50	0.4768	1.06853482		50	0.4219	1.24050144		50	0.4354	1.13478421		50	0.3072	1.97373548		50	0.3462	1.55553118		50	0.3462	1.55553118		50	0.3462	1.55553118	
0.2336	2.09787006	0.88927779		0.1753	2.51200805	0.87908811	0.4888	1.02167508	-1.43352545	0.4324	1.20955134	-0.56083188	0.5337	0.89698494	-0.18616714	0.499	1.0028796	-1.6399434	0.353	1.50224721	-0.18461521	0.3676	1.44477912	-0.7935692		0.3676	1.44477912	-0.7935692		0.3676	1.44477912			
0.2338	1.97821929		16	0.1775	2.49408798		16	0.4993	1.02021271		16	0.4424	1.17666676		16	0.5451	0.87399977		16	0.5489	0.86337744		16	0.3382	1.36511643		16	0.3382	1.36511643		16	0.3382	1.36511643	
0.2679	1.90021744	-0.00095694		0.1917	2.38305756	-0.00267741	0.5107	0.96944384	-3.74513406	0.4405	1.1669126	1.75939559	0.5910	0.756812	-2.76815114	0.5555	0.94813401	-3.27045663	0.4447	1.35506421	-1.74144205	0.3947	1.34116023	2.63056449		0.3947	1.34116023	2.63056449		0.3947	1.34116023			
0.2702	1.88748545	Mz		0.2005	2.11819625	Mz	0.5453	0.87487054	Mz	0.4709	1.08498118	Mz	0.5972	0.74370784	Mz	0.6254	0.67714115	Mz	0.412	1.27927284	Mz	0.4285	1.23275854	Mz		0.4285	1.23275854	Mz		0.4285	1.23275854			
0.301	1.73245996	0.81589189		0.2045	2.28989789	0.94108096	0.5827	0.77916819	-1.61304618	0.5334	0.906706	-0.5911219	0.6153	0.70110375	-0.63867322	0.6422	0.63890031	-1.55414667	0.438	1.19087715	-0.32688303	0.4307	1.21523449	-0.70264447		0.4307	1.21523449	-0.70264447		0.4307	1.21523449			
0.3213	1.63799326			0.2256	2.14814286		0.5983	0.784105276		0.5416	0.88489287		0.6151	0.70110319		0.6678	0.58250707		0.4382	1.19032854		0.4899	1.0294321			0.4899	1.0294321			0.4899	1.0294321			
0.3224	1.63306254	95	0.2272	2.13794718	95	0.6298	0.66702087	95	0.5582	0.8413886	95	0.6278	0.67163739	95	0.6278	0.67163739	95	0.7451	0.42449044	95	0.4499	1.15231338	95	0.5076	0.57822775	95	0.5076	0.57822775	95	0.5076	0.57822775	95	0.5076	0.57822775
0.3234	1.62894944	2.223658		0.2392	2.06369325	2.70117584	0.6379	0.64485923	1.21302093	0.5921	0.74029523	1.23677733	0.6472	0.62771118	1.10226346	0.7386	0.93858515	2.04302947	0.4664	1.100351	1.79512394	0.5445	0.67898863	1.60926808		0.5445	0.67898863	1.60926808		0.5445	0.67898863			
0.3241	1.62547533	5	0.2409	2.0606409	5	0.6994	0.51380594	5	0.6994	0.51380594	-1.12098055	0.6657	0.58705096	-2.46753255	0.6422	0.59035035	-4.74412097	0.8346	0.26084097	-1.77227607	0.4964	1.0041643	-1.360907	0.5579	0.84191442	-4.58492372		0.5579	0.84191442	-4.58492372		0.5579	0.84191442	
0.3461	1.57026721	Qj		0.2783	1.84527158	Qj	0.7507	0.41368811	Qj	0.7061	0.5205133	Qj	0.6664	0.5853474	Qj	0.8554	0.22532698	Qj	0.499	1.0028796	Qj	0.5829	0.77867311	Qj		0.5829	0.77867311	Qj		0.5829	0.77867311			
0.3496	1.51538499	0.86895115		0.2798	1.81751659	1.07163241	0.7669	0.38288639	1.82914548	0.7088	0.49654529	1.13782341	0.7081	0.49756314	1.59175996	0.6684	0.1700389	1.76275856	0.524	0.9323534	1.94252037	0.5939	0.7510717	1.79666093		0.5939	0.7510717	1.79666093		0.5939	0.7510717			
0.358	1.48195937			0.2839	1.8064022		0.7734	0.3707102		0.7293	0.43541185		0.7101	0.49349544		0.9236	0.11460895		0.5274	0.92302272		0.6031	0.73431688			0.6031	0.73431688			0.6031	0.73431688			
0.3591	1.47570324			0.2863	1.80418516		0.7793	0.35974624		0.7511	0.41291956		0.7254	0.46314743		0.9349	0.11362975		0.5475	0.88996194		0.6072	0.71975022			0.6072	0.71975022			0.6072	0.71975022			
0.3604	1.47211661			0.2877	1.79734767		0.8	0.32192537		0.7786	0.3645733		0.7432	0.42817397		0.9718	0.04126831		0.5581	0.84119733		0.6103	0.71240348			0.6103	0.71240348			0.6103	0.71240348			
0.3668	1.44682222			0.3075	1.7013273		0.8403	0.25102149		0.8206	0.28324653		0.78	0.3959253		1.0298	-0.04236382		0.5852	0.77299179		0.6345	0.65830238			0.6345	0.65830238			0.6345	0.65830238			
0.3741	1.41484923			0.3095	1.69197438		0.9358	0.09572706		0.8896	0.27072774		0.7639	0.38854102		1.0673	-0.09396496		0.5856	0.77200601		0.6546	0.60698082			0.6546	0.60698082			0.6546	0.60698082			
0.3858	1.37406333			0.3163	1.66602049		1.0338	-0.07560405		0.829	0.2705537		0.7812	0.35623313		1.0956	-0.13172006		0.6602	0.72212814		0.6936	0.52781973			0.6936	0.52781973			0.6936	0.52781973			
0.3981	1.36589589			0.3248	1.62284274		1.0807	-0.08974895		0.8324	0.27099193		0.7953	0.32938312		1.0991	-0.15253215		0.6861	0.69488312		0.7233	0.69346405			0.7233	0.69346405			0.7233	0.69346405			
0.3996	1.32336032			0.3316	1.59247652		1.1028	-0.14116988		0.8896	0.18345937		0.7852	0.32593813		1.1591	-0.21303234		0.6639	0.59597513		0.7283	0.64579138			0.7283	0.64579138			0.7283	0.64579138			
0.4086	1.29122797			0.332	1.5907314		1.1174	-0.16014437		0.8876	0.1701697		0.8	0.32192537		1.4119	-0.4976337		0.6644	0.59807103		0.7397	0.64349844			0.7397	0.64349844			0.7397	0.64349844			
0.4233	1.24023712			0.336	1.57345355		1.1499	-0.2015067		0.8936	0.16229754		0.8096	0.30471623		1.4438	-0.52866483		0.7036	0.50716832		0.7434	0.62785779			0.7434	0.62785779			0.7434	0.62785779			
0.4231	1.24023712			0.3421	1.5474989		1.1621	-0.21673239		0.9186	0.12249028		0.8124	0.29973532		1.45	-0.53604831		0.7071	0.50000961		0.7705	0.6312996			0.7705	0.6312996			0.7705	0.6312996			
0.4243	1.23751315			0.3423	1.54665372		1.1875	-0.24792542		0.9249	0.11262975		0.818	0.289648		1.6063	-0.68373558		0.7283	0.45739138		0.7913	0.63770048			0.7913	0.63770048			0.7913	0.63770048			
0.4261	1.22917514			0.3426	1.50471464		1.1946	-0.25891978		0.9186	0.12026124		0.818	0.289648		1.6063	-0.68373558		0.7283	0.45739138		0.7913	0.63770048			0.7913	0.63770048			0.7913	0.63770048			
0.4382	1.19012654			0.3583	1.48074753		1.309	-0.38464181		0.9366	0.09446426		0.8323	0.26516893		1.7084	-0.77263927		0.7512	0.41272754		0.8275	0.67316647			0.8275	0.67316647			0.8275	0.67316647			
0.4565	1.13130367			0.3615	1.46792003		1.3429	-0.42534428		0.948	0.0774038		0.8621	0.21407106		1.7143	-0.77761367		0.7635	0.3829665		0.8346	0.6064907			0.8346	0.6064907			0.8346	0.6064907			
0.4599	1.12059844			0.3824	1.38122334		1.3539	-0.43717149		0.9748	0.03862153		0.8849	0.17641217		1.7214	-0.78357575		0.7874	0.34482847		0.8702	0.6204136			0.8702	0.6204136			0.8702	0.6204136			
0.4617	1.11496293			0.3828	1.38312555		1.3801	-0.44647488		0.9808	0.02796888		0.8878	0.17021697		1.8113	-0.87286077		0.8061	0.31096664		0.8713	0.61992246			0.8713	0.61992246			0.8713	0.61992246			
0.4724	1.08159998			0.399	1.32552814		1.3913	-0.47642951		1.0087	-0.12265043		0.9105	0.13524793		1.898	-0.4795415		0.8225	0.2919103		0.8968	0.51714649			0.8968	0.51714649			0.8968	0.51714649			
0.4729	1.08038382			0.4253	1.23343681		1.4278	-0.51580899		1.1109	-0.15172767		0.9162	0.12626446		1.9113	-0.93454644		0.8251	0.27735677		0.9148	0.62847064			0.9148	0.62847064			0.9148	0.62847064			
0.4729	1.08038382			0.4318	1.2115546		1.4478	-0.53385781		1.1522	-0.2048943		0.9211	0.1185693		1.9199	-0.66969312		0.886	0.27661992		0.92	0.62092332			0.92	0.62092332			0.92	0.62092332			
0.4737	1.07794531			0.4333	1.20555165		1.5366	-0.61785743		1.1536	-0.20621334		0.9237	0.11450276		2.1196	-0.88378287		0.8913	0.16601558		0.9241	0.61387815			0.9241	0.61387815			0.9241	0.61387815			

PM-F11-56				PM-F11-51				PM-F11-52				PM-F11-53				PM-F11-54				PM-F11-55				PM-F11-56								
mm	gpi	results		mm	gpi	results		mm	gpi	results		mm	gpi	results		mm	gpi	results		mm	gpi	results		mm	gpi	results						
0.282	1.2161128	84	1.957	-0.9683556	84	0.2901	1.753627	84	0.2393	2.0639025	84	0.2254	2.1949224	84	0.1976	2.3193256	84	0.2127	2.2130918	84	0.2482	2.0104078	84	0.2841	1.8155191	1.2101308	84					
0.282	1.9257232	0.8183804	1.957	-0.9683556	50	0.3119	1.6080383	1.0058363	0.2768	1.8530648	1.0305754	0.2298	2.1215315	1.0658905	0.2651	1.9428723	1.2415952	0.2993	1.703211	1.1548377	0.2575	1.9573911	1.2144421	0.3219	1.8535191	1.2101308	84					
0.1148	1.8674745	50	1.957	-0.9683556	50	0.3219	1.6470061	50	0.2716	1.8804271	50	0.2942	1.7611592	50	0.2842	1.7611592	50	0.3065	1.7062609	50	0.2866	1.6148965	50	0.3231	1.6299156	50	0.3231	1.6299156	50			
0.121	1.6193493	-1.9723895	1.957	-0.9683556	0.8616128	0.3402	1.5171817	0.9139458	0.3484	1.4604265	-0.2044317	0.2967	1.7813185	0.3138385	0.3024	1.7545536	0.5590117	0.3065	1.7062609	0.4127748	0.3424	1.5461212	0.599713	0.3386	1.6055424	0.7011169	0.3386	1.6055424	0.7011169			
0.3225	1.6126153	16	4.464	-2.1581877	16	0.3729	1.4231276	16	0.3734	1.4211943	16	0.3235	1.6281461	16	0.3025	1.7497936	16	0.3106	1.688056	16	0.3472	1.5261484	16	0.3431	1.5248415	16	0.3431	1.5248415	16			
0.1312	1.5942134	-4.2042199	4.464	-2.1581877	-4.9068491	0.3965	1.3405594	-1.0462164	0.3782	1.4027687	-2.7139187	0.3518	1.5071587	-0.6761724	0.3121	1.6799055	-0.19911802	0.3235	1.6281461	-0.4774101	0.3494	1.5153546	-0.1523719	0.3474	1.5251744	-0.16791936	0.3474	1.5251744	-0.16791936			
0.3096	1.4159519	84	4.464	-2.1581877	84	0.4076	1.2947809	84	0.4089	1.2961912	84	0.359	1.4779151	84	0.3118	1.6720686	84	0.3848	1.3778074	84	0.3541	1.4977805	84	0.3507	1.5316788	84	0.3507	1.5316788	84			
0.1794	1.4148149	-1.7797062	4.464	-2.1581877	-4.6548065	0.41	1.2178114	0.8502616	0.4111	1.2754235	-0.8452678	0.4116	1.2867422	-0.8428255	0.3189	1.6448105	0.8487196	0.3078	1.3395908	0.8468412	0.3665	1.4481026	0.5538754	0.3604	1.4721161	0.541144	0.3604	1.4721161	0.541144			
0.4167	1.2429081	15	1.9068575	5	0.4463	1.1639444	0.4462	1.2177101	0.4441	1.1710362	0.4441	1.1710362	0.4441	1.1710362	0.4441	1.1710362	0.4441	0.3081	1.3287659	0.3081	1.3287659	0.3081	1.3287659	0.3081	1.3287659	0.3081	1.3287659	0.3081	1.3287659	0.3081		
0.4329	1.2078808	95	1.9068575	5	0.4464	1.1639444	95	0.4417	1.2118875	95	0.4453	1.1671406	95	0.4395	1.5411802	95	0.4154	1.26741616	95	0.3869	1.3899578	95	0.3835	1.3828982	95	0.3835	1.3828982	95	0.3835	1.3828982	95	
0.4441	1.1701032	1.7995562	15	1.9068575	-2.0057221	0.4460	1.1622098	1.6849973	0.4462	1.5947919	9128261	0.3472	1.5261484	0.3472	1.5261484	0.3472	1.5261484	0.3472	1.5261484	0.3472	1.5261484	0.3472	1.5261484	0.3472	1.5261484	0.3472	1.5261484	0.3472	1.5261484	0.3472		
0.4716	1.0845521	5	15	1.9068575	5	0.4465	1.1283481	5	0.4781	1.0646609	5	0.4744	1.0791499	5	0.4379	1.4212776	5	0.4095	1.1880549	5	0.4039	1.3071889	5	0.4053	1.302069	5	0.4053	1.302069	5	0.4053	1.302069	5
0.4747	1.0749025	-0.7003996	15	1.9068575	-4.9068491	0.459	1.1234244	-2.1842569	0.4953	1.0136149	-4.4184083	0.4926	1.0215023	-1.779971	0.4003	1.3208351	-1.4716134	0.462	1.1140252	-1.1581858	0.4139	1.2726358	-0.76302239	0.4089	1.2901812	-0.6844555	0.4089	1.2901812	-0.6844555	0.4089	1.2901812	-0.6844555
0.4876	1.0362211	84	15	1.9068575	84	0.462	1.1140252	84	0.5029	0.9164215	84	0.505	0.9164215	84	0.4153	1.2740299	84	0.467	1.0849625	84	0.4197	1.2525994	84	0.4125	1.2676989	84	0.4125	1.2676989	84	0.4125	1.2676989	84
0.4918	1.0138477	2.3464536	15	1.9068575	0.8014829	0.4620	1.1124012	1.08767276	0.512	0.9187036	1.86518789	0.5148	0.9578704	0.94927634	0.4261	1.2291756	0.94097915	0.4577	1.0718167	0.8481319	0.4275	1.2259311	0.7180042	0.4468	1.1564869	0.7180042	0.4468	1.1564869	0.7180042	0.4468	1.1564869	0.7180042
0.5063	0.9819271	15	1.9068575	5	0.52	0.9104815	0.527	0.9134712	0.5183	0.9411268	0.4317	1.2118875	0.4317	1.2118875	0.4317	1.2118875	0.4317	0.4857	1.0481838	0.4857	1.0481838	0.4857	1.0481838	0.4857	1.0481838	0.4857	1.0481838	0.4857	1.0481838	0.4857	1.0481838	0.4857
0.5379	0.7911031	15	1.9068575	5	0.5341	0.90427043	0.5349	0.91758214	0.5376	0.9242793	0.4318	1.2115456	0.4318	1.2115456	0.4318	1.2115456	0.4318	0.4857	1.0481838	0.4857	1.0481838	0.4857	1.0481838	0.4857	1.0481838	0.4857	1.0481838	0.4857	1.0481838	0.4857	1.0481838	0.4857
0.6051	0.7077901	15	1.9068575	5	0.5511	0.8540853	0.5511	0.8540853	0.5403	0.8811599	0.4358	1.1962156	0.4358	1.1962156	0.4358	1.1962156	0.4358	0.4857	1.0481838	0.4857	1.0481838	0.4857	1.0481838	0.4857	1.0481838	0.4857	1.0481838	0.4857	1.0481838	0.4857	1.0481838	0.4857
0.6178	0.6947625	15	1.9068575	5	0.5581	0.8413973	0.5581	0.8413973	0.5406	0.8873508	0.4394	1.1881819	0.4394	1.1881819	0.4394	1.1881819	0.4394	0.5083	0.8782961	0.5083	0.8782961	0.5083	0.8782961	0.5083	0.8782961	0.5083	0.8782961	0.5083	0.8782961	0.5083	0.8782961	0.5083
0.6295	0.60771807	15	1.9068575	5	0.5758	0.79635157	0.5584	0.84062204	0.5597	0.8726277	0.4484	1.1571203	0.4484	1.1571203	0.4484	1.1571203	0.4484	0.5236	0.9134551	0.5236	0.9134551	0.5236	0.9134551	0.5236	0.9134551	0.5236	0.9134551	0.5236	0.9134551	0.5236	0.9134551	0.5236
0.6468	0.4288011	15	1.9068575	5	0.5807	0.7841284	0.5618	0.8118943	0.5913	0.73803141	0.4512	1.1481512	0.4512	1.1481512	0.4512	1.1481512	0.4512	0.5255	0.9382248	0.5255	0.9382248	0.5255	0.9382248	0.5255	0.9382248	0.5255	0.9382248	0.5255	0.9382248	0.5255	0.9382248	0.5255
0.6962	0.5242136	15	1.9068575	5	0.6024	0.7799114	0.5750	0.8096948	0.5997	0.7176888	0.4573	1.1287763	0.4573	1.1287763	0.4573	1.1287763	0.4573	0.5174	0.9310212	0.5174	0.9310212	0.5174	0.9310212	0.5174	0.9310212	0.5174	0.9310212	0.5174	0.9310212	0.5174	0.9310212	0.5174
0.7151	0.4813779	15	1.9068575	5	0.5921	0.7568085	0.5732	0.80288289	0.604	0.72717319	0.4688	1.0925468	0.4688	1.0925468	0.4688	1.0925468	0.4688	0.5382	0.92083801	0.5382	0.92083801	0.5382	0.92083801	0.5382	0.92083801	0.5382	0.92083801	0.5382	0.92083801	0.5382	0.92083801	0.5382
0.818	0.398248	27	-4.7548479	30	0.6002	0.7364755	0.5814	0.73239041	0.6049	0.7252253	0.4763	1.070405	0.4763	1.070405	0.4763	1.070405	0.4763	0.539	0.89165328	0.539	0.89165328	0.539	0.89165328	0.539	0.89165328	0.539	0.89165328	0.539	0.89165328	0.539	0.89165328	0.539
0.8265	0.2793971	27	-4.7548479	30	0.6165	0.6979213	0.5989	0.7396071	0.6087	0.7161967	0.4792	1.0089127	0.4792	1.0089127	0.4792	1.0089127	0.4792	0.5406	0.8873508	0.5406	0.8873508	0.5406	0.8873508	0.5406	0.8873508	0.5406	0.8873508	0.5406	0.8873508	0.5406	0.8873508	0.5406
0.8351	0.2044413	27	-4.7548479	30	0.6276	0.6727706	0.6148	0.6971194	0.6148	0.6971194	0.504	0.9901245	0.504	0.9901245	0.504	0.9901245	0.504	0.5489	0.8796487	0.5489	0.8796487	0.5489	0.8796487	0.5489	0.8796487	0.5489	0.8796487	0.5489	0.8796487	0.5489	0.8796487	0.5489
1.0046	-0.0066212	27	-4.7548479	30	0.6475	0.6270426	0.6045	0.7261761	0.6132	0.6951677	0.5396	0.8986414	0.5396	0.8986414	0.5396	0.8986414	0.5396	0.5497	0.8832761	0.5497	0.8832761	0.5497	0.8832761	0.5497	0.8832761	0.5497	0.8832761	0.5497	0.8832761	0.5497	0.8832761	0.5497
1.0097	-0.1512929	27	-4.7548479	30	0.6529	0.6150085	0.6048	0.7246882	0.6282	0.67098848	0.5439	0.9762773	0.5439	0.9762773	0.5439	0.9762773	0.5439	0.5739	0.8811235	0.5739	0.8811235	0.5739	0.8811235	0.5739	0.8811235	0.5739	0.8811235	0.5739	0.8811235	0.5739	0.8811235	0.5739
1.0596	-0.0853194	27	-4.7548479	30	0.6546	0.6112952	0.6145	0.6181579	0.6279	0.62939495	0.5429	0.9293592	0.5429	0.9293592	0.5429	0.9293592	0.5429	0.5739	0.8811235	0.5739	0.8811235	0.5739	0.8811235	0.5739	0.8811235	0.5739	0.8811235	0.5739	0.8811235	0.5739	0.8811235	0.5739
1.1466	-0.1973801	27	-4.7548479	30	0.6616	0.5958362	0.6071	0.6051803	0.6346	0.6560752	0.5324	0.9040683	0.5324	0.9040683	0.5324	0.9040683	0.5324	0.5834	0.7774813	0.5834	0.7774813	0.5834	0.7774813	0.5834	0.7774813	0.5834	0.7774813	0.5834	0.7774813	0.5834	0.7774813	0.5834
1.1838	-0.1188413	27	-4.7548479	30	0.6694	0.5790545	0.6073	0.6053709	0.6415	0.64047541	0.539	0.89165328	0.539	0.89165328	0.539	0.89165328	0.539	0.5883	0.7653695	0.5883	0.7653695	0.5883	0.7653695	0.5883	0.7653695							

PB

PB-F1-S1				PB-F1-S4				PB-F2-S1				PB-F3-S2				PB-F3-S3				PB-F3-S4			
mm	phi	results	mm	phi	results	mm	phi	results	mm	phi	results	mm	phi	results	mm	phi	results	mm	phi	results	mm	phi	results
0.3645	1.45599697	84	0.5673	0.81780931	84	0.3337	1.58336302	84	0.1706	2.55128887	84	0.3208	1.64024008	84	0.3208	1.64024008	84	0.271	1.88361931	84	0.3208	1.64024008	84
0.5565	0.84553926	0.15011449	0.5961	0.74636741	0.07601859	0.5243	0.93152697	0.27550711	0.3237	1.62725697	0.36585654	0.3751	1.41464087	-0.38684145	0.3751	1.41464087	-0.38684145	0.3952	1.33933382	0.61584125	0.3751	1.41464087	-0.38684145
0.6133	0.70532918	50	0.6046	0.72594098	50	0.5438	0.87884451	50	0.5427	0.88176573	50	0.445	1.16811288	50	0.445	1.16811288	50	0.4086	1.29122797	50	0.445	1.16811288	50
0.6949	0.52511827	-0.90505195	0.6481	0.62570637	-1.10146401	0.5559	0.84709555	-0.7462898	0.5996	0.73792147	-1.17588881	0.5762	0.79535171	-2.34837701	0.5762	0.79535171	-2.34837701	0.4772	1.06732502	-0.29005316	0.5762	0.79535171	-2.34837701
0.6954	0.5240806	16	0.6939	0.52719587	16	0.5771	0.79310006	16	0.6107	0.71145823	16	0.5937	0.75218762	16	0.5937	0.75218762	16	0.4853	1.04304241	16	0.5937	0.75218762	16
0.7569	0.40182199	-2.9660091	0.7406	0.43322988	-2.51223343	0.5813	0.78263857	-1.81743967	0.653	0.61483999	-3.7103619	0.5952	0.74854724	-4.36630705	0.5952	0.74854724	-4.36630705	0.5252	0.92905332	-1.3246528	0.5952	0.74854724	-4.36630705
0.7598	0.39630503	Mz	0.7413	0.43186693	Mz	0.6211	0.68709672	Mz	0.6596	0.60033162	Mz	0.6477	0.62659705	Mz	0.6477	0.62659705	Mz	0.5379	0.89458254	Mz	0.6477	0.62659705	Mz
0.8147	0.29565669	-1.24031552	0.767	0.38269828	-1.17922628	0.6649	0.58878574	-0.76274078	0.6847	0.54645146	-1.50679806	0.7877	0.34427891	-2.36717517	0.7877	0.34427891	-2.36717517	0.5644	0.82520313	-0.33295491	0.7877	0.34427891	-2.36717517
0.8376	0.25566449		0.768	0.38081856		0.6661	0.58618436		0.6858	0.54413559		0.8358	0.25876815		0.8358	0.25876815		0.5824	0.77991114		0.8358	0.25876815	
0.8459	0.24143893	95	0.7816	0.35549462	95	0.704	0.50634838	95	0.7126	0.48883148	95	0.8955	0.15923332	95	0.8955	0.15923332	95	0.6016	0.73311733	95	0.8955	0.15923332	95
0.8499	0.23463301	0.81121285	0.7898	0.34043785	0.68860399	0.7413	0.43186693	1.00678616	0.7138	0.48640408	1.30193825	0.9348	0.09726954	1.15410663	0.9348	0.09726954	1.15410663	0.6218	0.68547168	1.32490971	0.9348	0.09726954	1.15410663
0.8506	0.23344527	5	0.8829	0.17967653	5	0.7466	0.42158902	5	0.7219	0.47012511	5	0.9517	0.07142062	5	0.9517	0.07142062	5	0.6541	0.6124117	5	0.9517	0.07142062	5
0.8759	0.19116031	-4.5235237	0.8921	0.16472126	-3.54840661	0.7654	0.38571093	-2.31682282	0.7318	0.45047487	-4.11433223	1.0118	-0.016924	-4.58492372	1.0118	-0.016924	-4.58492372	0.6574	0.60515152	-2.06821521	1.0118	-0.016924	-4.58492372
0.8912	0.16617746	Qi	0.9471	0.07841067	Qi	0.8217	0.28331393	Qi	0.765	0.38646508	Qi	1.2544	-0.3269947	Qi	1.2544	-0.3269947	Qi	0.6765	0.56383339	Qi	1.2544	-0.3269947	Qi
0.8941	0.16149053	1.58732431	0.9837	0.02370949	1.28903431	0.8342	0.26153257	1.02681381	0.7811	0.35641782	1.83970165	1.2607	-0.33422218	1.86441645	1.2607	-0.33422218	1.86441645	0.6816	0.55299808	0.99923335	1.2607	-0.33422218	1.86441645
0.9534	0.06884589		1.0049	-0.00705188		0.8386	0.25394312		0.8045	0.31383302		1.3278	-0.4090344		1.3278	-0.4090344		0.7247	0.46454027		1.3278	-0.4090344	
0.9542	0.06763584		1.0097	-0.01392659		0.9348	0.09726954		0.8352	0.25980419		1.415	-0.50079782		1.415	-0.50079782		0.7289	0.45620334		1.415	-0.50079782	
0.9705	0.04319952		1.0654	-0.09139441		0.9427	0.08512865		0.8428	0.24673569		1.5581	-0.63978242		1.5581	-0.63978242		0.7305	0.45303999		1.5581	-0.63978242	
0.9746	0.03711756		1.0692	-0.09653093		0.9779	0.03224088		0.8539	0.22785904		1.6431	-0.71641423		1.6431	-0.71641423		0.7356	0.43020087		1.6431	-0.71641423	
1.024	-0.03421543		1.0997	-0.13710885		0.9796	0.02973507		0.8929	0.1634281		1.7374	-0.7969233		1.7374	-0.7969233		0.7446	0.42545888		1.7374	-0.7969233	
1.026	-0.03703042		1.1017	-0.13973024		0.9808	0.02796888		0.9163	0.12610701		1.7891	-0.83922693		1.7891	-0.83922693		0.7668	0.38037452		1.7891	-0.83922693	
1.0293	-0.04166318		1.1137	-0.15535935		1.0507	-0.0713502		0.9273	0.10889102		1.9543	-0.96664377		1.9543	-0.96664377		0.7675	0.38175812		1.9543	-0.96664377	
1.0732	-0.1019181		1.1223	-0.16645696		1.0726	-0.1011113		0.9363	0.09495643		2.3082	-1.20675804		2.3082	-1.20675804		0.7747	0.36875804		2.3082	-1.20675804	
1.0795	-0.11036231		1.1647	-0.21995654		1.0883	-0.12207527		0.9672	0.04811344		2.3424	-1.22797707		2.3424	-1.22797707		0.7834	0.35217599		2.3424	-1.22797707	
1.0922	-0.12723599		1.1801	-0.2389071		1.0896	-0.12379756		1.0004	-0.00057696		2.5295	-1.33884092		2.5295	-1.33884092		0.7955	0.34502333		2.5295	-1.33884092	
1.1087	-0.14868778		1.2043	-0.26819255		1.1136	-0.1552298		1.0432	-0.06101526		2.5988	-1.37783396		2.5988	-1.37783396		0.8138	0.2972513		2.5988	-1.37783396	
1.1644	-0.21958489		1.2433	-0.31417179		1.1154	-0.15755984		1.0642	-0.08976855		2.8389	-1.5053193		2.8389	-1.5053193		0.8156	0.29406383		2.8389	-1.5053193	
1.1667	-0.22243176		1.2621	-0.33582338		1.1222	-0.16632841		1.0901	-0.12445943		2.8452	-1.50851731		2.8452	-1.50851731		0.8202	0.28594399		2.8452	-1.50851731	
1.168	-0.22403838		1.289	-0.36624917		1.1241	-0.16876896		1.0947	-0.13053445		3.0642	-1.6154968		3.0642	-1.6154968		0.8342	0.26534965		3.0642	-1.6154968	
1.1827	-0.24208212		1.3055	-0.3845992		1.1325	-0.17950953		1.1273	-0.28368236		3.2629	-1.70614034		3.2629	-1.70614034		0.8354	0.25945876		3.2629	-1.70614034	
1.2003	-0.26339281		1.3271	-0.40827363		1.1583	-0.21200771		1.223	-0.29042195		3.2731	-1.71064321		3.2731	-1.71064321		0.854	0.2276901		3.2731	-1.71064321	
1.2093	-0.27416987		1.3545	-0.43775669		1.1658	-0.22131843		1.2799	-0.35602808		3.2741	-1.71108391		3.2741	-1.71108391		0.8603	0.21708642		3.2741	-1.71108391	
1.2558	-0.32860394		1.3872	-0.47217181		1.23	-0.29865579		1.2889	-0.36613724		3.3265	-1.73399037		3.3265	-1.73399037		0.9169	0.12516264		3.3265	-1.73399037	
1.2573	-0.33032613		1.3977	-0.48305065		1.2387	-0.30882421		1.2939	-0.37172298		3.3491	-1.74375871		3.3491	-1.74375871		0.9411	0.08757932		3.3491	-1.74375871	
1.2747	-0.35015479		1.4356	-0.52164942		1.2414	-0.31196541		1.3517	-0.43477131		3.4216	-1.7746561		3.4216	-1.7746561		0.9499	0.07415182		3.4216	-1.7746561	
1.2764	-0.35207754		1.4866	-0.57201168		1.3043	-0.3832725		1.3732	-0.45753789		3.4281	-1.77739419		3.4281	-1.77739419		0.9533	0.06945129		3.4281	-1.77739419	
1.35	-0.43295575		1.5218	-0.60577364		1.3543	-0.43754365		1.4028	-0.48830521		3.4708	-1.79525305		3.4708	-1.79525305		1.0114	-0.01635355		3.4708	-1.79525305	
1.4309	-0.51691848		1.555	-0.63690919		1.3817	-0.46644046		1.4948	-0.57994756		3.5544	-1.82995957		3.5544	-1.82995957		1.0211	-0.03012391		3.5544	-1.82995957	
1.4961	-0.58120169		1.6922	-0.75889367		1.3905	-0.47559972		1.517	-0.601216		3.5809	-1.84030667		3.5809	-1.84030667		1.027	-0.03843586		3.5809	-1.84030667	
1.5224	-0.60634234		1.7324	-0.79276537		1.415	-0.50079782		1.5645	-0.6456962		3.589	-1.84356633		3.589	-1.84356633		1.0287	-0.04082196		3.589	-1.84356633	
1.5237	-0.60757374		1.841	-0.88048218		1.5113	-0.59578503		1.5836	-0.66320236		3.612	-1.85278222		3.612	-1.85278222		1.0494	-0.06956411		3.612	-1.85278222	
1.596	-0.67445495		1.8593	-0.894752		1.5172	-0.60140619		1.6872	-0.75462462		3.6167	-1.85465823		3.6167	-1.85465823		1.0516	-0.07258543		3.6167	-1.85465823	
1.6023	-0.68013854		1.8655	-0.89955475		1.5366	-0.61973642		1.7724	-0.82569725		3.8717	-1.95295065		3.8717	-1.95295065		1.0705	-0.09828396		3.8717	-1.95295065	
1.6471	-0.71992206		1.9133	-0.93605519		1.5607	-0.64218782		1.7972	-0.84574381		3.9574	-1.98453611		3.9574	-1.98453611		1.0888	-0.12273793		3.9574	-1.98453611	
1.6545	-0.72638915		1.9393	-0.95552792		1.5732	-0.65369656		1.8195	-0.86353475		4.1565	-2.05535183		4.1565	-2.05							

[illegible]

[illegible]

Appendix V

Diagenesis and Mineralogy

Each Miocene sample was stain using a solution composed of Alizarin red S Potassium Ferric Cyanide mixed with dilute hydrochloric acid. This stain died all calcite minerals red while leaving the dolomite grains their original color. This allowed for the use of background extraction (in JMicroVision™) to quantify the amount of calcite vs. dolomite in each sample. To determine the amount of dolomite for the entire rock volume, first the amount of porosity from background extraction was subtracted from 100. Then the measured amount of calcite was divided by the rock volume after porosity was subtracted out. This value was then multiplied by 100 to calculate a percentage and then subtracted from 100, providing the total amount of dolomite. The spreadsheet below contains the percentage of dolomite calculated from this analysis as well as the percentage of moldic porosity and cement from each sample. The moldic porosity and cement amounts were calculated from the point counting method described in Appendix III (and are included there as well). They are included in this appendix as these three criteria were used to distinguish the 6 diagenetic facies that were used for classification in Chapter 3. Informative photomicrographs are also located below.

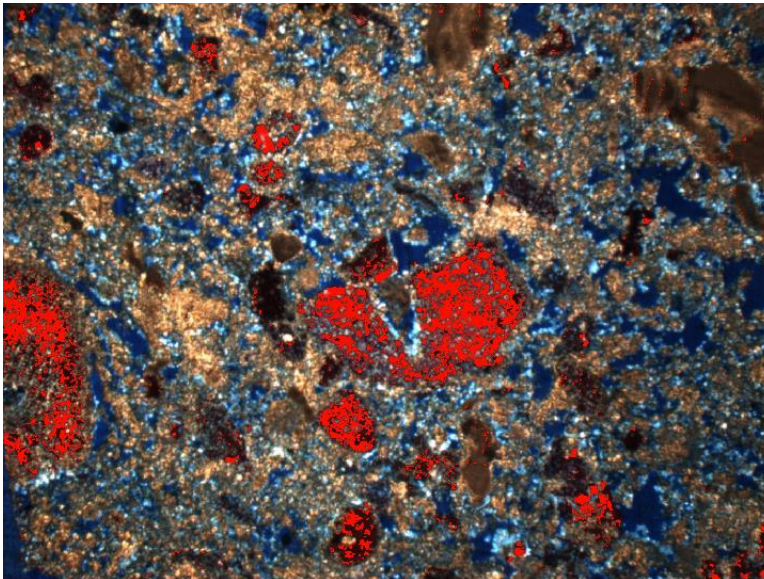
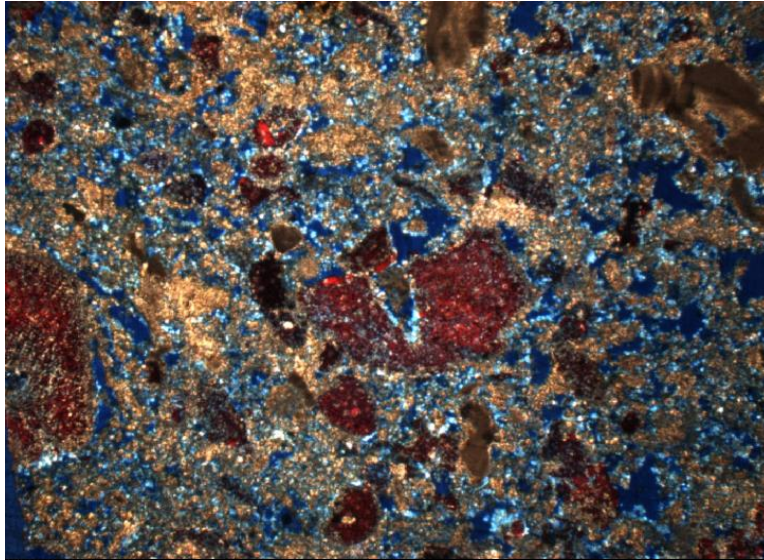
Section	% Moldic Porosity	% Cement	% Dolomite
RP-F1-S2	32	0	66.3
RP-F1-S3	20.8	0.4	99.0
RP-F1-S4	-	10	35.0
RP-F2-S1	27.2	0.8	-
RP-F2-S2	18	2.8	84.6
RP-F2-S3	0	3.2	62.0
RP-F2-S4	1.6	6.4	51.0
RP-F3-S1	1.2	1.6	0.0
RP-F3-S2	1.2	0.4	0.0
RP-F3-S3	6	4.8	50.0
RP-F4-S1	2	0.8	30.0
RP-F4-S2	1.2	2.8	30.0
RP-F4-S3	0.4	0.8	30.0
RP-F4-S4	0.4	19.8	20.0
RP-F5-S1	25.6	18	87.4
RP-F5-S2a	37	2	100.0
RP-F5-S2b	16	19	100.0
RP-F5-S4	6.4	28.8	51.1
RP-F5-S5	16	18.8	92.5
RP-F6-S1	0.4	1	0.0

RP-F6-S2	2.8	0	0.0
RP-F6-S3	1.2	0.2	0.0
RP-F7-S1a	1.2	0.2	0.0
RP-F7-S1b	0	0.8	0.0
RP-F7-S2	0.4	2	0.0
RP-F7-S4a	-	-	0.0
RP-F7-S9	0	0	0.0
RP-F8-S1	0	1.6	0.0
RP-F8-S2	0	1.6	0.0
RP-F8-S3	6	10.8	0.0
RP-F9-S2a	1.6	0.8	28.0
RP-F9-S2b	0.4	0.4	22.5
RP-F9-S3	0.8	3.2	35.5
RP-F10-S1	1.6	0.4	2.0
RP-F10-S2	0.8	0	1.0
RP-F10-S3a	0	0	0.0
RP-F10-S3b	0	0.8	0.0
RP-F10-S4	0.8	0	2.0
RP-F10-S5	0.4	0	0.0
RP-F11-S1	4.8		0.0
RP-F11-S2	10.2	34.4	0.0
RP-F11-S4a	10	39.2	0.0
RP-F11-S4b	9.2	45.6	0.0
RP-F11-S5	12	34.4	0.0
RM-F1-S1	10.6	10	49.4
RM-F1-S2	10	16	55.1
RM-F2-S1a	2.4	11	44.1
RM-F2-S1b	0.4	8.7	38.1
RM-F2-S2	1.6	28.4	
RM-F3-S1	15	3.2	58.0
RM-F3-S3	15.6	0.4	78.7
RM-F3-S4	10	2	85.1
RM-F3-S5	2.8	8.8	80.0
RM-F3-S6	10.8	4	81.5

RM-F4-S1	5.2	2.4	89.7
RM-F4-S3	8.8	0	65.9
RM-F4-S4	3.2	0	72.0
RM-F4-S6	3.2	2	74.7
RM-F4-S7	5.2	0.8	72.1
RM-F5-S2	1.6	0.4	65.9
RM-F5-S4	0.8	18.8	81.4
RM-F6-S1	26.4	0.4	98.6
RM-F6-S2	10	0	85.3
RM-F6-S3	15.6	2	97.5
RM-F7-S2	16.4	4.8	100.0
RM-F7-S3	34.8	1.6	92.4
RM-F7-S4	20.4	4	100.0
RM-F8-S1	16.8	1.6	95.5
RM-F8-S2	22.4	8	71.1
RM-F8-S3	1.6	1.6	29.9
RM-F8-S4	1.2	5.6	4.8
RM-F9-S1	0.4	39.6	0.0
RM-F9-S3	0	42.4	0.0
SP-F1-S1	10.8	2	100.0
SP-F1-S2	-	-	100.0
SP-F1-S3	18.4	0.8	100.0
SP-F2-S2	6.8	2.8	100.0
SP-F2-S3	10	3.2	100.0
SP-F2-S4	18.4	8.8	100.0
SP-F2-S5	21.2	6.8	96.9
SP-F2-S6	17.6	16	98.0
SP-F2-S7	33.2	7.2	98.0
SP-F2-S8	24.4	10.8	100.0
SP-F3-S1	8	0	100.0
SP-F3-S2	16.4	3.6	100.0
SP-F3-S3	7.6	2.8	100.0
SP-F4-S1	22	11.2	100.0
SP-F4-S3	18.4	8.8	100.0
SP-F4-S4	5.6	8.4	69.8
SP-F4-S5	-	-	76.1
SP-F4-S7	-	-	93.1

SP-F5-S1	6.8	5.6	78.8
SP-F5-S2	4	2.8	62.8
SP-F5-S3	8	6.4	88.9
SP-F5-S4	7.6	3.2	100.0
SP-F5-S6	13.2	3.2	100.0
SP-F5-S7	10.4	2.4	100.0
SP-F6-S1	16.4	3.6	84.0
SP-F6-S2	14.4	4.4	100.0
SP-F6-S3	13.2	6.4	100.0
SP-F7-S1	23.6	0.8	100.0
SP-F7-S2	22.4	4	100.0
SP-F7-S3	23.6	0.8	100.0
SP-F7-S4	37.2	7.2	100.0
SP-F7-S5	28.4	12.8	100.0
SP-F8-S1	10	15.8	75.0
SP-F9-S1	12.8	3.6	100.0
SP-F9-S2	-	-	99.0
SP-F10-S1	18.8	6.4	80.5
SP-F10-S2	11.2	7.6	60.9
SP-F10-S3	5.2	3.2	76.8
SP-F10-S4	10.4	8	57.5
SP-F11-S1	18	0.4	98.0
SP-F11-S2	14.4	0.8	95.1
SP-F11-S3	9.6	0.8	66.7
SP-F11-S4	15.2	1.2	50.6
SP-F11-S5	13.6	1.6	71.4
SP-F12-S1	7.3	3.6	-
SP-F12-S2	10.8	4.8	-
SP-F13-S1	12	4.4	75.9
SP-F13-S2	6	6.4	74.7
SP-F13-S3	10	4.8	77.5
SP-F13-S4	7.6	4.8	78.8
SP-F13-S5	9.2	4	64.7
SP-F13-S6	14.4	6	100.0
SP-F13-S8	12	2.8	100.0
SP-F13-S9	6.4	8.4	77.8
WF-F1-S1	4	5.2	-
SP-F14-S1	2.8	4.8	43.3
SP-F14-S2	3.6	4.4	75.0

SP-F14-S3	2.8	4.8	40.7
SP-F14-S4	3.6	2	55.7
SP-F14-S5	3.6	3.2	43.2
SP-F14-S6	4.4	0	18.8
SP-F14-S7	5.2	1.6	27.3
SP-F14-S8	3.2	2	9.2
WF-F5-S1	4.4	6.8	-
WF-F5-S2	4.8	3.2	-
WF-F5-S3	5.6	9.2	-
SP-F16-S1	3.6	1.2	29.0
SP-F16-S2	6.8	0.4	21.6
SP-F16-S3	6.8	3.6	20.9
SP-F16-S5	3.2	2.8	3.0
SP-F16-S6	6.8	2.8	12.6
SP-F16-S7	7.2	4.4	22.5
SP-F16-S10	6.8	8	16.9

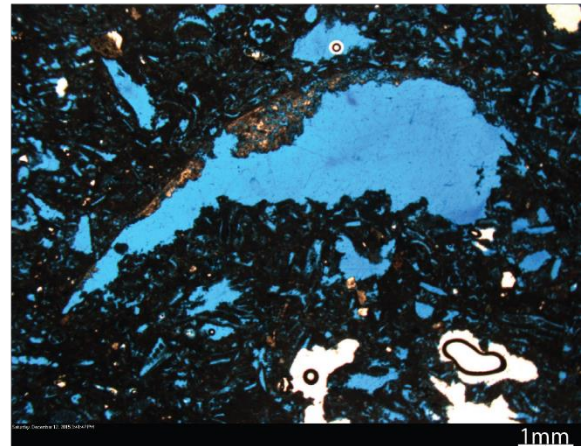


Top photomicrograph shows an example from the Miocene of a sample that has been overdolomitized. Red staining shows which minerals are calcite. The lower photomicrograph shows how background extraction can highlight and quantify calcite content.

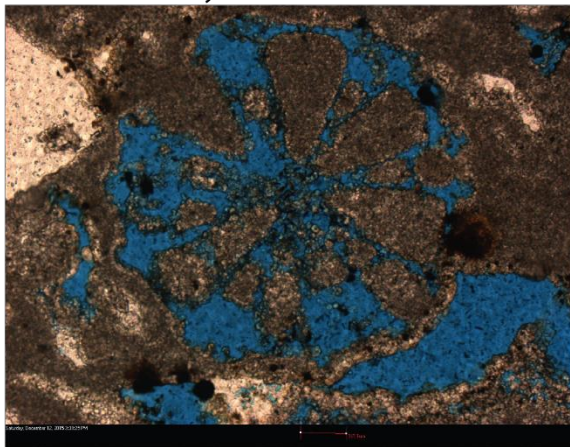
DF-3- High Cement, Isolated Moldic Pores- 100% Calcite



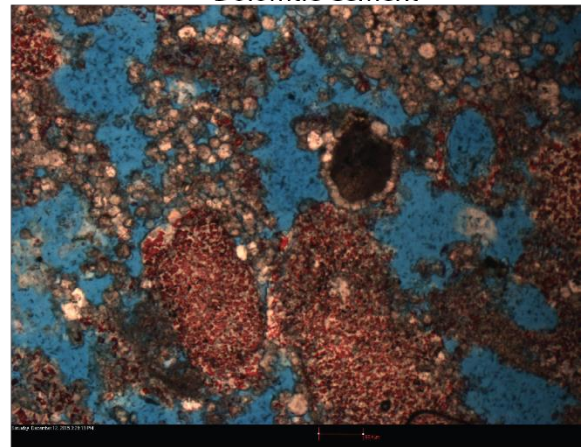
Bivalve Mold- 100% Dolomite



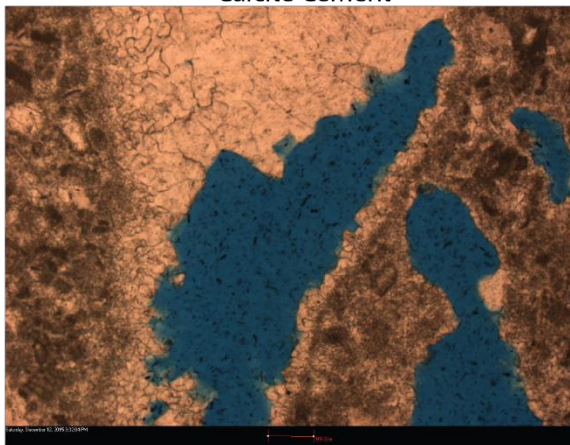
Partial Bryozoan Mold- 100% Dolomite



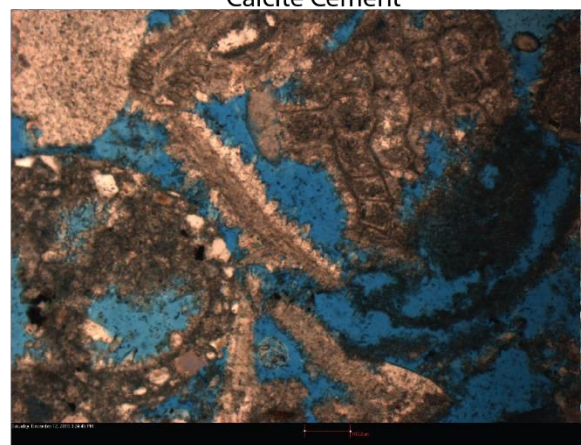
Dolomite Cement



Calcite Cement



Calcite Cement



This plate shows moldic pore types and dolomite and calcite cement.

Appendix VI

Miocene Paleobathymetric Quantification

The spreadsheet below contains the values of paleodepths for each Miocene lithofacies as measured by tracing time equivalent strata along corrected paleotopography.

Cycle #	Deepest Facies Water Depth (m)	Shallowest Facies Water Depth (m)	Amplitude (m)	Amplitude after subtraction of the thickness of the cycle before sea-level drop (m)
1	64.5	12.5	52	47
2	84	12.5	71.5	64.5
3	115	12.5	102.5	98.5
4	150	12.5	137.5	118.5
5	120	87	33	28
6	140	85	55	51
7	139	109	30	30


Appendix VII

Petrophysical Dataset

This appendix contains the full petrophysical dataset including porosity, permeability, and grain density for each sample. Values were split up by dataset (Pliocene and Miocene) and regressions were run for each. Both datasets show a normal distribution. Four samples were removed from the Pliocene dataset and five from the Miocene dataset as they plotted outside of 2.5 standard deviations from the mean distribution and are believed to reflect errors in measurement or damage to the core plugs. Graphs for both datasets are included below as well as spreadsheets that include the regression statistics, analysis of variation data, and the residual outputs for each sample.

Box plots were constructed in Excel™ and were constructed using five plot points: 1) box bottom (1st quartile), 2) box middle (median), 3) box top (3rd quartile), 4) whisker top (maximum), 5) whisker bottom (minimum). Spreadsheets for both Pliocene, Miocene, and diagenesis box plots are included below. Columns are color coded by lithofacies based on the keys in Appendix I

FZI or flow zone indicator values are displayed in graphs representing the vertical distribution of petrophysical values in each measured section. There are 7 FZI graphs for the Pliocene and 3 for the Miocene. These graphs show a combined petrophysical value for each sample and highlight flow zones within a section. FZI values are calculated according to the following equation: $\sqrt{(\phi/k)}$. This appendix also contains additional plots and correlations between petrophysical values and rock properties that weren't included in the text.

FILE NO.: NO-76262		 Weatherford [®] LABORATORIES		
ANALYST: Cotton				
ANALYST: Waller / Larocco				
DATE: 3/12/2015				
		Permeability	Porosity	
	Sample	Horizontal	Helium	Grain
Sample	Identification	Kair		Density
Number	feet	md	%	gm/cc
1	PT-F1-S1A	3733	49.8	2.70
2	PT-F1-S1B	6037	52.1	2.71
3	PT-F1-S3A	10957	49.2	2.72

4	PT-F1-S3B	9585	47.7	2.72
5	PT-F1-S3	5828	54.6	2.71
6	PT-F1-S4	2976	45.8	2.72
7	PT-F1-S4A	5266	54.0	2.75
8	PT-F1-S4B	8348	56.2	2.72
9	PT-F1-S5	4506	52.1	2.73
10	PT-F2-S1A	1809	47.0	2.67
11	PT-F2-S1B	903	41.0	2.69
12	PT-F2-S2	13226	55.3	2.60
13	PT-F2-S3	6647	49.7	2.73
14	PT-F2-S4	6298	54.4	2.72
15	PT-F2-S5A	250	42.8	2.66
16	PT-F2-S5B	220	39.4	2.68
17	PT-F2-S6	1440	44.6	2.68
18	PT-F2-S7	996	40.7	2.70
19	PT-S3A	4896	51.0	2.70
20	PT-S3B	7044	43.5	2.70
21	PT-S4A	3211	46.8	2.69
22	PT-S4B	3999	47.9	2.69
23	PW-F1-S1	206	36.6	2.69
24	PW-F1-S2A	799	33.7	2.71
25	PW-F1-S2B	130	33.6	2.71
26	PW-F1-S3	527	41.3	2.68
27	PW-F1-S4A	4559	44.0	2.79
28	PW-F1-S4B	5952	35.0	2.70
29	PW-F1-S5A	10324	53.6	2.76
30	PW-F1-S5B	13426	51.1	2.70
31	PW-F1-S6	21039	52.7	2.69
32	PW-F2-S5	753	42.4	2.71
33	PW-F2-S2	4543	46.3	2.70
34	PW-F3-S1A	7058	55.3	2.72
35	PW-F3-S1B	9919	54.0	2.72
36	PW-F3-S2	2484	46.1	2.70
37	PW-F3-S3A	1016	42.4	2.69
38	PW-F3-S3B	898	42.3	2.69
39	PW-F3-S4	3776	48.2	2.69
40	PW-F3-S5	194	38.3	2.68
41	PW-F3-S6	110	35.3	2.68

42	PW-F3-S7A	864	42.3	2.68
43	PW-F3-S7B	2118	50.2	2.68
44	PW-F4-S1	2927	49.1	2.70
45	PW-F4-S2	5004	47.6	2.70
46	PW-F5-S1	1531	47.3	2.68
47	PW-F5-S2	1180	46.9	2.69
48	PW-F6-S1A	1026	45.7	2.70
49	PW-F6-S1B	627	52.7	2.71
50	PW-F6-S2	2394	47.5	2.69
51	PW-F6-S3	2299	48.9	2.71
52	PW-F6-S4	558	44.8	2.70
53	PW-F6-S5	1912	50.0	2.70
54	PW-F6-S6	456	45.7	2.71
55	PW-F6-S7A	939	40.7	2.69
56	PW-F6-S7B	647	45.1	2.78
57	PW-F6-S8	2714	49.8	2.69
58	PW-F6-S9	4170	49.9	2.69
59	PW-F7-S1	6107	49.2	2.67
60	PR-F1-S1	11638	38.9	2.71
61	PR-F1-S3A	2780	39.2	2.70
62	PR-F1-S3B	5767	40.6	2.71
63	PR-F3-S3	1350	35.1	2.70
64	PR-F5-S2A	2354	47.7	2.72
65	PR-F5-S2B	296	34.3	2.72
66	PR-F7-S1	12810	49.7	2.72
67	PR-F7-S2	13137	55.8	2.70
68	PR-F8-S1	19422	53.6	2.72
69	PR-F11-S1	25825	44.1	2.72
70	PR-F13-S1	2176	42.5	2.72
71	PR-F13-S3A	10447	54.9	2.74
72	PR-F13-S3B	59	39.5	2.71
73	PR-F14-S1A	2290	40.6	2.70
74	PR-F14-S1B	7257	43.0	2.70
75	PR-F14-S4	8708	40.4	2.70
76	PR-F14-S6A	7325	44.4	2.68
77	PR-F14-S6B	5255	37.6	2.68
78	PR-F14-S8A	7863	58.1	2.72
79	PR-F14-S8B	6043	51.6	2.72

80	PR-F15-S1A	50.2	28.0	2.71
81	PR-F15-S1B	243	34.8	2.70
82	PR-F15-S2A	7883	48.6	2.72
83	PR-F15-S2B	9042	52.6	2.73
84	SP-F1-S2	252	38.5	2.80
85	SP-F2-S3	28	23.9	2.81
86	SP-F2-S6	273	28.3	2.76
87	SP-F2-S8	226	31.2	2.79
88	SP-F3-S1A	119	26.3	2.79
89	SP-F3-S1B	70.1	27.5	2.79
90	SP-F3-S3	236	29.2	2.81
91	SP-F4-S3A	62	33.2	2.78
92	SP-F4-S3B	134	38.3	2.79
93	SP-F5-S1	210	33.0	2.79
94	SP-F5-S2	171	33.6	2.76
95	SP-F5-S3A	1006	53.9	3.79
96	SP-F5-S3B	690	36.3	2.78
97	SP-F5-S4	209	29.2	2.78
98	SP-F5-S6	111	33.9	2.80
99	SP-F5-S7	52.7	31.9	2.79
100	SP-F8-S1A	1383	40.0	2.73
101	SP-F8-S1B	1018	38.5	2.71
102	SP-F9-S2	407	34.7	2.79
103	SP-F10-S1	394	39.5	2.77
104	SP-F13-S1	250	36.1	2.76
105	SP-F13-S3A	1788	40.8	2.81
106	SP-F13-S3B	1310	37.5	2.81
107	SP-F14-S1	84.4	30.9	2.75
108	SP-F14-S3A	91.5	37.6	2.78
109	SP-F14-S3B	105	38.7	2.79
110	SP-F14-S7A	190	47.8	2.78
111	SP-F14-S7B	74.7	45.5	2.74
112	SP-F14-S8A	102	37.5	2.76
113	SP-F14-S8B	75.2	36.2	2.77
114	SP-F16-S6	65.4	32.9	2.69
115	SP-F16-S10A	5794	30.9	2.69
116	SP-F16-S10B	33225	34.1	2.70
117	SP-F16-S10C	374	30.7	2.69

118	RP-F1-S2	14418	33.6	2.79
119	RP-F1-S3	26.4	28.6	2.77
120	RP-F2-S1	18299	40.1	2.77
121	RP-F2-S4	0.0144	13.8	2.81
122	RP-F3-S1	51.1	12.0	2.70
123	RP-F3-S2	2.27	16.5	2.70
124	RP-F3-S3	4.89	28.8	2.69
125	RP-F4-S2	0.0572	16.8	2.76
126	RP-F4-S3	950	20.7	2.71
127	RP-F5-S1	807	37.6	2.77
128	RP-F5-S5	666	50.4	2.78
129	RP-F6-S2A	2107	43.9	2.70
130	RP-F6-S2B	1908	43.6	2.70
131	RP-F6-S3	1270	46.6	2.70
132	RP-F7-S1	476	35.5	2.69
133	RP-F7-S5	128	35.7	2.70
134	RP-F7-S9	779	37.6	2.69
135	RP-F8-S1	5279	43.7	2.70
136	RP-F8-S1	5354	43.2	2.70
137	RP-F9-S3	2655	41.7	2.69
138	RP-F10-S1	851	37.1	2.68
139	RP-F10-S3	1247	39.3	2.70
140	RP-F10-S4	784	42.9	2.68
141	RP-F11-S1	10170	27.7	2.69
142	RP-F11-S3A	16917	32.0	2.69
143	RP-F11-S3B	0.213	14.5	2.57
144	RP-F11-S4A	0.451	10.9	2.55
145	RP-F11-S4B	664	13.2	2.57
146	RP-F11-S5A	2.27	12.3	2.54
147	RP-F11-S5B	0.166	14.1	2.56
148	WF-F2-S1A	57	37.1	2.73
149	WF-F2-S1B	27.8	36.8	2.74
150	WF-F2-S2	40.1	35.7	2.72
151	WF-F4-S1A	53.4	37.3	2.71
152	WF-F4-S1B	108	37.4	2.70
153	WF-F4-S2A	77.9	34.3	2.71
154	WF-F4-S2B	149	33.5	2.71

155	WF-F6-S3	309	32.9	2.70
156	WF-F6-S4	128	33.4	2.71
157	WF-F6-S5	182	35.2	2.71
158	PV-F1-S3A	386	37.4	2.66
159	PV-F1-S3B	90.7	33.2	2.66
160	PV-F2-S1	3807	40.4	2.67
161	PV-F3-S4A	2923	45.9	2.69
162	PV-F3-S4B	3679	44.3	2.69
163	PV-F4-S1	4861	50.4	2.68
164	PV-F4-S3A	823	35.6	2.67
165	PV-F4-S3B	3183	43.1	2.69
166	Beach Rhodo Facies	3266	38.2	2.70
167	Beach Coarse CF-C1 A	1006	39.7	2.69
168	Beach Coarse CF-C1 B	12458	41.9	2.69
169	PD-F1-S1A	3012	28.3	2.69
170	PD-F1-S1B	3371	36.4	2.69
171	PD-F1-S4A	8521	43.2	2.71
172	PD-F1-S4B	2035	41.3	2.68
173	PD-F1-S7	5948	38.4	2.70
174	PD-F3-S4A	7111	42.6	2.70
175	PD-F3-S4B	5867	42.8	2.69
176	PD-F3-S7A	1055	39.0	2.70
177	PD-F3-S7B	1536	42.3	2.69
178	PD-F4-S1A	346	38.7	2.70
179	PD-F4-S1B	83.2	33.5	2.69
180	PD-F4-S4	920	39.1	2.69
181	PD-F4-S5	46.1	33.2	2.70
182	PD-F5-S2	5383	40.0	2.70
183	PB-F1-S1A	185	33.8	2.66
184	PB-F1-S1B	8.39	35.3	2.66
185	PB-F1-S2	1146	32.4	2.68
186	PB-F1-S4	315	35.9	2.67
187	PB-F2-S1	825	31.8	2.69
188	PB-F3-S2	1358	45.0	2.67
189	PB-F3-S3	853	41.5	2.70
190	PB-F3-S4A	2203	44.8	2.71
191	PB-F3-S4B	839	46.2	2.69

192	PL-F2-S2A	0.729	16.0	2.71
193	PL-F2-S2B	0.325	16.4	2.71

194	SP-F1-S3	590	37.3	2.81
195	SP-F2-S2	142	28.6	2.78
196	SP-F2-S4	242	28.4	2.78
197	SP-F4-S4	102	35.7	2.76
198	SP-F6-S1A	362	38.1	2.78
199	SP-F6-S1B	155	32.0	2.78
200	SP-F6-S2A	157	30.0	2.78
201	SP-F6-S2B	272	34.4	2.79
202	SP-F6-S3	145	35.3	2.74
203	SP-F7-S1	115	36.8	2.79
204	SP-F7-S4	66.3	36.9	2.80
205	SP-F7-S5	228	38.2	2.79
206	SP-F9-S1	721	36.5	2.76
207	SP-F10-S3	426	37.1	2.75
208	SP-F11-S2A	701	34.2	2.80
209	SP-F11-S2B	690	35.0	2.80
210	SP-F11-S3	330	36.4	2.76
211	SP-F11-S4	365	33.4	2.77
212	SP-F12-S1A	313	35.4	2.72
213	SP-F12-S1B	335	36.2	2.72
214	SP-F12-S2A	643	39.4	2.74
215	SP-F12-S2B	432	39.9	2.75
216	SP-F13-S6A	1223	38.1	2.80
217	SP-F13-S6B	1256	39.0	2.80
218	SP-F14-S4	128	34.6	2.79
219	SP-F14-S5	217	40.5	2.78
220	SP-F14-S6	128	35.1	2.71
221	SP-F16-S1	49	38.6	2.71
222	SP-F16-S2	544	33.3	2.72
223	SP-F16-S3A	48.6	27.3	2.71
224	SP-F16-S3B	301	28.5	2.71
225	SP-F16-S7A	4.77	26.5	2.73
226	SP-F16-S7B	80.2	30.1	2.73

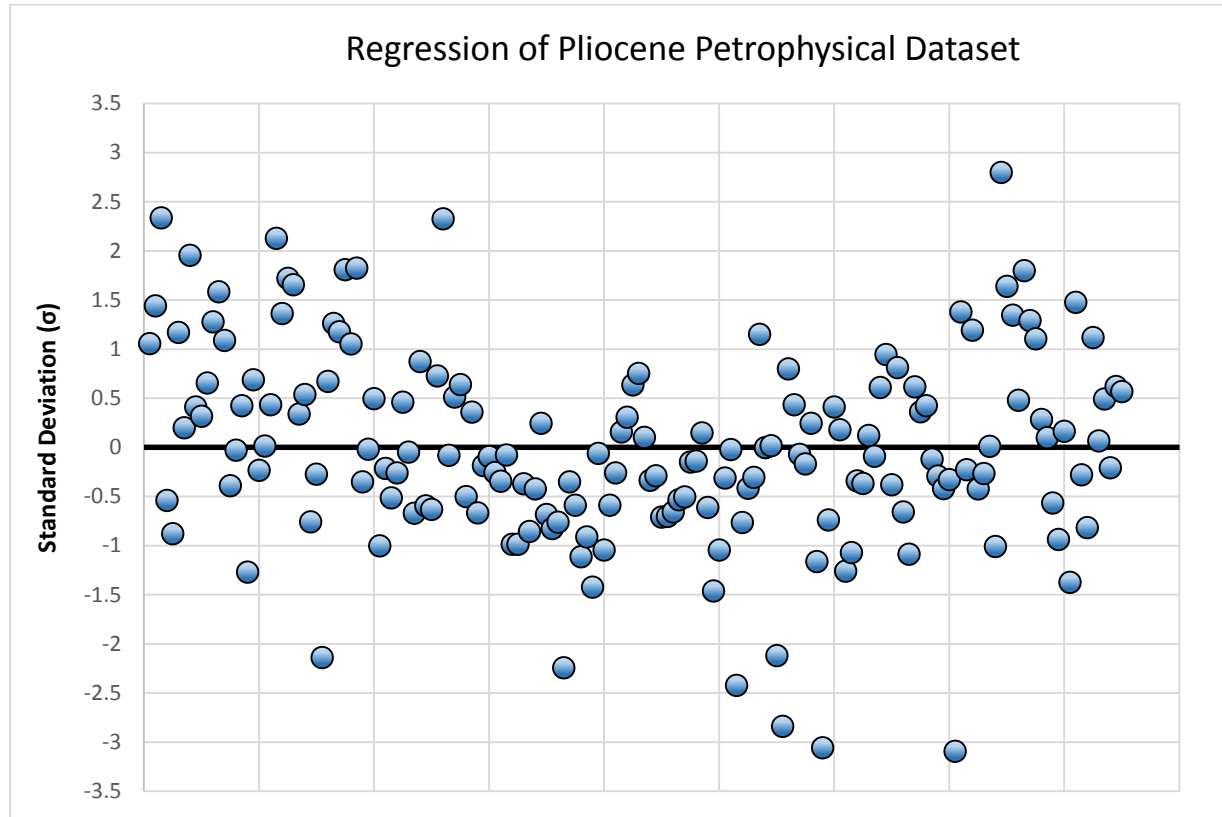
227	SP-F16	93.6	36.6	2.74
228	RM-F1-S1A	51.8	40.9	2.79
229	RM-F1-S1B	152	44.3	2.77
230	RM-F1-S2	1031	46.4	2.78
231	RM-F1-S4	2995	47.2	2.80
232	RM-F2-S1	1865	35.5	2.76
233	RM-F2-S2	231	32.1	2.78
234	RM-F4-S6A	46.3	29.6	2.76
235	RM-F4-S6B	53.5	29.7	2.77
236	RM-F4-S6C	1817	38.9	2.77
237	RM-F5-S1	1481	38.9	2.79
238	RM-F5-S2	5253	44.9	2.76
239	RM-F6-S1	4193	45.7	2.78
240	RM-F6-S2	40.5	37.3	2.78
241	RM-F7-S2A	1256	19.9	2.80
242	RM-F7-S2B	503	37.2	2.79
243	RM-F7-S2C	2191	39.1	2.79
244	RM-F7-S3	4679	40.8	2.77
245	RM-F7-S4	3867	35.7	2.80
246	RM-F8-S1	5590	20.8	2.80
247	RM-F8-S2	3698	42.2	2.80
248	RM-F8-S3	5814	45.5	2.70
249	RM-F8-S4	4810	36.1	2.69
250	RM-F9-S1	0.593	13.7	2.71
251	RM-F9-S2A	2641	29.8	2.70
252	RM-F9-S2B	3247	32.0	2.70
253	RM-F9-S3	3.64	11.4	2.71
254	RP-F1-S4	0.0113	2.9	2.65
255	RP-F2-S2	1922	34.7	2.73
256	RP-F2-S3	152	21.2	2.72
257	RP-F4-S1	2.16	18.3	2.73
258	RP-F4-S4A	0.0184	15.3	2.76
259	RP-F4-S4B	0.438	14.5	2.75
260	RP-F5-S4	12.8	26.0	2.75
261	RP-F6-S1A	384	36.9	2.68
262	RP-F7-S2B	781	37.8	2.69
263	RP-F7-S4	1670	42.6	2.69

264	RP-F7-S4	3611	44.5	2.71
265	RP-F7-S6A	1747	42.1	2.69
266	RP-F8-S2B	4761	40.7	2.69
267	RP-F9-S2	406	24.6	2.69
268	RP-F11-S2	0.0917	13.6	2.68
269	RP-TF-S1	15131	17.3	2.73
270	SP-F1-S1A	239	31.2	2.77
271	SP-F2-S7B	1749	31.6	2.80
272	SP-F4-S5	197	31.5	2.77
273	SP-F7-S2	70.3	33.7	2.79
274	SP-F7-S2	140	33.3	2.79
275	SP-F7-S3A	86.5	35.9	2.81
276	SP-F7-S3B	54	34.7	2.79
277	SP-F10-S2	903	39.6	2.72
278	SP-F10-S4A	540	36.3	2.76
279	SP-F11-S1B	1432	37.6	2.79
280	SP-F11-S3A	621	33.1	2.76
281	SP-F11-S5B	598	31.7	2.78
282	SP-F13-S2A	573	36.6	2.79
283	SP-F13-S2B	781	35.6	2.79
284	SP-F14-S2	396	45.1	2.75
285	SP-F16-S5A	11.3	27.3	2.67
286	SP-F16-S5B	12.5	26.3	2.67
287	SP-F16-S5C	7.13	25.7	2.67
288	PM-F1-S1	1596	37.9	2.70
289	PM-F2-S2	1946	41.3	2.69
290	PM-F6-S1	1806	44.2	2.69
291	PM-F6-S4	7439	52.4	2.71
292	PM-F6-S5	5014	47.6	2.69
293	PM-F7-S1	150	38.1	2.66
294	PM-F7-S2	3.45	30.4	2.67
295	PM-F7-S3	253	38.1	2.67
296	PM-F7-S4	9229	49.8	2.67
297	PM-F7-S5	765	38.0	2.69
298	PM-F7-S6	47.3	32.6	2.69
299	PM-F7-S7	315	41.4	2.66
300	PM-F8-S1	105	30.8	2.69
301	PM-F8-S2	55.5	27.6	2.69

302	PM-F8-S3	267	32.8	2.69
303	PM-F10-S1	4565	49.3	2.68
304	PM-F10-S2	3166	42.8	2.68
305	PM-F11-S3	1855	37.7	2.69
306	PM-F11-S5	1327	44.6	2.70
307	PM-F12S1	4061	42.8	2.68
308	PM-F12S2	2858	50.5	2.69
309	PM-F12-S3	3476	54.3	2.68
310	PM-F13-S1	6161	46.3	2.68
311	PM-F13-S2	5871	47.7	2.69
312	PM-F13-S3A	12807	51.4	2.68
313	PM-F13-S3B	10727	54.0	2.65
314	PM-F16-S2	8450	53.9	2.72
315	PM-F17-S1	16636	58.3	2.73
316	PR-F2-S2A	5948	34.9	2.68
317	PR-F2-S2B	108	32.3	2.67
318	PR-F2-S4	13.5	23.4	2.68
319	PR-F2-S5A	2591	38.1	2.70
320	PR-F2-S5B	1086	39.7	2.67
321	PR-F2-S6	7347	38.5	2.71
322	PR-F2-S7	4209	45.6	2.70
323	PR-F2-S8A	273	31.7	2.71
324	PR-F2-S8B	141	25.9	2.71
325	PR-F3-S1	5398	41.3	2.71
326	PR-F3-S2	2605	35.4	2.69
327	PR-F5-S3A	385	32.8	2.71
328	PR-F5-S3B	34.9	31.0	2.69
329	PR-F7-S3	10953	53.3	2.72
330	PR-F11-S2	26002	49.1	2.72
331	PR-F11-S4A	8647	40.9	2.71
332	PR-F11-S4B	6786	40.0	2.70
333	PR-F13-S2A	1777	40.2	2.72
334	PR-F13-S2B	296	39.1	2.71
335	PR-F14S2	17964	48.3	2.72
336	PR-F14S7A	580	40.0	2.71
337	PR-F14-S7B	1331	42.3	2.70
338	PR-F14-S7C	4000	44.8	2.70
339	PT-F1-S	8871	54.9	2.70

340	PT-F1-S1	939	38.3	2.70
341	PT-F2-S9A	26.8	37.1	2.69
342	PT-F2-S9B	175	36.3	2.69
343	PL-F1-S2	1710	42.1	2.70
344	WF-F1-S1	180	40.1	2.74
345	WF-F2-S4	79.8	39.5	2.76
346	WF-F3-S2	94.5	36.2	2.67
347	WF-F3-S3	61.4	31.1	2.75
348	WF-F5-S1	302	38.4	2.68
349	WF-F5-S2	536	42.9	2.69
350	WF-F5-S3	407	38.7	2.70
351	WF-F6-S1	4422	38.1	2.75
352	WF-F6-S6	30.6	26.7	2.68
353	SP-F4-S2A	354	38.9	2.75
354	SP-F4-S2B	483	40.2	2.75
355	SP-F13-S4	614	39.7	2.72
356	SP-F13-S7A	1028	41.8	2.76
357	SP-F13-S7B	155	39.3	2.76
358	SP-F13-S9A	90.7	40.9	2.75
359	SP-F13-S9B	123	37.3	2.73
360	RP-F7-S3A	1496	38.6	2.66
361	RP-F7-S3B	2325	39.4	2.69

Pliocene Dataset Regression Summary Output



<i>Regression Statistics</i>	
Multiple R	0.769618844
R Square	0.592313165
Adjusted R Square	0.589886457
Standard Error	0.532820499
Observations	170

ANOVA					
	<i>df</i>	<i>SS</i>	<i>MS</i>	<i>F</i>	<i>Significance F</i>
Regression	1	69.29403147	69.29403	244.081	1.47253E-34
Residual	168	47.69481094	0.283898		
Total	169	116.9888424			

	<i>Coefficients</i>	<i>Standard Error</i>	<i>t Stat</i>	<i>P-value</i>	<i>Lower 95%</i>	<i>Upper 95%</i>	<i>Lower 95.0%</i>	<i>Upper 95.0%</i>
Intercept	-0.316791958	0.22771132	-1.3912	0.166004	-0.766336275	0.132752358	-0.766336275	0.132752358
0.38869719	8.163980899	0.522558589	15.62309	1.47E-34	7.132353471	9.195608327	7.132353471	9.195608327

RESIDUAL OUTPUT					
<i>Observation</i>	<i>Predicted 4.06587835285739</i>	<i>Residuals</i>	<i>Standard Residuals</i>		
1	2.882688746	0.56135605	1.056686585		
2	2.99520141	0.765748542	1.441431355		
3	2.532874478	1.241496481	2.336970765		
4	2.319282132	-0.285858376	-0.538094693		
5	1.596868476	-0.466534708	-0.878196587		
6	2.791315911	0.622151502	1.171126858		
7	2.928319324	0.107510501	0.202375844		
8	2.82754965	1.03856039	1.954967497		
9	3.404524298	0.219654628	0.413473942		
10	2.267655666	0.168506981	0.317194526		
11	1.800608336	0.348610777	0.65621869		
12	3.052954414	0.679278466	1.278661633		
13	2.573818939	0.841988789	1.584944632		
14	2.5519759	0.578357869	1.088690505		
15	3.57858481	-0.206778352	-0.38923587		
16	2.486118541	-0.01482683	-0.027909759		
17	2.358793455	0.226667275	0.426674423		
18	2.216302312	-0.673476885	-1.267740839		
19	3.741458925	0.366090205	0.689121652		
20	4.242552887	-0.124056687	-0.233522088		
21	4.032008249	0.007524838	0.014164621		
22	4.056470869	0.231823081	0.436379619		
23	3.280554468	1.131485862	2.129888744		
24	3.690626546	0.724380208	1.363560344		
25	3.022508282	0.914357177	1.721169592		
26	2.951041854	0.880572001	1.657572981		
27	3.156915062	0.180743829	0.34022895		
28	2.962276421	0.287411007	0.541017337		

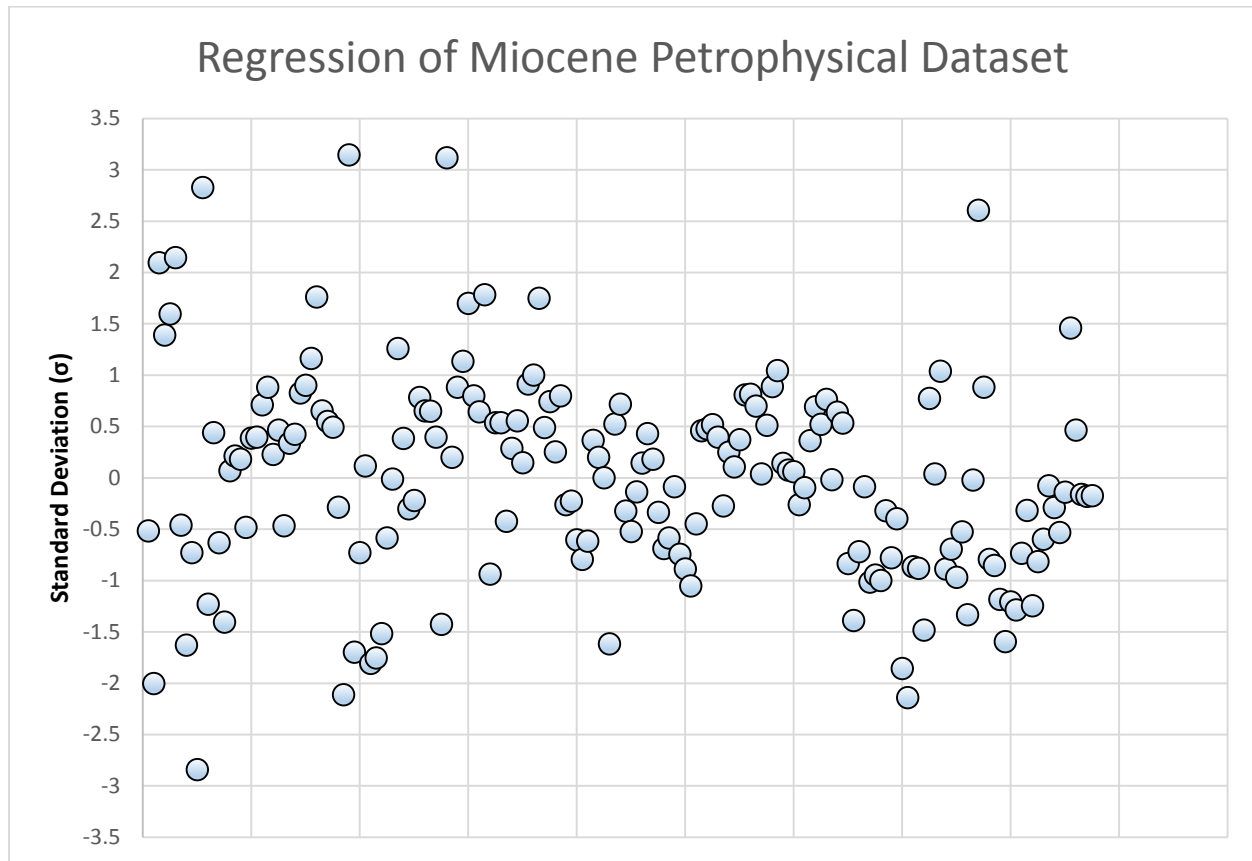
29	2.873786953	-0.402495242	-0.757649842
30	4.163643522	-0.144651927	-0.272290199
31	2.905676656	-1.134824644	-2.136173607
32	3.001363991	0.358471491	0.674780322
33	3.190167721	0.670589402	1.262305493
34	3.629438311	0.624964735	1.176422437
35	2.978488129	0.961430292	1.80977918
36	3.305573541	0.559234088	1.052692243
37	2.751301271	0.969271449	1.824539234
38	2.948992319	-0.185564325	-0.349302966
39	3.134086909	-0.009908853	-0.018652248
40	3.337042004	0.265017988	0.498865118
41	4.426733974	-0.531145699	-0.999819161
42	3.893950835	-0.112698241	-0.212141152
43	1.972081182	-0.271377465	-0.510836084
44	2.522130816	-0.136524542	-0.256991356
45	3.65181929	0.244872236	0.460943117
46	3.981099492	-0.02483499	-0.04674894
47	2.668326296	-0.354459076	-0.667227423
48	2.437179291	0.465367488	0.875999434
49	2.429508104	-0.315564752	-0.594013444
50	3.056929865	-0.33511925	-0.63082248
51	3.271806662	0.38706293	0.728600335
52	2.537535349	1.237127573	2.328746811
53	4.055417248	-0.041569252	-0.078249216
54	3.855211836	0.272734806	0.51339112
55	3.982204423	0.340820671	0.641554733
56	3.141860529	-0.265065553	-0.498954655
57	3.466047895	0.191294841	0.360089987
58	4.20163018	-0.352948526	-0.664383991
59	4.093164185	-0.096696295	-0.182019376
60	3.444735496	-0.049583905	-0.093335855
61	3.142295295	-0.135401588	-0.254877526
62	3.135909827	-0.18263349	-0.343786015
63	3.616724474	-0.039692489	-0.074716431
64	2.810735542	-0.522933812	-0.984361251
65	2.564011174	-0.522618489	-0.983767694
66	3.133332018	-0.196818275	-0.3704872
67	3.780549635	-0.454623679	-0.855775479
68	3.690710458	-0.224287735	-0.422195221
69	3.568004202	0.131313099	0.247181428

70	3.547379703	-0.362404512	-0.68218377
71	3.50962274	-0.437740732	-0.823995323
72	3.414736003	-0.403588642	-0.759708039
73	3.987733699	-1.190466158	-2.240912198
74	3.564165689	-0.185041543	-0.348318889
75	3.674179977	-0.312641006	-0.588509837
76	3.337798454	-0.591164255	-1.112797017
77	3.764863441	-0.483375553	-0.909897493
78	3.414522149	-0.755557306	-1.422247555
79	3.004281102	-0.03161551	-0.05951247
80	3.364554475	-0.553650195	-1.042181221
81	3.745715021	-0.312105178	-0.587501203
82	3.757163689	-0.137027634	-0.257938367
83	3.702053475	0.083774445	0.157695516
84	2.808210866	0.164454726	0.309566635
85	3.700266979	0.339424683	0.63892695
86	3.580844094	0.400748023	0.75436091
87	3.41904978	0.054583147	0.102746339
88	3.748582415	-0.176524425	-0.33228642
89	3.933818936	-0.15299776	-0.288000247
90	4.142161529	-0.376641986	-0.708984137
91	4.093679933	-0.372199078	-0.700620885
92	4.269569302	-0.347986861	-0.655044242
93	3.936711223	-0.282920036	-0.532563613
94	3.523971671	-0.266533104	-0.501717146
95	3.034262966	-0.078575216	-0.147908581
96	4.19434844	-0.072919922	-0.137263157
97	3.743332371	0.079293308	0.149260304
98	4.123475712	-0.324273056	-0.610405799
99	3.174405695	-0.776465686	-1.461605117
100	2.896734511	-0.55431183	-1.043426672
101	3.323090958	-0.164728466	-0.310081917
102	3.008884662	-0.010625324	-0.020000919
103	2.714070116	-1.285935322	-2.420621643
104	2.649034875	-0.405996827	-0.764241163
105	4.168030623	-0.220058044	-0.414233325
106	3.85090496	-0.161063551	-0.303183146
107	3.235391524	0.612427824	1.152823178
108	3.506726195	-8.58897E-05	-0.000161677
109	3.592123028	0.009828376	0.01850076
110	0.98775022	-1.125022692	-2.117722587

111	1.018855806	-1.506972445	-2.836697969
112	2.777242827	0.42579006	0.801499591
113	3.057731411	0.231411425	0.435604726
114	3.293145457	-0.036427711	-0.068570872
115	3.961045599	-0.08953104	-0.168531628
116	3.569503074	0.130681255	0.245992057
117	2.791976791	-0.615885532	-1.159331906
118	2.161835744	-1.624016649	-3.057019886
119	2.795492475	-0.392371953	-0.738593945
120	3.745361573	0.219793073	0.413734548
121	2.788016719	0.095644716	0.180039903
122	2.342683718	-0.667822578	-1.257097272
123	3.0670428	-0.568732247	-1.070571406
124	2.201768176	-0.180578877	-0.339918447
125	1.938411679	-0.194118696	-0.36540556
126	2.36152618	0.064985081	0.122326754
127	3.706252966	-0.046812184	-0.088118418
128	3.174959803	0.325551107	0.61281158
129	2.764948704	0.50339521	0.947582138
130	3.324477074	-0.201606151	-0.379499812
131	3.176159964	0.432473026	0.814079487
132	3.803860843	-0.347798619	-0.654689898
133	4.117986189	-0.576906421	-1.085958325
134	3.461930186	0.327721023	0.61689619
135	3.57589375	0.192818331	0.362957776
136	3.88144003	0.22600738	0.425432248
137	4.092554439	-0.062076158	-0.11685105
138	4.081676822	-0.154820113	-0.291430611
139	4.442456555	-0.221407643	-0.416773786
140	2.440961428	-0.173789699	-0.32713862
141	2.565966205	-1.642204244	-3.091255889
142	2.325787284	0.733397334	1.38053402
143	2.617378273	-0.119067719	-0.224130945
144	2.281831358	0.634622591	1.194602211
145	3.356173239	-0.223273469	-0.420285983
146	3.072400039	-0.141451008	-0.266264846
147	3.337398417	0.00561608	0.010571609
148	3.458320783	-0.534558823	-1.006243964
149	1.990644882	1.488210086	2.80138004
150	2.65585417	0.871904582	1.641257587
151	3.214015712	0.716474854	1.348679446

152	3.0525311	0.256033313	0.481952528
153	2.817402186	0.956968774	1.801380899
154	3.16470861	0.687222068	1.293614527
155	3.179853837	0.588562252	1.107899053
156	2.870740901	0.152511559	0.28708503
157	3.133277625	0.05311359	0.099980072
158	2.839703265	-0.300627166	-0.565895199
159	2.417800874	-0.497677547	-0.936819311
160	2.876155357	0.08763247	0.164957794
161	2.392534153	-0.728833228	-1.371942629
162	2.945352198	0.785672182	1.478935259
163	2.734132588	-0.147545284	-0.277736603
164	2.390894257	-0.43328697	-0.815611641
165	2.985523858	0.595059019	1.120128451
166	3.430569567	0.035259248	0.066371378
167	3.303579709	0.262150079	0.493466618
168	3.795710863	-0.108985242	-0.205151869
169	2.586091285	0.32930855	0.619884523
170	3.200208394	0.302628244	0.569661993

Miocene Dataset Regression Summary Output



<i>Regression Statistics</i>	
Multiple R	0.742652187
R Square	0.551532271
Adjusted R Square	0.548939972
Standard Error	0.682499427
Observations	175

ANOVA					
	<i>df</i>	<i>SS</i>	<i>MS</i>	<i>F</i>	<i>Significance F</i>
Regression	1	99.10382522	99.10383	212.758	6.08495E-32
Residual	173	80.58434601	0.465805		
Total	174	179.6881712			

	<i>Coefficients</i>	<i>Standard Error</i>	<i>t Stat</i>	<i>P-value</i>	<i>Lower 95%</i>	<i>Upper 95%</i>	<i>Lower 95.0%</i>	<i>Upper 95.0%</i>
--	---------------------	-----------------------	---------------	----------------	------------------	------------------	--------------------	--------------------

Intercept	- 0.850544 279	0.22241 875	- 3.824 07	0.000 183	- 1.289548 032	- 0.41154 0526	- 1.28954 8032	- 0.41154 0526
0.3358579 59	9.183679 946	0.62961 3197	14.58 623	6.08E -32	7.940967 465	10.4263 9243	7.94096 7465	10.4263 9243

RESIDUAL OUTPUT			
<i>Observation</i>	<i>Predicted</i> <i>4.158905</i>	<i>Residuals</i>	<i>Standard</i> <i>Residuals</i>
1	1.772470754	-0.350866754	-0.515574584
2	-0.585029049	-1.361890951	-2.001205167
3	2.836496761	1.425930239	2.0953065
4	2.336922774	0.946830226	1.391301953
5	1.093309997	1.088534003	1.599525916
6	0.248508615	1.459912385	2.145240929
7	0.668289041	-0.312263041	-0.458849081
8	1.797903504	-1.108594504	-1.629003444
9	0.829261603	-0.494807603	-0.72708577
10	0.689896688	-1.932496688	-2.839671087
11	1.05260003	1.92512397	2.828837385
12	0.476671082	-0.835201082	-1.227270597
13	2.606464185	0.300409815	0.44143158
14	1.536964346	-0.429754346	-0.631494479
15	3.779032757	-0.955558757	-1.404127931
16	2.536208748	0.048122252	0.070712342
17	3.177532496	0.146132504	0.214731673
18	3.155424338	0.125153662	0.183904706
19	3.430993328	-0.327189328	-0.480782234
20	2.413922641	0.263684359	0.387466046
21	2.621664249	0.270986751	0.398196408
22	2.690576242	0.484355758	0.711727503
23	2.763567653	0.602855347	0.885854506
24	3.066177088	0.156538912	0.230023174
25	3.239901952	0.317725048	0.466875125
26	2.423493431	-0.316283431	-0.464756768
27	3.012019036	0.230273964	0.338371766
28	2.602449677	0.289087323	0.424793956
29	3.15896708	0.56358492	0.828149311
30	3.113371221	0.615306779	0.90415103
31	2.885250475	0.792447525	1.164447183

32	1.407973298	1.200552702	1.764129697
33	2.980139636	0.443925364	0.652317817
34	2.554685458	0.375244542	0.551396068
35	2.758200811	0.337665189	0.496175792
36	3.08767477	-0.19335877	-0.284127425
37	0.398913552	-1.436543552	-2.110902035
38	2.086210699	2.142112301	3.147686826
39	0.482147319	-1.153767319	-1.695381792
40	0.149624672	-0.495444672	-0.728021901
41	0.275004174	0.081021826	0.119056006
42	0.447674025	-1.227564025	-1.803820981
43	2.906691677	-1.192361677	-1.752093548
44	3.213689406	-1.031845406	-1.516225918
45	3.409666298	-0.396407298	-0.582493284
46	3.483487509	-0.007090509	-0.010419016
47	2.411634159	0.859044841	1.262307362
48	2.100460905	0.263151095	0.386682451
49	1.869509143	-0.203928143	-0.299658393
50	1.87686258	-0.14850858	-0.218223154
51	2.725393308	0.533961692	0.784620014
52	2.72489243	0.44566257	0.654870521
53	3.277016628	0.443390372	0.651531683
54	3.350703611	0.271821389	0.399422853
55	2.576556135	-0.969101135	-1.424027524
56	0.977280023	2.121709977	3.117707012
57	2.56312695	0.13844105	0.20342961
58	2.737903317	0.602738683	0.885683076
59	2.896587361	0.773565639	1.13670155
60	2.429656066	1.157717934	1.701186949
61	3.022392985	0.545574015	0.801683525
62	3.325993827	0.438481173	0.644317953
63	2.467315344	1.214829656	1.7851087
64	0.409040947	-0.635990947	-0.934544993
65	0.194457414	0.366643586	0.538757555
66	2.011004167	0.367393833	0.539859992
67	2.687509003	-0.286108003	-0.42041605
68	2.574152536	0.196699464	0.289036345
69	1.772215034	0.380072966	0.558491106
70	1.345174385	0.101983615	0.149857914
71	1.759808562	0.624006438	0.916934581
72	1.75300734	0.68315566	1.003850298

73	2.051946546	1.190843454	1.749862625
74	2.018582962	0.335525038	0.493030987
75	1.568927832	0.506619168	0.744442055
76	1.672744686	0.172973314	0.254172398
77	1.828125195	0.544786805	0.800526774
78	2.726221024	-0.177218024	-0.260409709
79	2.836856734	-0.152909734	-0.224690346
80	2.202313885	-0.409921885	-0.602352042
81	2.665628325	-0.538523325	-0.791323021
82	2.427430043	-0.418830043	-0.615441967
83	2.044331604	0.250134396	0.367555307
84	2.184143222	0.138075778	0.202892868
85	2.230652811	0.002343189	0.003443155
86	4.102091824	-1.099493824	-1.61563062
87	2.480982175	0.357866825	0.525860708
88	1.829962078	0.490183922	0.720291589
89	2.264685683	-0.219362683	-0.322338389
90	2.076937295	-0.355126295	-0.521833687
91	2.651341017	-0.092632017	-0.136116384
92	2.090844867	0.099487133	0.146189506
93	1.902112925	0.293787075	0.431699919
94	2.310257849	0.124311151	0.182666694
95	2.38931688	-0.22794888	-0.334955216
96	2.526869956	-0.466171956	-0.685007655
97	2.243373081	-0.396418081	-0.582509129
98	2.204556118	-0.058428118	-0.085856104
99	2.442520501	-0.505504501	-0.742804127
100	2.334869046	-0.602475046	-0.88529568
101	2.536842174	-0.715328174	-1.051125597
102	2.661751664	-0.303816664	-0.446437711
103	2.826940876	0.313881124	0.461226743
104	2.68164144	0.32610656	0.479191181
105	2.503671879	0.354263121	0.520565312
106	2.337794076	0.271799924	0.399391311
107	2.779809762	-0.184313762	-0.270836408
108	2.784709907	0.170978093	0.251240558
109	2.555192021	0.074217979	0.10905822
110	2.478746628	0.253647372	0.372717383
111	2.605839896	0.550103104	0.808338709
112	2.290460673	0.555257327	0.815912486
113	2.362047807	0.476801193	0.700626588

114	2.492044202	0.026469798	0.038895549
115	2.213068057	0.349224943	0.513162056
116	2.186844472	0.606247528	0.890839082
117	2.064927383	0.711773617	1.045902419
118	2.397458654	0.098085346	0.144129676
119	2.471688474	0.053356526	0.078403748
120	2.767180393	0.041030607	0.060291658
121	2.811849895	-0.176365895	-0.259157563
122	2.462033111	-0.064093111	-0.094180423
123	2.511154283	0.247000717	0.362950581
124	2.420903	0.471748	0.693201269
125	2.896796482	0.355571518	0.522487911
126	2.595318981	0.521952019	0.766972625
127	2.799476181	-0.011308181	-0.016616595
128	2.651238426	0.436187574	0.640947666
129	2.734501563	0.364488437	0.535590712
130	2.756413805	-0.566081805	-0.831818312
131	2.902126865	-0.944519865	-1.387907036
132	2.578278699	-0.488373699	-0.717631592
133	1.983602398	-0.057260398	-0.084140221
134	3.287676291	-0.689981291	-1.013880093
135	2.603641085	-0.642220085	-0.943698283
136	2.699969888	-0.678780888	-0.997421871
137	2.323789138	-0.216579138	-0.318248161
138	2.865364438	-0.528904438	-0.777188726
139	2.377471182	-0.270261182	-0.397130236
140	3.541710672	-1.262956672	-1.855828042
141	3.328174886	-1.454853886	-2.137807813
142	2.597515074	-0.588915074	-0.865370233
143	2.475235698	-0.599017698	-0.880215345
144	2.698512448	-1.008316448	-1.481651731
145	2.207403141	0.528195859	0.776147519
146	1.659274414	0.027361586	0.040205971
147	1.771120137	0.707445863	1.039543081
148	1.656157721	-0.603079721	-0.886184207
149	1.568317796	-0.471407796	-0.692701363
150	1.510189235	-0.657099235	-0.965562172
151	2.173012886	-0.357434886	-0.525226003
152	1.584784291	-0.906266291	-1.331696038
153	1.916509978	-0.012335978	-0.018126871
154	1.988100207	1.774877793	2.608060952

155	1.970523764	0.602348236	0.885109341
156	2.50997181	-0.53869581	-0.791576476
157	2.835348195	-0.580075195	-0.852380638
158	2.56068726	-0.80481226	-1.182616311
159	2.528508435	-1.084463435	-1.593544496
160	2.42389519	-0.82075119	-1.206037473
161	2.776004183	-0.874001183	-1.284284679
162	2.474040369	-0.498608369	-0.732670735
163	2.003844083	-0.215676083	-0.316921183
164	2.573556332	-0.846015332	-1.243161394
165	2.587694442	-0.554270442	-0.814462326
166	2.296106037	-0.404569037	-0.594486399
167	2.224847541	-0.051661541	-0.075913084
168	2.676373929	-0.196366929	-0.288547708
169	3.090194358	-0.361029358	-0.530507833
170	2.702680562	-0.093086562	-0.136784306
171	2.650630577	0.994988423	1.462067115
172	2.171464371	0.318493629	0.468004502
173	2.215269835	-0.108059835	-0.158786502
174	2.381920225	-0.121849225	-0.179049063
175	1.602370395	-0.116649395	-0.17140827

Pliocene box plot input

Permeability											
	Box Bottom	121	11164	159.2	7730	2705	1998	2050	3353	1546	681
	Box Middle	65	717.25	155.8	1859	1802	1890	1227	2414	1500	673
	Box Top	191	627.75	4457	3524	4360	8576	2622	2936	2032	3844
	Whisker Top	191	627.75	4457	3524	4360	8576	2622	2936	2032	3844
	Whisker Bottom	65	717.25	155.8	1859	1802	1890	1227	2414	1500	673
Porosity											
	Box Bottom	30	51.892	34.86	49.47	45.22	37.28	34	39.3	37.9	34.9
	Box Middle	2.1	2.1826	4.501	3.182	5.258	4.988	5.783	1.577	4.77	8.96
	Box Top	1.6	0.8864	5.197	2.823	2.852	7.919	5.272	4.151	3.29	4.43
	Whisker Top	1.6	0.8864	5.197	2.823	2.852	7.919	5.272	4.151	3.29	4.43
	Whisker Bottom	2.1	2.1826	4.501	3.182	5.258	4.988	5.783	1.577	4.77	8.96

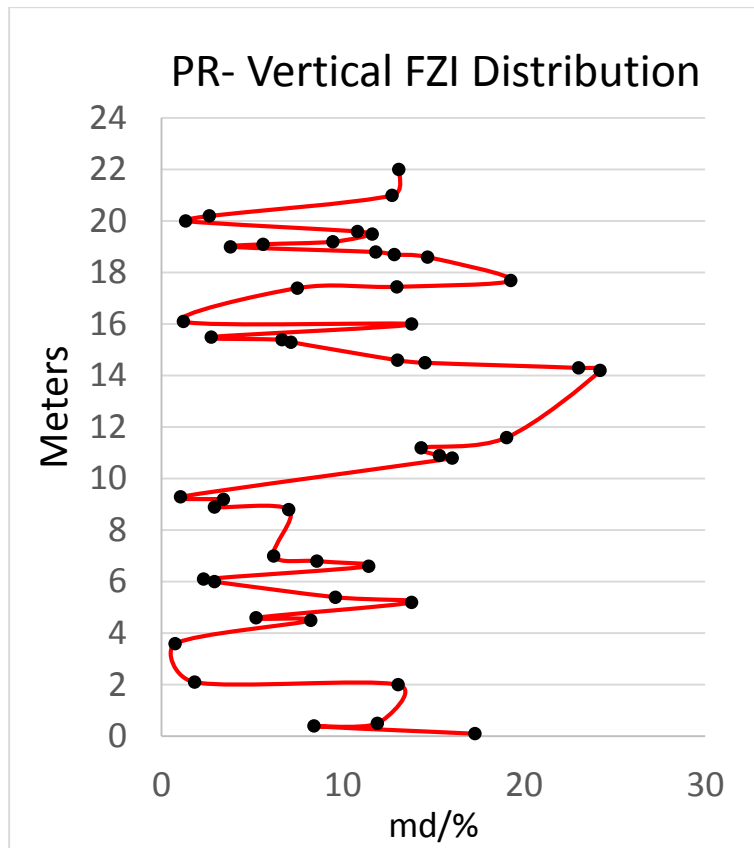
Miocene box plot input

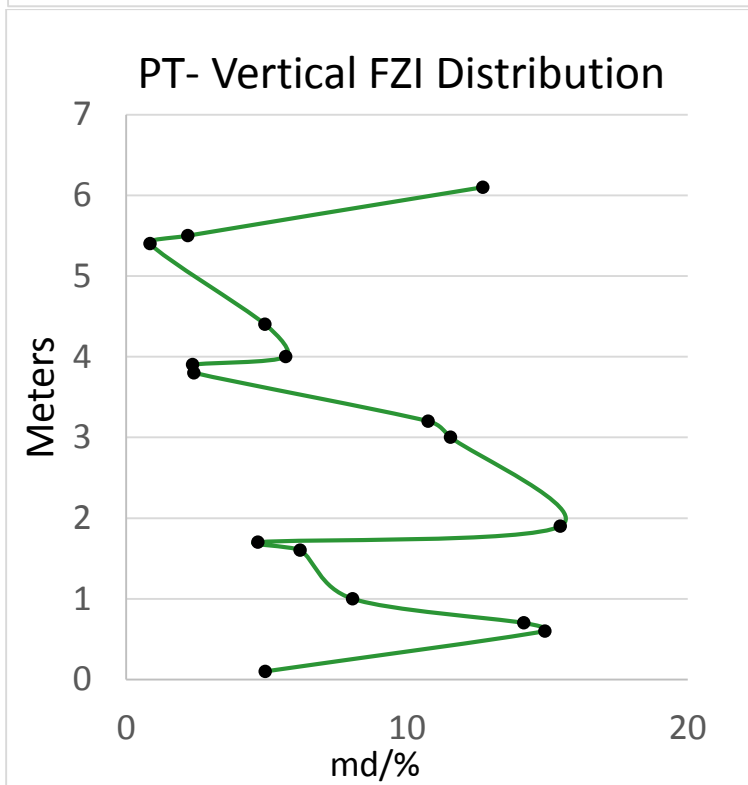
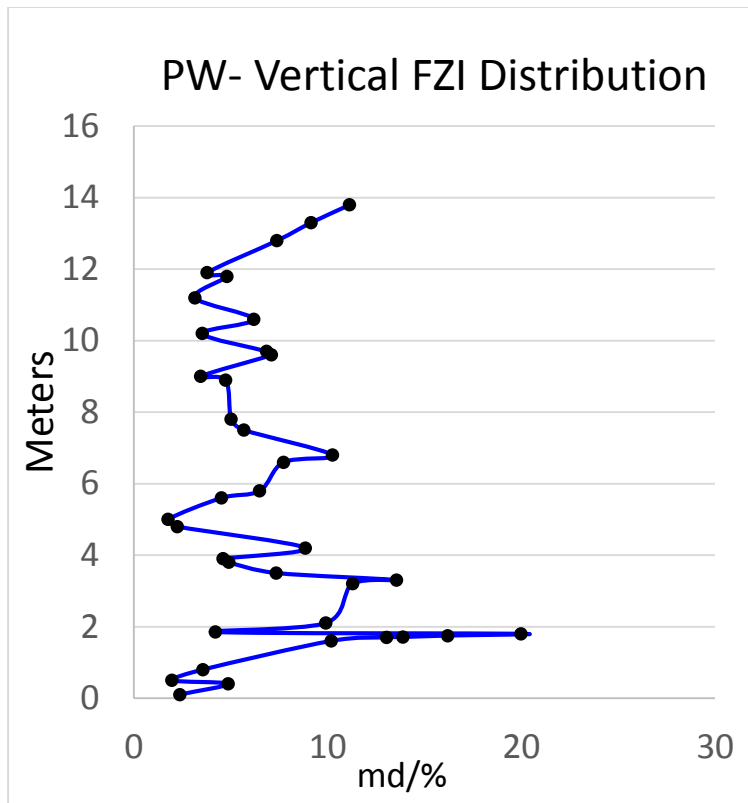
Permeability														
	Box Bottom	334	37.2	181.5	50.95	339	49.9	812	327.25	121.4	44.6	558	486	70.3
	Box Middle	331.9	37.11	153.5	50.94	338.97	3.6	684	286.75	68.65	39.8	164	78.5	16.3
	Box Top	2344	2589	2172	1447	988.5	882	1058	2600	408	230	331	78.5	70.8
	Whisker Top	2344	2589	2172	1447	988.5	882	1058	2600	408	230	331	78.5	70.8
	Whisker Bottom	331.9	37.11	153.5	50.94	338.97	3.6	684	286.75	68.65	39.8	164	78.5	16.3
Porosity														
	Box Bottom	23.75	16.58	27.8	22.75	22	29.7	37.05	34.4	26.38	30.4	37.7	35.2	34.6
	Box Middle	11.75	5.675	7.9	19.85	7.575	0.05	1.55	3.2	3.075	4.7	1.35	0.45	1.3
	Box Top	7.45	11.33	2.55	2.3	8.475	4.6	2.95	4.05	10.73	6.35	0.5	0.45	1.15
	Whisker Top	7.45	11.33	2.55	2.3	8.475	4.6	2.95	4.05	10.73	6.35	0.5	0.45	1.15
	Whisker Bottom	11.75	5.675	7.9	19.85	7.575	0.05	1.55	3.2	3.075	4.7	1.35	0.45	1.3

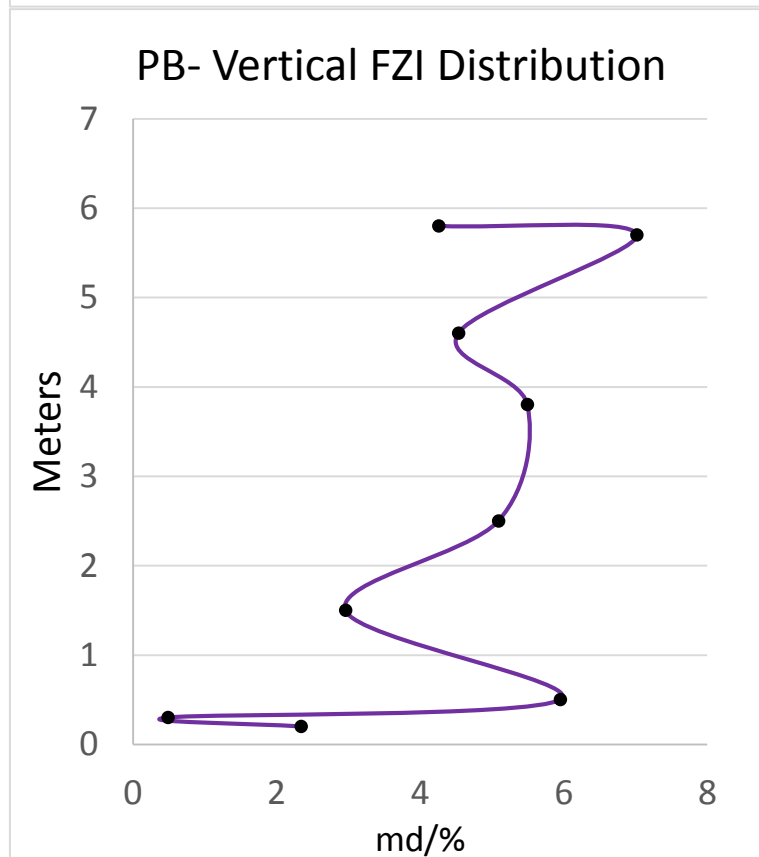
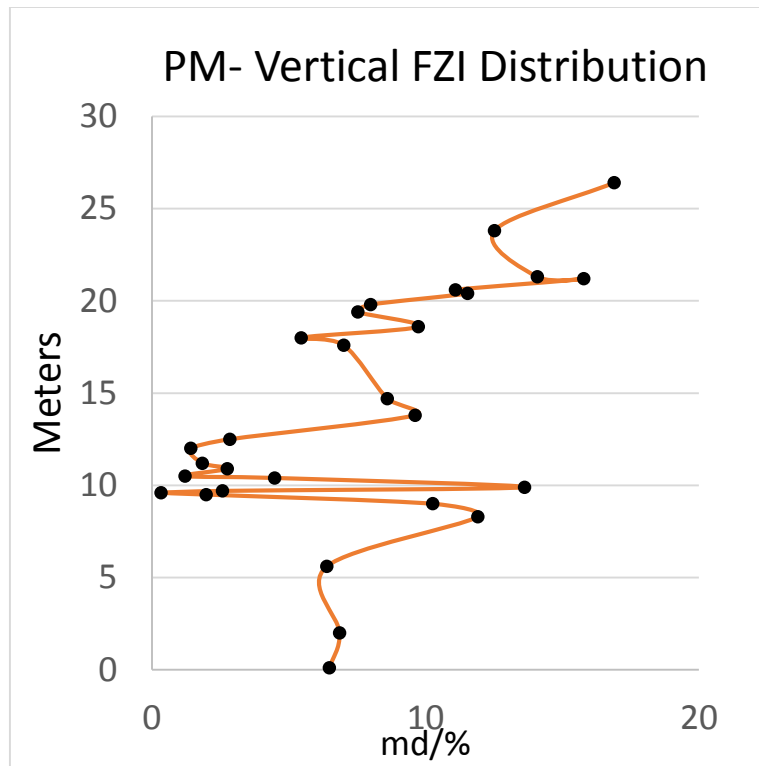
Diagenesis box plot input

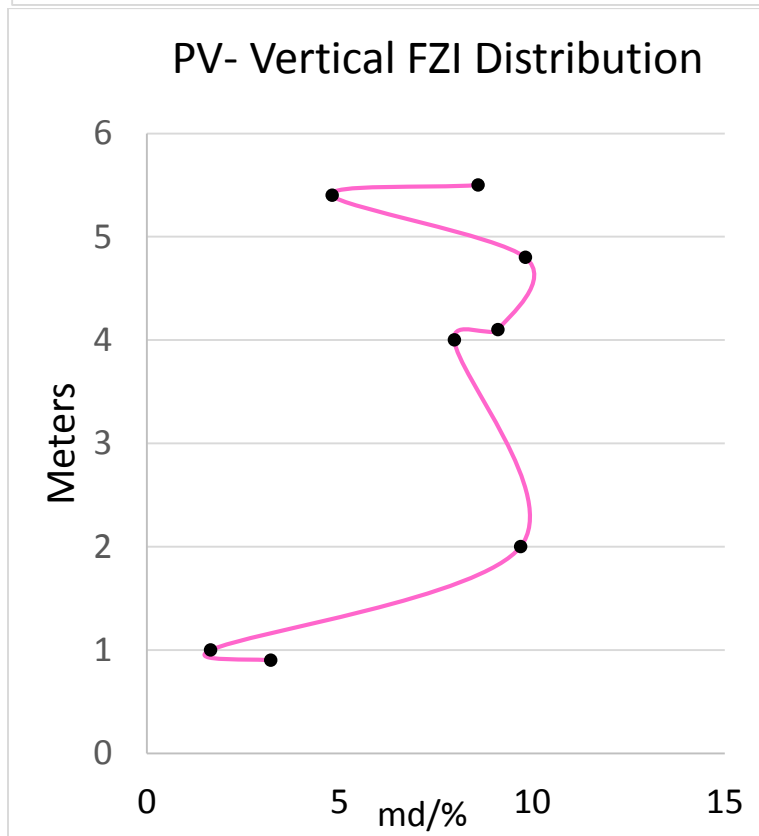
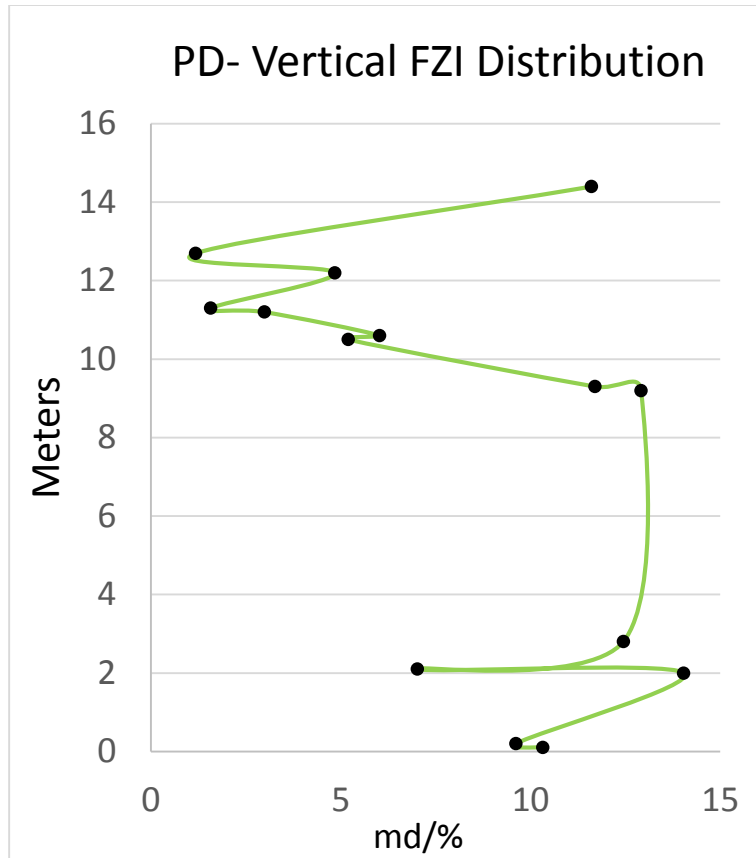
Permeability							
	Box Bottom	1270	64.03	0.27	195.70	403.72	32.10
	Box Middle	1267	63.97	0.26	169.30	403.28	10.90
	Box Top	9251	2843	75.74	2157.00	2223.00	887.00
	Whisker Top	9251	2843	75.74	2157.00	2223.00	887.00
	Whisker Bottom	1267	63.97	0.26	169.30	403.28	10.90
Porosity							
	Box Bottom	33.1	24.1	8.30	27.90	26.50	28.58
	Box Middle	9.663	12.10	5.38	8.00	12.00	7.38
	Box Top	7.764	5.80	15.33	4.90	5.95	8.97
	Whisker Top	7.764	5.80	15.33	4.90	5.95	8.98
	Whisker Bottom	9.663	12.10	5.38	8.00	12.00	7.38

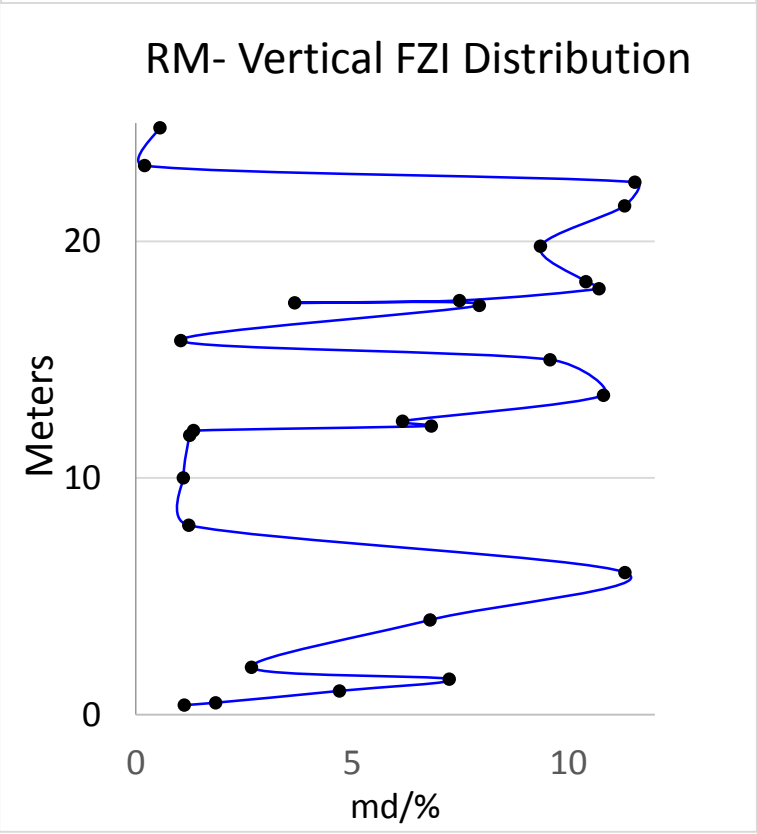
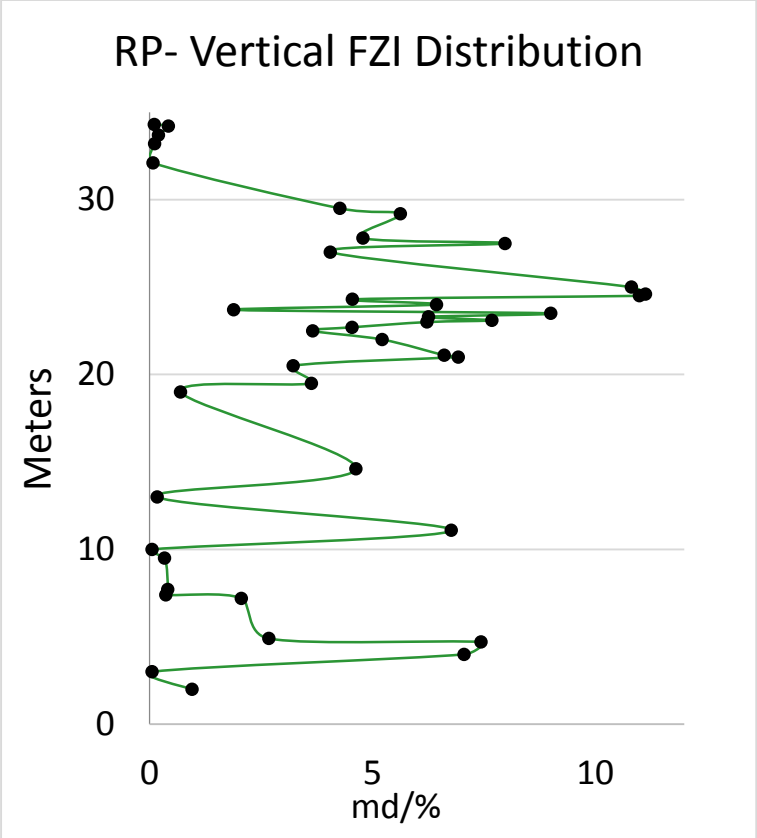
FZI Graphs

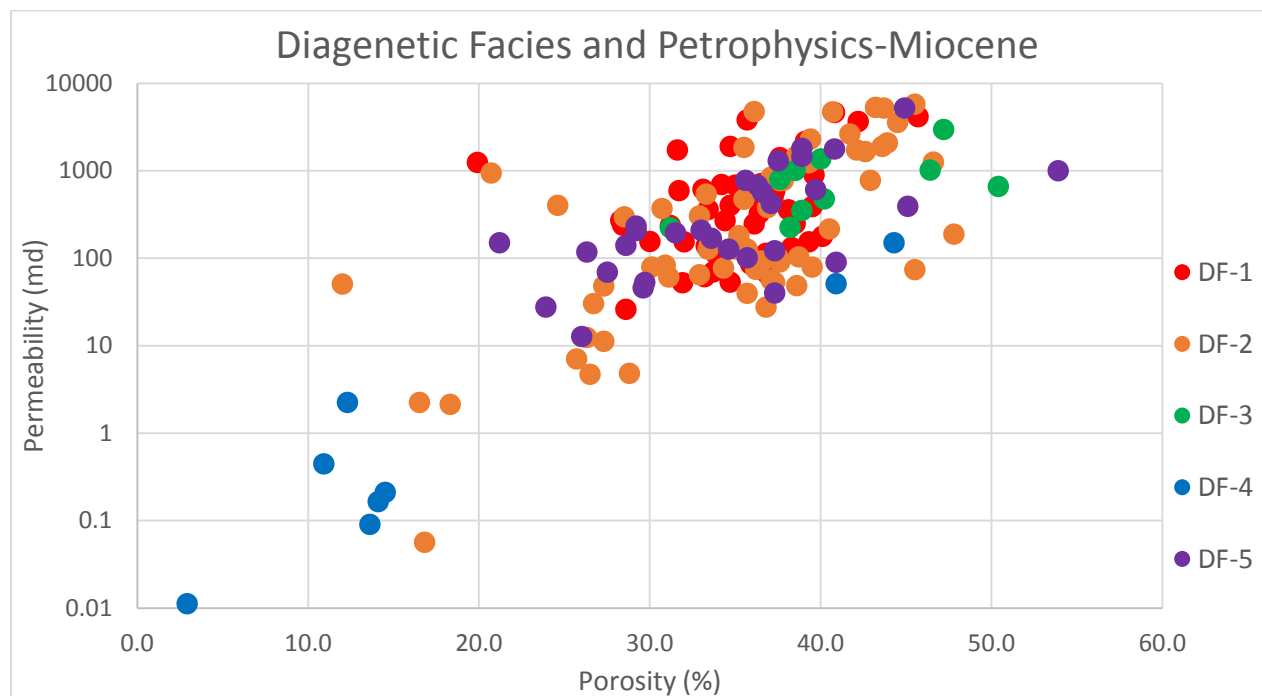
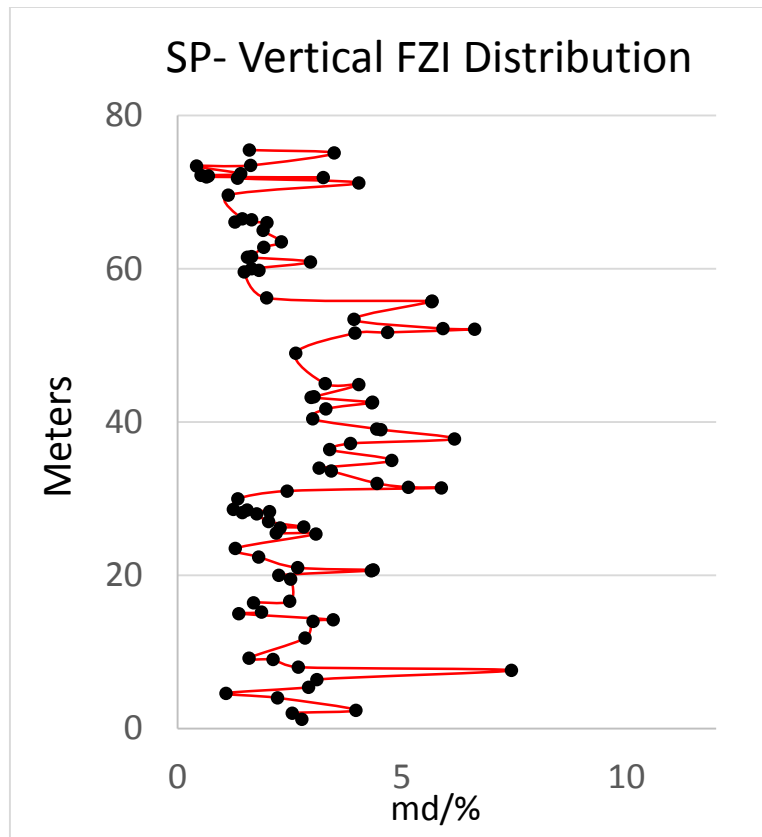




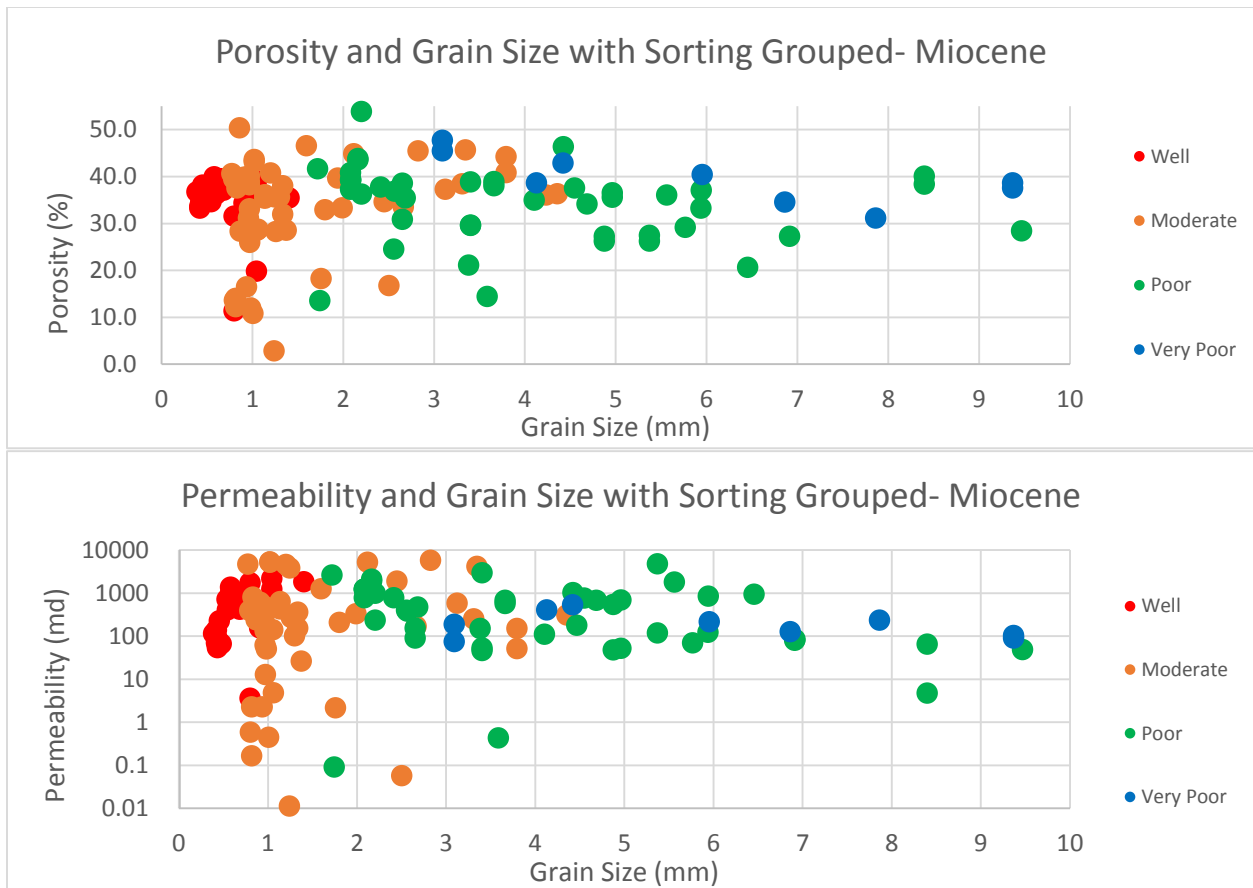




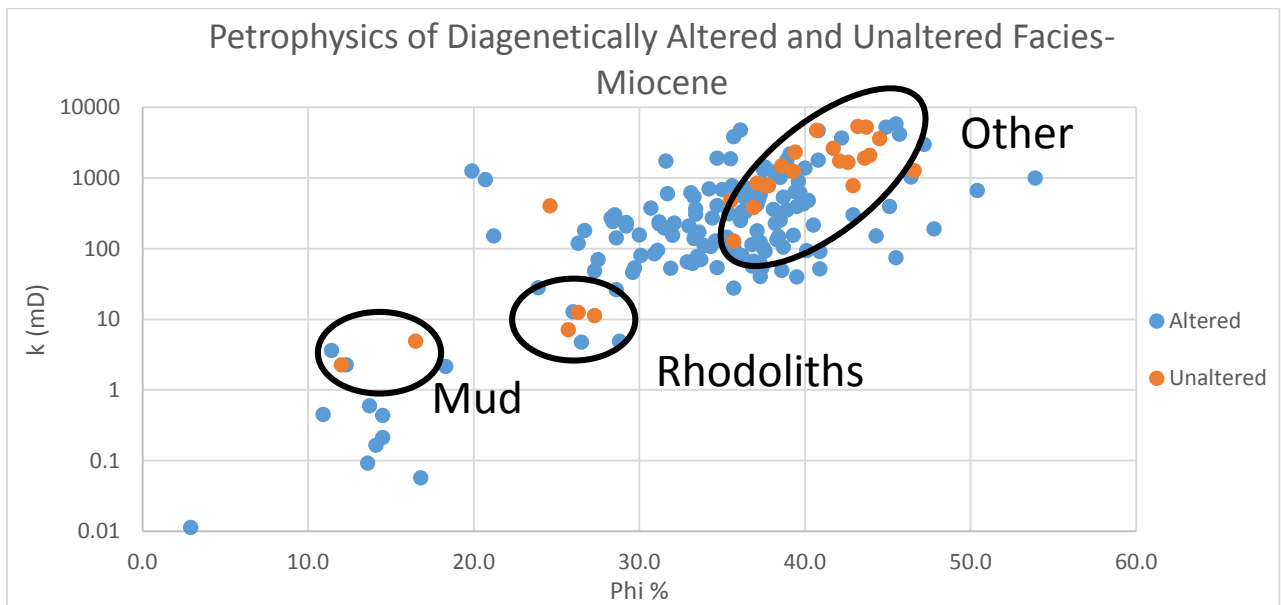




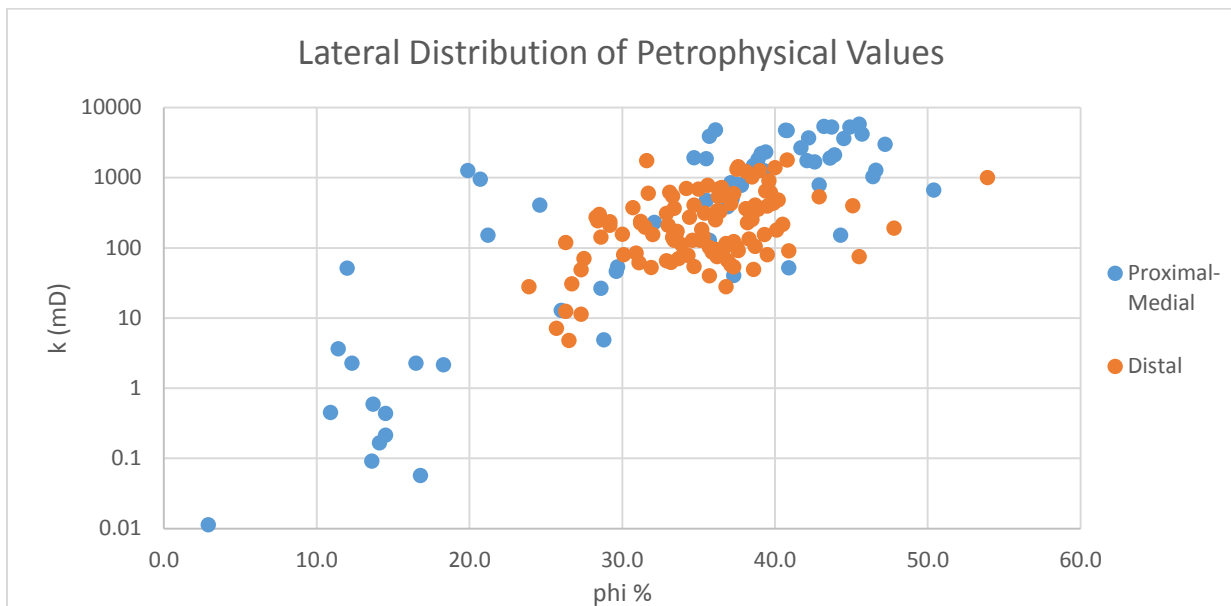
Petrophysical distribution of Miocene deposits separated by diagenetic facies.



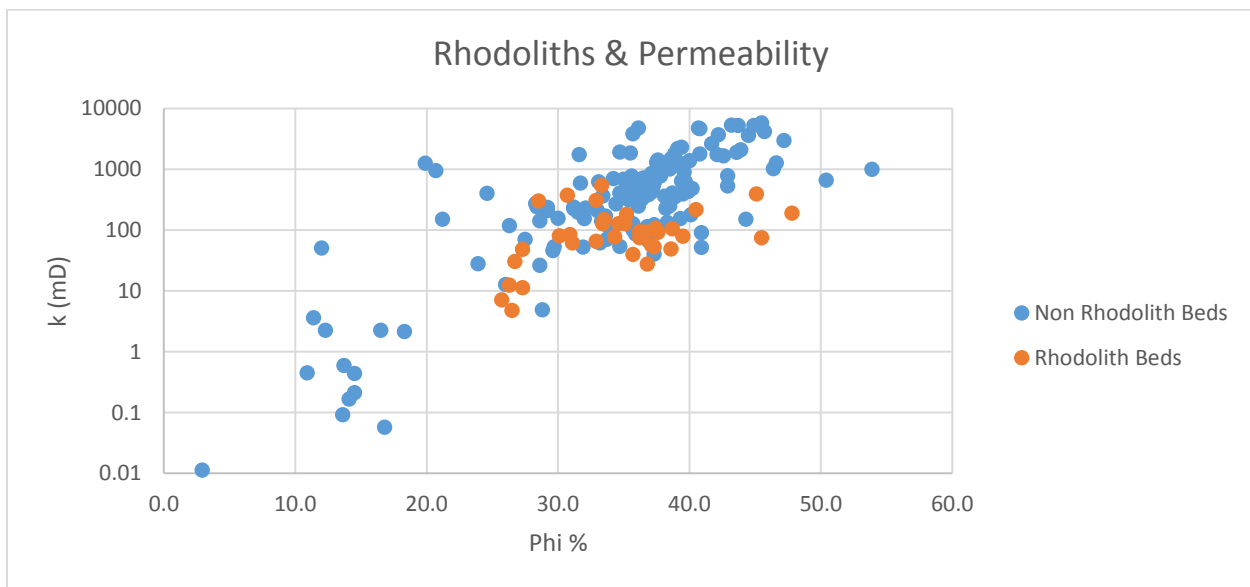
Porosity and Permeability of Miocene deposits plotted against grain size and grouped by grain sorting.



Petrophysical comparison of altered and unaltered Miocene deposits. The lower-value, unaltered Deposits are due to silt and rhodolith content.



Petrophysical comparison of petrophysical values based on paleotopographic position in Miocene deposits. Distal values group more consistently, and lower and higher than the proximal-medial samples.



Petrophysical comparison of rhodolith beds to strata that don't contain rhodoliths. Overall, rhodoliths beds/ rhodolith-rich facies plot significantly lower than the majority of other lithofacies.

Appendix VIII

T and F Test Results

Student T and F tests were run to measure the variance of mean petrophysical values (t-test) and the variance of range (f-tests). There were run to determine where or not certain differences between two datasets were statistically significant or random. Examples of these analyses are included below. If $p < .05$ then the null hypothesis is rejected and there is a statistically significant difference between the two datasets.

t-Test: Two-Sample Assuming Unequal Variances		
	<i>PS 1</i>	<i>PS2</i>
Mean	2.601049	2.359697
Variance	0.472188	0.230828
Observations	11	14
Hypothesized Mean Difference	0	
df	17	
t Stat	0.990161	
P(T<=t) one-tail	0.16799	
t Critical one-tail	1.739607	
P(T<=t) two-tail	0.335981	
t Critical two-tail	2.109816	

t-Test: Two-Sample Assuming Unequal Variances		
	<i>PS 1</i>	<i>PS3</i>
Mean	2.601049	2.769023
Variance	0.472188	0.132264
Observations	11	21
Hypothesized Mean Difference	0	
df	13	
t Stat	-0.7571	
P(T<=t) one-tail	0.231247	
t Critical one-tail	1.770933	
P(T<=t) two-tail	0.462494	
t Critical two-tail	2.160369	

Porosity

F-Test Two-Sample for Variances		
	<i>rud</i>	<i>pack</i>
Mean	0.354482	0.318269
Variance	0.005385	0.010266
Observations	112	52
df	111	51
F	0.524601	
P(F<=f) one-tail	0.00251	
F Critical one-tail	0.684086	

Permeability

F-Test Two-Sample for Variances		
	<i>rud</i>	<i>pack</i>
Mean	2.407353	2.310804
Variance	0.556541	0.984608
Observations	112	52
df	111	51
F	0.56524	
P(F<=f) one-tail	0.006616	
F Critical one-tail	0.684086	

Appendix IX

Petrel Input Data

This appendix contains data that was input into Petrel to develop the 3-D models. Each lithofacies for each dataset (Pliocene and Miocene) was assigned a discrete integer for representation throughout the model. UTM and kelly bushing data for pseudowells and pseudosections are also included. A Measured depth values and the facies code for the Miocene model is also included below to show the construction of each pseudowell. Pseudowells were assigned these values so that Petrel™ is able to populate the vertical section with an assigned facies with a particular thickness. Lastly, paleotopographic maps developed in Petrel for both field areas are shown below.

Pliocene Lithofacies	Petrel Input Lithofacies Integers
Silty Coralline Algae Packstone	1
Sorted Bryozoan Packstone	2
Silt-Gravel Coralline Algae Packstone	3
Sorted Coralline Algae-Bivalve Packstone	4
Interbedded Bivalve Packstone	5
Bryozoan-Coralline Algae Rudstone	6
Bivalve-Coralline Algae Rudstone	7
<i>Pecten</i> Rudstone	8
Ostreid-Pectinid Rudstone	9
Rhodolith Rudstone	10

Pliocene lithofacies input codes.

Miocene Lithofacies	Petrel Input Lithofacies Integers
Bryozoan-Echinoid Packstone	1
Bryozoan-Bivalve Packstone	2
Bivalve-Coralline Algae Packstone	3
Bryozoan-Ostreid Rudstone	4
Bryozoan-Pectinid Rudstone	5
Fragmented <i>Pecten</i> Rudstone	6
<i>Pecten</i> Rudstone	7
Globular Bryozoan-Clam Rudstone	8
Coralline Algae-Bivalve Rudstone	9
Rhodolith Rudstone	10
Massive Echinoid Packstone	11
Massive Planktonic Foraminiferal Wackestone	12
Bedded Planktonic Foraminiferal Wackestone	13

Miocene lithofacies input codes.

Pliocene input for some pseudowells

Pliocene				
Pseudowell Name	UTMs			KB (m)
pr	597688	4091341		35
pr1	597566	4091322		35
pr2	597880	4091350		35
ppsed	597875	4091275		25
ppsed1	597560	4091250		25
prep	597875	4091180		23
prep1	597560	4091180		23
pw	597900	4091075		20
pw1	597556	4091075		20
pt	597929	4090994		19
pt1	597567	4091005		19
pm	597925	4090908		18
pm1	597540	4090917		18
pb	597926	4090862		18
pb1	597547	4090829		18
pd	597912	4090821		17
pd1	597551	4090787		17
pv	597899	4090806		15
pv1	597563	4090755		15

Miocene input for all pseudowells

Miocene				
Pseudowell Name	UTMs			KB (m)
rp	589615	4084950		284
rp1	589778	4085120		284
rp3	589904	4085500		284
a1	589750	4084950		267
a2	589900	4085120		267

a3	589675	4084750		267
a4	590000	4085500		267
b1	589900	4084950		256
b2	589785	4084650		256
b3	590050	4085120		256
b4	590100	4085500		256
c1	589900	4084600		244
c2	590050	4084950		244
c3	590150	4085120		244
c4	590200	4085500		244
rm	589821	4084344		235
rm1	589983	4084600		235
rm2	590119	4084950		235
rm4	590237	4085120		235
rm5	590250	4085500		235
d1	590325	4084950		217
d2	590100	4084600		217
d3	590375	4085500		217
e1	590450	4084950		205
e2	590200	4084600		205
e3	590550	4085500		205
f1	590325	4084600		177
f2	590560	4084950		177
f3	590725	4085500		177
sp	590857	4085263		166
sp1	590661	4084950		166
sp2	590454	4084600		166
sp4	590857	4085500		166

Miocene Pseudosections Petrel

RP			RP3			A3			B2			C1		
	MD	Facies		MD	Facies		MD	Facies		MD	Facies		MD	Facies
	0	2		0	2		0	2		0	7		0	7
	3.1	7		3.1	7		0.5	7		4.5	3		3.75	1
	6.7	5		6.7	5		4.5	5		5.5	7		4.25	5
	7.9	1		7.9	1		5.5	2		10	4		5.25	7
	9.96	8		9.96	8		7	8		14	7		8.75	1
	11.6	5		11.6	5		9	5		18.5	4		9.75	5
	13.6	1		13.6	1		11.5	2		21	7		10.25	7
	19.4	5		19.4	5		16	5		26.5	1		15.25	1
	24.75	1		24.75	1		20.5	2		29	1		15.75	5
	26.75	5		26.75	5		23	5					16.5	6
	30.5	4		30.5	4		31	5					18	7
	34.3	4		34.3	4								24	2
													26	2
RP1			A1			A4			B3			C2		
	MD	Facies		MD	Facies		MD	Facies		MD	Facies		MD	Facies
	0	2		0	2		0	2		0	7		0	7
	3.1	7		0.5	7		0.5	7		4.5	3		3.75	1
	6.7	5		4.5	5		4.5	5		5.5	7		4.25	5
	7.9	1		5.5	2		5.5	2		10	4		5.25	7
	9.96	8		7	8		7	8		14	7		8.75	1
	11.6	5		9	5		9	5		18.5	4		9.75	5
	13.6	1		11.5	2		11.5	2		21	7		10.25	7
	19.4	5		16	5		16	5		26.5	1		15.25	1
	24.75	1		20.5	2		20.5	2		29	1		15.75	5
	26.75	5		23	5		23	5					16.5	6
	30.5	4		31	5		31	5					18	7
	34.3	4											24	2
													26	2
RP2			A2			B1			B4			C3		
	MD	Facies		MD	Facies		MD	Facies		MD	Facies		MD	Facies
	0	2		0	2		0	7		0	7		0	7
	3.1	7		0.5	7		4.5	3		4.5	3		- 20.25	1
	6.7	5		4.5	5		5.5	7		5.5	7		- 19.75	5
	7.9	1		5.5	2		10	4		10	4		- 18.75	7

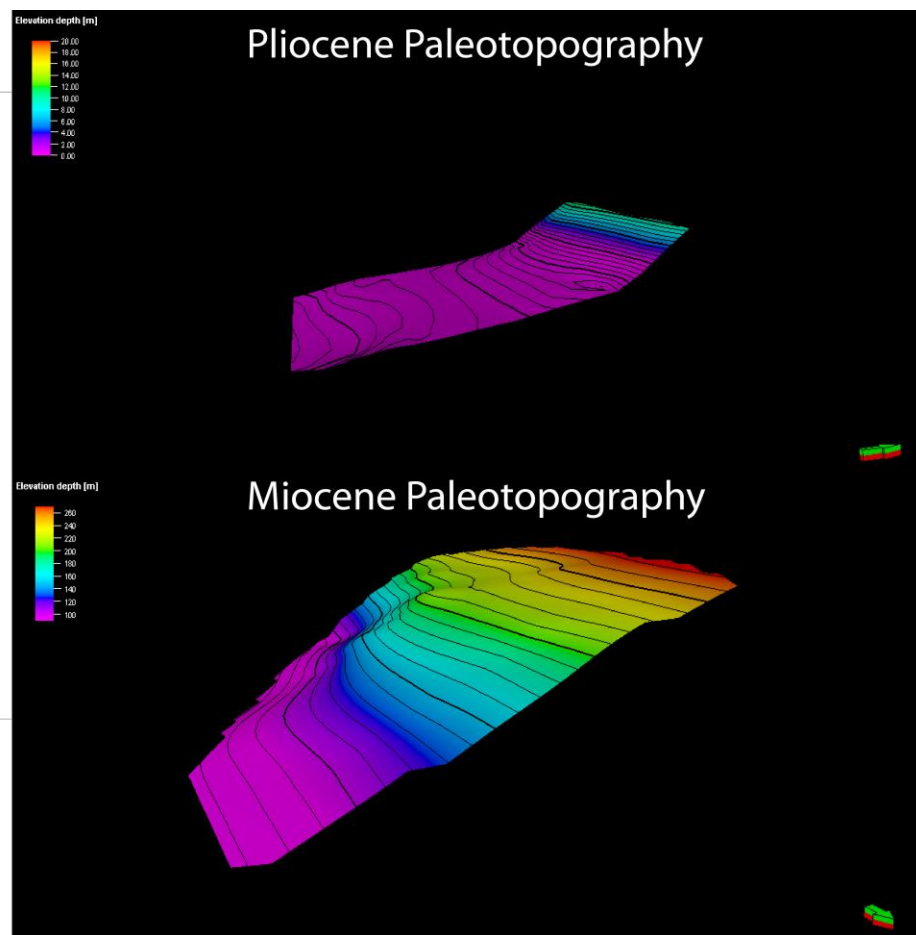
	9.96	8		7	8		14	7		14	7		-15.25	1
	11.6	5		9	5		18.5	4		18.5	4		-14.25	5
	13.6	1		11.5	2		21	7		21	7		-13.75	7
	19.4	5		16	5		26.5	1		26.5	1		-8.75	1
	24.75	1		20.5	2		29	1		29	1		-8.25	5
	26.75	5		23	5								-7.5	6
	30.5	4		31	5								-6	7

C4			RM2			RM5			D3			E3		
	MD	Facies		MD	Facies		MD	Facies		MD	Facies		MD	Facies
	0	7		0	2		0	2		0	5		0	10
	3.75	1		2	7		2	7		2	9		4	7
	4.25	5		6.5	3		6.5	3		11	5		7.5	9
	5.25	7		9.2	7		9.2	7		15	7		10.5	7
	8.75	1		10.8	2		10.8	2		20.5	4		24.5	7
	9.75	5		12.7	6		12.7	6		23	7		35.5	9
	10.25	7		16.8	7		16.8	7		28	9		42	7
	15.25	1		22.7	1		22.7	1		35	4		52	5
	15.75	5		24	4		24	4		36	5		54	1
	16.5	6		25	4		25	4		40	1		55	1
	18	7								42	1			
	24	2												
	26	2												
RM			RM3			D1			E1			F1		
	MD	Facies		MD	Facies		MD	Facies		MD	Facies		MD	Facies
	0	2		0	2		0	5		0	10		0	10
	2	7		2	7		2	9		4	7		5	9
	6.5	3		6.5	3		11	5		7.5	9		7.5	10
	9.2	7		9.2	7		15	7		10.5	7		14.5	7
	10.8	2		10.8	2		20.5	4		24.5	7		27	2
	12.7	6		12.7	6		23	7		35.5	9		30.5	7
	16.8	7		16.8	7		28	9		42	7		42.5	11
	22.7	1		22.7	1		35	4		52	5		44	9
	24	4		24	4		36	5		54	1		47	12
	25	4		25	4		40	1		55	1		51	9
							42	1					58	1
													60.5	7
													63.5	1

RM1			RM4			D2			E2				64	5
	MD	Facies		MD	Facies		MD	Facies		MD	Facies		67	5
	0	2		0	2		0	5		0	10			
	2	7		2	7		2	9		4	7			
	6.5	3		6.5	3		11	5		7.5	9			
	9.2	7		9.2	7		15	7		10.5	7			
	10.8	2		10.8	2		20.5	4		24.5	7			
	12.7	6		12.7	6		23	7		35.5	9			
	16.8	7		16.8	7		28	9		42	7			
	22.7	1		22.7	1		35	4		52	5			
	24	4		24	4		36	5		54	1			
	25	4		25	4		40	1		55	1			
							42	1						

F2			SP			SP2		
	MD	Facies		MD	Facies		MD	Facies
	0	10		0	10		0	10
	5	9		6.1	9		6.1	7
	7.5	10		8.5	10		8.5	10
	14.5	7		15.8	7		15.8	7
	27	2		26.7	3		26.7	3
	30.5	7		32.8	7		32.8	7
	42.5	11		38.4	11		38.4	11
	44	9		42.5	12		42.5	12
	47	12		43.7	11		43.7	11
	51	9		44.6	13		44.6	13
	58	1		48.2	2		48.2	2
	60.5	7		50.7	9		50.7	9
	63.5	1		56.6	3		56.6	3
	64	5		63.7	9		63.7	9
	67	5		67	3		67	3
				72	7		72	7
F3				75.7	7		75.7	7
	MD	Facies						
	0	10	SP1			WF		
	5	9		MD	Facies		MD	Facies
	7.5	10		0	10		0	13
	14.5	7		6.1	7		81	9
	27	2		8.5	10		89	13
	30.5	7		15.8	7		109	9

	42.5	11		26.7	3		122	13
	44	9		32.8	7		185	5
	47	12		38.4	11		212	5
	51	9		42.5	12			
	58	1		43.7	11			
	60.5	7		44.6	13			
	63.5	1		48.2	2			
	64	5		50.7	9			
	67	5		56.6	3			
				63.7	9			
				67	3			
				72	7			
				75.7	7			



Pliocene and Miocene paleotopography onto which the carbonates deposited. These were made in Petrel and were used for the models. The models are vertically exaggerated by 2x.

Appendix X

Reservoir Analog Modeling Workflow

The workflow for each of the eight models was the same as was the importation of data into Petrel. Once the data was imported and lithofacies displayed in pseudowells, well tops were selected based on stratigraphic correlations (Pugliano et al., 2015, Chapter 1). Well tops were selected at sequence and parasequence boundaries for each cycle. Picking well tops at such a detailed scale allowed for high-resolution control on lithofacies during population of the model. A polygon reflecting the orientation and geometry of the complexes from the field was then created, surrounding the dataset. The polygon was traced around the outcrop to represent a 3-D volume based on the actual geometry and size of the strata being modeled. For the Miocene model, facies thicknesses and measurements were all directly from outcrop. Pliocene models were constructed to represent a complete clinothem geometry, therefore facies were made to thin both in the most updip and down dip settings. Well tops were then converted into surfaces using the convergent interpolation algorithm. From the surfaces, a 3-D cellular grid was constructed with grid sizes of 5 meters for the Miocene model and 10 meters for the Pliocene models, allowing for details throughout the grid. Horizons were then created within the grid from the surfaces, which were then used as the framework for creating zones and layers that followed sequence and parasequence boundaries. Facies properties within the pseudowells were then upscaled to allow for variables to be populated throughout the 3-D model, away from the individual pseudowells (Schlumberger, Petrel 1, Petrel 1). As the goal of the models was to make a geologically sound representation of the outcrop, variogram values were selected only to provide a framework and guide for this goal, describing the variation in discrete data as spatial variation increases (Schlumberger, Petrel 1, Petrel 1). In addition, close pseudowell spacing and thorough understanding of lithofacies distribution allowed for the correct distribution of major and minor orientations. Property modeling was then implemented to populate the 3-D grid with lithofacies and petrophysical data. For the Pliocene models two types of models were made, close grid models that reflect a true clinothem geometry, and coarser block models.

Lithofacies Modeling

Within each zone, individual lithofacies percentages based on the amount of volume they comprise within the individual zone were calculated. Most zones contained more than one lithofacies and the sequential indicator simulation (SIS) was implemented to populate lithofacies throughout the 3-D grid (Deutsch and Journel, 1998; Schlumberger, Petrel 1). This method was selected as it allows for a stochastic population of the model from the upscaled well logs creating a pixel-based model that can produce multiple realizations of the data (Schlumberger, Petrel 1). For the zones that only contain one lithofacies, the indicator kriging algorithm was utilized, as it creates smooth data interpretations, but doesn't describe heterogeneities, which would be necessary if multiple facies were in the zone (Schlumberger, Petrel 1). Thirty-three realizations were run for each model type (Elton per. comm., 2015), allowing for the selection of the best option and to calculate the arithmetic mean of the 33 models to create probability models for individual lithofacies and for petrophysical modeling.

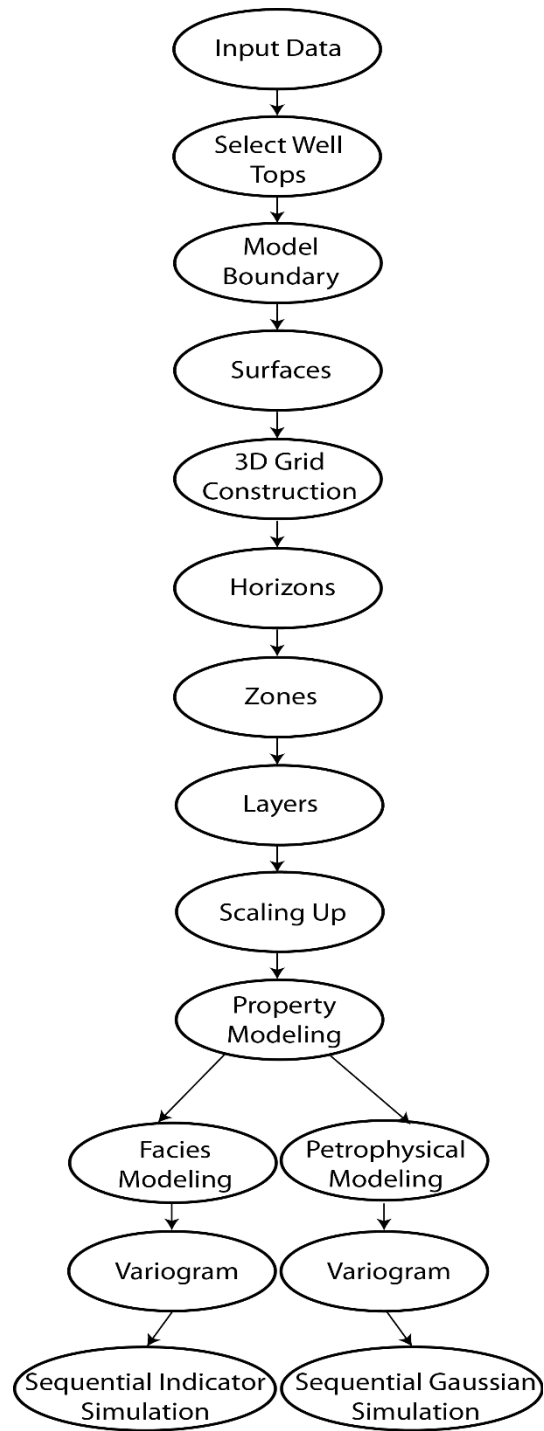
Petrophysical Modeling

Once property modeling of lithofacies was completed, petrophysical variables including the range, mean, and standard deviations were entered for lithofacies in each individual zone. This

creates a very specific distribution of petrophysical values based directly from where the values naturally derive. Using this methodology was especially important in the Miocene as diagenesis highly alters the distribution of petrophysical values. A lithofacies may have high petrophysical values in one location and significantly variable values in a different location. To distribute these values from upscaled pseudowells, the stochastic sequential Gaussian simulation was utilized (Corvi et al., 1992; Deutsch and Journel, 1998). This simulation used the separate input petrophysical parameters and variograms to describe how the porosity and permeability distribute away from the upscaled pseudowell data.

References

- Corvi, P., K. Heffer, P., King, Tyson, and G. Verly, 1992, Reservoir Character using expert knowleg, data, and statistics, Schlumberger, Oilfield Reviews, v.4, p. 25-39.
- Deutsch, C.V., and A. G., Journel, 1998, GSLIB Geostatistical software library and user's guide, 2nd ed.: New York, Oxford University Press, 369p.
- Schlumberger, Petrel Modeling Course 1

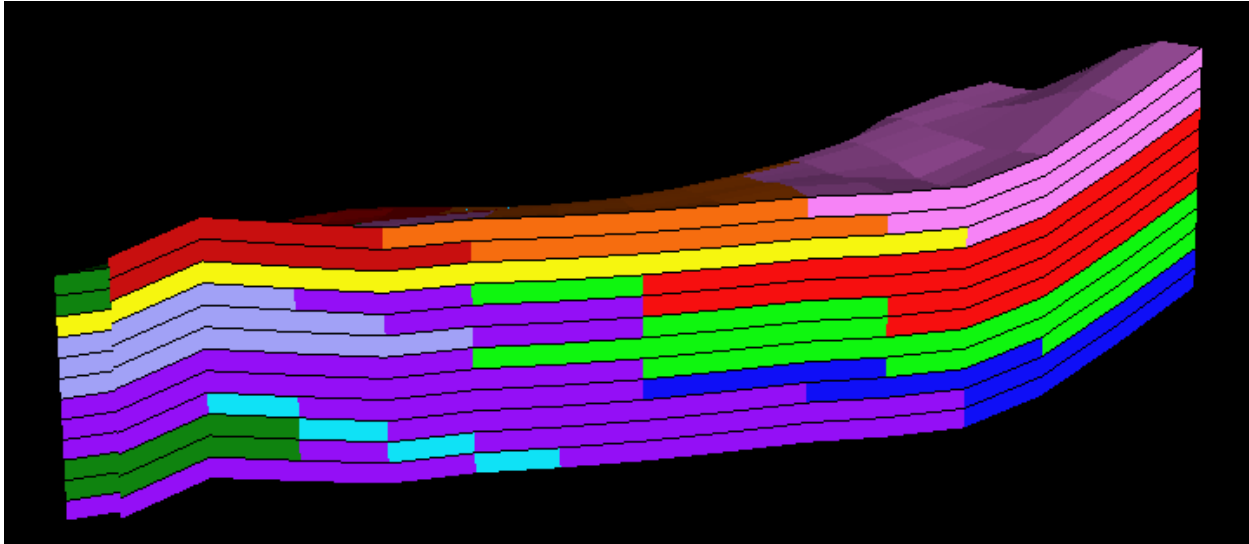


Workflow model for developing facies and reservoir analog models in Petrel.

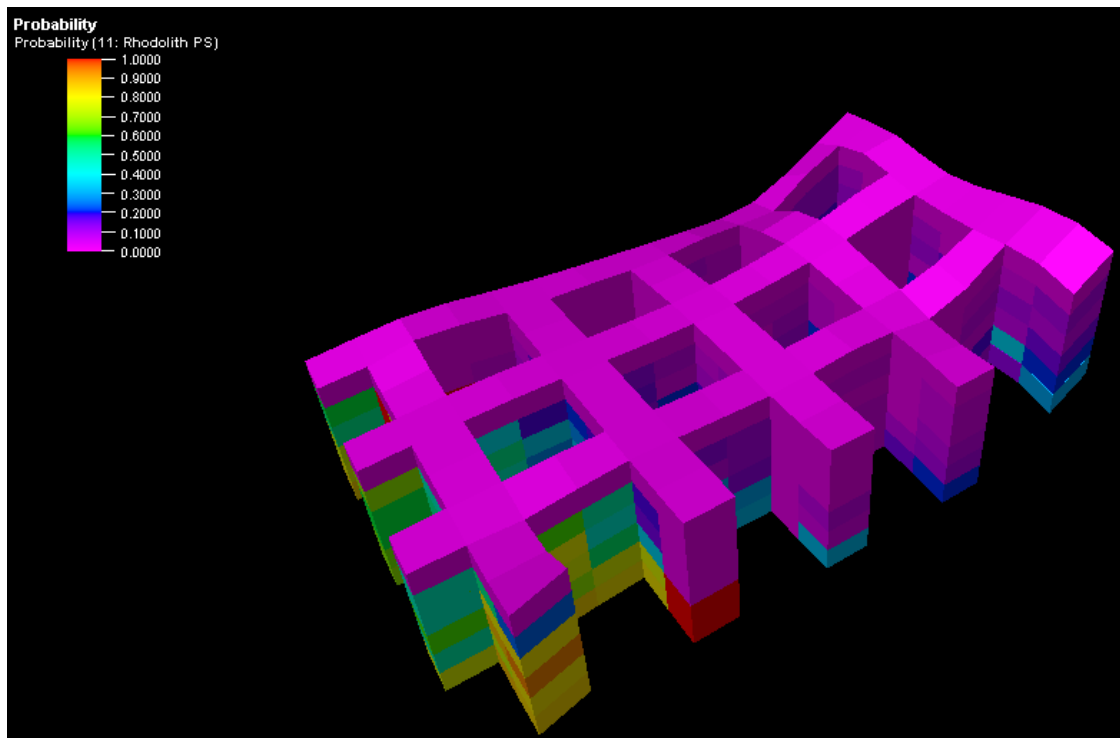
Appendix XI

Petrel Facies Models

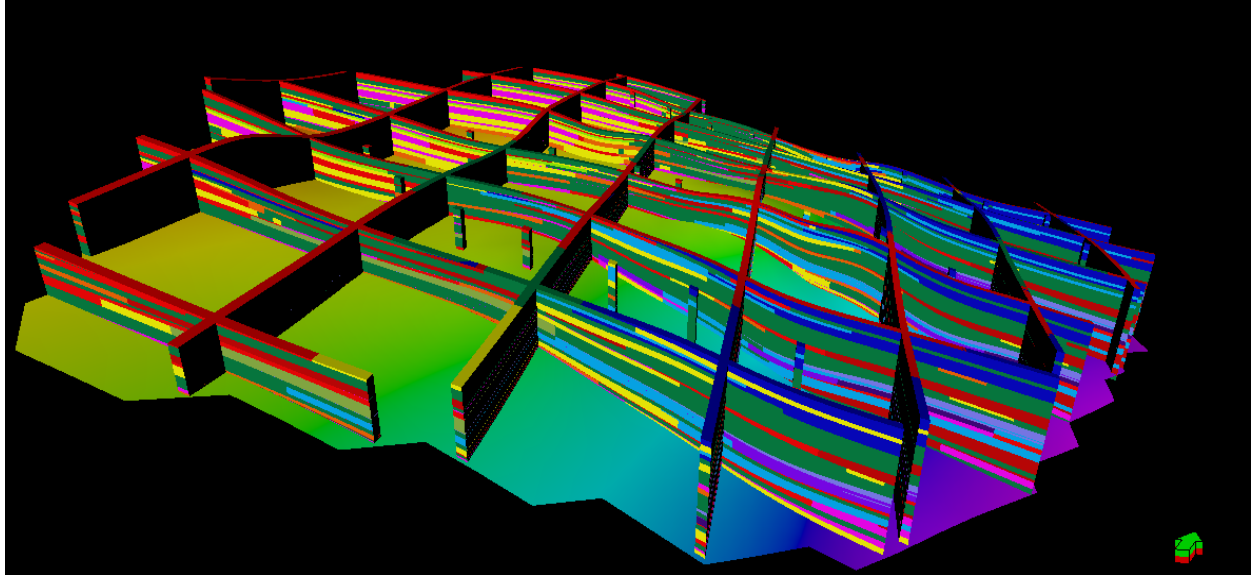
This appendix contains Petrel™ facies models not included in the text. Each facies model also contains a probability distribution model for each individual facies, one example from the block models is shown below.



Facies model of the entire Pliocene clinothem representing all six of the depositional profiles. This shows the variety of facies distribution that can occur from a diverse combination of each of the lateral profiles described throughout the heterozoan clinothem. The model is .6km in length.



An example of a facies probability map from the Pliocene clinothem, this represents the distribution of the Rhodolith Rudstone. This shows the likelihood of a facies being deposited in the clinothem. Rhodolith Rudstone has a 70-100% chance of distribution in the most distal regions of the clinothem. And 0-10% chance in the medial to proximal regions. The model is .6km in length.

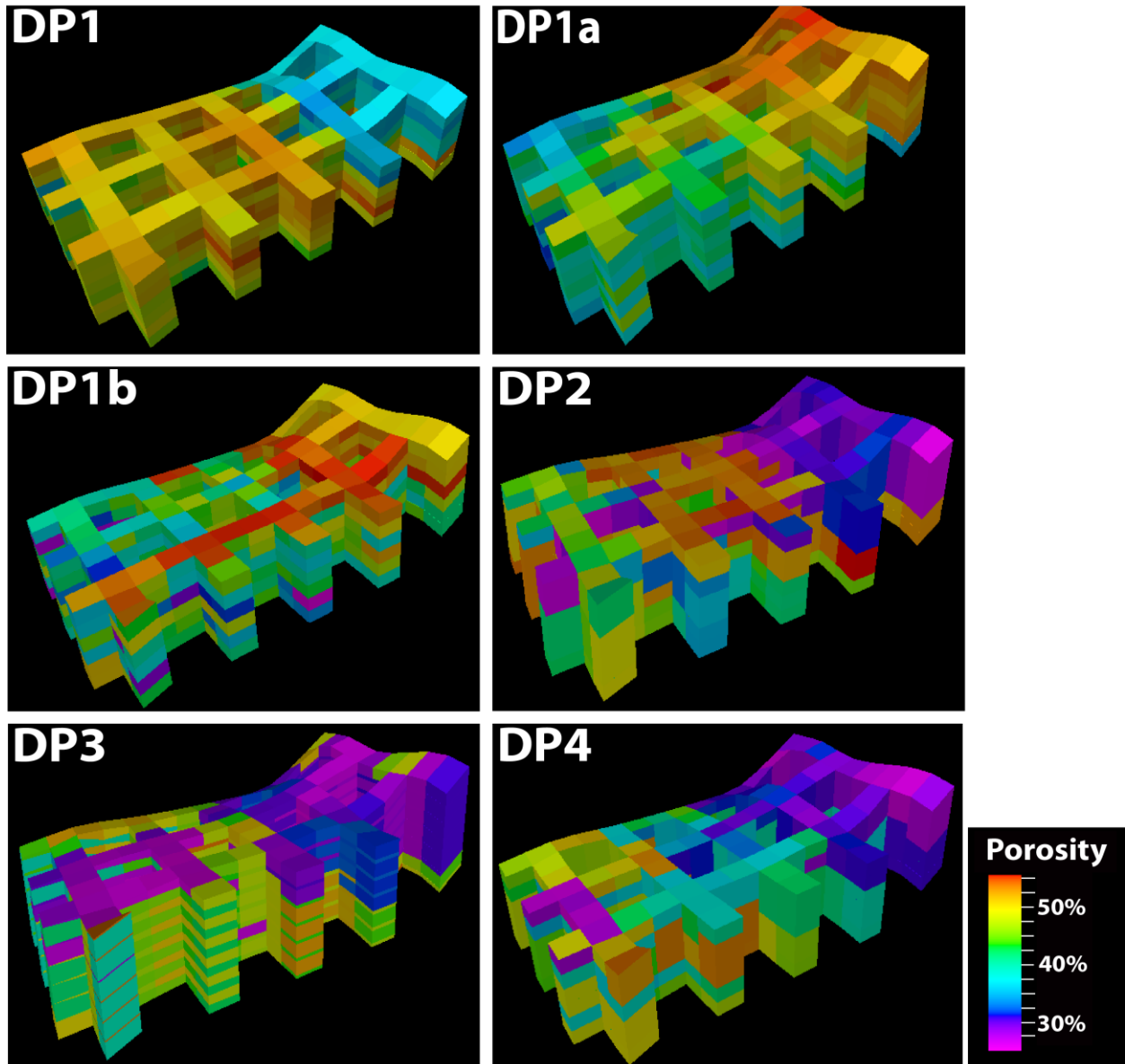


Fence diagram of the Miocene facies model. This image shows a different orientation than the facies model included within the text. The model is 1.3km in length.

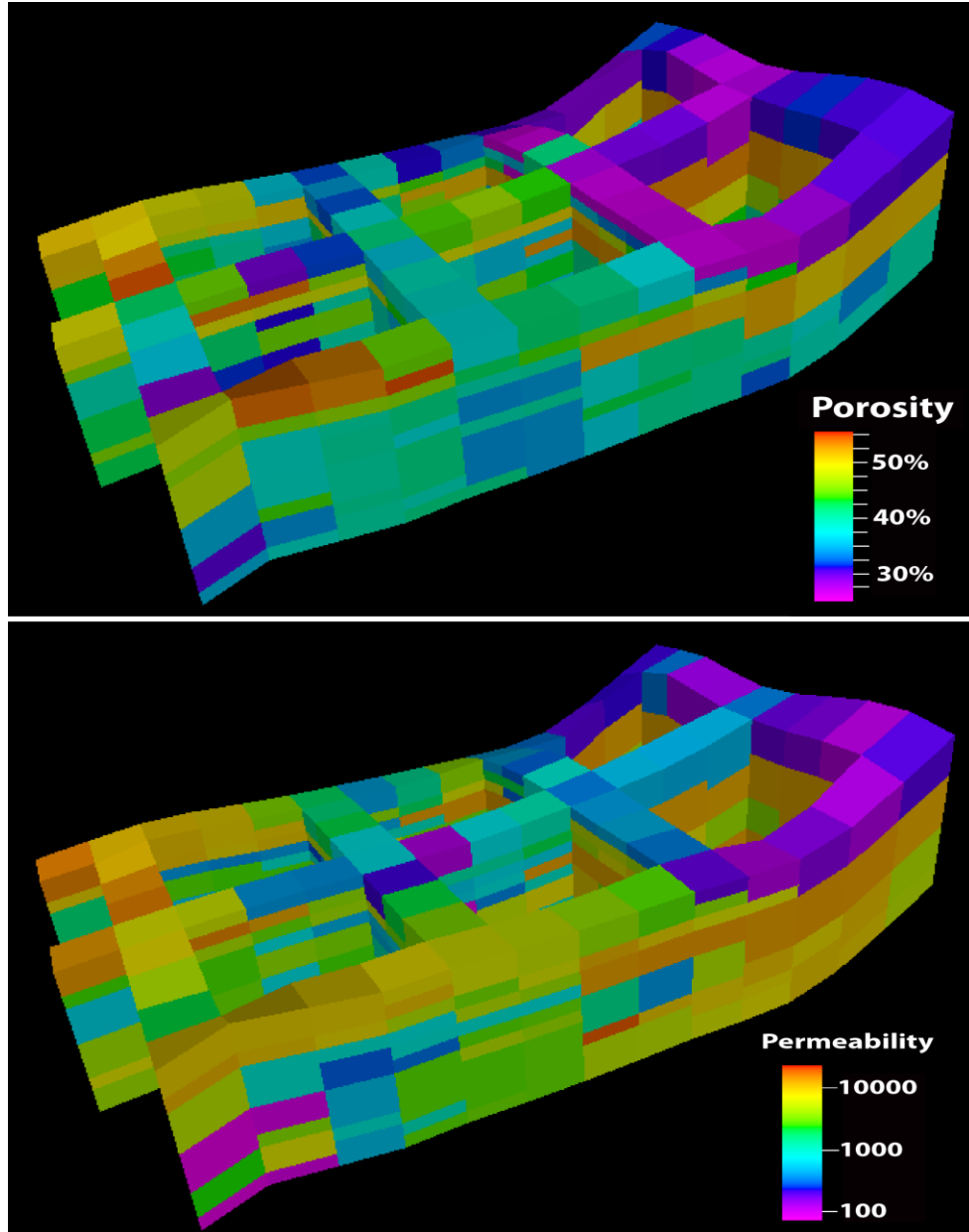
Appendix XII

Petrel Petrophysical Models

This appendix includes petrophysical models not included in the text.



Porosity block models for each of the lateral facies profiles in the Pliocene clinothem. Each model is .6 km long.



Petrophysical block models of the entire Pliocene clinothem. Note the diversity of petrophysical distribution dependent on which depositional profile is present (See Appendix XI). Petrophysical values are lowest in the most proximal regions and are highest in the lower proximal and medial regions. Each model is .6 km long.

APPENDIX XIII

Petrel Model Volumetrics

This appendix contains the volumetric data of pore space used to calculate the m³ and the amount of barrels each reservoir analog can hold. Mean porosity values are split by facies within each individual zone, they are then averaged for their particular zone and then multiplied by the bulk model volume which was calculated in Petrel™, and is based on the size of each zone within the model. Identical zone thicknesses were used within the individual Pliocene models and therefore those values remain constant, while the Miocene zones are highly variable and this variance is reflected in the bulk model volume.

Pliocene DP-1 Zones			Bulk Model Volume m ³	Mean Porosity for Zone	Pore Volume m ³	LF1	LF2	LF3	LF4	LF5	LF6	LF7		Zone Mean
Zone 1	0.3	1000000	300000	0.46	138000.0	53	43	42						46
Zone 2	0.3	1000000	300000	0.46	138000.0	53	43	42						46
Zone 3	0.3	1000000	300000	0.46	138000.0	53	43	42						46
Zone 4	0.3	1000000	300000	0.46	138000.0	53	43	42						46
Zone 5	0.3	1000000	300000	0.46	138000.0	53	43	42						46
Zone 6	0.3	1000000	300000	0.46	138000.0	53	43	42						46
Zone 7	0.3	1000000	300000	0.46	138000.0	53	43	42						46
Zone 8	0.3	1000000	300000	0.46	138000.0	53	43	42						46
Zone 9	0.3	1000000	300000	0.46	138000.0	53	43	42						46
Zone 10	0.3	1000000	300000	0.4175	125250.0	53	43	42	29					41.75
Zone 11	0.3	1000000	300000	0.4175	125250.0	53	43	42	29					41.75
Zone 12	0.3	1000000	300000	0.4175	125250.0	53	43	42	29					41.75
Zone 13	0.3	1000000	300000	0.4175	125250.0	53	43	42	29					41.75
Zone 14	0.3	1000000	300000	0.4175	125250.0	53	43	42	29					41.75
Zone 15	0.3	1000000	300000	0.4175	125250.0	53	43	42	29					41.75
Zone 16	0.3	1000000	300000	0.4175	125250.0	53	43	42	29					41.75
Zone 17	0.3	1000000	300000	0.416666667	125000.0	29	53	43						41.6666667
Zone 18	0.3	1000000	300000	0.416666667	125000.0	29	53	43						41.6666667
Zone 19	0.3	1000000	300000	0.416666667	125000.0	29	53	43						41.6666667
Zone 20	0.3	1000000	300000	0.416666667	125000.0	29	53	43						42
Total	10	1000000	1000000		2618750.0									

Pliocene DP-1A Zones			Bulk Model Volume m ³	Mean Porosity for Zone	Pore Volume m ³	ZONE 1							Zone Mean
						LF1	LF2	LF3	LF4	LF5			
Zone 1	0.3	1000000	300000	0.4475	134250.0	53	40	43	43				44.75
Zone 2	0.3	1000000	300000	0.4475	134250.0	53	40	43	43				44.75
Zone 3	0.3	1000000	300000	0.4475	134250.0	53	40	43	43				44.75
Zone 4	0.3	1000000	300000	0.442	132600.0	53	43	40	43	42			44.2
Zone 5	0.3	1000000	300000	0.442	132600.0	53	43	40	43	42			44.2
Zone 6	0.3	1000000	300000	0.442	132600.0	53	43	40	43	42			44.2
Zone 7	0.3	1000000	300000	0.442	132600.0	53	43	40	43	42			44.2
Zone 8	0.3	1000000	300000	0.442	132600.0	53	43	40	43	42			44.2
Zone 9	0.3	1000000	300000	0.442	132600.0	53	43	40	43	42			44.2
Zone 10	0.3	1000000	300000	0.442	132600.0	53	43	40	43	42			44.2
Zone 11	0.3	1000000	300000	0.442	132600.0	53	43	40	43	42			44.2
Zone 12	0.3	1000000	300000	0.442	132600.0	53	43	40	43	42			44.2
Zone 13	0.3	1000000	300000	0.442	132600.0	53	43	40	43	42			44.2
Zone 14	0.3	1000000	300000	0.442	132600.0	53	43	40	43	42			44.2
Zone 15	0.3	1000000	300000	0.4525	135750.0	53	43	43	42				45.25
Zone 16	0.3	1000000	300000	0.4525	135750.0	53	43	43	42				45.25
Zone 17	0.3	1000000	300000	0.4525	135750.0	53	43	43	42				45.25
Zone 18	0.3	1000000	300000	0.4525	135750.0	53	43	43	42				45.25
Zone 19	0.3	1000000	300000	0.4525	135750.0	53	43	43	42				45.25
Zone 20	0.3	1000000	300000	0.4525	135750.0	53	43	43	42				45.25
Total	10	1000000	1000000		2675850.0								

Pliocene DP-1B			Bulk Model Volume	Mean Porosity for Zone	Pore Volume					
Zones			m^3		m^3	LF1	LF2	LF3	LF4	Zone Mea
Zone 1	0.3	1000000	300000	0.426666667	128000.0	43	43	42		42.66667
Zone 2	0.3	1000000	300000	0.426666667	128000.0	43	43	42		42.66667
Zone 3	0.3	1000000	300000	0.426666667	128000.0	43	43	42		42.66667
Zone 4	0.3	1000000	300000	0.426666667	128000.0	43	43	42		42.66667
Zone 5	0.3	1000000	300000	0.426666667	128000.0	43	43	42		42.66667
Zone 6	0.3	1000000	300000	0.426666667	128000.0	43	43	42		42.66667
Zone 7	0.3	1000000	300000	0.426666667	128000.0	43	43	42		42.66667
Zone 8	0.3	1000000	300000	0.426666667	128000.0	43	43	42		42.66667
Zone 9	0.3	1000000	300000	0.4525	135750.0	43	43	42	53	45.25
Zone 10	0.3	1000000	300000	0.4525	135750.0	43	43	42	53	45.25
Zone 11	0.3	1000000	300000	0.4525	135750.0	43	43	42	53	45.25
Zone 12	0.3	1000000	300000	0.4525	135750.0	43	43	42	53	45.25
Zone 13	0.3	1000000	300000	0.4525	135750.0	43	43	42	53	45.25
Zone 14	0.3	1000000	300000	0.4525	135750.0	43	43	42	53	45.25
Zone 15	0.3	1000000	300000	0.4525	135750.0	43	43	42	53	45.25
Zone 16	0.3	1000000	300000	0.4525	135750.0	43	43	42	53	45.25
Zone 17	0.3	1000000	300000	0.4525	135750.0	43	43	42	53	45.25
Zone 18	0.3	1000000	300000	0.4525	135750.0	43	43	42	53	45.25
Zone 19	0.3	1000000	300000	0.4525	135750.0	43	43	42	53	45.25
Zone 20	0.3	1000000	300000	0.4525	135750.0	43	43	42	53	45.25
Total	10	1000000	1000000		2653000.0					

Pliocene DP-2			Bulk Model Volume	Mean Porosity for Zone	Pore Volume						
Zones			m^3		m^3	LF1	LF2	LF3	LF4	LF5	Zone Mean
Zone 1	0.3	1000000	300000	0.426666667	128000.0	43	43	42			42.6666667
Zone 2	0.3	1000000	300000	0.4525	135750.0	43	43	42	53		45.25
Zone 3	0.3	1000000	300000	0.4525	135750.0	43	43	42	53		45.25
Zone 4	0.3	1000000	300000	0.4525	135750.0	43	43	42	53		45.25
Zone 5	0.3	1000000	300000	0.46	138000.0	53	43	42			46
Zone 6	0.3	1000000	300000	0.4525	135750.0	43	43	42	53		45.25
Zone 7	0.3	1000000	300000	0.4525	135750.0	43	43	42	53		45.25
Zone 8	0.3	1000000	300000	0.4525	135750.0	43	43	42	53		45.25
Zone 9	0.3	1000000	300000	0.4525	135750.0	43	43	42	53		45.25
Zone 10	0.3	1000000	300000	0.42	126000.0	43	43	42	53	29	42
Zone 11	0.3	1000000	300000	0.42	126000.0	43	43	42	53	29	42
Zone 12	0.3	1000000	300000	0.42	126000.0	43	43	42	53	29	42
Zone 13	0.3	1000000	300000	0.42	126000.0	43	43	42	53	29	42
Zone 14	0.3	1000000	300000	0.42	126000.0	43	43	42	53	29	42
Zone 15	0.3	1000000	300000	0.42	126000.0	43	43	42	53	29	42
Zone 16	0.3	1000000	300000	0.42	126000.0	43	43	42	53	29	42
Zone 17	0.3	1000000	300000	0.42	126000.0	43	43	42	53	29	42
Zone 18	0.3	1000000	300000	0.42	126000.0	43	43	42	53	29	42
Zone 19	0.3	1000000	300000	0.42	126000.0	43	43	42	53	29	42
Zone 20	0.3	1000000	300000	0.42	126000.0	43	43	42	53	29	42
Total	10	1000000	1000000		2602250.0						

Pliocene DP-3			Bulk Model Volume	Mean Porosity for Zone	Pore Volume				
Zones			m^3		m^3	LF1	LF2	LF3	Zone Mean
Zone 1	0.2308	1000000	230800	0.47	108476.0	51	43		47
Zone 2	0.2308	1000000	230800	0.41	94628.0	51	43	29	41
Zone 3	0.2308	1000000	230800	0.41	94628.0	51	43	29	41
Zone 4	0.2308	1000000	230800	0.41	94628.0	51	43	29	41
Zone 5	0.2308	1000000	230800	0.41	94628.0	51	43	29	41
Zone 6	0.2308	1000000	230800	0.41	94628.0	51	43	29	41
Zone 7	0.2308	1000000	230800	0.41	94628.0	51	43	29	41
Zone 8	0.2308	1000000	230800	0.41	94628.0	51	43	29	41
Zone 9	0.2308	1000000	230800	0.41	94628.0	51	43	29	41
Zone 10	0.2308	1000000	230800	0.41	94628.0	51	43	29	41
Zone 11	0.2308	1000000	230800	0.41	94628.0	51	43	29	41
Zone 12	0.2308	1000000	230800	0.41	94628.0	51	43	29	41
Zone 13	0.2308	1000000	230800	0.41	94628.0	51	43	29	41
Total	10	1000000	1000000		1244012.0				

Pliocene DP-4			Bulk Model Volume	Mean Porosity for Zone	Pore Volume						
Zones			m^3		m^3	LF1	LF2	LF3	LF4	LF5	Zone Mea
Zone 1	0.3	1000000	300000	0.4375	131250.0	40	52	40	43		43.75
Zone 2	0.3	1000000	300000	0.4375	131250.0	40	52	40	43		43.75
Zone 3	0.3	1000000	300000	0.4375	131250.0	40	52	40	43		43.75
Zone 4	0.3	1000000	300000	0.408	122400.0	40	52	40	43	29	40.8
Zone 5	0.3	1000000	300000	0.408	122400.0	40	52	40	43	29	40.8
Zone 6	0.3	1000000	300000	0.408	122400.0	40	52	40	43	29	40.8
Zone 7	0.3	1000000	300000	0.408	122400.0	40	52	40	43	29	40.8
Zone 8	0.3	1000000	300000	0.408	122400.0	40	52	40	43	29	40.8
Zone 9	0.3	1000000	300000	0.408	122400.0	40	52	40	43	29	40.8
Zone 10	0.3	1000000	300000	0.408	122400.0	40	52	40	43	29	40.8
Total	10	1000000	1000000		1250550.0						

Miocene			Bulk Model Volume	Mean Porosity for Zone	Pore Volume									
Zones			m^3		m^3	LF1	LF2	LF3	LF4	LF5	LF6	LF7	LF8	Zone Mean
Zone 1	2	1000000	2000000	0.359333333	718666.7	33.8	36.2	33.8	44	31	36.8			35.93333333
Zone 2	2	1000000	2000000	0.294666667	589333.3	13	40.8	34.6						29.46666667
Zone 3	3	1000000	3000000	0.2985	895500.0	13	31	40.8	34.6					29.85
Zone 4	1	1000000	1000000	0.2985	298500.0	13	31	40.8	34.6					29.85
Zone 5	3	1000000	3000000	0.289	867000.0	25	31	25	34.6					28.9
Zone 6	2	1000000	2000000	0.329857143	659714.3	33.8	12.6	34.5	44.7	31	40.8	33.5		32.98571429
Zone 7	3	1000000	3000000	0.343375	1030125.0	42.5	13.1	34.5	44.7	31	40.8	33.5	34.6	34.3375
Zone 8	3	1000000	3000000	0.3705	1111500.0	40.8	39.3	33.5	34.6					37.05
Zone 9	4	1000000	4000000	0.3705	1482000.0	40.8	39.3	33.5	34.6					37.05
Zone 10	3	1000000	3000000	0.362	1086000.0	33.8	36.2	34.5	44.7	31	37			36.2
Zone 11	6	1000000	6000000	0.369	2214000.0	38	36.2	34.5	44.7	31	37			36.9
Zone 12	8	1000000	8000000	0.339	2712000.0	31	36.8							33.9
Zone 13	2	1000000	2000000	0.340833333	681666.7	33.8	36.2	33.8	44.7	31	25			34.08333333
Zone 14	2	1000000	2000000	0.361666667	723333.3	33.8	36.2	34.5	44.7	31	36.8			36.16666667
Zone 15	7	1000000	7000000	0.335571429	2349000.0	19	36.2	34.5	44.7	31	32.7	36.8		33.55714286
Zone 16	1	1000000	1000000	0.306	306000.0	44.7	31	25	25	25	38.5	25		30.6
Zone 17	5	1000000	5000000	0.34225	1711250.0	31	36.8	33.5	35.6					34.225
Zone 18	0	1000000	0	0.3295	0.0	44.7	31	25	33.5	38.5	25			32.95
Zone 19	7	1000000	7000000	0.335166667	2346166.7	21.7	31	40.8	33.5	38.5	35.6			33.51666667
Zone 20	1	1000000	1000000	0.3464	346400.0	33.8	36.2	44.7	25	33.5				34.64
Zone 21	2	1000000	2000000	0.357857143	715714.3	33.8	36.2	34.5	44.7	31	36.8	33.5		35.78571429
Zone 22	4	1000000	4000000	0.36	1440000.0	33.8	36.2	44.7	31	36.8	33.5			36
Zone 23	2	1000000	2000000	0.359	718000.0	33.8	36.2	33.8	44.7	31				35.9
Zone 24	2	1000000	2000000	0.3596	719200.0	33.8	44.7	31	36.8	33.5				35.96
Zone 25	2	1000000	2000000	0.37125	742500.0	33.8	36.2	33.8	44.7					37.125
Total	77	1000000	77000000		26463570.2									

APPENDIX XIV

Compaction Algorithms

This appendix contains porosity compaction results for calcite samples from both field areas showing compaction down to 2,000m in 500m increments. A modified version of the Athy's compaction equation for grain-rich carbonates was used to calculate these porosity values. The equation is included below in the spreadsheet.

Compaction Algorithm										
$\exp(-z/k)*\phi$										
Compaction Coefficient (k)										
3990										
RP	Porosity	Depth (m)	Depth (m)	Depth (m)	Depth (m)	Depth (m)	Depth (m)	Depth (m)	Depth (m)	Depth (m)
		4000	3500	3000	2500	2000	1500	1000	500	
	RP-F6-S1	36.9	13.5	15.3	17.4	19.7	22.3	25.3	28.7	32.5
	RP-F6-S2A	43.9	16.1	18.2	20.7	23.4	26.6	30.1	34.1	38.7
	RP-F6-S2B	43.6	16.0	18.1	20.6	23.3	26.4	30.0	34.0	38.5
	RP-F6-S3	46.6	17.1	19.4	22.0	24.9	28.2	32.0	36.3	41.1
	RP-F7-S1	35.5	13.0	14.8	16.8	19.0	21.5	24.4	27.7	31.4
	RP-F7-S2B	37.8	13.9	15.7	17.8	20.2	22.9	26.0	29.4	33.4
	RP-F7-S3A	38.6	14.1	16.0	18.2	20.6	23.4	26.5	30.0	34.0
	RP-F7-S3B	39.4	14.4	16.4	18.6	21.0	23.8	27.0	30.6	34.7
	RP-F7-S4a	42.6	15.7	17.7	20.1	22.8	25.8	29.3	33.2	37.6
	RP-F7-S4b	44.5	16.3	18.5	21.0	23.8	27.0	30.6	34.7	39.3
	RP-F7-S5	35.7	13.1	14.8	16.8	19.1	21.6	24.5	27.7	31.5
	RP-F7-S6	42.1	15.4	17.5	19.8	22.5	25.5	28.9	32.7	37.1
	RP-F7-S9	37.6	13.8	15.6	17.7	20.1	22.8	25.8	29.3	33.2
	RP-F8-S1a	43.7	16.0	18.2	20.6	23.3	26.4	30.0	34.0	38.5
	RP-F8-S1b	43.2	15.8	18.0	20.4	23.1	26.1	29.6	33.6	38.1
	RP-F8-S2	40.7	14.9	16.9	19.2	21.7	24.6	27.9	31.7	35.9
	RP-F10-S1	37.1	13.6	15.4	17.5	19.8	22.5	25.5	28.9	32.7
	RP-F10-S3	39.3	14.4	16.3	18.5	21.0	23.8	27.0	30.6	34.7
	RP-F10-S4	42.9	15.7	17.8	20.2	22.9	26.0	29.4	33.4	37.8
	RP-F11-S1	27.7	10.2	11.5	13.1	14.8	16.8	19.0	21.6	24.5
	RP-F11-S2	13.6	5.0	5.7	6.4	7.3	8.2	9.3	10.6	12.0
	RP-F11-S3A	32.0	11.7	13.3	15.1	17.1	19.4	22.0	24.9	28.2
	RP-F11-S3B	14.5	5.3	6.0	6.8	7.8	8.8	10.0	11.3	12.8
	RP-F11-S4A	10.9	4.0	4.5	5.1	5.8	6.6	7.5	8.5	9.6
	RP-F11-S4B	13.2	4.8	5.5	6.2	7.1	8.0	9.1	10.3	11.6
	RP-F11-S5A	12.3	4.5	5.1	5.8	6.5	7.4	8.4	9.5	10.8
	RP-F11-S5B	14.1	5.2	5.9	6.7	7.6	8.6	9.7	11.0	12.5
RM	RM-F9-S1	13.7	5.0	5.7	6.5	7.3	8.3	9.4	10.7	12.1
	RM-F9-S2A	29.8	10.9	12.4	14.1	15.9	18.1	20.5	23.2	26.3
	RM-F9-S2B	32.0	11.7	13.3	15.1	17.1	19.4	22.0	24.9	28.2
	RM-F9-S3	11.4	4.2	4.7	5.4	6.1	6.9	7.8	8.9	10.0
PR	PR-F1-S1	38.9	14.3	16.2	18.3	20.8	23.5	26.7	30.3	34.3
	PR-F1-S3A	39.2	14.4	16.3	18.5	20.9	23.7	26.9	30.5	34.6
	PR-F1-S3B	40.6	14.9	16.9	19.1	21.7	24.6	27.9	31.6	35.8
	PR-F2-S2A	34.9	12.8	14.5	16.5	18.7	21.1	24.0	27.2	30.8
	PR-F2-S2B	32.3	11.8	13.4	15.2	17.3	19.6	22.2	25.1	28.5
	PR-F2-S4	23.4	8.6	9.7	11.1	12.5	14.2	16.1	18.2	20.7
	PR-F2-S5A	38.1	14.0	15.8	17.9	20.3	23.1	26.1	29.6	33.6
	PR-F2-S5B	39.7	14.6	16.5	18.7	21.2	24.1	27.3	30.9	35.1
	PR-F2-S6	38.5	14.1	16.0	18.2	20.6	23.3	26.4	30.0	34.0
	PR-F2-S7	45.6	16.7	19.0	21.5	24.4	27.6	31.3	35.5	40.2
	PR-F2-S8A	31.7	11.6	13.2	14.9	16.9	19.2	21.7	24.6	27.9
	PR-F2-S8B	25.9	9.5	10.8	12.2	13.9	15.7	17.8	20.2	22.9
	PR-F3-S1	41.3	15.1	17.2	19.5	22.1	25.0	28.3	32.1	36.4
	PR-F3-S2	35.4	13.0	14.7	16.7	18.9	21.4	24.3	27.6	31.2
	PR-F3-S3	35.1	12.9	14.6	16.6	18.8	21.3	24.1	27.3	31.0
	PR-F5-S2A	47.7	17.5	19.8	22.5	25.5	28.9	32.8	37.1	42.1
	PR-F5-S2B	34.3	12.6	14.3	16.2	18.3	20.8	23.6	26.7	30.3
	PR-F5-S3A	32.8	12.0	13.6	15.5	17.5	19.9	22.5	25.5	28.9
	PR-F5-S3B	31.0	11.4	12.9	14.6	16.6	18.8	21.3	24.1	27.4
	PR-F7-S1	49.7	18.2	20.7	23.4	26.6	30.1	34.1	38.7	43.9
	PR-F7-S2	55.8	20.5	23.2	26.3	29.8	33.8	38.3	43.5	49.3
	PR-F7-S3	53.3	19.5	22.2	25.1	28.5	32.3	36.6	41.5	47.0
	PR-F8-S1	53.6	19.7	22.3	25.3	28.6	32.4	36.8	41.7	47.3
	PR-F11-S1	44.1	16.2	18.3	20.8	23.5	26.7	30.3	34.3	38.9
	PR-F11-S2	49.1	18.0	20.4	23.1	26.2	29.7	33.7	38.2	43.3
	PR-F11-S4A	40.9	15.0	17.0	19.3	21.9	24.8	28.1	31.8	36.1
	PR-F11-S4B	40.0	14.7	16.6	18.9	21.4	24.2	27.5	31.2	35.3
	PR-F13-S1	42.5	15.6	17.7	20.1	22.7	25.8	29.2	33.1	37.5
	PR-F13-S2A	40.2	14.7	16.7	18.9	21.5	24.3	27.6	31.3	35.4
	PR-F13-S2B	39.1	14.3	16.3	18.4	20.9	23.7	26.8	30.4	34.5
	PR-F13-S3A	54.9	20.1	22.8	25.9	29.3	33.2	37.7	42.7	48.4
	PR-F14-S1A	40.6	14.9	16.9	19.2	21.7	24.6	27.9	31.6	35.9
	PR-F14-S1B	43.0	15.8	17.9	20.3	23.0	26.0	29.5	33.4	37.9
	PR-F14-S2	48.3	17.7	20.1	22.8	25.8	29.3	33.2	37.6	42.6
	PR-F14-S4	40.4	14.8	16.8	19.0	21.6	24.5	27.7	31.4	35.6
	PR-F14-S6A	44.4	16.3	18.5	20.9	23.7	26.9	30.5	34.5	39.1
	PR-F14-S6B	37.6	13.8	15.6	17.7	20.1	22.8	25.8	29.2	33.2
	PR-F14-S7A	40.0	14.7	16.6	18.9	21.4	24.2	27.5	31.1	35.3
	PR-F14-S7B	42.3	15.5	17.6	19.9	22.6	25.6	29.0	32.9	37.3
	PR-F14-S7C	44.8	16.4	18.6	21.1	23.9	27.1	30.7	34.8	39.5
	PR-F14-S8A	58.1	21.3	24.2	27.4	31.1	35.2	39.9	45.2	51.3
	PR-F14-S8B	51.6	18.9	21.5	24.3	27.6	31.2	35.4	40.1	45.5
	PR-F15-S1A	28.0	10.3	11.7	13.2	15.0	17.0	19.3	21.8	24.7
	PR-F15-S1B	34.8	12.8	14.5	16.4	18.6	21.1	23.9	27.1	30.7
	PR-F15-S2A	48.6	17.8	20.2	22.9	26.0	29.4	33.4	37.8	42.9
	PR-F15-S2B	52.6	19.3	21.9	24.8	28.1	31.9	36.1	41.0	46.4

PW	PW-F1-S1	36.6	13.4	15.2	17.2	19.5	22.1	25.1	28.5	32.3
	PW-F1-S2A	33.7	12.4	14.0	15.9	18.0	20.4	23.2	26.3	29.8
	PW-F1-S2B	33.6	12.3	14.0	15.9	18.0	20.4	23.1	26.2	29.7
	PW-F1-S3	41.3	15.2	17.2	19.5	22.1	25.0	28.4	32.2	36.5
	PW-F1-S4A	44.0	16.1	18.3	20.7	23.5	26.6	30.2	34.2	38.8
	PW-F1-S4B	35.0	12.8	14.5	16.5	18.7	21.2	24.0	27.2	30.8
	PW-F1-S5A	53.6	19.7	22.3	25.3	28.6	32.4	36.8	41.7	47.2
	PW-F1-S5B	51.1	18.8	21.3	24.1	27.3	31.0	35.1	39.8	45.1
	PW-F1-S6	52.7	19.3	21.9	24.8	28.1	31.9	36.2	41.0	46.5
	PW-F2-S5	42.4	15.5	17.6	20.0	22.6	25.7	29.1	33.0	37.4
	PW-F2-S2	46.3	17.0	19.3	21.8	24.8	28.1	31.8	36.1	40.9
	PW-F3-S1A	55.3	20.3	23.0	26.1	29.6	33.5	38.0	43.1	48.8
	PW-F3-S1B	54.0	19.8	22.5	25.5	28.9	32.7	37.1	42.0	47.7
	PW-F3-S2	46.1	16.9	19.2	21.7	24.6	27.9	31.6	35.9	40.6
	PW-F3-S3A	42.4	15.5	17.6	20.0	22.6	25.7	29.1	33.0	37.4
	PW-F3-S3B	42.3	15.5	17.6	19.9	22.6	25.6	29.0	32.9	37.3
	PW-F3-S4	48.2	17.7	20.0	22.7	25.7	29.2	33.1	37.5	42.5
	PW-F3-S5	38.3	14.1	15.9	18.1	20.5	23.2	26.3	29.8	33.8
	PW-F3-S6	35.3	12.9	14.7	16.6	18.9	21.4	24.2	27.5	31.1
	PW-F3-S7A	42.3	15.5	17.6	19.9	22.6	25.6	29.0	32.9	37.3
	PW-F3-S7B	50.2	18.4	20.9	23.7	26.8	30.4	34.5	39.1	44.3
	PW-F4-S1	49.1	18.0	20.4	23.1	26.2	29.7	33.7	38.2	43.3
	PW-F4-S2	47.6	17.5	19.8	22.4	25.4	28.8	32.7	37.0	42.0
	PW-F5-S1	47.3	17.4	19.7	22.3	25.3	28.7	32.5	36.8	41.8
	PW-F5-S2	46.9	17.2	19.5	22.1	25.0	28.4	32.2	36.5	41.3
	PW-F6-S1A	45.7	16.8	19.0	21.6	24.4	27.7	31.4	35.6	40.3
	PW-F6-S1B	52.7	19.3	21.9	24.9	28.2	31.9	36.2	41.0	46.5
	PW-F6-S2	47.5	17.4	19.8	22.4	25.4	28.8	32.6	37.0	41.9
	PW-F6-S3	48.9	17.9	20.3	23.0	26.1	29.6	33.6	38.0	43.1
	PW-F6-S4	44.8	16.4	18.6	21.1	23.9	27.1	30.7	34.8	39.5
	PW-F6-S5	50.0	18.3	20.8	23.6	26.7	30.3	34.3	38.9	44.1
	PW-F6-S6	45.7	16.8	19.0	21.5	24.4	27.7	31.4	35.6	40.3
	PW-F6-S7A	40.7	14.9	16.9	19.2	21.7	24.6	27.9	31.7	35.9
	PW-F6-S7B	45.1	16.5	18.8	21.3	24.1	27.3	31.0	35.1	39.8
	PW-F6-S8	49.8	18.3	20.7	23.5	26.6	30.1	34.2	38.7	43.9
	PW-F6-S9	49.9	18.3	20.8	23.5	26.7	30.2	34.3	38.8	44.0
	PW-F7-S1	49.2	18.1	20.5	23.2	26.3	29.8	33.8	38.3	43.4
PT	PT-F1-S1	38.3	14.0	15.9	18.0	20.5	23.2	26.3	29.8	33.8
	PT-F1-S3A	49.2	18.1	20.5	23.2	26.3	29.8	33.8	38.3	43.4
	PT-F1-S3B	47.7	17.5	19.9	22.5	25.5	28.9	32.8	37.2	42.1
	PT-F1-S4	45.8	16.8	19.0	21.6	24.5	27.7	31.4	35.6	40.4
	PT-F1-S1A-lat	49.8	18.3	20.7	23.5	26.6	30.2	34.2	38.8	43.9
	PT-F1-S1B-lat	52.1	19.1	21.7	24.5	27.8	31.5	35.8	40.5	45.9
	PT-F1-S3-lat	54.6	20.0	22.7	25.8	29.2	33.1	37.5	42.5	48.2
	PT-F1-S4A-lat	54.0	19.8	22.5	25.5	28.9	32.7	37.1	42.0	47.7
	PT-F1-S4B-lat	56.2	20.6	23.4	26.5	30.0	34.0	38.6	43.7	49.6
	PT-F1-S5-lat	52.1	19.1	21.7	24.6	27.8	31.6	35.8	40.6	46.0
	PT-F2-S1A	47.0	17.3	19.6	22.2	25.1	28.5	32.3	36.6	41.5
	PT-F2-S1B	41.0	15.1	17.1	19.4	21.9	24.9	28.2	31.9	36.2
	PT-F2-S2	55.3	20.3	23.0	26.1	29.5	33.5	37.9	43.0	48.7
	PT-F2-S3	49.7	18.2	20.7	23.4	26.6	30.1	34.1	38.7	43.9
	PT-F2-S4	54.4	20.0	22.6	25.6	29.1	32.9	37.3	42.3	48.0
	PT-F2-S5A	42.8	15.7	17.8	20.2	22.9	25.9	29.4	33.3	37.7
	PT-F2-S5B	39.4	14.4	16.4	18.6	21.0	23.8	27.0	30.6	34.7
	PT-F2-S6	44.6	16.4	18.5	21.0	23.8	27.0	30.6	34.7	39.3
	PT-F2-S7	40.7	14.9	16.9	19.2	21.8	24.7	28.0	31.7	35.9
	PT-F2-S9A	37.1	13.6	15.4	17.5	19.8	22.5	25.5	28.9	32.8
	PT-F2-S9B	36.3	13.3	15.1	17.1	19.4	22.0	24.9	28.3	32.0
	PT-S3A	51.0	18.7	21.2	24.1	27.3	30.9	35.1	39.7	45.0
	PT-S3B	43.5	16.0	18.1	20.5	23.3	26.4	29.9	33.9	38.4
	PT-S4A	46.8	17.2	19.5	22.1	25.0	28.4	32.2	36.5	41.3
	PT-S4B	47.9	17.6	19.9	22.6	25.6	29.0	32.9	37.3	42.2
PM	PM-F1-S1	37.9	13.9	15.8	17.9	20.3	23.0	26.0	29.5	33.4
	PM-F2-S2	41.3	15.2	17.2	19.5	22.1	25.0	28.4	32.2	36.5
	PM-F6-S1	44.2	16.2	18.4	20.8	23.6	26.8	30.4	34.4	39.0
	PM-F6-S4	52.4	19.2	21.8	24.7	28.0	31.7	36.0	40.8	46.2
	PM-F6-S5	47.6	17.5	19.8	22.4	25.4	28.8	32.7	37.0	42.0
	PM-F7-S1	38.1	14.0	15.8	18.0	20.4	23.1	26.1	29.6	33.6
	PM-F7-S2	30.4	11.1	12.6	14.3	16.2	18.4	20.8	23.6	26.8
	PM-F7-S3	38.1	14.0	15.9	18.0	20.4	23.1	26.2	29.7	33.6
	PM-F7-S4	49.8	18.3	20.7	23.5	26.6	30.1	34.2	38.7	43.9
	PM-F7-S5	38.0	14.0	15.8	17.9	20.3	23.0	26.1	29.6	33.6
	PM-F7-S6	32.6	12.0	13.5	15.4	17.4	19.7	22.4	25.4	28.7

	PM-F7-S7	41.4	15.2	17.2	19.5	22.2	25.1	28.5	32.3	36.6
	PM-F8-S1	30.8	11.3	12.8	14.5	16.5	18.7	21.2	24.0	27.2
	PM-F8-S2	27.6	10.1	11.5	13.0	14.8	16.7	19.0	21.5	24.4
	PM-F8-S3	32.8	12.0	13.6	15.5	17.5	19.9	22.5	25.5	28.9
	PM-F10-S1	49.3	18.1	20.5	23.2	26.3	29.9	33.8	38.4	43.5
	PM-F10-S2	42.8	15.7	17.8	20.2	22.9	25.9	29.4	33.3	37.7
	PM-F11-S3	37.7	13.9	15.7	17.8	20.2	22.9	25.9	29.4	33.3
	PM-F11-S5	44.6	16.4	18.6	21.0	23.8	27.0	30.6	34.7	39.3
	PM-F12S1	42.8	15.7	17.8	20.2	22.9	25.9	29.4	33.3	37.7
	PM-F12S2	50.5	18.5	21.0	23.8	27.0	30.6	34.7	39.3	44.5
	PM-F12-S3	54.3	19.9	22.6	25.6	29.0	32.9	37.3	42.3	47.9
	PM-F13-S1	46.3	17.0	19.3	21.8	24.7	28.0	31.8	36.0	40.8
	PM-F13-S2	47.7	17.5	19.8	22.5	25.5	28.9	32.7	37.1	42.1
	PM-F13-S3A	51.4	18.9	21.4	24.2	27.5	31.2	35.3	40.0	45.4
	PM-F13-S3B	54.0	19.8	22.5	25.5	28.9	32.7	37.1	42.0	47.6
	PM-F16-S2	53.9	19.8	22.4	25.4	28.8	32.6	37.0	41.9	47.5
	PM-F17-S1	58.3	21.4	24.2	27.5	31.2	35.3	40.0	45.4	51.4
PB										
	PB-F1-S1A	33.8	12.4	14.1	15.9	18.1	20.5	23.2	26.3	29.8
	PB-F1-S1B	35.3	13.0	14.7	16.6	18.9	21.4	24.2	27.5	31.2
	PB-F1-S2	32.4	11.9	13.5	15.3	17.3	19.6	22.2	25.2	28.6
	PB-F1-S4	35.9	13.2	14.9	16.9	19.2	21.8	24.7	28.0	31.7
	PB-F2-S1	31.8	11.7	13.2	15.0	17.0	19.3	21.9	24.8	28.1
	PB-F3-S2	45.0	16.5	18.7	21.2	24.0	27.3	30.9	35.0	39.7
	PB-F3-S3	41.5	15.2	17.3	19.6	22.2	25.1	28.5	32.3	36.6
	PB-F3-S4A	44.8	16.4	18.6	21.1	23.9	27.1	30.7	34.8	39.5
	PB-F3-S4B	46.2	17.0	19.2	21.8	24.7	28.0	31.8	36.0	40.8
PD										
	PD-F1-S1A	28.3	10.4	11.8	13.3	15.1	17.1	19.4	22.0	24.9
	PD-F1-S1B	36.4	13.4	15.1	17.2	19.5	22.1	25.0	28.3	32.1
	PD-F1-S4A	43.2	15.9	18.0	20.4	23.1	26.2	29.7	33.7	38.2
	PD-F1-S4B	41.3	15.1	17.2	19.5	22.1	25.0	28.3	32.1	36.4
	PD-F1-S7	38.4	14.1	16.0	18.1	20.5	23.3	26.4	29.9	33.9
	PD-F3-S4A	42.6	15.6	17.7	20.1	22.8	25.8	29.3	33.2	37.6
	PD-F3-S4B	42.8	15.7	17.8	20.2	22.9	25.9	29.4	33.3	37.8
	PD-F3-S7A	39.0	14.3	16.2	18.4	20.9	23.7	26.8	30.4	34.4
	PD-F3-S7B	42.3	15.5	17.6	19.9	22.6	25.6	29.0	32.9	37.3
	PD-F4-S1A	38.7	14.2	16.1	18.2	20.7	23.4	26.5	30.1	34.1
	PD-F4-S1B	33.5	12.3	13.9	15.8	17.9	20.3	23.0	26.1	29.6
	PD-F4-S4	39.1	14.4	16.3	18.4	20.9	23.7	26.9	30.4	34.5
	PD-F4-S5	33.2	12.2	13.8	15.6	17.7	20.1	22.8	25.8	29.3
	PD-F5-S2	40.0	14.7	16.6	18.8	21.4	24.2	27.4	31.1	35.3
PV										
	PV-F1-S3A	37.4	13.7	15.5	17.6	20.0	22.6	25.7	29.1	33.0
	PV-F1-S3B	33.2	12.2	13.8	15.6	17.7	20.1	22.8	25.8	29.3
	PV-F2-S1	40.4	14.8	16.8	19.1	21.6	24.5	27.8	31.5	35.7
	PV-F3-S4A	45.9	16.8	19.1	21.6	24.5	27.8	31.5	35.7	40.5
	PV-F3-S4B	44.3	16.3	18.4	20.9	23.7	26.9	30.4	34.5	39.1
	PV-F4-S1	50.4	18.5	21.0	23.8	26.9	30.5	34.6	39.2	44.4
	PV-F4-S3A	35.6	13.0	14.8	16.8	19.0	21.5	24.4	27.7	31.4
	PV-F4-S3B	43.1	15.8	17.9	20.3	23.0	26.1	29.6	33.5	38.0